Studies on Contribution of Astrocyte Secreted Proteins on Neuronal Health in Models of Alzheimer's Disease

Thesis submitted for the degree of

Doctor of Philosophy (Science)

In Biochemistry

By

Sukanya Sarkar

Regn.no: 02640/Ph.D.(Sc.)Proceed/2019

Department of Biochemistry

University of Calcutta

2022

This thesis work is dedicated
to
'Maa' & 'Baba'

ACKNOWLEDGEMENT

"For my part, I am almost contended just now, and very thankful. Gratitude is a divine emotion: it fills the heart, but not to bursting; it warms it, but not to fever."

Charlotte Bronte

Standing at the end of the six-year adventure (PhD) that I just had, I look back and try to remember where it all began. I see a much younger Sukanya uncertain of her inner calling working at a job, enjoying every bit of the science but yet something did not feel right. It was because she wanted to do her own science and have her own 'Eureka' moments. Each passing day she became more and more certain of what she wanted and although her fate presented her with many challenges including a last minute cancellation of PhD interview, she fought through them with all her might finally joining the laboratory of Dr. Subhas C. Biswas. There is a quote that goes "It takes a village to raise a child". My laboratory and my family is my village that raised me, fed me and shaped me into what I am today. It is my pleasure to thank each one of them from the bottom of my heart.

My parents **Srimati Chhanda Sarkar** and **Sri Manab Kumar Sarkar** are my strength. They are the pillars of my existence. They sacrificed many pleasures of their own to build me. I know I have them beside me whenever I need them, imbibing from them the very zeal for life. Maa has taught me that nothing is impossible for a girl if her heart is in the right place and to passionately do her part, leaving the rest to Almightly. Her deep confidence in me is my constant motivation in life and career. My Baba is a creative person and he has always balanced out my life with his humor. He has gifted me the biggest power of

forgiveness which I am still in the process of emulating in my life. I hope to make them proud everyday in every aspect.

I have always been intrigued by the brain. The 'brain' and the 'mind' are inseparable. I have seen in my childhood how much the diseases of the mind are stigmatized in our society. Hence, I knew I wanted to investigate the unknown crevices of the mind and work with diseases of the brain. I got acquainted with **Dr. Subhas C. Biswas** during my Masters at Biochemistry department, University of Calcutta. He is a passionate teacher and I was an inquisitive student. He answered all my questions very patiently and I knew that I wanted to work with him because only a patient scientist can have an unbiased perspective of science. Today, I can proudly say that he gave me that and more. It is difficult to put to words what role he has played in shaping me during the past six years. Besides being a very perceptive scientist, he is an honest and kind human being. PhD is not only a journey with science but greatly impacts your overall life. Dr. Biswas has been a very understanding mentor and taught me critical insights of life that helped me sail through the stormy phases of my tenure. He also gave me absolute freedom in science and that really pushed me beyond my limits. He made me believe that science can be great even with a small honest step at a time. I am thankful and grateful that he chose me as his student and I found him as my mentor. I convey my deepest gratitude to Dr. Subhas C. Biswas for his immense contribution to this thesis starting from its inception.

The initial few years into my PhD, the long conversations I had with **Dr. P.K. Sarkar** (INSA Honorary Scientist, IICB), in Room 242 were really brain-storming. While he told stories of Harvard, I would imagine those for myself and how science thrived so

beautifully even in those days when amenities were limited. He taught me to bring perfection to my scientific endeavors and provided critical insights on my thesis work. I thank him deeply for his infectious enthusiasm and admire him for his deep knowledge in neuroscience. I also thank **Dr. Sumantra Das** (former H.O.D. of CBP Dept., CSIR-IICB) for his kind words to me from time-to-time and his straight-forward attitude towards life and science. Scientists like them are inspirations for many.

I also thank **Dr. Arun Bandyopadhyay**, Director, CSIR-IICB for providing me the institutional facilities and financial support for carrying out my research work. I highly acknowledge **Council of Scientific and Industrial Research (CSIR)-Government of India** for providing me the laboratory support. I deeply convey my gratitude to **Department of Science and Technology (DST) - INSPIRE** for providing me the independent fellowship that supported me throughout my tenure.

Coming to my laboratory village that raised me in these six years my heart feels with warm emotions. It has been my second home where I have spent my mornings, my nights, my weekends and my holidays getting absorbed in the whole essence of **'My Lab'**. I care for each and every instrument of my lab and convey my deep gratitude to them for helping me with the acquisition of all my thesis data. I thank my lab with all my heart for listening to my laughter and my complaints equally and non-judgmentally. My lab-mates have been the part and parcel of my tenure and have supported me all throughout. I remember the number of times the address of the village (lab-shift) changed from Room 247 to Room 239 and then back to Room 247 - from rickety room to fancy interiors. Without the collective efforts of all my colleagues it would have been

impossible. The whole laboratory has been arranged and still being maintained by the incessant hard work of my colleagues and hope that it only grows bigger and better in the coming days.

I feel fortunate to learn a lot of things from my seniors. In my earliest days, the person that completely supported and taught me animal handling and experimentation is **Ramesh**. Besides our fights like Tom and Jerry, he constantly emphasized the value of promptness and with him there was not a single moment of dullness. Although we had our share of differences, we have a bond of friendship that stood the test of time and distance. I am deeply grateful for his contribution in my training and to my work. **Kusumikadi** is my go-to-person in my lab and she had a patient ear to my problems. She is a person I really admire for her intellect and her scientific collaboration with me is sure to bear the best fruits. **Subhalakshmidi** taught me the nitty-gritty of cell culture and kept me motivated cheering me up every time I was upset on the face of experimental failures. She has a zeal for trying new things and I think that had brushed on me. I thank her with all my heart. **Hrishitadi** has a 'calmness' to her that I deeply admire and her creative personality is reflected through her work – experimental design to thesis writing – she does everything with panache. I really enjoyed our scientific partnership. **Anoyda** is the most helpful person around and has a solution to all my technical bottlenecks. It's just so much fun with him around us. **Pallabidi** has been really kind to me and every time we had a scientific conversation it generated not just new but brilliant ideas. We often shared our philosophical views on life and women empowerment in STEM. **Akashda** and I had a cute relationship and I really admire his meticulous nature of teaching and his

great taste in fashion. I have been fortunate to learn a lot from **Pamapadi** while working towards our common goal and I am grateful to **Rebeccadi** for her help at the time when I most needed her. I thank my super seniors **Suraiyadi** and **Priyankarda** for their support and insights whenever I looked up to them.

Diptesh is my dearest junior and his presence itself makes every environment lighter and so much easier. Hope that he achieves whatever dreams he has and also brings to fruition the project we have been working towards. I have closely worked with **Naqiya** and love her sense of organization and thorough understanding of her job. **Soumita** is a ball of energy and her enthusiasm be it in work or at play (Ooty) is contagious. I thoroughly enjoyed exchanging knowledge with you guys and have fond memories. The new kids around – **Angshuman** and **Ananya** – I wish you all the best for your PhD adventures.

My own training in the lab would not be complete without my trainees **Ashish**, **Souvik** and **Chayan** with whom I shared great bonds. Each of them taught me things that would greatly help me when I emerge as an independent scientist myself.

I would like to extend my heartfelt gratitude to **Dr. B.N. Srikumar** and his lab members especially **Keerthana** from NIMHANS Bangalore for believeing in my project and providing me the amenities, the space and the training to perform the electrophysiology experiments that is an integral part of this thesis.

My acknowledgement will be so incomplete without mentioning the **Rats and Mice of IICB** who all sacrificed their life for this project and without them all these work would not have been possible. Hope they rest in peace.

I am thankful towards my friends that have kept me sane through my PhD tenure. **Ritapa**, **Pranay** and **Umesh** have been the victims of my regular rants and chatting (rather blabbering) with them over a cup of tea relieved me of my day's stress. I do not know how my life would have turned out if I did not have these stress-relievers in my life. My friends who are a call away **Ahana, Shreo, Dams, Aruna, Tilo, Nilu, Avishek** and **SukG** have really kept me sane and happy. My IICBian mates – **Varsha, Aleepta, Priya, Dipayan, Debanjan, Moumita, Priyanka** and **Debajyoti** – have been really my 'friends in need' and I am deeply grateful that I had found them. I found a beautiful collaborator-turned friend in **Anindita** and am thankful that she believed in me throughout the time we pursued our work together. I feel fortunate that I am blessed with some really good people in my life who have unconditionally helped me, made me believe that there is still goodness in this world and have been surprise saviors during all my last-moment revision times. I deeply thank them all. **IICB theatre** days shall also remain ever-etched in my mind as the happiest moments I have spent in IICB.

I extend my gratitude to **Dr. Aditya Konar**, **Dr. Joy Chakraborty**, **Dr. Suvendra Nath Bhattacharya**, **Dr. Krishnananda Chattopadhyay, Dr. Nahid Ali, Dr. Partha Chakraborty, Dr. Rupasri Ain, Dr. Uday Bandhyopadhyay** and **Dr. Sucheta Tripathy** and their lab members for all the facilities they provided to me. I thank the staffs of animal facility especially **Shambhuda** and **Laluda** for consistently maintained and providing animals for my research work. I extend my special thanks to **Gobindada** who is a dear member of our lab, has been a great help. His hard working jovial nature and helpful attitude have always put a smile on my face. I thank **Sounakda** and **Tapasda** for their technical support

during STED imaging and western blot development respectively. I am grateful to **Vignesh** for his immense technical expertise to bring back to life most of the instruments that broke down in my tenure. **IICB canteen** has been the place where I had the best moments with my friends and the canteen staff always gave me that extra tea, I thank them deeply. The essential space and help that **IICB central library** provided me whenever I went there will remain precious to me.

I want to extend my sincere gratitude to all my teachers, who have always motivated me to strive for excellence and pursue my dream incessantly. My heartfelt appreciation to all of my teachers who played a significant role in building my character and special thanks to my teachers from my school B.D. Memorial International especially **Sutopa Ma'am, ND ma'am** and **Suman Sir**, tuition teachers **Roy Ma'am** and **Neelanjana Ma'am**, all the teachers from St. Xavier's College Kolkata – **AKM sir, SSC ma'am, MMG ma'am, MM ma'am, RM sir** and others, and all the faculties Department of Biochemistry, University of Calcutta - **Prof. Anirban Siddhanta (Head), Prof. Maitrayee DasGupta, Prof. Sanjay Ghosh, Prof. Prasanta Kumar Bag, Prof. Maitree Banerjee, Dr. Sanghamitra Sen Gupta, Dr. Anindita Ukil, Dr. Geetanjali Sundarum, Dr. Ishani Deb, Prof. Anjan Kr. Dasgupta, Prof. Krishanu Chakrabarti, Prof. Santasree Majumder, Prof. Mrinal Kanti Poddar** who have been a constant source of inspiration.

Finally, I am grateful for the strongest and hard working yet simple family I have got without whom conceiving this dream would not be possible. I thank my **Thamma** for being so patient and jolly with me all her life and always wanting to see 'Dr.' before my name, my **Didan** for being the inspiration for my research and **Dadu** whom I lost early

but thank him for his intellectual genes. **Nadi** I hope whenever you are you are still your enigmatic self exuding a tranquility that is rare. You strong ideologies in life and sense of independence as a woman are what I would like to inculcate in my life. I also covey my deepest regards to my new family members – **Srimati Manju Rawat** (Mother-in-law) and **Sri Paduman Singh Rawat** (Father-in-law) for showing their deep love, care and understanding for me and my work that I could ever ask for and actually nurturing me throughout my PhD tenure like their own daughter. Your blessings are my motivation. **Yaminidi** has been a guide to me and her honest and lovable nature lifts my mood every time I speak to her. Her respect towards my work and enthusiasm about life in general is a constant inspiration.

Finally, life would have been nothing without the two most important persons besides my parents in my life, **Rohan (husband)** and **Sammani (sister). Rohan** is my friend, philosopher and guide whose utter conviction in me overwhelms me. I know 'he is there' - elicits a feeling that cannot be contested on and gives me the constant courage to chase my dreams and fight when life pulls me down. He has come in my life like a blessing from the Universe and with him I have started believing that tomorrow would be an even better day. He keeps me humble, patient and kind. His perspective towards life is very simple and there is only positivity around him. I feel very fortunate to be his partner and believe that without his undented support I would not have come this far. **Sammani (Dimpi)** has grown from my younger sister to my best friend. From sharing our day-to-day struggles to exploring places together, we have grown together in every way. She is my confidante and my soul. Her creative insights have significantly helped me in

my thesis work and I am ever-grateful to her for being always there for me. I just hope the best things happen to both of you and dedicate this thesis to you both.

I thank the **ALMIGHTY** for the courage to hold my head high each day and work towards my goal consistently with an undivided focus.

- Sukanya

ABSTRACT

Astrocytes are integral players in maintaining normal brain homeostasis and are the ones to respond first to any pathological insult to brain including Alzheimer's disease (AD). They go through 'reactive astrogliosis' which is increasingly being recognized as a defence mechanism rather than an offensive one. Astrocytes undergo drastic changes at the molecular, morphological and functional levels, secreting an array of cytokines, early in AD. The identity and the function/s of these cytokines remain elusive. We show that amyloid-β (Aβ) induces a state of reactivity and elicits a cytokine pool from primary astrocytes as early as 6h. We detected tissue inhibitor of matrix metalloproteinase-1 (TIMP-1) as a major neuroprotective candidate in this secretome through neuron-astrocyte co-culture studies. In primary neurons, TIMP-1 inhibited both Aβ-induced - FOXO3a-mediated apoptosis and impaired autophagy flux - by increasing Akt^{S473} phosphorylation. Furthermore, we detected that CD63 is the receptor responsible for TIMP-1 binding on neurons and mediating Akt signaling through knockdown studies. Interestingly, we detected significantly reduced levels of TIMP-1 in the hippocampi and cortices of two to ten month old 5xFAD mice, an advanced transgenic model of AD, compared to age-matched wild-type mice. Hence, intracerebroventricular injection of exogenous TIMP-1 in Aβ-induced rat model and in 5xFAD mouse specifically contributed towards inhibiting apoptosis, preventing autophagic deregulation and decreasing Aβ plaques in the hippocampus. TIMP-1 further ameliorated cognitive deficits in behavioral tests in both the animal models. We found improved synaptic protein expressions and spine F/G actin content in pure synaptosomal preparations from hippocampi and cortices of TIMP-1-treated 5xFAD mice. TIMP-1 increased long term potentiation (LTP) at the Schaffer collateral-CA1 synapses in acute hippocampal slices from 5xFAD mice in electrophysiology experiments. We unveil that inhibition of GSK3β activity by improved Akt signaling in TIMP-1-treated 5xFAD mice mediates LTP induction. Further, our results show that brain derived neurotrophic factor (BDNF) is also released in the hippocampus as a result of TIMP-1 injection in 5xFAD mouse. Thus, TIMP-1 emerges as a major neuroprotective cytokine secreted by reactive astrocytes early in response to Aβ that

ameliorates cognitive deficits by improving synaptic health in rodent models and has an exciting prospect in AD therapeutic research.

Key words: Reactive astrocytes, astrogliosis, Alzheimer's disease, Aβ, synaptic plasticity, apoptosis, autophagy, cytokine, neuroprotection

ABBREVIATIONS

Aβ: Amyloid Beta

ACh: Acetylcholine

ACM: Astrocyte Conditioned Medium

AD: Alzheimer'sDisease

ApoE4: Apolipoprotein E4

APP: Amyloid Precursor protein

BDNF: Brain derived neurotrophic factor

Bim: Bcl-2 interacting mediator of cell death

BSA: Bovine serum albumin

CINC: Cytokine-induced neutrophil chemoattractant

CNTF: Ciliary neurotrophic factor

CNS: Cental nervous system

CSF: Cerebro Spinal Fluid

CXCL: C-X-C motif chemokine ligand

DAA: Disease-associated astrocytes

DIV: Days in vitro

DLB: Dementia with Lewy Bodies

DMEM: Dulbecco's modified Eagle medium

DMSO: Dimethyl Sulphoxide

E18: Embryonic day 18

ELISA: Enzyme linked immunosorbent assay

EOAD: Early onset Alzheimer's disease

FBS: Fetal Bovine Serum

FOXO3a: Forkhead box transcriptor factor 3a

FTD: Frontotemporal dementia

GAPDH: Glyceraldehyde 3-phosphate dehydrogenase

G-CSF: granulocyte colony stimulating factor

GFAP: Glial Fibrillary Acidic protein

GFP: Green fluorescent protein

H2-D1: histocompatibility 2, D region locus 1

HFIP: 1,1,1,3,3,3-hexafluoro-2-propanol

HRP: Horse radish peroxidase

IFN: Interferon

ILs: Interleukins

ICAM-1: Intercellular adhesion molecule-1

PARP: Poly(ADP-ribose) polymerase

NFT: Neurofibrillary Tangle

TNF-α: Tumour Necrosis Factor- α

LIF: leukemia inhibitory factor

LOAD: Late onset AD

LPS: lipopolysaccharide

LRP1: lipoprotein receptor-related protein 1

MCI: Mild Cognitive Imapirment

MCP-1: monocyte chemoattractant protein-1

MIP-1α: Macrophage inflammatory protein-1 α

mTOR: molecular Target of Rapamycin

NSAIDs: nonsteroidal anti-inflammatory drugs

NF-κβ: nuclear factor kappa light chain enhancer of activated B cells

NFT: Neurofibrillary tangle

OSM: oncostatin M

PSEN: Presenilin

S100β: S100 calcium-binding protein β

SSP1: Sporulation-specific protein 1

TBI: Traumatic brain injury

TBS: Tris-buffered saline

TBST: Tris-buffered saline tween 20

TGFβ: transforming growth factor β

TIMP-1: Tissue inhibitor of matrix metalloproteinase-1

VEGF: Vascular endothelial growth factor

CONTENTS

LIST OF FIGURES

Materials and Methods

Results and Discussions

PART-I

PART-II

PART-III

Summary and Conclusion

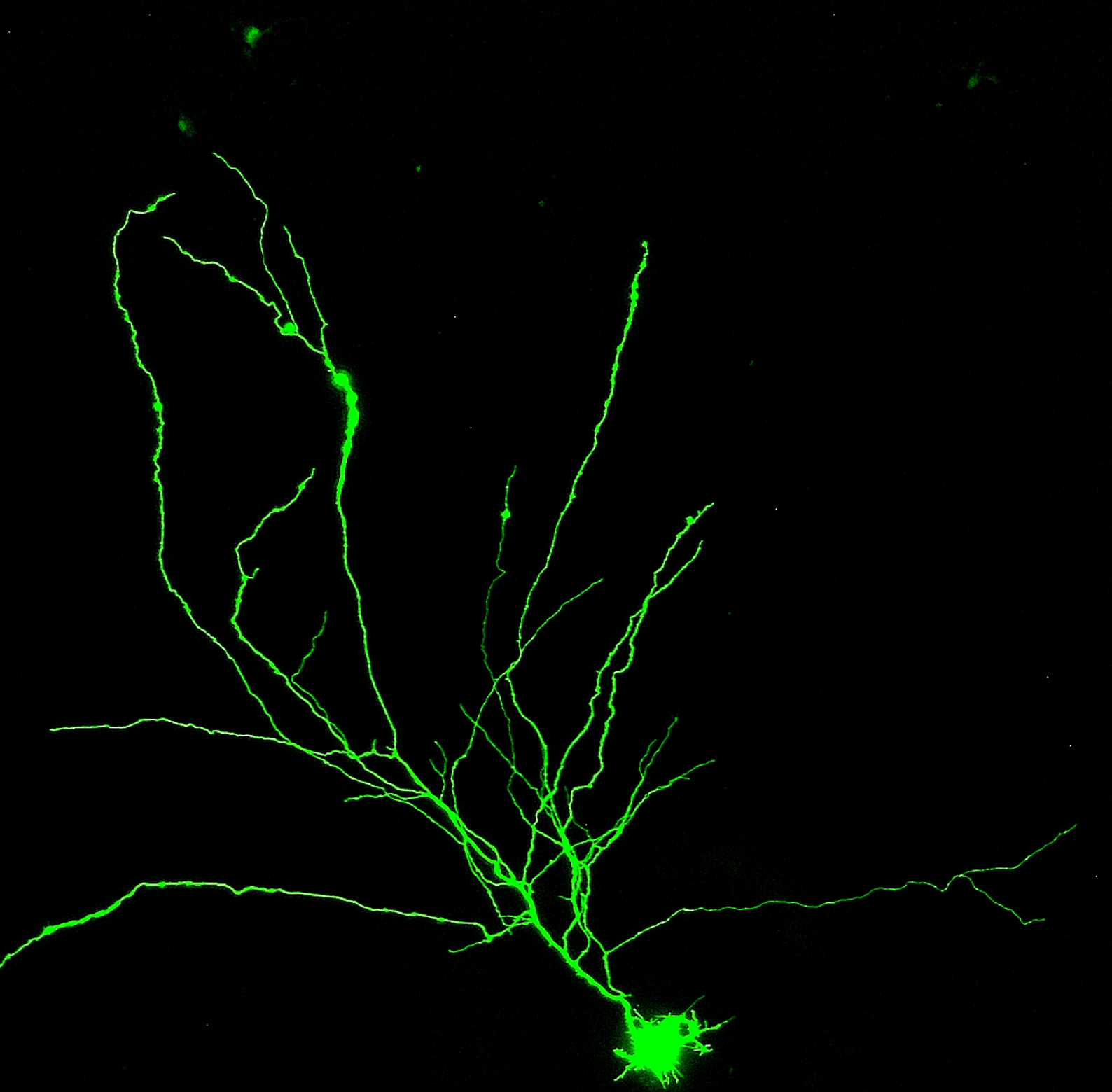

INTRODUCTION

INTRODUCTION

"The mind is like an iceberg; it floats with one-seventh of its bulk above water."

-Sigmund Freud

Gabriel Garcia Marquez's novel - 'One Hundred Years of Solitude' narrates the story of a small village plagued with a 'disease of memory loss' and how one man incessantly tried to remind himself of the items of his house, only to sadly fall prey to the same disease. That was a story, but in real life we do have a devastating disease that steals a person off his/her memories. The disease is Alzheimer's disease (AD). AD is a progressive neurodegenerative disorder that causes depletion of memory and subsequent death in oblivion. While modern medicine has extended the average human life span up to 80 years, many age-related diseases have surfaced, the major being AD. Back in 1906, Sir Alois Alzheimer's in the state asylum in Frankfurt, Germany examined a 51-year old female patient, Auguste Deter. Auguste D. had grown increasing jealous of her husband, started showing signs of cognitive deficits, was unable to orient herself in her own home and complained of confusion and paranoia. Five years later, under Sir Alois Alzheimer's observation, she died but her brain autopsy revealed exquisite details that made her and her doctor's names ever-etched in the history of neuroscience. Sir Alzheimer performed silver staining in her brain and detected what we nowknow as the most important pathological hallmarks of Alzheimer's disease – extracellular deposits outside neurons (amyloid-β plaques), tangled protein fibers inside neuron (neurofibrillary tangles) and a shrunken brain (brain atrophy) (Bondi et al., 2017). The major reason behind the

transition of the discoverer's name from the scientific field to the household is the immense epidemiological sensation AD has created. Currently, according to World Alzheimer's report 2021, 55 million people in the world are suffering from dementia and the number is 6.5 million in the age group of 65 years and above for AD-relateddementia in the US itself (https://www.alzint.org/resource/world-alzheimer-report-2021/). AD has also created a huge economic burden as the average annual expenses incurred for this disease crossed $1.3 trillion in 2020 alone. Sixty to 80% of all the dementia cases are caused due to AD. However, further investigations revealed that a little below 50% were actually pure AD while the majority was detected as mixed dementias (Murray et al., 2011). Other types of dementia involve vascular dementia, frontotemporal dementia, Parkinson's disease-related dementia, Lewy body dementia, etc., among which Lewy body dementia and vascular dementia are often associated with AD. However, each of these disease accounts for a maximum of 10% among the total dementia cases (Barker et al., 2002). The major risk factor for AD is the inevitable process of aging (Qiu et al., 2009), others being specific genetic mutations (mutations in amyloid precursor protein (APP) or presinilin1 or presenilin2) and the presence of ε4 allele in ApoE gene, family history and cardiovascular diseases. Alzheimer's association report of 2020 suggests that educational background, social life of a person and any history of traumatic brain injury are lesser known risk factors for AD (2020). Most of the cases of AD however do not have a genetic basis, expect for the correlation with ApoEε4 allele, and are categorized as late-onset Alzheimer's disease (LOAD, 65 year and above) while less than 5% of AD patients have early-onset AD (EOAD).

Memory is the part and parcel of our everyday living. The way we react to the world is dictated by our ability to learn, then construct and retrieve our memory. Hippocampal-dependent episodic memory or autobiographical memory is the worst hit by AD (Park and Lee, 2021), however other forms of memory less reliant on the hippocampus and more on amygdala, striatum, cerebellum etc. (implicit memory) are eventually damaged as the patient transitions from an asymptomatic phase (with evidence of Aβ plaques i.e. Pre-clinical AD), through mild cognitive impairment (MCI) to the severe form of AD which ultimately proves to be fatal. Interestingly, enough evidences suggest that abnormal protein depositions (Aβ plaques and tau aggregates) accumulate ten to fifteen years before the appearance of clinical cognitive deficits. At the beginning of the 21st century intensive work has been done on the MCI-related to AD phase in order to restrict the disease before the advent of drastic clinical symptoms. The current decade is observing a rise in search of suitable biomarkers to detect the disease at its earliest that is in the pre-clinical stage since this prodromal phase holds the highest potential for clinicallypreventative interventions. Even the very recent FDA approved (amidst controversies) Aβ antibody from Biogen, Aducanumab, was shown to be effective in clearing Aβ plaques in early-phase AD (MCI-related to AD and Mild AD) and provided partial recovery in cognitive functioning (Cummings et al., 2021) re-emphasizing the importance of targeting AD at its prodromal phase. Hence, in this work our major effort has been directed to unveil targets in the prodromal phase of AD.

Aducanumab research also points to the fact that the most targeted hypothesis in AD has been the 'amyloid cascade hypothesis'. According to this hypothesis, APP is cleaved along

the amyloidogenic pathway giving rise to $A\beta_{1-42}$ (the toxic peptide), that eventually aggregates to form oligomers and finally plaques triggering the initiation of the disease. Several reports from our laboratory have contributed to the understanding of molecular mechanisms by which oligomeric Aβ induces cell death pathways such as apoptosis (Akhter et al., 2014; Sanphui and Biswas, 2013) and autophagy (Saleem and Biswas, 2017) in neurons revealing important targets in the process. Yet modern research groups highly contradict the solo importance of this hypothesis, especially due to the continued failures of Aβ-targeting drugs (except the controversial Aducanumab) and believe that enhanced research should be focused on the tau hypothesis and more importantly the immune (neuroinflammation) hypothesis. A recent report even revised the amyloid cascade hypothesis stating that the depositions of Aβ plaques and abnormal tau are indicators of proteopathic stress and are preceded by a very complex cellular phase involving critical interactions of the neurons with glia and the vasculature (De Strooper and Karran, 2016). Hence, it is imperative that AD is studied from a perspective where there is an association between the major AD hypotheses; especially the amyloid hypothesis and the immune hypothesis should be focused with an integration of glial cells.

Astrocytes are the most abundant of the glial cells, the non-neuronal cells in the central nervous system (CNS). The fact that they play critical roles in maintaining brain homeostasis especially in terms of supplying energy and anti-oxidants to neurons andregulating neurotransmitter balance at synapses, make them exceptional candidates to study when situations turn hostile for the brain. A failure in their ability to perform the

normal functioning under disease conditions is now considered the propelling force behind the eventual aggressive CNS changes in AD (De Strooper and Karran, 2016). From a cellular point of view, astrocytesremain in close communication with neurons and other glial cells through an exchange of cytokine and chemokine molecules. Since cytokines and chemokines are considered integral factors of the immune mechanism of the brain, studying astrocytes in AD has become more relevant than ever.

AD research has progressed immensely in the last few decades and has divulged key cellular processes that underlie disease pathogenesis. Given the multi-factorial nature of AD, understanding the basic cellular or molecular level interactions that lead to the eventual synaptic and neuronal loss underpinning clinical symptoms is a pre-requisite for a subsequent cost-effective translational phase in AD research. With the advent of sophisticated neuroimaging techniques like PET, fMRI, CT etc. and identification of AD-specific CSF and plasma biomarkers, a silver lining is in view in the diagnosis horizon. However, there are miles to go before a successful drug can be marketed because to date the rate of failures in AD clinical trials has been 99.6% (Cummings et al., 2014). Hence, sustained research in AD is of utmost importance and is the focus of this thesis work.

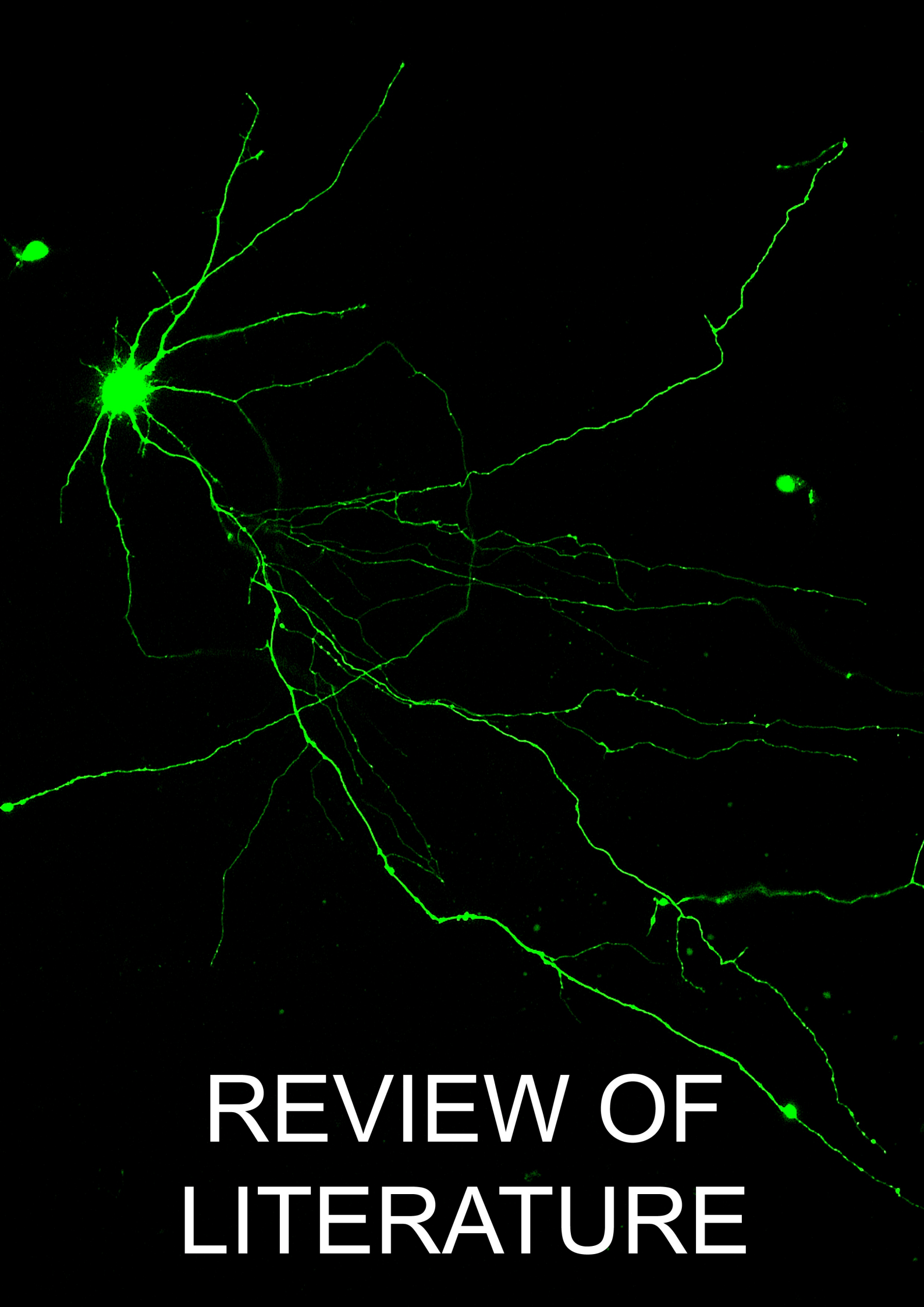

REVIEW OF LITERATURE

REVIEW OF LITERATURE

1. Alzheimer's disease

1.1. Historical perspective

In the 37th meeting of German Psychiatrists from the South-Western regions that was convened in Tübingen on 3rd November, 1906, German psychiatrist and neuro-anatomist Alois Alzheimer (Fig. 1) reported a unique case study of one of his patients showing "A peculiar severe disease process of the cerebral cortex". At that time, Alois Alzheimer was a lecturer at the Munich University Hospital. He was a contemporary of Emil Kraepelin. Sir Alzheimer described a 51-year-old woman Auguste Deter (Figure 1), who was under his care. Auguste Deter was observed carefully at Frankfurt Psychiatric hospital, since 1901, following her admission for paranoia, memory loss, sleeplessness, aggressive behavior and progressive state of mental confusion, for five years, until she died (Bondi et al., 2017). Following the death of Auguste D., Alois Alzheimer performed histological staining and detected neuritic plaques and neurofibrillary tangles in her brain that as we see now have become the major hallmarks of the disease. While Alzheimer was not keen to give the disease his name, his mentor-coworker Kraeplin coined and named the disease "Alzheimer's disease' in his honor in his own book 'Handbook of Psychiatry' in 1910. However, despite an enthuastic response from Kraeplin the remaining of the medical community showed little interest in his work. However around 1911 the medical community in Europe and the United States started using Alzheimer's observations of the disease for the diagnosis of patients. It raised little interest in the meeting despite an enthusiastic response from Kraepelin. Three more cases were reported by Alzheimer in

1909. He also detected a "plaque-only" variant in 1911, much later in 1998 the original specimens were re-examined and and it was identified as a different stage of Alzheimer's disease. Sir Alzheimer demised in 1915, aged 51 years, following his promotion as the Chairman of Psychiatry in Breslau, much long before the whole world got to know his name. Much later in the 1980s that the work of Alzheimer gained its due recognition and the field accelerated hugely. During this time, AD associated neuropsychological symptoms were profiled to show how this disease is different from other forms of dementia (Bondi et al., 2017). While the 1990s saw investigations into the various cognitive systems affected by the neurotoxic element, in 2000s scientists mainly took an interest in divulging the prodromal stages of AD that is mild cognitive disorder (MCI) before the actual appearance of disease symptoms. The last 10-20 years has seen the rise in imaging techniques such as PET and fMRI and advancement in the field of biomarkers to diagnose AD in its pre-clinical stage before the actual memory decline. Although Alois Alzheimer made the pathbreaking discovery of AD more than 110 years ago, we are still in a complicated mesh searching for a complete cure of AD.

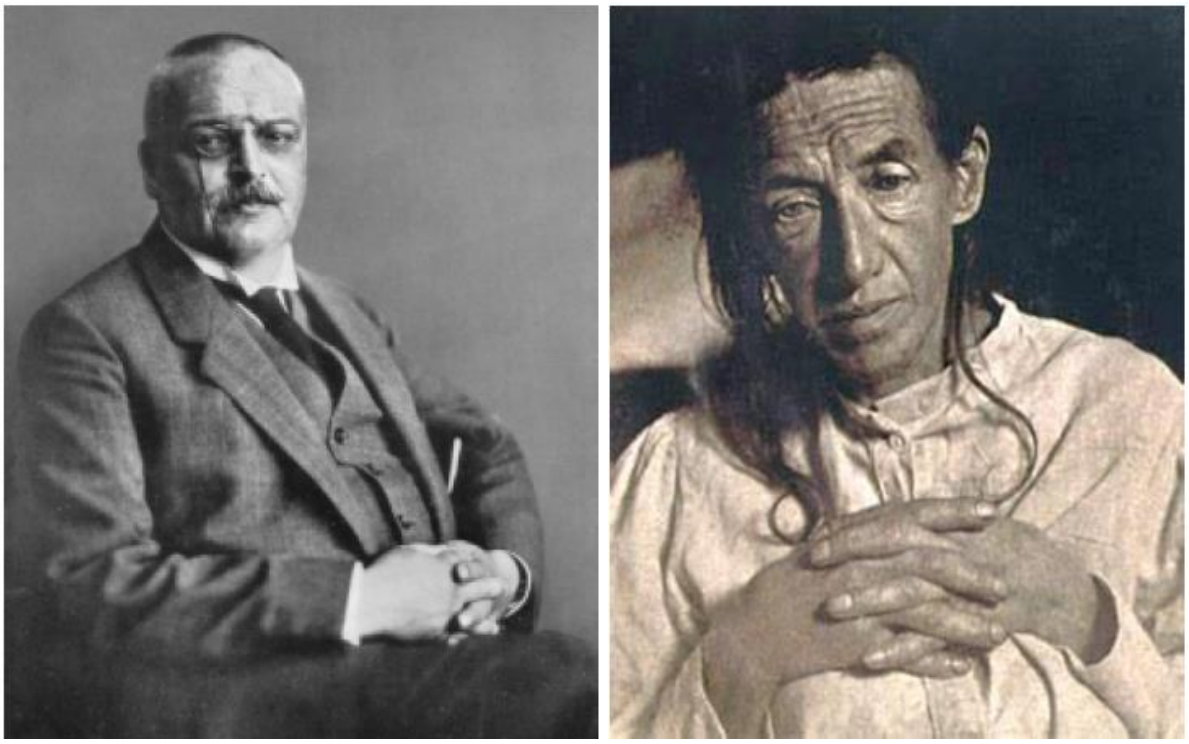

Fig.1: (Left) Alois Alzheimer (Photo courtesy: Prof. Manual Graeber) (Bratisl Lek Listy 2006; 107(9-10): 343-345). (Right) His patient Mrs. Auguste Deter. (Photo courtesy: http://alz.org).

1.2. Symptoms

Alzheimer's disease is a neurodegenerative disorder in which neuronal degeneration occurs way before the actual clinical symptoms surface. The symptoms of AD deteriorate over time. The rate of AD progression is not the same in every patient. On an average, a person diagnosed with AD survives for four to eight years, but some patients may survive longer, sometimes as long as two decades, depending on other factors. Progress of AD is very slow. It is best to define the stages in AD as a function of its most prominent pathological hallmarks - the Aβ plaques and the neurofibrillary tangles since 90% of the AD cases have been identified/diagnosed by pathologists to date with the presence of these histopathological lesions in the brains from AD patients.

General staging: Although AD progression is a continuous process, roughly five stages in AD progression have been described as a general guide - Pre-clinical AD, Mild Cognitive Impairment (MCI) related to AD, mild dementia due to AD, moderate dementia related to AD and severe dementia related to AD (https://www.mayoclinic.org/diseases-conditions/alzheimers-disease/in-depth/alzheimers-stages/art-20048448).

1.2.1. **Pre-clinical AD** may be defined as a phase when the brain of an individual displays significant level of plaques but no dementia. It actually precedes the clinical alterations. Advanced imaging techniques have revealed that non-demented individuals often have plaque burdens resembling that in persons with clinical AD (Swerdlow, 2007). This phase may last for decades without any noticeable symptoms.

1.2.2. **Mild Cognitive Impairment (MCI) due to AD** - The earliest recognizable clinical phase of AD may start with MCI. Patients in MCI phase show mild alterations in their thinking and memory abilities (Morris, 2006). However, these clinical changes do not confirm AD and hence imaging techniques or other laboratory-level methods are used to confirm the presence of pathological hallmarks of AD. Measuring CSF $A\beta_{1-42}$ either by using biochemical technique or positron emission tomography imaging, it has been shown that amyloid positive patients with MCI were more likely to be clinically diagnosed for AD within two years (Jack et al., 2010).

1.2.3. **Mild dementia stage** - Most of the AD patients are diagnosed in this stage, that is, the mild dementia stage since the extent of damage to thinking and memory of the individual starts affecting his/her daily life and he/she starts losing memory of recent events, is unable to make judgements and to solve common problems. Major symptoms

include:

- Unable to remember new names of people they have met
- Loses the ability to plan or organize things
- Cannot recollect newly gained information
- Misplaces valuable belongings
- Asks the same question repeatedly

1.2.4. **Moderate dementia stage** - It is then downhill from here as the patients continue to progressively deteriorate sequentially through the moderate dementia stage where the person starts requiring help for day-to-day activities.Major symptoms include:

- Loses track of date or month
- Starts forgetting personal details like address or phone number
- Unable to respond to instructions
- Struggle with multi-step tasks like house cleaning
- Becomes extremely moody or withdrawn especially under socially stressful situations
- Unable to cook for themselves
- Unable to choose clothing depending on season or weather
- Sleep disorders

- Tends to get lost or wander around meaninglessly
- Show changes in personality like increased suspiciousness, inability to trust and starts having delusions

1.2.5. **Severe dementia stage**- In this AD stage where alongside the cognitive losses hitting a rock bottom, physical abilities become compromised. Major symptoms include:

- Unable to swallow food
- Erratic or uncontrolled bowel movements
- Unable to dress themselves
- Starts losing weight
- Develops rashes and other skin infections
- Highly disturbed sleep patterns
- Pneumonia
- Struggle in walking

The three final stages in AD may be cumulitively assigned as "advanced or late-AD stage". Aβ accumulation attains a plateau at the beginning of clinical dementia. Interestingly, memory dysfunctions correspond more with tau aggegation that begins at the medial temporal lobe and spreads to neocortex in the clinical phases of AD (Long and Holtzman, 2019). It is worth mentioning again that AD is not an all-or-nothing entity, even the stages defined are rather arbitrary. Fig.2 shows the general clinical

staging of AD.

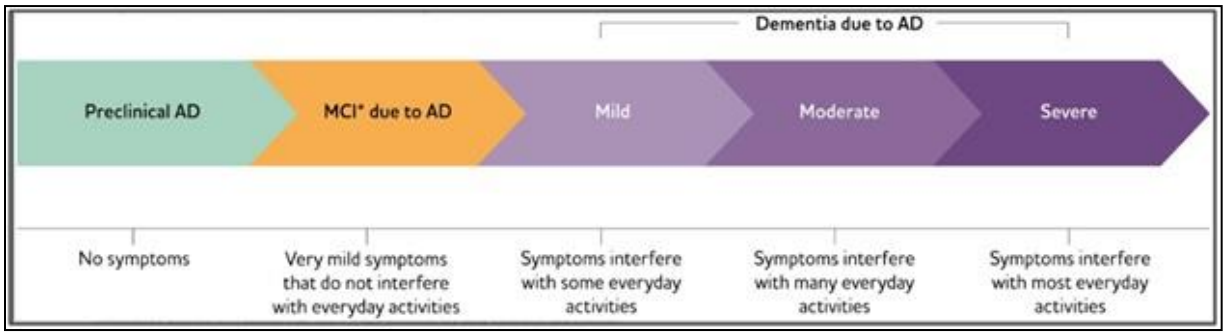

Fig.2: Stages in Alzheimer's disease. MCI = Mild Cognitive Impairment Alzheimer's Association Report (2020)

AT(N) classification – In recent times, National Institute on Aging and Alzheimer's association (NIA-AA) developed a "research framework". They described that "Alzheimer's disease" is a biological term that can be defined on the basis of biomarkers identifying the major hallmarks of AD: Aβ (A), phosphorylated tau (T) and neurodegeneration (N), named as the AT(N) classification (Jack et al., 2018). This classification is not oriented around clinical manifestations. Earlier, it has been mentioned that Alzheimer's disease must rather be regarded as a continuum than be restricted to the three symptomatic changes especially because the symptomatic phase of the disease can extend across 20 or more years (Dubois et al., 2016). The AT(N) classification was thus described to study AD stages as a function of biomarkers to help researchers to delineate the several pathological events that actually underpin the outcome of cognitive decline. It was not proposed for clinical practice (Jack et al., 2018).

The **"framework"** was defined based on two factors:

- AD-staging based on biomarkers
- AD-staging based on severity of cognitive deterioration

AD-staging based on biomarkers

A person with biomarker-based detection of Aβ depositionbut negative for tau biomarker (A+T-) would be identified as "Alzheimer's pathologic change". A person will only be categorized as "Alzheimer's disease" positive if he/she is positive for both Aβ and tau (A+T+). Alzheimer's pathologic change and Alzheimer's disease are included within "Alzheimer's continuum" independent of the clinical symptoms as shown in Fig.3 (Jack et al., 2018). Hence, presence of Aβ is the determining criteria for including a person within the "Alzheimer's continuum" while presence of the pathological form of tau further determines the person's inclusion in "Alzheimer's disease" category. Hence, it may be interpreted that Aβ is the most crucial component in categorizing and further including a person in "Alzheimer's disease".

Biomarker profiles and categories

AT(N) profiles	Biomarker category	
A-T-(N)-	Normal AD biomarkers	
A+T-(N)-	Alzheimer's pathologic change	Alzheimer's continuum
A+T+(N>	Alzheimer's disease	
A+T+(N)+	Alzheimer's disease	
A+T-(N)+	Alzheimer's and concomitant suspected non Alzheimer's pathologic change	
A-T+(N)-	Non-AD pathologic change	
A-T-(N)+	Non-AD pathologic change	
A-T+(N)+	Non-AD pathologic change	

Fig.3: Biomarker based Alzheimer's disease AT(N) classification. A=Amyloid-β, T=Tau, N=Neurodegeneration (Jack et al., 2018)

AD-staging based on severity of cognitive deterioration

Cognitive decline in AD occurs in a continuous manner. Two cognitive systems were presented to describe the stages in cognitive impairment not dependent on the biomarker profiles – "syndromal categorical cognitive staging" and "numeric clinical staging". The "syndromal categorical cognitive staging" is comprised of three groups – cognitively unimpaired (CU), MCI and dementia, the latter sub-categorized into mild, moderate and severe dementia. A CU person shows a cognitive activity in the range expected for him/her. A person in the MCI stage displays a cognitive activity less than that individual's expected range. The individual can still carry out day-to-day work without any help but starts struggling with more complicated daily functionings. During the dementia stage, a prominent decline in cognitive performance is noticed in the person and he/she starts requiring assistance in daily-life.

"Numeric clinical staging" scheme recruits participants from the Alzheimer's continuum and classification is beyond the traditional categories. This staging system elaborates the sequential events that lead to the development of AD starting from the detection of pathologic biomarkers of AD in an individual without any symptoms. In this system however there are six stages - Stage-1 to 6 (Jack et al., 2018).

Stage-1 identifies asymptomatic individuals with an evidence of biomarkers similar to that in the "Alzheimer's continuum". Stage-2 identifies those with initial clinical manifestations

of the pathologic identifiers of the "Alzheimer's continuum", not essentially expressed as cognitive dysfunctions, and hence similar to "Preclinical AD" in the NIA-AA guideline, 2011 (Sperling et al., 2011).

In Stage-3, patients show cognitive deficits yet not full-blown dementia and are similar to those in the "MCI" stage in "syndromal categorical cognitive staging".

In Stages 4-6 patients show a progressive decline in cognitive functions impacting their daily-life activities and are similar to "mild", "moderate" and "severe dementia" stages of the "syndromal cognitive staging" scheme. As per the NIA-AA research framework, an individual can be carefully categorized into stages with a combination of biomarker profile and cognitive staging elucidated in any one of the two schemes (Jack et al., 2018).

1.3. Incidence and Prevalence of AD

According to the World Alzheimer Report 2021, the 7th leading cause of mortality globally is dementia and it creates the highest monetary burden on the society. At present there are more than 55 million people living with dementia in the world among which less than 25% are actually diagnosed and in low-income countries the percentage of diagnosed dementia patients go down to less than 10%. The number of people suffering from dementia is rising on a daily basis and is predicted to reach 78 million by 2030 (https://www.alzint.org/resource/world-alzheimer-report-2021/). According to Alzheimer's Association Report 2022, among Americans in the age group of 65 years or above approximately 6.5 million are living with AD-related dementia and predicted to reach 13.8 million cases by 2060 in America itself. Fig.4 shows the number and

percentage of people, aged 65 years or older, living with AD-related dementia and Fig. 5 presents the estimated number of aged people to be living with AD in another 30 years according to Alzheimer's Association Report 2020 (2020). As per the latest AD-related morbidity report in 2019, 121,499 deaths were recorded. In USA, AD was the sixth leading cause of death in 2019 but in 2020 and 2021, it has moved to seventh position as COVID-19 entered the ranks. Yet AD remains the 5th leading cause of death in Americans in the 65 years or above age group. The World Health Organization (WHO) has developed a global action plan to diagnose at least 50% of the people thought to bsuffering from dementia in 50% of the world's nations by 2025. However, COVID-19 pandemic has largely delayed this plan. An estimated 16 billion hours of care was provided by more than 11 million family members and care-givers to AD and other dementia patients in 2021 alone. Unpaid care-giving costs are estimated to $271.6 billion in 2021 in the US. All of these are excluding the mental health and negative physical conditions of the patient's family members and health-givers especially during pandemic (2022). In the low and middle income countries the monetary burden on the society has already gone up to an alarming state. In the Indian front, 3.7 million people are reported to be suffering from dementia according to Dementia India report of World Alzheimer's Report 2010. In low and middle-income countries including India we see a major lack in accessibility to modern technology and trained health care professionals. Additionally, there are taboos and lack of awareness about AD dementia. There have been several breakthroughs in the diagnosis front with the advent of plasma based biomarkers of AD. However, COVID-19 pandemic has enhanced the probability ofcognitive decline in patients and hampered dementia research big time. Moreover, during the two years of

pandemic the AD patients had limited access to help in terms of care-givers and routine checkups and assessment of disease progression. As the global population is ageing, the number of dementia patients is increasing proportionally especially because AD is a disease of ageing or we can say age is the biggest risk factor for AD.

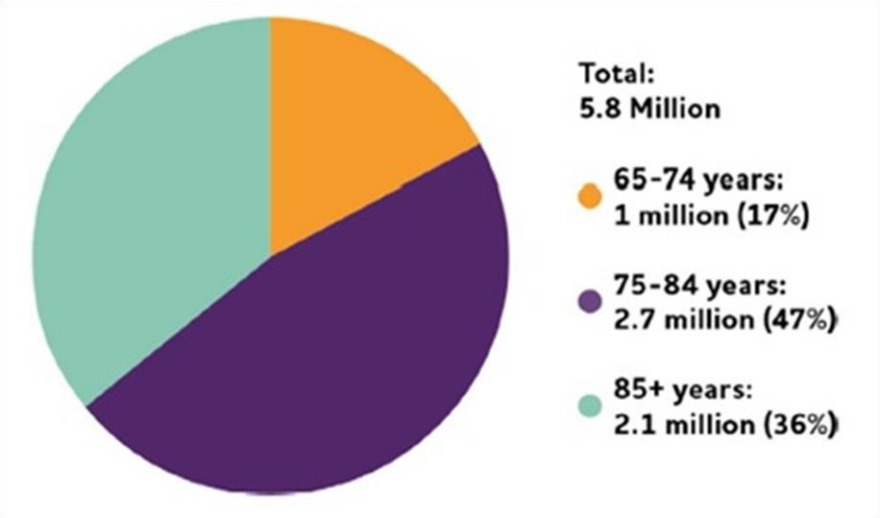

Fig.4: Number and percentage of people at or above 65 years of age living with Alzheimer's dementia in the US according to Alzheimer's Association Report (2020)

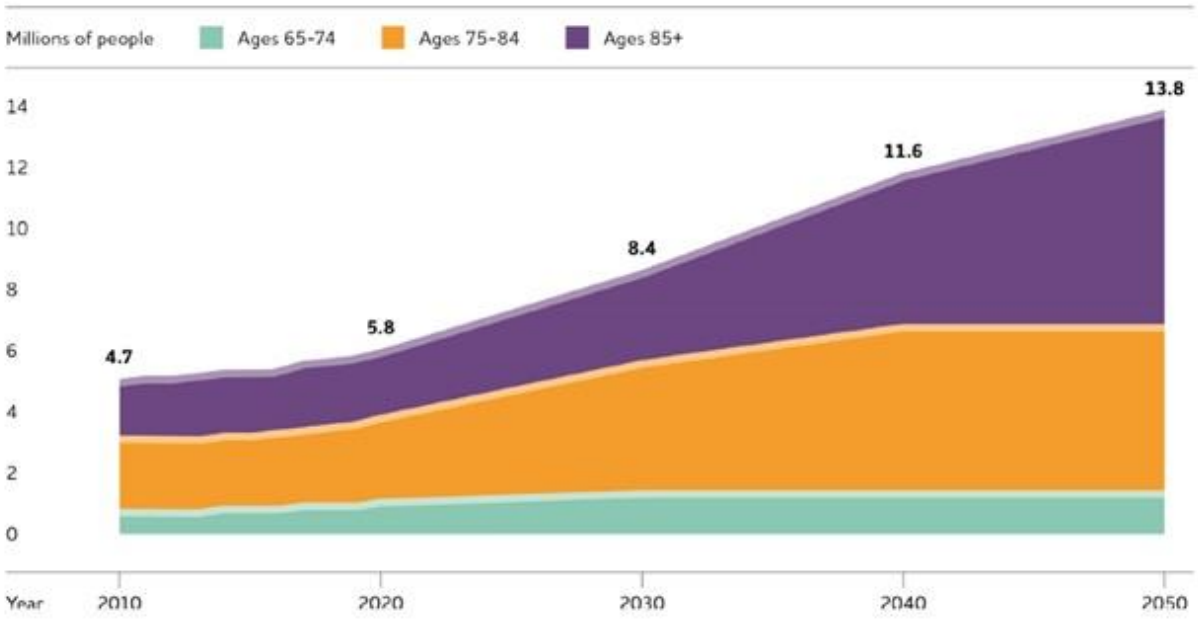

Fig.5: Projected number of people of 65 or above years of age (total and by age) to be living with dementia in the coming decades in the US according to Alzheimer's Association Report (2020).

The number of women suffering from AD or dementia is more than men (Hebert et al., 2013). Among the 5.8 million people in the 65 and above age group living with AD in the US (according to Alzheimer's Association 2020 report), 3.6 million are women while 2.2 million are men. Moreover, in the age group of 71 or above, 16% of women suffers from AD or other dementia while it is only 11% among men shown in Fig. 6 (Plassman et al., 2007). This staggering bias towards the female gender may be due to the on an average the longer lifespan of women than men and higher aging population in women means the prevalence of AD is more. However, when it comes to actual risk in developing AD between men and women, there are inconclusive reports suggesting that the difference between men and women further depends upon age and/or their place of origin/living.

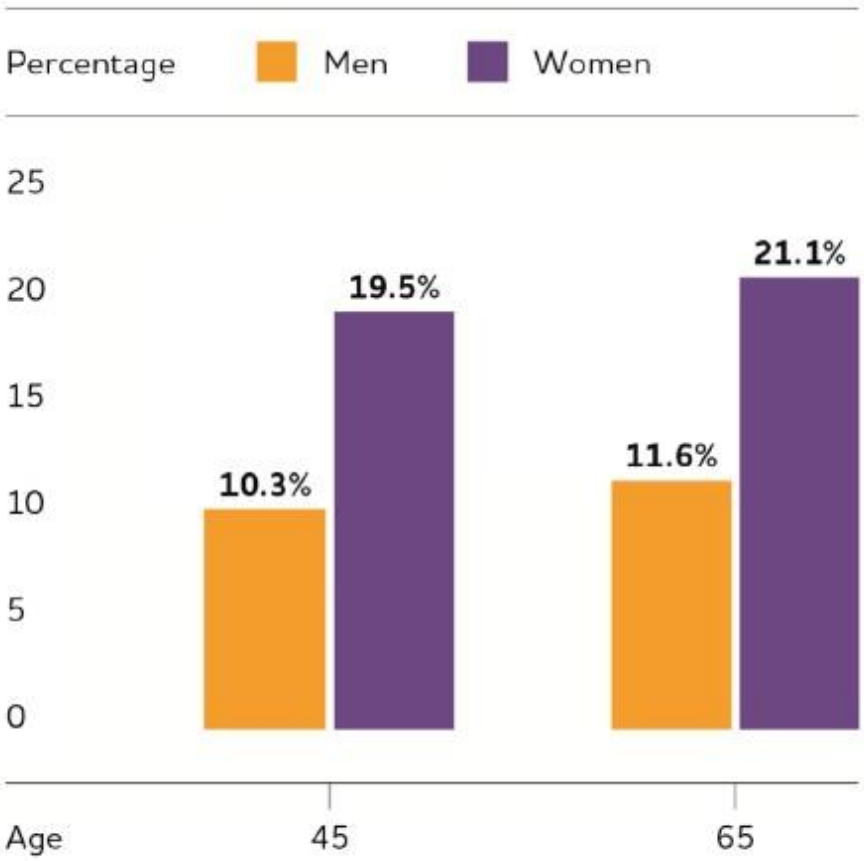

Fig.6: The gender bias in Alzheimer's disease showing the estimated risk of men versus women to acquire AD-related dementia (Chene et al., 2015).

1.4. Types of AD

1.4.1. **Early onset Alzheimer's disease (EOAD)** – Although AD is more prevalent in the age group of 65 and above, a small proportion of the disease occur below the age 65 and has a more devastating effect on the patients with lower relative rate of survival. EOAD cases accounts for less than 5% of the patients diagnosed with AD (DeTure and Dickson, 2019). Interestingly, the very first reported patient Auguste Deter suffered with EOAD with symptoms arising in her late 40s and finally got diagnosed at 51. She struggled with cognitive deficits, sleep disorders, language impairment, paranoia,

aggressive behaviors, mood swings and delusions. Histological analysis of her brain following her demise revealed plaque depositions and neurofibrillary tangles (NFT) in her brain, the major hallmarks of the disease. People with Down syndrome are at ahigher risk of developing AD with reports suggesting the appearance of AD-associated pathological hallmarks by the age 40 and the clinical symptoms surface at around 50. By the age of 65, most Down syndrome patients suffer from dementia (Ballard et al., 2016). Interestingly, Down syndrome patients have partial or full chromosome 21 trisomy and APP gene is located on chromosome 21 (Kang et al., 1987). Hence, in Down syndrome patients there is an over-expression of APP gene putting them at a very high risk of AD. EOAD is also linked to defects in specific region of chromosome 14. Additionally, myclonus, sudden shock-like involuntary muscle jerk is often observed in EOAD patients (Beagle et al., 2017).

1.4.2. **Late onset AD (LOAD)** is the most common type of AD that occurs in people in the 65 and above age group. EOAD is closely related tospecific gene mutations while LOAD may or may not have a genetic basis. However, the primary genetic risk factor for LOAD is APOEε4 allele. In APOEε4 heterozygotes the odds ratio is 3 whereas in individuals homozygous for APOEε4 the ratio goes upto 12 when compared to persons carrying APOEε3/ε3 (non-carriers) allele (Lane et al., 2018). Some additional risk factors for LOAD are TREM2, ADAM10 and PLD3 (Jansen et al., 2019; Karch and Goate, 2015).

1.4.3. **Familial AD (FAD)** is a very uncommon form of AD running dominantly inherited in families and makes up less than 1% of all AD cases. Although it is often seen as a sub-category of EOAD, its pathological and clinical presentations identify more with LOAD.

The major causal genetic mutations responsible for FAD are in amyloid precursor protein (APP), presenilin 1 (PSEN1) and PSEN2 genes. The average age of onset for FAD is 46.2 years but it can occur as early as 20 years of age (Ryman et al., 2014).

1.5. Risk factors

1.5.1. **Age** – It is the greatest of all risk factors for AD.The percentage of people suffering from AD increases drastically with aging. Notably, 3% of people in the age group 65-74, 17% in the age group of 75-84 and 32% in the age group of 85 and above suffers from Alzheimer's dementia. Ofnote is that Alzheimer's dementia is not normal consequence of aging and aging alone is not the absolute cause of AD (Hebert et al., 2013).

1.5.2. **Genetics** – Several genes are closely associated with the increased risk of AD. Apolipoprotein E4 (ApoE4) is the most important genetic risk factor for LOAD. ApoE is responsible for cholesterol transport in the brain and every person inherits either of the three of its alleles – ε2, ε3 or ε4 from each parent. Some ethnic group may have a higher risk of inheriting ε4 allele over the other. For example, higher number of African Americans inherits at least one copy of ε4 allele when compared with European Americans (Evans et al., 2003; Gu et al., 2020; Rajan et al., 2017).Moreover, persons carrying the ε4 allele are more prone to Aβ accumulation (Jansen et al., 2015)and AD-related dementia at a younger age than those carrying the ε3 or ε2 allele of ApoE gene (Spinney, 2014).

Other uncommon genes that increase the risk of AD are those already mentioned for FAD. Those are specific mutations in APP, PSEN1 and PSEN2 associated with Aβ

processing. Individuals carrying these mutations are almost guaranteed to suffer from AD if they have a normal life duration. Additionally, trisomy 21 in Down syndrome individuals put them at a higher risk for AD.

1.5.3. **Family history** – Although family history of AD is not an essential factor for a person to develop AD, yet individual with a first-degree relative (a parent or a sibling) who has AD is more likely to develop AD than others (Green et al., 2002; Loy et al., 2014). Moreover, those who have more than one number of first-degree relatives suffering from AD are at a higher risk for the disease (Lautenschlager et al., 1996). In this type of cases when AD runs in a family both genetic and/or non-genetic (shared lifestyle or food habits) factors may be responsible for developing AD.

In addition to the above most important risk factors for AD, some additional modifiable risk factors are discussed below according to the Alzheimer's Association Report 2020.

1.5.4. **Cardiovascular disease risk factors** – For a healthy functioning of the energy-intensive brain, healthy pumping of oxygenated blood by the heart is a pre-requisite. Smoking and diabetes increase the risk ofcardiovascular diseases which is often associated with the appearance of dementia (Choi et al., 2018; Gudala et al., 2013; Vagelatos and Eslick, 2013). Especially, the age at which the risk factors of cardiovascular disorders including hypertension, mid-life obesity and high cholesterol develop often sees the advent of dementia (Meng et al., 2014; Ronnemaa et al., 2011; Solomon et al., 2009). WHO recommends that an active lifestyle with lots of physical exercise, healthy vitamin rich diet and management of cardiovascular risk factors can help in delaying the advent of dementia if not prevent it (Stephen et al., 2021).

1.5.5. **Education** – Reportedly, individuals with longer duration of formal education are at a reduced risk of AD than those with low educational background (Evans et al., 2003; Sando et al., 2008; Stern, 2012). It is believed that years of education as well as intellectually demanding mid-life career creates a 'cognitive reserve' in the brain that can actually help them to perform cognitive brain functions even when faced with a pathological insult such Aβ accumulation or tau phosphorylation (Fisher et al., 2014; Then et al., 2014). "Cognitive reserve" is the brain's ability to retain brain plasticity and make efficient utilization of interconnected brain networks to continue carrying out cognitive functioning in the face of insult (Stern, 2002). Besides formal education, engagement in mentally-stimulating activities such as playing Sudoku or intellectually interactive social activities in late-life can greatly develop cognitive reserve. However, one cannot practically rule out the beneficial aspects of long years of formal education leading to a better socio-economic condition giving leverage to these people to lead a healthy lifestyle, good nutrition and better access to healthcare facilities. Hence, whether the level of education or the socio-economic development associated with formal education is the reason behind lower AD, risk in individuals needs to be scientifically ascertained in the coming years.

1.5.6. **Social and cognitive engagement** – Studies show that staying mentally and socially active reduces the risk of developing AD (Johnsen et al., 2022; Staff et al., 2018). Additionally a socially and intellectually active lifestyle helps in building cognitive reserve. However, the mechanisms underpinning such observations are still lacking. Moreover, whether cognitive impairments restrict a person to interact socially leading to

the observation needs to be researched upon before drawing a conclusion.

1.5.7. **Traumatic brain injury (TBI)** – TBI increases dementia risk (Fann et al., 2018). It is a perturbation of normal brain functions due to injury or blow to the head or due to accidental perforation of the skull by any external object. Even mild TBI enhances the risk of developing dementia by two-fold (Barnes et al., 2018). Notably, a person with a history of TBI develops AD at a lower age than those without any past record of TBI (LoBue et al., 2017). However, whether TBI directly causes AD or induces other conditions leading to the development of AD remains elusive.

1.6. Pathophysiology of AD

1.6.1. **Aβ plaques** - AD is associated with extracellular senile plaques composed majorly of Aβ protein, intraneuronal formation of NFT due to tau protein hyperphophorylation, dramatic neuroinflammation, significant damage of neurons and synapses in the brain (De Strooper and Karran, 2016). Aβ is an amino acid peptide fragment generated due to the cleavage of amyloid precursor protein (APP) successively either by α- and γ-secretases or by β- and γ-secretases. The latter set of enzymes generates Aβ1-40 or Aβ1-42 peptides. Generation and subsequent deposition of excess of Aβ1-42 leads to the formation of Aβ oligomers and fibrils further aggregating into extracellular plaques (Kim and Tsai, 2009). Mutations in APP or subunits of γ-secretase, PSEN1/PSEN2 or SorL1 or ApoE, all responsible for amyloid production, processing and/or trafficking are strongly related to the development of AD. Thus, providing a strongly testimony for the crucial role of Aβ in the pathogenesis of AD.

1.6.2. Neurofibrillary tangles - NFT is directly linked to neurodegeneration and is shown to be proportional to the development of symptomsin cognitive decline of AD. Tau protein is majorly located in the neuronal axons and is known to stabilize microtubules. NFT is formed within the neurons when two helical filaments of abnormally hyperphosphorylated tau come together. Intriguingly, Aβ deposition has been shown to be responsible for the progress in tau pathology as well as AD-related neurodegeneration (Wang et al., 2016a).

1.6.3. **Synapse and Neuron loss** – Extensive synapse and neuron loss seem to be the most evident feature of an advanced-stage AD brain as imaged in many autopsy studies. While synaptic failure is seen as an early phenomenon in AD much before the appearance of clinical symptoms, loss of neurons is concomitant with drastic cognitive changes in an AD patient. Indeed, loss of neurons in the nucleus basalis of Meynert causes Acetylcholine (ACh) deficiency, the neurotransmitter highly implicated in brain signaling. Further loss of serotonergic and adrenergic neurons lead to sleep disorders and dysphoria in AD (Meeks et al., 2006).

Another important pathological feature observed by several groups around the world is extensive **reactive astrogliosis** in the AD brain. While astrocyte reactivity (explained in later sections) is not exclusive to AD, it has been detected in the vicinity of Aβ plaques as well as NFTs, increasing linearly along AD progression (Serrano-Pozo et al., 2011). Additionally, tau can accumulate within astrocytes in AD. Further, astrocytes activity can be influenced by tau aggregation leading towards detrimental effects on both astrocytes and neurons (Kahlson and Colodner, 2015). The major pathological hallmarks of AD are

shown in Fig.7.

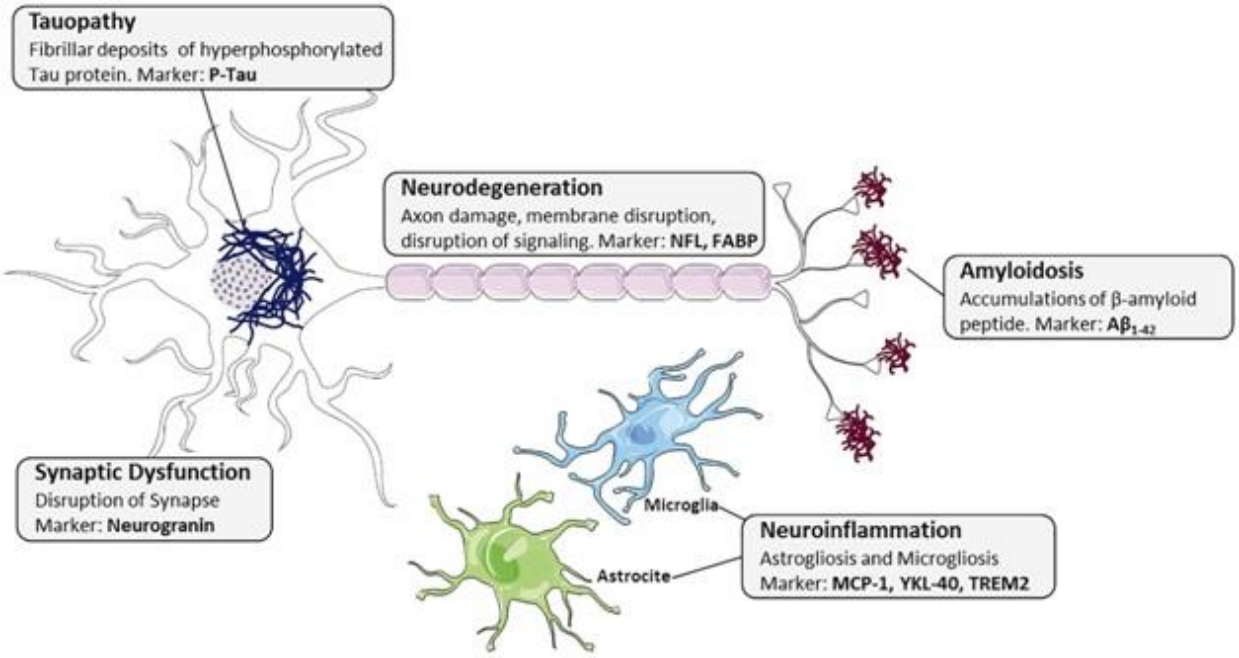

Fig.7: The pathological hallmarks of Alzheimer's disease. (https://doi.org/10.1515/almed-2020-0090)

1.7. Current hypotheses in AD and related anti-AD therapy

1.7.1. **Amyloid cascade hypothesis-** Hardy and Higgins proposed "amyloid cascade hypothesis" in 1992. According to this hypothesis, abnormal processing, accumulation and clearance of $A\beta_{1-42}$ is at the centreof AD pathogenesis (Hardy and Higgins, 1992). APP is a transmembrane protein that is hydrolysed by either α, β, γ or η secretases along any of the three pathways shown in Fig.8 to produce a C-terminal fragment. Notably, when APP undergoes hydrolysis in the amyloidogenic pathway, Aβ1-42 is released by the sequential action of β and γ secretases (Fan et al., 2019). However, there are many

controversies with this hypothesis especially because of lack of proof for any direct connection between Aβ load and rate of cognitive deterioration in cases of sporadic AD (Nelson et al., 2012a). This lead to extensive revisions of the hypothesis with the latest proposal by Bart De Strooper and Eric Karran (De Strooper and Karran, 2016). They suggested that AD pathogenesis entails an intricate and lengthy cellular phase comprising feedback and feed-forward reactions of glial cells and vasculature. They further proposed that Aβ and tau accumulations are the risk factors in sporadic AD and their aggregation is an indication of enhanced proteopathic stress. Aberrant clearanceof Aβ and abnormal tau depositions, the impairment in the neurovascular unit, abnormal activity of the neuronal network, dysfunctions in the astrocyte and microglialnormal functions and the plausible possible gain-of-toxic functions underpins the cellular phase of the disease. They emphasize on the cellular level role of astrocytes in maintaining the brain homeostasis and that shift from their normal functioning under AD circumstances leads to aggressive progress of disease pathogenesis (De Strooper and Karran, 2016).

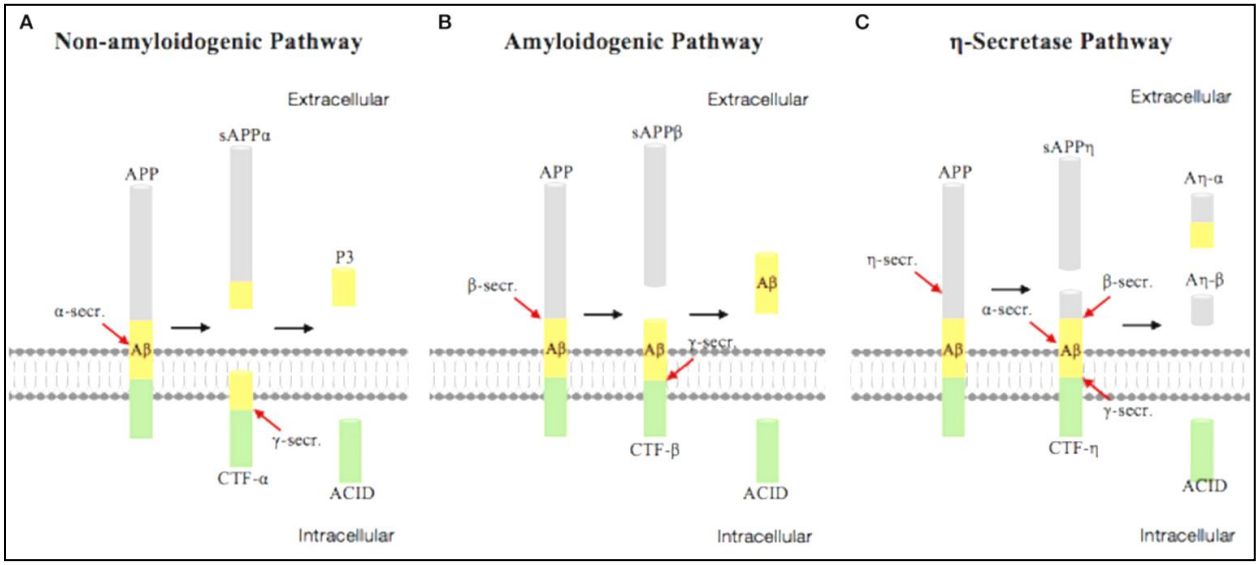

Fig.8: Schema depicting the three pathways of Amyloid precursor protein (APP) cleavage. The amyloidogenic pathway generating the toxic Aβ is shown in (B). The non-amyloidogenic pathways are shown in (A) and (C). CTF=C-terminal fragment, AICD=APP intracellular domain (Fan et al., 2019).

The direct strategy in Anti-Aβ therapy is by inhibiting β or γ secretase (Chang et al., 2004; McConlogue et al., 2007; Wong et al., 2004). However, these strategies are not devoid of its side effects for example targeting γ secretase can wrongly target notch signaling pathway (Klaver et al., 2010; Olry et al., 2005; van Es et al., 2005). Aβ immuno-therapywas thought to be an alternative approach. The first potential anti-Aβ vaccine (AN1792) by ELAN displayed favourable effects on memory functioning but was banned due to harmful side effects like meningoencephalitis (Gilman et al., 2005; Holmes et al., 2008). Passive immunotherapy did not perform any better. Several antibodies against Aβ underwent clinical trials but eventually failed namely Crenezumab (Genentech) (Bouter et al., 2015; Ultsch et al., 2016), Bapineuzumab (Pfizer/Johnson & Johnson) (Laskowitz and Kolls, 2010), solanezumab (Eli Lily) (Bouter et al., 2015)and ponezuman (Pfizer/Johnson & Johnson) (Landen et al., 2013). Only recently another anti-Aβ antibody Aducanumab (Biogen) underwent two independent phase 3 clinical trials in which one was a success while the other raised controversies yet was approved by FDA (Cummings et al., 2021). However, the scientific community cannot completely ignore the role of Aβ in AD pathogenesis especially because even today presence of Aβ is considered a pre-requisite for AD diagnosis. The new search is for combinatorial therapies that can be used along with anti-Aβ therapies to prevent AD progression or even cure AD.

1.7.2. **Tau hypothesis**–In 1988, Claude Wischik detected tau in plaques of AD brains reporting that tau may be the cause of Alzheimer's dementia (Wischik et al., 1988). NFT are comprised of tau proteins. Tau undergoes many post translational modifications, like phosphorylation, arginine mono-methylation, lysine acetylation, lysine mono- and di-methylation, lysine ubiquitylation etc. (Morris et al., 2015). In AD, tau proteins are abnormally hyperphosphorylated, decreasing its affinity for the microtubules and then they aggregate together in axons leading towards loss of neuronal plasticity. The failure of anti-Aβ therapy has drawn the attention of the scientific community towards the tau hypothesis especially because tau accumulation could be directly linked to the rate of cognitive decline (Brier et al., 2016).

There are some new strategies that have targeted tau hyperphosphorylation. Various drugs have been developed that can stabilize microtubules, modify kinases and phosphatases activities directed at tau modifications as shown in Fig.9. However, even these efforts suffered failures in clinical trials. TRx0237 (LMTM) that has shown the ability to block tau aggregation at pre-clinical levels failed as it showed toxicity and lack of efficacy in phase III clinical trials (Gauthier et al., 2016). Tau-directed active vaccines namely ACI35 and AADvac-1 and passive vaccines namely RG6100 and ABBv-8E12 are presently in different phases of clinical trial (Li and Gotz, 2017; Novak et al., 2017). Even immunoglobulin (IVIG), the single passive vaccine, was not successful in phase III clinical trials and was unable to fulfill the major targets in mild-to moderate AD patients (Li and Gotz, 2017).

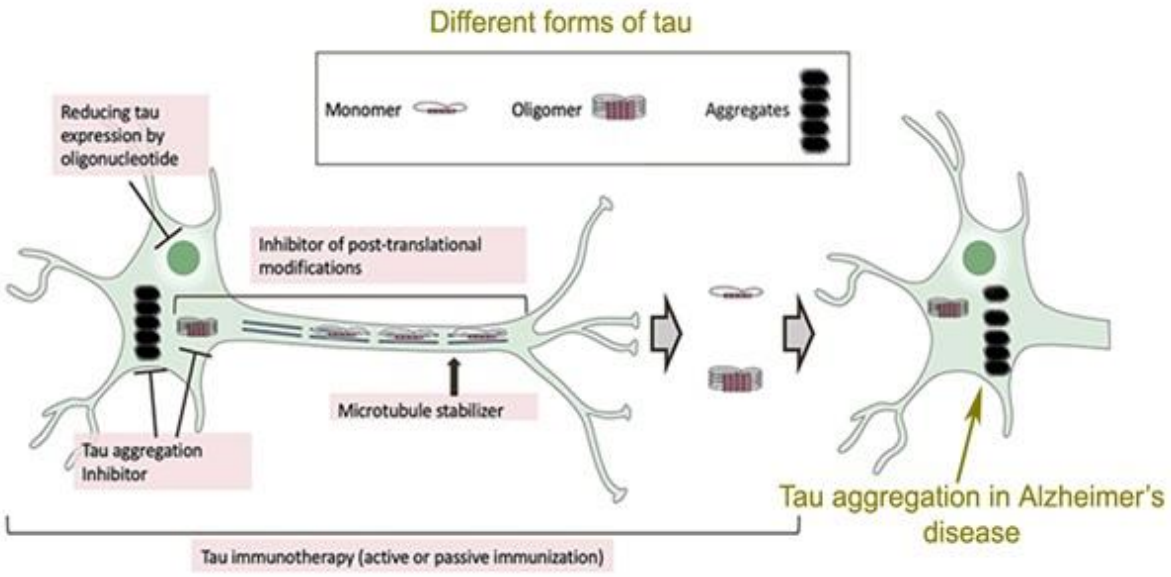

Fig.9: Tau hypothesis of Alzheimer's disease and possible strategies targeting abnormal tau-mediated damages in neurons (modified from (Soeda and Takashima, 2020)

1.7.3. **Inflammation hypothesis -** Neuroinflammation and reactive gliosis are hallmarks of AD (Calsolaro and Edison, 2016). Recent body of literature suggests that both astrocytes and microglia play crucial roles in AD pathogenesis. The processes of long-term synaptic plasticity and activity-dependent synaptic strengthening underpin the changes in cognitive behaviors and are driven by the changes in LTP. Astrocytes are the major glialcells recruited for neurotransmitter homeostasis at synapses and play an important role on synaptic activity. Both astrocytes and microglia surround the Aβ plaques in AD and starts secreting a plethora of cytokine and chemokine molecules. Initially these factors were thought to be predominantly detrimental and hence non-steroid anti-inflammatory drugs (NSAIDs) were tried to treat AD and were indeed successful at the pre-clinical level only to fail at the clinical phase (Ozben and Ozben, 2019). This emphasizes that the cytokines secreted by reactivated astrocytes and microglia may

possess a beneficial role rather than detrimental. New report on PD-1 checkpoint blockade has shown positive results in terms of memory recovery (Baruch et al., 2016). The new era of glial research has divulged many new targets against which new drugs can be designed for AD therapy.

1.7.4. **Cholinergic and oxidative stress hypothesis -** Acetylcholine (ACh) is one of the most crucial neurotransmitter in a healthy brain regulating normal functioning including learning and memory functions, sleep and wake cycle, sensory information, response to stress and attention (Hasselmo et al., 1992; Sarter and Bruno, 1997). However, in AD heavy damage in cholinergic neurons were detected and directly correlated with AD-related dementia. The cholinergic hypothesis was tested with cholinesterase inhibitors in the treatment of AD as shown in Fig. 10. Tacrine was the first AChE inhibitor approved for clinical practice (Brinkman and Gershon, 1983; Summers et al., 1986), following which several other AChE inhibitors are now available in the market namely rivastigmine, donepezil, and galantamine approved by US FDA (Panza et al., 2019). However, these drugs also present a number of side effects including vomiting, nausea and diarrhea (Graham et al., 2017). Another drug approved by FDA is memantine, a NMDA receptor antagonist have positive effects on memory scores in cognitive test (Kishi et al., 2017). Nonetheless, side-effects of memantine include hypotension and fainting (Gallini et al., 2008). Notably, none of these drugs provide a cure for AD and are prescribed by doctors to provide symptomatic relief to the patients.

Oxidative stress is also thought to be an important causal factor for AD pathogenesis. Brain is the most energy intensive organ of the body, utilizing higher amount of oxygen

as compared to other tissues and undergoes mitochondrial respiration generating ROS in the process. AD has been strongly correlated with cell-level oxidative stress involving enhanced rate of oxidation of proteins, lipid peroxidation, glycoloxidation and protein nitration besides accumulation of Aβ (Cheignon et al., 2018). Aβ can in turn induce oxidative stress (Butterfield et al., 2007). Thus, the application of anti-oxidant compounds was thought to provide protection against Aβ and cognitive impairments. However, the anti-oxidant strategy was questioned because it is a single mechanism among the multiple mechanisms underpinning AD and not AD-specific and hence, was proposed as a part of combination therapy. Hence, no such anti-oxidant molecule has progressed to clinical trials.

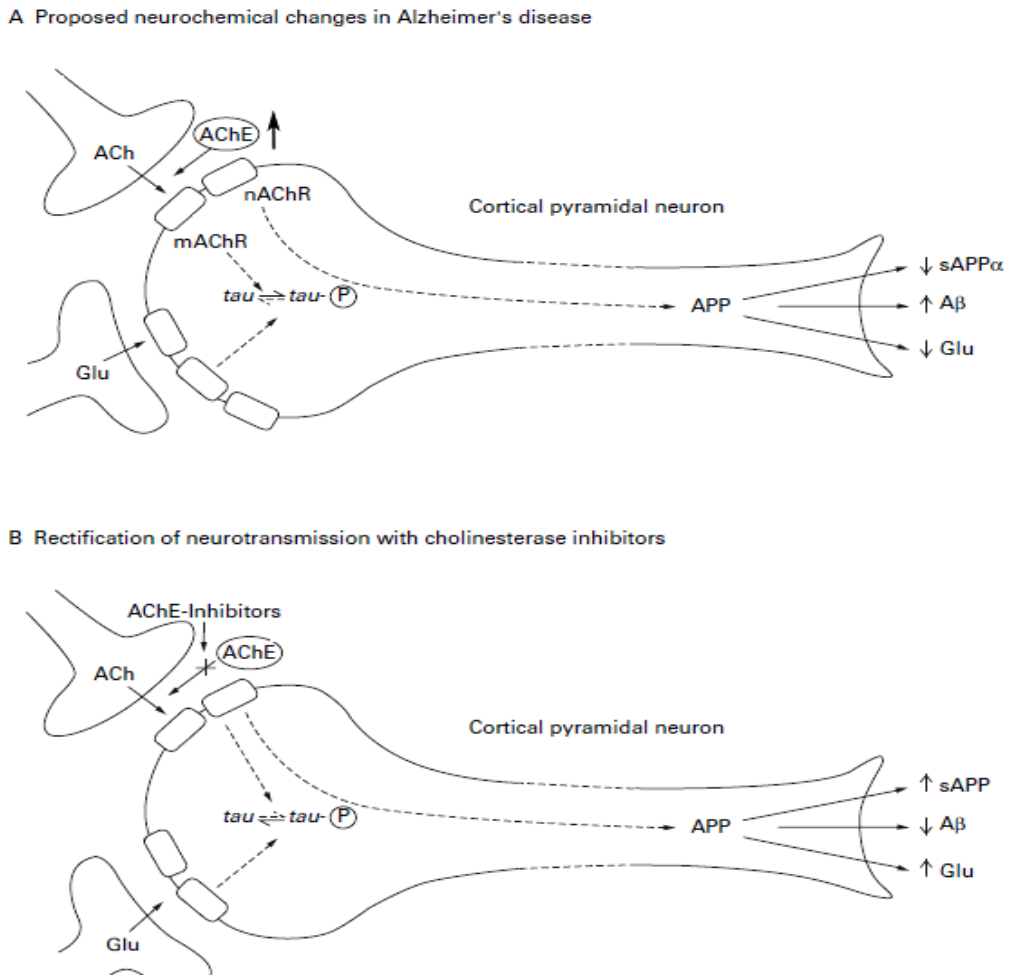

Fig.10: The Cholinergic hypothesis of Alzheimer's disease and the role of Acetylcholine esterase (AChE) inhibitors. (Modified from (Babic, 1999)).

1.7.5. **Glucose hypometabolism** – Glucose hypometabolism is a common feature of the prodromal stage of AD and can be correlated to cognitive deterioration (Daulatzai, 2017; Du et al., 2018). The scientific community today is majorly interested in targeting AD in the early phase before the advent of irreversible damages. Hence, targeting glucose hypometabolism has emerged as a major therapy in AD. However, to date there are no drugs targeting glucose hypometabolism in an early AD brain. Nevertheless, this strategy has been successfully utilized as biomarker for early AD diagnosis. 18FDG-PET imaging is

now being used by clinicians to predict neurodegenerative disorders including AD (Nasrallah and Dubroff, 2013).

Unfortunately, anti-AD drug development has a very high failure rate of 99.6% from 2002 – 2012 according to statistical reports (Cummings et al., 2014). Hence, this indicates that there is a huge knowledge gap in understanding the multi-factorial and complex mechanisms leading to AD pathogenesis and that has been the major barrier in anti-AD therapy development. This has encouraged the scientific community to engage in further search for a hypothesis that can best fit AD pathogenesis.

2. Astrocytes

2.1. Introduction to glial cells

The non-neuronal cells of the brain that perform critical functions to maintain the brain homeostasis under healthy physiological conditions for the neurons to effectively carry out their signaling are known as glial cells. The three major types of CNS glial cells are – Astrocyte, microglia and oligodendroglia.

2.1.1. **Astrocytes** – Astrocytes account for 20-40% of all glial cells in the CNS depending on the region within the brain. Astrocyte, named after its star-like morphology, has often been debated for its constitution not only because of the diversity in its types and subtypes but also because the kinds of similarity it has with other types of cell in the CNS (Oberheim et al., 2012). From Kimelberg's review, the criteria that maybe used for defining astrocytes are – Non-excitability, K+ gradient-induced very negative membrane potential, uptake of gamma amino butyric acid (GABA) and glutamate by astrocyte-

specific transporters, intermediate filament bundles, glycogen granules, cell processes encompassing synapses and blood vessels, gap junctions comprised of connexins (Kimelberg, 2010). The astrocytes will be discussed in details in later parts.

2.1.2. **Microglia**– They constitute 0.5% -16% of total cell population depending on the region of human brain (Lawson et al., 1992). They can be considered as the resident macrophage-like cells in the CNS responsible for the brain's defense system orchestrating inflammatory response to any foreign insult. Additional roles of microglia include trophic support to neurons during development, maintenance of neuronal excitability, phagocytosis of apoptotic cells, damaged cells and debris, maintenance of synapses, myelin turnover and finally provide protection to the neurons. In response to any toxic stimulus, the microglia undergo drastic transformation in terms of morphology, proliferation, phagocytic ability, antigen presentation and starts secreting a number of pro- and anti-inflammatory cytokine and chemokine molecules (Bachiller et al., 2018). The microglial cells are thoroughly in communication with astrocytes, neurons and oligodendroglia under normal physiological conditions as well as under pathological circumstances. Similar to astrocytes, microglial activation in response to any pathological stimulus is considered as a dynamic process and goes beyond the traditional detrimental (M1) and neuroprotective (M2) phenotypes (Tang and Le, 2016). A broad array of reactive microglia profiles in neurodegenerative diseases has been recently elaborated (De Biase et al., 2017; Keren-Shaul et al., 2017). Interestingly, ApoE (expressed by astrocytes) whose ε4 allele is considered the major genetic risk factor for AD can regulate microglial activity through TREM2 receptor leading towards loss of neurons in an acute model of

neurodegeneration (Krasemann et al., 2017). Thus, microglia are another important glial cell besides astrocytes showing high dynamicity in disease scenario.

2.1.3. **Oligodendroglia**– They are the myleinating cells of the CNS and create insulating myelin sheath around axons for optimum transmission of electrical impulses along the axonal length. The origin of oligodendrocytes is from oligodendrocyte progenitor cells (OPCs) and during the stage of development they are under the influence of several neurotransmitters and other neuron-derived factors. A single oligodendrocyte can myelinate 30-40 axons and each myelin sheath can extend up to 50-100 μm along the axon forming internodes that are punctuated by the nodes of Ranvier (Butt and Ransom, 1989). Massive white matter degeneration and myelin loss are important pathological features of AD. It has been shown that increasing the activity of oligodendroglia, in turn enhances myelin renewal that alleviated hippocampus related cognitive deficits in APP/PS1 mice model of AD (Chen et al., 2021).

2.2. Astrocytes in AD

2.2.1. **Physiological role and subtypes**: Astrocytes are the major cells responsible forthe maintenance of brain homeostasis by regulation of ionic balance at the synapse. They help in uptaking excess glutamate and convert it to glutamine via the glutamate-glutamine cycle to prevent glutamate excitotoxicity. They are the supplier of energy to neurons through the lactate shuttle and also provide antioxidants such as glutathione and ascorbic acid to the neurons. Astrocyte-dependency of neuron via the lactate shuttle and the glutamate-glutamine cycle is shown in Fig.11. Role of astrocytes has been further elucidated inthe regulation of neuronal excitation-inhibition balance, in the functioning

of synapses, in the development of learning and memory and in the maintenance of blood brain barrier integrity in the CNS (Arranz and De Strooper, 2019; Burda and Sofroniew, 2014; Giaume et al., 2007; Pekny et al., 2016; Valori et al., 2019; Verkhratsky et al., 2017).

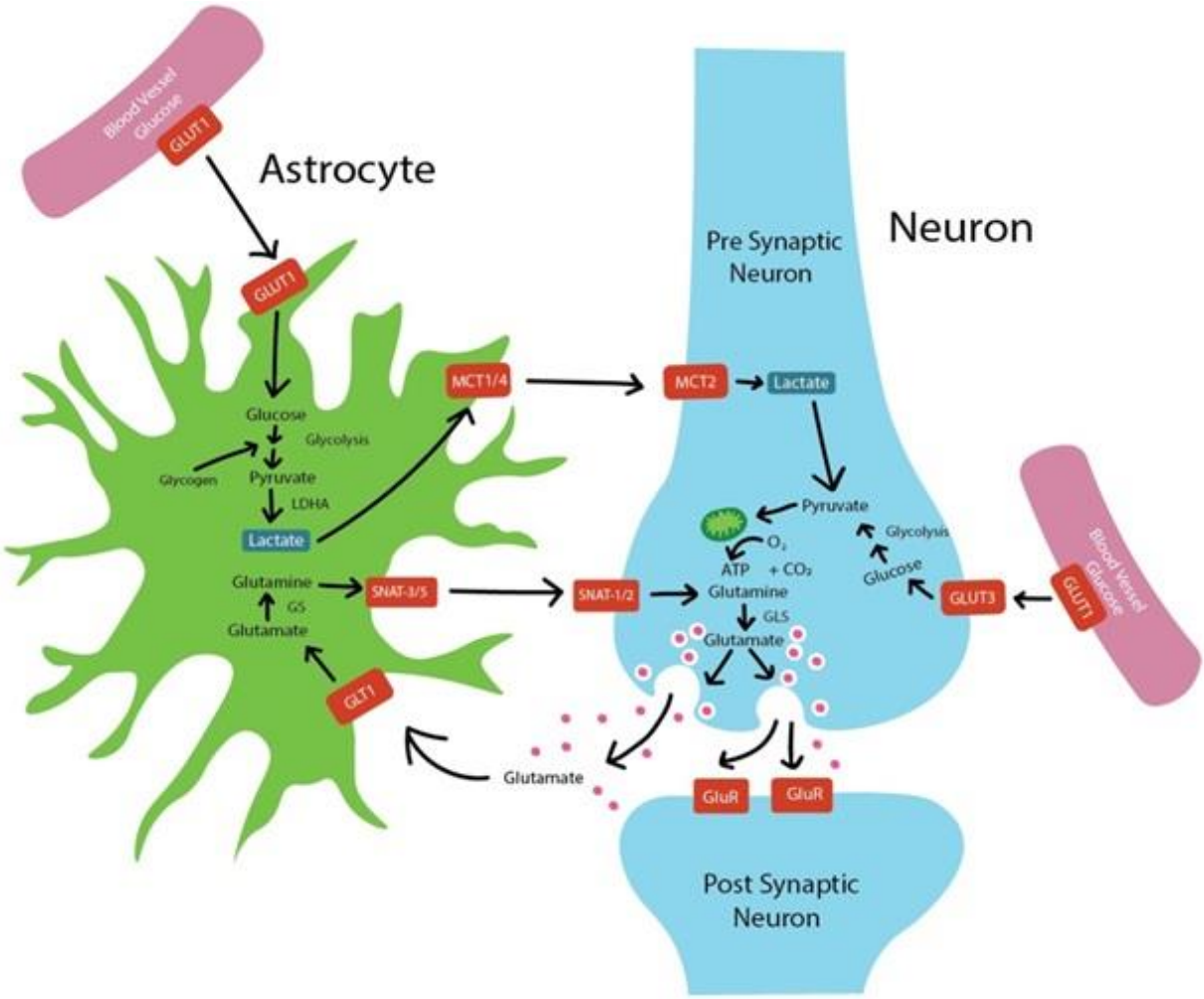

Fig.11: Astrocyte-neuron lactate shuttle and glutamate-glutamine cycle: The simplified cartoon illustrates the lactate shuttle and the glutamate-glutamine cycle at play between astrocyte and neurons. Glucose is transported to the astrocyte from blood vessels via the GLUT1 transporter where part of it is metabolized to lactate through pyruvate by LDHA enzyme. The lactate is then released outside via the MCT1/4 transporter and is taken up by the neuron via MCT2. The lactate forms the major source of energy for neurons in

brain and is converted to pyruvate by LDHB and eventually oxidized in mitochondria releasing ATP. The neuron may also directly uptake glucose via GLUT3. Neurotransmitter glutamate is rapidly taken up by the astrocytes from the synaptic cleft via GLT-1 and is further converted into glutamine by GS. Glutamine is then transferred to the neurons via SNATs and is the substrate for glutamine to glutamate synthesis via GLS which is then released extracellularly. Glutamate uptake by astrocytes can trigger the uptake of glucose from the nearby blood vessels and enhance aerobic glycolysis. Aerobic glycolysis may also be influenced by the catabolism of intracellular stores of glycogen within astrocytes. GS: glutamine synthetase; LDHA: lactate dehydrogenase isoenzyme A; LDHB: lactate dehydrogenase isoenzyme B; GLUT1: glucose transporter 1; GLUT3: glucose transporter 3; MCT1/4: monocarboxylate transporter 1 or 4; MCT2: monocarboxylate transporter 2; SNAT1/2 or SNAT3/5: glutamine transporters; GLS: glutaminase; GluR: receptor for glutamate; GLT-1: glutamate transporter 1

Based on morphology and anatomical location, astrocytes may be classified in two major groups – protoplasmic astrocytes of the grey matter and fibrous astrocytes of the white matter. Protoplasmic astrocytes, having a more complex morphology with fine branching processes, organize themselves into distinct domains or territories without any interaction or overlap between cells adjacent to each other. This organization into domains is assumed to play a central role in coordinating blood flow and synaptic activity (Oberheim et al., 2012). The domain of a single astrocyte in the hippocampus can encompass approximately 1,40,000 synapses. Contrarily, fibrous astrocytes have long processes that are less complex than the protoplasmic astrocytes which contact axons as well as set up perivascular end-feet. Arranged along the white matter tracts, fibrous astrocytes do not organize themselves into domains (Garwood et al., 2017). Besides this oversimplified classification of astrocytes, various other morphological types has been determined in the human cortex that are evolutionary unique to human (higher primates), for example – interlaminar astrocyte found in superficial cortex (Oberheim et

al., 2009; Oberheim et al., 2006). The diversity of astrocytes is further discussed by Verkhratsky et al. 2019 (Figure 12)(Verkhratsky et al., 2019).

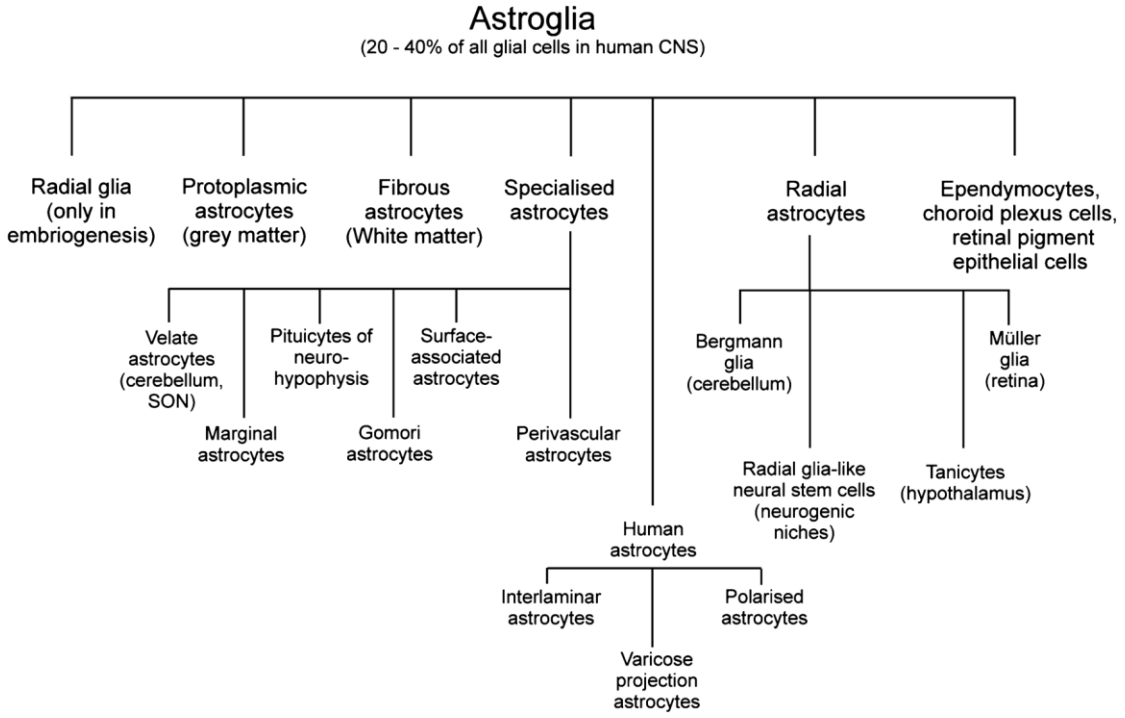

Fig.12: Astrocyte Diversity (Verkhratsky et al., 2019)

2.2.2. Astrocyte reactivity

Neuropathologies in general can be broadly pictured as the failure in brain homeostasis where astrocytes are the major homeostatic cells. Hence, any perturbation in their ability to maintain the inherent balance will dictate the survival or death of neurons thus determining the consequence of the pathological insult. A basic contribution of astrocyte to neuropathology was highlighted by Alois Alzheimer, Santiago Ramon-y-Cajal, Franz Nissl, Rio-Hortega and William Lloyd Andriezen, the latter commenting that the astrocytes "exhibit a morbid hypertrophy in pathological conditions" (Andriezen, 1893). It is now well accepted that neurological disorders are accompanied by astrocytic

hypertrophy and microglial activation together referred to as reactive gliosis (Verkhratsky et al., 2019). Earlier, reactive astrogliosis was considered as a non-specific reaction to a pathological insult as a part of neuroinflammation that formed the basis of neurological disorders. However, current research has disclosed very specific and distinct functions of reactive astrocytes from neurodegenerative disease perspective. The response generated against a pathological insult represented by reactive astrogliosis and microglial activation is now majorly considered to be protective at least at the initial stages. Given the complexity in astrocyte behavior over time, with disease progression, and being dragged to the extent of pathologic severity, reactive astrocytes may turn detrimental and contribute to neuronal death. However, it is also thought that the formation of astroglial scar limits the area of damage and by secreting several neurotoxic factors including pro-inflammatory cytokines and chemokines, surrounding astrocytes and microglia exterminate the pathologically affected neurons and thus protect the neuronal cells and circuits lying outside the damaged area (Morizawa et al., 2017; Wakida et al., 2018). Following such a clearance, neuroglia promotes vascularization, reforms blood-brain barrier, initiates synaptogenesis and induces re-myelination (Anderson et al., 2016; Burda and Sofroniew, 2017; Verkhratsky et al., 2017). Pathological modifications in the morphology of astrocytes are complicated and are specific to disease stage and disease model. The variations are dependent on alterations along the development of disease as reviewed by Verkhratsky et al. 2019 (Figure 13). Three major categories defined based on the manifestations of astrogliopathology are – “reactive astrogliosis”, “astrodegeneration with astroglial atrophy and loss of function” and “pathological remodeling”. The latter

two groups are together identified as "astrocytopathies" to distinguish them from reactive astrogliosis.

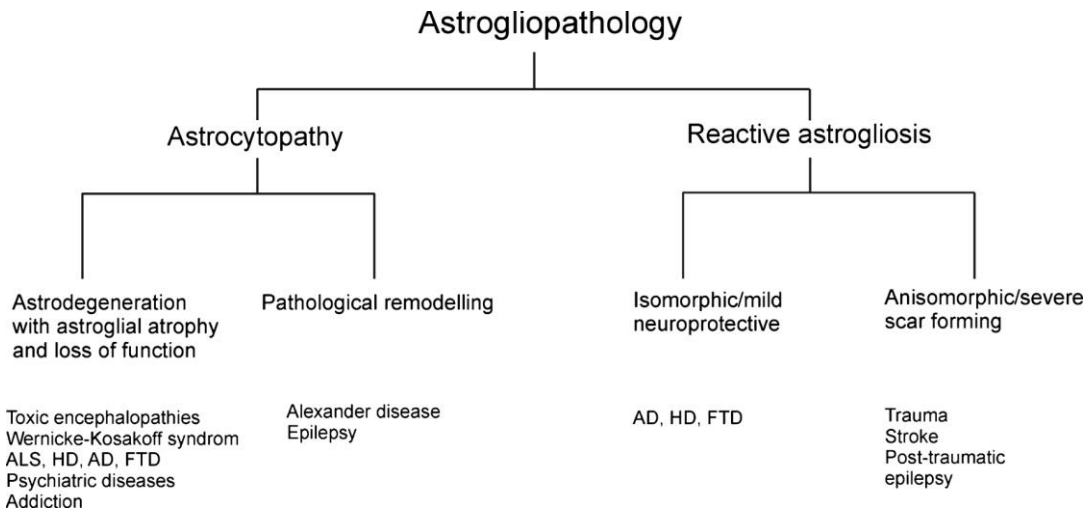

Fig.13: Astrogliopathology classification (Verkhratsky et al., 2019)
AD: Alzheimer's disease; ALS: amyotrophic lateral sclerosis; HD: Huntington's disease; FTD: frontotemporal dementia

Recent findings show that astrocytes go through dramatic changes at the morphological, functional, biochemical and transcriptional levels to give rise to a heterogeneous population when faced with any pathological insult (Escartin et al., 2019). However, some of the alternations may reverse while other changes are more long-term. Such a population of astrocytes is called reactive astrocytes. A series of publications in recent times based on single-cell transcriptomics and proteomics data elude towards a range of functional variations in reactive astrocytes that influence the evolution of disease in different manners (Anderson et al., 2014). In 2021, a world-wide consensus report from glial biologists on the term to describe the astrocyte reaction was decided as either 'reactive astrogliosis' or 'astrocyte reactivity'. They further updated the definition – a

hugely complicated disease-stage and disease-specific occurrence involving all of astrocytes' reactive states in which 'state' indicates a transient or long-term remodeling of astrocytes(Escartin et al., 2021). Astrocyte reactivity may be classified on the basis of the nature of the pathological stimulus which may be external or cell-autonomous in its origin (Fig. 14).

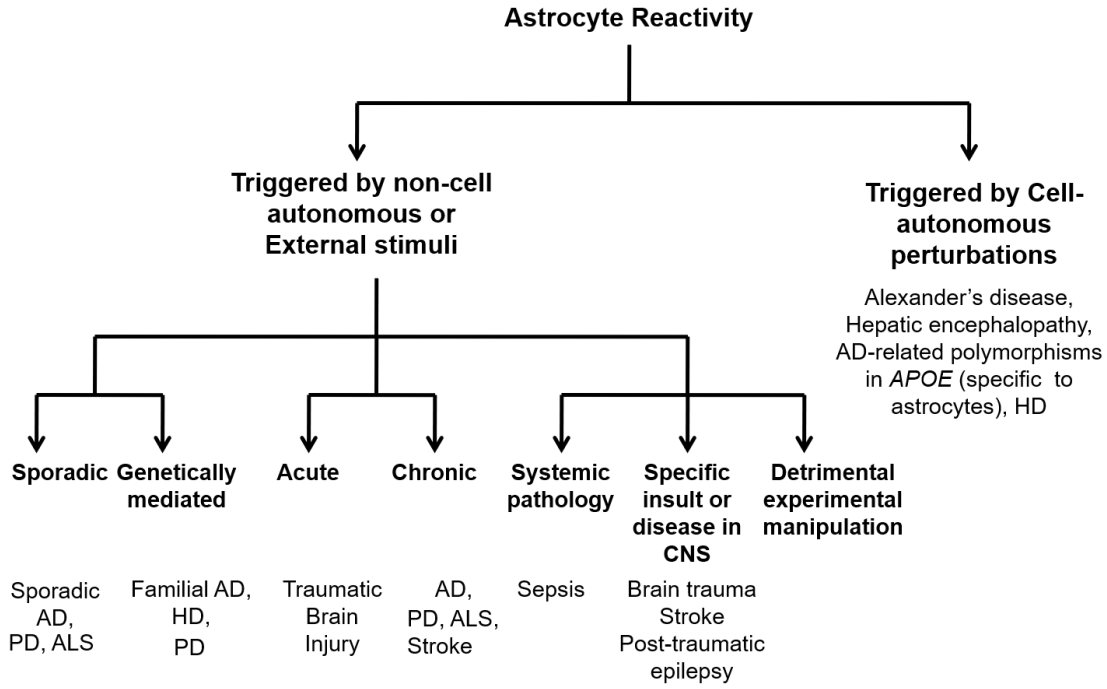

Fig.14: Classification of Astrocyte reactivity based on the nature of stimuli: Astrocyte reactivity is defined as the response of the astrocytes to any pathologicalstimulus. AD, Alzheimer's disease; PD, Parkinson's disease; ALS, Amyotrophic lateral sclerosis; HD, Huntington's disease. Ishan Patro et al. (Eds): The Biology of Glial Cells: Recent Advances, 978-981-16-8312-1, 521150_1_En, (Chapter 9 by Sarkar et al. 2022)

2.2.3. Neurotoxic and neuroprotective aspects of reactive astrocytes

Enhanced levels of glial fibrillary acidic protein (GFAP), s100β or vimentin proteins that are used to identify hypertrophic astrocytes are hugely observed in AD post-mortem

brains (Verkhratsky et al., 2016). Reactive astrocytes are detected in the vicinity of senile plaques (Fig. 15) and have transcriptomic profiles showing upregulation of pro-inflammatory cytokines detected in AD models of rodent and in AD patient samples (Li et al., 2011). Moreover, upon the blockage of astrocyte reactivity in APP/PS1 mice, neuroinflammation was alleviated and there was significant amelioration of cognitive deficits beside a reduction in Aβ load (Furman et al., 2012). Reactive astrocyte-secreted pro-inflammatory cytokines act in an autocrine pathway enhancing the secretion of Aβ from the reactive astrocytes themselves (Blasko et al., 2000). The pro-inflammatory cytokines can further regulate the nearby microglia influencing their ability to phagocytose Aβ (Koenigsknecht-Talboo and Landreth, 2005). They can also influence neurons directly, upregulating caspase-3 activity in them besides increasing abnormal tau phosphorylation and pushes the cell towards neuronal death (Garwood et al., 2011).The reactive astrocyte itself loses their ability to uptake glutamate and starts secreting GABA, thus transforms into a state that is detrimental towards neurons.

Interestingly, reactive astrocytes were found within the brain much before the appearance of Aβ plaques (Wang et al., 2018). Indeed, when astrocyte reactivity was inhibited in a rodent model of AD, AD-related pathological hallmarks were found to be upregulated (Kraft et al., 2013). Reactive astrocytes also posses the ability to uptake and clear Aβ demonstrated in an *in vitro* model of mouse astrocytes (Wyss-Coray et al., 2003). Reports of Aβ-containing astrocytes are already present in earlier literature in brain samples of aged persons (Funato et al., 1998), in entorhinal cortex (Thal et al., 2000) and near to the amyloid plaques in human (Kurt et al., 1999; Yamaguchi et al.,

1998). Reactive astrocytes restricts the amyloid plaques from propagating to the nearby healthy neurons restricting further damage (Sofroniew, 2009). Once the reactive astrocytes uptake Aβ, they can degrade it through the lysosomal pathway especially in the early phase of AD since it has been shown that enhancing lysosomal biogenesis within astrocytes by overexpression of transcription factor EB increased the rate of Aβ phagocytosis followed by Aβ degradation in APP/PS1 mice (Xiao et al., 2014). Aβ may further be degraded by reactive astrocytes with the increased expression of Aβ-degrading enzymes namely neprilysin, Insulin degrading enzyme, endothelin-converting enzyme-2 and matrix metalloproteinases (MMPs) (Carter et al., 2019). These indicate that reactive astrocyte may have a beneficial paradigm in its functionality and partakes in Aβ clearance especially in the prodromal stage of the disease. Thus the phenomenon of astrocyte reactivity is not a simple phenomenon rather it sees a transition in astrocyte function from being protective in the initial phase to a detrimental phenotype in the late-stage AD. Additionally, reports show that the domain organization of reactive astrocytes remains intact even in AD (Oberheim et al., 2008) and astrocytes do not proliferate at least in animal models of the disease (Sirko et al., 2013).

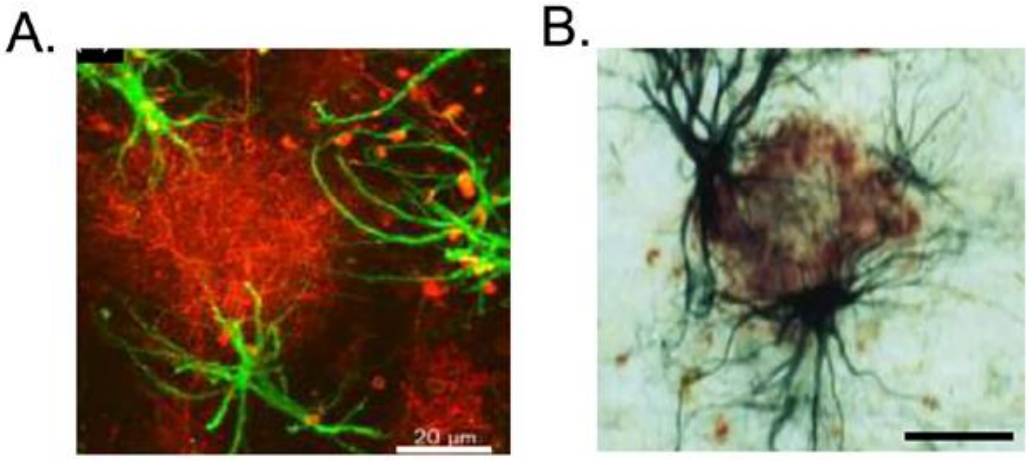

Fig.15: Reactive astrocytes surrounding Aβ plaque: (A) GFAP (green) and Aβ (red) in the hippocampus of 3xTgAD mice, scale bar 20 μm (Olabarria et al., 2010) (B) GFAP (black) and Aβ (brown) in the hippocampus of a human AD patient, scale bar 50 μm (Pike et al., 1995). The similarity between the two images is noticeable.

2.2.4. Reactive astrocyte subtypes in AD

A decade ago, a major transcriptomic profiling of reactive astrocytes by Barres group revealed that astrocytes can have disparate transcriptomes depending on the nature of the external insult (Liddelow and Barres, 2017; Zamanian et al., 2012). They utilized two different mouse models – ischemic model induced by occluding Middle Cerebral Artery and a neuroinflammation model induced by lipopolysaccharide (LPS). High throughput transcriptomic profiling of reactive astrocytes in these two models revealed that the astrocyte transcriptomic profile of one was distinctively different from the other. Few years later in a review from the same group the reactive astrocytes from the ischemic model was named the A2 astrocytes and from the LPS model as the A1 astrocyte (Liddelow and Barres, 2017). A1 reactive astrocyte profile saw an upregulation of detrimental genes essentially encoding pro-inflammatory cytokines. The A2 astrocyte, on the other hand, expressed genes that coded for beneficial proteins. Hence A1 and A2 were essentially the detrimental and beneficial astrocyte subtypes respectively. A1 astrocytes have the potential to trigger various genes of the complement cascade system especially C3 that reportedlyhas a harmful effect on synapses by activation of NF-κβ pathway. Other pro-inflammatory genes that were upregulated within A1 astrocytes are H2-D1, SSP1, Serping1, CXCL1, CXCL2, Ggta1 etc. (Zamanian et al., 2012). Conversely, A2 reactive astrocyte subtype expressed enhanced levels of various neurotrophic molecules

including some of them that are implicated in anti-oxidative pathways such as Arginase-1, Nrf2, PTX3, SPHK1 and TM4SF1 (Zamanian et al., 2012). These genes are involved in the promotion of neuronal viabilityand in the induction of thrombospondins that are known to help synapse repair. However, they indicated that A1 and A2 may be the two terminals of a heterogenous population of astrocytes that are generated. More recently, single-cell and single-nucleus RNA sequencing reports revealed that a specific subtype of reactive astrocytes, detected by a mix of A1 and A2 reactive transcripts, is highly unregulated in mouse models and patient brain samples of neurodegenerative disease which also included AD (Grubman et al., 2019; Habib et al., 2020; Zhou et al., 2020). Habib et al termed this subtype of reactive astrocytes as disease-associated astrocytes (DAA). DAA were present in the initial stage (pre-cognitive decline) in AD and their number started increasing with the progress of disease. DAA-like populations started to appear with age in both wild type mice and in human brains. DAA were majorly detected in the vicinity of Aβ plaques, both in the hippocampus and the subiculum that means the areas, most sensitive to damage in AD. Hence, it may be inferred that there are many reactive astrocytes that are way more complex and numerous beyond the oversimplified A1/A2 nomenclature. It is imperative that we unveil the molecular switch that causes the transition of reactive astrocyte from the beneficial phenotype to the detrimental phenotype. In fig. 16, we have depicted the probable reactive astrocyte subtypes in AD upon treatment with Aβ and named the detrimental subtype – A1-like astrocyte and the protective one – A2-like astrocyte to allude to the heterogeneity of reactive astrocytes beyond A1/A2 nomenclature.

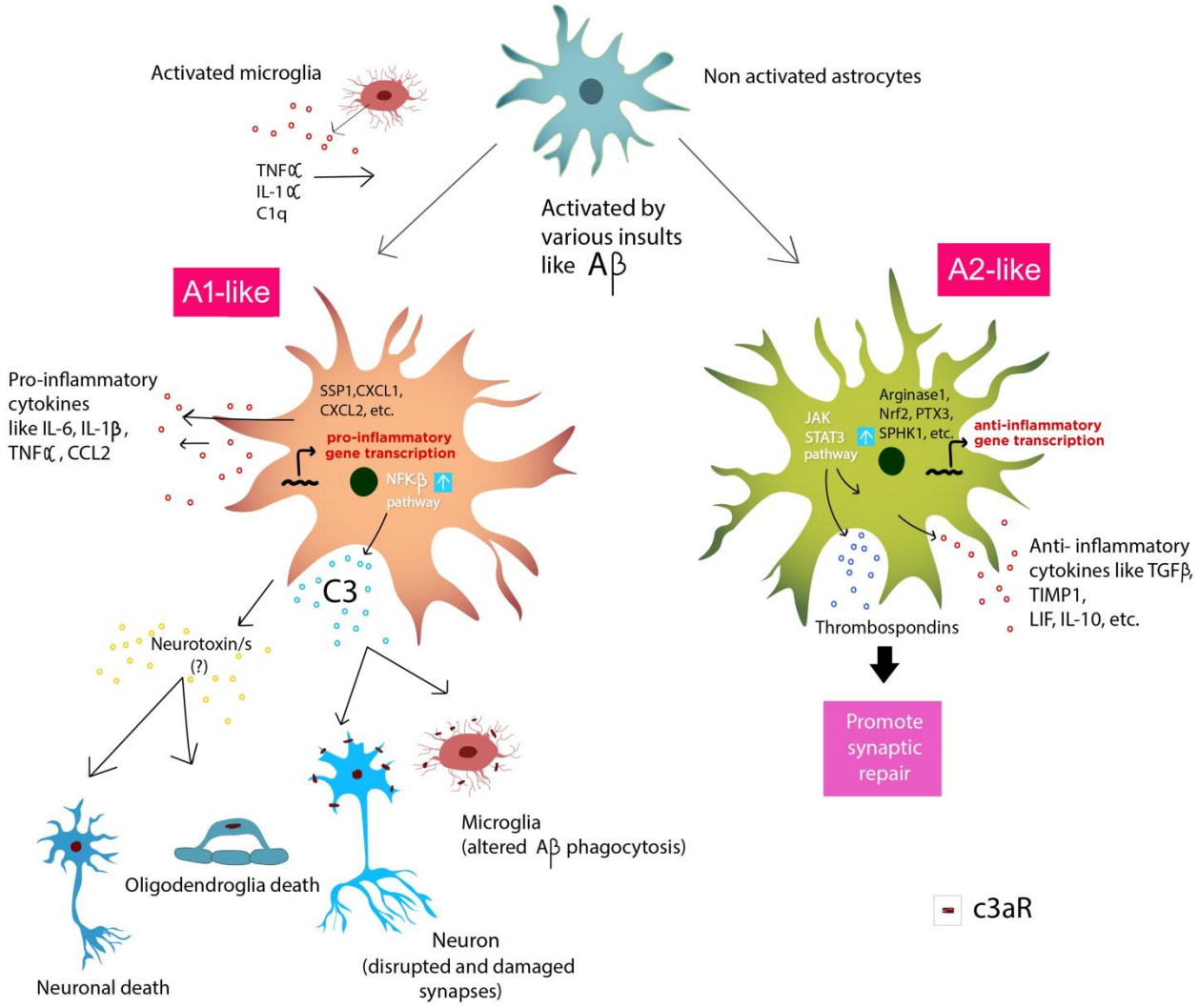

Fig.16: Schema showing astrocyte reactivation in Alzheimer's disease: Astrocyte reactivity in response to Aβ in Alzheimer's disease has been shown. The subtypes are broadly classified as A1-like (detrimental) and A2-like (beneficial) reactive astrocytes. However there are many more subtypes present that are disease and disease-stage specific. A1-like astrocytes have a distincttranscriptomic profile fromA2-like astrocytes. A1-like reactive astrocyte may be generated under the influence ofcytokinesTNFα, IL-1α and C1q from activated microglia. The secretome profiles of A1-like and A2-like astrocytes are very different. Ishan Patro et al. (Eds): The Biology of Glial Cells: Recent Advances, 978-981-16-8312-1, 521150_1_En, (Chapter 9 by Sarkar et al. 2022)

2.2.5. Role of astrocyte secreted cytokines

Astrocyte derived cytokine and chemokine molecules can either affect the neurons directly orregulate the action of microglia on neuronsin the CNS. The intercellular communication between neuronal and non-neuronal cells is a highly complex in nature and majorly mediated by cytokines along autocrine or paracrine pathways. Cytokines are defined as a heterogeneous population of small proteins that play crucial role in communication among cells and are rapidly secreted as a result of a CNS insult. They can be exciting molecules in studying the various stages in AD progression and are valuable from a translational perspective.

IL-1β which belongs to the IL-1 cytokine family is recognized as a prominent pro-inflammatory cytokine which has been found in the plasma and CSF of human AD samples (Brosseron et al., 2014). Interestingly, they were secreted by reactive astrocytes (Sofroniew, 2015). IL-1β is known to initiate the series of immune responses in AD and also induces the cleavage of APP along the amyloidogenic pathway in neurons (Griffin et al., 1998). Along an autocrine pathway IL-1β can trigger IL-6 secretion from astrocytes and also induces an enhanced expression of s100β in them. Further IL-1β enhamces iNOS activity (Rossi and Bianchini, 1996) and the excess release of macrophage colony stimulating factorpaving the way towards neuronal degeneration (Rubio-Perez and Morillas-Ruiz, 2012). IL-1β can further increase neuronal AChE activity and its own synthesis, and further reactivation of astrocyte themselves through a vicious loop (Griffin et al., 1998; Mrak and Griffin, 2001).

IL-6, expressed in reactive astrocytes by an upstream IL-1β can trigger both pro-inflammatory and anti-inflammatory signaling in neuronal cells (Sofroniew, 2015). IL-6

binds to the receptor, gp130, which is also a common receptor for many growth factors including ciliary neurotrophic factor (CNTF), oncostatin M (OSM), leukemia inhibitory factor (LIF) as well as another cytokine- IL-11. Following binding to gp130, IL-6 can trigger the JAK-STAT pathway enhancing the growth of neurons. Conversely, IL-6 can also have a negative impact on neurogenesis especially during the developmental phase (John et al., 2005). There are contradictory reports on IL-6 in literature. IL-6 can inhibit the secretion of proinflammatory cytokines including IL-1β and TNFα (John et al., 2005). Conversely, some reports elucidate that IL-6 promotes APP synthesis (Vandenabeele and Fiers, 1991). In the AD scenario, IL-6 can induce ERK1/ERK2 pathway as well as STAT3 pathways (Schumann et al., 1999). It may additionally direct the production of acute phase proteins in neurons like α2-macroglobulin and metallothionine (Akiyama et al., 2000; Bauer et al., 1993; Ganter et al., 1991).

A critical pro-inflammatory cytokine, TNFα, may also be secreted from reactive astrocytes and is reported to trigger toxic cell cycle processes in the post-mitotic neurons contributing towards AD pathogenesis (Yamamoto et al., 2007). Soluble form of TNFα has the capability to bind to its receptor TNFR1 which has an intracellular 'death domain', thus further activating neuroinflammation and neuronal death in neurodegenerative disorders including AD, PD, ALS and MS (Akiyama et al., 2000; Antel et al., 1996).

Fractalkine or CX3CL1 is a cytokine that under physiological conditions are primarily expressed in neurons but under abnormal circumstances may be released by the astrocytes of the CNS (Hughes et al., 2002; Pereira et al., 2001). Findings allude that the

fractalkine-CX3CR1 signaling may play a crucial role in AD (Chen et al., 2016). Upon the binding of fractalkine with its receptor CX3CR1 on the surface of neurons in the hippocampus, pro-survival Akt pathway is induced further ensuring neuroprotection (Meucci et al., 2000). CXCL8, is another cytokine, that can be expressedin astrocytes and microglia besides neurons under the influence of Aβ and maintains the viability and health of neurons by enhancing the release of brain derived neurotrophic factor (BDNF) and also by preventing Aβ-induced apoptotic death of neurons along autocrine or paracrine pathways (Ashutosh et al., 2011).

Astrocytes may also influence neuronal health by regulating microglial functions; all these mediated by cytokine molecules. The cytokine TGF-β secreted from reactive astrocytes blocks neuroinflammatory processes by modulating microglial activation. Intriguingly, IL-10 is the cytokine that is released by activated microglia acts as an upstream regulator of TGF-β secretion from astrocytes. It can be thus inferred that astrocyte plays an essential role in dictating IL-10-induced anti-inflammatory responses which includes a reduced expression of pro-inflammatory IL-1β while increasing the production of anti-inflammatory fractalkine receptor (CXCR1) as well as IL-4 receptor (IL-4Rα) in microglia (Cekanaviciute et al., 2014; Norden et al., 2014). GFAP-IL-6 mice, where there is overproduction of IL-6 from astrocytes, have enhanced levels of microglial activation and chronic neuroinflammation. Coherently, the neuroinflammation further induces synapse loss of calbindin-containing neurons and hence severe learning and memory deficits were detected in this mouse model (Heyser et al., 1997). Thus, we may conclude that cytokine plays essential yet some play pleiotrophic role in AD depending on disease-stage and

hence are crucial candidates for future investigation.

2.2.6. Astrocyte subtype-based therapies – emerging role of cytokines

As we have seen that there is a possible transition in secretomes of reactive astrocyte subtypes along the AD continuum, astrocyte subtype-targeted therapeutic approach seems to be a new paradigm in AD treatment and the cytokines emerge as exciting candidates.

A1 or A1-like astrocytes are induced in AD by the action of three specific cytokines - IL-1α, TNFα and C1q secreted from reactive microglia in an LPS model of neuroinflammation. Mechanisms to block the reactivity the of the detrimental A1-like astrocytes is targeted by either inhibiting microglial reactivity or by blocking the action of microglia-secreted cytokines – IL-1α, TNFα and C1q. NLY01 (Yun et al., 2018) or exendin4 (Goncalves et al., 2016; Gullo et al., 2017; Lee et al., 2018) are being used to prevent or abrogate the activation of microglia as both of them are agonists of long-acting glucagon-like peptide-1 receptor and hence are considered useful for treating AD. TNFα inhibitor such as Etanercept is already being used in the market for the treatment of rheumatoid arthritis and its use has been correlated with reduced risk of developing AD in aged population in comparison to control population (Chou et al., 2016; Ekert et al., 2018). However, in phase-2 clinical trial Etanercept failed to qualify as a drug for AD treatment (Decourt et al., 2017). Besides TNFα targeting, C1q is also targeted by antibodies while for IL-1α, a recombinant antagonist (Anakinra) has been designed. Both are now undergoing clinical trials (Lansita et al., 2017; Liddelow and Barres, 2017). A1-like astrocyte released IL-1α, IL-6 and IFNγ can influence the nearby neurons towards a detrimental fate by inducing

enhanced caspase-3 activity and excessive abnormal tau phosphorylation. Minocycline can inhibit the above-mentioned cytokine from being released thus preventing neuron death downstream even under Aβ exposure (Garwood et al., 2010). A1-like astrocyte can also be inhibited by using inhibitors against C3 (Lian et al., 2015; Lian and Zheng, 2016) or by targeting C3aR (C3 receptor) (Lian et al., 2016; Lian et al., 2015). NSAIDs can also be used to inhibitthe secretion of pro-inflammatory cytokines and thus preventing neurodegeneration in AD (Gasparini et al., 2004; Sastre and Gentleman, 2010). Unfortunately, till date NSAIDs are unable to show any positive resultin clinical trials for AD (de Jong et al., 2008). Additionally, glucocortocoids are thought to diminish release of IL1α, IL1β and IL-6 from the A1-like astrocytes (Fakhoury, 2018; Szczepanik and Ringheim, 2003). The major reason for the failures of A1-like astrocyte or pro-inflammatory cytokine-targeted therapies in AD is the lack of appreciation of the fact that reactive astrocytes have disparate cytokine profiles across the different stages in AD.

A2-like reactive astrocyte secreted anti-inflammatory cytokines may be utilized as novel drug candidates in AD therapy. Injection of TGFβ through the intranasal (IN) route in an Aβ-infused rat model of AD ameliorated learning and memory impairmentsas well as apoptotic cell death of neurons (Chen et al., 2015). In another study, intra-hippocampal injection of TGFβ in a mouse model of AD alleviated AD-associated cognitive dysfunctions and synaptic deregulation by activating PI3K/Akt/Wnt/β-catenin pathway (Hu et al., 2019). These reports re-emphasize the importance cytokine-mediated therapeutic approaches in AD. Additional reports show that injection of exogenous IFNβ through the IN route which is known to be secreted by both neurons and glia can

improve cognitive functioning of AD rats model by regulating apoptotic cell death and inducing hippocampal neurogenesis (Chavoshinezhad et al., 2019). On the other hand, injection of IL-10, an anti-inflammatory cytokine, through the intravenous route in an Aβ-injected mouse model as well as in a LPS-induced inflammation model in mice, attenuated the excess release of pro-inflammatory cytokines namely IL-1α, IL-1β, IL-6 and MCP-1 in the hippocampi and cortices (Szczepanik and Ringheim, 2003). Injection of IL-33 through the intraperitoneal (i.p.) route in APP/PS1 mice decreased the Aβ plaque burden by increasing the phagocytic activity of microglia, by attenuating the transcription of pro-inflammatory genes and by enhancing cognitive abilities (Fu et al., 2016). In recent past, Guha et al. have shown that i.p. injection of ICAM-1 alleviates cognitive deficits not only in an Aβ-infused rat model of AD but also in an advanced transgenic mouse model of AD, 5xFAD by targeting the proinflammatory NF-κβ pathway (Guha et al., 2022). Subcutaneous injection of granulocyte colony stimulating factor (G-CSF) in Aβ-infused mice as well as in transgenic Tg2576 mice (overexpressing mutant APP with Swedish mutation, characterized by elevated levels of Aβ and amyloid plaques) prominently improved cognitive activity. It was observed that G-CSF also triggered mobilization of bone marrow-derived hematopoietic stem cells and neurogenesis in the vicinity of Aβ plaques. Interestingly, G-CSF is available in the market for the treatment of chemotherapy-induced neutropenia. Hence, further work with G-CSF may unveil interesting results to facilitate its use cytokine-dictatedtherapy in AD (Tsai et al., 2007). However, all these cytokines are being still tested at the pre-clinical levels and needs to be further validated before starting clinical trials. A list of probable A1-like and A2-like

astrocyte secreted cytokine based putative targets for the treatment of AD is presented in Table 1.

A1-like astrocyte targeted strategies in AD treatment					
Target	**Therapeutic molecule/drug**	**Experimental model**	**Route of drug/moleculeadministration**	**Age of administration**	**Reference**
		Cytokine-based inhibition			
TNFα	Etanercept (TNFα inhibitor, used in standard RA therapy)	Human AD patients[1]	s.c.	Average age, 76.5 years	(Chou et al., 2016)
		Human AD patients[#]	s.c.	Average age, 72.4±9.7 years	(Butchart et al., 2015)
		Human AD patients[#2]	perispinal	Average age, 76.7±10.9 years	(Tobinick et al., 2006)
	Xpro1595 (TNFα inhibitor)	TgCRND8 mice	s.c.	1-month old (Pre-plaque stage)	(Cavanagh et al., 2016)
	TNFR2:Fc (anti-TNFα biologics)	$A\beta_{25-35}$-injected mice	s.c.	6-week old (2nd, 4th and 6th day following Aβ administration)	(Detrait et al., 2014)
	3,6'-dithiothalidomide (small molecule TNFα inhibitor)	3xTg-AD Mice	i.p.	4-month old (Pre-plaque stage with mild intraneuronal Aβ)	(Gabbita et al., 2012)
		$A\beta_{1-42}$-injected mice	i.p.	3-month old (Administered 7days prior to Aβ injection)	(Russo et al., 2012)
	Thalidomide (small molecule TNFα inhibitor)	APP23 mice	i.p.	Long term treatment- 9 to 12-month-old, Short term treatment – 12-month old	(He et al., 2013)
	Infliximab (monoclonal anti-TNFα antibody)	$A\beta_{1-42}$-injected mice	i.c.v.	6-week old (co-administered with Aβ)	(Kim et al., 2016)
		APP/PS1 mice	i.c.v.	12-month old	(Shi et al., 2011)
	XENP345 (Dominant negative TNFα inhibitor selective for soluble TNF)	3xTg-AD mice	i.c.v.	4.5-month old	(McAlpine et al., 2009)

C1q	ANX005 (anti-C1q antibody)	Sprague-Dawley (SD) rats	i.v.	8-9 weeks	(Lansita et al., 2017)
		Cynomolgus monkeys	i.v.	2-4 years	
	ANX-M1 (anti-C1q antibody)	$A\beta_{1-40}$-oligomer injected mice	i.p. and i.c.v.	3-month old (co-administered with Aβ)	(Hong et al., 2016)
IL1α	Anakinra (recombinant IL1α receptor antagonist)	McGill-Thy1-APP-TG rats	s.c.	6-month old (Pre-plaque stage)	(Qi et al., 2018)
IL-6, MCP-1	Minocycline (an antibiotic)	Htau mice	i.p.	3-4 month old	(Garwood et al., 2010)
IL1β, TNFα, IL-6	NSAIDs - Ibuprofen	Human AD patients#	oral	≥65 years	(Pasqualetti et al., 2009)
		Tg2576 mice	oral	3-month old (Pre-plaque Stage with high levels of soluble Aβ)	(Eriksen et al., 2003)
	Indomethacin	Human AD patients#	oral	Average age 78±2 years	(Rogers et al., 1993)
		Human AD patients#	oral	Average age 72.7±6.9 years	(de Jong et al., 2008)
	Naproxen	Human AD patients#	oral	Average age 74.1±7.8 years	(Aisen et al., 2003)
IL1α, IL1β, IL-6, MCP-1	Glucocorticoids (prednisolone and dexamethasone)	$A\beta_{1-42}$-injected mice	i.p.	50-60 days old (30 min prior to Aβ injection by i.c.v.)	(Szczepanik and Ringheim, 2003)
			Microglial activation inhibition		
Glucagon-like peptide-1 receptor agonists	Exendin-4[3]	Streptozotocin (STZ) injected rat AD model	i.p.	Male mature rats weighing between 200-220 g (Administered for 14 days following i.c.v. STZ)	(Solmaz et al., 2015)
		$A\beta_{1-42}$-injected rat	i.p.	6-8 weeks (weighing 180±20g, administeredfrom Day-1 to Day-14 following Aβ i.c.v. on Day-1)	(Garabadu and Verma, 2019)

NF-κβ	NSAIDs-Indomethacin	Tg2576 mice	oral	8-month old	(Sung et al., 2004)
	Aspirin	Tg2576 mice	s.c.	12-month old	(Medeiros et al., 2013)
C3	C3aR antagonist	APP/TTA double transgenic mice	i.p.	8-month old	(Lian et al., 2015)
	C3aR antagonist or genetic deletion of C3aR	APP/TTA mice	i.p.	7.25-month old	(Lian and Zheng, 2016)
A2-like astrocyte targeted strategies in AD treatment					
TIMP-1	-do-	$A\beta_{1-42}$-injected rat	i.c.v.	Adult male SD rats weighing 280-320 g (Administered on the 7th day following Aβ i.c.v.)	(Saha et al., 2020b)
ICAM-1	-do-	$A\beta_{1-42}$-injected rat	i.p.	Adult male SD rats weighing 280-320 g (Drug injection started on the 7th day following Aβi.c.v.)	S. Guha, R. K. Paidi, P. Saha, S.C. Biswas (Unpublished)
		5xFAD mice	i.p.	6-month old	
TGFβ	-do-	$A\beta_{1-42}$-injected rat	i.c.v.	4-month old (1 hour before Aβi.c.v.)	(Chen et al., 2015)
			i.n.	(7^{th}-day after Aβi.c.v.)	
		3xTg mice	i.c.v.	2-3 month	(Hu et al., 2019)
IL-10	-do-	$A\beta_{1-42}$-injected mice	i.v.	50-60 days old (Administered 10 min before the Aβi.c.v. injection)	(Szczepanik and Ringheim, 2003)
IFNβ	-do-	Lentiviral (LV) mediated overexpression of mutant APP in hippocampus of adult rat	i.n.	12 week old male Wister rats (240-260g) (Administered on Day-23 following icv of LV-APP and continued on	(Chavoshinezhad et al., 2019)

				alternate days till day-48)	
IL33	-do-	APP/PS1 mice	i.p.	6-25 month old mice	(Fu et al., 2016)
G-CSF	-do-	Tg2576 mice	s.c.	10-12 month old	(Tsai et al., 2007)
		$A\beta_{1-42}$-injected mice	s.c.	8-week old (Administration started onthe7thday following Aβ i.c.v.)	

Table 1: Probable A1-like and A2-like astrocyte subtype-specific therapeutic targets in Alzheimer's disease (AD) (Sarkar and Biswas, 2021)

Abbreviations: C3aR - C3 receptor, i.c.v. - intracerebroventricular, i.n. - intranasal, i.p. – intraperitoneal, i.v. – intravenous, NSAIDs - nonsteroidal anti-inflammatory drugs, RA – rheumatoid arthritis, s.c. – subcutaneous, TNFR2:Fc - TNF receptor 2 fused to a Fc domain, -do- - same as the previous cell

#Probable AD according to National Institute of Neurological and Communicative Disorders and Stroke and the Alzheimer's Disease and Related Disorders Association (NINCDS-ADRDA) Criteria

[1]As per International Classification of Diseases, Ninth Revision (ICD-9) code for rheumatoid arthritis (RA), along with a diagnosis of AD made at least 120 days after the diagnosis of RA

[2]Diagnostic and Statistical Manual of Mental Disorders, Fourth Edition (DSM-IV) criteria for AD, mild-to-severe AD

[3]A site-specific pegylated form of exendin-4, NLY01 produced by Neuraly company (http://www.ddpharmatech.com/) has been approved for Phase 2B trial in patients with MCI due to AD after it was well-tolerated in Phase-1 trial (NCT03672604) in healthy volunteers.

3. Study of cognitive dysfunctions in AD

3.1. Memory loss in AD – Learning and memory are the two critical qualities of our

brain. While learning helps us to acquire new information, memory helps us to retain the knowledge for a lifetime. However, the debilitating disease, AD, is often called a memory thief and has emerged as the most notorious player in the loss of learning and memory processes. Memory is defined as the process of encoding, storing, consolidating and retrieving information of any external or internal stimuli that can be utilized by the nervous system to respond properly to a new stimulus (Jahn, 2013). Memory can be broadly classified as short-term and long-term memory. While short-term memory (working memory) lasts for seconds to minutes and is limited in its capacity, long-term memory is more complex, unlimited in its capacity and lasts for many years. In short-term memory formation, sites in frontal and parietal lobes are responsible (Miller, 1956). Long-term memory is stored by de novo synthesis of proteins and alternations in neuronal networks across different regions of the cortex especially the medial temporal lobe. Long-term memory is sub-divided into implicit (non-declarative) and explicit (declarative) memories. Explicit memories depend on a deliberate or conscious retrieval of memory. This group is again sub-categorized into episodic memory (dependent on context, mostly personal experience) and semantic memory (independent of context, mostly facts). The memory classification is shown in fig. 17. Semantic memory loss can be detected many years before the actual diagnosis of AD and is mainly presented as loss of verbal memory, loss of words and fluency, as the first set of symptoms (Verma and Howard, 2012). However, episodic memory is the worst hit in AD (Park and Lee, 2021). Notably, in all these memory formations especially in the consolidation step hippocampus is responsible for converting short-term memory to long-term memory. In AD, patients suffer a huge damage to the hippocampus hence hippocampus-dependent

recognition and spatial memories are the worst hit. AD patients show progressive deterioration in their working memory and attention as well. Further, the frontal subcortical dependent executive functions that impair the ability to plan and perform in a goal-oriented manner are eventually damaged (Jahn, 2013). The AChE inhibitors and NMDA inhibitors help to improve concentration and attention in the mild-to-moderate AD patients but are unable to prevent further damages (Pepeu and Giovannini, 2010; Pepeu et al., 2013).

In clinical practice, several types of behavioral tests are performed to assess the cognitive functions of an individual namely CERAD (Consortium to establish a registry for Alzheimer's disease) test, the MMSE (Mini mental state examination) and also scaling systems like the CDR (clinical dementia rating) scale (Morris, 1997; Morris et al., 1989; Morris et al., 1988). Further, mental deficits in planning, attention and execution are scored in Winconsin card sorting test, the Stroop test, the Tower of London test, the Boston naming test, the clock drawing, trail making test etc. (Jahn, 2013).

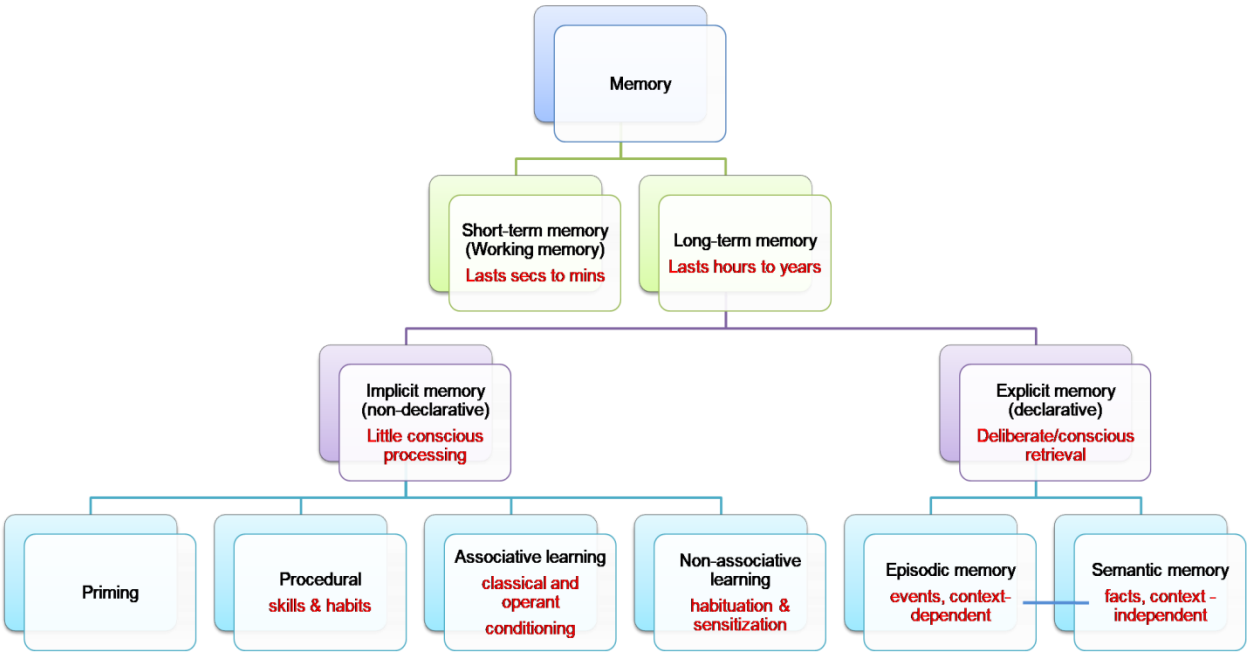

Fig.17: Classification of memory interpreted from Principles of Neural Science (5th edition).

3.2. Animal models in AD research - Animal models have become an important tool to study several diseases because they can recreate the disease circumstances to an extent that recapitulates the disease progression in humans. In AD, several peptide-induced (for ex. Aβ-injected) as well as genetically manipulated transgenic models are available now. Although none of them is an absolute model given the complexity of AD in humans, atleast it helps us to decipher specific molecular mechanisms underlying disease pathogenesis and to test potential therapeutic agents at the preclinical level. In intra-hippocampal Aβ-injected model of rats, direct effect of Aβ on neurons and glia has been revealed and has further divulged many important aspects of Aβ-directed disease pathogenesis. However, these models recapitulate only those pathways that are triggered by Aβ and hence rejected by many biologists who are not in support of the amyloid

cascade hypothesis. However, genetically manipulated transgenic mice have become the prevalent work-horses in most laboratories to delineate the different aspects of AD. The first was modeled by over-expressing the APP gene in mice and named as PD-APP mice in 1995 (Games et al., 1995). Mice are especially suitable because the Aβ plaques detected in the transgenic mouse brain structurally resemble those that are found in human AD brain (Yang et al., 2000). Research work with transgenic mice have revealed numerous aspects of AD including the higher toxicity of Aβ oligomers compared to plaques (Haass and Selkoe, 2007), that there is intraneuronal Aβ accumulation prior to plaque deposition (Billings et al., 2005; Oddo et al., 2003), the connection between Aβ and tau (Blurton-Jones and Laferla, 2006) etc. With time, more advanced models have emerged bearing mutations in the APP, PSEN1 and PSEN2 genes as well as mutations in tau genes to encompass multiple hallmarks of AD. The most extreme APP/PS1 FAD transgenic model in mice as of today is 5xFAD carrying five mutations (Swedish, London and Florida in the APP gene and two mutations in the PSEN1 gene). They represent a very robust model where at 6 weeks of age the mice develop intraneuronal Aβ and by 2 months Aβ plaques can be observed in the brain (Drummond and Wisniewski, 2017). The most commonly used transgenic mouse models of AD are listed in Table 2. However, due to immense failure of drugs that were pre-clinically tested in rodent models, later in clinical trials, have questioned the use of the available transgenic mouse models in AD research. The questions that are being raised with their translational values are

- The disparity in species between mice and humans – incomplete models, altered

targets, difference in immune response

- Heterogeneity in humans enrolled in clinical trials as well as there are co-morbidities in humans as opposed to mice models which are in-bred under the laboratory settings
- Most of the current animal models do not show enough loss of synapses or neurons unlike human patients and hence the transgenic mice may represent the prodromal phase of AD.
- Most of the current mice models are FAD, whereas most of the human cases are sporadic AD.

More recently mouse model carrying ApoEε4 variant as well as a specific TREM2 variant are being developed by the MODEL-AD consortium, based in the US with the main target to recapitulate the pathological features of LOAD. Moreover, scientists around the world have starting exploring non-human primates including marmosets and rhesus macaques as models of AD and are thought to have higher translational relevance.

Animal Models	Details
$A\beta_{1-42}$-injected mouse/rat	$A\beta_{1-42}$ oligomer injected intracerebroventricularly into the mouse/rat brain (in most cases into hippocampus)
$A\beta_{1-40}$-injected mouse	$A\beta_{1-40}$ oligomer injected intracerebroventricularly into the mouse brain
$A\beta_{25-35}$-injected mouse	$A\beta_{25-35}$ oligomer injected intracerebroventricularly into the mouse brain
STZ-injected rat	Streptozotocin (STZ) injected intracerebroventricularly into the rat brain
APP/PS1	Double-transgenic mice incorporated with a murine/human amyloid precursor protein (APP) construct with the Swedish double mutation and also the exon-9–deleted presenilin 1 (PSEN1) mutation (APPswe +

	PSEN1/dE9)
APP/TTA	Double-transgenic mice with an APP transgene bearing the Swedish and Indiana mutations under a tetracycline-responsive promoter
APP23	Transgenic AD mice that express mutated human Swedish double mutation (βAPP) under a neuron-specific and murine origin Thy-1 promoter
Tg2576	Transgenic AD mice overexpressing the Swedish mutation (KM670/671NL) of APP (isoform 695) with high levels of Aβ plaques
3xTgAD	Transgenic AD mouse model that expresses mutant human genes APPswe, PS1M146V and tauP301L
5xFAD	Transgenic AD mice overexpressing 5 mutations - K670N/M671L (Swedish), V717I (London) and I716V (Florida) mutations in human APP (695), and L286V and M146L mutations in human PSEN1
TgCRND8	Mice that express both Swedish and Indiana mutations of APP 695 (KM670/671NL+V717F) under the PrP gene promoter.
Htau	Transgenic AD mice created by mating 8c mice, expressing the whole wild-type human gene, with the tau knock-out mice
McGill-Thy1-APP-TG rat	Transgenic rat that expresses human APP751 with Indiana and Swedish mutations under the regulation of the murine Thy1.2 promoter.
https://www.alzforum.org/	

Table 2: Commonly used transgenic mouse models in Alzheimer's disease (Sarkar and Biswas, 2021).

3.3. Behavioral tests in rodent models of AD – The medial-temporal lobe is the part of the brain mostly implicated in explicit or declarative memory (Scoville and Milner, 1957). Hippocampus is the most important part of the medial temporal lobe responsible for spatial memory and is the most vulnerable to damage in AD (O'Keefe and Dostrovsky, 1971; Squire et al., 1993; Squire and Zola-Morgan, 1991). Most of the rodent behavioral tests assess hippocampal-dependent memory. Tests that are generally used in AD are Morris water maze (MWM), radial arm maze (RAM), T/Y maze, fear conditioning test, novel objective recognition test, active and passive avoidance tests etc. (Puzzo et al.,

2014). Additionally, some anxiety and exploratory behaviors are tested through open-field (locomotion) test and elevated plus maze test which add additional attributes in studying AD-related changes, even if these tests are not specific to AD (Samaey et al., 2019). RAM is used to test short-term memory whereas MWM is used to test long-term memory where the test protocols can be modified in different ways to assess various types of memories including semantic memory (Puzzo et al., 2014). MWM is used to test hippocampal-dependent spatial memory where the mouse generally has to find a hidden submerged platform using visual cues (Morris et al., 1982). Fear conditioning tests are used to test implicit memory. The two types of implicit memory are associative (classical and operant memory) and non-associative learning (habituation and sensitization). Fear conditioning is an associative learning process based on the classical Pavlovian conditioning containing a conditional stimulus (CS), generating a weak response that is unrelated to the task to be learned (light or sound) and an unconditional stimulus (US) that can generate a particular behavioral response (for ex. salivation for food or freezing against shock). It is particularly useful in estimating both contextual and emotional aspects of memory and integrates hippocampus and amygdala respectively in the same task (Puzzo et al., 2014). Novel object recognition test helps in the assessment of recognition memory and is dependent on the innate ability of rodents to prefer a novel object over an object with which it was made familiar early on. It is not a typical hippocampal-dependent memory but by increasing the interval between training and test phase from minutes to hours, this test can be useful to estimate hippocampal-dependent long-term memory (Hammond et al., 2004). Finally, active and passive avoidance tests are also employed to check associative learning and memory. Active avoidance test is

based on fear-motivated response of a rodent to actively avoid an aversive stimulus (Vanderwolf, 1964). In passive avoidance test, the animal is tested for its ability to refrain from entering a darker chamber where it has previously received an aversive stimulus (van der Poel, 1967). In our study, we have employed some of the most important cognitive behavioral tests to understand the changes in hippocampal memory in models of AD.

4. AD is a synaptic failure

4.1. Role of Aβ oligomers - Neurochemical analysis of AD patient brains revealed thatthe enzymes that help in the production of AChE are significantly reduced (Davies and Maloney, 1976). Interestingly, the Aβ containing neuritic plaques were localized in the hippocampal and basal forebrain-neocortical region tracts that were enriched in cholinergic neurons. Neuronal loss was also observed along these pathways. A significant reduction in neurotransmitters occurs along the course of AD progression, however these early symptoms occurred in association with the loss ofcholinergic and glutamatergic synapses in AD (Small et al., 2001). Morphometric analyses of frontal and temporal cortical sections of brains, 2 to 4 years following onset of clinical symptoms of AD, showed that there is approximately 35% loss in synapse number in the AD cortex (Davies et al., 1987). Indeed, it was found that synapse loss correlated more with the observed cognitive deficits compared to plaque, NFT or neuronal loss (Terry et al., 1991). Expression levels of several pre- and post-synaptic markers including synaptophysin, SNAP25, PSD95 were also found to be reduced in AD brain. Furthermore, several *ex vivo* and *in vivo* electrophysiological studies revealed that both basal synaptic

transmission and LTP, implicated in strengthening of synapses, are hampered in the hippocampus in models of AD (Selkoe, 2002). Interestingly, Aβ has been directly shown to cause synaptic dysfunction in Aβ-producing transgenic mouse models of AD. However, it has been shown that oligomeric Aβ and not Aβ plaques per se are associated with a subset of synapses in the vicinity of plaques in AD patients. Furthermore, the levels of toxic oligomers are found to be enhanced in the patient's CSF compared to controls (Bilousova et al., 2016; Herskovits et al., 2013; Koffie et al., 2012). Moreover, oligomeric Aβ directly inhibits LTP but increases LTD in excitatory synapses, thus leading towards cognitive decline in AD (Wang et al., 2016b). However, there is huge controversy about the type and size of Aβ oligomers that propagates synaptic dysfunctions. Recently, Type 2 Aβ oligomers (detected by OC antibody) and not Type 1 (detected by A11 antibody) Aβ oligomers were shown to actually cause synaptotoxicity (Pickett et al., 2016). Moreover, the toxic Aβ oligomers causing synaptic deregulation can be either intraneuronal (Wirths et al., 2012) or extracellular (Takeda et al., 2013) in its origin. It is proposed that Aβ oligomers can bind to post-synaptic receptors and mediate their synaptotoxicity (Um et al., 2013). This is especially supported by the fact that the post-synaptic receptors lie close to the post-synaptic plasma membrane where APP cleavage occurs, giving rise to Aβ. Hence, this creates a clear case of proximity-based interaction between Aβ oligomers and specific receptors, including both ionotropic and metabotropic glutamate receptors, on post-synaptic surface, now acting as toxin receptorsshown in fig. 18 (Jarosz-Griffiths et al., 2016). Aβ binding leads to increased ubiquitination of AMPAR, following which they are degraded by the proteasomal degradation pathway leading to reduction in surface

AMPAR number, dendritic spine density and the strength of synapses (Rodrigues et al., 2016). Other receptors that can help mediate Aβ oligomer-induced synaptic toxicity includes specific NMDARs, mGluR5, EphrinA4, Sigma2/PGRMC1 and a-7 nicotinic receptor (Forner et al., 2017).

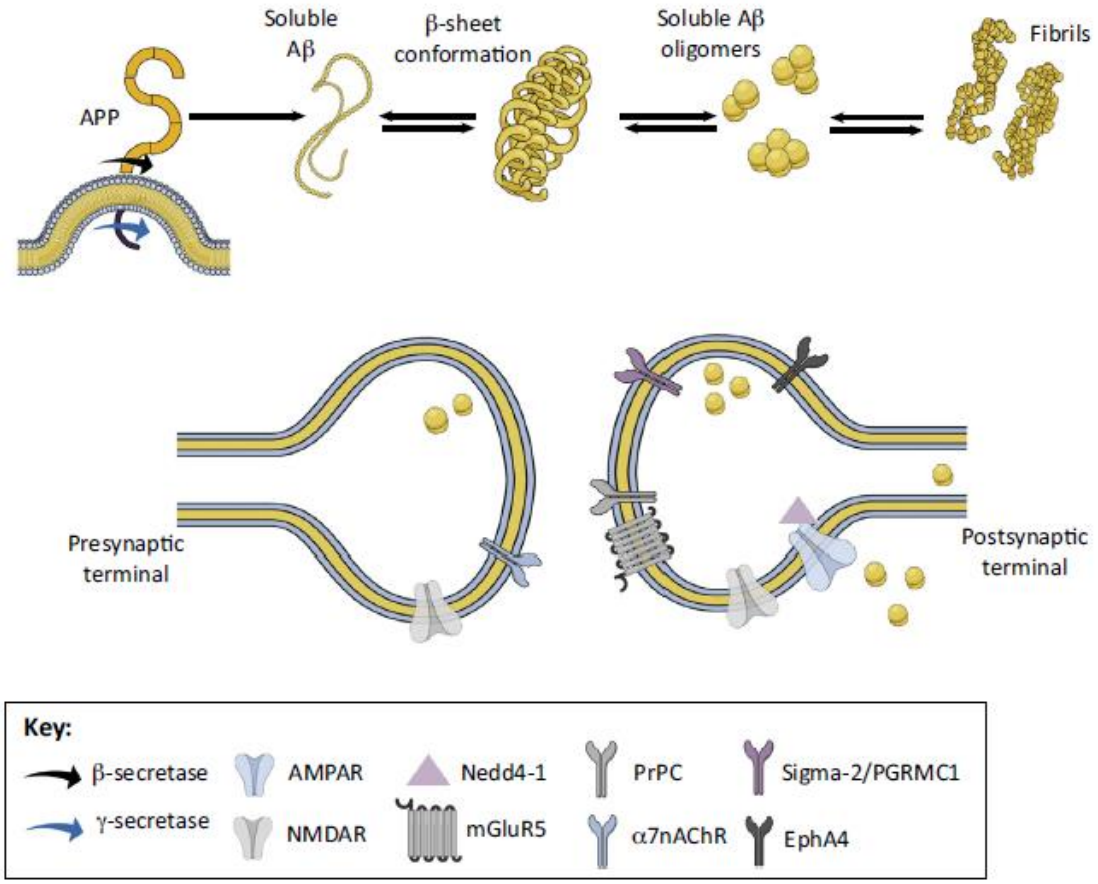

Fig.18: Aβ oligomer formation and synaptotoxicity induced by them: Aβ oligomers are formed due to the aggregation of β-sheets of $A\beta_{1-42}$ following amyloidogenic cleavage of APP. The oligomer thus formed reduces the number of AMPA receptors on the post-synaptic membrane and dampens the synaptic strength through binding with NMDAR. Additional synaptic receptors may play as Aβ receptors including mGluR5, α7nAChR, EphA4 and Sigma-2/PGRMC1 (Forner et al., 2017)

4.2. Role of tau - A growing body of literature suggests that tau plays a critical role in synaptic functioning and is detected in dendrites, pre-synaptic and post-synaptic compartments (reviewed in (Forner et al., 2017)). Tau can modulate the transfer of mitochondria to the pre-synaptic terminal and helps in efficient vesicle releases. Tau can be released into the extracellular space and can regulate synaptic signaling through specific receptors such as mAChRs. Tau acting as a scaffolding protein helps in the localization of glutamatergic receptors at the post-synaptic compartments of dendritic spines. Furthermore, the phosphorylating kinases of tau that is GSK3β and p38/MAPK are localized in the post-synaptic sites that are implicated in long-term synaptic plasticity regulation (Kimura et al., 2014; Regan et al., 2015). Such huge array of tau-regulated physiological synaptic processes may be damaged in AD (Pooler et al., 2014). In AD scenario, due to increased phosphorylation of tau, it loses its affinity for axonal microtubules and gets migrated to the somatodendritic compartments and into spines where it may disrupt normal synaptic functioning shown in fig. 19 (Izzo et al., 2014; Jadhav et al., 2015). Under physiological conditions, tau can further interact directly with a tyrosine kinase, Fyn, and helps in its localization to the post-synaptic membrane where it can modulate the functioning of PSD95/NMDAR complex (Mondragon-Rodriguez et al., 2012; Pooler et al., 2014). However, in AD, more dendritic tau means more scaffolding of Fyn and hence an excess of Fyn in the post-synaptic sites causing more NMDARs stabilization and consequently increased PSD95/NMDAR complex formation that can to lead to the excitotoxicity observed in AD (Usardi et al., 2011). Hence, it may be inferred that both oligomeric Aβ and hyperphosporylated tau cooperate to contribute to the synaptic dysfunctions observed in AD.

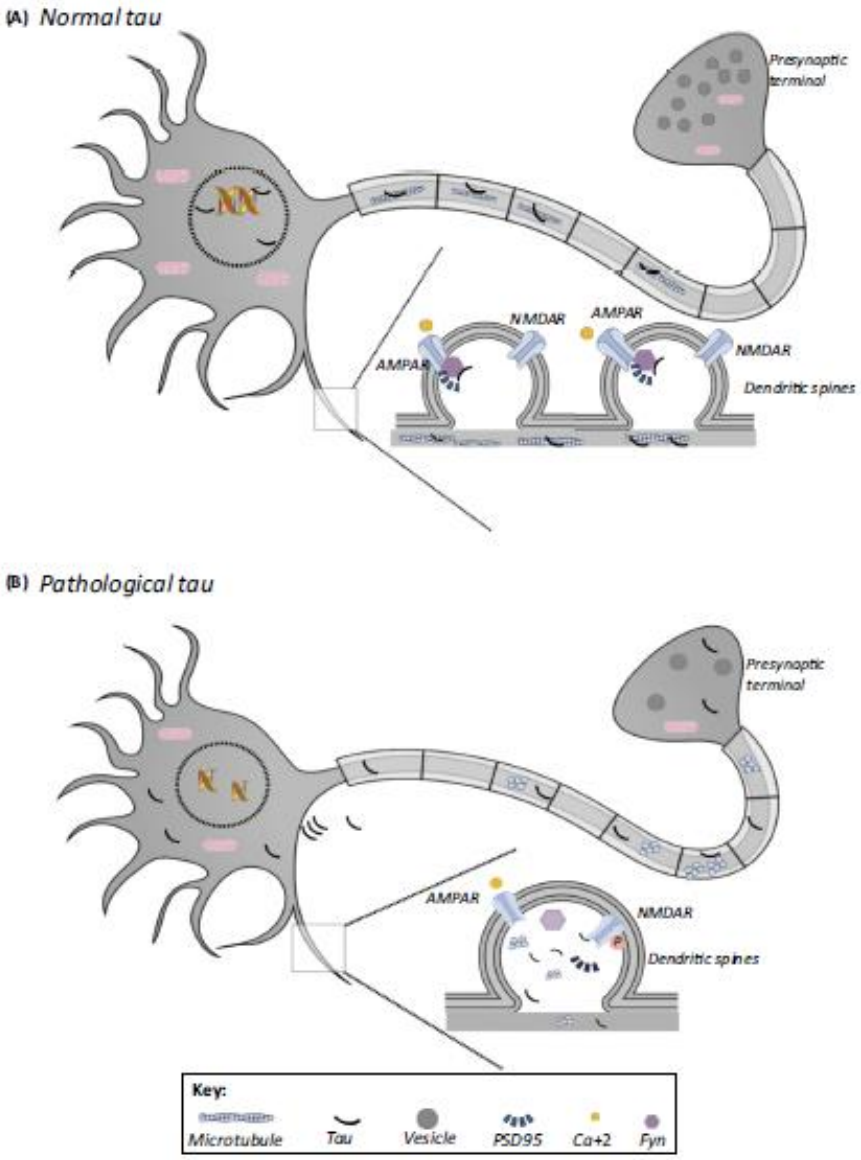

Fig.19: Role of tau in synaptic dysfunction in AD: (A) Under physiological conditions, tau is mainly localized in the axon (stabilizing microtubules) and also in the nucleus of the neuron (stabilizing DNA). It also directly interacts with a tyrosine kinase, Fyn that stabilizes the interaction between NMDAR and PSD95(Forner et al., 2017). Thus playing an active role in strengthening of synapses and hence spine number. (B) Under pathological scenario including AD, tau gets hyperphosphorylated and reduces its affinity for microtubules and migrates to the somatodendritic as well as the pre- and post-synaptic compartments. However, it is not longer detected in the nucleus while its enhanced presence in the post-synaptic compartment causes the increased interaction between Fyn and tau reducing Fyn's interaction with NMDAR, thus interfering with

PSD95/NMDAR stability. A reduction is synaptic strength and spine number is observed as a consequence.

5. Conclusion to the Review of Literature

I started the review of literature by refreshing the readers' memory about the origin of Alzheimer's disease and how Alois Alzheimer was able to predict the most important pathological hallmarks of the disease more than 110 years ago simply by silver staining. Next, I detailed an up-to-date literature about the symptoms and staging in AD with a special mention of the updated AT(N) classification by NIA-AA. Then, I mentioned the current prevalence and incidence of AD emphasizing that AD is still the 7th leading cause of death globally and shows a gender bias. After that, I discussed about the types of AD, the risk factors and the major pathological hallmarks of AD. Finally I ended the part 1 of the review on AD by elaborating on the current hypotheses in AD and the related hypothesis-based therapies in AD showing that clinical trials in AD have a very high percentage of failures. Section 2 was about Astrocytes and I discussed their role in details in AD especially since they become reactivated in AD scenario and display both neuroprotective and neurotoxic functions. Section 3 was concerned with cognitive dysfunctions in AD and I highlighted topics including the nature of memory loss in AD, the current animal models utilized in AD research and finally elucidated on the array of behavioral tests that are used for the assessment of cognitive functions in AD rodent models. In the final section, section 4, I discussed that AD is largely regarded as a disease of synaptic failure and presented evidences of Aβ and abnormal tau that are now known to regulate synaptic dysfunctions in AD. I have attempted to agglomerate all the relevant information from scientific literature that will help the reviewers to understand my

rationale behind initiating the subject of my thesis research work and the ensuing work itself.

AIMS & OBJECTIVES

AIMS & OBJECTIVES

Alzheimer's disease is the most prevalent neurodegenerative disorder creating havoc in the aging population worldwide. AD has created a huge economical and emotional burden on the society. Unfortunately, there is no cure to date except for few drugs that provide symptomatic relief. Although AD research has progressed in the biomarker front, consistent translational level failures in therapy are making the scientific world question the very basis of the disease. Hence, rigorous basic research in AD is imperative. AD is a multi-factorial disease and there are many hypotheses related to its generation. The most popular is the 'amyloid cascade hypothesis'. Nevertheless, recent view is that Aβ should not be seen as the sole factor for causing the disease. It is thought that the non-neuronal cells of the brain, especially astrocytes, may have a pivotal role in AD pathogenesis and is one of the first responders to Aβ insult. The complete understanding of astrocyte reactivity in AD and their role on neuronal health is still lacking.

Astrocytes in various neurodegenerative diseases were earlier considered to be playing a detrimental role. However, a wealth of literature now indicates that astrocytes may instead be the defensive sentinels in the brain against any pathological insult. Astrocytes undergo a phenomenon called astrocyte reactivity in several neurodegenerative diseases including in AD. We hypothesize that reactive astrocytes in the early phase of AD progression play a protective role but in the later phases of AD, reactive astrocytes turn detrimental towards neurons. Interestingly, during each of these stages reactive astrocytes communicate with the neurons and the other glial cells in the CNS via cytokines and

chemokines. The astrocyte 'reactive state' specific identity and functional role of these chemical mediators remain elusive in AD and is the main focus of this research.

PART I

AIM: To study the kinetics of astrocyte reactivity and to understand the role of a major secretory protein – tissue inhibitor of matrix metalloproteinase 1 (TIMP-1) on neurons against Aβ treatment.

Specifics objectives:

I. To decipher the kinetics of astrocyte reactivity in response to Aβ *in vitro*
II. To unravel the secretome profiles of Aβ responsive reactive astrocytes and their effects on neurons against Aβ toxicity
III. To identify the major astrocyte-secreted neuroprotective cytokine following Aβ treatment
IV. To investigate the neuroprotective efficacy of TIMP-1 on neurons *in vitro*
V. To identify the mechanism/s behind TIMP-1-mediated neuroprotection against Aβ

PART II

AIM: To investigate the role of TIMP-1 on Aβ plaque load, neuronal health and cognitive functions in animal models of Alzheimer's disease (AD).

Specifics objectives:

I. To establish an Aβ-induced AD model in rat to study the role of TIMP-1 *in vivo*

II. To study the effect of TIMP-1 on Aβ plaque load and apoptosis in Aβ-injected rat model of AD

III. To investigate the function of TIMP-1 injection on behavioral deficits in Aβ-injected rats

IV. To study the effect of TIMP-1 injection on Aβ plaque load and cell death pathways in an advanced transgenic model of AD – 5xFAD mouse

V. To elucidate the role of TIMP-1 on cognitive deficits in 5xFAD mice

PART III

AIM: To reveal the synaptic underpinnings of cognitive improvement rendered by TIMP-1.

Specifics objectives:

I. To delineate the changes in pre- and post-synaptic markers following TIMP-1 treatment in 5xFAD mice

II. To study the effect of TIMP-1 on spine morphology and spine density in 5xFAD mouse brain

III. To elucidate the electrophysiological changes underlying the synaptic plasticity alterations in TIMP-1 treated 5xFAD mice

IV. To investigate the molecular pathways involved in TIMP-1 mediated synaptic changes in 5xFAD mice

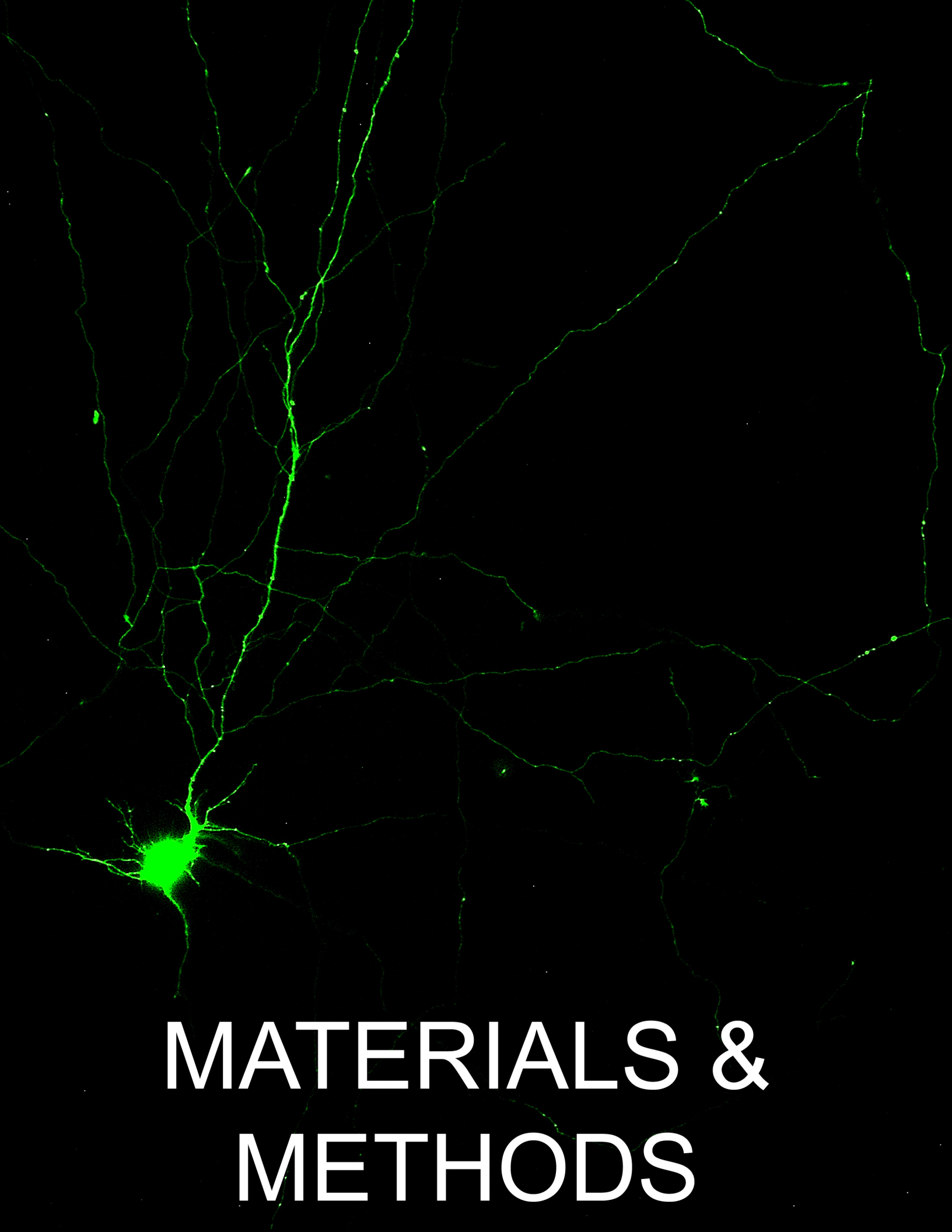

MATERIALS & METHODS

MATERIALS & METHODS

Materials:

Cell culture media DMEM, DMEM-F12, Neurobasal medium, B27 supplement, Fetal Bovine Serum, Horse Serum, Penstrep antibiotic, Lipofectamine 2000, Alexa Fluor and Sypro Ruby were purchased from Invitrogen. Insulin, progesterone, putrescine, selenium, Apo-transferrin, NGF, poly-D-lysine (PDL), DMSO, HFIP were purchased from Sigma. Primary culture instruments were from Paul's Instruments, India. Cell culture dishes, plates and flasks were purchased from BD Falcon, Corning and Nunc. Aβ (1–42) was purchased from American Peptide. ECL reagent and PVDF membrane were purchased from GE Healthcare and Takara. Trypsin and BSA was purchased from SRL. All other fine chemicals were locally obtained. List of antibodies used for this work and their sources has been given in Table 1.

Antibody	Species raised	Application	Source
GFAP	rabbit	ICC IHC	Abcam
s100β	rabbit	ICC	Abcam
Vimentin	rabbit	ICC	CST
Nestin	rabbit	ICC	Merck
Ki67	rabbit	ICC	Abcam
MAP2	rabbit	ICC	SCBT
phospho-Akt (Ser473)	rabbit	WB	CST
phospho-Akt	rabbit	WB	CST

(Thr308)			
Akt	rabbit	WB	CST
phospho-FOXO3a	rabbit	WB	CST
FOXO3a	rabbit	ICC WB	CST
BIM	rabbit	WB	Abcam
PUMA	rabbit	WB	Novus biologics
Bcl2	rabbit	WB	CST
Bcl-xl	rabbit	WB	CST
pH2Ax	rabbit	IHC WB	CST
Cleaved Caspase 3	rabbit	WB	CST
PARP	rabbit	WB	CST
phospho-mTOR	rabbit	WB	CST
mTOR	rabbit	WB	CST
ATG5	rabbit	WB	Novus biologics
p62	mouse	WB ICC IHC	Novus biologics
LC3B	rabbit	WB ICC IHC	CST
LAMP-1	rabbit	WB ICC IHC	Abcam
TIMP-1	mouse	WB	SCBT

		IHC	
TIMP-1	rabbit	ICC IHC	Merck
CD63	mouse	WB ICC	SCBT
IL-1β	rabbit	WB	SCBT
NFκβ	rabbit	WB	CST
CD11b	rabbit	IHC (DAB)	Abcam
COX-2	rabbit	IHC (DAB)	Abcam
Aβ	rabbit	IHC	Abcam
phospho-ULK1	rabbit	IHC	CST
PSD-95	rabbit	IHC WB	Merck
SNAP-25	mouse	IHC WB	SCBT
Synaptophysin1	mouse	WB	Synaptic systems
Homer1	mouse	WB	Synaptic systems
CAMKIIα	mouse	WB	SCBT
Actin	rabbit	WB	Sigma
GAPDH	rabbit	WB	CST
phospho-Cofilin	rabbit	WB	CST
Cofilin	rabbit	WB	CST
phospho-GSK3β (Ser9)	rabbit	WB	CST
GSK3β	rabbit	WB	CST
BDNF	rabbit	WB	SCBT

Table 1: List of antibodies. WB=western blot, ICC=immunocytochemistry, IHC=immunohistochemistry, CST=Cell Signaling Technology, SCBT=SantaCruz Biotechnology

Primary Cell Cultures:

Astrocyte primary culture: Primary astrocytes were cultured following protocol that has been described earlier (Saha et al., 2020b). In short, 0-1 day old Sprague Dawley (SD) rat pups were acquired from the animal facility, the brain was taken out and the meninges were separated out with care. Neo-cortex parts were dissected out and sectioned into very small pieces. Following this, the tissue pieces were trypsinized for 20 min at 37°C. The trypsinized tissues were triturated in DMEM (Gibco) + 10% fetal bovine serum (FBS) (Gibco) medium. Next, the tissue suspension was allowed to pass through nylon mesh to remove clumps. The single cell suspension was then centrifuged and the pellet was resuspended in fresh medium. The cells were finally counted and plated onto PDL (Sigma-Aldrich, St. Louis, MO, USA) coated plates. Astrocytes were maintained for 13-14 days *in vitro* (DIV) during which on every alterate day the spent medium was changed with fresh DMEM+10%FBS.

Primary Cortical Neuron Cultures: Primary cortical neuron culture was carried out according to the protocol elucidated earlier (Park et al., 1998; Troy et al., 2000). Briefly, the neocortex regions of E16-18 rat brain were dissected out and put into serum-free medium (DMEM/F12 [1:1]) added with 6 mg/ml D-glucose, 100 µg/ml transferrin, 25 µg/ml insulin, 20 nM progesterone, 60 µM putrescine, 30 nM selenium) and triturated into a single cell suspension. The cells were plated on PDL coated plates. The neurons were given treatment on 7DIV following plating with oligomeric beta-amyloid (Aβ 1-42).

Astrocyte-neuron coculture: The astrocyte-neuron coculture model was developed by transferring astrocyte conditioned medium (ACM) from the various treatment conditions to primary neuron culture (Nagai et al., 2007).

Preparation of oligomeric Aβ:

Lyophilized $A\beta_{1-42}$ peptide (American peptide, Sunnyvale, CA, USA) was dissolved in 100% 1,1,1,3,3,3 hexafluoro-2-propanol (HFIP) (sigma-aldrich) to 1 mM followed by centrifugation in a speed vac (Eppendorf, Hamburg, Germany). The peptide pellet was re-suspended in DMSO (Sigma-Aldrich) at 5 mM and sonicated in a 37ºC water bath for 10 min. Then, it was diluted in phosphate buffer saline [PBS: NaCl (137 mmole/L), KCL (2.7 mmole/L), Na_2HPO_4 (10 mmole/L), KH_2PO_4 (2 mmole/L), pH7.2] and SDS (0.2%) (Merck) to 400 µM and incubated for 6-18 h at 37ºC. Lastly, PBS was added to attain a concentration of 100 µM and re-incubated for 18-24 h at 37ºC. This preparation of Aβ was checked for oligomeric species by SDS-PAGE followed by Sypro Ruby protein gel staining.

Treatments on cells:

14 DIV astrocyte cultures were given treatment with 1.5 μM of Aβ for various time points as mentioned in the figures. For the neutralization experiment, neuron cultures were treated with TIMP-1 neutralizing antibody (Abdserotec) at 1 μg/ml concentration, in the presence or absence of Aβ, added to the ACM.

Cortical neurons were treated with 1.5 μM Aβ for 24 h, rat recombinant TIMP-1 protein (R&D system) at 100 ng/ml for 24 h, and with ACM transferred from different treatment conditions that have been mentioned in figures for 24 h and 48 h.

Transfection studies:

Plasmid Maxi kit (Qiagen, Waltham, MA, USA) was used to prepare the plasmid DNA constructs. For survival assay, primary cortical neurons were transfected with 0.5 μg of pSIREN-GFP empty scrambled construct in cortical medium using lipofectamine 2000 (Invitrogen) (Life technologies, Grand Island, NY, USA). Post 6 h of incubation at 37ºC in 5% CO_2, lipofectamine added medium was changed with fresh cortical medium. 48 h following transfection, neurons were given treatment with Aβ and ACM from the various treatment conditions. GFP-expressing viable neurons were imaged at 0 h, 24 h and 48 h under fluorescent microscope and representative images are given in figures.

Primary neurons were introduced with siCD63 (Thermo scientific) or scrambled siRNA (negative control) on Day-4 following plating according to the manufacturer's protocol at 100 pmole/well (50 nM) of a 6-well tissue culture plate with the help of Lipofectamin 2000. Successful knockdown was verified after 72h of incubation by western blot with CD63 antibody. On Day-7 following plating, the cells were treated according to experimental paradigm.

Survival assay: Survival assay of neurons was carried out using a protocol called nuclei buffer couning method as elaborated earlier (Rukenstein et al., 1991; Sanphui et al., 2013; Troy et al., 2002). Lysis of the cells was performed in a detergent containing buffer that dissolves plasma membrane but not the nuclear membrane. The intact nuclei were then counted in a haemocytometer.

Immunocytochemistry:

Immunocytochemistry was carried out as per the protocol mentioned earlier (Biswas et al., 2005; Biswas et al., 2007). In brief, cells (astrocytes or neurons) cultured on glass cover slips were fixed in 4% paraformaldehyde (Sigma) in PBS for 15 min at room temperature (RT). 3% goat serum in 0.3% Triton X-100 in PBS was used to block the cells for 1-2 h. Cells were incubated with primary antibody and incubated overnight at 4˚C. Next, cells were given three washes and then incubated with secondary antibody Alexa fluor 546/488 for 1-2 h at RT. Nuclei were stained with Hoechst 33342 at a concentration of 1 μg/ml in PBS for 30 min at RT. Pictures were otained with the help of LeicaCTR4000 fluorescence microscope or Leica Sp8 STED microscope at different magnifications as mentioned in individual cases. In case of colocalization studies, Pearson's correlation coefficient was calculated from images taken at 60x magnification using Leica Sp8 software. The corrected total cell fluorescence (CTCF) was calculated by using integrated density of staining, area of the cell, and the background fluorescence of different experimental conditions. CTCF=Integrated density – (area of selected cell x mean fluorescence of background readings).

Preparation of cell or tissue lysate:

Post treatment, cells were given PBS washes, collected through scraping in PBS and then pelleted by centrifugation at 800 g at 4ºC for 5 min. In case of tissues, following microdissection of the required region of the rat or mouse brain, the tissue was immediately collected in RIPA buffer. Alternatively in case of culture, cells were lysed by RIPA buffer (Sigma) along with phosphastase inhibitor (Roche) and protease inhibitor mix (Takara). Each tube contents were sonicated by 2-3 pulses on ice to breakdown

genetic material and incubated for 30 min on ice with intermittent vortexing. The lysed cells/tissue was then mixed with 5x sample buffer so that the final contents are in 1x sample buffer concentration. The protein concentration was checked by Lowry method.

Western blotting:

Proteins (50-60 μg) from each of the treated conditions were run in SDS-PAGE. Next, protein gels were transferred to PVDF membranes (GE Healthcare). After blocking with 5% bovine serum albumin (BSA, Merck) for 1 h at RT, the membranes were incubated with primary antibodies overnight at 4ºC. Membranes were given three washes with TBST [1.5 M NaCl, 1 M Tris (pH7.5), 0.1% Tween20] after which blots were given incubation with HRP-tagged secondary antibody for 1-2 h at RT. Protein bands were detected on ChemiDoc MP imaging system (BIO-RAD) using ECL reagents (Takara) following three washes with TBST. Band intensities were analyzed by NIH ImageJ software.

ELISA:

This assay utilizes the quantitative sandwich enzyme immunoassay method. A monoclonal antibody specific for rat TIMP-1 was pre-coated onto a microplate obtained from the manufacturer. Standard, control and samples were added to the wells. Any rat-origin TIMP-1 present in the samples gets bound to the immobilized antibody. Following washes to remove unbound proteins, an enzyme-linked polyclonal antibody specific for rat TIMP-1 was pipetted into the wells. Next, further washes were given to remove any excess antibody-enzyme reagent and the substrate solution was added. A blue product

present at the end of the enzymatic reaction turns yellow when the stop solution was added. The intensity of the color measured, is proportional to the level of rat TIMP-1 present in the sample added in the first step.

Cytokine array:

The cytokine composition of the secretomes from astrocytes with or without Aβ treatment was investigated by Proteome profiler rat cytokine array kit (R&D system). ACM from untreated and Aβ-treated astrocytes were collected and then conjugation with biotinylated antibodies was carried out. Next, this cocktail was incubated with cytokine array membranes (embedded with 29 cytokines antibodies) for 16-18 h at 4°C. Next, membranes were given washes and streptavidin-HRP conjugates were added. Chemiluminescence was checked in UVP bioimager.

Animal housing and care:

Adult SD rats with weights in the range of 280-320 g or 6-month-old male 5xFAD mice were housed three in each cage at 24 ± 2 °C, with 12 to 12 h light-dark cycle, optimum humidity (60 ± 5 %) and access to food and water *ad libitum* in the animal house of CSIR-Indian Institute of Chemical Biology, Kolkata. All the studies were conducted following the Institutional Animal Ethics Committee (IAEC) and according to the National Guidelines (CPCSEA) on the essential care and usage of animals in laboratory research (Indian National Science academy, INSA, New Delhi, 2000).

Sterotaxic procedures:

The experimental rats were divided into 5 groups, namely, Control, only TIMP1 (5 ng), only Aβ and Aβ + TIMP1 (2.5 ng and 5 ng). The control group received icv injection of 10 *µ*l of Phosphate buffer saline whereas the Aβ group received oligomeric Aβ at 2.25 *µg*/side of the brain (bilateral injection). In case of mice, the groups were WT (C57/BL6), 5xFAD, 5xFAD+aCSF, TIMP-1 (5 ng) and 5xFAD+TIMP-1 (5 ng). WT mice were alternatively injected with aCSF (icv) but WT+aCSF group was eventually excluded in the further experiments since no difference was observed in the initial behavioral tests.

Rats were anesthetized with Sodium thiopentone (50 mg/kg. i.p.) in 0.9% normal saline following the protocol mentioned earlier (Paidi et al., 2015). The rodents were placed in a stereotactic frame (Stoelting, MO, USA) with the incision bar positioned at the Bregma point at the beginning of the experiment. The body temperature of the rodents was kept at 37°C with the help of a homeothermic blanket (Harvard apparatus, U.K.). Oligomeric Aβ was infused bilaterally into the hippocampus (lateral, ±0.21 cm from the bregma; anteroposterior, -0.36 cm; dorsoventral, -0.28 cm, according to the atlas of Paxinos and Watson) at 4.5 µg, in a final volume of 10 µl (5 µl per side). The flow rate was maintained at 0.5 µl/min with the help of a worker-bee syringe pump (BAS, West Lafayette, USA). Aβ was allowed to diffuse for an extra 5 min after delivery. Exact volume of PBS was bilaterally injected in each control rat.

Six days post Aβ or PBS infusion, rat recombinant TIMP1 (rrTIMP1) was injected at a dose of 2.5 ng or 5 ng per animal (dissolved in aCSF) in a total volume of 5 µl into the ventricle (lateral, 0 cm from the bregma; anteroposterior, -0.36 cm; dorsoventral, -0.38

cm) and allowed to diffuse for an extra 5 min. The experimental schedule for rats is shown in Fig. 1.

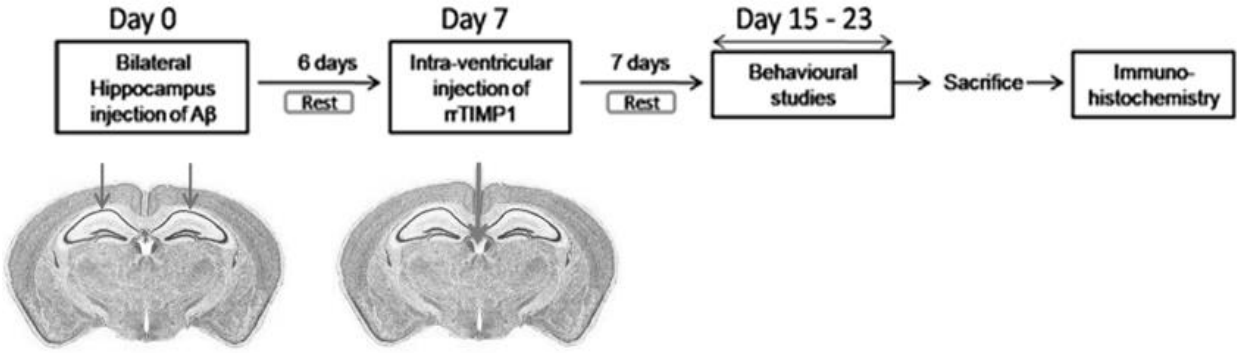

Fig.1: Experimental schedule in rats.

For mice, a combination of ketamine (100 mg/kg IP) and xylazine (10 mg/kg IP) in 0.9% normal saline was used for anesthetization for a short duration for the stereotaxic surgery. Mice were placed in a suitable stereotaxic frame and TIMP-1 (5 ng) in a total volume of 5 μl was injected icv into the ventricle (lateral, 0 cm from the bregma; anteroposterior, -0.16 cm from bregma; dorsoventral, -0.22 cm from bregma) and allowed to diffuse for an additional 5 min. The experimental schedule for mice is shown in Fig. 2.

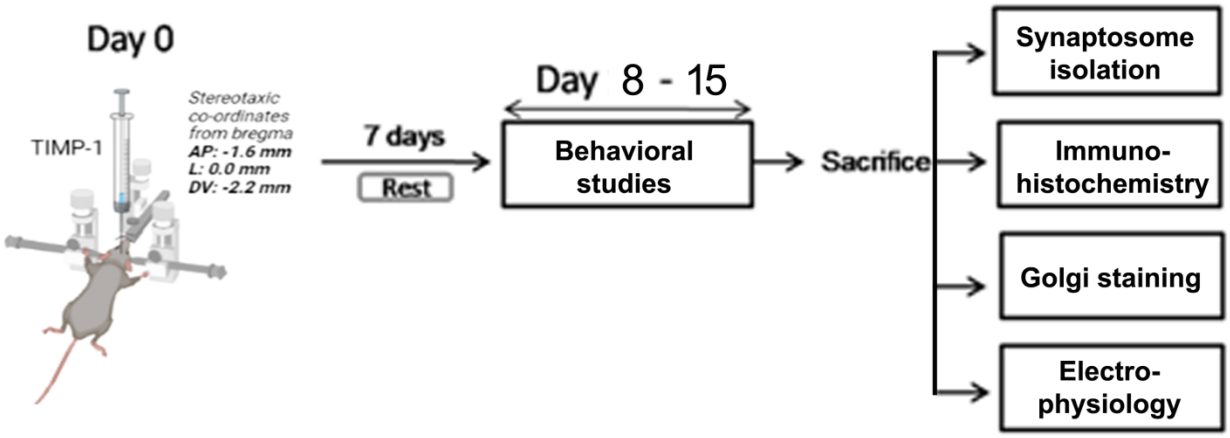

Fig.2: Experimental schedule in mice.

Behavioral assessments:

To investigate Aβ-induced memory loss and their restoration with TIMP1, rats from each of the experimental groups were tested successively by open-field test, novel object recognition test, passive avoidance test, contextual fear conditioning test, cue-dependent fear conditioning test and elevated plus maze test (cognition and anxiety) beginning on the Day-15 following Aβ or PBS infusion. Similarly for mice, both WT and 5xFAD transgenic mice were treated with TIMP-1 and similar format (except for mice-based alterations) of behavioral protocols were followed starting on Day-8 following TIMP-1 infusion. Passive avoidance test was not performed in mice due to restriction in apparatus adjustment in accordance to mice. Total number of rats in each group is shown in Table 1 and the number of mice in each experimental group in Table 2.

	Experimental Animal Groups				
Cognitive tests	CON	TIMP-1	Aβ	Aβ+TIMP-1 (2.5 ng)	Aβ+TIMP-1 (5 ng)
Locomotion	9	4	5	3	4
Novel-object recognition	6	6	8	3	6
Elevated-plus maze	11	7	9	3	7
Passive avoidance	12	10	6	3	7
Contextual fear conditioning	6	4	7	3	6
Cue-dependent fear conditioning	10	6	7	3	7

Table 2: Number of rats involved in behavioral experiments.

	Experimental Animal Groups			
Cognitive tests	WT	5xFAD	5xFAD+ aCSF	5xFAD+ TIMP-1
Locomotion	9	9	5	5
Novel-object recognition	11	10	8	8
Elevated-plus maze	12	12	8	10
Contextual fear conditioning	9	6	4	9
Cue-dependent fear conditioning	8	4	4	7

Table 3: Number of mice involved in behavioral experiments.

Locomotion

Locomotor activities in rodents can be estimated by the open field test (Crusio, 2001). The open field test (locomotion) apparatus (IR Actimeter, Panlab) consists of a open field plexiglas area with photocell emitters and recorders placed across the perimeter of the area (278×236×300 mm), shown in fig. 3. These emitters and recorders construct an x-y grid of invisible infrared rays. Rodents, put inside this area, cause beam breaks during movement and the data is recorded and analyzed by the analyzer. The rodents were placed in the area for a 10 min period and the distance traversed by individual animal was evaluated.

Fig.3: The open field test (locomotion) apparatus (Panlab, Harvard apparatus)

Novel Object Recognition (NOR)

Rats and mice display an inherent tendency to explore a new object over a familiar object (Ennaceur, 2010). This tendency to investigate the novel object indicates the

involvement of recognition memory dependent on hippocampus especially because the time interval between training and test is kept at 24h. Thus, in this test a rodent is placed in a rectangular box (50 cm x 30 cm) with two identical (same diameter, same color, and same length) objects fixed at parallel corners and the animal is allowed to explore them for 5 min on Day-1 of the test. On Day-2, one of the identical objects was replaced with a differently colored and shaped object and the animal was given 5 min to explore the objects in the NOR box to evaluate novel object recognition. A schematic representation of the two day NOR protocol is shown in fig.4. The length of time spent in exploring each of the objects on both the days was calculated and discrimination and preference index derived from Day-2 data. The length of time spent in exploring novel object was termed as TN and time spent at familiar object termed as TF values. Discrimination index (DI) and preference index (PI) were derived according to the formulas – DI = (TN-TF)/(TN+TF), PI = TN/ (TN+TF)*100(Antunes and Biala, 2012).

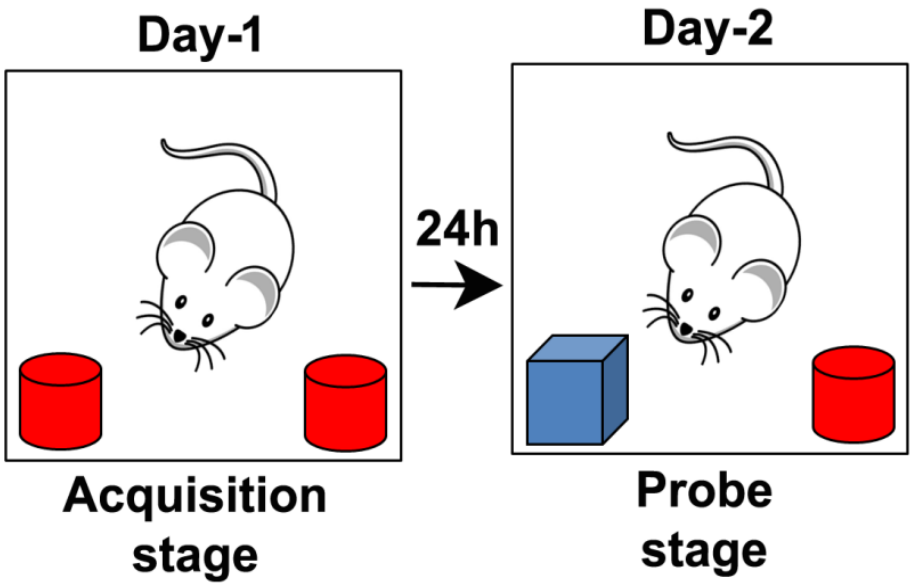

Fig.4: Schema showing the novel object recognition (NOR) test protocol.

Passive Avoidance test

The instrument comprises of two chambers with same dimensions however, one is a white-colored (well-lit) chamber and the other is a dark-colored chamber separated by a software-controlled guillotine door (Panlab), shown in fig.5. Initially, the animals were allowed to habituate for 5 min in the compartments. In the acquisition stage (Day-1), the animal was kept in the white compartment with door-open condition. It is the inherent tendency of rodents to move towards a darker area but as soon as it travelled to the darker chamber it received a mild foot-shock (0.7 mA for 2 sec). On Day-2 (Probe stage), same test was performed to evaluate its memory and learning, by assessing retention time in white chamber or latency to the dark chamber. Animals that remembered the shock from Day-1 will associate the dark chamber with the negative stimulus and avoid it while animals with memory loss will cross over to the dark chamber. The latency (sec) in crossing through the gate between the chambers was measured (Senechal et al., 2008).

Fig.5: Passive avoidance test apparatus (Panlab, Harvard Apparatus)

Fear Conditioning Test

These tests are utilized to study changes in hippocampus-dependent associative (implicit) memory. It is also helpful to evaluate amygdala-hippocampus communication. Here, each rodent is put in a sound-proof box with a stainless-steel grid floor which can supply the shock stimulus and is fitted with a recorder for recording the freezing behavior. Freezing behavior is defined as the complete loss of movement in the animal except for breathing. The fear conditioning box is shown in fig. 6. Diluted vanilla essence was added in this box as an odour cue. Animals were handled once per day for three days and habituated inside the experimentation room before the start of the actual behavioral tests. Only one animal was allowed in the experimentation room at a time (Hamann et al., 2002).

Fig.6: Apparatus for fear conditioning tests (Panlab, Harvard Apparatus)

Contextual fear conditioning test

On Day-1 (acquisition), the animal was put in the conditioning box and given a 2 min habituation period. Following habituation, the animal was given four sessions of an unconditional stimulus (each session- 89 sec pre-shock interval; 0.7 mA for rat/0.4 mA for mouse, 1s footshock) terminating in a 2 min resting period (10 min total). On Day-2 (Probe day), the animal was returned to the same box under the same context for an 8 min period but without any shock (Fig. 7). Freezing behavior was assessed by PACKWIN 2.0 software (Panlab). A normal animal behavior on Day-1 is response to the unconditional stimuli and its freezing behavior on Day-2 in apprehension of the shock is showed in fig.8 as recorded by the PACKWIN software (Bubser et al., 2014).

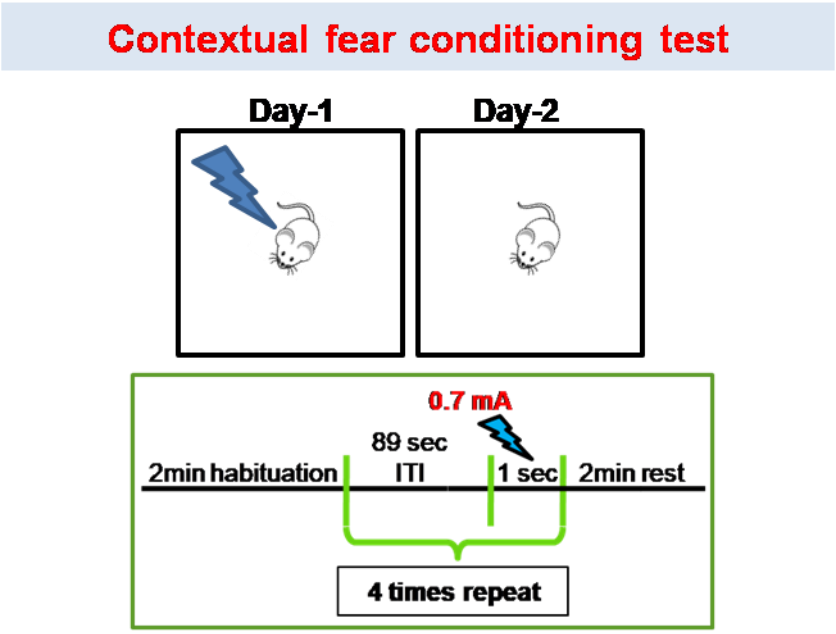

Fig.7: Schema shows the experimental protocol for contextual fear conditioning test

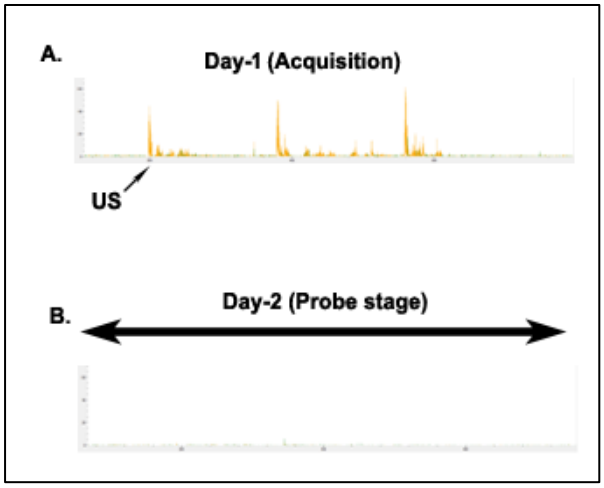

Fig.8: Freezing signals recorded in fear conditioning test: (A) Shows the movements of the animal on Day-1 of fear conditioning test in response to the unconditioned stimuli (US, footschock). (B) No movement (freezing response) on Day-2 of the test

Cue-dependent fear conditioning test

On the Day-1 (acquisition), the animals were put in the vanilla extract scented conditioning box initially for a 2 min period. After the habituation, four 29-sec sessions of light and sound (90 dB, 4000 Hz for rats; 80 dB, 2500 Hz for mice) co-terminating with a foot shock (0.6 mA, 1 sec for rat; 0.4 mA, 1 sec for mouse) were supplied with an inter-trial interval of 1 min, following this a 2-min rest period was given before the rodent was taken out of the box (10 min in total). On Day-2 (probe), the context of the box was altered from that of Day-1. Rodents were given same sessions of light and sound as on Day-1 but without the shocks (Fig. 9). Freezing behavior was recorded in the 8 min duration of the probing experiment by PACKWIN 2.0 software (Panlab) (Bubser et al., 2014).

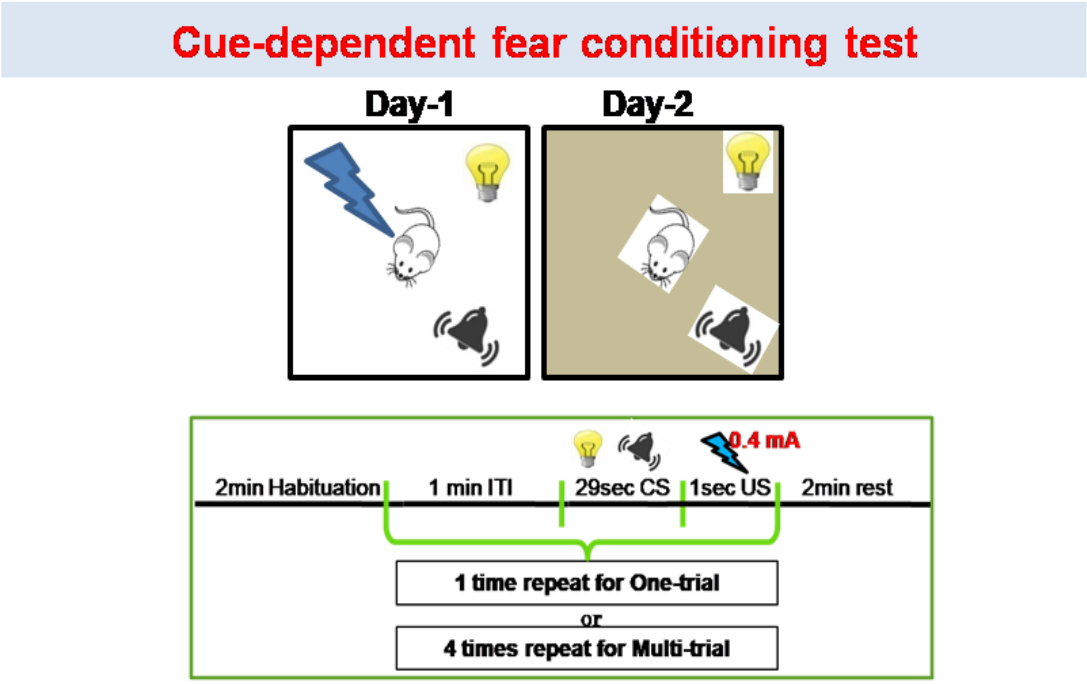

Fig.9: Schema shows the experimental protocol for cue-dependent fear conditioning test. Only the multi-trial cue-dependent experiment was performed.

Elevated plus maze (EPM) test

EPM test is used to study anxious behavior and cognitive abilities in rodents (Belzung and Griebel, 2001). The apparatus consists of a plus-shaped wooden platform elevated at a height of 60 cm from the ground comprising of two open arms (50 cm x 10 cm, with a very small, 1 cm, wall) opposite to one another and at right angles to the two closed arms of same dimensions fitted with high walls (50 cm) as shown in fig. 10. On Day-1, the animal was placed at the extreme end of an open arm facing outwards and allowed to investigate the plus maze without any intervention. The time elapsed before the rodent first entered the closed arm was recorded as the initial transfer latency (ITL) and the test was stopped at that point. On Day-2, the animal was returned to the plus maze

in a similar manner and the transfer latency to the closed arm was recorded as retention transfer latency (RTL). The maximum time given per animal was 5 min.

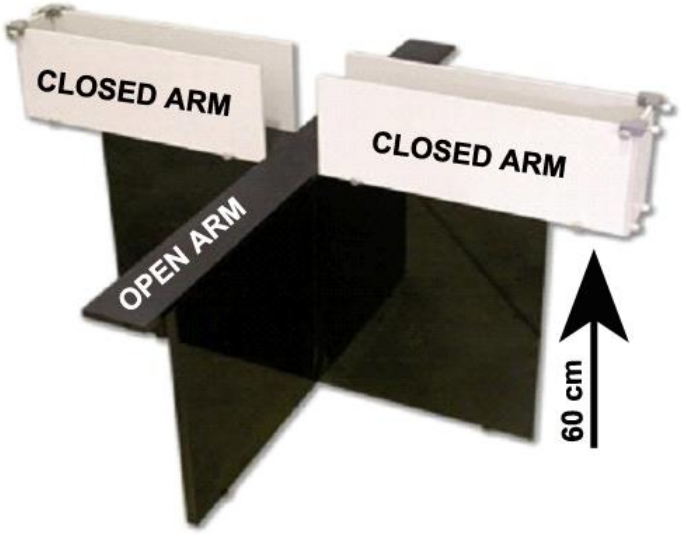

Fig.10: The elevated plus maze (EPM) test apparatus

Immunohistochemistry

Animal was perfused transcardially under anaesthesia of 1g/kg of urethane in 0.9% NaCl solution (i.p.) with cold 100 mM PBS (pH 7.4) following which it was allowed to get fixed with 4% (w/v) PFA. Immediately after, the animal was sacrificed and the brain was taken out. The intact brain was put in 4% PFA and kept at 4°C for 24-48 h. Next, following fixation, the PFA was changed with 30% (w/v) sucrose solution in PBS for cryopreservation at 4°C. Coronal sections (20 μm thick) were obtained, such that the hippocampal and the cortical regions remained intact, with the help of a cryotome (Thermo Shandon, Pittsburg, PA, USA) and then transferred onto gelatin-coated slides. The cryosectioning steps are shown in fig.11. The cryosections were then washed with

PBS before permeabilization with PBS + 0.4% Triton-X for 40 min. Next, sections were rinsed with PBS + 0.1% Triton-X (PBST) thrice carefully. Then, the sections were blocked with 4% BSA in 0.1% PBST for 1-2 h at RT. Primary antibodies prepared in blocking solution were added to the slices and incubated for 48 h at 4°C. Following multiple PBST washes, the sections were incubated with Alexa fluor-tagged secondary antibodies in blocking solution and kept for 2 h at RT. Next, Hoechst solution was added to the sections for nuclei staining and incubated for 30 min at RT. Further washes were given to remove excess stain and then the sections were mounted with Prolong Gold Antifade with DAPI (Invitrogen) on coverslips for microscopic study.

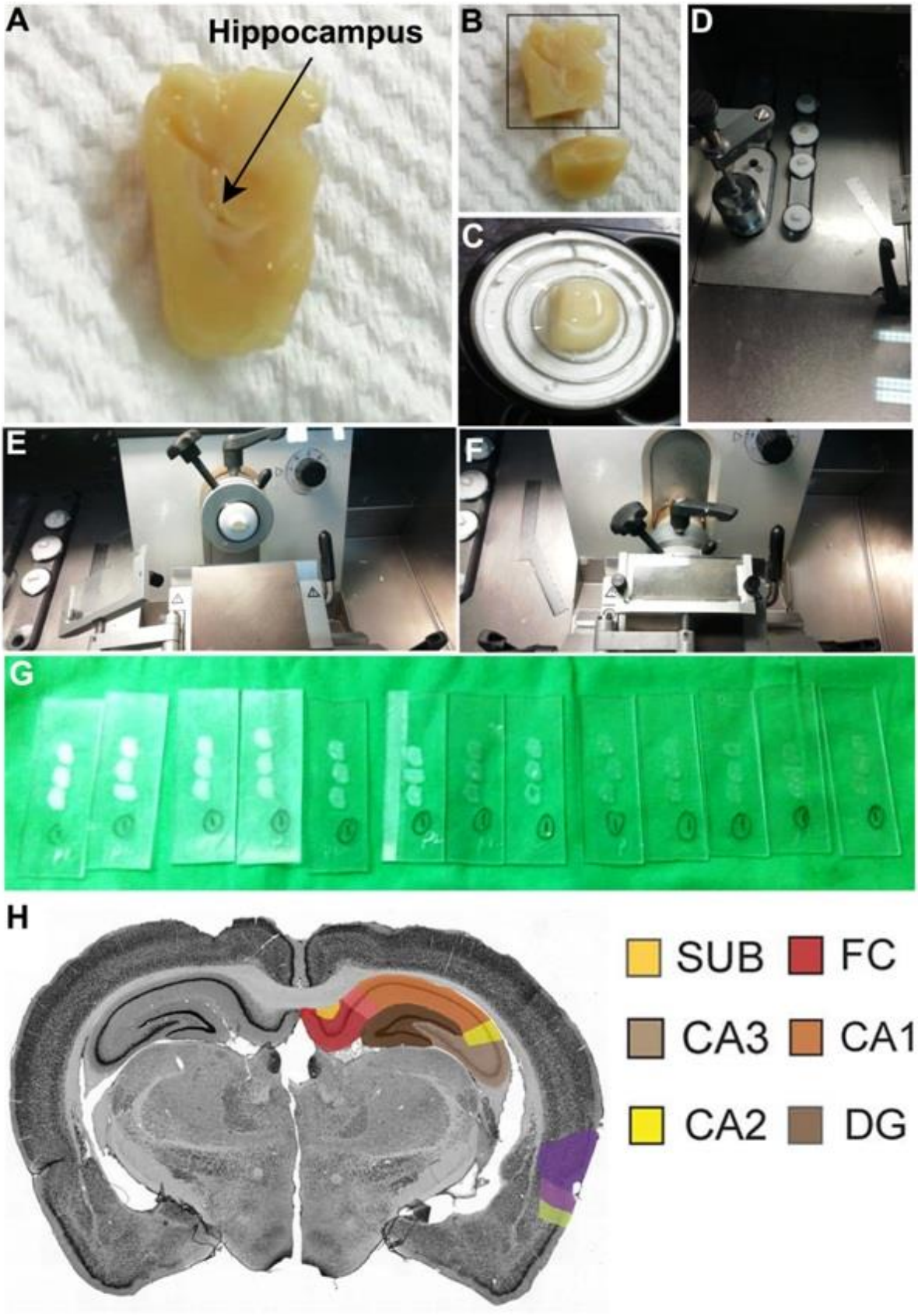
A
Hippocampus
B
C
D
E
F
G
H
SUB
FC
CA3
CA1
CA2
DG

Fig.11: Steps of cryosectioning for coronal sections of the mouse brain comprising of the hippocampus. (A) Fixed mouse brain cut in half (one of the hemispheres shown), (B) Frontal lobe is cut away, only the lower portion is used for cryosectioning, (C) Brain part fixed on the brain holder with cryogel, (D) Brains allowed to freeze inside the cryotome (E-F). The process of cryosectioning (G), Coronal sections on gelatin-coated slides (H), Coronal section of the brain showing the various parts of the hippocampus (Kjonigsen et al., 2011). SUB=Subiculum, FC=Fasciolarum Cinereum; CA= Cornu Ammonis.

TUNEL assay

TUNEL assay was performed using Clonetech ApoAlert DNA Fragmentation kit (Takara) according to the manufacturer's protocol. Following rehydration and fixation, the tissues were digested in Proteinase K solution (20 μg/ml, diluted from the main stock provided in the kit) for 20 min. PBS washes were given to terminate the reaction and then 4% PFA in PBS was added to the slices for further fixation. Following few more washes with PBS, Equilibriation buffer was added to the tissue slices and incubated for 10 min at RT. Next, a solution containing the nucleotide mix and Tdt enzyme was added to the sections and kept for 1 h in dark at 37°C. The tailing reaction was stopped by the addition of 2XSSC buffer (provided in the kit) for 15 min at RT. Next, PBS washes were given followed by addition of Hoechst for 30 min at 37°C. The sections were then mounted onto coverslips with Prolong Gold Antifade with DAPI for microscopic analysis. Percent apoptotic cells were deduced by dividing the number of TUNEL-positive cells with the total number of cells (Hoechst stained nuclei) multiplied by 100.

Isolation of synaptosomes

Synaptosomes were isolated from adult mouse brain by the method described earlier (Gharami and Biswas, 2020). Briefly, the freshly dissected mouse brain tissue (hippocampus or cortex) was homogenized in an isotonic sucrose gradient buffer (diluted

to 1X from a stock of 4X Gradient buffer - 1.28 M sucrose, 4 mM EDTA, 20 mM Tris, pH 7.4). The homogenized suspension was then centrifuged at 1000g for 10 min at 4°C to separate supernatant and debris. The supernatant was then loaded onto a discontinuous Percoll gradient composed of three layers – 3% (vol/vol), 10% (vol/vol) and 23% (vol/vol) percoll. The gradient was then centrifuged at 31,000 g for 5 min at 4°C (excluding acceleration and decceleration time). The synaptosomes separate as a layer between 10% and 23% percoll layers. The synaptosome layer was collected, diluted in artificial cerebro-spinal fluid (aCSF) and centrifuged to remove percoll contamination. The final synaptosomal pellets were re-suspended in 1x sample buffer before protein estimation for SDS-PAGE run. Alternatively, for determination of Filamentous/Globular (F/G) actin content ratio, the synaptosomal pellet was further fractionated into the cytoskeleton and cytoplasmic fractions. Accordingly, the synaptosomal pellet was resuspended in a Mg^{2+}-containing buffer (50 mM Tris, 2 mM $MgCl_2$, pH 7.4) and vortexed while maintaining the suspension on ice. Next, TritonX-100 was added to the suspension at a final concentration of 0.5% and kept on ice for 20-30 min. Then, it was allowed to centrifuge at 12,000 g for 10 min at 4°C. The pellet thus obtained is the cytoskeleton or PSD fraction containing F actin while the supernatant contains all the cytosolic proteins including G actin. Each of the fractions was resuspended in 1x sample buffer for western blot analysis. A schema for the protocol is shown in fig. 12.

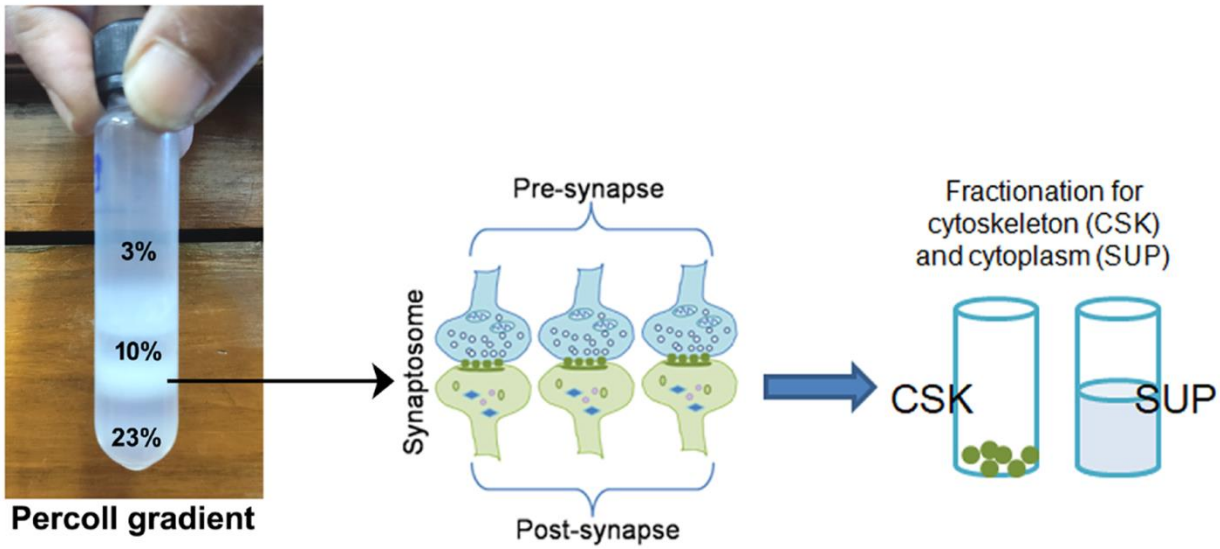

Fig.12: Steps for synaptosome isolation and sub-fractionation into cytoskeleton (CSK) and cytoplasmic (supernatant, SUP) fractions

Golgi-cox impregnation and staining procedure

Golgi-cox staining was performed according to the protocol described previously (Zhong et al., 2019). Briefly, the brain of the mouse was taken out and immediately submerged in the impregnation solution - a mixture of 5 parts by volume of Solution A (5% potassium dichromate in DW), 5 parts by volume of Solution B (5% mercuric chloride in DW), 4 parts by volume of Solution C (5% potassium chromate in DW) and 10 parts by volume of distilled water (DW), and kept in dark at RT. The solution was changed after 24 h, following which the brain was kept in the solution for 2 weeks. Next, the brain was transferred to Solution D, a cryoprotectant solution prepared by mixing 20 g of sucrose and 15 ml glycerol in 100 ml of DW and kept at 4°C in dark for 24 h following which fresh cryoprotectant solution was added. A period of 2-3 days was given for the brain to sink to the bottom. Sectioning was done at -25°C in a cryotome and 100-200

μm thick slices were collected on gelatine-coated glass slides. The sections were allowed to dry for some time, then, washed twice with DW and stained with 20% ammonium solution for 10 min in dark. Following two more washes with DW, sections were dehydrated through 50%, 70%, 95% and 100% (twice) ethanol for 5 min in each. The sections were removed off fat by xyline wash twice for 5 min each. The sections were mounted in DPX reagent, covered with a coverslip and allowed to dry at RT for 3-4 days in dark before bright-field microscopic analysis.

Electrophysiology

14 days following TIMP-1 injection, mice were anesthetized in a 5% gaseous isoflurane chamber (Aerrane, Baxter Healthcare Corporation; Fluovac, Harvard Apparatus, USA) and perfused transcardially at a speed of 45 ml/min using a peristaltic pump (Cole Palmer, USA) with cold (7-8°C) aCSF, which was continuously bubbled with carbogen (5% CO2 and 95% O2, Chemix Special Gases and Equipments, India). The composition of aCSF is given below (Table 4):

Sl. No.	Chemical*	Concentration (in mM)
1	NaCl	118
2	KCl	2.5
3	NaH_2PO_4	1.5
4	$NaHCO_3$	25
5	$C_6H_{12}O_6$	25
6	$MgCl_2$	1.3
7	$CaCl_2$	2.2

Table 4: The chemical composition of artificial cerebro-spinal fluid

*Sigma Aldrich (St. Louis, MO, USA)

The pH of aCSF was adjusted to 7.4 with an osmolarity of 310-320 mOsm/L

The set-up for performing perfusion before slicing is shown in Fig. 13

Fig.13: Set-up for perfusion of mice for *ex vivo* slice electrophysiology

The brain was immediately shelled out of the skull and submerged in ice-cold carbogenated aCSF. The hemispheres were separated and positioned on the tissue holder with a cyanoacrylate adhesive. The tissue holder was then fitted to the tray and 400µm thick viable para-sagittal slices were taken from each mouse by a vibratome (Leica VT, 1200S, Leica Biosystems, Germany) with a blade speed of 0.14 mm/s and amplitude 1.20 mm. A representative mouse brain has been shown and the parasagittal plane has been marked (Fig. 14). The slices were then kept in a brain slice keeper (BSK4-Quad, Automate

Scientific Inc CA, USA) in carbogenated aCSF at RT. The detailed set-up is shown in fig. 15.

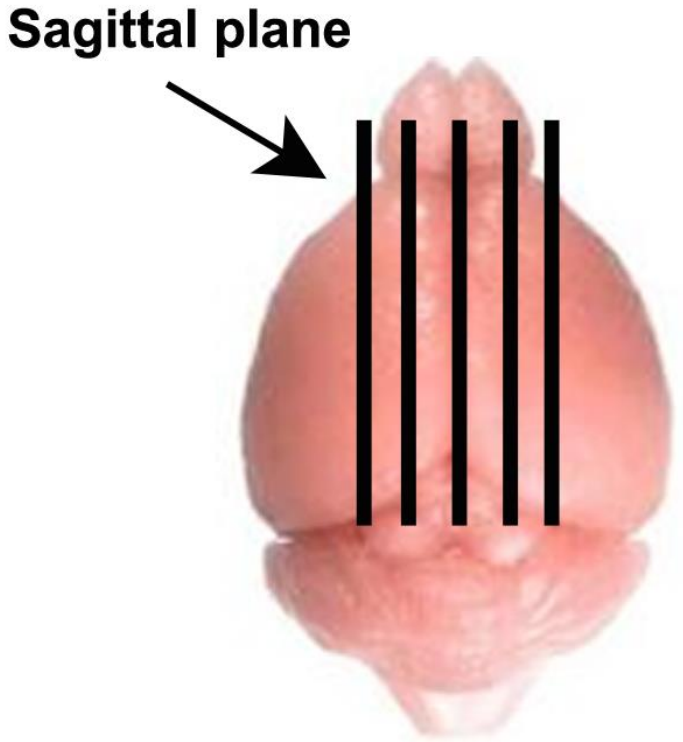

Fig.14: Mouse brain showing the para-sagittal plane

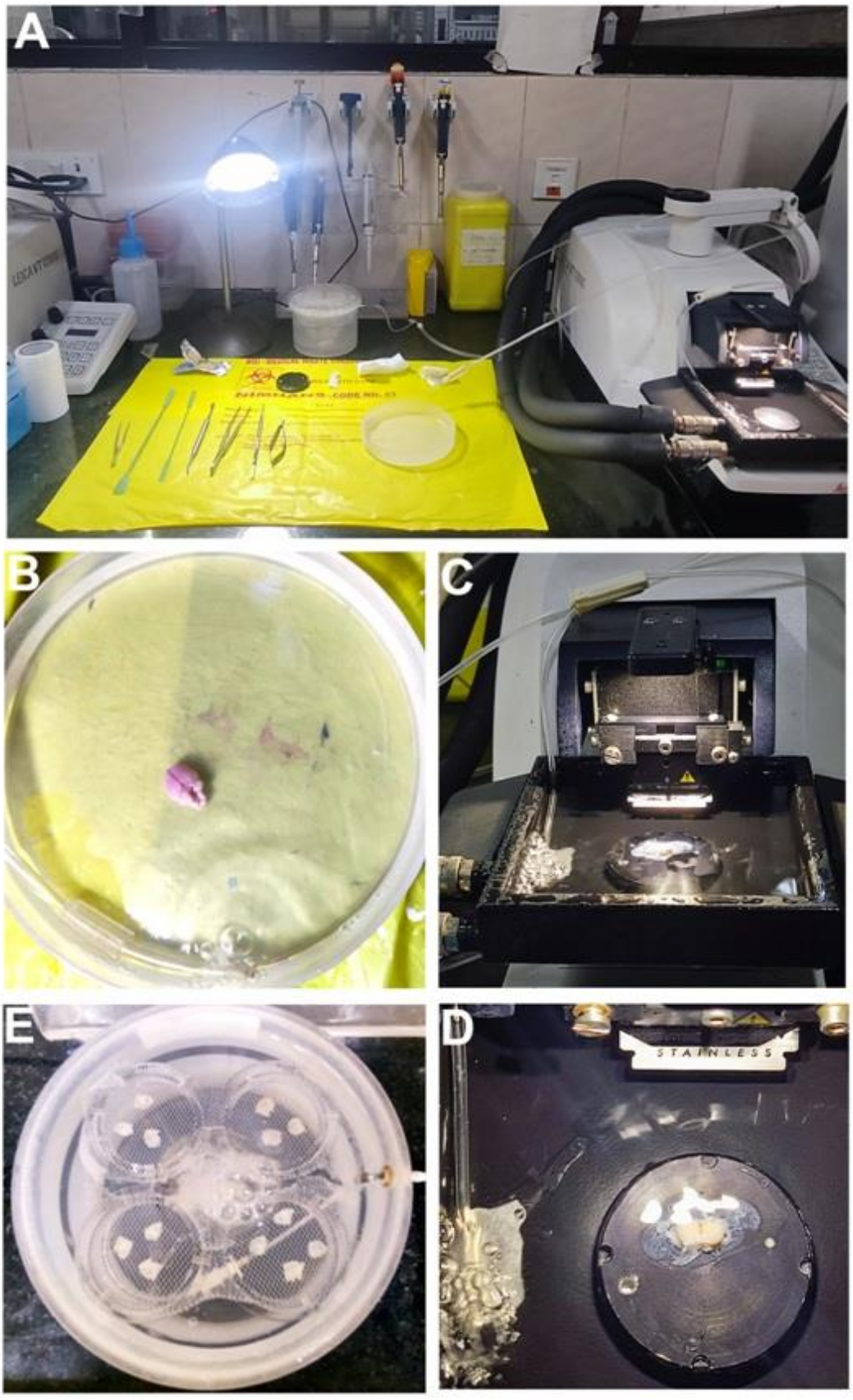
A
B
C
E
D
STAINLESS

Fig.15: Whole set-up for obtaining acute hippocampal slices: (A) The set-up of instruments, the brain slice keeper (middle) and the vibratome (right) on the table before starting the experiment are shown. (B) Shelled out brain placed in a plastic petri-plate submerged in continuously carbogenated aCSF. (C-D) The brain was taken on a tissue holder and slices were cut on a vibratome. (E) Slices were immediately transferred into a brain slice keeper and incubated for 2h at RT.

For extracellular Field Excitatory Postsynaptic Potential (fEPSP) recordings, 2h following incubation at RT, the brain sections were transferred to a recording chamber (Warner instruments, USA), constantly supplied with carbogen-saturated aCSF (32°C) with the help of a Minipuls Evolution peristaltic pump (Gilson Inc USA). The flow rate was maintained at 2 ml/min. The whole set-up along with the associated apparatus is shown in fig.16. Platinum-iridium cluster bipolar electrodes (Frederick Haer Company Inc, ME, USA) were positioned on the section with the help of stereo zoom microscope (Olympus, Japan) to stimulate Schaffer collateral-commissural fibre synapses (Fig. 17).

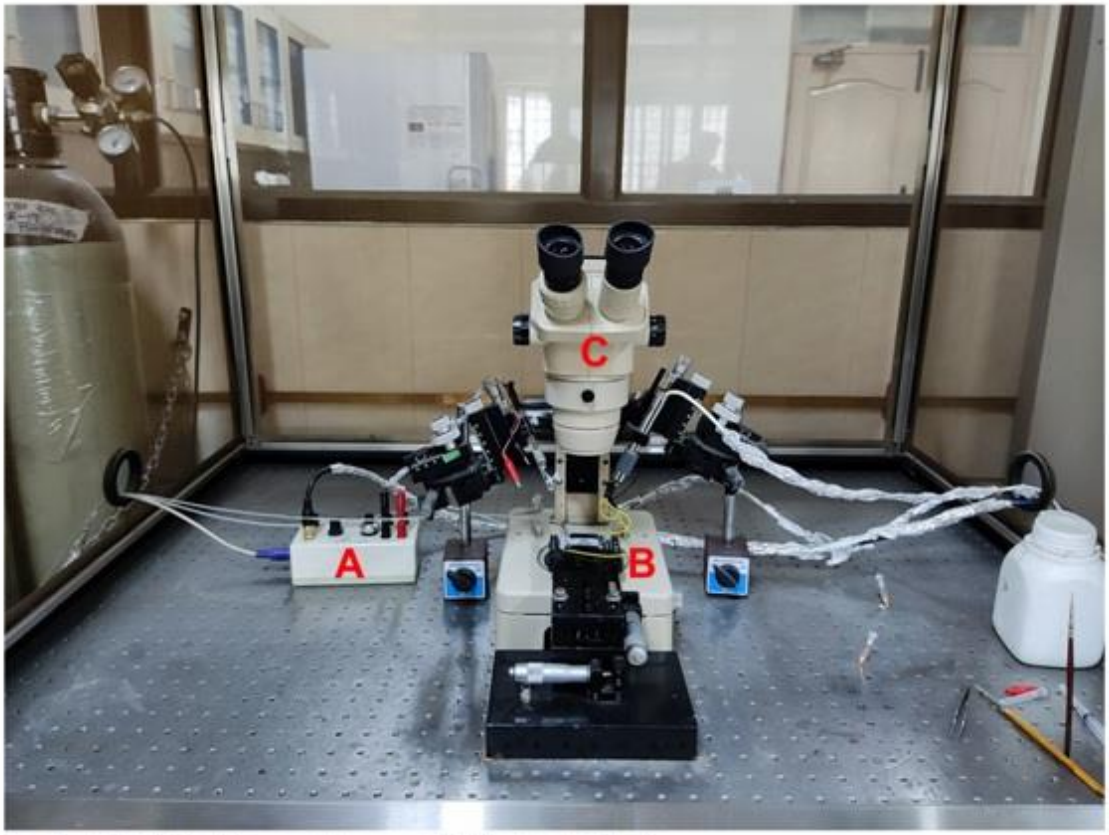
A
B
C


D

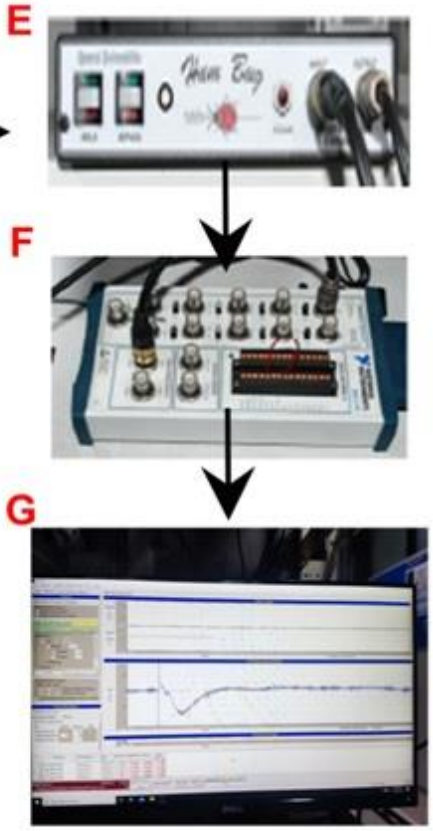
E
F
G

Fig.16: Schema showing the set-up for recording field excitatory postsynaptic potentials (fEPSPs) in acute hippocampal slices: (A) Stimulus isolator unit (B) Slice recording chamber (C) Stereo-zoom microscope (D) Differential amplifier (E) 50/60 Hz noise eliminator (F) Analog-digital convertor (G) Computer with data acquisition board and software.

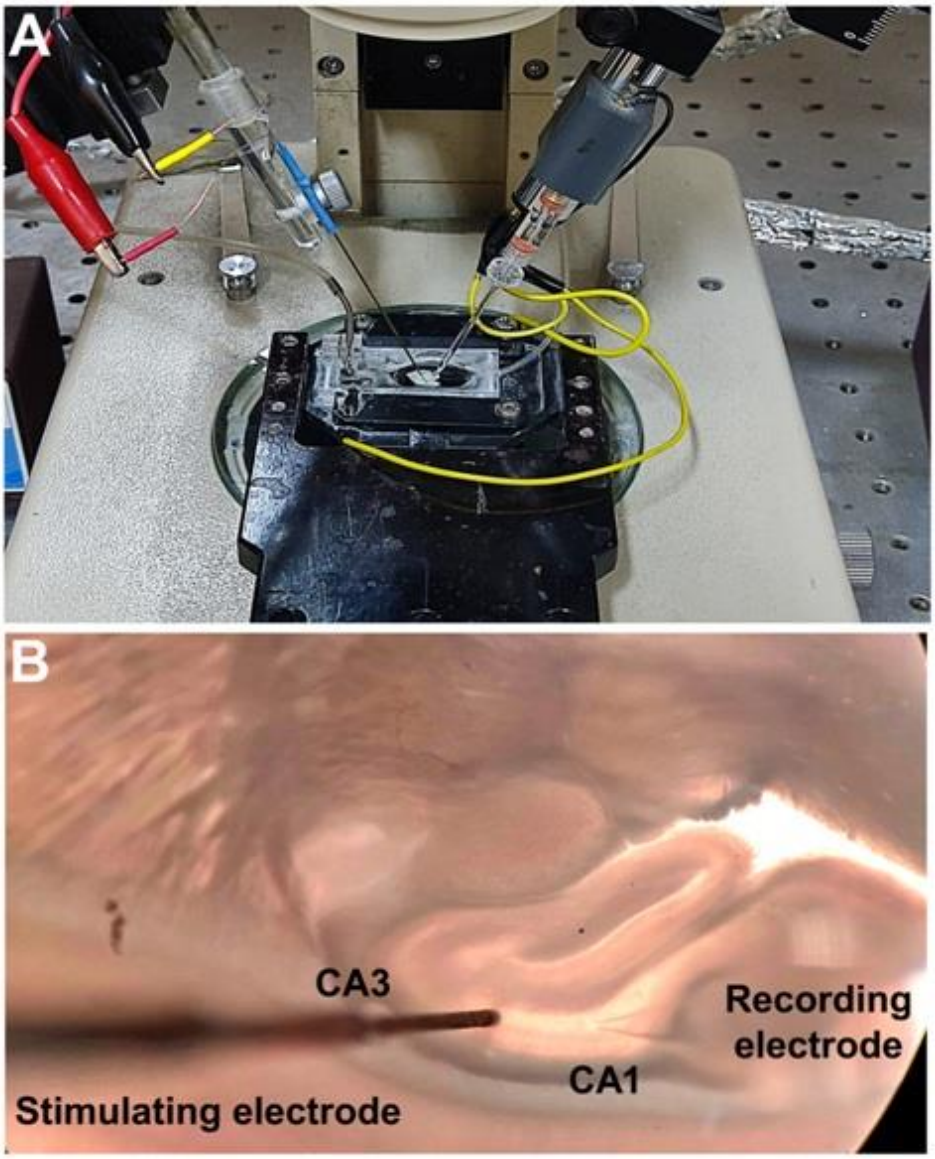

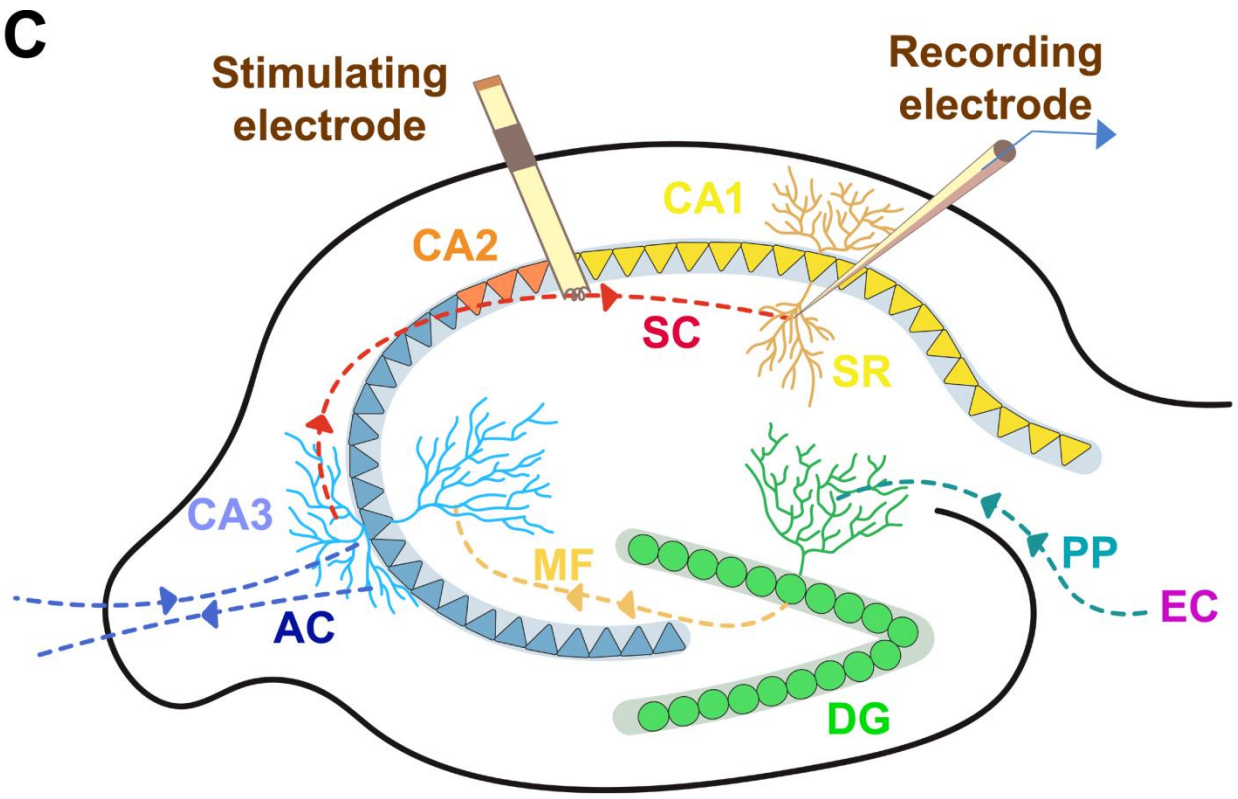

Fig.17: Positioning of the electrodes for recordingfield excitatory postsynaptic potentials (fEPSPs) in acute hippocampal slices: (A) Slice recording chamber with a slice perfused continuously with carbogenated-aCSF (B) The placement of the stimulating electrode at CA3 and the recording electrode at CA1 in the acute hippocampal slice under the stereo-microscope. (C) Schema showing the different regions of the hippocampus – CA1, CA2, CA3, Dentate gyrus (DG) – and the Entorhinal cortex (EC). The dotted lines mark the connecting fibres – Schaffer collateral (SC), Mossy fibres (MF), Perforant pathway (PP), Associational commissural fibres (AC). SR= Stratum radiatum is where the recording electrode is placed in the CA1 region.

Borosilicate glass microelectrode (Sutter instruments, USA) filled with 2M NaCl was used as recording electrode upon being fixed to an electrode holder with silver wire. The electrode was then positioned in the stratum radiatum layer of the CA1 region of dorsal hippocampus, and readings were acquired while the slices remained immersed. fEPSPs were induced by administering 0.1-ms width square wave pulses with the help of a

stimulus isolator in a constant current mode that produced fEPSP with a typical stimulus artefact, fibre volley and a negative deflection shown in fig. 18.

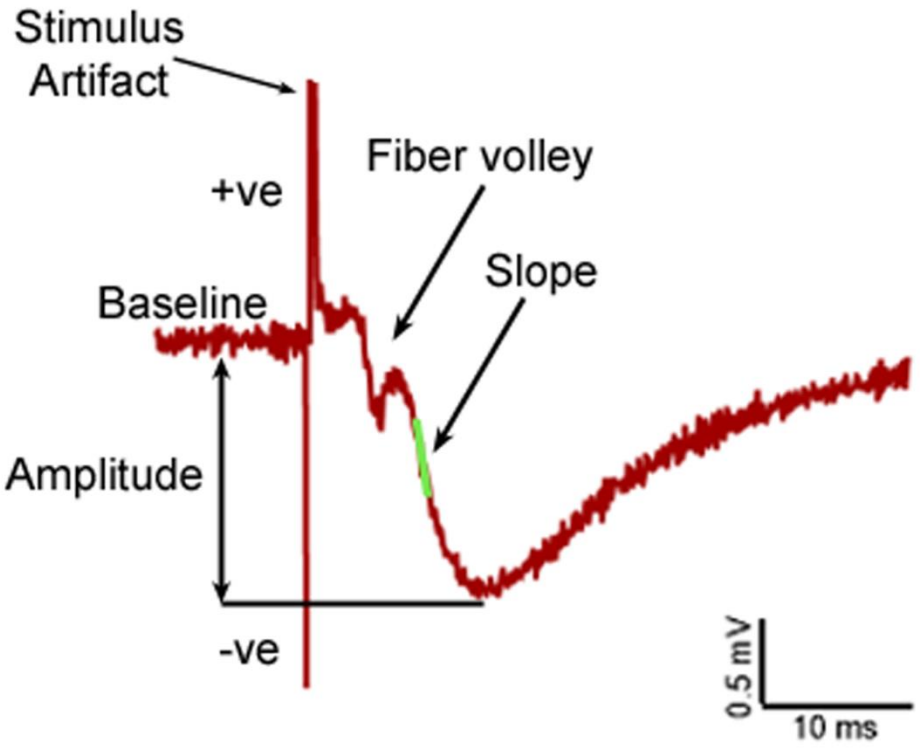

Fig.18: Representative fEPSP tracing with a characteristic stimulus artefact, a fiber volley and a negative deflection (slope in green and amplitude are marked).

fEPSPs were induced at a test stimulus frequency of 0.033Hz during the whole experimental duration. A steady baseline of minimum 20 min was noted prior to the assessment of the main electrophysiological factors. The studies conducted sequentially as described earlier (Subhadeep et al., 2021). Briefly, the steps are as follows:

(i) **Input-output (I-O) relationship** was measured by elevating the input current strength (by 20 μA increment) until population spike was observed. The stimulus current strength for the test was kept at a number that evoked a 40% of the maximum fEPSP slope value.

(ii) **Paired-pulse facilitation (PPF)** was determined by supplying two pulses in close succession with inter-stimulus intervals (ISI) ranging from 30-300 ms with an increment of 30ms. Paired-pulse ratio (PPR) was calculated by dividing the slope of fEPSP2 by fEPSP1.

(iii) Following 20 min of baseline recording, **post-tetanic potentiation** (PTP), **short-term potentiation** (STP) and **long-term potentiation** (LTP) were evoked by a single theta burst stimulation (TBS, 4 pulses/burst at 100 Hz, 20 bursts with 200-ms interval) shown in fig. 19. Recordings were carried out up to 60 min following TBS induction. Slices that displayed stable readings for a minimum of 60 min post TBS were the ones utilized for analysis of PTP, STP and LTP. The average slopes of fEPSPs normalised to baseline recorded between 20^{th}-30^{th} min (for STP) and 40^{th}-60^{th} min (for LTP) post TBS were utilised for statistical comparisons.

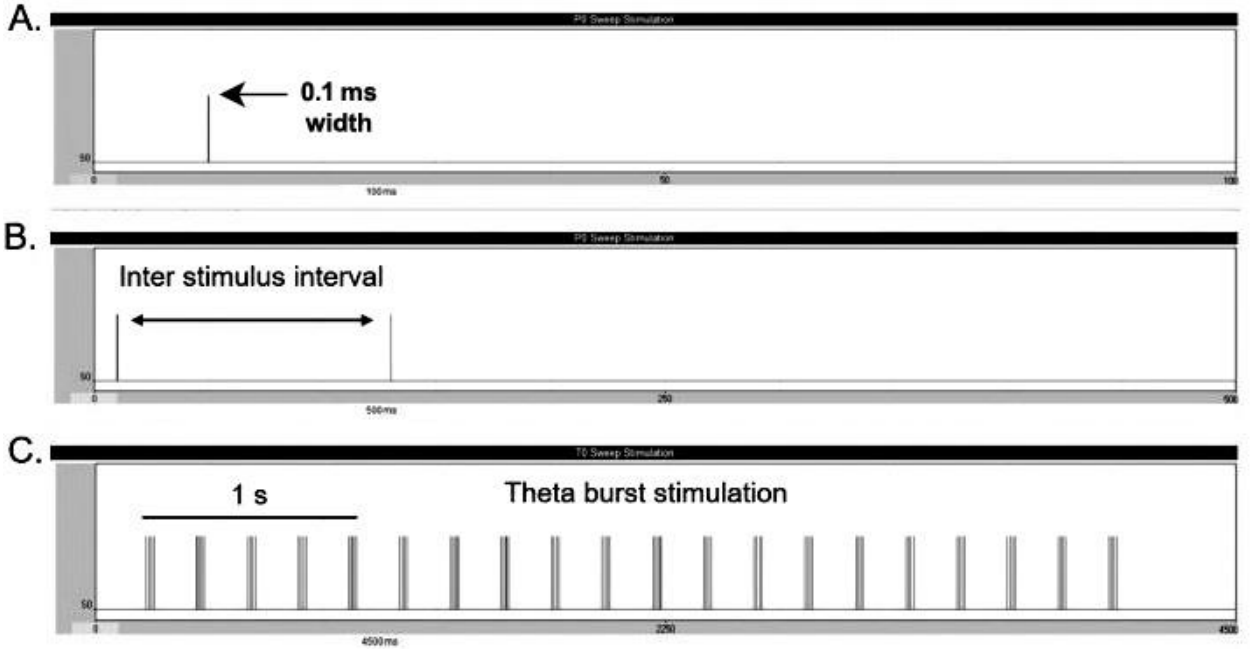

Fig.19: Schema showing the protocol for stimulus used to obtain (A) Baseline (B) Paired pulse facilitation (C) Theta burst stimulation

The fEPSP recordings were amplified using a differential amplifier (A-M systems, USA) and digitised with the help of a digitiser (National Instruments, USA). A noise eliminator (Humbug, Quest scientific) was utilised to eliminate the effect of electrical interference on the recordings. The data were acquired and analysed using WinLTP® v2.3 software (WinLTP Ltd, UK).

Statistical Analysis:

All data was analysed and graphs were created by using Prism software (v8.0, GraphPad Inc, USA). For comparing more than two experimental groups, one way ANOVA analysis followed by tukey's multiple comparison post hoc test was used in all the experiments. For analysis of significant difference between only two groups unpaired student's t-test was used. However, in case of the input-output curve and PPF curve, two-way ANOVA followed by tukey's multiple comparison post hoc analysis was used to calculate the effect of TIMP-1. All data is presented as mean ± standard error of mean (SEM) of at least 3 experiments, and $p < 0.05$ was considered to be statistically significant.

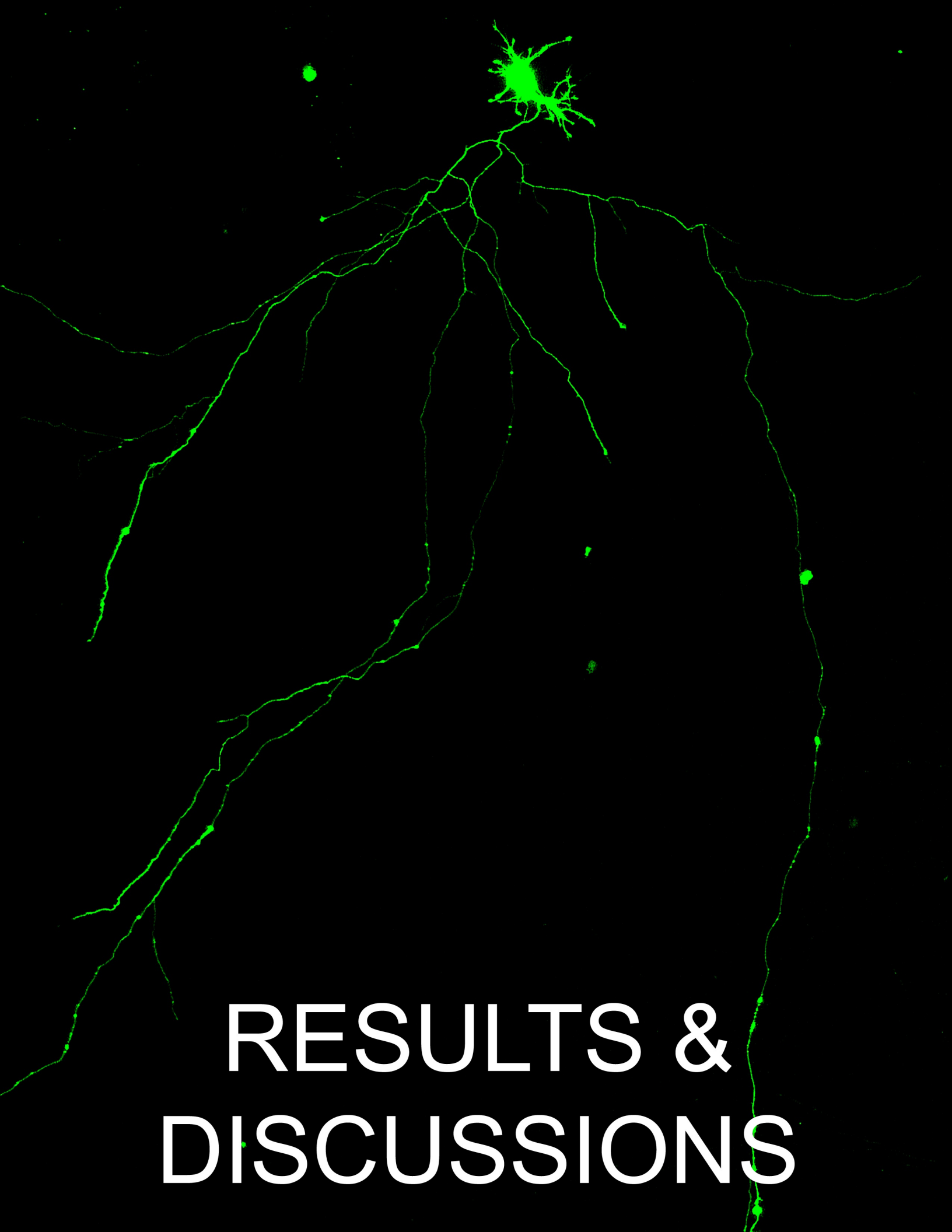

RESULTS & DISCUSSIONS

PART I

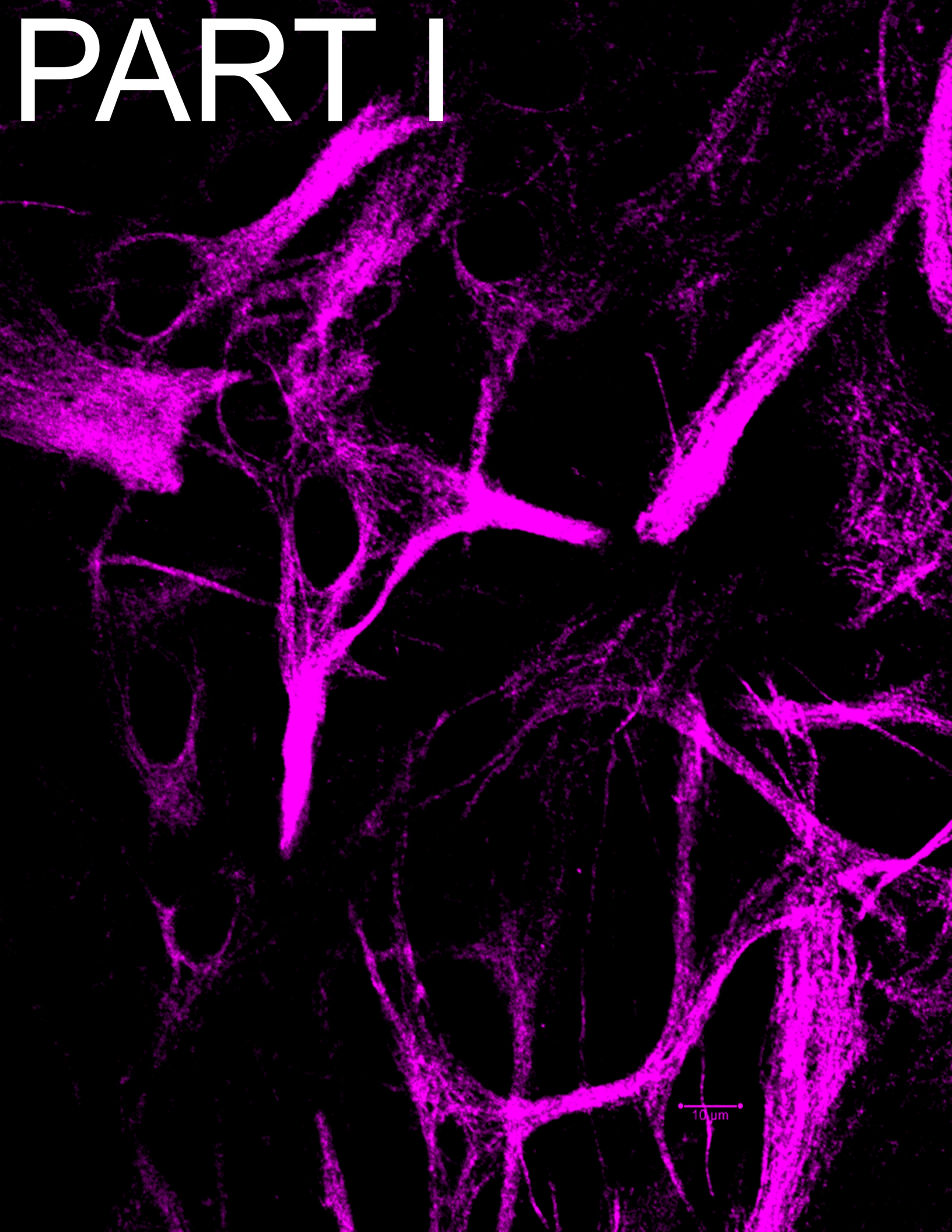

Part I: Aβ-induced reactive astrogliosis and the emergence of tissue inhibitor of matrix metalloproteinase 1 (TIMP-1)

PART- I: Aβ-induced reactive astrogliosis and the emergence of Tissue inhibitor of matrix metalloproteinase 1 (TIMP1)

Tissue inhibitor of matrix metalloproteinase 1 (TIMP-1) has been widely studied for its role in maintaining tissue integrity especially in cancer biology. In recent times it has also gained significant limelight in neurodegenerative diseases. It has surfaced as a major factor in deciding the path of disease progression. The versatile functionality of TIMP-1 is due to its two-domain structure – one responsible for metalloproteinase inhibition and other for cytokine-like cellular signalling. This unique feature of TIMP-1 gives rise to its complex interactome comprising numerous proteases and cell-surface proteins that induce several downstream signalling pathways. TIMP-1 inhibits the enzymatic activity of at least ten out of the sixteen presently known soluble matrix metalloproteinases (MMPs) - MMP-1, MMP-2, MMP-3, MMP-7, MMP-8, MMP-9, MMP-10, MMP-11, MMP-12 and MMP-13 (Baker et al., 2002). It was initially discovered as a collagenase inhibitor. MMPs are upregulated in cancer, so it was thought TIMP-1 may play a role in prevention of invasion and metastasis. While some reports show that TIMP-1 display anti-invasive and anti-metastatic properties (Cruz-Munoz and Khokha, 2008; Khokha, 1994), clinical results show increased level of TIMP-1 in blood and tissue in cancer patients (Jackson et al., 2017). This was an interesting twist and allured towards a more complex role of TIMP-1 in disease scenario.

The N-terminal domain (NTD) of TIMP-1 binds to metalloproteinases and inhibits their function. Metalloproteinases are known to remodel extracellular matrix in an irreversible manner but their functions may extend well beyond this role. Cell membrane bound

TIMP-1 can also target ADAM-10 (a disintegrin and metalloproteinase 10). ADAM-10 regulates cell surface protein composition by driving the cleavage of various cell surface receptors or releasing active cytokines by cleaving their pro-forms which in turn switches on/off specific signalling pathways. So, TIMP-1 by its NTD not only orchestrates MMP activities in the extracellular environment but also modulates intracellular signalling pathways by inhibiting ADAM-10 activity on cell surface (Murphy, 2011). The C-terminal domain (CTD) of TIMP-1 can bind to pro-MMP9 as well as tetraspanin - CD63. Complex of TIMP-1's CTD with its target's pro-form i.e. pro-MMP9 can in turn bind to ADAM-10 on cell surface leading to the cleavage of pro-MMP9 to MMP-9. Alternatively, pro-MMP9-TIMP1 complex can bind to CD44 on cell surface initiating JAK2/PI3K/Akt pathway that prevents apoptosis (Lambert et al., 2009). CD63 was the first identified cell-surface receptor of TIMP-1 and can induce MAPK pathway in breast cancer cells (Jung et al., 2006). TIMP-1-CD63 binding leads to integrinβ1 signalling but the mechanism remains elusive. TIMP-1 bound CD63 can also trigger FAK signalling in an integrin independent manner activating PI3K and MAPK pathways downstream (Liu et al., 2005; Termini and Gillette, 2017). TIMP-CD63 induced PI3K signalling essentially induce pro-survival pathways, tumor growth and angiogenesis (Cui et al., 2015). CD82, another tetraspanin, was recently identified as a binding partner of TIMP-1 through its NTD (Zhang et al., 2017). TIMP-1-CD82 binding leads to the endocytosis of TIMP-1. LRP-1 is another important receptor that can not only bind to free-TIMP-1 but also can interact with MMP/TIMP-1 complexes. While TIMP-1-LRP1 initiates pathways responsible for modulating neuronal morphology, MMP-TIMP-1 complexes are endocytosed upon binding with LRP-1 and finally degraded. The multi-functionality of TIMP-1 arises from

the competition among the different binding partners of TIMP-1 for their corresponding attachment domain which is highly influenced by the context, TIMP-1:MMP ratio and the binding affinities of the partners. Higher levels of TIMP-1 compared to MMPs means there is free TIMP-1 available to bind to cognate cell-surface receptors such as CD63, CD82 and LRP-1. An equal amount of MMPs and TIMP-1 means there is complex formation of TIMP-1 with MMPs followed by its cell surface binding to either CD44 for signalling or LRP-1 for degradation. During pathological insult, when the levels of MMPs are higher compared to TIMP-1, MMP-9 activity increases, as a result more pro-MMP9s are cleaved and hence the CTD of TIMP-1 becomes free for binding and signalling through CD63. This shows that although the different binding partners of TIMP-1 and their functions are independent of each other, they are interconnected via their dependency on the external context. TIMP-1's activity may be influenced by the presence of other three members of the TIMP family namely – TIMP-2, TIMP-3 and TIMP-4. This is because they all share the same two-domain structure and hence can bind to MMPs as well as cell surface receptors namely TIMP-2 with integrin α3β1, TIMP-3 with VEGFR2 while the surface receptor of TIMP-4 is yet to be discovered (Grunwald et al., 2019).

In recent times, TIMP-1 has drawn considerable attention in CNS disorders including AD, ischemia and HAND (HIV-associated Neurocognitive Disorder) (Ashutosh et al., 2012; Kaczmarek et al., 2002). Especially, an increased secretion of TIMP-1 is observed in case of inflammatory processes associated with various CNS diseases (Gardner and Ghorpade, 2003; Jaworski, 2000; Khuth et al., 2001; Suryadevara et al., 2003). Reportedly, TIMP-1 is almost exclusively expressed by astrocytes in white matter lesion and plays a

neuroprotective role by inhibiting MMP activities (Althoff et al., 2010). A more recent investigation revealed that TIMP-1 and MMPs levels greatly vary in the plasma between neurodegenerative disorder patients (FTD, DLB and AD) and healthy controls signifying the importance to study TIMP-1 in neurodegenerative disorders (Tuna et al., 2018). Earlier reports also indicated a correlation between reactivated astrocytes and TIMP-1. Reportedly, TIMP-1 that is upregulated early in response to an inflammatory insult to the brain is initially secreted from neurons but later on astrocytes becomes the major source of TIMP-1 and also detected in the CSF of AD patients (Inspector et al., 2005; Wang et al., 2014). In a recent report delineating astrocyte heterogeneity along inflammatory profiles, a TIMP-1 expressing reactive astrocyte subtype was detected in white matter tracts that were suggested to partake in ECM remodelling, neuroprotection and remyleination (Hasel et al., 2021).

There are reports that suggest that TIMP-1 plays an anti-apoptotic role especially while acting on the cell in a MMP-independent manner. Indeed, overexpression of TIMP-1 or treatment of cells with recombinant TIMP-1 reduces the vulnerability of cell lines to apoptosis (Guedez et al., 1998). TIMP-1 can also induce the expression of IL-10 which can itself act as an anti-apoptotic factor (Guedez et al., 2001). In MCF7 and MCF10A cell lines, both epithelial origins, TIMP-1 induces FAK/PI3K signalling that protects cells against intrinsic and extrinsic apoptotic pathways (Li et al., 1999; Liu et al., 2003; Liu et al., 2005).

Hence, there still lies a lacuna in understanding the neuroprotective role of TIMP-1 especially in AD. The question remains as to when reactive astrocytes starts if at all

producing TIMP-1 during AD progression. Is it induced in response to Aβ oligomers on astrocytes? How astrocytes react morphologically as well as in terms of their secretory profiles? What is the mechanism by which astrocyte-secreted TIMP-1 tries to protect neurons in AD? Which receptor among those discussed above is actually responsible for mediating TIMP-1's neuroprotective effect in AD? We have addressed all these questions in this work.

Results

Kinetic study of astrocyte reactivity in response to Aβ *in vitro*

Astrocyte reactivity is a phenomenon that occurs under any kind of pathological situation in the brain. The term encompasses changes in astrocytes at the functional, morphological as well as at the transcription and secretion levels (Escartin et al., 2021). These reactive astrocytes are a complex and heterogeneous population and their attributes varies across different neurodegenerative diseases and at different disease stages. Indeed, distinct population of reactive astrocytes may render contrasting effects on neuronal heath. Numerous reports suggest that astrocytes are one of the earliest responsive cells to any kind of damage to the brain and their initial reactivity is often seen as a defence mechanism to nullify the detrimental effect of the toxin. Aβ accumulation is a consequence of imbalance between Aβ production and its clearance which progressively leads to AD. Hence, with time, a slow increase in Aβ content is the major reason for AD pathogenesis. Reactive astrocytes are implicated in uptaking and clearing Aβ plaques (Basak et al., 2012). Indeed ablation of reactive astrocytes leads to

elevated plaque levels (Kraft et al., 2013). However, with increasing time, the astrocytes loss their ability to either uptake or degrade Aβ plaques following phagocytosis. These plaque-positive astrocytes eventually turn out to be detrimental and contribute to secondary plaque formation. Hence, it is essential to study the transition of astrocyte from being a friend to a foe in response to Aβ (Garwood et al., 2017). We characterized astrocyte reactivity in response to Aβ oligomers *in vitro* and simultaneously analyzed their effect on neuronal health in co-culture models.

Kinetics of astrocyte reactivity was studied upon exposure of primary astrocytes to oligomeric Aβ in culture at three time points – 6h, 16h and 24h. Astrocyte reactivity was checked by quantifying the expression level of astrocyte-specific markers – GFAP, S100β, vimentin and nestin by immunocytochemistry. Morphological analysis in terms of GFAP expression was also performed. Ki67 staining was used as the standard marker to quantify cell proliferation. GFAP expression and related morphological analysis in response to Aβ treatment has previously been shown by our laboratory (Saha et al., 2020a). Astrocytes showed enhanced reactivity as evidenced by the morphological changes from flat polygonal astrocytes to long process bearing hypertrophic cells and the change in perimeter was calculated (Fig. 1A, E, *$p \leq 0.05$). Cell proliferation was also found to be increased by 2.5 fold in Aβ-treated astrocytes compared to control as evident from the increased number of Ki67 positive cells at 6h (Fig. 1A, F, *$p \leq 0.05$). However, the upregulation in GFAP expression level was not significant at 6h (Fig. 1A, D). At 16h and 24 h time points both GFAP expression and astrocyte perimeter showed a significant increase when compared to control (Fig. 1B–E) but no further increase in cell

proliferation was observed at these time points (Fig. 1F). Similar kinetics of astrocyte reactivation was observed when stained with S100β (Fig. 1 G-H), vimentin (Fig 1I-J) and nestin (Fig 1K-L) reconfirming that astrocytes become reactive displaying visible hypertrophic morphology as early as 6h following Aβ treatment which was detected till 24h. These results reaffirm that astrocytes become reactive early in response to Aβ treatment *in vitro*.

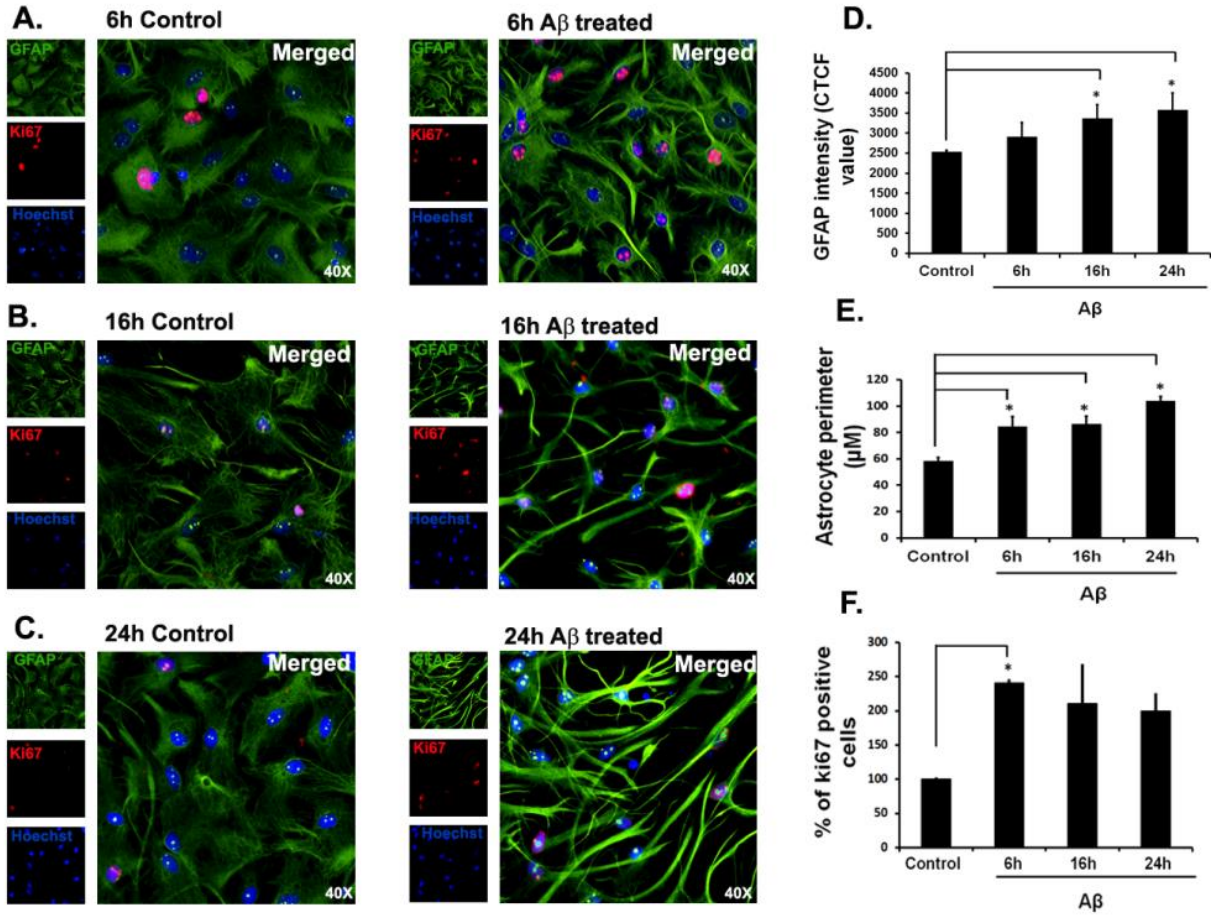

.

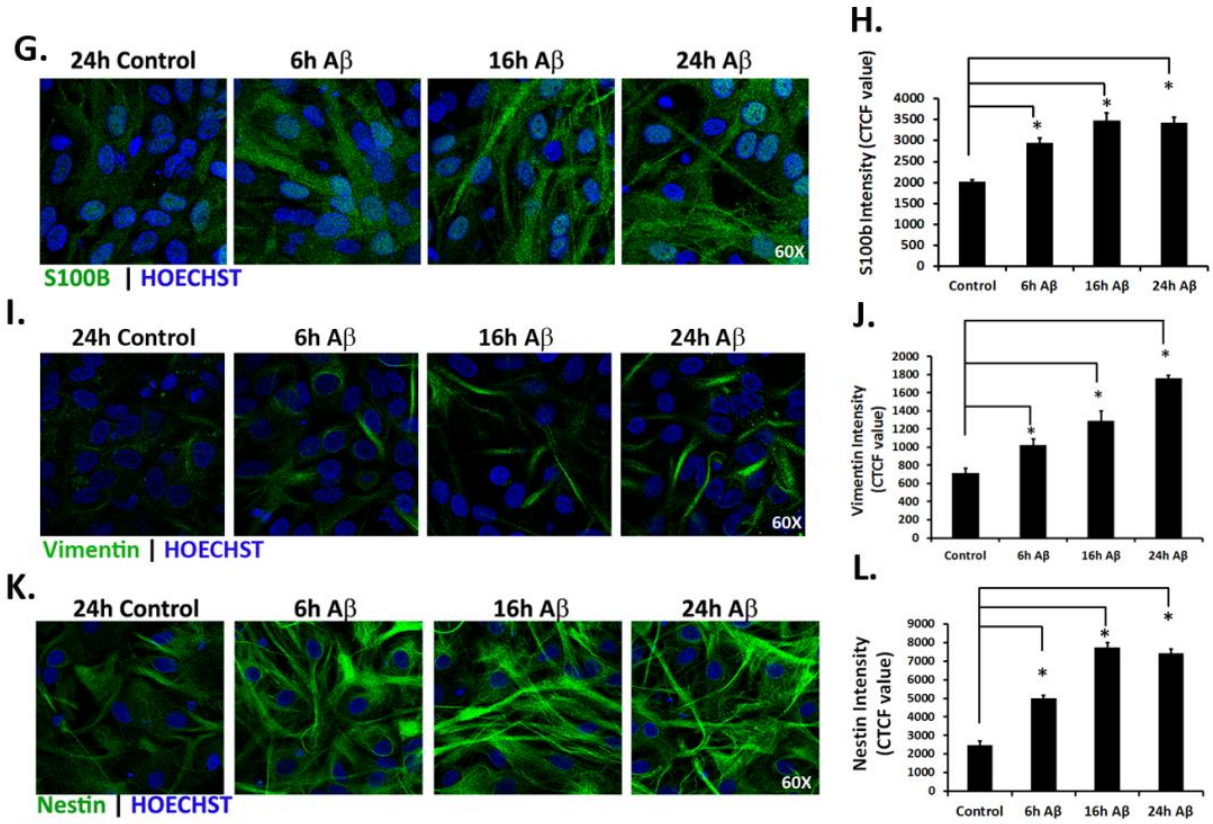

Fig.1: Time kinetics of primary astrocytes reactivity following Aβ treatment. Aβ (1.5 μM) treatment to mature primary astrocytes at 14DIV resulted in astrocyte reactivity observed at 6 h (A), 16 h (B) and 24 h (C) following immunocytochemical staining with GFAP, Ki67 and Hoechst at 40x magnification. Bar diagrams represents GFAP intensity expressed as CTCF value (D), astrocyte perimeter in μm (E) and percentage of ki67 positive cells (F) across the three different time points following Aβ treatment and compared to control (untreated) cells. Values are expressed as Mean±SEM from three independent experiments where *p≤0.05. Primary astrocytes were also stained with other astrocyte specific markers at the three time points along with Hoechst for the nuclei and compared to 24h untreated control cells as indicated with s100β (G), Vimentin (I) and Nestin (K). Confocal images were taken at 60x magnification. The changes in CTCF values are represented as bar graphs for s100β (H), vimentin (J) and nestin (L). Values are expressed as Mean±SEM from three independent experiments where *p≤0.05.

Astrocyte conditioned media from Aβ-treated astrocytes is protective towards neurons

The role of reactive astrocytes in AD remains controversial. It may play a beneficial or detrimental role in various disease scenarios. Initially, astrocytes may play a beneficial

role and then eventually turn detrimental towards neurons as observed in acute inflammation versus chronic inflammatory diseases (Gardner and Ghorpade, 2003). Their effect on neurons is mainly mediated by a plethora of cytokines secreted at different time points. Hence, it is important to study the effect of secretomes of reactive astrocytes at different time points, following their reactivity upon Aβ treatment, on neurons to understand when they transition from being neuroprotective to neurotoxic.

Astrocyte conditioned media (ACM) from Aβ-treated astrocytes were collected at 6h, 16h and 24h and transferred on GFP-transfected cortical neurons, either treated with or without Aβ as mentioned in Fig 2 A-C. The neurons under various treatment conditions were imaged at 0h, 24 h and 48h to study the changes in neuronal morphology and also cell viability was estimated by nuclei counting method at 24 h following Aβ treatment. Figs 2A-C depicts that treatment of Aβ on primary cortical neurons lead to progressive loss of neuronal processes. Additionally, Fig 2D shows that in terms of viability, Aβ treatment in the absence of ACM leads to 40% loss in percent cell viability at 24 h ($p<0.05$). In presence of ACM from control astrocytes (C-ACM) or ACM from Aβ-treated astrocytes (Aβ-ACM), overall neuronal health and viability was protected significantly upto 48 h. Interestingly, 6h Aβ-ACM rendered neuroprotection upto 48 h better, in terms of retention of neuronal processes and viability, in contrast to 16h Aβ-ACM or 24 h Aβ-ACM (Fig. 2A–D, $p \leq 0.05$). C-ACM was unable to protect neurons against Aβ toxicity upto 48 h.

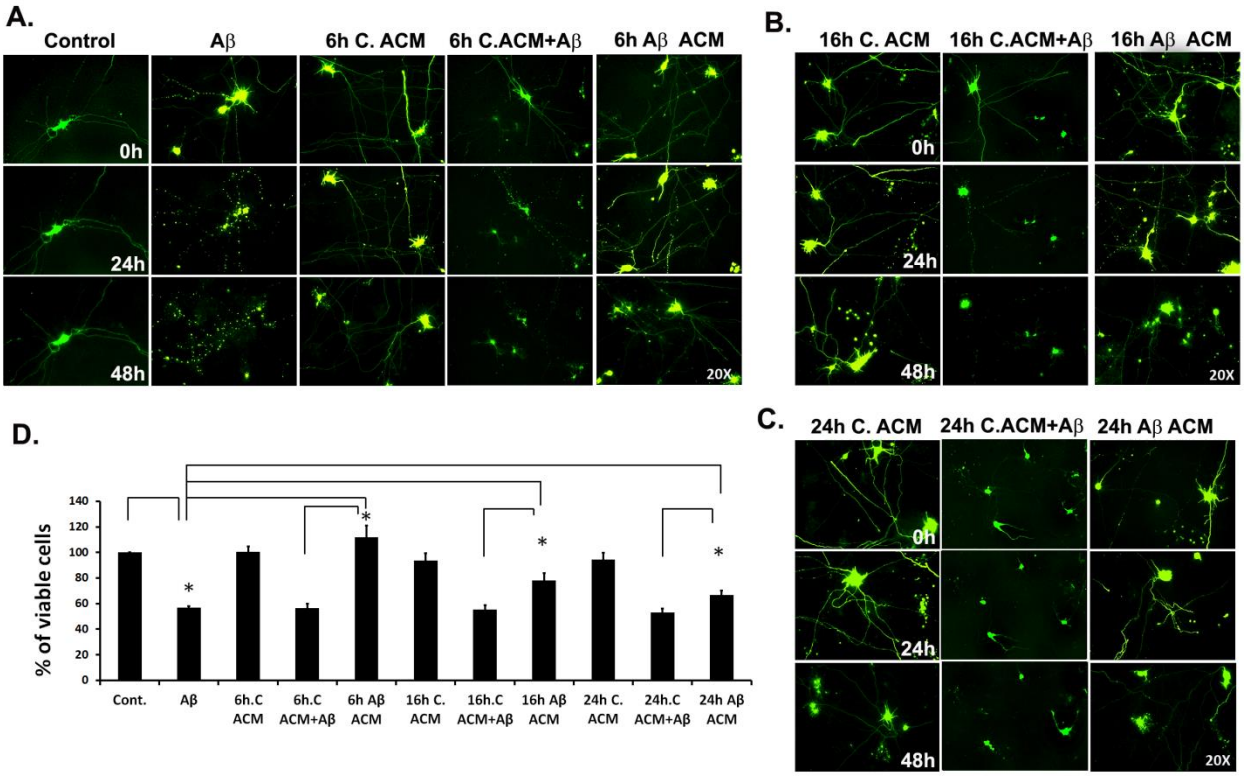

Fig.2: Effect of astrocyte conditioned media (ACM) from Aβ-treated astrocytes on neuron health. (A-C) 6DIV cortical neurons were GFP transfected and treated with control ACM (C-ACM) or Aβ-ACM from different time points 6h, 16 h and 24 h with or without Aβ as indicated, besides the neurons directly treated with Aβ. Live cells were imaged under fluorescence microscopy at 0h, 24h and 48 h at 20x magnification. Following 24h incubation with ACM, live cells were counted by nuclei buffer counting method and represented as a bar diagram (D). Values are expressed as means of five different experiments where *p≤0.05.

TIMP-1 is enriched in 6h ACM following Aβ -treatment

As observed in Fig 2, 6h Aβ-ACM provides the highest protection to neurons even in the presence of Aβ in terms of cell morphology and viability. Hence, we wanted to delineate the composition of cytokines present in this neuroprotective 6h Aβ-ACM versus 6h C-ACM. We performed cytokine arraysfor 29 common cytokines with C-ACM and Aβ-

ACM from 6h, 16h and 24h. We found that TIMP-1 was significantly up-regulated in the 6h Aβ-ACM versus 6 h C-ACM but decreased at 16 h and 24 h (Fig. 3A-E). This was an interesting finding given that TIMP-1 was already highlighted by Ashutosh et al to posses neuroprotective abilities against staurosporine in HIV-induced dementia model (Ashutosh et al., 2012) and as mentioned earlier TIMP-1 levels varied greatly in the CSF (Lorenzl et al., 2003) and plasma of AD patients (Tuna et al., 2018) when compared to healthy controls. Some additional cytokines levels namely sICAM-1, CINC-1, MIP-1α, VEGF and IL-2 also varied between the control and the treated groups as tabulated in Fig.3D at each time points. Coherently, ELISA data revealed that secreted TIMP-1 levels were increased by almost four-fold in the ACM of Aβ-treated astrocytes at 6h compared to control (Fig. 3F, $p < 0.05$). Intriguingly, while TIMP-1 was mostly referred in literature as a neuroprotective cytokine in consistence with our results and detected at reduced levels at the later time points, some pro-inflammatory cytokines – Fracktalkine, MIP3α and CINC-2α/β were increased at 16h and 24h (Fig 3A-D). Collectively, these data suggest that TIMP-1 is a major cytokine responsible for rendering the neuroprotective property of 6h Aβ-ACM.

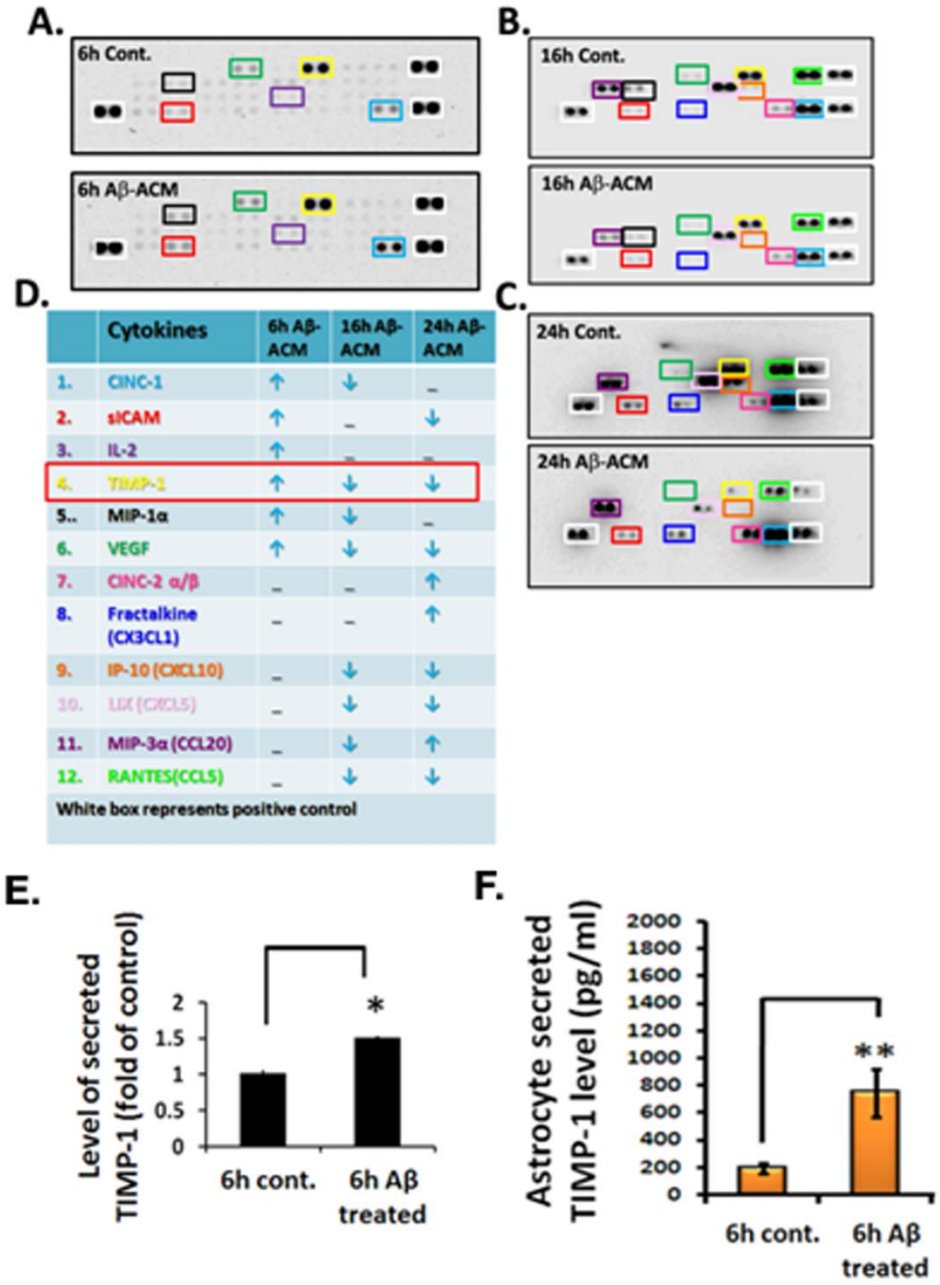

Fig.3: TIMP-1 is rapidly secreted by Aβ-treated astrocytes. Primary astrocytes (14 DIV) were exposed to Aβ at 1.5 μM concentration for 6h, 16h and 24h as indicated and ACM was utilized for cytokine array and compared to control ACM (A-C). (D) The cytokines that were significantly altered are tabulated and the color codes correspond to those present in individual blots. The increase in concentration of each cytokine was analyzed in comparison to control and gradual change (increase or decrease) across the given time

points are indicated. (E) Bar graph represents the densitometric analysis of TIMP1 dots from (A) i.e. 6h control and Aβ-ACM, *p≤0.05. (F) Bar graph shows ELISA results for TIMP1 at pg/ml level in control ACM versus Aβ-ACM. Values are expressed as means of three different experiments where **p≤0.05.

Aβ-ACM devoid of TIMP-1 loses its neuroprotective ability

TIMP-1 being a major cytokine that was significantly increased in 6h Aβ-ACM we wanted to analyze the specific contribution of TIMP-1 in the secretome in rendering the neuroprotective effect. Hence, we used a neutralizing antibody against TIMP-1 (TIMP-1-Nab) in 6h Aβ-ACM and compared it with TIMP-1 enriched 6h Aβ-ACM for changes in its role in protecting primary neurons against Aβ toxicity. Cortical neuron cultures were treated with Aβ, ACM, 6h Aβ-ACM, 6h ACM+Nab+TIMP-1 and 6h Aβ-ACM+NabTIMP-1 and the changes in cell viability were assessed 24h later by nuclei buffer counting method. It was observed that Aβ caused around 50% death in primary cortical neurons and 6h C-ACM and 6h Aβ-ACM were able to retain cell viability upto 100% compared to control cells and was consistent with our previous results. Neutralizing TIMP-1 in 6h C-ACM reduced neuronal viability by only 10-20% (not significant) when transferred on cortical neurons which may be due to the presence of other neuroprotective factors while addition of Nab TIMP-1 to 6h Aβ-ACM resulted in complete loss of protection rendered by 6h Aβ -ACM on neurons (compared to control, $p < 0.05$). The latter confirms that TIMP-1 is essential for rendering the neuroprotective ability of 6h-Aβ-ACM (Fig 4).

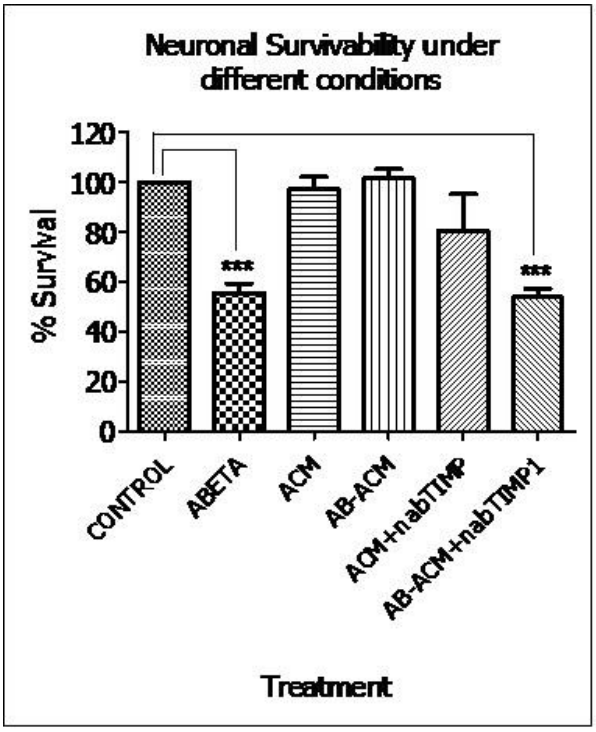

Fig.4: Neutralization of TIMP-1 from early Aβ-ACM abrogates its neuroprotective ability. Primary cortical neurons (6DIV) were treated with Aβ (1.5 μM), C-ACM (6h), Aβ-ACM (6h) , C-ACM+Nab (TIMP-1 neutralizing antibody) and Aβ-ACM+Nab for 24 h and bar graph represents the results from viability assay by nuclei buffer counting method. Values are expressed as Mean±SEM of three independent experiments where ***$p \leq 0.05$.

Rat recombinant TIMP-1 protects primary neurons against Aβ toxicity

Data that showed TIMP-1 mediates the neuroprotective property of 6h Aβ-ACM and emerges as an essential component of early hour reactive astrocyte secretome prompted us to further understand the role of rat recombinant TIMP-1 (rrTIMP-1) on neuronal health and viability. Hence, we treated 6DIV primary cortical neurons with rrTIMP-1 in presence or absence of Aβ for 24h and then performed immunocytochemical studies with MAP2 antibody. Neuronal viability under similar treatment conditions after 24h was assessed by nuclei buffer counting method. It was observed that TIMP-1 at 100 ng/ml

provided significant neuroprotection against Aβ toxicity in terms of neurite length and overall cell morphology (Fig 5A). TIMP-1 also provided significant protection in terms of cell viability against Aβ by recovering percent viability by approximately 40% at 24h following Aβ treatment while cells treated with TIMP-1 in absence of Aβ retained intact morphology and viability (Fig 5B, $p<0.05$). All further experiments with rrTIMP-1 were conducted at a dose of 100 ng/ml. All rrTIMP-1 henceforth is referred as TIMP-1.

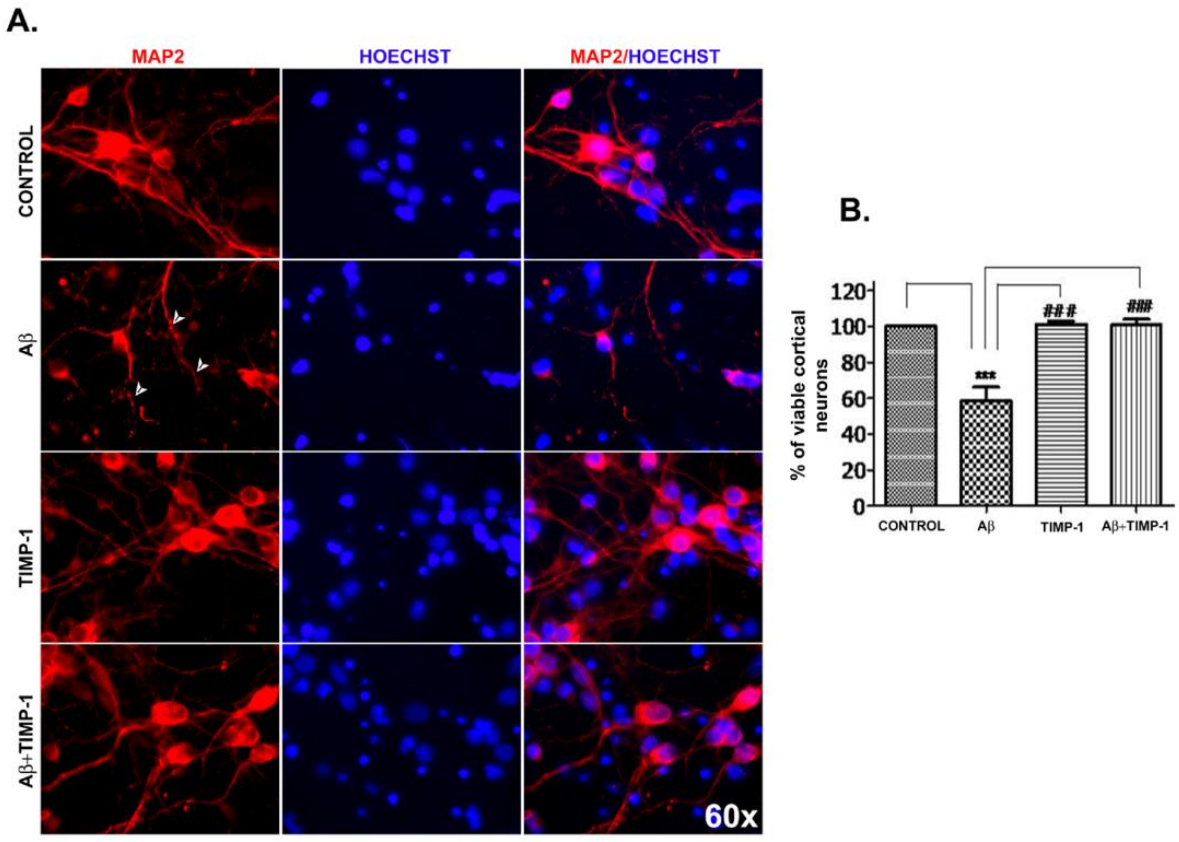

Fig.5: Addition of rat recombinant TIMP-1 to cortical neurons protects them against Aβ. 6DIV primary cortical astrocytes were treated with Aβ, rrTIMP-1 or Aβ along with rrTIMP-1 (Aβ+TIMP-1). Cells were fixed at 24h and immunocytochemistry was performed with MAP2 antibody followed by nuclei staining with Hoechst. Images were taken at 60x magnification. The white arrowheads indicate degenerating neuritis. (B) Neurons were also assessed for viability by nuclei buffer counting method 24 h following

treatments. Values are expressed as Mean±SEM of three independent experiments where **p≤0.05 (compared to control), ###p≤0.05 (compared to Aβ).

TIMP-1 plays a protective role by inhibiting the pro-apoptotic pathway and activating Akt in Aβ treated primary neurons

We wanted to explore the mechanisms behind TIMP-1 mediated protection of neurons against Aβ -induced toxicity. TIMP-1 binds to CD63 and activates Akt pathway and is responsible for inducing anti-apoptotic pathway in thyroid cancer (Bommarito et al., 2011). PI3K/Akt pathway is interrupted upon Aβ treatment to rat cortical neurons (Chen et al., 2009). Moreover, earlier reports from our lab show that Aβ treatment to cortical neurons causes the dephosphorylation of Akt and its downstream target FOXO3a. Dephosphorylation of FOXO3a at Ser253 induces its nuclear translocation and hence leading to increased transcription of pro-apoptotic genes BIM and PUMA (Akhter et al., 2014; Sanphui and Biswas, 2013).

Primary neurons were treated with TIMP-1 in the presence or absence of TIMP-1 besides the controls (untreated and Aβ-treated neurons) for 24h. Western blot analysis shows that treatment of Aβ alone on cortical neurons led to a significant decrease in the level of Akt phosphorylation (s473) compared to untreated control cells. This reduction in phosphorylation level of Akt was reversed upon rrTIMP-1 co-treatment with Aβ as observed from the densitometric analysis of pAkt/tAkt levels from whole cell lysates (Fig. 6A-B). Corresponding levels of Actin and tAkt remained unchanged across all treatment groups. The direct downstream target of pAkt i.e. FOXO3a's phosphorylation levels

were found to be significantly increased in the TIMP-1 treated Aβ neurons in contrast to the levels observed upon Aβ treatment alone in western blot analysis. Corroborating the results, when immunocytochemistry was performed 24h following Aβ treatment with FOXO3a antibody, increased staining of FOXO3a was observed in the Hoechst-stained nuclei in Aβ-treated neurons whereas co-localization of FOXO3a puncta and Hoechst was negligible in case of Aβ+TIMP-1 treated cells, almost comparable to untreated cells (Fig. 6C). This indicated towards decreased translocation of FOXO3a to the nucleus upon TIMP-1 treatment to Aβ-treated cells due to FOXO3a's increased phosphorylation by activated Akt. Moreover, phospho-FOXO3a level was reduced compared to control in Aβ-treated cells but preserved when co-treated with TIMP-1 in total cell lysates (Fig. 6D-E). FOXO3a in the nucleus acts as a transcription factor for several pro-apoptotic genes, BIM and PUMA being the most prominent ones as shown by our group earlier (Akhter et al., 2014; Sanphui and Biswas, 2013). We found upregulation of FOXO3a target proteins, BIM and PUMA in Aβ neurons and their levels were significantly reduced in Aβ+TIMP-1 treated cells at 24h (Fig. 6D, F-G). Interestingly, anti-apoptotic protein Bcl-2 level was elevated upon TIMP-1 treatment to Aβ-treated cells compared to only Aβ-treated cells while the level of Bcl-xl, another anti-apoptotic protein, remained unchanged across the treatment groups (Fig 6D, H-I). Western blot results further revealed increased levels of apoptotic mediators cleaved Caspase3 and DNA damage marker phosphoH2AX in Aβ-treated neurons that were both downregulated in the Aβ+TIMP-1 treated group (Fig 6D, J-K). Thus, these results strongly suggest that TIMP-1 protects neurons against Aβ cytotoxicity by preventing apoptosis through activation of Akt/FOXO3a/Caspase axis.

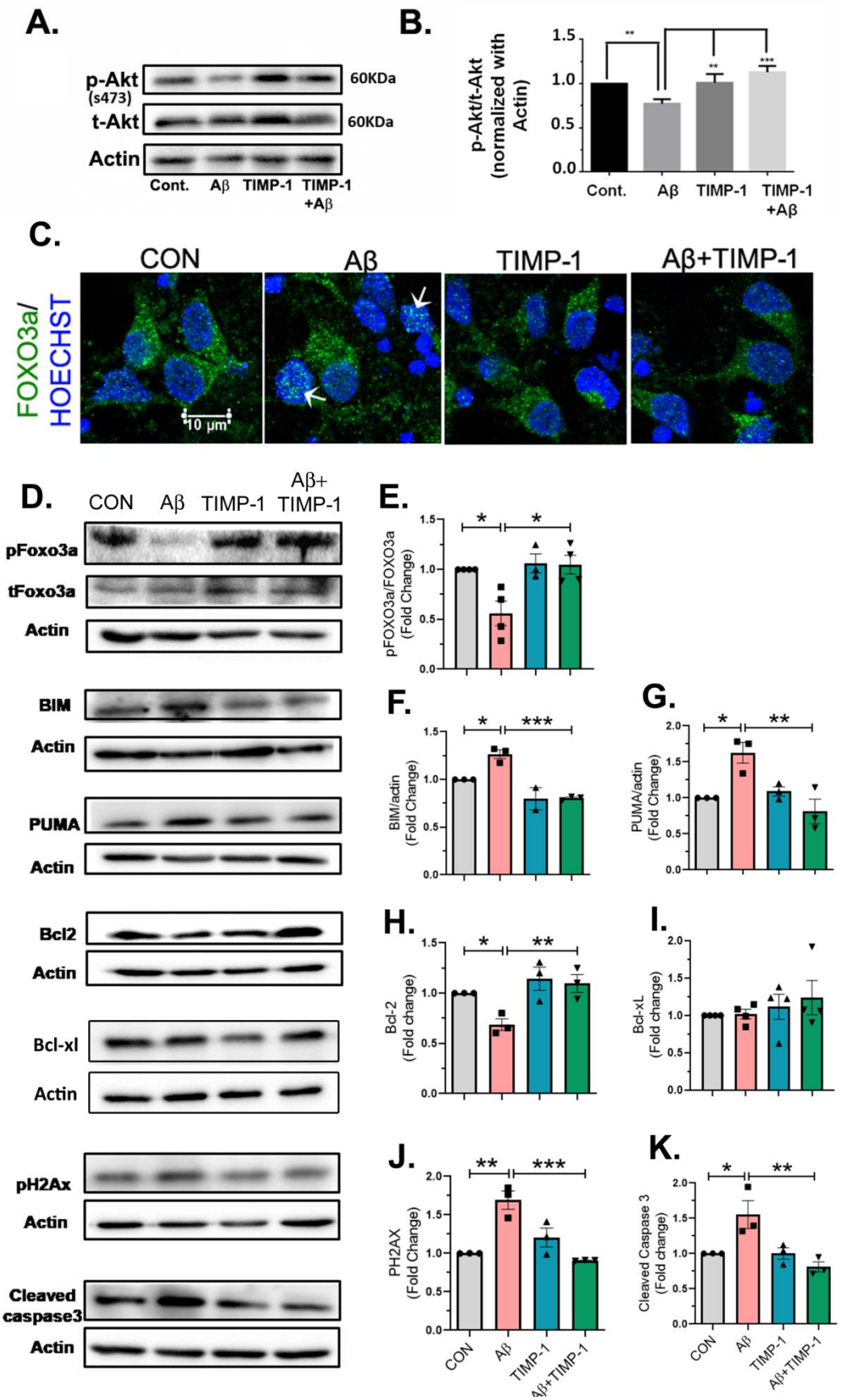
A.
p-Akt (s473)
t-Akt
Actin
60KDa
60KDa
Cont.
Aβ
TIMP-1
TIMP-1 +Aβ
B.
p-Akt/t-Akt (normalized with Actin)
1.5
1.0
0.5
0.0
**
**
***
Cont.
Aβ
TIMP-1
TIMP-1 +Aβ
C.
CON
Aβ
TIMP-1
Aβ+TIMP-1
FOXO3a/ HOECHST
10 μm
D.
CON
Aβ
TIMP-1
Aβ+ TIMP-1
pFoxo3a
tFoxo3a
Actin
BIM
Actin
PUMA
Actin
Bcl2
Actin
Bcl-xl
Actin
pH2Ax
Actin
Cleaved caspase3
Actin
E.
pFOXO3a/FOXO3a (Fold Change)
F.
BIM/actin (Fold Change)
G.
PUMA/actin (Fold Change)
H.
Bcl-2 (Fold change)
I.
Bcl-xL (Fold change)
J.
PH2AX (Fold Change)
K.
Cleaved Caspase 3 (Fold change)
CON
Aβ
TIMP-1
Aβ+TIMP-1

Fig.6: TIMP-1 protects primary cortical neurons against apoptosis. Primary cortical neurons (6DIV) were treated with Aβ, TIMP-1 and Aβ+TIMP-1 besides control and following 24 h of treatment, cell lysates were collected and subjected to western blot assay. (A) Represents immunoblots probed with phospho (s473) Akt, total Akt (tAkt) and Actin. (B) Densitometric analysis of the pAkt/t-Akt is represented as a bar graph where each bar represents values expressed as Mean±SEM of 3 independent experiments where **p<0.01 and ***p<0.001. (C) Immunocytochemistry with FOXO3a (green) antibody followed by nuclei staining with Hoechst (blue) was also performed. White arrow indicates co-localization of green dots in the nuclei in the Aβ-treated neurons. (D) The representative panel of immunoblots from neuron sample lysates probed with pro- and anti-apoptotic markers are shown along with the corresponding loading control or actin from the same blot. (E-F) Bar graphs represent normalized densitometric analysis for each protein showing the fold change upon treatment with respect to control. Values are expressed as Mean±SEM. One way ANOVA followed by Tukey's post hoc test was used for comparison among the groups.*p<0.05, **p<0.01, ***p<0.001

TIMP-1 corrects impaired autophagy flux in Aβ treated primary neurons

Autophagy is another cell death pathway highly implicated in AD. Akt is known as a common upstream regulator of both apoptotic and autophagic pathways (Fig. 7A). Earlier report from our laboratory shows that Aβ treatment on primary cortical neurons leads to increased accumulation of autophagic bodies including p62, LC3B and lysosomal marker LAMP1 inside primary cortical neurons, preventing their clearance leading to an impaired autophagy flux (Saleem and Biswas, 2017). Hence, we wanted to investigate whether TIMP-1 has any effect on impaired autophagy flux induced by Aβ in neurons. We performed western blots from lysate of primary cortical neurons treated under the same conditions as in Fig. 6, 24h following treatment. We found decreased level of phosphorylation of mTOR (Fig. 6B-C), phospho-mTOR negatively regulates autophagy initiation and mTOR is also the direct target of Akt. We found increased levels of ATG5

(an upstream marker indicating elongation of autophaghagosome), p62 (cargo adaptor and the most crucial determinant of autophagy flux) and LC3B-II following Aβ treatment. Lysosome numbers were also found to be increased, identified by LAMP1 (lysosomal marker), under Aβ treatment to cortical neurons indicating that although autophagy was induced by Aβ, the flux was impaired eventually. Addition of TIMP-1 to Aβ-treated neurons improved autophagy flux by reversing the levels of ATG5, p62, LC3BII and LAMP1 to the level of untreated control. Primary neurons treated under the same conditions for 24 h and immunocytochemistry was also performed with p62, LC3B and LAMP1 antibodies. CTCF values revealed increased expression of these proteins in neurons in Aβ-treated conditions but Aβ+TIMP-1 co-treatment reduced their expression levels significantly (Fig 7, $p<0.05$). Hence, we understood that both apoptosis and autophagy pathways are regulated by TIMP-1 through phosphorylation of a common upstream kinase, Akt and through this TIMP-1 helps to maintain cell viability even under Aβ toxicity.

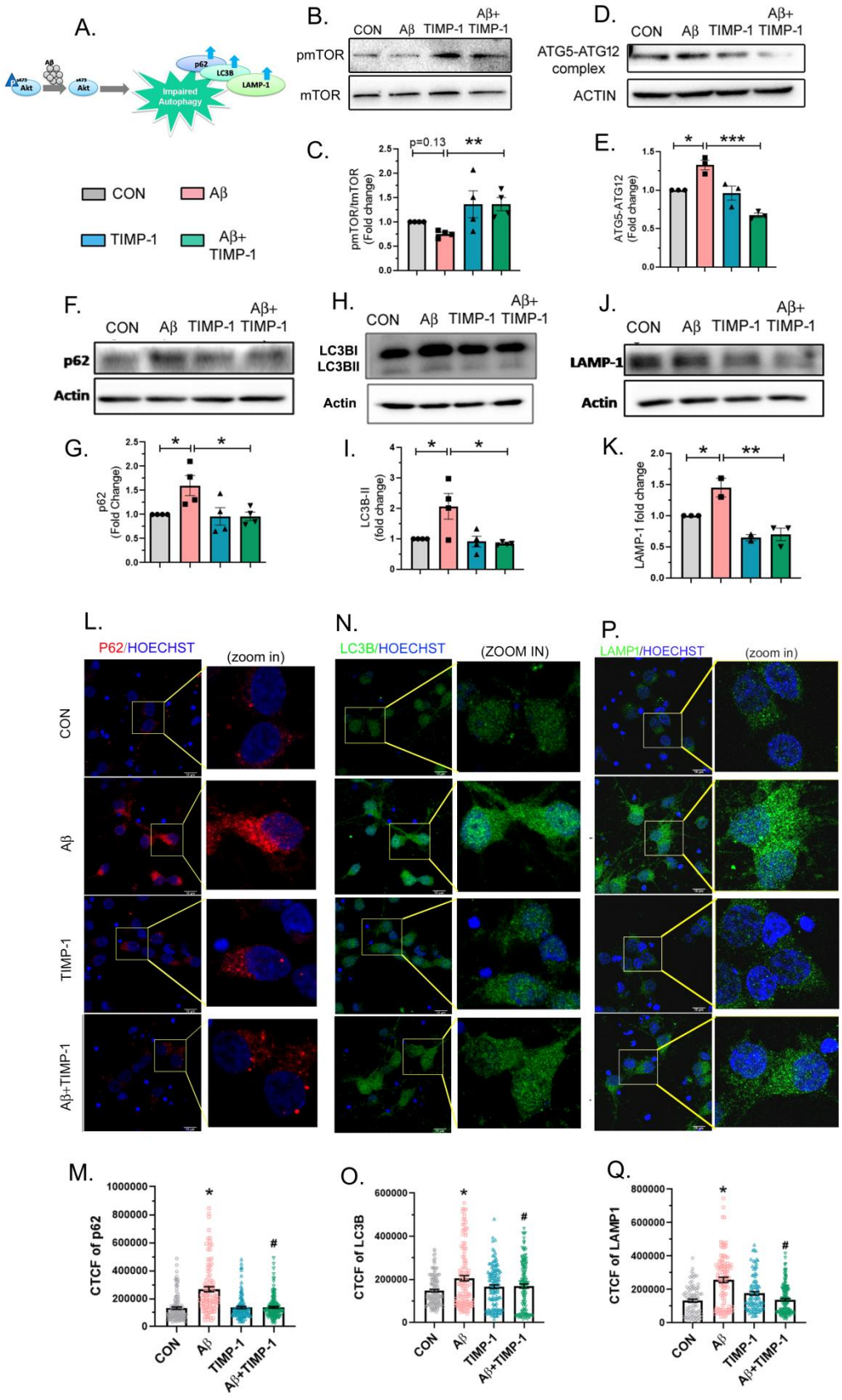
A.
Aβ
p-Akt
Akt
Impaired Autophagy
p62
LC3B
LAMP-1
CON
Aβ
TIMP-1
Aβ+ TIMP-1
B.
CON Aβ TIMP-1 Aβ+ TIMP-1
pmTOR
mTOR
C.
p=0.13
**
pmTOR/tmTOR (Fold change)
D.
CON Aβ TIMP-1 Aβ+ TIMP-1
ATG5-ATG12 complex
ACTIN
E.
*
***
ATG5-ATG12 (Fold change)
F.
CON Aβ TIMP-1 Aβ+ TIMP-1
p62
Actin
G.
*
*
p62 (Fold Change)
H.
CON Aβ TIMP-1 Aβ+ TIMP-1
LC3BI
LC3BII
Actin
I.
*
*
LC3B-II (fold change)
J.
CON Aβ TIMP-1 Aβ+ TIMP-1
LAMP-1
Actin
K.
*
**
LAMP-1 fold change
L.
P62/HOECHST
(zoom in)
CON
Aβ
TIMP-1
Aβ+TIMP-1
N.
LC3B/HOECHST
(ZOOM IN)
P.
LAMP1/HOECHST
(zoom in)
M.
CTCF of p62
CON Aβ TIMP-1 Aβ+TIMP-1
O.
CTCF of LC3B
CON Aβ TIMP-1 Aβ+TIMP-1
Q.
CTCF of LAMP1
CON Aβ TIMP-1 Aβ+TIMP-1

Fig.7: TIMP-1 addition ameliorates autophagy flux in Aβ-treated neurons. (A) Schematic showing Akt inactivation by Aβ is the cause of impaired autophagy flux in neurons. Primary cortical neurons were treated with Aβ, TIMP-1 and Aβ+TIMP-1 besides control and following 24 h of treatment cell lysates were collected and subjected to western blot assay. Representative blots along with individual blot loading control or actin are shown along with densitometric analysis of proteins – pmTOR/mTOR (B-C), ATG 5-12 complex (D-E), p62 (F-G), LC3B II (H-I) and LAMP1 (J-K). Bar graphs represent normalized densitometric analysis for each protein showing the fold change upon treatment with respect to control. Values are expressed as Mean+SEM. One way ANOVA followed by Tukey's post hoc test was used to compare among the groups, *$p<0.05$, **$p<0.01$, ***$p<0.001$. Immunocytochemistry was performed 24 h following treatment, cells were fixed and stained with p62 (red), LC3B (green) and LAMP1 (green) as indicated in the panels along with Hoechst for nuclei staining in blue. Confocal images were taken at 63x magnification (scale bar = 10 μm). A zoom-in panel has been shown for each protein to highlight the change in intensity within individual cell. Corresponding CTCF values were calculated from 90-150 cells from three independent experiments and represented as Mean±SEM. *$p<0.05$, compared to control (CON) #$p<0.05$, compared to Aβ

Exogenous TIMP-1 binds with CD63 on neuronal surfaces inducing Akt phosphorylation

TIMP-1 may mediate its pro-survival role by binding to CD63 receptor on cell surface as discussed earlier. To check whether CD63 binding is responsible for mediating TIMP-1 induced protection on Aβ-treated primary neurons, we conducted a co-localization study in primary cortical neurons treated with TIMP-1 compared to untreated primary cortical neurons and found that exogenously added rrTIMP-1 remains bound to CD63 receptor on the neuronal cell surface till 16h following treatmentas evident from the increased Pearson's correlation coefficient between TIMP-1 and CD63 (Fig. 7A-B). To further study the direct role of CD63 in TIMP-1 mediated signalling pathway, RNAi technology was utilized. CD63 was downregulated by adding siCD63 (commercially purchased – mentioned in methods section) at 100 nM to 4DIV primary cortical neurons for 72h and

the extent of downregulation was validated by western blot analysis (Fig. 7C). Following 48h of siCD63 treatment, the neurons were treated with or without TIMP-1 in the presence or absence of Aβ for another 24 h. Western blot analysis was done to check the changes in expression level of pAkt (s473) in each treatment groups where CD63 has been downregulated versus in those similarly treated groups where there was no prior CD63 downregulation (Fig 8D-E). It was observed that pAkt level, an important downstream target of CD63/integrin signalling (Grunwald et al., 2019), was significantly reduced upon Aβ treatment compared to control siCD63 treated neurons and the results were comparable to the change we observed between similar groups in normal control siRNA treated neurons. However, the pAkt level that was improved upon TIMP-1 treatment to Aβ treated group in control siRNA treated cells was absent in Aβ+TIMP-1 treated cells where CD63 receptor has been downregulated. This confirms that TIMP-1 not only binds to CD63 on neuronal surface but also is actively involved in mediating Akt activation implicated in TIMP-1 mediated protection to neurons against Aβ toxicity.

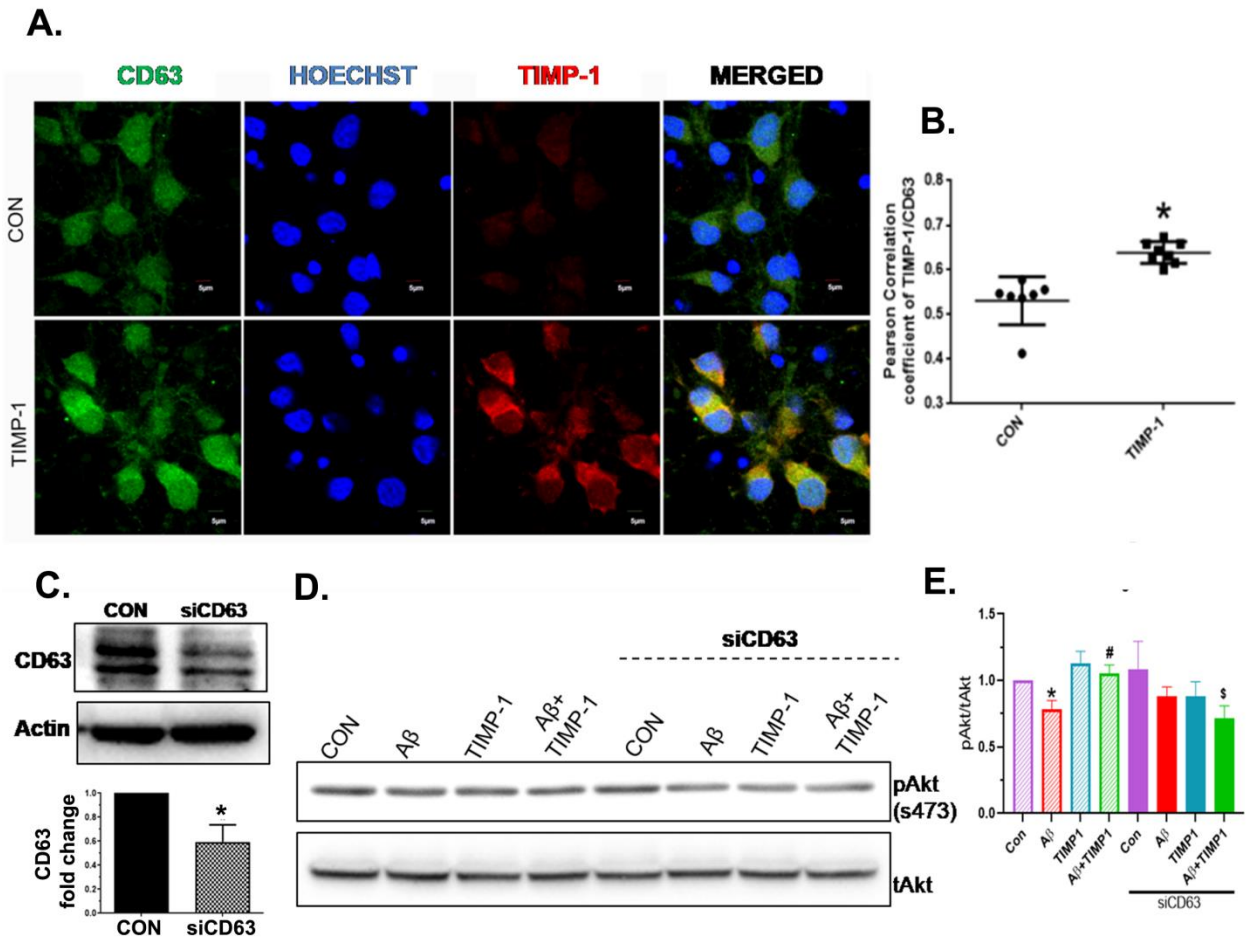

Fig.8: TIMP-1 binds to CD63 on neurons and improves Akt phosphorylation. (A) Primary cortical neurons (6DIV) were treated with or without TIMP-1 and then fixed after 16h following treatment. Cells were immunostained with CD63 (green) and TIMP-1 (red) antibodies followed by Hoechst (blue) for nuclear staining. Merged panel shows the co-localization between the two proteins in yellow. Images were taken in confocal microscope and scale bar is shown (5 μm). (B) Pearson correlation coefficient between TIMP-1 and CD63 were calculated from 2-3 images each from three independent experiments. Values are shown in scatter dot plot as Mean±SEM, unpaired t-test was performed, *p<0.0002. (C) Primary cortical neurons were either treated with siCD63 or siCON at 4DIV and after 72h cells lysates were collected and probed with CD63 antibody. Representative CD63 probed immunoblots are shown along with Actin, densitometric analysis is shown as a bar graph where values are expressed in Mean+SEM, unpaired t-test was performed, *p<0.0001. (D) Primary neurons were transfected with siCD63 on 4DIV and on 6DIV the cells were treated with or without Aβ, TIMP-1 or co-treated with Aβ+TIMP-1 alongside cells without CD63 downregulation but treated similarly. After 24h following treatment, cell lysates were blotted with pAkt (s473) and

total Akt (tAkt). Representative immunoblots are shown. (E) Bar graph represents densitometric quantification of pAkt blots normalized with tAkt and the fold change with respect to control is shown. Values are expressed in Mean+SEM, unpaired t-test was performed to compare between two groups at a time, *p=0.0034, compared to Con (without siCD63). #p=0.0211, compared to Aβ (without siCD63) and $p=0.0165, compared to Aβ+TIMP-1 (without siCD63).

Discussion

The scientific world has recently shifted their focus to the role of glia in neurodegenerative diseases. Astrocyte the most abundant of the glial cells takes the highest throne because it is now vital in the progression of neurodegenerative diseases besides their well-known indispensible homeostatic functions in the CNS (Arranz and De Strooper, 2019; Verkhratsky et al., 2017). Astrocyte reactivity is now seen as a first response to any kind of neurological insult. It may be defined as a set of molecular, functional, morphological and transcriptional change in the astrocytes in a very context specific manner. This phenomenon usually gives rise to a heterogeneous population of reactive astrocyte subtypes. Initially, Barres group classified reactive astrocytes into beneficial – A2 (ischemic stress) and detrimental – A1 (LPS treatment) subtypes (Liddelow and Barres, 2017). Now, the delineation of astrocyte subtypes in an inflammatory model in response to LPS treatment to the mouse brain provides critical insights into the location specific reactive astrocyte populations in this model (Hasel et al., 2021). Habib et al also detected DAA as the disease associated astrocyte subtype in AD (Habib et al., 2020). However, in AD we may broadly try to understand reactive astrocytes on the basis of their role in directing neuronal fate – neuroprotective or neurotoxic.

Previous reports suggest that astrocyte reactivity may indeed be a defensive mechanism against Aβ toxicity in the brain. Astrocyte reactivity was detected much before Aβ plaques accumulated in AD brain which may be seen as an early attempt by reactive astrocytes to nullify the Aβ insult (Wang et al., 2018). Indeed, inhibition of astrocyte reactivity propagated plaque pathology in AD models (Kraft et al., 2013). Further, Aβ are phagocytosed and degraded by reactive astrocytes (Wyss-Coray et al., 2003) and Aβ-loaded astrocytes were also detected surrounding Aβ plaques (Funato et al., 1998; Thal et al., 2000). However, several body of research also associate astrocyte reactivity with deleterious effect on neuron health (Furman et al., 2012; Garwood et al., 2011). Reactive astrocytes putatively protect neurons from Aβ toxicity by four mechanisms – by phagocytosing and degrading Aβ plaques (Xiao et al., 2014), by secreting Aβ degrading enzymes (Carter et al., 2019) and by forming glial scar and inhibiting the spread of Aβ to the healthy neurons (Pekny et al., 2014). However, a fourth highly complex mechanism is in play, orchestrated by several cytokines and chemokine molecules secreted by the reactive astrocytes, that dictates the fate of the neurons (Garwood et al., 2011). The identity of the cytokines has become a major area of research since it is hypothesized that specific cytokines may mediate the initial beneficial role of the astrocytes in the acute phase of neuroinflammation or in the prodromal stage of AD. Thus, they make up an exciting pool of therapeutic targets that may be possibly mimicked for cytokine-based therapy in AD. The reactive astrocytes may eventually with chronic activation of the disease or late-stage AD may become detrimental through secretion of pro-inflammatory cytokines. Hence, it was important to address the kinetics of astrocyte reactivity and

corresponding secretion profiles to understand the temporal changes in astrocyte phenotypes – neurotrophic to neurotoxic.

In our work, we first checked the temporal changes in mature primary astrocyte morphology and proliferation in response to Aβ treatment. We used four different astrocyte-specific markers and found that primary astrocytes become reactive as early as 6h following Aβ treatment in terms of increase in cell perimeter, proliferation and marker expression. The extent of reactivity increased from 6 h to 16 h to 24 h, at the latter there was long processes and highest marker expressions but the proliferation did not increase beyond 6h. In the control, the cell morphology and number remained unaltered. This result shows that proliferation is more of an immediate response to any pathological insult followed by observable changes in morphology.

Next we determined the role of Aβ-treated astrocytes from different time points on neuronal health. GFP expressing neurons were treated with astrocyte-conditioned medium from each time point – 6h, 16h and 24h and morphological changes were assessed at 24h and 48h while viability calculated at 24h. We observed that Aβ-ACM from all the time points protected the neurons till 48 h against Aβ toxicity when compared to those neurons treated with Aβ alone. ACM from the control astrocytes from each time point was unable to do the same. Moreover, the highest protection was elicited by the 6h Aβ-ACM (around 100%) compared to the viability seen with 16h Aβ-ACM (80%) and 24h Aβ-ACM (60%) and the decrease was gradual. This indicates that there is an enrichment of neuroprotective factors in 6h-Aβ ACM but a gradual reduction in their concentration over time or there may be a gradual secretion of other detrimental

factors. This is in coherence with earlier reports that show that acute exposure to a pathological insult may induce protective response yet the same insult if persists for a longer duration, making it chronic, can play a detrimental role (Van Eldik and Wainwright, 2003).

We next performed a cytokine array for 29 different cytokine molecules and found that TIMP-1 was one of the cytokines that was significantly enhanced in the 6h Aβ-ACM in comparison to ACM from untreated astrocytes. Moreover, its level subsequently decreased at the later time points. This is the first attempt in deciphering the secretome composition of Aβ-treated astrocytes as early as 6h as opposed to an earlier report where TIMP-1 was detected in Aβ-treated astrocyte secretome at 48h. Interestingly, the level of secreted TIMP-1 was not significantly altered at 48h between C and Aβ-ACM (Garwood et al., 2011).

Differential alterations in TIMP-1 level have been detected in primary human astrocytes and from CSF and tissue samples of HAND patients. In primary astrocyte culture, TIMP-1 level was found to be increased in response to pro-inflammatory IL-1β insult but in the advance-stage neurological samples, TIMP-1 level was found to be significantly reduced compared to healthy donors pointing towards a differential regulation of TIMP-1 in acute versus chronic disease activation (Gardner and Ghorpade, 2003). Hence, TIMP-1 may be a potential neuroprotective candidate since studies in TIMP-1 KO mouse reveals the positive role of TIMP-1 in learning and memory processes (Jourquin et al., 2005). In order to check whether TIMP-1 is essential for neuronal survival, we neutralized TIMP-1 from the 6h Aβ-ACM and transferred onto neurons. We found that there was significant

loss of cell viability upon TIMP-1 neutralization in Aβ-ACM and not in Control ACM, the latter may be because of the presence of other active neuroprotective molecules in Control ACM that replenish the loss of TIMP-1 under physiological condition. Hence, it may be concluded that TIMP-1 is essential for the survival of neurons at least at the early hours following Aβ exposure and poses as a neuroprotective molecule as reported earlier (Gardner and Ghorpade, 2003). Recombinant TIMP-1 rescues human neurons from the toxicity induced by staurosporine (Ashutosh et al., 2012). We found that co-treatment of TIMP-1 with Aβ on primary cortical neurons directly prevented them from Aβ-induced neurite loss and cell death. Earlier, TIMP-1 overexpression has proven to have a beneficial effect on neuronal health (Tejima et al., 2009).

Aβ is known to upregulate cell-death pathways namely apoptosis and autophagy. Aβ increases the translocation of FOXO3a to the nucleus and thereby increasing the transcription of pro-apoptotic proteins BIM (Sanphui and Biswas, 2013) and PUMA (Akhter et al., 2014). Additionally, BIM and PUMA cooperate and both are required for Aβ-induced death of neurons (Akhter et al., 2014). The upstream pathway that is compromised in this signaling is PI3K/Akt. Akt is the major protein kinase for FOXO3a phosphorylation and as a result FOXO3a is retained in the cytosol. Akt is also highly implicated in TIMP-1 mediated apoptotic regulation as previously reported (Grunwald et al., 2019). We found that TIMP-1 significantly improves the level of Akt phosphorylation at S473 even in the presence of Aβ when Aβ and TIMP-1 were co-treated to primary cortical neurons. Subsequently, pAkt upregulates FOXO3a phosphorylation in presence of TIMP-1 as opposed to Aβ only treated condition and prevents FOXO3a translocation

to the nucleus. As a result, we observed significant reductions in the protein levels of pro-apoptotic BIM and PUMA in TIMP-1 treated neurons when compared to treatment with Aβ alone. Thus, BIM and PUMA are that major apoptotic molecules activated by Aβ through Akt/FOXO3a axis and this pathway is inhibited by TIMP-1. Further cleaved caspase 3 and pH2Ax levels were also reduced upon TIMP-1 treatment to Aβ-treated cells. Both of which reaffirm our results that TIMP-1 prevents apoptotic cell death. Several reports suggest a delicate regulation between anti-apoptotic proteins Bcl2 and Bcl-xL upon treatment with TIMP-1. TIMP-1 regulates apoptosis in UT-7 erythroid cell line by activating JAK2/PI3K/Akt/Bcl2-associated death promoter pathway leading to the release of anti-apoptotic Bcl-xl (Lambert et al., 2003). Few other reports suggest the role of Bcl2 in TIMP-1 mediated pro-survival pathways (Guo et al., 2006; Li et al., 1999). Overexpression of Bcl2 leads to the upregulation of TIMP-1 in breast epithelial cells and hence prevents apoptosis and this is independent of TIMP-1's MMP-9 dependent activity (Li et al., 1999). While TIMP-1's suppression of apoptosis in lymphoma cells is correlated with enhanced expression of Bcl-xl and not Bcl2, another report suggests an upregulation of Bcl2 and not Bcl-xl following overexpression of TIMP-1 in lung adenocarcinoma cell line (Nalluri et al., 2015). Interestingly, both these anti-apoptotic protein levels are maintained upon TIMP-1 treatment against staurosporine toxicity in neuronal cells (Ashutosh et al., 2012). Thus, it seems interesting to observe how TIMP-1's regulation of these anti-apoptotic proteins varies under different circumstances – disease and disease stage. In our Aβ-treated cellular model, we found that Bcl2 level that was downregulated in the presence of Aβ, was stabilized in the presence of TIMP-1 but there was no significant change in Bcl-xl levels under the different treatment conditions. Thus, our

results reveal concomitant activation of Akt/FOXO3a pathway that reduce BIM and PUMA levels on one hand and induction of Bcl2 on the other hand in response to TIMP-1 treatment in Aβ-induced primary cortical neurons. Most likely these pathways cooperate to provide enhanced protection against Aβ.

Autophagy is a cell death pathway implicated in response of Aβ treatment to primary neurons as well as rat models of AD (Saleem and Biswas, 2017). Akt is a common upstream regulator of autophagy through PI3k/Akt/mTOR pathway. Aβ treatment to primary cortical neurons impaired autophagy flux such that upregulated levels of adaptor p62, central marker for detecting autophagy flux was observed. Increase in p62 puncta within the cell along with an increase in LC3B expression and an accumulation of lysosomal bodies detected with LAMP-1 indicated that although autophagy was induced but not completed upon Aβ treatment leading to the accumulation of these detrimental bodies within Aβ-treated neurons and our results were in accordance to earlier reports published by us and others (Saleem and Biswas, 2017). TIMP-1 treatment to these cells improved autophagic flux and hence expression levels of p62, LC3B and LAMP1 was found to be decreased. This indicates that Akt signalling induced by TIMP-1 can correct impaired autophagy flux observed with Aβ treatment to neurons. Thus, two parallel cell death pathways are regulated by TIMP-1 treatment to Aβ neurons.

While several evidence points to the fact that prevention of apoptosis by TIMP-1 mainly occurs in a MMP-9 independent manner, not much is known about the autophagy pathway. Importantly, CD63 has been identified to be responsible for TIMP-1 binding and inducing the downstream Akt signaling in many different cell types (Ries and Sastre,

2016). A recent review emphasises that presence of an excess of free or unbound TIMP-1, like in our system where TIMP-1 is added exogenously, mimicking the early stage response of astrocytes to Aβ, increases the chances of TIMP-1 binding to CD63 as opposed to its other MMP-inhibitory domain binding cell surface receptors to induce the downstream signalling pathways (Grunwald et al., 2019). Additionally, we did not observe any MMP-9/MMP-2 inhibitory activity in the different treatment groups of our cellular model (data not shown). In order to check whether TIMP-1 binds to CD63, we performed a co-localization study where we treated the neurons with recombinant TIMP-1 and then performed immunocytochemistry with CD63 and TIMP-1. As expected, we observed increased co-localization between TIMP-1 and CD63 in the TIMP-1 treated neurons versus the untreated ones on the cell surface. Further, we found that upon siRNA mediated inhibition of CD63 expression in neurons, phosphorylation of Akt was reduced significantly even in the TIMP-1 treated Aβ neurons and was almost comparable to Aβ only treated cells. This indicated that CD63 is the major binding partner of TIMP-1 and CD63 silencing directly impacts the TIMP-1 directed signalling pathway in Aβ-treated neurons. However, whether in our system TIMP-1 is acting completely in an MMP independent manner cannot be totally ruled out, it is not the focus of this work since we are hugely interested in the intracellular signalling pathways induced by TIMP-1 which many reports suggest is an MMP-independent activity.

PART II

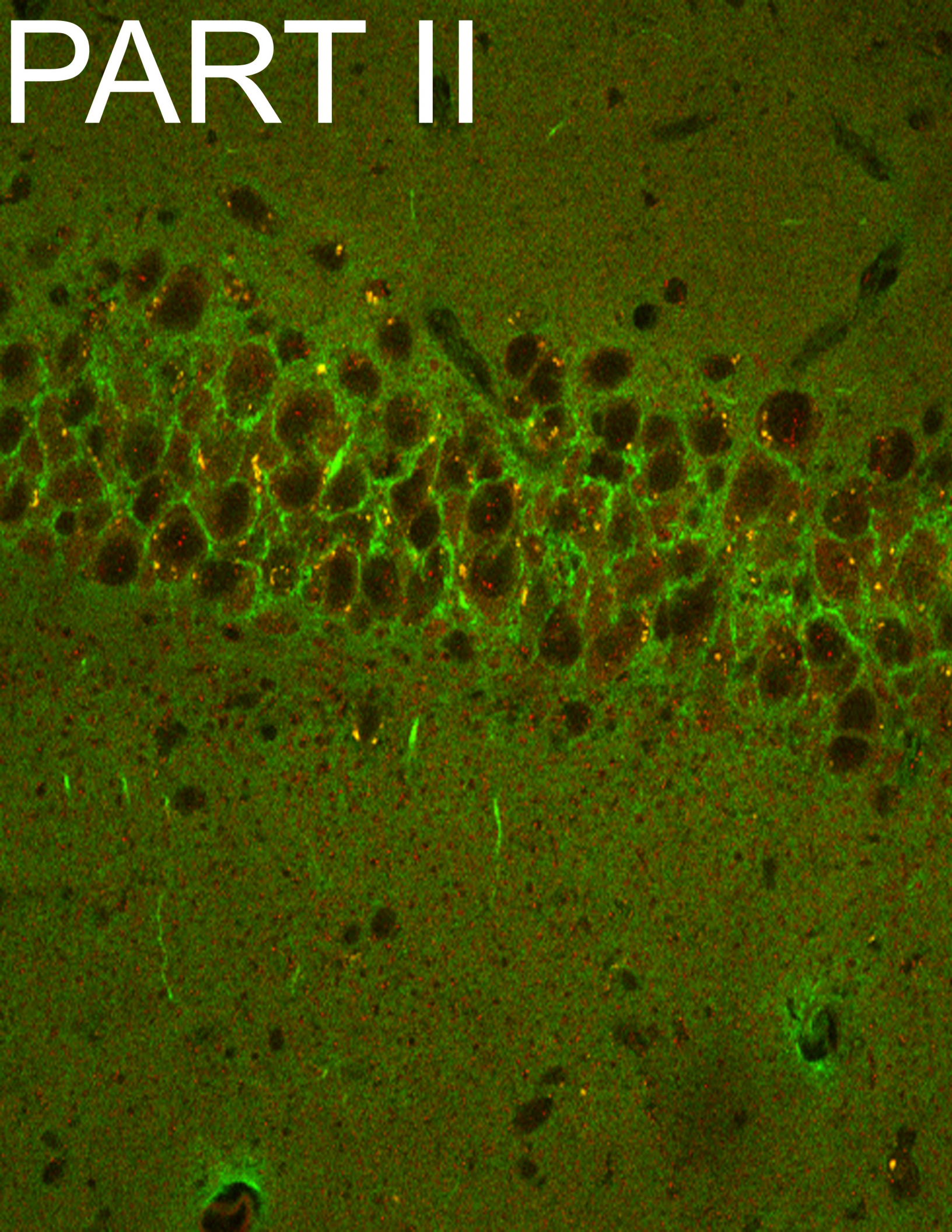

Part II: TIMP-1 ameliorates cognitive deficits in animal models of Alzheimer's disease (AD)

PART- II: TIMP-1 ameliorates cognitive deficits in animal models of Alzheimer's disease (AD)

In Part-I, we observed that TIMP-1 shows neuroprotective properties in an *in vitro* model of AD. So, we wanted to study its effect in rodent models ofAD. Animal studies in AD are essential in understanding the underpinning molecular mechanisms at play in the diseased condition. A complete rodent model should replicate the major hallmarks of AD including Aβ plaque deposits, neurofibrillary tangles, chronic inflammation and neuronal loss resulting in cognitive deficits. Hippocampus is the most sensitive area in AD and one of the earliest affected regions of the brain (O'Keefe and Dostrovsky, 1971). Prefibrillar forms of Aβ, along with its various soluble and insoluble forms, are regarded as the causative factor for learning and memory disruption (Walsh and Selkoe, 2004). Several groups across the world have targeted Aβ and numerous attempts have been made to reduce the unregulated levels of Aβ in AD therapy and have even proceeded to human clinical trials. An antibody based therapeutic drug named Aducanumab (BIIB037) was recently developed by Biogen. Aducanumab is an antibody which targets Aβ and has a possible role in its clearance (Alzheimer's News Today; https://alzheimersnewstoday.com/aducanumab/). Effect of Aducanumab includes a decline in Aβ plaque level by binding to neurotoxic oligomeric form of Aβ in the brain and improvement in cognitive performance in animal models of AD at the laboratory level. It moved into phase 3 clinical trials – EMERGE and ENGAGE. The EMERGE trial was successful in terms of its ability to improve cognitive functions and behaviors in MCI and mild AD patients while ENGAGE was not so as to say higher dose and longer

duration of antibody treatment was used to show positive outcomes in the participants. As of 2021, the use of Aducanumab has been given accelerated approval by US Food and Drug Administration (FDA) for marketing but has remained controversial to date (Cummings et al., 2021). This shows that reduction of Aβ may be a good way of predicting the neuroprotective potential of a candidate drug besides assessing the correlated changes in cognitive behavior and learning memory.

Intrahippocampal injection of Aβ in rodent brain is a well accepted animal model of AD. It is the most useful model for short-term study on AD-related changes in specific brain regions. This stereotaxic model provides the researchers with an alternate *in vivo* perspective to study AD (Facchinetti et al., 2018). The most important feature of a peptide injected rodent brain to be used as an AD model is the progressive loss of learning and memory activities as previously reviewed (McLarnon and Ryu, 2008). This model is also best suited to study inflammatory changes in an AD brain especially in terms of reactive astrogliosis as well as microglial activation. Concomitantly, several pro-inflammatory cytokines are secreted as a result of Aβ injection in the brain namely TNFα, ILβ etc. (Sipos et al., 2007). As we have already mentioned that the best assessment of a peptide-induced model is in the depreciation of cognitive functions of the rat to be suitably studied for therapeutic validation in AD. We conducted several learning and memory tests with the Aβ-infused rats and studied the influence of TIMP-1 on these animals' cognitive behaviors (see "Materials and Methods" for test details). Alongside neuroimaging, cognitive function tests are regarded as reliable and standard assessment systems to check the improvement in learning and memory functions in rodents

following drug treatment. For these experiments, freshly prepared Aβ was infused bilaterally into the hippocampus of rat. A battery of behavioral tests including open-field test (locomotion), NOR test, EPM test, passive avoidance test and fear conditioning tests were performed. Spatial learning and memory, working memory and fear memory are all affected by Aβ injection in the hippocampi of a rat brain and the above mentioned tests assess the loss of these hippocampus-dependent memories (Puzzo et al., 2014). Here in our study we have focused on analyzing the effect of TIMP-1 on the AD-related cognitive impairments seen in Aβ-infused rats besides deciphering TIMP-1's role in protecting neurons against apoptotic cell death, and its role in clearing Aβ deposits from the Aβ-infused rat brains. We went on to check the effect of TIMP-1 treatment in an advanced transgenic mouse model of AD that is 5xFAD. Genetically mutated mouse models are now recognized as critical tools to obtain a detailed insight into the role played by various therapeutic agents along the temporal scale of the disease. Additionally, they help in divulging the functionality of different active and inactive genes associated with AD. Several mouse models have been developed namely APP/PS1 by mutating the APP gene and the presinilin gene, 3xTg and the most advanced 5xFAD (Table 2 in 'Review of literature' section has been provided with the most common transgenic AD mouse models used for preclinical studies). Several other transgenic models include tau mutant mice (Kitazawa et al., 2012) as well as mice bearing mutations in ADAM10 and ADAM17 (Lee et al., 2003; Schroeder et al., 2009). In order to estimate the effective nature of a therapeutic strategy or to predict its success at the clinical level, delineating the molecular basis of the disease at the preclinical level is an imperative step. Hence, we attempt to divulge the main signaling pathway/s that is activated by TIMP-1

treatment to Aβ-infused rats and 5xFAD mice and the key players in this process mediating the neuroprotective functions of TIMP1.

Stereotactic Aβ injection in rat shows features of an inflammatory model of AD

In our study, we used stereotaxy to inject Aβ 1-42 oligomers bilaterally close to the hippocampal CA1 region in adult rat brains as mentioned in the "Materials and Methods" section. On day-23 following the Aβ injection, we found significantly increased levels of two important pro-inflammatory markers – Pro-IL-1β and NF-kβ through western blot analysis of the hippocampal tissue compared to control (PBS-infused) rat brain (Fig 1A-B, $p<0.01$). Additionally, we observed significant enhancement in astrocyte marker, GFAP, intensity (Fig 1C-D) as well as cell perimeter (Fig 1C, E) when compared to PBS infused hippocampal sections near the site of Aβ infusion through immunohistochemical studies. We further detected increased microglial activation quantified by the significantly increased number of CD11b (Fig. 1 F-G) and Cox-2 (Fig 1 H-I) positive cells in the Aβ-injected rat hippocampal regions near the site of injection compared to the PBS infused brain. We concluded that this model is well suited to study the neuroprotective properties of TIMP-1 to obtain an *in vivo* paradigm of cytokine-mediated therapy in AD.

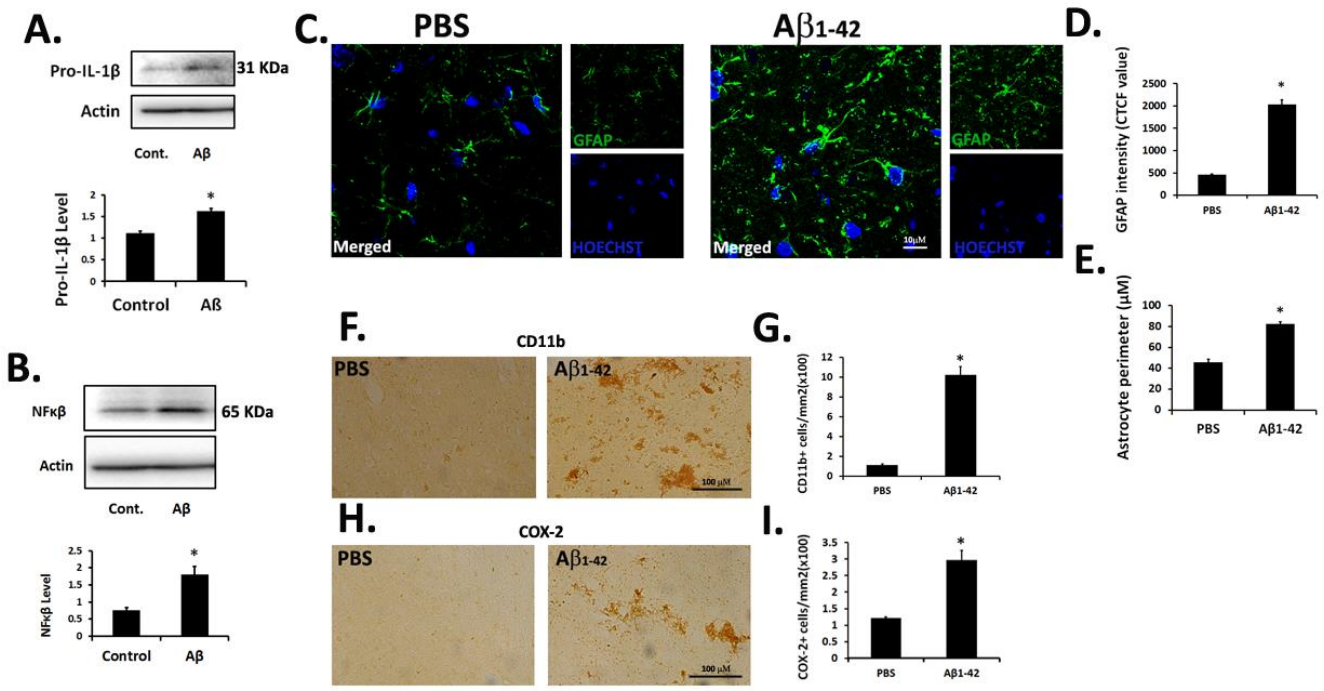

Fig.1: Aβ -injected rat displays neuroinflammatory hallmarks. 23 days following Aβ infusion, western blot analysis of hippocampal tissue from Aβ-infused rat brains showed significant upregulation of proinflammatory markers pro-IL-1β(A) and NF-kβ (B).Densitometric analysis by ImageJ software are expressed as Mean±SEM from three blots (n=3). *p<0.05. (C) Immunofluorescence studies in rat hippocampal coronal sections showincreased expression of astrocyte marker, GFAP, in Aβ infused rat brains compared to PBS-infused rats. scale bar=10 μm.Quantitative analyses reveal GFAP intensity in terms of CTCF values (D) and astrocyte morphology in terms of astrocyte perimeter (μm) (E). Immunohistochemical studies in rat hippocampus show increased expression of reactive microglia markers, CD11b (F) and COX-2 (H) in Aβ-injected rat brains vs. PBS-injected brain. Bar graphs represent quantitative analysis of the number of CD11b+ (G) and COX-2+ (I) cells/mm^2 respectively (n= 3 in both the groups, *p<0.05).

TIMP-1 reduces Aβ deposition and prevents apoptosis in Aβ-injected rat brains

We were next interested in studying the role of TIMP-1 on the major pathological hallmark of AD that is Aβ deposition and neuronal health. For this purpose we injected 5 ng of rrTIMP-1 intracerebroventricularly at 1ng/μl concentration. Immunohistochemistry

was performed in coronal sections through the hippocampus and stained with TIMP-1 antibody revealing generous spreading of TIMP-1 in the hippocampal and cortical regions as opposed to control rats in this method (Fig 2A). Aβ deposition was significantly increased in the hippocampal region in Aβ injected rats 23 days following infusion when compared to PBS infused rat brain through immunofluorescence studies. TIMP1 was able to decrease the Aβ deposition significantly as evident from the decrease in plaque number (Fig 2Bi-ii, $p<0.0001$) and plaque burden percentage (Fig 2Bi,iii, $p<0.0001$). Additionally, we detected an increased number of apoptotic cells in the Aβ-infused rats as opposed to PBS–injected rat brains through TUNEL assay in rat coronal sections (Fig 2Ci-ii). As evident from our *in vitro* studies, there is a reduction in apoptosis following TIMP-1 treatment in Aβ-treated neurons. Expectedly, we observed reduced numbers of TUNEL-positive cells in the TIMP-1 injected Aβ-infused rats in the hippocampal regions contrary to Aβ-only rats reinforcing our earlier results that TIMP-1 prevents apoptotic cell death in AD models (Fig 2Ci-ii). In Part-I we further showed that TIMP-1 can improve Akt phosphorylation even upon Aβ treatment to neurons. Hence, we wanted to check whether similar mechanism is in play *in vivo*. We found that indeed TIMP-1 injection improved phosphorylated Akt levels in Aβ-infused rat hippocampus compared to Aβ-only rats analyzed through western blot studies (Fig. 2D-E). Further downstream we found that levels of pro-apoptotic protein, BIM (Fig 2F-G), and also PARP cleavage (Fig 2 H-I, substrate of caspase 3) were reduced significantly in the TIMP-1 treated Aβ rat hippocampus denoting that TIMP-1 is acting along the Akt/BIM/caspase axis to prevent apoptosis in Aβ-injected rats.

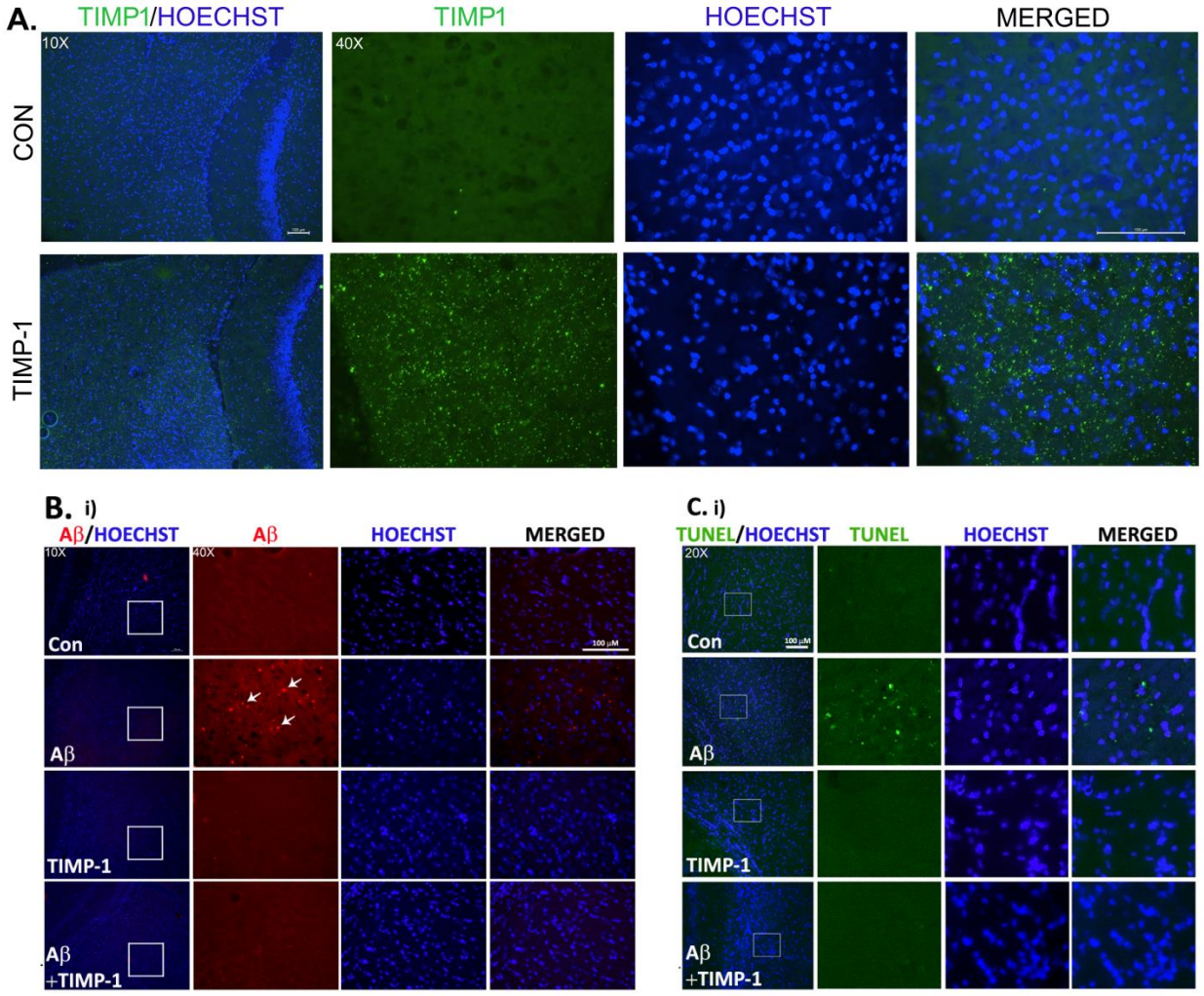
A.
TIMP1/HOECHST
TIMP1
HOECHST
MERGED
10X
40X
CON
TIMP-1
B. i)
Aβ/HOECHST
Aβ
HOECHST
MERGED
10X
40X
100 μM
Con
Aβ
TIMP-1
Aβ
+TIMP-1
C. i)
TUNEL/HOECHST
TUNEL
HOECHST
MERGED
20X
100 μM
Con
Aβ
TIMP-1
Aβ
+TIMP-1

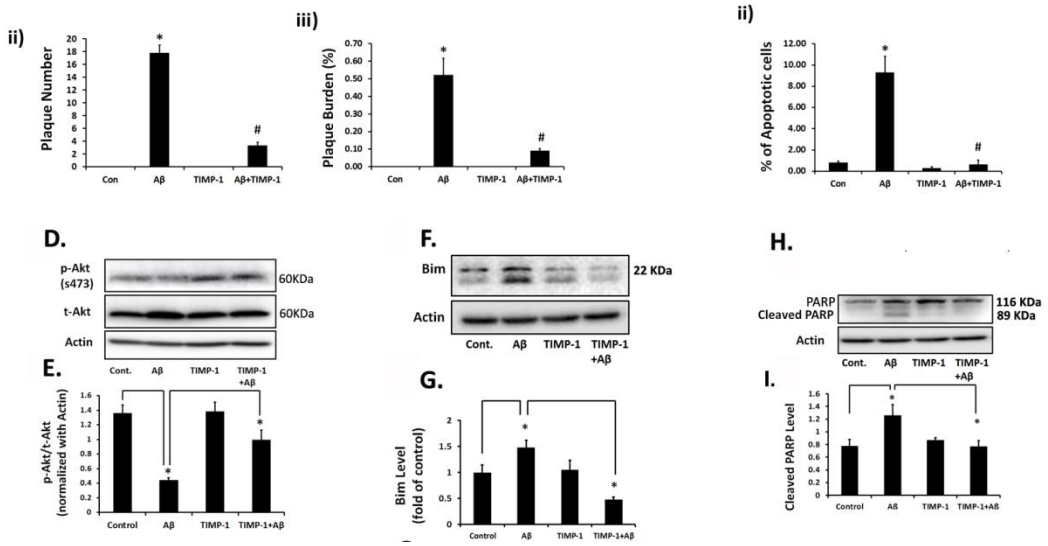

Fig.2: TIMP-1 induced neuroprotection and prevention of apoptosis in Aβ-infused rats.(A) 23 days following intracerebroventricular TIMP-1 injection, coronal sections through the hippocampus were obtained and stained with TIMP-1 antibody (green) followed by nuclei staining by hoechst (blue) and compared to untreated PBS-infused rats. Images were taken at 10x magnification (merged images are shown in left panel, scale bar – 100 um) and at 40x magnification (scale bar – 100 um).(Bi) Immunohistochemistry was performed with Aβ antibody (red) to detect Aβ 1-42 deposits in the Aβ-infused rat brains 23 days post infusion in the hippocampal and cortical regions near the site of infusion. TIMP-1 treatment was given at 5ng dose. Images were taken at 10x magnification (left panel, scale bar – 100 um). White box indicates region of interest near the site of infusion that was zoomed in to image the slices at 40x (scale bar – 100 um). White arrows indicate Aβ plaques at 40x magnification. The plaque number (ii) and plaque burden percentage (iii) are shown as bar graphs. (n = 3 for each group, 3 slices of each rat brain at 40x). *p < 0.0001,#p < 0.0001. (Ci) TUNEL assay in Aβ-infused coronal rat sections show the apoptotic cells (green puncta) colocalized with the nuclei (blue) imaged at 20x (left panel, scale bar – 100 um). White box indicates the region of interest chosen for zooming and magnified images are shown in the remaining panels - TIMP-1, Hoechst and merged (left to right). Percentage of apoptotic cells are counted and represented as bar graphs in (ii). Values are expressed as Mean+SEM (n = 3 in each group, 3 slices of each rat brain, 500 cells/slice at 20x); *p < 0.0001, #p < 0.0001. (*) indicates p-values in comparison to control group and (#) indicates p-values in comparison to Aβ group. Hippocampal tissues from the four groups were subjected to western blot analysis with phospho (s473) Akt, total Akt (tAkt) (D-E), BIM (F-G) and

PARP (H-I) antibodies. Following densitometric analyses by ImageJ, values are expressed as Mean+SEM of three independent experiments; *p < 0.01.

TIMP-1 reduces anxiety and enhances cognitive ability of Aβ-infused rat

After 15 days of Aβ infusion, we started behavioral tests since cognitive deficits were observed at this time, earlier shown by us (Guha et al., 2022). First we have performed open field test. This test is popularly known to assess locomotor activity and anxious behavior in rats. In the 10-min period of the test, the Aβ infused group displayed a significant increase in total distance travelled in an open field as compared to the values of vehicle infused control group (Fig. 3A). Groups of Aβ-infused rats administered with 2.5 ng and 5 ng of rrTIMP1 on the 7^{th} day following Aβ infusion showed reduced total distance travelled in open field compared to the Aβ group. However, only the 5 ng rrTIMP1 treated group delivered significant results (Fig. 3B; $p<0.01$). Hence, the Aβ induced hyperlocomotor activity of rat at an early testing period in an open field environment was corrected by 5 ng dose of rrTIMP1.

Next, we performed novel object recognition test. The novel object recognition test examines the hippocampus dependent working memory in rodents (Antunes and Biala, 2012). Novel object recognition memory was significantly impaired in animals 15 days post Aβ infusion in comparison to the control group denoted by reduced novel object exploration time compared to familiar object (Fig. 3C(i), decreased discrimination index (Fig 3C(ii) and reduced preference index (Fig. 3C(iii)). Aβ induced deficits were ameliorated with pronounced effect at 5 ng dose of rrTIMP1, depicting that rrTIMP1 may be effective in improving long-term recognition and learning memory. The lower dose

(2.5 ng) of rrTIMP1 was also improving the detrimental effect of Aβ but without any significant value. rrTIMP1 injection alone did not display any significant effect on the cognition of animals without Aβ infusions.

We have also performed elevated plus-maze (EPM) test which helps to estimate anxiety and changes in cognition in animal models (Paidi et al., 2022). In order to test for cognition, we placed the animal at the edge of the open arm and recorded the time taken by it to move into the closed arm. This time in seconds is known as the initial transfer latency or the ITL. On the probe day, we placed the animal on the outer edge of the open arm exactly similar to the previous day and recorded the time in seconds that the subject takes to move to the closed arm. This time period is known as the retention transfer latency or the RTL. In Fig 3D, latency is the time elapsed before the rodent moves from the open to the close arm in EPM. Aβ-infused rats showed a longer RTL than ITL which is in stark contrast to the other groups where RTL was significantly reduced compared to ITL. The difference between ITL and RTL (ITL-RTL) is utilized as the parameter to record memory and learning changes through EPM test. The Aβ-infused group produced a negative value for ITL-RTL as shown in (Fig. 3D). Interestingly, rrTIMP-1 treated Aβ-infused rats generated positive values for ITL-RTL and further divulged that only the higher dose was statistically significant compared to Aβ group.

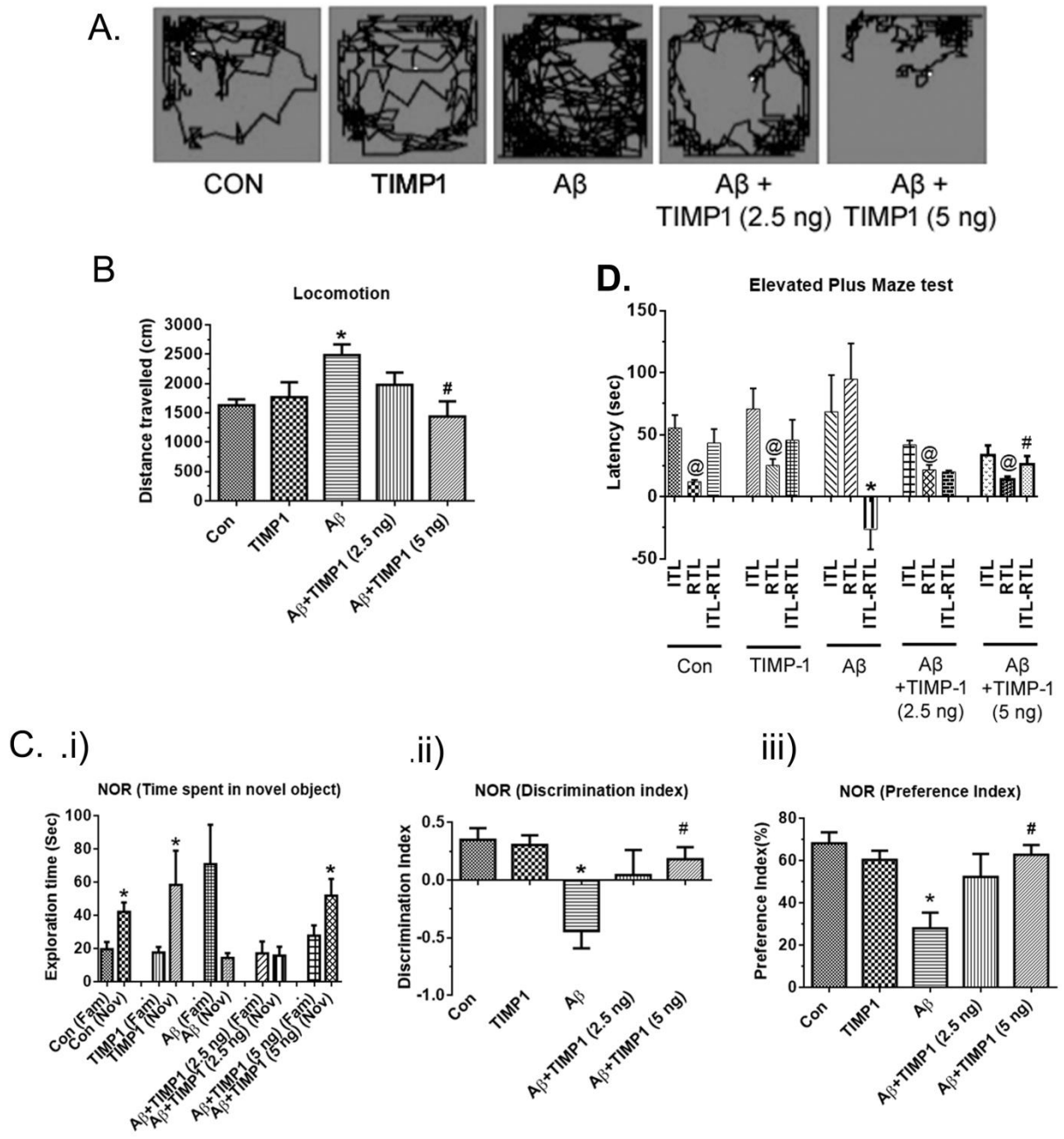

Fig.3: TIMP-1 improves cognitive functions of Aβ-infused rats. A battery of behavioral tests was performed in five groups of rats – PBS-infused (CON), TIMP-1 infused (TIMP-1), Aβ-infused (Aβ), Aβ+TIMP-1 (2.5 ng) and Aβ+TIMP-1 (5 ng). Locomotion or open-field test – representative infra-red images of the path travelled by the rats in each group (A) and the total distance travelled was recorded in cm in 10 min in the open arena. *p < 0.01, #p < 0.01. Novel object recognition (NOR) test – Day-2 results are shown as exploration time (sec) with familiar (fam) and novel (nov) objects (Ci, *p < 0.05),

discrimination index (Cii, *p < 0.05, #p < 0.05) and percentage preference index (Ciii, *p < 0.05, #p< 0.05). Elevated plus maze (EPM) test represents the latency (sec) that is the time taken by the rat to reach the closed arm recorded on Day-1 at initial transfer latency (ITL) and on Day-2 as retention transfer latency (RTL) and their difference (ITL-RTL), @p < 0.05,*p < 0.05, #p < 0.05 (D). All the bar graphs in this figure represent values expressed as Mean±SEM. (*) indicates p-values in comparison to control group and (#) indicates p-values in comparison to Aβ group, (@) indicates comparison between ITL and RTL within each group in EPM test. Number of animals used in each test is given in Table-2 in 'Materials & Methods' section.

TIMP-1 reverses learning and memory deficits in Aβ infused rats

The passive avoidance test is a fear-induced test used to understand learning and memory in rodent models of different central nervous system disorders. Passive avoidance test involves two chambers, one is brightly illuminated, and the other is dark. The chambers are connected to one another via a path through which animals can easily travel from one chamber to the other. On the acquisition day, we place the animals in the bright chamber. Rodents have an inherent tendency to go to dark areas. The machine is set in such a way that as soon as the subject enters the dark chamber, it receives a mild foot shock. So the subject immediately gets back to the bright chamber. On the probe day, we again place the subject in the bright chamber. Subjects would generally passively avoid the dark chamber due to their fear memory and choose to stay in the bright chamber without moving to the dark one, despite their natural preference for the dark chamber. This is a standard test for learning and memory. Passive avoidance evaluation of learning and memory showed that intrahippocampal Aβ infusion significantly alters the rate of acquisition learning compared to vehicle infused animals. Latency in Fig. 4A shows the time spent by individual animal in the light chamber prior to stepping into the dark

chamber during the 300 sec period following 5 min habituation. Fig. 4A(i) depicts the latency of the animal to step into the dark chamber of each group during acquisition training on Day 1. The probe test was carried out 24 h post training (Fig. 4A(ii)). In comparison to the control group, injection of Aβ significantly induced memory and learning deficiency in animals in passive avoidance test. Both the TIMP1-injected groups showed recovery in memory and learning performances, as portrayed through increased latency periods, especially in the 5ng TIMP-1 infused Aβ rats.

Contextual fear conditioning is an associative memory and learning task in which a response to an unconditional stimulus (foot shock) gets associated with a specific context. We measured the percentage freezing during that time period when the animals are anticipated to receive a foot shock. Freezing is a conditioned response to the unconditional stimulus that the subjects received on the acquisition day. Percentage freezing has a positive correlation with the retention in fear memory. Injection of Aβ induced detrimental effects on the acquisition of contextual fear conditioning, recorded 24 h later, shown as reduced percent value for freezing behavior (Fig 4B(i)). In this test, there was a dose-dependent recovery from Aβ-induced diminution in percentage of freezing by rrTIMP1. Animals infused with the higher dose (5 ng) of rrTIMP1 showed a significant increase in percent freezing but the recovery in percent freezing with the lower dose (2.5 ng) was not statistically significant from Aβ-infused rats. Animals injected with rrTIMP1 alone had no effect on contextual fear conditioning.

Cue-dependent fear conditioning test assesses memory and learning in animals responding to an unconditional stimulus (foot shock) associated with conditional stimuli

(light and sound). Impaired acquisition of cue-dependent fear conditioning training was evidenced 24 h following 1st day of acquisition. Aβ-infused rats displayed a marked diminution in percent freezing on the 2nd day of the test (probe stage) (Fig. 4B(ii)). Injection of rrTIMP1 in wild type rats did not induce any significant changes. However, upon injection of rrTIMP-1 in Aβ-infused rats, the animals displayed a dose-dependent recovery in percentage of freezing on Day-2; however, only the 5 ng dose showed statistical significance (Fig. 4B(ii)). Taken together, these results indicate that TIMP-1 reduces anxiety, confers improvement in cognition, learning and memory impaired by Aβ infusion in rats.

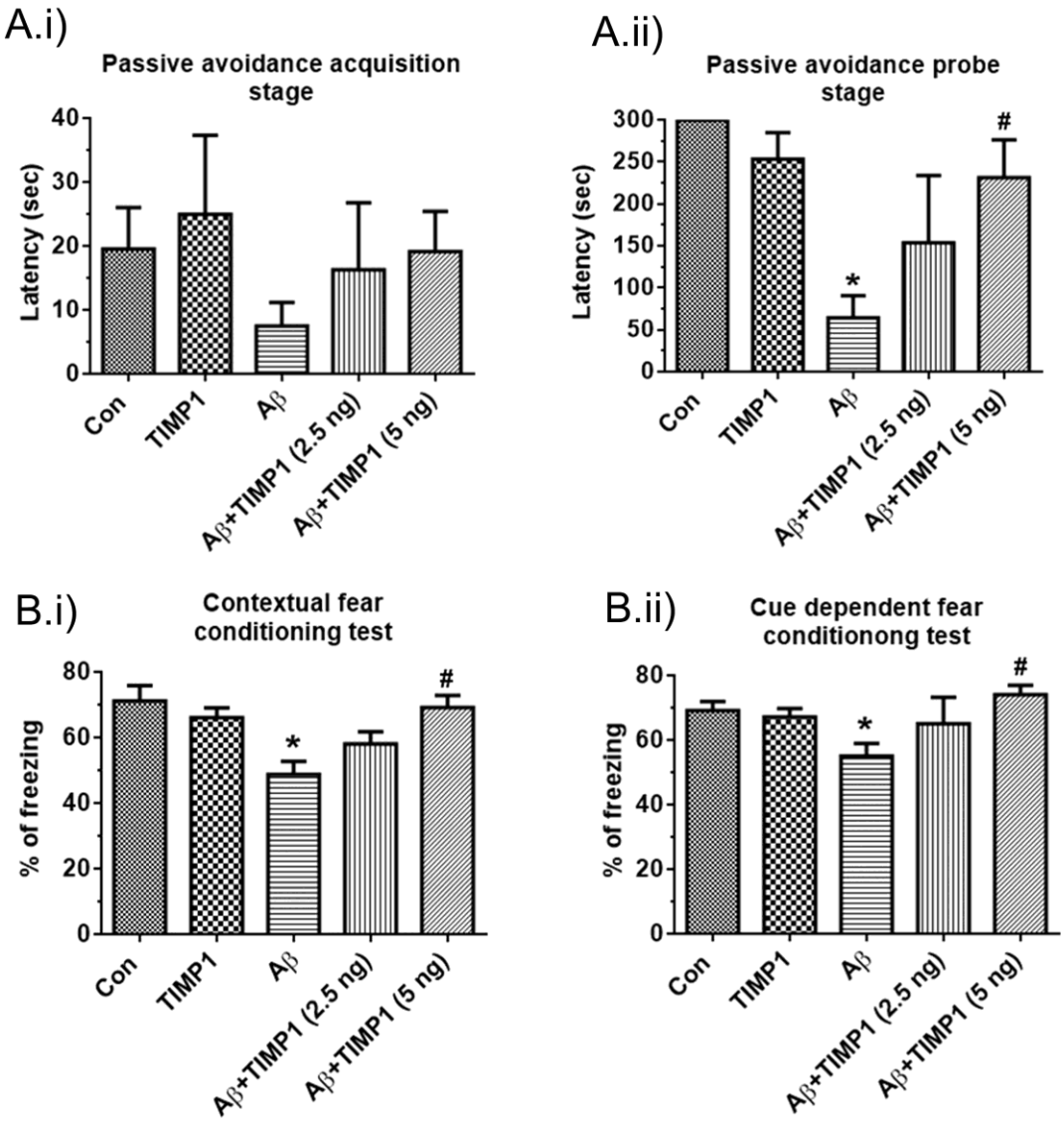

Fig.4: TIMP-1 ameliorates fear memory in Aβ -infused rats. Passive avoidance test shows the latency (sec) to the dark chamber on day-1 (acquisition stage, A.i) and on day-2 (probe stage, A.ii) of the test, *p<0.0001, #p<0.001. (Bi) Contextual fear conditioning test shows the percentage freezing time of rats in the different groups on Day-2 (probe stage) of the test, *p<0.005, #p<0.005. (Bii) Cue-dependent fear conditioning test shows the percentage freezing time of rats in the different groups on Day-2 (probe stage) of the test, *p< 0.05, #p< 0.01. In all the bar graphs in this figure, values are expressed as Mean±SEM. (*) indicates p-values compared to Control group and (#) indicates p-values compared to Aβ group.Number of animals used in each test is given in Table-2 in 'Materials & Methods' section.

TIMP-1 levels are reduced in 5xFAD mice across different age groups

We already showed that TIMP-1 was able to ameliorate the behavioral deficiencies of Aβ -injected rat model of AD. The Aβ-infused model gave us a significant estimate of the direct effect of TIMP-1 on Aβ-induced damages in the rat brain. However, the underlying mechanisms of AD pathogenesis extend way beyond just those observed as a direct effect of Aβ oligomers. Hence, we wanted to study the role of TIMP-1 in a more established and robust model of AD. 5xFAD is a familial AD mouse model with five different mutations (Table-2 in 'Review of literature') and is utilized as a benchmark model inapproximately 10% of all AD animal studies (AlzPED; https://alzped.nia.nih.gov/). 5xFAD mouse starts developing Aβ plaques as early as 2-4 months, inducing extensive reactive astrogliosis, microgliosis, synaptic and overall neuronal loss (Forner et al., 2021). Hence, we thought this model is a standard robust transgenic model to confirm our results from Aβ-induced rat model for better validation as well as we expected that this model would provide us a window to study additional features of AD pathogenesis. To begin with we first checked the levels of TIMP-1 (secreted form, 25 kDa) in the 5xFAD mice compared to C57/BL6 mice across different age groups to study TIMP-1 level across age.We detected TIMP-1 was markedly reduced in the hippocampal (Fig 5A-B) and cortical tissues (Fig 5C-D) in western blot analysis at 2 months and from 4–10 months compared to age-matched C57/BL6 mice as the wild type (WT) group. Moreover, the level of change in TIMP-1 was prominent (4 times reduced compared to WT) from 6 month onwards. Hence, all subsequent experiments were performed in 6-month-old 5xFAD mice. This was an interesting finding and hence, it meant that

intracerebroventricular injection of TIMP-1 in the 5xFAD mouse will uniquely help us to determine the changes directed by the exogenous TIMP-1 only without much contribution of the endogenous TIMP-1.

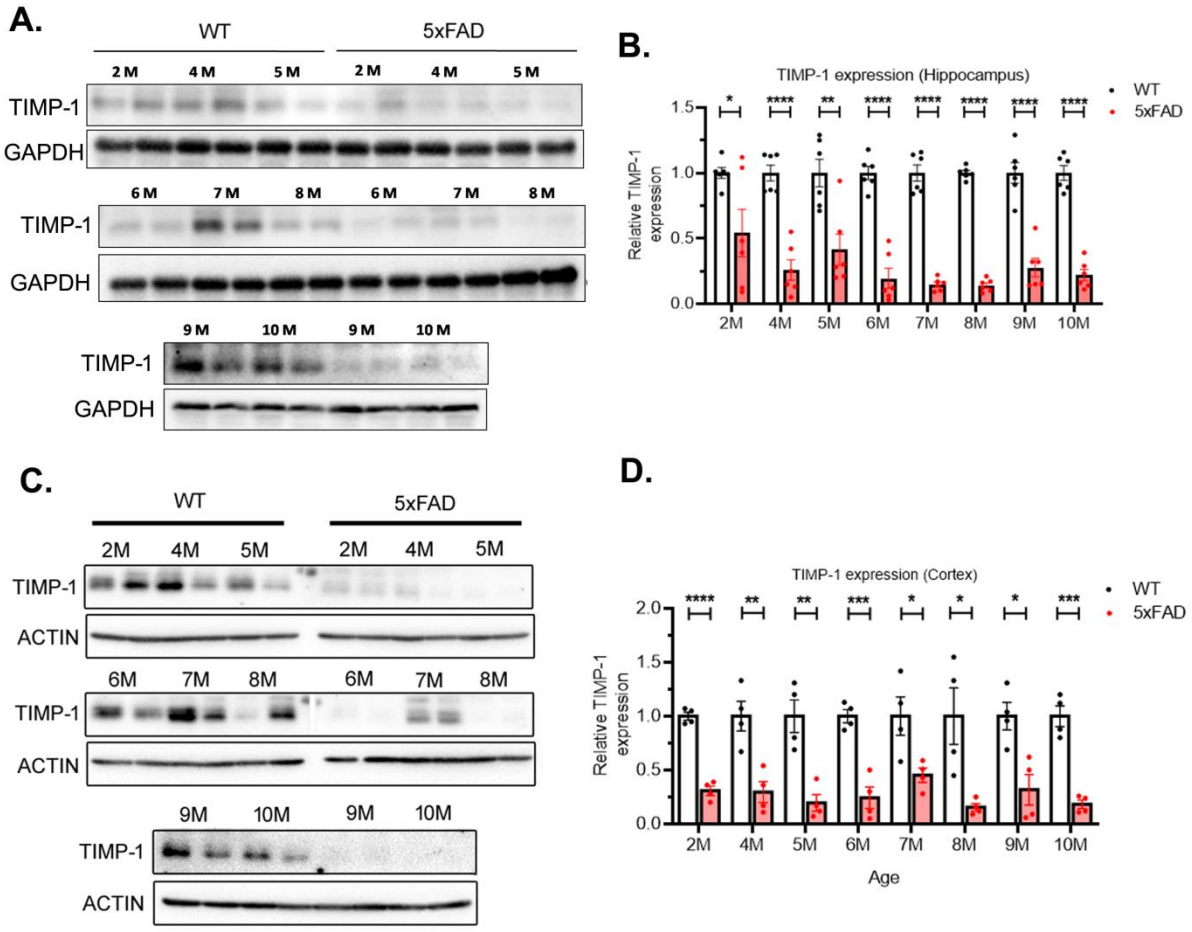

Fig.5: Expression of TIMP-1 across ages in 5xFAD mice. Whole tissue lysates were obtained from WT (C57BL6) and 5xFAD male mice hippocampi (A-B) and cortices (C-D) of different ages as indicated – 2 months (2M), 4M to 10M. Western blot analyses were done with TIMP-1 antibody using GAPDH or Actin as the loading control as indicated. Representative TIMP-1 blots from hippocampal (A) and cortex (C) whole tissues are shown where two consecutive lanes indicate protein levels in two different animals of each age group. Densitometric analysis are shown for hippocampal (B) and cortex (D) blots, showing relative TIMP-1 expression in each 5xFAD group vs. age-matched WT mice where WT protein expression is considered as 1.0.Results in graph are represented as Mean±SEM where *p<0.05, **p<0.01, ***p<0.001 and ****p<0.0001.

TIMP-1 injection clears Aβ plaques and prevents apoptosis in 5xFAD mice

We intracerebroventricularly injected TIMP-1 in 5xFAD mice and on the 8th day following treatment checked for the presence of TIMP-1 in the hippocampus since we have already found that in Aβ-infused rat model, effect of TIMP-1 was observed after 14 days following TIMP-1 treatment. We found through immunohistochemical analysis that TIMP-1 staining was significantly increased in the hippocampus of 5xFAD+TIMP-1 treated mice compared to untreated 5xFAD mice as shown by TIMP-1 count in Fig. 6 A-B.As previously performed, we first wanted to see the effect of TIMP-1 on Aβ plaque deposition in the hippocampal CA1 region of 5xFAD mice. For this we utilized coronal sections from mice sacrificed 14 days following treatment, in coherence to rat model timeline. We found that TIMP-1 treatment significantly reduced the plaque deposition in terms of plaque burden and plaque number in 5xFAD mice (Fig.6 C-E). Next, we checked whether apoptosis and the underlying apoptotic pathway are hampered in 5xFAD model. We performed TUNEL assay in coronal sections and found that there is a significant increment in the number of TUNEL positive cells in the hippocampal regions of 5xFAD mice compared to WT mice through immunohistochemistry. However, in TIMP-1 treated 5xFAD mice the number of TUNEL positive cells was significantly reduced (Fig. 6 F-G). Coherently, we detected decreased phosphorylation levels of Akt not only at ser473 (Fig 6 H-I) but also at thr308 (Fig 6 H, J) in 5xFAD mice compared to WT controls, both of these phosphorylations are strongly implicated in pro-survival pathway regulations, through western blot analysis. TIMP-1 was able to improve Akt phosphorylation levels in 5xFAD mice similar to the results we found in our earlier model. This reaffirms that even in 5xFAD, Akt is the upstream regulator of apoptosis.

Additionally, we checked for a downstream marker of apoptosis-related DNA damage that is phosphoH2Ax in TIMP-1 treated 5xFAD mice through western blot analysis and immunohistochemistry 14 days following treatment. We observed that TIMP-1 treatment abrogated the levels of pH2Ax in 5xFAD mice to a level comparable to WT mice in western blot analysis of hippocampal tissue (Fig. 6H, K) and immunohistrochemistry in hippocampal (Fig. 6L-M) and cortical areas (Fig. 6O-P).

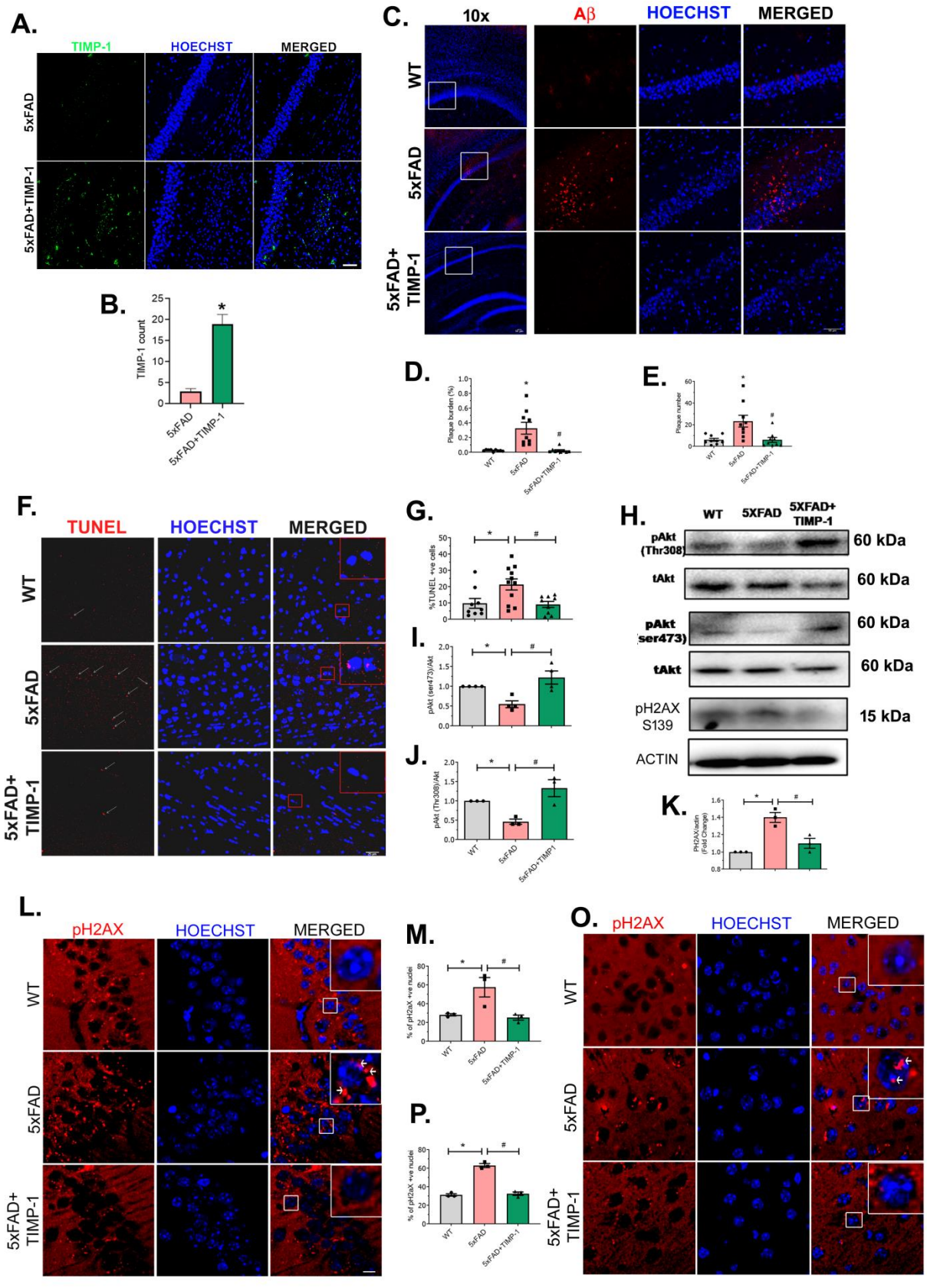
A.
TIMP-1
HOECHST
MERGED
5xFAD
5xFAD+TIMP-1
B.
TIMP-1 count
5xFAD
5xFAD+TIMP-1
C.
10x
Aβ
HOECHST
MERGED
WT
5xFAD
5xFAD+ TIMP-1
D.
Plaque burden (%)
E.
Plaque number
F.
TUNEL
HOECHST
MERGED
G.
%TUNEL +ve cells
H.
WT
5XFAD
5XFAD+ TIMP-1
pAkt (Thr308)
tAkt
pAkt ser473)
pH2AX S139
ACTIN
60 kDa
15 kDa
I.
J.
K.
L.
pH2AX
M.
% of pH2aX +ve nuclei
O.
P.

Fig.6: TIMP-1 injection in 5xFAD mice clears Aβ plaques and rescues from apoptosis. 14 days following intracerebroventricular TIMP-1 injection, animals were transcardially perfused and brains fixed. (A) Coronal sections were obtained from 5xFAD and TIMP-1 treated 5xFAD mice (5xFAD+TIMP-1) besides WT mice as indicated and stained with TIMP-1 antibody. Representative images were obtained in confocal microscope scale bar- 50 μm (B) Shows quantitative analysis for TIMP-1 immunoreactivity in the hippocampus shown as TIMP-1 count (n = 3 in each group, 3 slices of each mouse brain at 20x), *p<0.0001, compared to 5xFAD. (C) Immunohistochemistry was performed with Aβ antibody (red) to detect $A\beta_{1-42}$ deposits in the 5xFAD mouse brains in the hippocampal CA1 region. TIMP-1 treatment was given at 5 ng dose and observed 14 days post treatment. Images were taken at 10x magnification (left panel, scale bar – 50 μm). White box indicates region of interest in the CA1 region that were further imaged at 40x (scale bar – 50 μm). The plaque number (D, *p = 0.0054, #p = 0.0051) and plaque burden percentage (E, *p = 0.0004, #p = 0.0004) are shown as bar graphs. (n = 3 in each group, 3 slices of each mouse brain at 40x). (F) TUNEL assay in 5xFAD mice sections show the apoptotic cells (red puncta highlighted with white arrow) colocalized with the nuclei (blue) imaged at 40x (scale bar – 25 μm). Right panel shows the merged image where the red box demarcates the nuclei zoomed in for better viewing of the colocalization in the inset. (G) Percentage of TUNEL positive cells were calculated and values are expressed as Mean±SEM (n = 3 in each group, 3-4 slices of each mouse brain, 250 cells/slice at 20x); *p < 0.0231, #p < 0.0162. (H) Representative western blots show hippocampal tissue from each of the groups probed with pAkt (S473), pAkt (T308) and pH2Ax with the respective loading controls, either total Akt (tAkt) or actin, as indicated. Densitometric analyses for pAkt (s473)/tAkt (I, *p <0.05, #p <0.05), pAkt (t308)/tAkt (J,*p < 0.05, #p < 0.05) and pH2Ax (K, *p < 0.05, #p < 0.05) are shown. Values are expressed as Mean±SEM (n=3-4 animals per group). Immunohistochemistry of coronal sections of mice in 5xFAD group shows increased pH2ax puncta (red) colocalized with nuclei (blue) in the hippocampus (L) and in cortex (O). Images were taken under confocal microscope at 100x (scale bar- 10μm). White box shown in the merged panel demarcates a single nucleus zoomed for higher magnification viewing (inset). Quantitative analysis shows the % of pH2ax positive nuclei in hippocampus (M, *p = 0.0367, #p = 0.0246) and cortex (P, *p < 0.0001, #p < 0.0001), n=3 mice/group. (*) indicates p-values in comparison to WT group and (#) indicates p-values in comparison to 5xFAD group.

TIMP-1 treatment improves autophagy flux in 5xFAD mice

As shown through our *in vitro* results in Ch-1, TIMP-1 treatment corrects autophagy flux in Aβ -treated neurons and that Akt is the common upstream regulator by which TIMP-1 modulates both autophagy and apoptotic pathways. Since we found a protective role of TIMP-1 against apoptosis through Akt regulation in 5xFAD mice, we wanted to check what is happening to the other interconnected cell death pathway that is autophagy. We found that TIMP-1 was able to increase the inhibitory phosphorylation level of ULK-1 that prevents autophagy induction compared to untreated 5xFAD mice. In the latter, the level of pULK-1 was decreased compared to WT mice evident from immunohistochemical staining in the cortex (Fig 7 A, C) and hippocampal (Fig 7 B, D) slices indicating that autophagy induction is significantly higher in 5xFAD mouse brains compared to WT mice. However, we observed increased levels of p62 (Fig 7 E-H), LC3B (Fig 7 I-L) and LAMP1 (Fig 7 M-P) in the hippocampus and cortex of 5xFAD mice compared to WT mice indicating that although autophagy is induced more in 5xFAD mice compared to WT, the pathway is eventually impaired leading to the increased accumulation of autophagosomes and lysosomes in the transgenic mouse brain. TIMP-1 was able to ameliorate the level of these proteins in 5xFAD to the WT level indicating that TIMP-1 treatment improves autophagy flux.

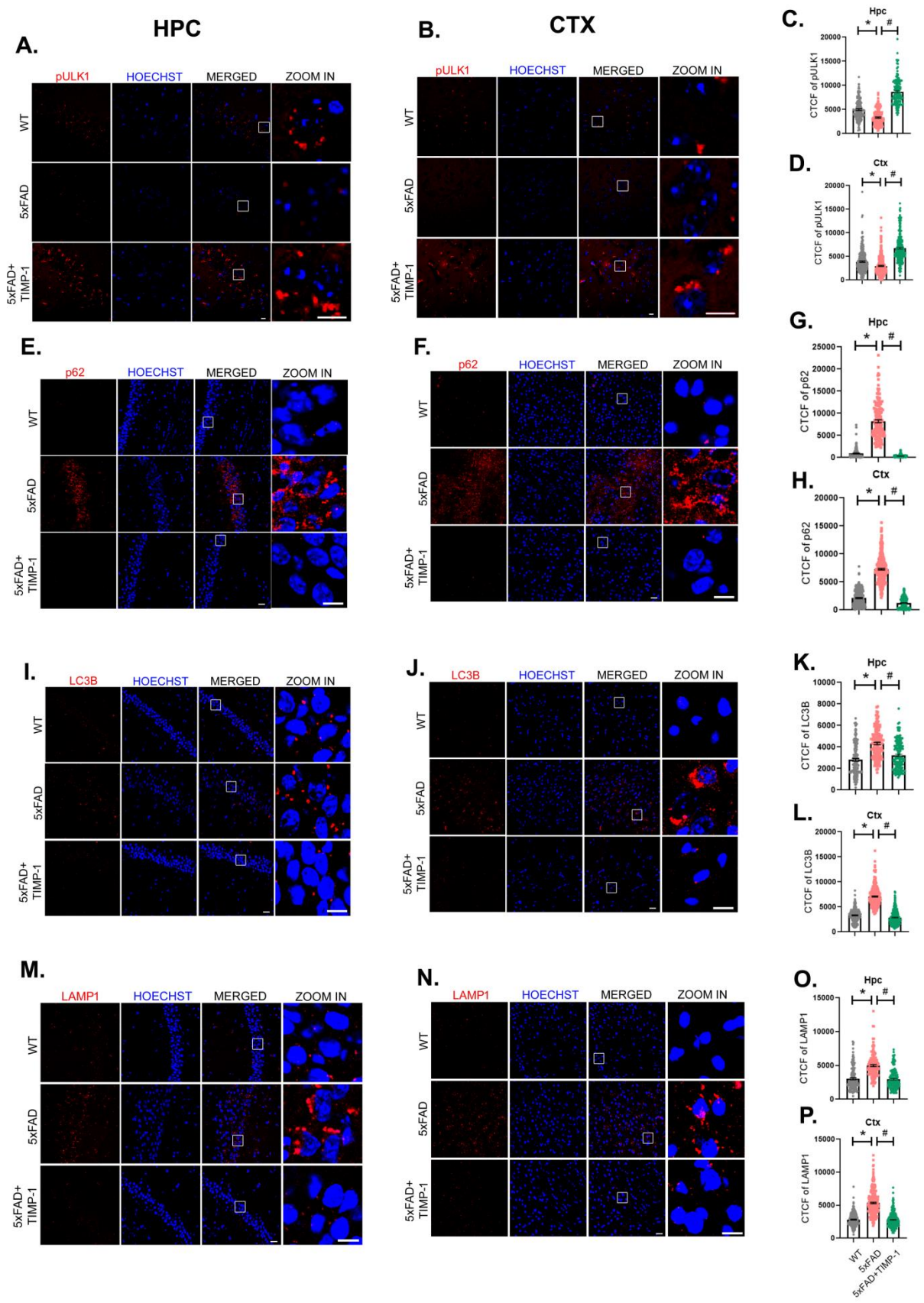
HPC
CTX
A.
B.
C.
D.
E.
F.
G.
H.
I.
J.
K.
L.
M.
N.
O.
P.
pULK1
p62
LC3B
LAMP1
HOECHST
MERGED
ZOOM IN
WT
5xFAD
5xFAD+ TIMP-1
Hpc
Ctx
CTCF of pULK1
CTCF of p62
CTCF of LC3B
CTCF of LAMP1

Fig.7: TIMP-1 injection in 5xFAD mice protects against impaired autophagy. 14 days following TIMP-1 injection, immunohistochemistry was performed in hippocampal and cortical slices and CTCF was calculated for pULK1 (A-D, Hpc*p < 0.0001, #p < 0.0001;Ctx*p < 0.0001, #p < 0.0001), p62 (E-H, Hpc*p < 0.0001, #p < 0.0001; Ctx*p < 0.0001, #p < 0.0001), LC3B (I-L, Hpc*p < 0.0001, #p < 0.0001; Ctx*p < 0.0001, #p < 0.0001) and LAMP1 (M-P, Hpc*p < 0.0001, #p < 0.0001; Ctx, *p < 0.0001, #p < 0.0001). n = 3 animals per group, 50 cells/animal from hippocampus (Hpc) and 100 cells/animal from cortex (Ctx) quantified from 40x images. Scale bar = 25 μm

TIMP-1 injection rescues cognitive deficits in 5xFAD mice

TIMP-1 was injected intracerebroventricularly by stereotaxic injection and behavioral tests were started on day-8 following injection as shown by the schematic in (Fig 8A). Initially, we performed locomotion test as it is useful to determine the exploratory activity in rodents. In the exploration time of 10 min, both the 5xFAD transgenic animals and aCSF infused 5xFAD mice travelled a longer distance (in cm) compared to the values of the WT animals. However, TIMP-1 treated 5xFAD mice exhibited a significant decline in the total distance travelled in the open field arena compared to 5xFAD mice (Fig 8. B-C).

Novel Object Recognition (NOR) test was used to estimate recognition memory of 5xFAD mice which is a hippocampus dependent memory, in comparison to WT mice (Fig 8D). On the first day (Acquisition stage), WT mice, 5xFAD, 5xFAD+aCSF and 5xFAD+TIMP-1 animals showed similar exploration time with the familiar objects (data not shown). On the second day, while WT mice spent more time with the novel object in the same NOR box, 5xFAD and 5xFAD+aCSF groups were unable to discriminate the novel object from the familiar one and spent almost equal time with both the objects. However, treatment with TIMP-1 ameliorated this deficit and the 5xFAD+TIMP-1 mice

spent markedly more time with the novel object in comparison to the familiar object (Fig 8E). This was further validated by calculating the discrimination index (DI, Fig. 8F) and preference index (PI, Fig. 8G) percentage.

In order to evaluate memory ability in EPM test, we recorded ITL and RTL of the different treated mice groups on day-1 and day-2 respectively. We further calculated ITL-RTL to show the difference in transfer latencies of each group between the two days. We found that 5xFAD showed longer RTL than ITL and 5xFAD+aCSF showed similar ITL and RTL. However, upon treatment with TIMP-1, 5xFAD mice had a shorter RTL than ITL similar to WT group indicating than TIMP-1 treatment was able to improve learning and memory significantly (Fig 8H-I).

Fear conditioning tests were performed to assess the fear memory related association between hippocampus and the amygdala. For fear conditioning test, we utilized two different test paradigms- context dependent fear conditioning and cue-based fear conditioning test. In contextual fear conditioning test, on day-1 (acquisition stage) all the groups of mice received four shock stimuli in a particular time interval. We calculated the mean of the percentage freezing in the four trials on day-2 of the test (probe stage) during the shock stimuli under the same context and found that freezing percentage were significantly reduced in the transgenic groups compared to the WT mice. TIMP-1 treatment significantly improved the percentage freezing level in 5xFAD mice (Fig 8J-K).

In cue-dependent fear conditioning test, mice were exposed to an unconditional stimulus (foot shock) associated with conditional stimuli (light and sound) on day-1 (Acquisition).

On day-2, the mice were exposed to the conditional stimuli only and freezing behavior was assessed (Probe stage). Percentage freezing was significantly reduced in the 5xFAD and 5xFAD+TIMP-1 mice groups compared to WT mice. TIMP-1 administration reversed the freezing percentage to a level comparable with the WT group. Hence, both these associative learning and memory functions were found to be impaired in the 5xFAD model of AD but were corrected significantly with TIMP-1 treatment (Fig 8L-M).

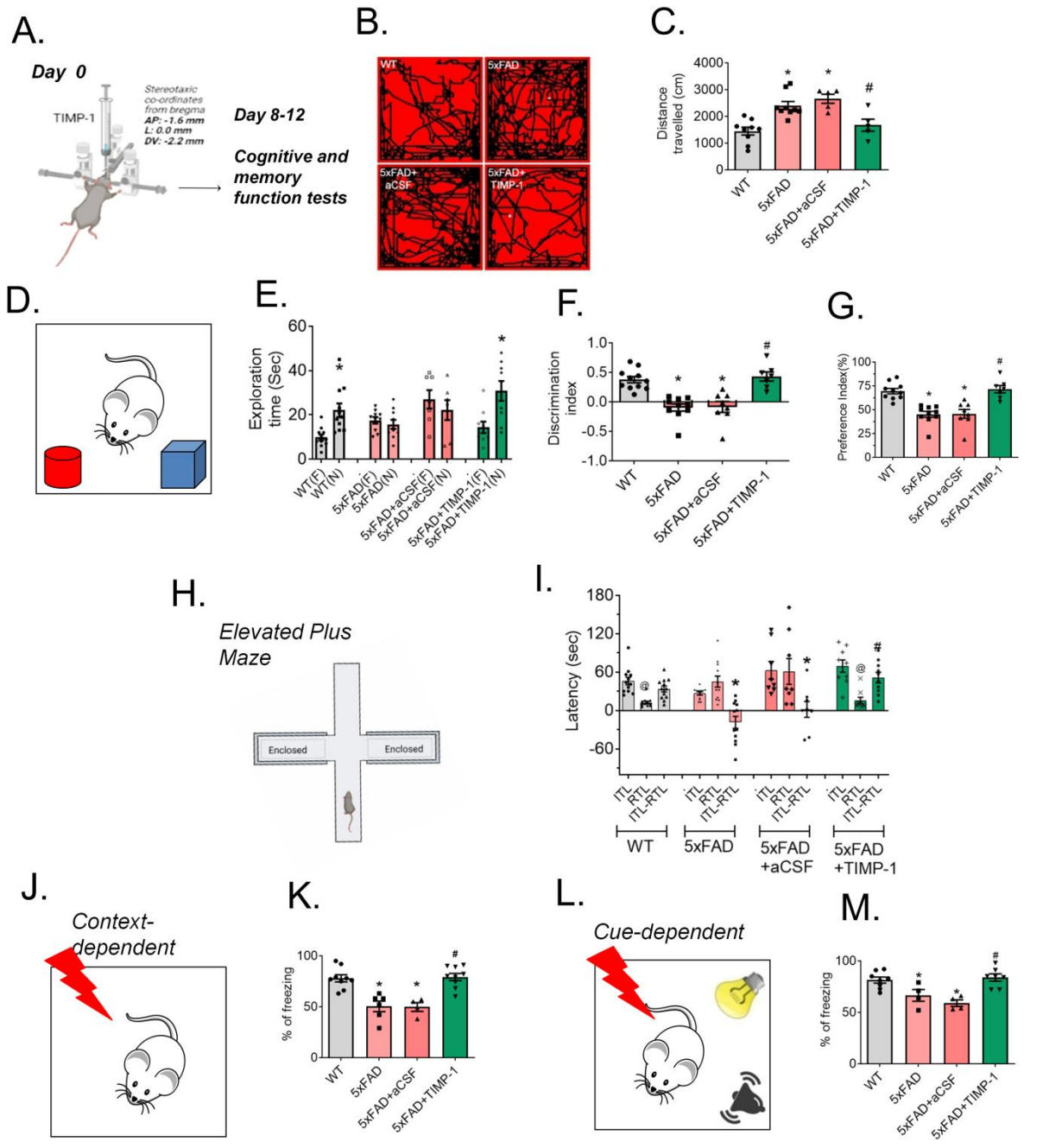

Fig.8: Cognitive deficits are corrected in 5xFAD mice following TIMP-1 treatment. A battery of behavioral tests was performed in four groups of mice – WT, 5xFAD, 5xFAD+aCSF and 5xFAD+TIMP-1 on day-8 following intracerebroventricular TIMP-1 infusion as shown by a schematic in (A). Locomotion or open-field test – representative infra-red images of the path travelled by mice in each group (B) and the total distance travelled was recorded in cm in 10 min in the open arena,*$p < 0.001$, #$p < 0.05$. (C). Novel object recognition (NOR) test – Schematic showing the day-2 scenario – with one

novel and one familiar object (D), results are shown as exploration time (sec) with familiar (F) and novel (N) objects within each group (E, *p < 0.01), discrimination index (F, *p < 0.0001, #p < 0.0001) and percentage preference index (G, *p < 0.0001, #p < 0.0001). Elevated plus maze (EPM) test, schematic shown in (H) represents the latency (sec) that is the time taken by the mouse to reach the closed arm recorded on day-1 at initial transfer latency (ITL) and on day-2 as retention transfer latency (RTL) and their difference (ITL-RTL), @p ≤ 0.0001,*p < 0.05, #p < 0.001 (I). (J) Shows the schematic and (K) the graphical representation of contextual fear conditioning test showing the percentage freezing time of mice in the different groups on day-2 (probe stage) of the test, *p<0.001, #p<0.001. (L) Shows the schematic and (M) the graphical representation of cue-dependent fear conditioning test shows the percentage freezing time of mice in the different groups on day-2 (probe stage) of the test, *p < 0.01, #p < 0.001. In all the bar graphs in this figure, values are expressed as Mean±SEM. (*) indicates p-values compared to WT group and (#) indicates p-values compared to 5xFAD group. No significant difference is observed between 5xFAD and 5xFAD+aCSF groups in all the behavioral tests. Number of animals used in each test is given in Table-3 in 'Materials & Methods' section.

Discussion

Reversal of memory deficits in AD patients has been a major challenge of clinicians and researchers worldwide. Various animal models have been implicated for this purpose at the preclinical level. The search for the most suitable animal model that replicates all the features of a human AD patient is incessant. Yet there are various suitable animal models available in the market now either peptide or chemical induced or genetic that mimics the essential hallmarks of AD serving specific purpose. We used two different animal models of AD – Aβ-infused rat and 5xFAD transgenic mouse. In the intrahippocampal Aβ-injected models, injected oligomeric Aβ serves as the toxic prion-like component spreading from the injected region to the surrounding regions of the brain (Katzmarski et al., 2020). Eventually, we observe that the Aβ-infused rats not only lose their

hippocampal dependent memory like recognition memory (NOR, EPM, Passive avoidance test), but shows additional complex memory deterioration where amygdala and prefrontal cortex are involved that is loss of fear memory acquisition (fear conditioning tests) as well as disinhibition behavior (hyperlocomotion and loss of thigmotaxis). Hence, we employ this model to study the short-term effects of TIMP-1 on the deficits directly induced by Aβ infusion. We found that TIMP-1 infusion restored learning and memory deficits of the Aβ-infused rats. Earlier reports show that reactive astrocytes may have a role in engulfing and clearing Aβ plaques and hence play a protective role (Wyss-Coray et al., 2003), however the exact molecular mechanisms remain elusive. We predict that secretion of TIMP-1 by the reactivated astrocytes in AD may be one mechanism of Aβ clearance from the AD brain. A report has earlier shown that TIMP-1 was able to reactivate the astrocytes and such reactivated astrocytes in the vicinity of Aβ-plaques in turn enhances the level of their MMPs that can degrade Aβ (Hernandez-Guillamon et al., 2009). Here, we show that TIMP-1 partakes in a neuroprotective role by clearing Aβ plaques from hippocampus and nearby cortical regions in the Aβ-infused rat brain. However, the exact mechanism by which TIMP-1 drives this clearance still needs to be divulged.

5xFAD mouse is one of the most advanced transgenic models of AD available to date. We found that endogenous TIMP-1 expression was significantly lower in the 5xFAD mice (hippocampus and cortex) across ages from as early as 2 months to 10 months when compared to the age-matched wild type mice. Moreover, the level of TIMP-1 was more than five-fold less than that of age-matched wild type from 6-month of age onwards.

This was an interesting data and although we did not calculate that reduction in TIMP-1 level in the 5xFAD mice specifically as a function of age, our result corroborated to some extent with an earlier report by Py et al. (Py et al., 2014). Although they have shown that in 5xFAD mice, TIMP-1 level increased progressively from 4 month to 6 month but its level reduces at 6 months with the initiation of neurodegeneration indicating that TIMP-1 may play a beneficial role in the prodromal stage of AD. A strong body of evidence by Ghorpade group shows that there is a biphasic regulation of TIMP-1 in response to acute vs. chronic inflammatory insults associated with HIV-related neurocognitive disorders (Gardner and Ghorpade, 2003). Their *in vitro* work in primary human astrocytes as well as *in vivo* results from HIV-1 transactivator of transcription (Tat) transgenic mouse model reveal that TIMP-1 is upregulated in response to an acute inflammatory stimulus but are reduced during chronic inflammatory insult (Joshi et al., 2020; Suryadevara et al., 2003). Coherently, they observed decreased levels of TIMP-1 from the CSF and brain tissue samples of HAND patients indicative of chronic neuroinflammation (Suryadevara et al., 2003). They hypothesize that secretion of TIMP-1 in response to acute inflammation is an attempt by the brain to protect and repair the neuronal damage due to the insult. However, in case of prolonged presence of the inflammatory insult, TIMP-1 mediated neuroprotective effect is lost due to the downregulation of TIMP-1 expression. They emphasize that the reduction in TIMP-1 protein level under chronic situation ultimately drives the neurons towards a detrimental fate. Additionally, they report that TIMP-1 secretion is exclusively mediated by the reactive astrocytes; this is consistent with our results in Part-I where we show that TIMP-1 is being released by reactive astrocytes while responding to Aβ treatment *in vitro*.

However, there are some contradictory reports. In APP/PS1 transgenic AD mice, MMP-2 and MMP-9 reportedly help in the degradation of Aβ plaques and the function of these proteases are inhibited by TIMP-1 treatment (Yin et al., 2006). Seizure mediated loss of neurons are restored in the hippocampus in a TIMP-1 KO model and is dependent on the MMP-inhibitory role of TIMP-1. Interestingly, these TIMP-1 KO mice also showed severe deterioration in learning and memory functions which are in coherence with our results (Jourquin et al., 2005). Moreover, utility of the 5xFAD model in our study to test the effect of exogenous TIMP-1 on cognitive behaviors and signaling pathway becomes magnanimously specific due to the low endogenous expression level of TIMP-1 in 5xFAD mice compared to WT. Hence, whatever effects we are observing in the 5xFAD mice is a direct effect of the exogenous TIMP-1 alone without much contribution of the endogenous TIMP-1.

We also enquired about the underpinning mechanisms at play by which TIMP-1 mediates its neuroprotective functions in these models of AD. Taking cue from our *in vitro* results, we found that indeed TIMP-1 was responsible for preventing apoptotic cell death by activating Akt *in vivo* leading to the downregulation of downstream apoptotic markers such as BIM, PARP cleavage and pH2Ax. Akt is implicated in the protection of neurons in AD models as reported by our group and others (Bommarito et al., 2011). TIMP-1 has been shown to prevent apoptosis in different models across different diseases and is responsible for upregulating various signaling pathways namely FAK, MAPK and PI3K/Akt pathways (Jung et al., 2006; Song et al., 2016). However, TIMP-1 mediated recovery in apoptosis was observed in the hippocampal tissue but not in the cortices in

western blot assay while in immunohistochemical study pH2Ax levels were downregulated in 5xFAD mice by TIMP-1 both in the hippocampal and cortical areas. This discrepancy may be because super resolution immunofluorescence studies are more sensitive and help in detection of even small level changes in the protein expression across different and specific brain regions while in western blot change in specific protein expression across groups should be at a particular threshold level to be detected by this method significantly. We hypothesize that may be changes in the signaling is not significantly altered in the cortices in response to TIMP-1 as in the hippocampi of 5xFAD mice and hence we are unable to observe any significant difference in the whole cortex level. Earlier report suggests that following birth TIMP-1 is majorly expressed by hippocampal pyramidal cells and cerebellar granule cells (Fager and Jaworski, 2000). We observed that TIMP-1 corrected impaired autophagy flux in our both *in vitro* and *in vivo* models. Interestingly Akt seems to be the common upstream mediator of both apoptosis and autophagy regulation by TIMP-1 in 5xFAD since Akt/mTOR pathway has been previously shown to be involved in autophagy dysregulation in 5xFAD mice (Saha et al., 2021).

Thus our results indicate that TIMP-1 can be used as a cytokine based therapy in AD in coherence to other cytokines that are reportedly neuroprotective *in vivo* namely ICAM-1, TGFβ, IL-10, IFN-β, IL-33 and G-CSF (Table-1 in 'Review of literature'). TIMP-1 not only rescues AD-related cognitive deficits in both the models of AD but also promotes neuronal survival by regulating both apoptosis and autophagy pathways through common upstream regulator Akt.

PART III

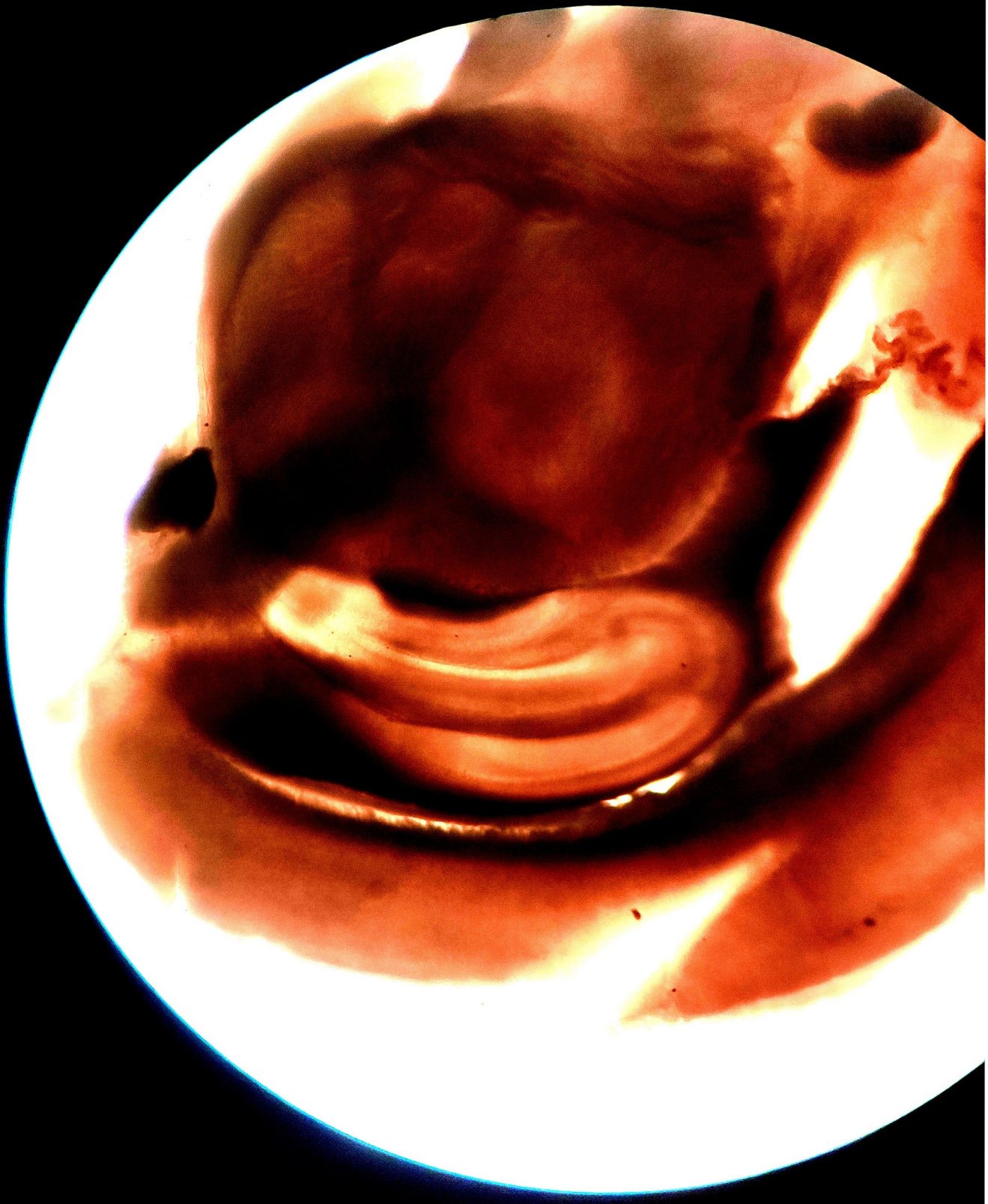

Part III: TIMP-1 on synaptic plasticity in AD: deciphering underpinning mechanisms of cognitive recovery

PART- III: TIMP-1 on synaptic plasticity in AD: deciphering underpinning mechanisms of cognitive recovery

Synaptic plasticity, defined as the activity-dependent changes in the strength of synaptic connections in-between neurons, forms the basis of memory storage in the brain (Singh and Abraham, 2017). Similar to numerous other physiological supports provided by the astrocytes to neurons, their role is undeniable in regulating synaptic transmission and synaptic plasticity (Garwood et al., 2017). The tripartite synapse, a term coined around 20 years ago (Araque et al., 1999), is used to define the close proximity between the pre- and post-synaptic neuronal processes to the astrocytic elements (Auld and Robitaille, 2003). This close positioning enables the astrocyte to interact with the neurons through a plethora of gliotransmitters and other neuro-active molecules across the synapse mediating synaptic communication and memory formation in the brain. Neurotransmitters are released from the pre-synaptic cleft triggering metabotropic or ionotropic receptors on the astrocyte surface (Garwood et al., 2017). In response, there is a transient elevation in calcium levels within the astrocytes which is dependent on the intensity of external signal. For example, upregulation in astrocytic Ca^{2+} levels has been reported upon activation of pyramidal neurons in hippocampus through the stimulation of metabotropic glutamate receptor on the astrocyte surface (Porter and McCarthy, 1996). The astrocytes, in turn, release a plethora of gliotransmitters such as glutamate, GABA, D-serine, ATP etc. which have the ability to influence synaptic plasticity by modifying long-term potentiation (LTP) and long-term depression (LTD) (Singh and Abraham, 2017). LTP is associated with generation of new dendritic spines, enhancement

of post-synaptic densities and spine head enlargement of neurons, all of which are markers of a healthy synapse. LTD, on the other hand, is associated with spine shrinkage as well as spine loss leading to weakening of synapses. LTP and LTD are thus considered experimental indicators of synaptic plasticity. Thus, it can be inferred that this bidirectional astrocyte-neuron communication demonstrates the active participation of astrocytes in memory formation (Gibbs et al., 2008; Zorec et al., 2015). Additionally, astrocytes also modulate synaptic signaling by efficient removal of inhibitory and excitatory neurotransmitters, released in the synaptic cleft, via specialized astrocytic transporters. The rate of clearance of the neurotransmitters maneuvers the extent of post-synaptic activation (Garwood et al., 2017). Thus, both release and uptake of neurotransmitters can modulate the synaptic activity and a single synaptic firing can be quickly communicated to neighboring astrocyte-neuron network. Astrocytes also secrete several cytokines that modulate synaptic plasticity in brain under normal physiological situation. For example, TNF-α can induce either membrane internalization or insertion of AMPA receptor subunits at the excitatory synapses depending on the activity involved (Habbas et al., 2015). TNF-α is also involved in synaptic scaling, defined as a coordinated modulation of a population of synapses to adjust their strength in accordance to long-term alterations in network activity. Additionally, it can also regulate astrocytic glutamate release and thus indirectly influence synaptic activity. Similarly, other cytokines from astrocytes such as IL-6, IL-2, IL-1β, IL-10, IFN-γ and IFN-α are involved in modulating synaptic plasticity (Singh and Abraham, 2017).

Astrocytes, as described, being a major contributor in maintaining synaptic plasticity plays a crucial role in maneuvering synaptic dysfunction and loss in AD. Synaptic dysfunction is

an early event in AD that proceeds towards memory dysfunction. Synaptic scaling as well as both LTP and LTD are perturbed in various animal models of AD (Cheng et al., 2009; Rowan et al., 2014; Selkoe, 2008). Reactive astrocytes in AD secrete several factors that can influence synaptic plasticity. GABA secreted by reactive astrocytes prevents excitatory neurotransmission and further prevents LTP induction. By inhibiting GABA release from reactive astrocytes in AD, several AD-related cognitive deficits are ameliorated (Acosta et al., 2017). On the other hand, ATP is also released by Aβ treatment to astrocytes that protects neurons from Aβ-triggered dysfunction in LTP in vitro (Jung et al., 2012). Thus, this mechanism may be one of the defensive weapons employed by the cells to protect synaptic damage and further prevent memory impairment. However, cytokines like TNF-α are robustly released from reactivated astrocytes in response to Aβ (Johnstone et al., 1999) and when TNF-α induction was silenced, it reduced Aβ-dependent suppression of LTP (Wang et al., 2005) and cognitive deficits (Alkam et al., 2008). Furthermore in advanced stages of AD, reactive astrocytes also profusely secrete pro-inflammatory cytokines including IL-1β, IL-6, IFN-γ etc. (Benzing et al., 1999; McGeer and McGeer, 2010) that are capable of inhibiting LTP (Singh and Abraham, 2017). Thus, we found evidence in literature that there are both good and bad factors that are released by reactive astrocytes in AD that can modulate synaptic health, LTP/LTD ratio and finally underlie the changes we observe in terms of cognitive behaviors. So, in Part-III we address the mechanisms underpinning the recovery in learning and memory we observed by TIMP-1 injection in 5xFAD mice in Part-II. Progressive changes in synaptic structure and functions often precede the actual neuronal loss and finally memory deficits that we

observe in AD. Thus, we focus our research on delineating the changes at the synaptic level from biochemical and electrophysiological perspectives.

Results

TIMP-1 improves synaptic health in both Aβ-infused rat brain and 5xFAD mice

In AD, loss of synaptic efficacy especially in the hippocampus may be seen as the earliest and the most prominent cause of neurodegeneration and the subsequent loss of memory especially in the early clinical phase of the disease. Moreover, oligomeric Aβ accumulation is detected as the main causal factor for the synaptic failure (Selkoe, 2002). In an early AD model developed by delivering AAV-based APP and PS1 genes in a 2-month old mouse brain, loss of post-synaptic protein PSD95 was observed and correlated to loss of LTP and memory impairment (Audrain et al., 2016). We checked for the levels of standard pre-synaptic marker synaptosomal-associated protein 25 (SNAP25) (Greber et al., 1999) and post–synaptic marker, post-synaptic density 95(PSD95) (Gylys et al., 2004), two prominent well-recognized markers to estimate changes in synaptic plasticity in both Aβ-induced model of AD and 5xFAD mice.

In Aβ-induced rat, 23 days following Aβ infusion through immunofluorescence studies in the hippocampus, we found significant decrease in the expressions of PSD95 (1A-B) and SNAP25 (1C-D). However, in the TIMP-1 treated Aβ-infused rats, the level of expression of both PSD95 and SNAP25 were significantly recovered.

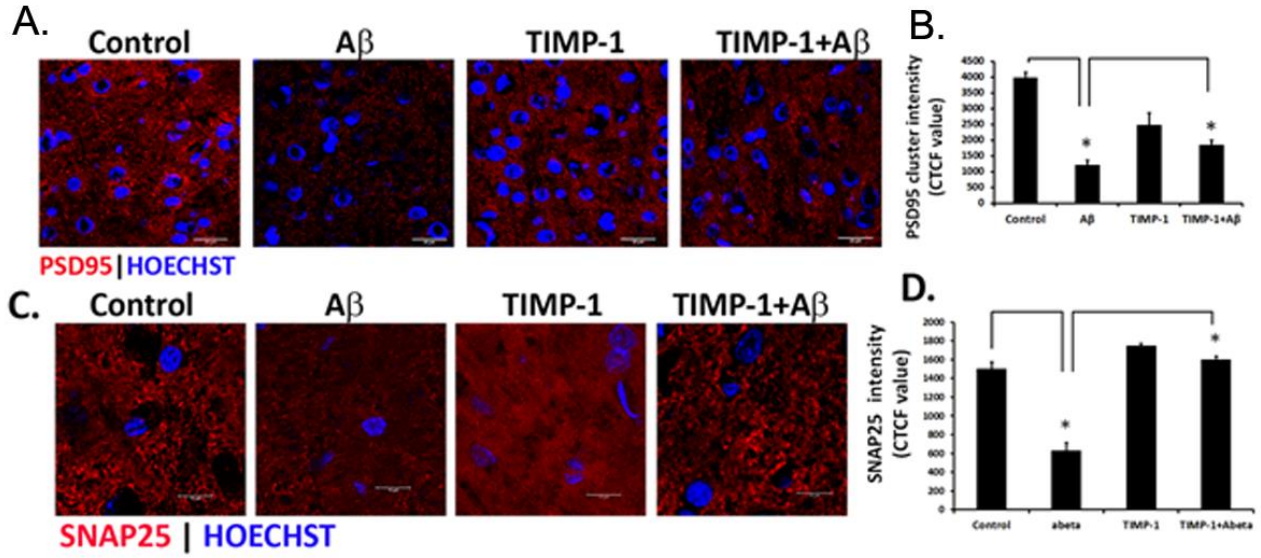

Fig.1: TIMP-1 improves synaptic protein expressions in Aβ-infused rat. (A-C) Immunocytochemistry technique was used in control, Aβ, TIMP-1 and Aβ+TIMP-1 injected coronal sections of rat brain with PSD95 and SNAP25 antibodies. Hippocampal regions were imaged at 40x magnification with the help of a confocal microscope (zoomed in images shown, scale bar = 20 μm for PSD95; scale bar = 10 μm for SNAP25). (B-D) CTCF values are presented as bar diagrams for each of the synaptic markers, *$p<0.05$.

We further checked whether similar changes occur in our 5xFAD model. We found that indeed both SNAP25 and PSD95 levels were significantly decreased in 6-month old 5xFAD mice both in the cortex and hippocampus in immunofluorescence studies. However, TIMP-1 injection in 5xFAD mice significantly improved both SNAP25 fluorescence intensities in the CA1 hippocampus (Fig 2A, C) and cortex (Fig 2E, G) and also PSD95 intensities in the CA1 hippocampus (Fig 2B, D) and cortex (Fig 2F, H). We performed whole tissue western blot analysis and found significant recovery in the expression levels of SNAP25 (Fig 2I, K) and PSD95 (Fig 2J, L) in the hippocampal tissue of TIMP-1 treated 5xFAD mice when compared to the untreated 5xFAD mice. However,

no significant changes were observed in these synaptic protein levels in the TIMP-1 treated 5xFAD group in the cortical tissues (data not shown). This discrepancy between immunofluorescence data and immunoblotting may be because of the technical constraint of western blotting in detecting very low level changes in protein expressions between groups or we may also infer that since we are utilizing whole cortex for immunoblotting, the changes if any, in any particular cortical layer is not captured properly by immunoblotting. Hence, our results were consistent with AD-related degradation in synaptic protein markers in both Aβ-induced rat model and 5xFAD mice and TIMP-1 was able to improve these protein levels indicating better synaptic health and integrity.

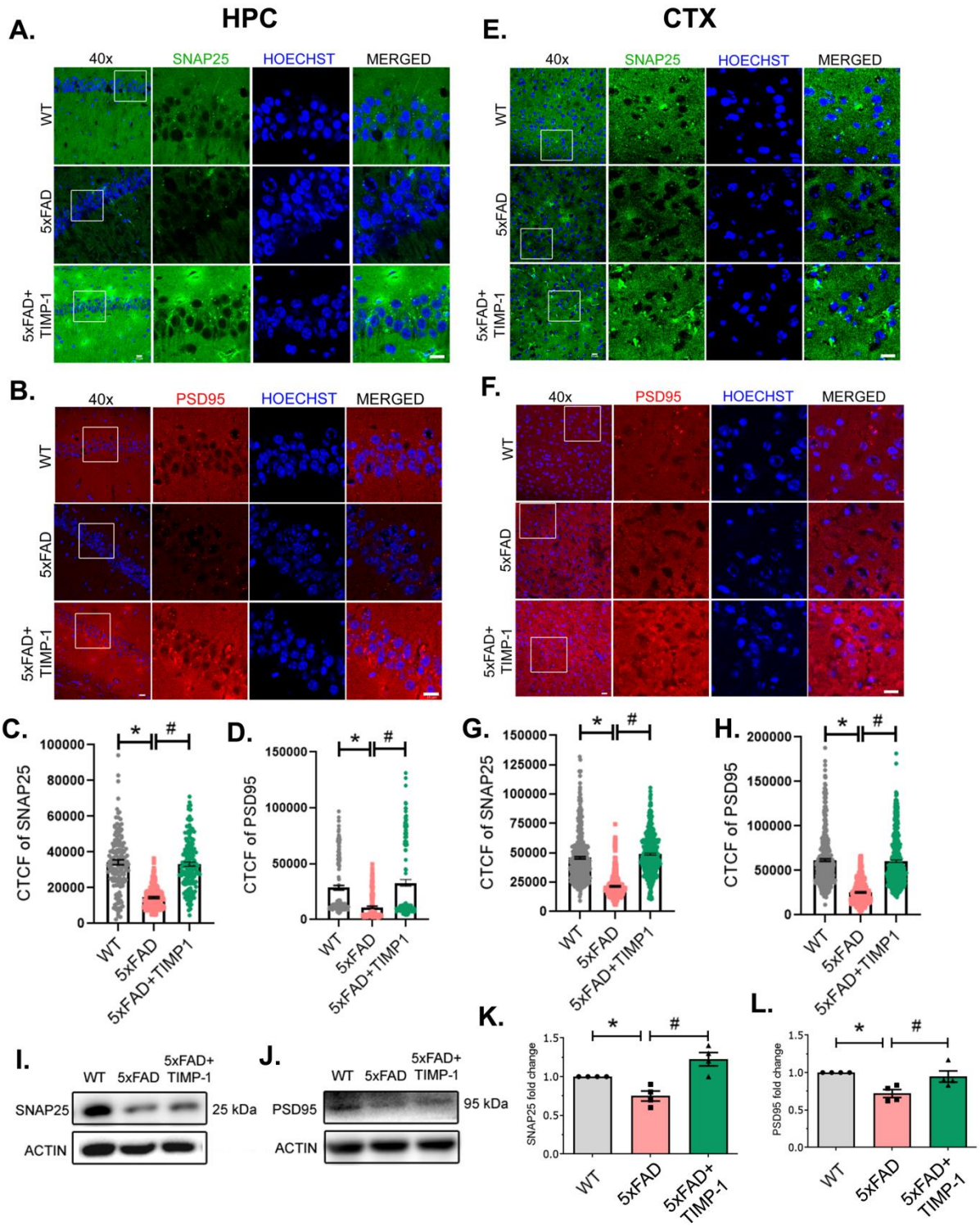

Fig.2: TIMP-1 improves synaptic protein expressions in 5xFAD mouse. Immunohistochemical analysis was performed on WT, 5xFAD and 5xFAD+TIMP-1 infused mice brain sections with SNAP25 (green) and PSD95 (red) antibodies from

hippocampus and cortex as indicated. Images were taken at 40x magnification under confocal microscope (white box indicate the regions under 40x selected for further zooming), scale bar = 15μm. Zoom-in pictures are represented (scale bar = 15μm). Bar diagrams are representing the Mean±SEM values of intensities of both the markers as CTCF values, n = 3 animals per group, 50 cells/animal from hippocampus (Hpc) and 150 cells/animal from cortex (Ctx) quantified from 40x images from Hpc(C, *p<0.0001, #p<0.0001; D, *p<0.0001, #p<0.0001) and Ctx (G, *p<0.0001, #p<0.0001; H, *p<0.0001, #p<0.0001). Western blot was performed from the hippocampal whole tissue lysates for SNAP25 (I) and PSD95 (J). Corresponding densitometric analyses are shown from K-L. Values are expressed as Mean±SEM, n = 4 animals per group where *p<0.05, #p<0.001 in (K) and *p<0.05, #p<0.05 in (L). (*) indicates p-values compared to WT group and (#) indicates p-values compared to 5xFAD group.

TIMP-1 mediated recovery in synaptic protein expressions occurs at the nerve terminal

Although we detected positive changes in synaptic proteins SNAP25 and PSD95 in whole tissue levels through immunohistochemical and western blot analyses with TIMP-1 treatment in 5xFAD mice, the assay systems were not sufficient to specify the localization of these proteins particularly at the nerve terminals or rather to understand whether the changes rendered by TIMP-1 is specifically a synaptic phenomenon. For this purpose, we isolated synaptosomes following a protocol described earlier (Gharami and Biswas, 2020). Synaptosomes are essentially isolated suspensions of nerve terminals, by careful mechanical shearing from mouse brain tissue, constituting cytoplasm, synaptic vesicles, cytoskeleton and mitochondria ensheathed by a membranous sac. These pre-synaptic nerve terminals often remain attached with the membrane of the post-synapse and the post-synaptic density proteins as observed by electron microscopy imaging earlier. Hence, synaptosomes are viable suspensions that structurally and functionally replicate nerve terminals in vivo and are quite useful to assess synaptic changes in response to a drug treatment. Here we isolated viable synaptosomes from the four treatment groups of

mice – WT, 5xFAD, WT+TIMP-1 and 5xFAD+TIMP-1 and then performed western blot analysis to determine the content of specific synaptic proteins under each condition. PSD-95, CaMKIIα and Homer 1 are implicated in excitatory synapse functioning and excitotoxicity of glutamatergic synaptic system is one of the hallmarks of AD (Wang et al., 2002; Wilcox et al., 2011). PSD95 is considered as the most important determinant in deciding the ratio of theexcitatory to inhibitory synaptic contacts (Prange et al., 2004). Additionally, pre-synaptic protein expressions undergo drastic changes in AD (Greber et al., 1999) and some including SNAP-25 are now strongly considered as CSF-based biomarkers of AD (Kivisakk et al., 2022). 14 days post TIMP-1 injection we isolated cortical and hippocampal synaptosomes from the mice brains of each treatment groups and performed western blot analysis to determine the changes in pre-synaptic proteins – SNAP25 (Fig 3A-C) and Synaptophysin (Fig 3A, D-E) and post-synaptic proteins PSD95 (Fig 3A, F-G) and HOMER 1 (Fig 3A, H-I). We also checked an excitatory synaptic marker – CAMKIIα level in our treatment groups. We observed that the expressions of pre and post synaptic markers were significantly lower in the 5xFAD group when compared to the WT group both in the cortical and hippocampal synaptosomes preparations. TIMP-1 treatment in 5xFAD was able to recover the level of SNAP25 significantly in the synapse of the cortex (Fig. 3A-B) and hippocampus (Fig 3A, C) comparable to WT SNAP25 level. TIMP-1 was unable to significantly recover the level of synaptophysin both in the cortex (Fig 3A, D) and in the hippocampal (Fig 3A, E) synaptosomes preparations. The level of PSD95 was significantly improved by TIMP-1 injection in 5xFAD mice both in the synapses of cortex (Fig 3A, F) and hippocampus (Fig 3A, G). HOMER1 level was significantly improved in the TIMP-1 treated 5xFAD cortex

(Fig 3A, H) but not significantly in the hippocampus (Fig 3A, I), although there was a trend. Interestingly, the level of CAMKIIα was found to be much higher in the hippocampal synaptosomes of the 5xFAD mice when compared to WT mice and its level was significantly reduced in the TIMP-1-treated 5xFAD group indicating that TIMP-1 was able to prevent the increased excitotoxicity in the 5xFAD mice synapses (Fig 3A, K). The cortical level of CAMKIIα remained unchanged among all the groups (Fig 3A, J).

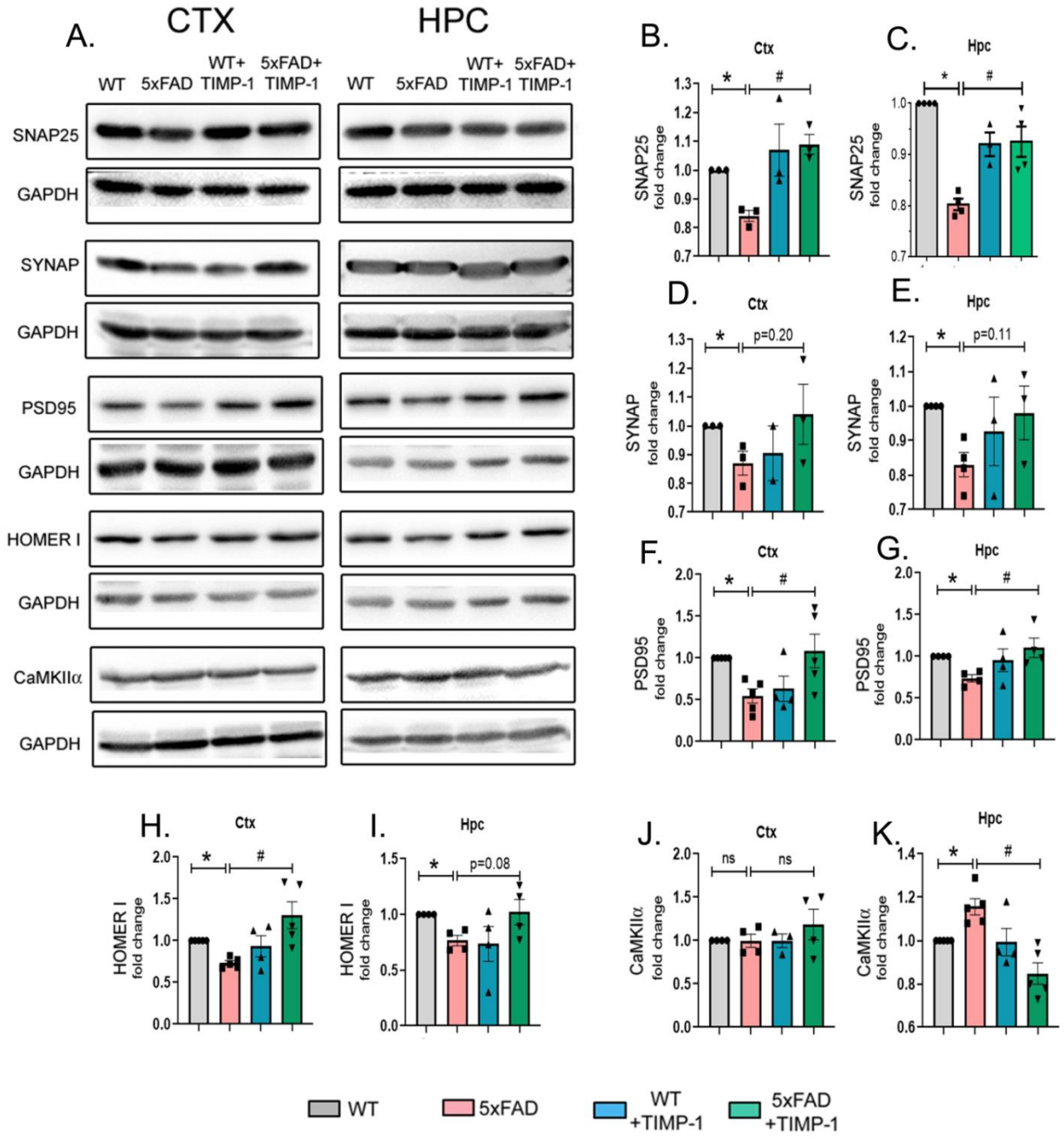

Fig.3: TIMP-1 differentially modulates synaptic protein expressions detected in isolated synaptosomes. Western blot was performed from synaptosomes isolated from cortex or hippocampus of the four treated groups. Representative blots for the panel of synaptic proteins are shown in (A). Densitometric analysis for pre-synaptic markers SNAP25 (B, *p=0.0358, #p=0.0491; C, *p<0.0001, #p<0.01) and Synaptophysin I (D, *p=0.0354; E, *p=0.003), post-synaptic markers - PSD95 (F, *p=0.0007, #p=0.0397; G, *p=0.0008, #p=0.0260) and HOMER1 (H, *p<0.0001, #p=0.0081; I, *p=0.0024) and

excitatory synaptic marker CAMKIIα (J;K, *p=0.0472, #p=0.0112) are shown as bar graphs. Values are expressed as Mean±SEM, n = 3-5/ group where (*) indicates p-values compared to WT group and (#) indicates p-values compared to 5xFAD group.Here, n represents number of independent synaptosome isolations.

TIMP-1 corrects deficits in synaptic spine density and spine shape in 5xFAD mice

Dendritic spines are the protrusions from the dendrites of a neuron and constitute a synapse when they communicate with a nearby axon. Dendritic or synaptic spines are highly dynamic in their size, shape and density and their changes are strongly correlated with learning and memory. Evidence suggests that accumulation of Aβ in rodent models of AD causes loss in the number of synapses, further causing damage in synaptic plasticity and disruption of neuronal networks (Kivisakk et al., 2022). We performed Golgi staining and obtain high resolution 120x bright-field images of cortical or hippocampal sections, 14 days following TIMP-1 injection in 5xFAD mouse to study changes in spine density.Fig 4A-D sequentially show the approximate locations of the brain from where the hippocampal and cortical stretches were imaged and used for calculations. We found thatthe number of spines/10 μm was significantly increased in both hippocampus (Fig 4E-F) and cortex (Fig 4G-H) of 5xFAD mice treated with TIMP-1 compared to untreated 5xFAD mice and was comparable to the untreated WT brain spine density in each region. The spine density was unaltered in the TIMP-1 injected WT mice. Notably, the spine density in the hippocampus was more than 2-fold than that detected in the cortex in the WT mice. Thus, TIMP-1 was able to improve the spine densities, both in the hippocampus and cortex, which were abrogated in the 5xFAD mice.

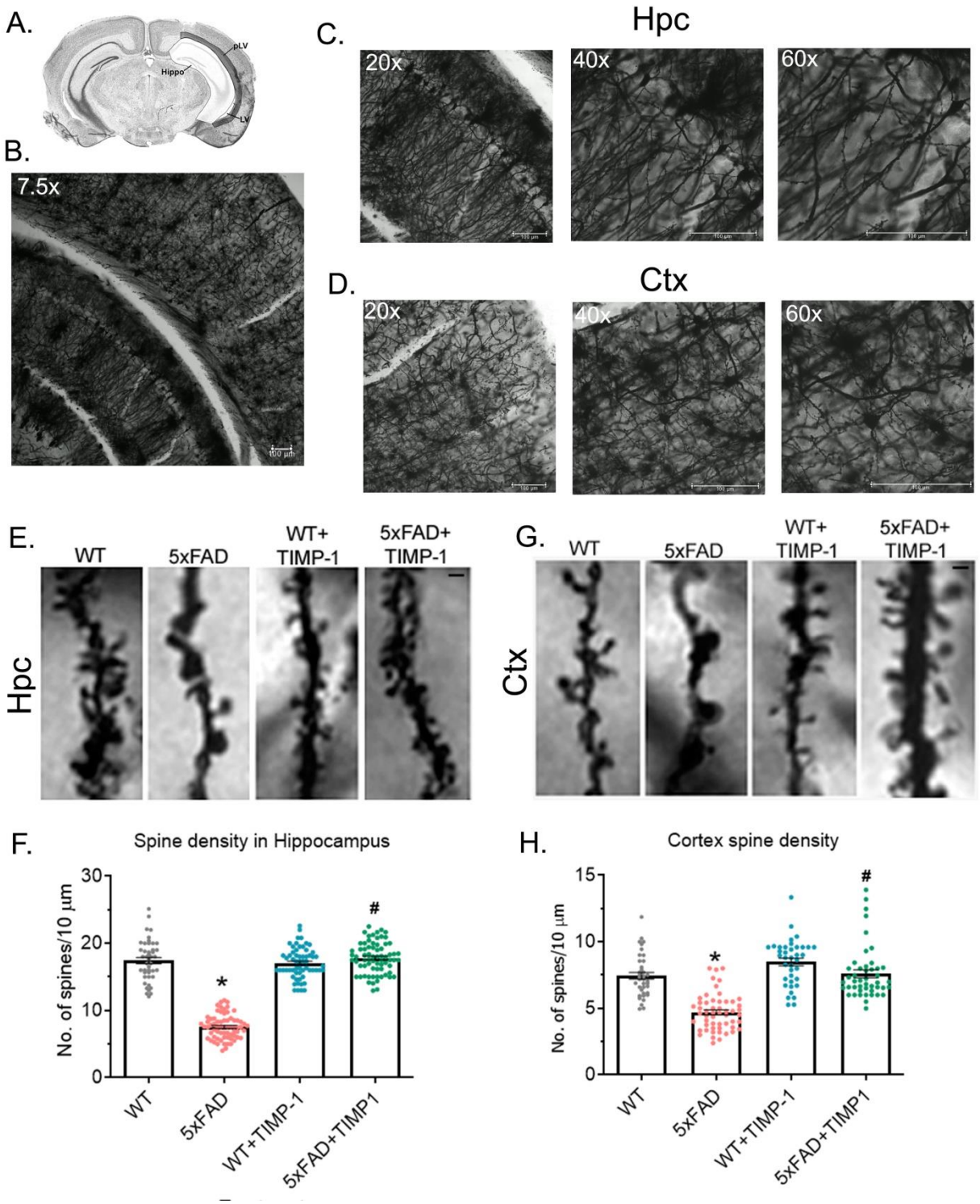

Fig.4: TIMP-1 restores spine density in the hippocampus and cortex of 5xFAD mouse to the normal physiological level. (A) The representative coronal slice of a brain showing the CA1 region of the hippocampus and the cortex targeted for spine density calculation

following Golgi staining. (B) Shows the region of the hippocampus and cortex zoomed for higher magnification imaging indicated by white boxes. Panels show the sequential zoom-in (20x-40x-60x) done to locate a particular dendrite for counting in hippocampus (Hpc, C) and cortex (Ctx, D). Scale bar indicates 100 μm. Panel shows representative images of 15 μm segment of dendrites with spines imaged at 120x in hippocampus (E) and cortex (G) from the four treatment groups, scale bar = 1 μm. Number of spines/10μm is quantified from each group and presented as a bar graph for hippocampus (F, *p<0.0001, #p<0.0001) and cortex (H, *p<0.0001, #p<0.0001). n=3 animals per group, 40-80 dendritic stretches/group from each region were used, values are presented as Mean±SEM, (*) indicates p-values compared toWT group and (#) indicates p-values compared to 5xFAD group.

Besides synaptic spine density, spine shape is yet another morphological aspect of synapses that are altered in an activity-dependent form of plasticity. Synaptosome proves to be a unique tool in quantifying changes in spine shape in terms of its actin content. Changes in spine shape are regulated by dynamic alterations in the cytoskeletal actin content that is change in the ratio of filamentous versus globular form of actin in synaptosome. Notably, shrinkage of dendritic spine is one of the pathological attributes of AD. We fractionated the viable synaptosomes further into the cytoskeletal fraction constituting the filamentous (F) actin and the supernatant fraction constituting the globular (G) actin (Fig. 5A). The ratio of F/G actin indicates the change in spine shape. We found that the ratio was significantly reduced in the hippocampal fractions from the 5xFAD mice when compared to WT group. However, treatment with TIMP-1 helped to improve the actin content of the spine as indicated by an increased F/G actin ratio in the 5xFAD mice (Fig. 5B-C). Spine shape and maturation are correlated to stabilization of actin cytoskeleton. Phosphorylation of Cofilin is the major factor for the stabilization of actin cytoskeleton and thereby helps the spine to attain maturation followed by spine enlargement. We found that the phosphorylation level of Cofilin was significantly lower

in the 5xFAD mice when compared to WT mice. However, in the 5xFAD+TIMP-1 group, the level of phosphoCofilin was significantly improved indicating the role of TIMP-1 in inducing spine maturation and hence the improvement in spine shape (Fig 5D-E).

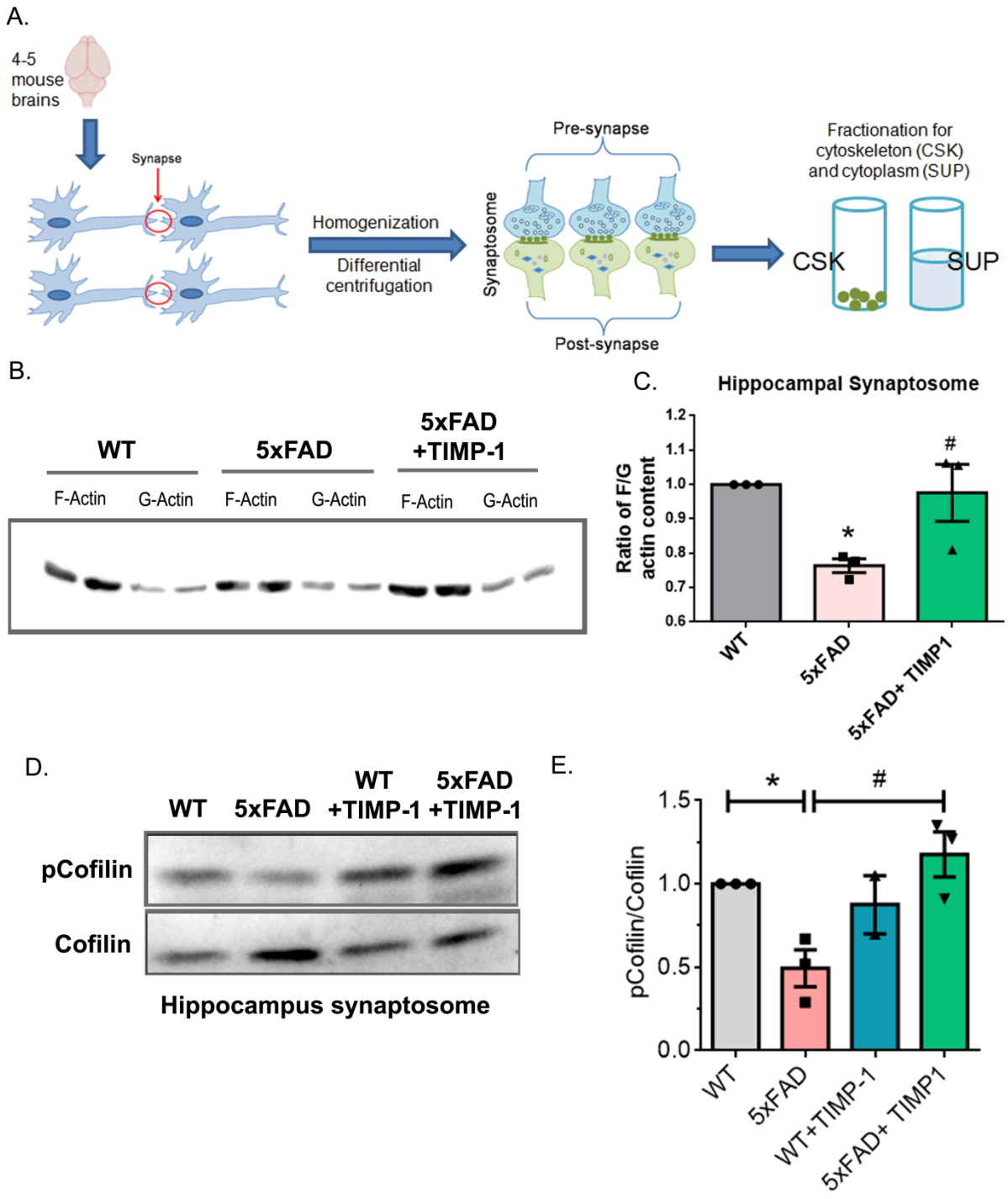

Fig.5: TIMP-1 improves spine shape in 5xFAD mice. (A) Schema showing the procedure for synaptosome isolation from 4-5 mouse brains followed by fractionation to obtain the cytoskeleton (CSK) and cytoplasmic/supernatant (SUP) fractions. (B) Representative immunoblot from hippocampus synaptosome showing filamentous (F, in CSK fraction) actin and globular (G, in SUP fraction) actin contents in each group of mice. Results from two mice are shown in consecutive lanes marked by the group name in the blot. (C) Densitometric analysis of F/G actin content is represented as Mean±SEM where n=3/group, *p=0.0340, #p=0.05. (D) Representative blot for hippocampal synaptosome phosphoCofilin and Cofilin are shown. (E) Densitometric analysis is presented as Mean±SEM where n=3/group, *p<0.05, #p<0.01. Here, n represents number of independent synaptosome isolations.

TIMP-1 improves basal synaptic transmission but did not affect short-term plasticity in the hippocampal schaffer collateral-CA1 synapses in 5xFAD mice

In order to determine whether basal synaptic transmission at Schaffer collateral-CA1 synapses is affected in 5xFAD mice compared to WT mice, we checked input-output (I-O) relationship curve in the hippocampal slices from the four treatment groups. Fig 6A shows the representative fEPSP traces of four experimental groups as indicated across different current stimulus intensities (20 – 300 μA with 20 μA increments). Fig 6B shows the quantitative analysis of the I-O curve. Two-way ANOVA followed by Tukey's post-hoc test revealed that in the 5xFAD slices, the fEPSP responses across the different current intensities were significantly lower than the untreated WT mice as indicated. TIMP-1 was able to improve the fEPSP slope values in 5xFAD significantly at several current intensities as indicated, the highest being at 260 μA current strength (#p=0.0483). Fig 6C shows the area under curve (AUC) interpreting the graph we obtained in Fig 6B with better clarity. Next we also wanted to study the effect of TIMP-1 treatment in 5xFAD on short-term plasticity by determining the paired-pulse facilitation (PPF) ratio at the Schaffer collateral-CA1 synapses. PPF helps in evaluating the alterations in pre-synaptic activity and

neurotransmitter release probability by administering two consecutive stimulating pulses with a short inter-stimulus interval (ISI). PPF ratio remained unaltered among the four experimental groups (Fig 6D). Fig 6E shows the AUC depicting the results we obtained in Fig 6D for clarity. Hence, we may conclude that the probability of pre-synaptic neurotransmitter release remained unaltered at the Schaffer collateral-CA1 synapses in 5xFAD mice and there was no further change with TIMP-1 treatment.

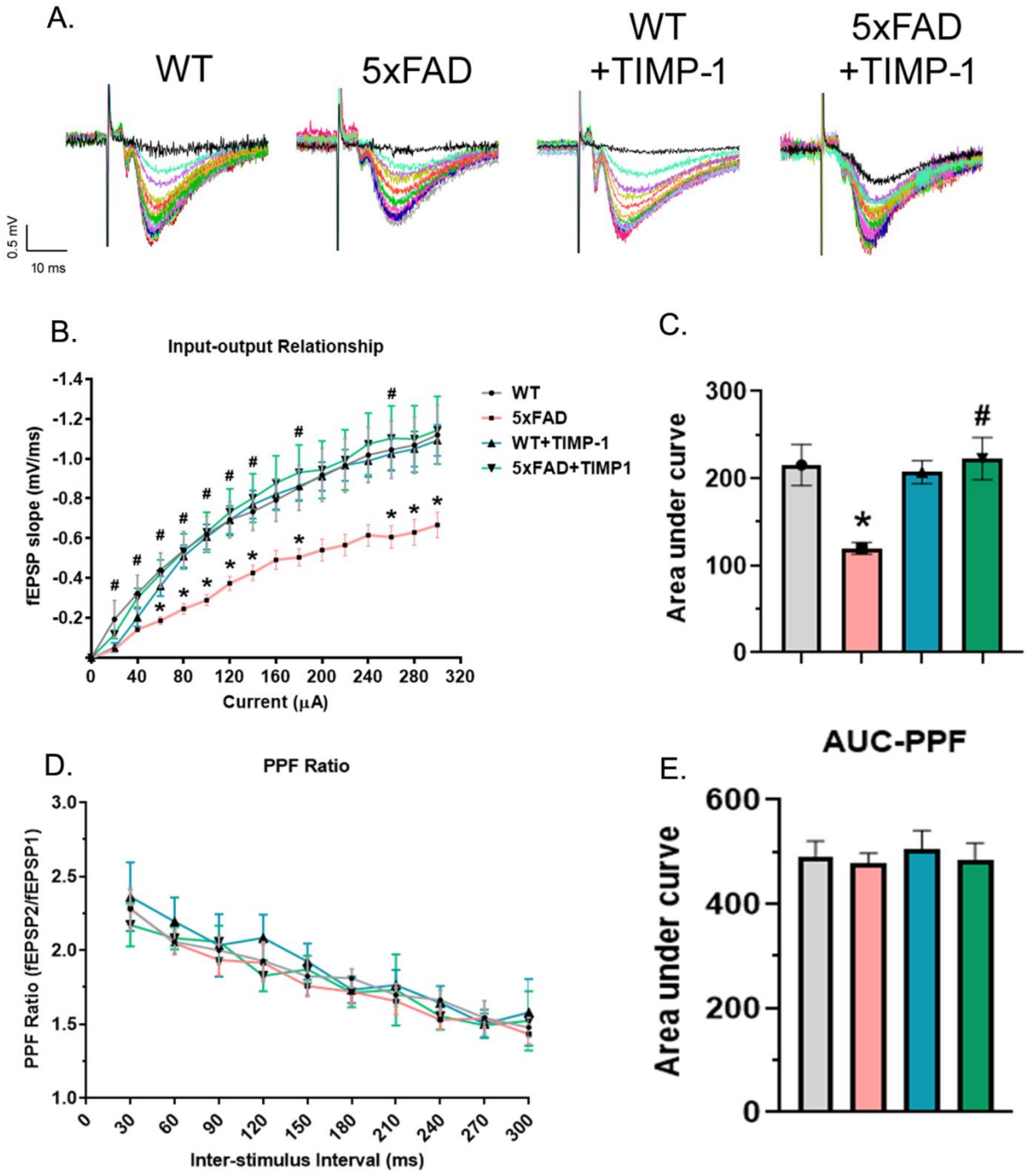

Fig.6: Deregulated basal synaptic transmission at Schaffer collateral-CA1 synapses in 5xFAD mouse is restored by TIMP-1 but paired pulse facilitation ratio remains unaffected in all the groups. (A) Representative fEPSP traces of slices from the four treatment groups are shown across increasing current stimulus strength. Each color curve represents field

responses (fEPSP) to schaffer collateral stimulation along different intensities of current stimulus (20 – 300 μA with 20 μA increments) (B) Input-output relationship (fEPSP slopes along a step-wise rise in stimulus intensity) is represented by calculating the mean value of all the slices in each group at each stimulus current strength from 20 – 300 μA (n= 9-15 slices/group, N=5-6 mice/group) where *p<0.05, #p<0.05. (C) Area under curve calculated from the graph shown in (B) where values are presented as Mean±SEM, *p=0.0153, #p=0.0103. (*) indicates p-values compared toWT group and (#) indicates p-values compared to 5xFAD group.(D) PPF ratio of all the four groups across increasing inter-stimulus interval ranging from 30 to 300 ms. (E) Area under curve calculated from the graph shown in (D), where values are presented as Mean±SEM (n= 9-15 slices/group, N=5-6 mice/group).

TIMP-1 ameliorates deficit in long-term potentiation in the hippocampal schaffer collateral-CA1 synapses in 5xFAD mice

LTP and LTD are the cell-level determinants of cognitive activities. LTP/LTD regulation forms the basis of synaptic plasticity which in turn modulates learning and memory. Several reports suggest that disruption of LTP occurs even before the appearance of Aβ plaques or any cognitive deficits in transgenic models of AD (Audrain et al., 2016; Jacobsen et al., 2006). Further, both synthetic as well as natural Aβ oligomers reportedly inhibit LTP *ex vivo* and *in vivo* respectively. Aβ can eventually lead to a downregulation of LTP and related processes and upregulation of LTD (Walsh et al., 2002). We next wanted to study whether the level of LTP expression was different between the WT and 5xFAD hippocampal slices. We also predicted that changes in basal synaptic transmission induced by TIMP-1 in 5xFAD mice may have a contribution towards LTP induction in hippocampal slices of mice. We evaluated synaptic potentiation at three different plasticity time points - Post-tetanic potentiation (PTP, 1 min post TBS), short-term potentiation (STP, 21st-30th min post TBS) and LTP (40th-60th min post TBS). Fig 7A shows

the representative tracings of pre- and post-TBS fEPSP in each of the treatment groups. Fig 7B shows the time course of normalized fEPSP response of the four treatment groups each initiating with a baseline of 20 min and continuing for another 60 mins post-TBS. Fig 7C shows the AUC for better interpretation of the graph shown in Fig 7B elucidating a diminished AUC in 5xFAD group compared to the other treatment groups while it was significantly improved in the TIMP-1 treated 5xFAD group. One-way ANOVA analysis showed that there was no significant change in PTP (Fig 7D) and STP (Fig 7E) among the treatment groups. One way ANOVA followed by Tukey's post hoc test showed that LTP induction was significantly lower in the 5xFAD hippocampal slices compared to WT mice. However, TIMP-1 treatment in 5xFAD mice significantly improved the level of LTP induction while TIMP-1 treatment to WT mice did not show any alteration when compared to the WT group (Fig7F).

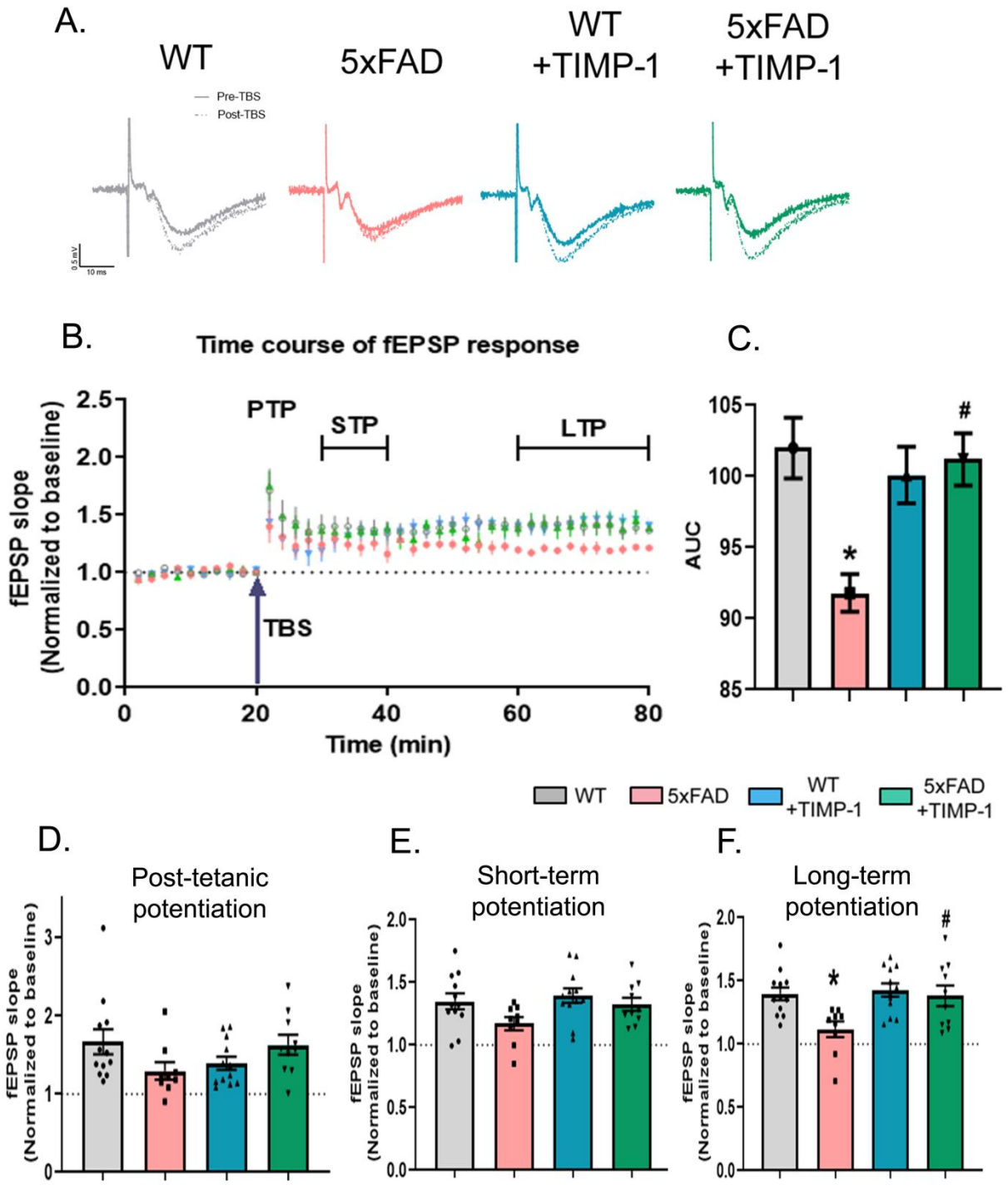

Fig.7: TIMP-1 improved the magnitude of long-term potentiation induced in 5xFAD mice. (A) Representative fEPSP tracings of slices from WT, 5xFAD, WT+TIMP- and 5xFAD+TIMP-1 mice. Solid line represents pre-TBS response (baseline) and dotted line represents post-TBS response. Note the decrease in the magnitude of LTP in 5xFAD

(pink) compared to WT (grey) and increase in LTP in 5xFAD+TIMP-1 (green) group compared to 5xFAD. (B) Time course of fEPSP responses with 20 min pre-TBS and 60 min post-TBS. Note the time segments post-TBS demarcated for calculating post-tetanic potentiation (PTP), short-term potentiation (STP) and long-term potentiation (LTP). (C) Area under curve calculated from the graph shown in (B). Values are presented as Mean±SEM, *p = 0.0088, #p = 0.0207. (*) indicates p-values compared toWT group and (#) indicates p-values compared to 5xFAD group. (D) Bar graph represents post-tetanic potentiation (1 min post-TBS). (E) Bar graph represents short-term potentiation (21st-30th min) post-TBS. (F) Bar graph represents long-term potentiation (40-60 min post-TBS) showing significant induction in LTP in 5xFAD+TIMP-1 slices compared to slices from untreated 5xFAD mice. Values are presented as Mean±SEM (n= 9-12 slices/group, N=5-6 mice/group),*p = 0.0165, #p = 0.0355. (*) indicates p-valuecompared toWTgroup and (#) indicates p-value compared to 5xFAD group.

TIMP-1 inhibits GSK3β activity and causes BDNF secretion in 5xFAD mice

GSK3β is an important regulator of LTP/LTD signaling implicated in synaptic changes in the brain (Bradley et al., 2012). We have already detected Akt as an important modulator in TIMP-1 mediated neuroprotection in vitro (Ch-1) and in vivo (Ch-2). Additionally, we found that TIMP-1 improves LTP induction in 5xFAD mice. We hypothesized that since Akt phosphorylation both at s473 and t308 leads to GSK3β (ser9) phosphorylation and there is a recovery in LTP, TIMP-1 may have a role in GSK3β signaling. Indeed we found that TIMP-1 increased GSK3β phosphorylation in the hippocampal whole tissue level versus significantly reduced phosphorylation level in untreated 5xFAD mice (Fig 8A-B). Further analysis of synaptosomes confirmed that TIMP-1–directed increase in pGSK3β level in 5xFAD mice takes place at synapses both from cortex (Fig 8C-D) and hippocampus (Fig. 8C, E). Brain Derived Neurotrophic Factor (BDNF) is known to play a role in GSK3β inhibition (Jain et al., 2013). Interestingly, in western blot analysis from whole tissue hippocampus we found significant induction in

BDNF levels upon treatment of 5xFAD mice with TIMP-1 compared to untreated 5xFAD mice (Fig 8F-G). Thus, we may conclude that the signaling pathway responsible for LTP induction in response to TIMP-1 treatment in 5xFAD mice is BDNF-regulated Akt/GSK3β pathway.

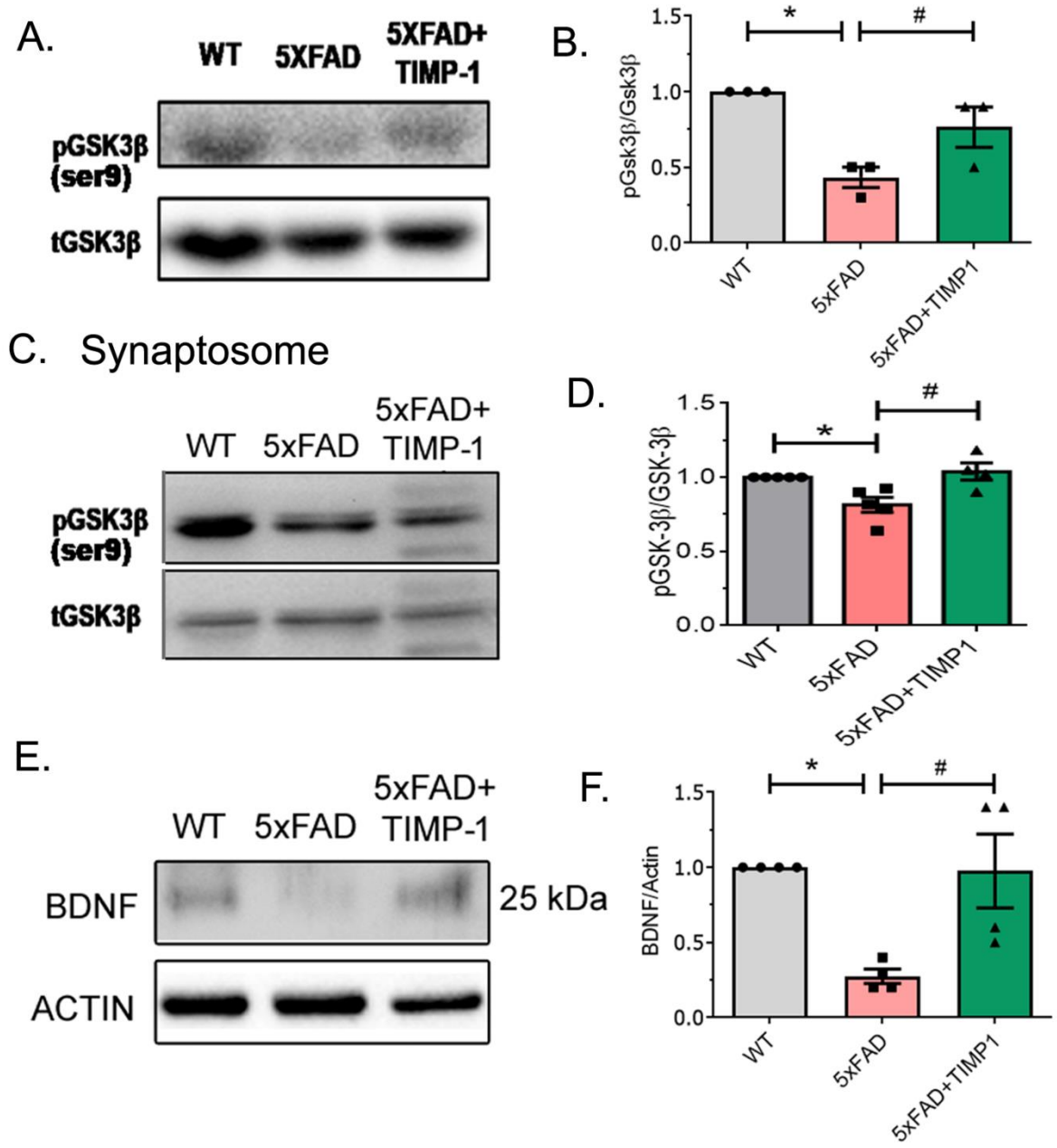

Fig.8: TIMP-1 inactivates GSK3β and induces BDNF expression in 5xFAD mice. (A) Representative blot from whole hippocampal tissue lysates showing phosphoGSK3β (ser9) and total GSK3β levels in the same blot. (B) Shows the densitometric analysis of hippocampal pGSK3β/GSK3β. Values are presented as Mean±SEM (n= 3 mice/group),*p< 0.01, #p < 0.05. (C) Representative blot from synaptosomal lysates showing phosphoGSK3β (ser9) level from hippocampus. (D) Densitometric analyses of hippocampal pGSK3β/GSK3β from synaptosomes represented as Mean±SEM (n= 3/group),*p = 0.0202, #p = 0.0094. Here, n represents number of independent synaptosome isolations. (E) Representative blot from whole hippocampal tissue lysates showing BDNF level and corresponding actin. (F) Shows the densitometric analysis of the normalized hippocampal BDNF level. Values are presented as Mean±SEM (n = 3 mice/group),*p< 0.05, #p < 0.05.

Discussion

Findings strongly suggest that synaptic dysfunctions precede Aβ deposition, neuronal damage and cognitive loss and are thus recognized as one of the earliest phenomena in AD (Audrain et al., 2016). Thus, deciphering the role of TIMP-1 in the earliest stage of AD may present as an effective neuroprotective strategy. We found that TIMP-1 significantly improved the levels of pre- and post-synaptic proteins, SNAP25 and PSD95, in 5xFAD mouse especially in the hippocampus at the whole tissue level and both in cortex and hippocampus, when specifically synaptic localization was studied in the synaptosomes. However, no recovery in synaptophysin level was observed with TIMP-1 treatment and in case of HOMER1 we did not find any significant change in hippocampus unlike in cortex. Hence, not all types of synaptic protein expressions are altered by TIMP-1, at least not equally in individual brain regions. Both SNAP25 (Greber et al., 1999) and PSD95 (Gylys et al., 2004) levels are found to be decreased in tissue samples of AD patients but interestingly their CSF levels are found to be increased in AD patients such that now both of SNAP25 and PSD95 are proposed as important biomarkers for early AD diagnosis and

can be correlated with cognitive decline (Kivisakk et al., 2022). While the authors show SNAP25 is more AD specific, PSD95 shows overall promise as a neurodegenerative disease marker for synaptic deterioration. In our study we find that SNAP25 and PSD95 levels are recovered by TIMP-1 and not the levels of other two synaptic markers. Intriguingly, the two highly correlated proteins are localized in two different synaptic compartments while the two pre- or two post-synaptic proteins were not responding to TIMP-1 treatment equally. This is in coherence to an earlier report suggesting that there may be a differential response of different synaptic proteins in AD brain (Shimohama et al., 1997). Additionally, not all of the synaptic components alter equally in the CSF of AD patients (Brinkmalm et al., 2018; Clarke et al., 2019; Shimohama et al., 1997). Increased expressions of synaptic protein may not simply mean improving the number of synaptic contacts between pre- and post-synaptic terminals but they may have some additional role in determining the type of synapse (excitatory/inhibitory), their shape as well as number in the newly formed synaptic contacts (Prange et al., 2004). We further observe there is an increase in level of CAMKIIα in the hippocampus and not in the cortex in the 5xFAD mice compared to WT mice. Increase in CAMKIIα may indicate increased excitotoxicity in 5xFAD that has been reported in AD earlier (Lauterborn et al., 2021). TIMP-1 was able to prevent this CAMKIIα-mediated excitotoxicity in the hippocampus.

We further found that TIMP-1 corrected loss of spine density and spine shape in 5xFAD mice. Shape and size of dendritic spines or in other words that of excitatory synapses are altered due to LTP/LTD changes. While LTP leads to the enlargement of dendritic spine, LTD induction leads to spine shrinkage. Besides spine loss, structural reorganization of

synapses is an important aspect of AD pathology, to an extent, that dynamic regulation of spines can help develop cognitive resilience against memory loss in aged people with AD pathology (Boros et al., 2017). Actin cytoskeleton plays a pivotal role in spine dynamics both from structural and functional perspectives. They can regulate the post-synaptic receptor trafficking and hence modulate post-synaptic response of a synapse. Spine actin dynamics is also directly responsible in regulating synaptic strength in other words spine shape and size. The organization of spine actin is intricately regulated by several signaling pathways among which cofilin emerges as the most important factor for spine stabilization. We show that phosphorylated cofilin (inactive form) level is decreased in synaptosomes isolated from 5xFAD mice when compared to WT mice. This means cofilin becomes hyperactive in 5xFAD mice capable of forming rod-shaped actin/cofilin bundles in the neuronal cytoplasm, blocking axonal trafficking and responsible for synaptic dysfunctions leading towards synaptic loss and is consistent with earlier reports in models of AD (Bamburg et al., 2010; Deng et al., 2016; Liu et al., 2022). Indeed, Aβ oligomers and fibrils have been directly implicated in inducing cofilin/actin rods following a long exposure time (Davis et al., 2011; Mendoza-Naranjo et al., 2012) and phospho-cofilin is found to be decreased in 7-month old APP/PS1 mice (Woo et al., 2015). Additionally modulation of upstream kinases of cofilin (inactivating cofilin) for example, PAK inactivation has been correlated with loss of social recognition in old 3xTg mice (Arsenault et al., 2013). Moreover, over-expression of LIMK1 in APP/PS1 mice hippocampus, another key kinase for cofilin phosphorylation, leads to an improvement in LTP and social memory in the transgenic AD model (Zhang et al., 2021). However, there are also some contradictory reports that indicated high phospho-cofilin

levels in models of AD (Barone et al., 2014; Fowler et al., 2014; Heredia et al., 2006) and that inactivation of cofilin leads to abnormal spine morphogenesis and deterioration of synaptic plasticity (Zhou et al., 2009). Rush et al show that phospho-cofilin level is increased in the PSD-enriched fraction from cortex of APP/PS1 mouse as well as in those isolated from the cortex of human AD patients (Rush et al., 2018). However, this report focuses on the PSD-enriched fraction specifically while we have performed our experiments with whole synaptosomes from the cortex and hippocampus containing both CSK and cytoplasmic elements. This discrepancy may be because the post-synaptic compartments are the immediate targets of Aβ oligomers and may produce differential results from that of whole synaptosomes especially because actin/cofilin rod formation is a cytoplasmic phenomenon.

Brain stores information through alterations in fine synaptic structures and efficiencies in signal transmission by processes of LTP and LTD. Hence, LTP/LTD regulation forms the underpinning mechanism regulating synaptic plasticity and in turn learning and memory functions. We utilized acute hippocampal slices from mouse brains and recorded field extracellular postsynaptic potential (fEPSP) to study the alterations in glutamatergic synaptic transmission and synaptic plasticity in 5xFAD mice and checked whether TIMP-1 can regulate them. We found that in 5xFAD mice the basal level CA3-CA1 synaptic strength was dampened through assessment of input-output relationship compared to WT C57/BL6 mice. Slices from the 5xFAD mice displayed significantly less fEPSP response and population spike along with increase in stimulus intensities in comparison to the WT mice slices. However, TIMP-1 treated 5xFAD mice showed a significant improvement in

fEPSP response and the 5xFAD+TIMP-1 slice I/O curve (fEPSP along current stimulus intensity) overlapped with that obtained from the WT mice. The impairment in synaptic strength in 5xFAD mice in I/O curve mirrors the changes we have already observed biochemically in 5xFAD mice that is decrease in synaptic density, shrinkage of individual spines indicative of synaptic strength deterioration and finally may also reflect changes in AMPAR-mediated transmission (Hoover et al., 2010; Smith and McMahon, 2018). Paired pulse facilitation ratio (PPR) helps us to quantify the changes in pre-synaptic neurotransmitter release probability induced by either increased calcium flux or the presence of ready-to-release pre-synaptic vesicles when triggered with the first stimulus (Citri and Malenka, 2008). We did not find any alterations in PPR among the four treatment groups indicating that the reduction in fEPSP values in 5xFAD slices in I/O relationship study was not due to reduced pre-synaptic activity nor decreased neurotransmitter (glutamate) release from the pre-synaptic terminals but due to modulations in post-synaptic activity (Nelson et al., 2012b). Further, we did not observe any change in post-tetanic potentiation (PTP) among the groups. PTP quantifies the initial sharp upregulation in fEPSP slope values in the first 2-3 mins after TBS. Interestingly, both PPR and PTP measure changes in short-term plasticity and also the probability of release of neurotransmitters from the pre-synaptic terminals (Citri and Malenka, 2008). Hence, in 5xFAD short-term plasticity remained unaltered when compared to WT mice and TIMP-1 did not have any effect on it. Intriguingly, the magnitude of LTP induction calculated from the 40^{th}-60^{th} min following TBS at the Schaffer collateral-CA1 synapses in 5xFAD mice slices was significantly lower compared to WT mice. In WT brain slices, the potentiation saw a peak in the PTP phase and then

dropped at STP following which the curve remained stable and maintained during the total 60 mins of post-TBS recording. However, in 5xFAD even after a successful PTP phase following TBS, the potentiation curve saw a gradual decline throughout the 60 min run time. However, the induction did not go back to the basal synaptic transmission level indicating that although the magnitude of LTP induction was significantly dampened in the 5xFAD mice, it was not completely abrogated even after 60 min following TBS. Our results are consistent with a previousreport that showed that both basal synaptic transmission (AMPAR-dependent synaptic regulation) and LTP (NMDAR-dependent synaptic plasticity) at Schaffer collateral-CA1 synapses are reduced in 5xFAD mice compared to WT mice at 6 months of age but not below 4-months of age. LTP reduction in 5xFAD was correlated to hippocampal-dependent memory deficits in this model and impairment in LTP rather than in basal synaptic transmission was regarded as the major causal factor for the hippocampal-dependent memory impairment. In our study, TIMP-1 treatment ameliorated this partial impairment in LTP induction in 5xFAD mice. Hence, we may speculate that recovery in LTP underlie the observable hippocampal-dependent learning and memory improvements with TIMP-1 treatment in 5xFAD we have observed in our behavioral tests in Part-II.

Increased GSK3β activity has been often correlated with impairment in spatial learning and memory and inhibition of LTP (Hernandez et al., 2002; Hooper et al., 2007). Additionally, active GSK3β (dephosphorylated form) interferes with Ca^{2+}-dependent SNARE complex formation thus negatively regulating synaptic vesicle fusion at the pre-synaptic terminal (Zhu et al., 2010). We found that in whole tissue lysate of

hippocampus of 5xFAD mice the level of pGSK3β was significantly upregulated compared to WT mice. This means that in 5xFAD mice GSK3β remains more active and thus can reciprocally regulate SNARE complex formation by weakening the association between different SNARE proteins namely SNAP25, syntaxin, synaptotagmin etc. In our study although we have checked the level of pre-synaptic and SNARE protein - SNAP25, in hippocampus (whole tissue and synaptosome) we did not study the changes in their association with the other pre-synaptic proteins. Activation of GSK3β reduces release of glutamate from pre-synaptic terminal (Zhu et al., 2007). However, in our electrophysiological study (PPF test) we did not observe any difference in pre-synaptic neurotransmitter release probabilities at the schaffer collateral-CA1 synapses among the treatment groups following the first stimulus. We may speculate that some different mechanism is coming to the rescue, nullifying the effect of activated GSK3β at the pre-synaptic terminal in 5xFAD mice. Hence, the same mechanism may be maintaining a normal level of pre-synaptic neurotransmitter release in 5xFAD in the PPF test. Additionally, we have not checked the pGSK3β level specifically in the pre-synaptic terminal of the hippocampal synapse. Intriguingly, GSK3β is also associated with the post-synaptic density in dendritic spines, regulates NMDAR-dependent synaptic plasticity (Peineau et al., 2009) and NMDAR trafficking (Chen et al., 2007; Zhang et al., 2014). GSK3β is considered as the most important switch for LTP/LTD regulation at glutamatergic synapses. Enhanced activity of GSK3β leads to upregulation of NMDA-depenedent LTD while inhibition of GSK3β activity leads to induction of NMDA-dependent LTP (Hooper et al., 2007). Hence, increase in pGSK3β (inactive form) level in TIMP-1-treated 5xFAD tissue mirrors an upregulation of LTP and corroborates with our

electrophysiological data. Since in the electrophysiological study we found that LTP induction in 5xFAD+TIMP-1 mice slices is dependent on changes at the post-synaptic level, we predict that the change we are observing in our biochemical analysis is a reflection of the phosphorylation changes in GSK3β at the post-synaptic compartment and not at the pre-synaptic terminal. Additionally, we have earlier seen that there is increased Akt activity following TIMP-1 treatment to 5xFAD mice. Hence, we predict that the main signaling mechanism in play is along the PI3K/Akt/GSK3β pathway that regulates the phosphorylation of GSK3β at ser9 and in turn its kinase activity, more prominently in the post-synaptic compartment.

Finally, we checked the BDNF levels as BDNF plays an integral role in hippocampal synaptic plasticity. Earlier studies have shown that induction of LTP in the CA1 region of the hippocampus was able to enhance BDNF mRNA level (Patterson et al., 1992). In a BDNF knockout mouse line, LTP induction gets impaired and that application of exogenous BDNF or its over-expression restored the impairment in LTP. BDNF-TrkB signaling has been directly implicated during the period of synaptic stimulation for LTP induction and has been regarded as the critical regulator for LTP induction following TBS. Hence, it was imperative to check the level of BDNF expression, the most important regulator directly impacting LTP induction, in the 5xFAD versus WT mice to reaffirm the changes we have observed in terms of LTP induction in our electrophysiological experiment. We found that in 5xFAD mice there was more than 4-fold decrease in BDNF expression level in the hippocampus. This result was consistent with previous reports that show a decrease in BDNF level in models of AD including 5xFAD mice compared to

controls (Kimura and Ohno, 2009). Interestingly, TIMP-1 was able to improve BDNF expression level in 5xFAD mice comparable to the level found in WT mice. Hence, we may conclude that TIMP-1 is improving LTP induction in 5xFAD mice by upregulating BDNF expression.

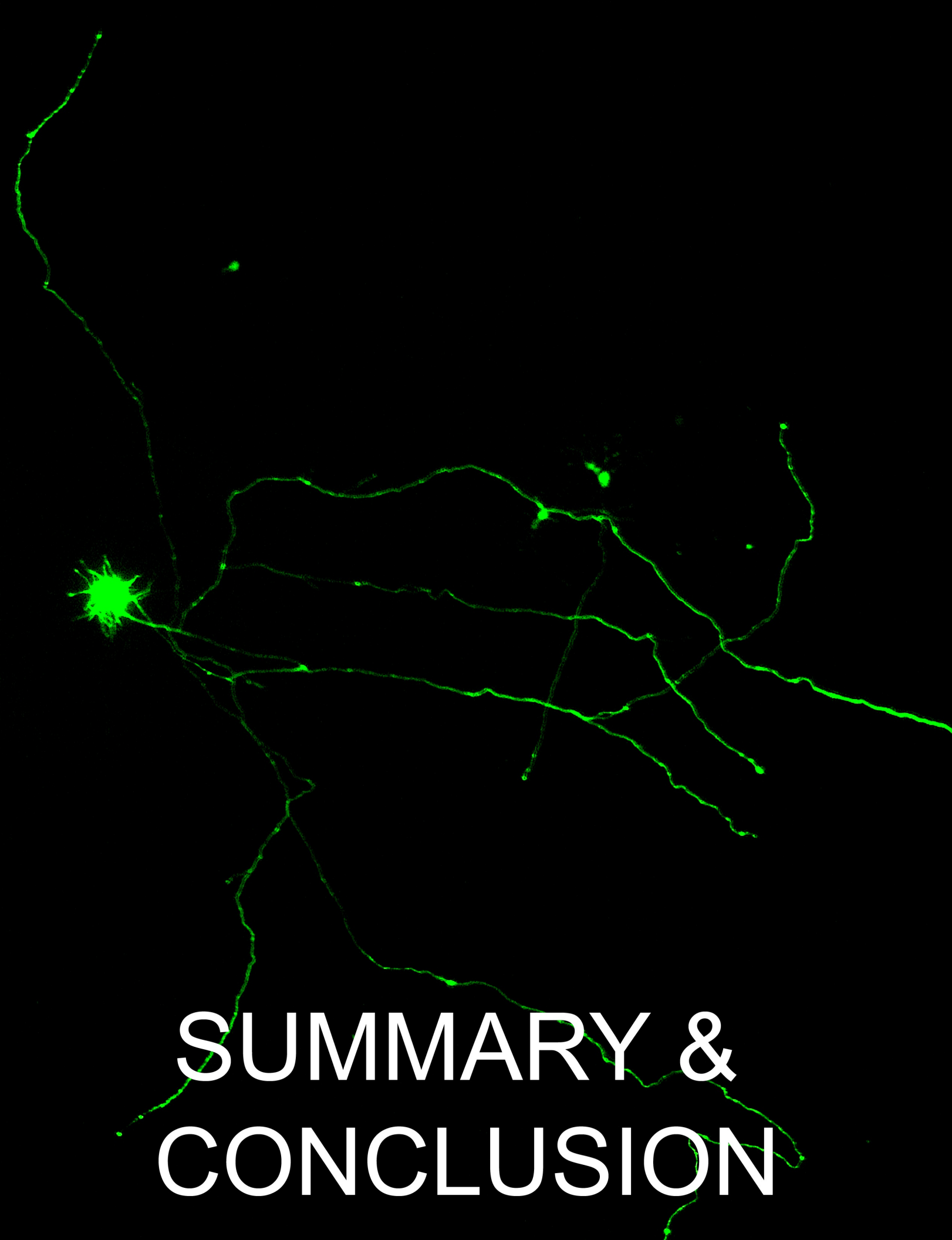

SUMMARY & CONCLUSION

SUMMARY

PART-I

In response to Aβ, primary astrocytes become reactive as early as 6 h and secrete a plethora of molecules, enriched in anti-inflammatory cytokines. We found that tissue inhibitor of matrix metalloproteinase 1 (TIMP-1) is an essential neuroprotective cytokine in this early hour reactive astrocyte conditioned medium. TIMP-1 mediates its neuroprotection by binding to cell surface receptor CD63, increasing the phosphorylation of Akt at ser473 downstream. Further, TIMP-1 inhibits Aβ-induced FOXO3a-mediated apoptosis and corrects impaired autophagy flux.

Major findings:

- Astrocytes become reactive as early as 6 h following Aβ treatment *in vitro.*
- Astrocyte-condition medium (ACM) from 6 h Aβ-treated astrocytes has a protective effect on neurons while the 16 h and 24 h Aβ-ACMs do not.
- Tissue inhibitor of matrix metalloproteinase 1 (TIMP-1) cytokine is enriched in 6 h Aβ-ACM.
- Recombinant TIMP-1 has a protective effect on neurons against Aβ toxicity.
- TIMP-1 upregulates AKT phosphorylation in Aβ-treated neurons and prevents Aβ-directed apoptosis by acting along AKT/FOXO3a/BIM/PUMA axis.
- TIMP-1 corrects Aβ-induced impaired autophagy induction as well as accumulation of p62, the cargo adaptor protein, through activation of common apoptosis-autophagy upstream regulator, AKT.
- TIMP-1 binds to CD63 receptor on neuronal surface to mediate its neuroprotective effect.

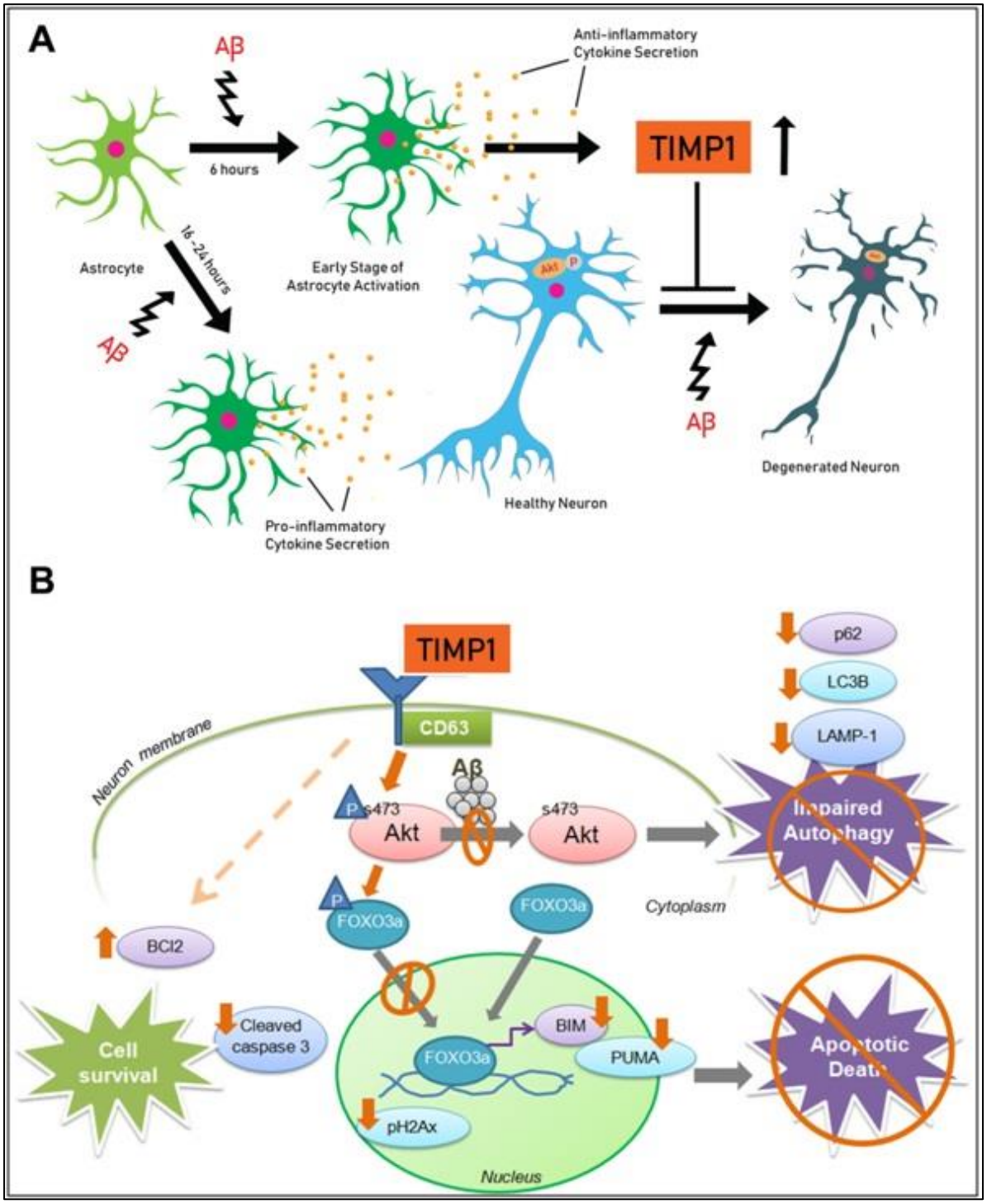

Fig.1: Astrocyte-secreted TIMP-1 is neuroprotective *in vitro*. (A) Astrocyte reactivity in response to Aβ treatment (B) TIMP-1 mediated inhibition of apoptosis and improvement in autophagy flux in Aβ-treated neurons.

PART-II

We used two different animal models of AD - Aβ-injected rats and 5xFAD mice. Following intracerebroventricular TIMP-1 injection we found that there was significant reduction in Aβ plaque load as well as in apoptotic cell death in the hippocampal regions of both these models. Interestingly, both the rodent models of AD showed improved learning and memory abilities following TIMP-1 injection tested through a battery of cognitive behavioral tests. Hence, we conclude that TIMP-1 has the ability to ameliorate cognitive functioning in AD.

Major findings:

- Injection of TIMP-1 in both Aβ-injected (bilaterally) rat and 5xFAD transgenic mouse reduces Aβ plaque load in the hippocampal regions of brain.
- TIMP-1 injection prevents cell death in the CA1 region of the hippocampus in both rat and mouse models of AD by inhibiting apoptosis and improving autophagic flux.
- TIMP-1 injection in both the AD models significantly improves the animals' cognitive behaviors (both explicit and implicit memories) in a battery of learning and memory tests.

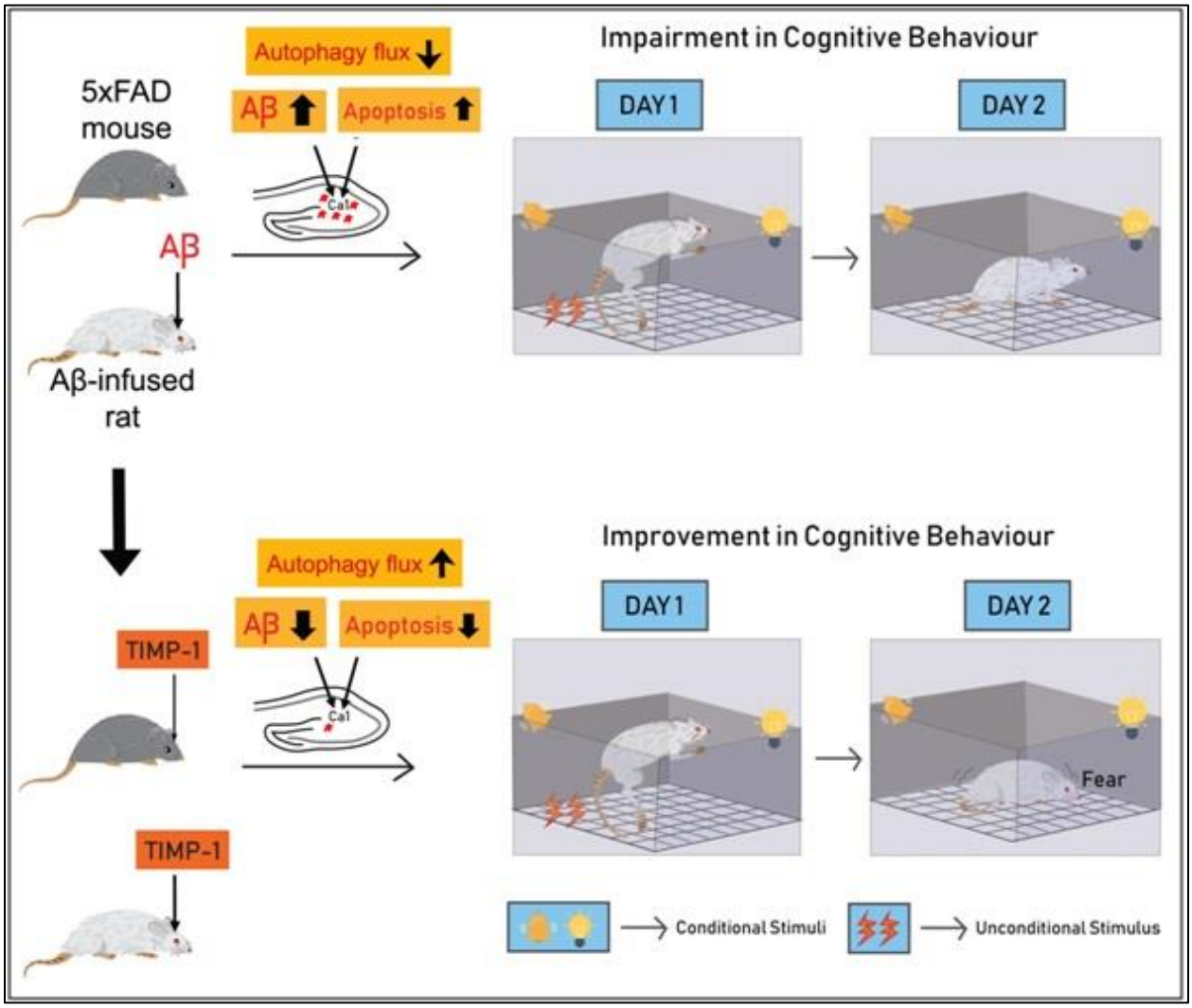

Fig.2: TIMP-1 injection ameliorates cognitive behaviors in animal models of Alzheimer's disease

PART-III

In this part, we investigated the underpinning mechanisms of cognitive recovery in 5xFAD mice following TIMP-1 injection. We show that there is significant improvement in synaptic protein expressions in both total tissue level as well as in isolated synaptosome preparations. We detected that there is improvement in spine density and size in both hippocampus and cortex of TIMP-1 treated 5xFAD mice. Functionally, we show that there is an increase in basal synaptic transmission and long-term potentiation at the Schaffer collateral CA1 synapses in 5xFAD mice injected with TIMP-1. Further, our data reveal that there is inhibition of GSK3β activity (known as a LTP/LTD switch) upon increased phosphoryation by Akt, in 5xFAD mice treated with TIMP-1. Additionally, we found that BDNF level, a neurotrophic factor, is increased significantly in the hippocampus following TIMP-1 injection in 5xFAD mice.

Major findings:

- TIMP-1 injected 5xFAD mice show improvement in pre-synaptic (SNAP-25) and post-synaptic (PSD-95) protein expressions in both hippocampus and cortex.
- TIMP-1 increases spine density and spine size in 5xFAD mice.
- TIMP-1 improves basal synaptic transmission and increases magnitude of long-term potentiation induction at Schaffer-collateral CA1 synapses in 5xFAD mice.
- TIMP-1 inhibits GSK3β activity and induces BDNF secretion from neurons in 5xFAD mice.

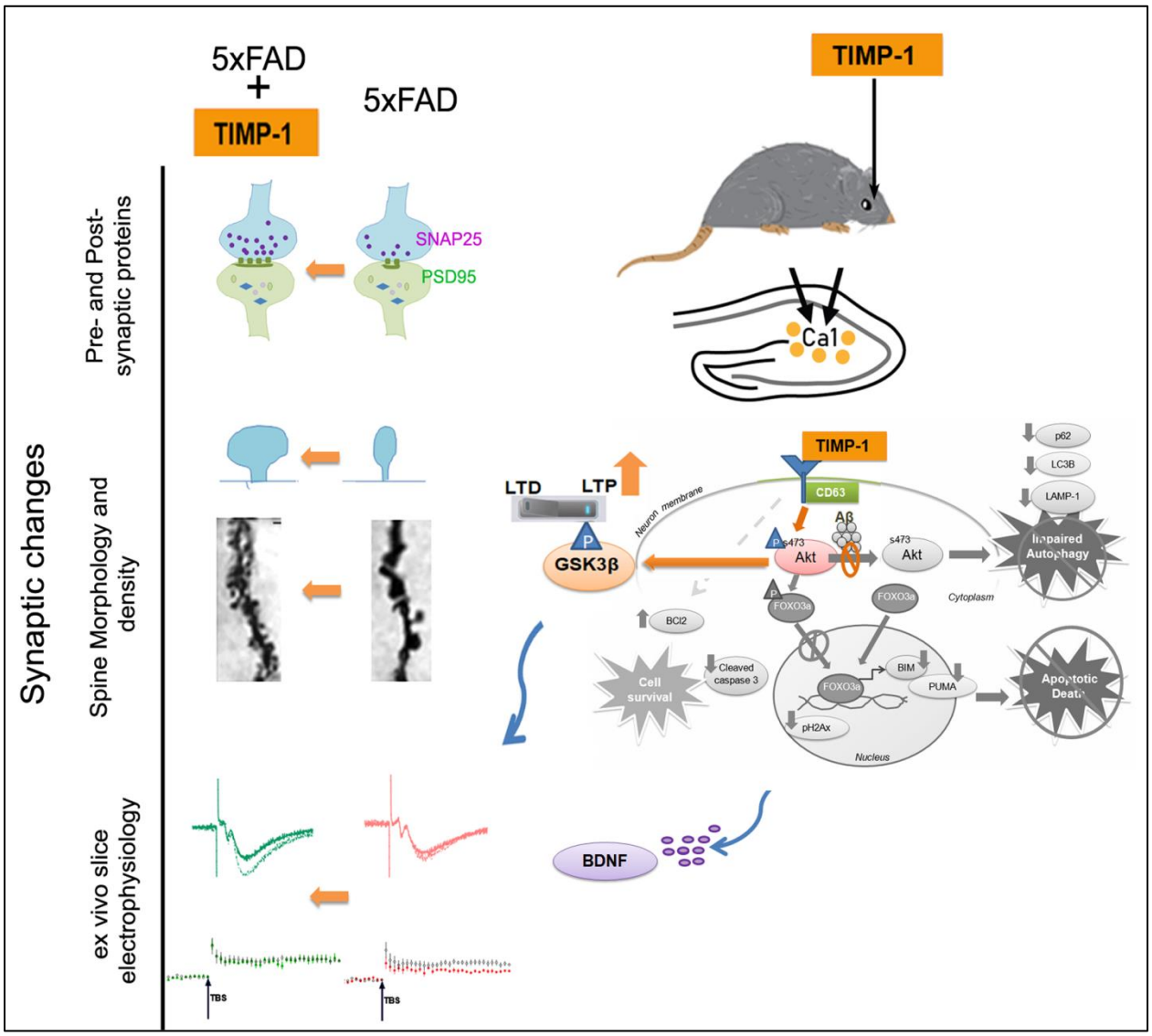

Fig.3: TIMP-1 corrects synaptic dysfunctions in 5xFAD mice – improving synaptic protein expressions, spine morphology and density, and long term potentiation at Schaffer collateral-CA1 synapses.

CONCLUSION

The phenomenon of 'astrocyte reactivity' encompasses several reactive states of astrocytes. During disease pathogenesis of neurodegenerative diseases including Alzheimer's disease (AD), consequent reactive astrocyte heterogeneity may be broadly classified, functionally, as beneficial and detrimental. In Part-I, we tried to explore the secretome profiles of reactive astrocytes in response to oligomeric Aβ *in vitro*. We show that application of previously standardized sub-lethal dose of Aβ in primary astrocytes render them reactive in terms of enhanced expressions of specific astrocyte markers, increased cell perimeter and proliferation as early as 6h. We found that the astrocyte-conditioned medium (ACM) from 6h Aβ-treated astrocytes protected neurons against Aβ toxicity while the 16h and 24h Aβ-ACM failed to do so, rather was detrimental to neurons. We further revealed that a cytokine, tissue inhibitor of matrix metalloproteinase 1 (TIMP-1) was greatly enhanced in the 6h secretome of astrocytes following Aβ treatment. We further established that TIMP-1 was the major contributing factor in rendering the neuroprotective effect of 6h Aβ-ACM since neurtralization of TIMP-1 caused diminution of the neuroprotective efficacy. Our results further revealed that recombinant TIMP-1 protected neurons against Aβ-induced death by disinhibition of Akt signaling pathway. TIMP-1 prevented apoptosis by restricting Aβ-induced Akt-regulated FOXO3a translocation to the nucleus and in the process downregulated the expression of pro-apoptotic proteins BIM and PUMA. Interestingly, TIMP-1 also improved the level of Bcl2 but not Bcl-xl in Aβ-treated neurons alluring towards a differential regulation of

anti-apoptotic proteins by TIMP-1. Earlier reports suggest that TIMP-1 may regulate the expression of either Bcl-xl (Lambert et al., 2003) or Bcl-2 (Nalluri et al., 2015) or both (Ashutosh et al., 2012) albeit in different models. We may thus infer that there are two different pathways in TIMP-1 mediated inhibition of apoptosis in Aβ-treated neurons. Whether these two pathways are independent or cooperate together have not been addressed in our work. TIMP-1 further improved autophagy flux, deregulated under the influence of Aβ, in neurons. Autophagy has been implicated as another major cell death pathway besides apoptosis under Aβ-treated conditions. Additionally, they cooperate in mediating neurotoxicity in AD (Saha et al., 2021). AD is a proteopathic disease and hence clearance of autophagosomal bodies containing toxic cargos is a pre-requisite for the smooth functioning of cells. We show that TIMP-1 was able to restore the homeostatic level of autophagic flux by regulating the upstream Akt kinase that was also involved in apoptosis pathway indicating a common regulator point manipulated by TIMP-1 in correcting both these cell death pathways. Finally, we elucidate that all these beneficial aspects of TIMP-1 are mediated by its binding on the neuronal surface with its cognate receptor CD63 in an MMP-independent manner. However, whether this beneficial effect of TIMP-1 in cell models could be translated in animal models remained to be examined and hence, was taken up in Part-II.

We employed two different animal models – Aβ-infused rat (mimicking sporadic AD) and 5xFAD mouse (mimicking familial AD) for delineating the role of TIMP-1 in AD brain. We found that both in Aβ-infused rats and 5xFAD mice, exogenous TIMP-1 reduced the Aβ plaque load. One predicted mechanism may be that TIMP-1 can

reactivate astrocytes surrounding Aβ plaques in a manner such that they start an overproduction of MMPs and contribute to the clearance of Aβ (Hernandez-Guillamon et al., 2009). TIMP-1 was further able to ameliorate cognitive functioning in both these models tested through a battery of behavioral tests. While positive results from novel object recognition and passive avoidance tests indicated a TIMP-1 mediated improvement in hippocampal-dependent spatial memory (explicit memory) in both the AD models, fear-conditioning test results allured towards an alleviation of implicit memory deficits (involving amygdala) directed by TIMP-1. Hence, both explicit and implicit memories that are damaged in the advanced stage of AD are attenuated by TIMP-1 treatment. In coherence to our Part-I results, TIMP-1 further prevented apoptotic pathway in the hippocampus while correcting the toxic levels of autophagic markers both in the hippocampus and cortical areas in the models. All these pre-clinical data emphasize the value of TIMP-1 as a therapeutic candidate in AD. Interestingly, we found that the endogenous level of TIMP-1 in 5xFAD mice especially from 6 month of age onwards was strongly reduced when compared to age-matched wild type mice. The Ghorpade group has extensively reported that TIMP-1 may be a neuroprotective candidate that they found was reduced in CSF and tissue samples of HAND patients compared to healthy controls but was increased when acute inflammatory insult was given to primary astrocytes in culture (Ashutosh et al., 2012; Suryadevara et al., 2003). Coherently, our report suggests that TIMP-1 is secreted early by reactivated astrocytes as a response to Aβ (acute system) and indeed plays a neuroprotective role in AD brain when supplemented from an exogenous source leading towards cognitive recovery. Neuronal death is an advanced-stage effect of AD while behavioral changes start

comparatively earlier to the loss of neurons. Hence, the next obvious question was to understand the immediate alterations in synaptic functioning that underlie cognitive changes mediated by TIMP-1.

Synaptic plasticity changes in brain form the immediate basis of any observed cognitive changes. In AD, synaptic dysfunction is regarded as the earliest of phenomena even before Aβ plaques, memory impairment and neuron loss. In Part-III, we found that TIMP-1 injection improved the levels of specific pre-synaptic (SNAP-25) and post-synaptic (PSD-95) proteins in both the models of AD. However, we found that not all pre- and post-synaptic proteins were equally affected in the 5xFAD mice by TIMP-1 treatment. TIMP-1 was however able to inhibit increased excitotoxicity (reduced CAMKIIα level) in the hippocampus of 5xFAD mice but not in the cortex. These results were obtained specifically in pure synaptosomes and hence provide a direct picture of the synapse level changes in protein composition following TIMP-1 treatment. Next, we observed improved dendritic spine density as well as spine shape in both hippocampus and cortex of TIMP-1 treated 5xFAD mice compared to the untreated 5xFAD animals. Both spine density and spine shape are important correlates of synaptic plasticity. Besides, the changes in spine density (i.e. number) and the dynamic alterations in spine morphology can impart cognitive resilience in aged AD patients. We found that there was an improved filamentous versus globular actin content in sub-fractionated synaptosomal preparations from TIMP-1 treated 5xFAD mice. Spine actin dynamics is an important determinant of spine shape and size. We inferred that spine size was improved by TIMP-1 infusion in 5xFAD mice. We further revealed a diminished activity of cofilin (implicated

in destabilizing actin) in 5xFAD mice following TIMP-1 treatment while cofilin remained hyperactive in 5xFAD animals. All these data corroborates earlier reports showing cofilin hyperactivity directed cofilin/actin rod formation mediating synaptic dysfunctions as a direct effect of Aβ oligomer treatment (Bamburg et al., 2010; Deng et al., 2016; Liu et al., 2022). We substantiated our biochemical results with ex vivo electrophysiology in acute hippocampal slices along the Schaffer collateral-CA1 synapses. LTP and LTD regulations are the cellular coordinates of synaptic changes (strength, shape, size or number) underlying cognitive functioning. Our results show that TIMP-1 treatment not only improved the basal synaptic transmission in 5xFAD mice but also upregulated the magnitude of LTP induction following a high frequency stimulation compared to untreated 5xFAD mice. However, there was no change in pre-synaptic activity. In connecting the dots as to how TIMP-1 may directly regulate LTP, we found the same Akt in action. We detected that Akt activation upon TIMP-1 treatment inhibited GSK3β activity in 5xFAD mice by improving phosphorylation at Ser9. GSK3β is not only regarded as an LTP/LTD switch but also is known to regulate SNARE protein fusion dynamics (Zhu et al., 2010). Interestingly, we also found an upregulated expression of BDNF in the hippocampus of TIMP-1 injected 5xFAD mice. Thus, the above evidence is strong enough to state that TIMP-1 has a direct implication on several regulators of synaptic plasticity and this explains the mechanistic basis of TIMP-1 mediated cognitive recovery in AD models.

This work elucidates, in a detailed approach, the mechanisms by which reactive astrocyte-secreted TIMP-1 mediates neuroprotection, synaptic improvement and

cognitive recovery in models of AD. This shows that reactivated astrocytes in early AD plays a defensive role against the initial insult by secreting an important neuroprotective cytokine, TIMP-1. Eventually the TIMP-1 levels go down along AD progression resulting in the failure of neuroprotection. It remains to be understood why and how TIMP-1 level decreases with AD progression. Is there a molecular regulator upstream of TIMP-1 in astrocytes? Do astrocytes themselves enter a distinct reactive state along AD progression and stop secreting TIMP-1? All these need to be answered to understand the whole story of TIMP-1. Nevertheless, our work re-emphasizes the importance of astrocyte reactivity in AD and that studying these cells can divulge critical information about novel targets that can be addressed for therapeutic intervention. We propose TIMP-1 as a candidate molecule in cytokine-mediated treatment of AD.

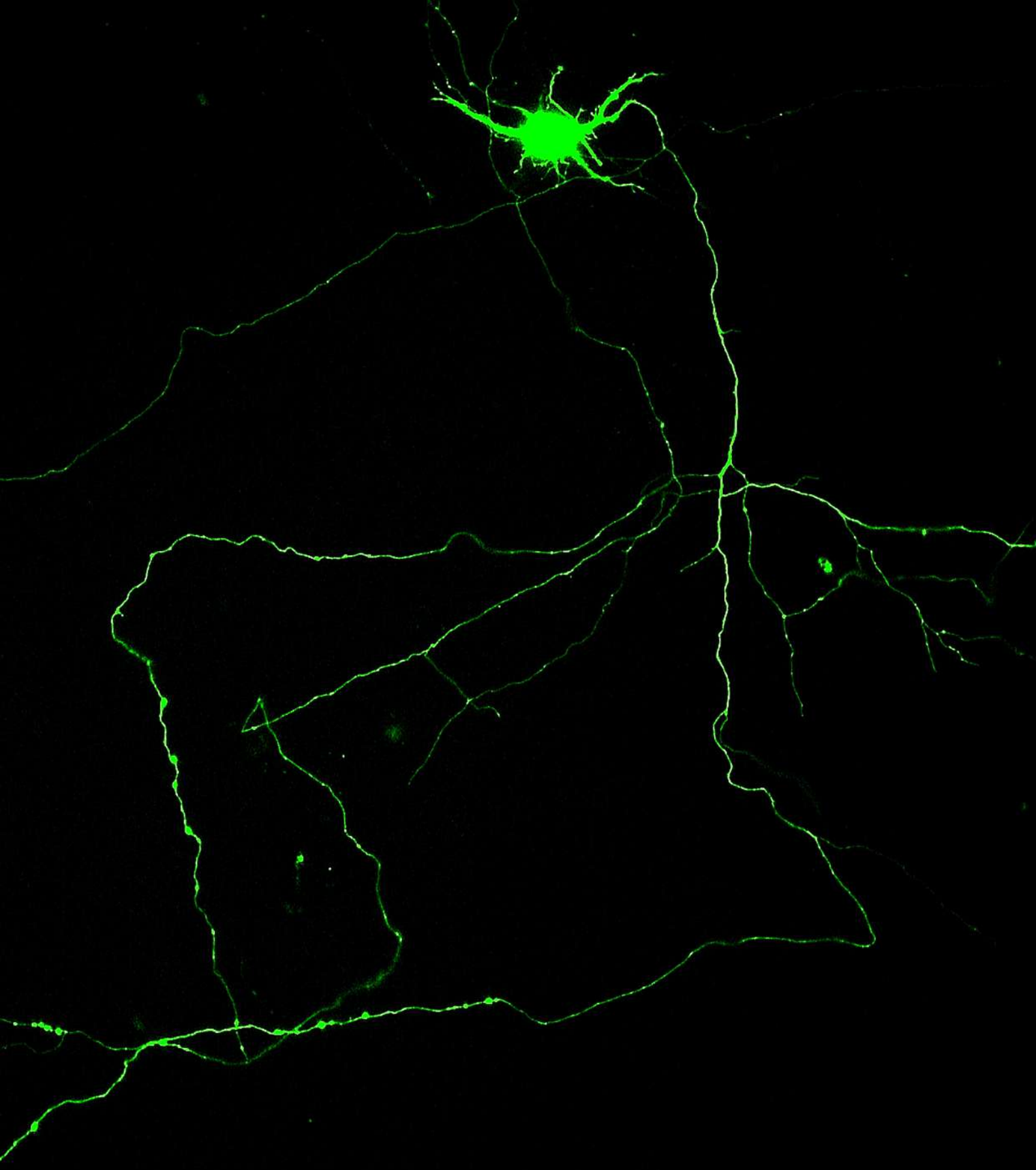

BIBLIOGRAPHY

BIBLIOGRAPHY

(2020). 2020 Alzheimer's disease facts and figures. Alzheimers Dement.

(2022). 2022 Alzheimer's disease facts and figures. Alzheimers Dement *18*, 700-789.

Acosta, C., Anderson, H.D., and Anderson, C.M. (2017). Astrocyte dysfunction in Alzheimer disease. J Neurosci Res *95*, 2430-2447.

Aisen, P.S., Schafer, K.A., Grundman, M., Pfeiffer, E., Sano, M., Davis, K.L., Farlow, M.R., Jin, S., Thomas, R.G., and Thal, L.J. (2003). Effects of rofecoxib or naproxen vs placebo on Alzheimer disease progression: a randomized controlled trial. JAMA *289*, 2819-2826.

Akhter, R., Sanphui, P., and Biswas, S.C. (2014). The essential role of p53-up-regulated modulator of apoptosis (Puma) and its regulation by FoxO3a transcription factor in beta-amyloid-induced neuron death. J Biol Chem *289*, 10812-10822.

Akiyama, H., Barger, S., Barnum, S., Bradt, B., Bauer, J., Cole, G.M., Cooper, N.R., Eikelenboom, P., Emmerling, M., Fiebich, B.L*., et al.* (2000). Inflammation and Alzheimer's disease. Neurobiol Aging *21*, 383-421.

Alkam, T., Nitta, A., Mizoguchi, H., Saito, K., Seshima, M., Itoh, A., Yamada, K., and Nabeshima, T. (2008). Restraining tumor necrosis factor-alpha by thalidomide prevents the amyloid beta-induced impairment of recognition memory in mice. Behav Brain Res *189*, 100-106.

Althoff, G.E., Wolfer, D.P., Timmesfeld, N., Kanzler, B., Schrewe, H., and Pagenstecher, A. (2010). Long-term expression of tissue-inhibitor of matrix metalloproteinase-1 in the murine central nervous system does not alter the morphological and behavioral phenotype but alleviates the course of experimental allergic encephalomyelitis. Am J Pathol *177*, 840-853.

Anderson, M.A., Ao, Y., and Sofroniew, M.V. (2014). Heterogeneity of reactive astrocytes. Neurosci Lett *565*, 23-29.

Anderson, M.A., Burda, J.E., Ren, Y., Ao, Y., O'Shea, T.M., Kawaguchi, R., Coppola, G., Khakh, B.S., Deming, T.J., and Sofroniew, M.V. (2016). Astrocyte scar formation aids central nervous system axon regeneration. Nature *532*, 195-200.

Andriezen, W.L. (1893). The Neuroglia Elements in the Human Brain. Br Med J *2*, 227-230.

Antel, J.P., Becher, B., and Owens, T. (1996). Immunotherapy for multiple sclerosis: from theory to practice. Nat Med *2*, 1074-1075.

Antunes, M., and Biala, G. (2012). The novel object recognition memory: neurobiology, test procedure, and its modifications. Cogn Process *13*, 93-110.

Araque, A., Parpura, V., Sanzgiri, R.P., and Haydon, P.G. (1999). Tripartite synapses: glia, the unacknowledged partner. Trends Neurosci *22*, 208-215.

Arranz, A.M., and De Strooper, B. (2019). The role of astroglia in Alzheimer's disease: pathophysiology and clinical implications. Lancet Neurol *18*, 406-414.

Arsenault, D., Dal-Pan, A., Tremblay, C., Bennett, D.A., Guitton, M.J., De Koninck, Y., Tonegawa, S., and Calon, F. (2013). PAK inactivation impairs social recognition in 3xTg-AD Mice without increasing brain deposition of tau and Abeta. J Neurosci *33*, 10729-10740.

Ashutosh, Chao, C., Borgmann, K., Brew, K., and Ghorpade, A. (2012). Tissue inhibitor of metalloproteinases-1 protects human neurons from staurosporine and HIV-1-induced apoptosis: mechanisms and relevance to HIV-1-associated dementia. Cell Death Dis *3*, e332.

Ashutosh, Kou, W., Cotter, R., Borgmann, K., Wu, L., Persidsky, R., Sakhuja, N., and Ghorpade, A. (2011). CXCL8 protects human neurons from amyloid-beta-induced neurotoxicity: relevance to Alzheimer's disease. Biochem Biophys Res Commun *412*, 565-571.

Audrain, M., Fol, R., Dutar, P., Potier, B., Billard, J.M., Flament, J., Alves, S., Burlot, M.A., Dufayet-Chaffaud, G., Bemelmans, A.P*., et al.* (2016). Alzheimer's disease-like APP processing in wild-type mice identifies synaptic defects as initial steps of disease progression. Mol Neurodegener *11*, 5.

Auld, D.S., and Robitaille, R. (2003). Glial cells and neurotransmission: an inclusive view of synaptic function. Neuron *40*, 389-400.

Babic, T. (1999). The cholinergic hypothesis of Alzheimer's disease: a review of progress. J Neurol Neurosurg Psychiatry *67*, 558.

Bachiller, S., Jimenez-Ferrer, I., Paulus, A., Yang, Y., Swanberg, M., Deierborg, T., and Boza-Serrano, A. (2018). Microglia in Neurological Diseases: A Road Map to Brain-Disease Dependent-Inflammatory Response. Front Cell Neurosci *12*, 488.

Baker, A.H., Edwards, D.R., and Murphy, G. (2002). Metalloproteinase inhibitors: biological actions and therapeutic opportunities. J Cell Sci *115*, 3719-3727.

Ballard, C., Mobley, W., Hardy, J., Williams, G., and Corbett, A. (2016). Dementia in Down's syndrome. Lancet Neurol *15*, 622-636.

Bamburg, J.R., Bernstein, B.W., Davis, R.C., Flynn, K.C., Goldsbury, C., Jensen, J.R., Maloney, M.T., Marsden, I.T., Minamide, L.S., Pak, C.W*., et al.* (2010). ADF/Cofilin-actin rods in neurodegenerative diseases. Curr Alzheimer Res *7*, 241-250.

Barker, W.W., Luis, C.A., Kashuba, A., Luis, M., Harwood, D.G., Loewenstein, D., Waters, C., Jimison, P., Shepherd, E., Sevush, S*., et al.* (2002). Relative frequencies of Alzheimer disease, Lewy body, vascular and frontotemporal dementia, and hippocampal sclerosis in the State of Florida Brain Bank. Alzheimer Dis Assoc Disord *16*, 203-212.

Barnes, D.E., Byers, A.L., Gardner, R.C., Seal, K.H., Boscardin, W.J., and Yaffe, K. (2018). Association of Mild Traumatic Brain Injury With and Without Loss of Consciousness With Dementia in US Military Veterans. JAMA Neurol *75*, 1055-1061.

Barone, E., Mosser, S., and Fraering, P.C. (2014). Inactivation of brain Cofilin-1 by age, Alzheimer's disease and gamma-secretase. Biochim Biophys Acta *1842*, 2500-2509.

Baruch, K., Deczkowska, A., Rosenzweig, N., Tsitsou-Kampeli, A., Sharif, A.M., Matcovitch-Natan, O., Kertser, A., David, E., Amit, I., and Schwartz, M. (2016). PD-1 immune checkpoint blockade reduces pathology and improves memory in mouse models of Alzheimer's disease. Nat Med *22*, 135-137.

Basak, J.M., Verghese, P.B., Yoon, H., Kim, J., and Holtzman, D.M. (2012). Low-density lipoprotein receptor represents an apolipoprotein E-independent pathway of Abeta uptake and degradation by astrocytes. J Biol Chem *287*, 13959-13971.

Bauer, J., Ganter, U., Abel, J., Strauss, S., Jonas, U., Weiss, R., Gebicke-Haerter, P., Volk, B., and Berger, M. (1993). Effects of interleukin-1 and interleukin-6 on metallothionein and amyloid precursor protein expression in human neuroblastoma cells. Evidence that interleukin-6 possibly acts via a receptor different from the 80-kDa interleukin-6 receptor. J Neuroimmunol *45*, 163-173.

Beagle, A.J., Darwish, S.M., Ranasinghe, K.G., La, A.L., Karageorgiou, E., and Vossel, K.A. (2017). Relative Incidence of Seizures and Myoclonus in Alzheimer's Disease, Dementia with Lewy Bodies, and Frontotemporal Dementia. J Alzheimers Dis *60*, 211-223.

Belzung, C., and Griebel, G. (2001). Measuring normal and pathological anxiety-like behaviour in mice: a review. Behav Brain Res *125*, 141-149.

Benzing, W.C., Wujek, J.R., Ward, E.K., Shaffer, D., Ashe, K.H., Younkin, S.G., and Brunden, K.R. (1999). Evidence for glial-mediated inflammation in aged APP(SW) transgenic mice. Neurobiol Aging *20*, 581-589.

Billings, L.M., Oddo, S., Green, K.N., McGaugh, J.L., and LaFerla, F.M. (2005). Intraneuronal Abeta causes the onset of early Alzheimer's disease-related cognitive deficits in transgenic mice. Neuron *45*, 675-688.

Bilousova, T., Miller, C.A., Poon, W.W., Vinters, H.V., Corrada, M., Kawas, C., Hayden, E.Y., Teplow, D.B., Glabe, C., Albay, R., 3rd*, et al.* (2016). Synaptic Amyloid-beta Oligomers Precede p-Tau and Differentiate High Pathology Control Cases. Am J Pathol *186*, 185-198.

Biswas, S.C., Liu, D.X., and Greene, L.A. (2005). Bim is a direct target of a neuronal E2F-dependent apoptotic pathway. J Neurosci *25*, 8349-8358.

Biswas, S.C., Shi, Y., Sproul, A., and Greene, L.A. (2007). Pro-apoptotic Bim induction in response to nerve growth factor deprivation requires simultaneous activation of three different death signaling pathways. J Biol Chem *282*, 29368-29374.

Blasko, I., Veerhuis, R., Stampfer-Kountchev, M., Saurwein-Teissl, M., Eikelenboom, P., and Grubeck-Loebenstein, B. (2000). Costimulatory effects of interferon-gamma and interleukin-1beta or tumor necrosis factor alpha on the synthesis of Abeta1-40 and Abeta1-42 by human astrocytes. Neurobiol Dis *7*, 682-689.

Blurton-Jones, M., and Laferla, F.M. (2006). Pathways by which Abeta facilitates tau pathology. Curr Alzheimer Res *3*, 437-448.

Bommarito, A., Richiusa, P., Carissimi, E., Pizzolanti, G., Rodolico, V., Zito, G., Criscimanna, A., Di Blasi, F., Pitrone, M., Zerilli, M.*, et al.* (2011). BRAFV600E mutation, TIMP-1 upregulation, and NF-kappaB activation: closing the loop on the papillary thyroid cancer trilogy. Endocr Relat Cancer *18*, 669-685.

Bondi, M.W., Edmonds, E.C., and Salmon, D.P. (2017). Alzheimer's Disease: Past, Present, and Future. J Int Neuropsychol Soc *23*, 818-831.

Boros, B.D., Greathouse, K.M., Gentry, E.G., Curtis, K.A., Birchall, E.L., Gearing, M., and Herskowitz, J.H. (2017). Dendritic spines provide cognitive resilience against Alzheimer's disease. Ann Neurol *82*, 602-614.

Bouter, Y., Lopez Noguerola, J.S., Tucholla, P., Crespi, G.A., Parker, M.W., Wiltfang, J., Miles, L.A., and Bayer, T.A. (2015). Abeta targets of the biosimilar antibodies of Bapineuzumab, Crenezumab, Solanezumab in comparison to an antibody against Ntruncated Abeta in sporadic Alzheimer disease cases and mouse models. Acta Neuropathol *130*, 713-729.

Bradley, C.A., Peineau, S., Taghibiglou, C., Nicolas, C.S., Whitcomb, D.J., Bortolotto, Z.A., Kaang, B.K., Cho, K., Wang, Y.T., and Collingridge, G.L. (2012). A pivotal role of GSK-3 in synaptic plasticity. Front Mol Neurosci *5*, 13.

Brier, M.R., Gordon, B., Friedrichsen, K., McCarthy, J., Stern, A., Christensen, J., Owen, C., Aldea, P., Su, Y., Hassenstab, J.*, et al.* (2016). Tau and Abeta imaging, CSF measures, and cognition in Alzheimer's disease. Sci Transl Med *8*, 338ra366.

Brinkmalm, G., Sjodin, S., Simonsen, A.H., Hasselbalch, S.G., Zetterberg, H., Brinkmalm, A., and Blennow, K. (2018). A Parallel Reaction Monitoring Mass Spectrometric Method for Analysis of Potential CSF Biomarkers for Alzheimer's Disease. Proteomics Clin Appl *12*.

Brinkman, S.D., and Gershon, S. (1983). Measurement of cholinergic drug effects on memory in Alzheimer's disease. Neurobiol Aging *4*, 139-145.

Brosseron, F., Krauthausen, M., Kummer, M., and Heneka, M.T. (2014). Body fluid cytokine levels in mild cognitive impairment and Alzheimer's disease: a comparative overview. Mol Neurobiol *50*, 534-544.

Bubser, M., Bridges, T.M., Dencker, D., Gould, R.W., Grannan, M., Noetzel, M.J., Lamsal, A., Niswender, C.M., Daniels, J.S., Poslusney, M.S.*, et al.* (2014). Selective activation of M4 muscarinic acetylcholine receptors reverses MK-801-induced behavioral impairments and enhances associative learning in rodents. ACS Chem Neurosci *5*, 920-942.

Burda, J.E., and Sofroniew, M.V. (2014). Reactive gliosis and the multicellular response to CNS damage and disease. Neuron *81*, 229-248.

Burda, J.E., and Sofroniew, M.V. (2017). Seducing astrocytes to the dark side. Cell Res *27*, 726-727.

Butchart, J., Brook, L., Hopkins, V., Teeling, J., Puntener, U., Culliford, D., Sharples, R., Sharif, S., McFarlane, B., Raybould, R.*, et al.* (2015). Etanercept in Alzheimer disease: A randomized, placebo-controlled, double-blind, phase 2 trial. Neurology *84*, 2161-2168.

Butt, A.M., and Ransom, B.R. (1989). Visualization of oligodendrocytes and astrocytes in the intact rat optic nerve by intracellular injection of lucifer yellow and horseradish peroxidase. Glia *2*, 470-475.

Butterfield, D.A., Reed, T., Newman, S.F., and Sultana, R. (2007). Roles of amyloid beta-peptide-associated oxidative stress and brain protein modifications in the pathogenesis of Alzheimer's disease and mild cognitive impairment. Free Radic Biol Med *43*, 658-677.

Calsolaro, V., and Edison, P. (2016). Neuroinflammation in Alzheimer's disease: Current evidence and future directions. Alzheimers Dement *12*, 719-732.

Carter, S.F., Herholz, K., Rosa-Neto, P., Pellerin, L., Nordberg, A., and Zimmer, E.R. (2019). Astrocyte Biomarkers in Alzheimer's Disease. Trends Mol Med *25*, 77-95.

Cavanagh, C., Tse, Y.C., Nguyen, H.B., Krantic, S., Breitner, J.C., Quirion, R., and Wong, T.P. (2016). Inhibiting tumor necrosis factor-alpha before amyloidosis prevents synaptic deficits in an Alzheimer's disease model. Neurobiol Aging *47*, 41-49.

Cekanaviciute, E., Dietrich, H.K., Axtell, R.C., Williams, A.M., Egusquiza, R., Wai, K.M., Koshy, A.A., and Buckwalter, M.S. (2014). Astrocytic TGF-beta signaling limits inflammation and reduces neuronal damage during central nervous system Toxoplasma infection. J Immunol *193*, 139-149.

Chang, W.P., Koelsch, G., Wong, S., Downs, D., Da, H., Weerasena, V., Gordon, B., Devasamudram, T., Bilcer, G., Ghosh, A.K.*, et al.* (2004). In vivo inhibition of Abeta production by memapsin 2 (beta-secretase) inhibitors. J Neurochem *89*, 1409-1416.

Chavoshinezhad, S., Mohseni Kouchesfahani, H., Ahmadiani, A., and Dargahi, L. (2019). Interferon beta ameliorates cognitive dysfunction in a rat model of Alzheimer's disease: Modulation of

hippocampal neurogenesis and apoptosis as underlying mechanism. Prog Neuropsychopharmacol Biol Psychiatry *94*, 109661.

Cheignon, C., Tomas, M., Bonnefont-Rousselot, D., Faller, P., Hureau, C., and Collin, F. (2018). Oxidative stress and the amyloid beta peptide in Alzheimer's disease. Redox Biol *14*, 450-464.

Chen, J.F., Liu, K., Hu, B., Li, R.R., Xin, W., Chen, H., Wang, F., Chen, L., Li, R.X., Ren, S.Y.*, et al.* (2021). Enhancing myelin renewal reverses cognitive dysfunction in a murine model of Alzheimer's disease. Neuron *109*, 2292-2307 e2295.

Chen, J.H., Ke, K.F., Lu, J.H., Qiu, Y.H., and Peng, Y.P. (2015). Protection of TGF-beta1 against neuroinflammation and neurodegeneration in Abeta1-42-induced Alzheimer's disease model rats. PLoS One *10*, e0116549.

Chen, P., Gu, Z., Liu, W., and Yan, Z. (2007). Glycogen synthase kinase 3 regulates N-methyl-D-aspartate receptor channel trafficking and function in cortical neurons. Mol Pharmacol *72*, 40-51.

Chen, P., Zhao, W., Guo, Y., Xu, J., and Yin, M. (2016). CX3CL1/CX3CR1 in Alzheimer's Disease: A Target for Neuroprotection. Biomed Res Int *2016*, 8090918.

Chen, T.J., Wang, D.C., and Chen, S.S. (2009). Amyloid-beta interrupts the PI3K-Akt-mTOR signaling pathway that could be involved in brain-derived neurotrophic factor-induced Arc expression in rat cortical neurons. J Neurosci Res *87*, 2297-2307.

Chene, G., Beiser, A., Au, R., Preis, S.R., Wolf, P.A., Dufouil, C., and Seshadri, S. (2015). Gender and incidence of dementia in the Framingham Heart Study from mid-adult life. Alzheimers Dement *11*, 310-320.

Cheng, L., Yin, W.J., Zhang, J.F., and Qi, J.S. (2009). Amyloid beta-protein fragments 25-35 and 31-35 potentiate long-term depression in hippocampal CA1 region of rats in vivo. Synapse *63*, 206-214.

Choi, D., Choi, S., and Park, S.M. (2018). Effect of smoking cessation on the risk of dementia: a longitudinal study. Ann Clin Transl Neurol *5*, 1192-1199.

Chou, R.C., Kane, M., Ghimire, S., Gautam, S., and Gui, J. (2016). Treatment for Rheumatoid Arthritis and Risk of Alzheimer's Disease: A Nested Case-Control Analysis. CNS Drugs *30*, 1111-1120.

Citri, A., and Malenka, R.C. (2008). Synaptic plasticity: multiple forms, functions, and mechanisms. Neuropsychopharmacology *33*, 18-41.

Clarke, M.T.M., Brinkmalm, A., Foiani, M.S., Woollacott, I.O.C., Heller, C., Heslegrave, A., Keshavan, A., Fox, N.C., Schott, J.M., Warren, J.D.*, et al.* (2019). CSF synaptic protein concentrations are raised in those with atypical Alzheimer's disease but not frontotemporal dementia. Alzheimers Res Ther *11*, 105.

Crusio, W.E. (2001). Genetic dissection of mouse exploratory behaviour. Behav Brain Res *125*, 127-132.

Cruz-Munoz, W., and Khokha, R. (2008). The role of tissue inhibitors of metalloproteinases in tumorigenesis and metastasis. Crit Rev Clin Lab Sci *45*, 291-338.

Cui, H., Seubert, B., Stahl, E., Dietz, H., Reuning, U., Moreno-Leon, L., Ilie, M., Hofman, P., Nagase, H., Mari, B.*, et al.* (2015). Tissue inhibitor of metalloproteinases-1 induces a pro-tumourigenic increase of miR-210 in lung adenocarcinoma cells and their exosomes. Oncogene *34*, 3640-3650.

Cummings, J., Aisen, P., Lemere, C., Atri, A., Sabbagh, M., and Salloway, S. (2021). Aducanumab produced a clinically meaningful benefit in association with amyloid lowering. Alzheimers Res Ther *13*, 98.

Cummings, J.L., Morstorf, T., and Zhong, K. (2014). Alzheimer's disease drug-development pipeline: few candidates, frequent failures. Alzheimers Res Ther *6*, 37.

Daulatzai, M.A. (2017). Cerebral hypoperfusion and glucose hypometabolism: Key pathophysiological modulators promote neurodegeneration, cognitive impairment, and Alzheimer's disease. J Neurosci Res *95*, 943-972.

Davies, C.A., Mann, D.M., Sumpter, P.Q., and Yates, P.O. (1987). A quantitative morphometric analysis of the neuronal and synaptic content of the frontal and temporal cortex in patients with Alzheimer's disease. J Neurol Sci *78*, 151-164.

Davies, P., and Maloney, A.J. (1976). Selective loss of central cholinergic neurons in Alzheimer's disease. Lancet *2*, 1403.

Davis, R.C., Marsden, I.T., Maloney, M.T., Minamide, L.S., Podlisny, M., Selkoe, D.J., and Bamburg, J.R. (2011). Amyloid beta dimers/trimers potently induce cofilin-actin rods that are inhibited by maintaining cofilin-phosphorylation. Mol Neurodegener *6*, 10.

De Biase, L.M., Schuebel, K.E., Fusfeld, Z.H., Jair, K., Hawes, I.A., Cimbro, R., Zhang, H.Y., Liu, Q.R., Shen, H., Xi, Z.X.*, et al.* (2017). Local Cues Establish and Maintain Region-Specific Phenotypes of Basal Ganglia Microglia. Neuron *95*, 341-356 e346.

de Jong, D., Jansen, R., Hoefnagels, W., Jellesma-Eggenkamp, M., Verbeek, M., Borm, G., and Kremer, B. (2008). No effect of one-year treatment with indomethacin on Alzheimer's disease progression: a randomized controlled trial. PLoS One *3*, e1475.

De Strooper, B., and Karran, E. (2016). The Cellular Phase of Alzheimer's Disease. Cell *164*, 603-615.

Decourt, B., Lahiri, D.K., and Sabbagh, M.N. (2017). Targeting Tumor Necrosis Factor Alpha for Alzheimer's Disease. Curr Alzheimer Res *14*, 412-425.

Deng, Y., Wei, J., Cheng, J., Zhong, P., Xiong, Z., Liu, A., Lin, L., Chen, S., and Yan, Z. (2016). Partial Amelioration of Synaptic and Cognitive Deficits by Inhibiting Cofilin Dephosphorylation in an Animal Model of Alzheimer's Disease. J Alzheimers Dis *53*, 1419-1432.

Detrait, E.R., Danis, B., Lamberty, Y., and Foerch, P. (2014). Peripheral administration of an anti-TNF-alpha receptor fusion protein counteracts the amyloid induced elevation of hippocampal TNF-alpha levels and memory deficits in mice. Neurochem Int *72*, 10-13.

DeTure, M.A., and Dickson, D.W. (2019). The neuropathological diagnosis of Alzheimer's disease. Mol Neurodegener *14*, 32.

Drummond, E., and Wisniewski, T. (2017). Alzheimer's disease: experimental models and reality. Acta Neuropathol *133*, 155-175.

Du, X., Wang, X., and Geng, M. (2018). Alzheimer's disease hypothesis and related therapies. Transl Neurodegener *7*, 2.

Dubois, B., Hampel, H., Feldman, H.H., Scheltens, P., Aisen, P., Andrieu, S., Bakardjian, H., Benali, H., Bertram, L., Blennow, K.*, et al.* (2016). Preclinical Alzheimer's disease: Definition, natural history, and diagnostic criteria. Alzheimers Dement *12*, 292-323.

Ekert, J.O., Gould, R.L., Reynolds, G., and Howard, R.J. (2018). TNF alpha inhibitors in Alzheimer's disease: A systematic review. Int J Geriatr Psychiatry *33*, 688-694.

Ennaceur, A. (2010). One-trial object recognition in rats and mice: methodological and theoretical issues. Behav Brain Res *215*, 244-254.

Eriksen, J.L., Sagi, S.A., Smith, T.E., Weggen, S., Das, P., McLendon, D.C., Ozols, V.V., Jessing, K.W., Zavitz, K.H., Koo, E.H.*, et al.* (2003). NSAIDs and enantiomers of flurbiprofen target gamma-secretase and lower Abeta 42 in vivo. J Clin Invest *112*, 440-449.

Escartin, C., Galea, E., Lakatos, A., O'Callaghan, J.P., Petzold, G.C., Serrano-Pozo, A., Steinhauser, C., Volterra, A., Carmignoto, G., Agarwal, A.*, et al.* (2021). Reactive astrocyte nomenclature, definitions, and future directions. Nat Neurosci *24*, 312-325.

Escartin, C., Guillemaud, O., and Carrillo-de Sauvage, M.A. (2019). Questions and (some) answers on reactive astrocytes. Glia *67*, 2221-2247.

Evans, D.A., Bennett, D.A., Wilson, R.S., Bienias, J.L., Morris, M.C., Scherr, P.A., Hebert, L.E., Aggarwal, N., Beckett, L.A., Joglekar, R.*, et al.* (2003). Incidence of Alzheimer disease in a biracial urban community: relation to apolipoprotein E allele status. Arch Neurol *60*, 185-189.

Facchinetti, R., Bronzuoli, M.R., and Scuderi, C. (2018). An Animal Model of Alzheimer Disease Based on the Intrahippocampal Injection of Amyloid beta-Peptide (1-42). Methods Mol Biol *1727*, 343-352.

Fager, N., and Jaworski, D.M. (2000). Differential spatial distribution and temporal regulation of tissue inhibitor of metalloproteinase mRNA expression during rat central nervous system development. Mech Dev *98*, 105-109.

Fakhoury, M. (2018). Microglia and Astrocytes in Alzheimer's Disease: Implications for Therapy. Curr Neuropharmacol *16*, 508-518.

Fan, L., Mao, C., Hu, X., Zhang, S., Yang, Z., Hu, Z., Sun, H., Fan, Y., Dong, Y., Yang, J.*, et al.* (2019). New Insights Into the Pathogenesis of Alzheimer's Disease. Front Neurol *10*, 1312.

Fann, J.R., Ribe, A.R., Pedersen, H.S., Fenger-Gron, M., Christensen, J., Benros, M.E., and Vestergaard, M. (2018). Long-term risk of dementia among people with traumatic brain injury in Denmark: a population-based observational cohort study. Lancet Psychiatry *5*, 424-431.

Fisher, G.G., Stachowski, A., Infurna, F.J., Faul, J.D., Grosch, J., and Tetrick, L.E. (2014). Mental work demands, retirement, and longitudinal trajectories of cognitive functioning. J Occup Health Psychol *19*, 231-242.

Forner, S., Baglietto-Vargas, D., Martini, A.C., Trujillo-Estrada, L., and LaFerla, F.M. (2017). Synaptic Impairment in Alzheimer's Disease: A Dysregulated Symphony. Trends Neurosci *40*, 347-357.

Forner, S., Kawauchi, S., Balderrama-Gutierrez, G., Kramar, E.A., Matheos, D.P., Phan, J., Javonillo, D.I., Tran, K.M., Hingco, E., da Cunha, C.*, et al.* (2021). Systematic phenotyping and characterization of the 5xFAD mouse model of Alzheimer's disease. Sci Data *8*, 270.

Fowler, S.W., Chiang, A.C., Savjani, R.R., Larson, M.E., Sherman, M.A., Schuler, D.R., Cirrito, J.R., Lesne, S.E., and Jankowsky, J.L. (2014). Genetic modulation of soluble Abeta rescues cognitive and synaptic impairment in a mouse model of Alzheimer's disease. J Neurosci *34*, 7871-7885.

Fu, A.K., Hung, K.W., Yuen, M.Y., Zhou, X., Mak, D.S., Chan, I.C., Cheung, T.H., Zhang, B., Fu, W.Y., Liew, F.Y.*, et al.* (2016). IL-33 ameliorates Alzheimer's disease-like pathology and cognitive decline. Proc Natl Acad Sci U S A *113*, E2705-2713.

Funato, H., Yoshimura, M., Yamazaki, T., Saido, T.C., Ito, Y., Yokofujita, J., Okeda, R., and Ihara, Y. (1998). Astrocytes containing amyloid beta-protein (Abeta)-positive granules are associated with Abeta40-positive diffuse plaques in the aged human brain. Am J Pathol *152*, 983-992.

Furman, J.L., Sama, D.M., Gant, J.C., Beckett, T.L., Murphy, M.P., Bachstetter, A.D., Van Eldik, L.J., and Norris, C.M. (2012). Targeting astrocytes ameliorates neurologic changes in a mouse model of Alzheimer's disease. J Neurosci *32*, 16129-16140.

Gabbita, S.P., Srivastava, M.K., Eslami, P., Johnson, M.F., Kobritz, N.K., Tweedie, D., Greig, N.H., Zemlan, F.P., Sharma, S.P., and Harris-White, M.E. (2012). Early intervention with a small molecule inhibitor for tumor necrosis factor-alpha prevents cognitive deficits in a triple transgenic mouse model of Alzheimer's disease. J Neuroinflammation *9*, 99.

Gallini, A., Sommet, A., and Montastruc, J.L. (2008). Does memantine induce bradycardia? A study in the French PharmacoVigilance Database. Pharmacoepidemiol Drug Saf *17*, 877-881.

Games, D., Adams, D., Alessandrini, R., Barbour, R., Berthelette, P., Blackwell, C., Carr, T., Clemens, J., Donaldson, T., Gillespie, F.*, et al.* (1995). Alzheimer-type neuropathology in transgenic mice overexpressing V717F beta-amyloid precursor protein. Nature *373*, 523-527.

Ganter, U., Strauss, S., Jonas, U., Weidemann, A., Beyreuther, K., Volk, B., Berger, M., and Bauer, J. (1991). Alpha 2-macroglobulin synthesis in interleukin-6-stimulated human neuronal (SH-SY5Y neuroblastoma) cells. Potential significance for the processing of Alzheimer beta-amyloid precursor protein. FEBS Lett *282*, 127-131.

Garabadu, D., and Verma, J. (2019). Exendin-4 attenuates brain mitochondrial toxicity through PI3K/Akt-dependent pathway in amyloid beta (1-42)-induced cognitive deficit rats. Neurochem Int *128*, 39-49.

Gardner, J., and Ghorpade, A. (2003). Tissue inhibitor of metalloproteinase (TIMP)-1: the TIMPed balance of matrix metalloproteinases in the central nervous system. J Neurosci Res *74*, 801-806.

Garwood, C.J., Cooper, J.D., Hanger, D.P., and Noble, W. (2010). Anti-inflammatory impact of minocycline in a mouse model of tauopathy. Front Psychiatry *1*, 136.

Garwood, C.J., Pooler, A.M., Atherton, J., Hanger, D.P., and Noble, W. (2011). Astrocytes are important mediators of Abeta-induced neurotoxicity and tau phosphorylation in primary culture. Cell Death Dis *2*, e167.

Garwood, C.J., Ratcliffe, L.E., Simpson, J.E., Heath, P.R., Ince, P.G., and Wharton, S.B. (2017). Review: Astrocytes in Alzheimer's disease and other age-associated dementias: a supporting player with a central role. Neuropathol Appl Neurobiol *43*, 281-298.

Gasparini, L., Ongini, E., and Wenk, G. (2004). Non-steroidal anti-inflammatory drugs (NSAIDs) in Alzheimer's disease: old and new mechanisms of action. J Neurochem *91*, 521-536.

Gauthier, S., Feldman, H.H., Schneider, L.S., Wilcock, G.K., Frisoni, G.B., Hardlund, J.H., Moebius, H.J., Bentham, P., Kook, K.A., Wischik, D.J.*, et al.* (2016). Efficacy and safety of tau-aggregation inhibitor therapy in patients with mild or moderate Alzheimer's disease: a randomised, controlled, double-blind, parallel-arm, phase 3 trial. Lancet *388*, 2873-2884.

Gharami, K., and Biswas, S.C. (2020). Glutamate treatment mimics LTP- and LTD-like biochemical activity in viable synaptosome preparation. Neurochem Int *134*, 104655.

Giaume, C., Kirchhoff, F., Matute, C., Reichenbach, A., and Verkhratsky, A. (2007). Glia: the fulcrum of brain diseases. Cell Death Differ *14*, 1324-1335.

Gibbs, M.E., Hutchinson, D., and Hertz, L. (2008). Astrocytic involvement in learning and memory consolidation. Neurosci Biobehav Rev *32*, 927-944.

Gilman, S., Koller, M., Black, R.S., Jenkins, L., Griffith, S.G., Fox, N.C., Eisner, L., Kirby, L., Rovira, M.B., Forette, F.*, et al.* (2005). Clinical effects of Abeta immunization (AN1792) in patients with AD in an interrupted trial. Neurology *64*, 1553-1562.

Goncalves, A., Lin, C.M., Muthusamy, A., Fontes-Ribeiro, C., Ambrosio, A.F., Abcouwer, S.F., Fernandes, R., and Antonetti, D.A. (2016). Protective Effect of a GLP-1 Analog on Ischemia-Reperfusion Induced Blood-Retinal Barrier Breakdown and Inflammation. Invest Ophthalmol Vis Sci *57*, 2584-2592.

Graham, W.V., Bonito-Oliva, A., and Sakmar, T.P. (2017). Update on Alzheimer's Disease Therapy and Prevention Strategies. Annu Rev Med *68*, 413-430.

Greber, S., Lubec, G., Cairns, N., and Fountoulakis, M. (1999). Decreased levels of synaptosomal associated protein 25 in the brain of patients with Down syndrome and Alzheimer's disease. Electrophoresis *20*, 928-934.

Green, R.C., Cupples, L.A., Go, R., Benke, K.S., Edeki, T., Griffith, P.A., Williams, M., Hipps, Y., Graff-Radford, N., Bachman, D.*, et al.* (2002). Risk of dementia among white and African American relatives of patients with Alzheimer disease. JAMA *287*, 329-336.

Griffin, W.S., Sheng, J.G., Royston, M.C., Gentleman, S.M., McKenzie, J.E., Graham, D.I., Roberts, G.W., and Mrak, R.E. (1998). Glial-neuronal interactions in Alzheimer's disease: the potential role of a 'cytokine cycle' in disease progression. Brain Pathol *8*, 65-72.

Grubman, A., Chew, G., Ouyang, J.F., Sun, G., Choo, X.Y., McLean, C., Simmons, R.K., Buckberry, S., Vargas-Landin, D.B., Poppe, D.*, et al.* (2019). A single-cell atlas of entorhinal cortex from individuals with Alzheimer's disease reveals cell-type-specific gene expression regulation. Nat Neurosci *22*, 2087-2097.

Grunwald, B., Schoeps, B., and Kruger, A. (2019). Recognizing the Molecular Multifunctionality and Interactome of TIMP-1. Trends Cell Biol *29*, 6-19.

Gu, Y., Beato, J.M., Amarante, E., Chesebro, A.G., Manly, J.J., Schupf, N., Mayeux, R.P., and Brickman, A.M. (2020). Assessment of Leisure Time Physical Activity and Brain Health in a Multiethnic Cohort of Older Adults. JAMA Netw Open *3*, e2026506.

Gudala, K., Bansal, D., Schifano, F., and Bhansali, A. (2013). Diabetes mellitus and risk of dementia: A meta-analysis of prospective observational studies. J Diabetes Investig *4*, 640-650.

Guedez, L., Courtemanch, L., and Stetler-Stevenson, M. (1998). Tissue inhibitor of metalloproteinase (TIMP)-1 induces differentiation and an antiapoptotic phenotype in germinal center B cells. Blood *92*, 1342-1349.

Guedez, L., Mansoor, A., Birkedal-Hansen, B., Lim, M.S., Fukushima, P., Venzon, D., Stetler-Stevenson, W.G., and Stetler-Stevenson, M. (2001). Tissue inhibitor of metalloproteinases 1 regulation of interleukin-10 in B-cell differentiation and lymphomagenesis. Blood *97*, 1796-1802.

Guha, S., Paidi, R.K., Goswami, S., Saha, P., and Biswas, S.C. (2022). ICAM-1 protects neurons against Amyloid-beta and improves cognitive behaviors in 5xFAD mice by inhibiting NF-kappaB. Brain Behav Immun *100*, 194-210.

Gullo, F., Ceriani, M., D'Aloia, A., Wanke, E., Constanti, A., Costa, B., and Lecchi, M. (2017). Plant Polyphenols and Exendin-4 Prevent Hyperactivity and TNF-alpha Release in LPS-Treated In vitro Neuron/Astrocyte/Microglial Networks. Front Neurosci *11*, 500.

Guo, L.J., Luo, X.H., Xie, H., Zhou, H.D., Yuan, L.Q., Wang, M., and Liao, E.Y. (2006). Tissue inhibitor of matrix metalloproteinase-1 suppresses apoptosis of mouse bone marrow stromal cell line MBA-1. Calcif Tissue Int *78*, 285-292.

Gylys, K.H., Fein, J.A., Yang, F., Wiley, D.J., Miller, C.A., and Cole, G.M. (2004). Synaptic changes in Alzheimer's disease: increased amyloid-beta and gliosis in surviving terminals is accompanied by decreased PSD-95 fluorescence. Am J Pathol *165*, 1809-1817.

Haass, C., and Selkoe, D.J. (2007). Soluble protein oligomers in neurodegeneration: lessons from the Alzheimer's amyloid beta-peptide. Nat Rev Mol Cell Biol *8*, 101-112.

Habbas, S., Santello, M., Becker, D., Stubbe, H., Zappia, G., Liaudet, N., Klaus, F.R., Kollias, G., Fontana, A., Pryce, C.R.*, et al.* (2015). Neuroinflammatory TNFalpha Impairs Memory via Astrocyte Signaling. Cell *163*, 1730-1741.

Habib, N., McCabe, C., Medina, S., Varshavsky, M., Kitsberg, D., Dvir-Szternfeld, R., Green, G., Dionne, D., Nguyen, L., Marshall, J.L.*, et al.* (2020). Disease-associated astrocytes in Alzheimer's disease and aging. Nat Neurosci *23*, 701-706.

Hamann, S., Monarch, E.S., and Goldstein, F.C. (2002). Impaired fear conditioning in Alzheimer's disease. Neuropsychologia *40*, 1187-1195.

Hammond, R.S., Tull, L.E., and Stackman, R.W. (2004). On the delay-dependent involvement of the hippocampus in object recognition memory. Neurobiol Learn Mem *82*, 26-34.

Hardy, J.A., and Higgins, G.A. (1992). Alzheimer's disease: the amyloid cascade hypothesis. Science *256*, 184-185.

Hasel, P., Rose, I.V.L., Sadick, J.S., Kim, R.D., and Liddelow, S.A. (2021). Neuroinflammatory astrocyte subtypes in the mouse brain. Nat Neurosci *24*, 1475-1487.

Hasselmo, M.E., Anderson, B.P., and Bower, J.M. (1992). Cholinergic modulation of cortical associative memory function. J Neurophysiol *67*, 1230-1246.

He, P., Cheng, X., Staufenbiel, M., Li, R., and Shen, Y. (2013). Long-term treatment of thalidomide ameliorates amyloid-like pathology through inhibition of beta-secretase in a mouse model of Alzheimer's disease. PLoS One *8*, e55091.

Hebert, L.E., Weuve, J., Scherr, P.A., and Evans, D.A. (2013). Alzheimer disease in the United States (2010-2050) estimated using the 2010 census. Neurology *80*, 1778-1783.

Heredia, L., Helguera, P., de Olmos, S., Kedikian, G., Sola Vigo, F., LaFerla, F., Staufenbiel, M., de Olmos, J., Busciglio, J., Caceres, A.*, et al.* (2006). Phosphorylation of actin-depolymerizing factor/cofilin by LIM-kinase mediates amyloid beta-induced degeneration: a potential mechanism of neuronal dystrophy in Alzheimer's disease. J Neurosci *26*, 6533-6542.

Hernandez-Guillamon, M., Delgado, P., Ortega, L., Pares, M., Rosell, A., Garcia-Bonilla, L., Fernandez-Cadenas, I., Borrell-Pages, M., Boada, M., and Montaner, J. (2009). Neuronal TIMP-1 release accompanies astrocytic MMP-9 secretion and enhances astrocyte proliferation induced by beta-amyloid 25-35 fragment. J Neurosci Res *87*, 2115-2125.

Hernandez, F., Borrell, J., Guaza, C., Avila, J., and Lucas, J.J. (2002). Spatial learning deficit in transgenic mice that conditionally over-express GSK-3beta in the brain but do not form tau filaments. J Neurochem *83*, 1529-1533.

Herskovits, A.Z., Locascio, J.J., Peskind, E.R., Li, G., and Hyman, B.T. (2013). A Luminex assay detects amyloid beta oligomers in Alzheimer's disease cerebrospinal fluid. PLoS One *8*, e67898.

Heyser, C.J., Masliah, E., Samimi, A., Campbell, I.L., and Gold, L.H. (1997). Progressive decline in avoidance learning paralleled by inflammatory neurodegeneration in transgenic mice expressing interleukin 6 in the brain. Proc Natl Acad Sci U S A *94*, 1500-1505.

Holmes, C., Boche, D., Wilkinson, D., Yadegarfar, G., Hopkins, V., Bayer, A., Jones, R.W., Bullock, R., Love, S., Neal, J.W.*, et al.* (2008). Long-term effects of Abeta42 immunisation in Alzheimer's disease: follow-up of a randomised, placebo-controlled phase I trial. Lancet *372*, 216-223.

Hong, S., Beja-Glasser, V.F., Nfonoyim, B.M., Frouin, A., Li, S., Ramakrishnan, S., Merry, K.M., Shi, Q., Rosenthal, A., Barres, B.A.*, et al.* (2016). Complement and microglia mediate early synapse loss in Alzheimer mouse models. Science *352*, 712-716.

Hooper, C., Markevich, V., Plattner, F., Killick, R., Schofield, E., Engel, T., Hernandez, F., Anderton, B., Rosenblum, K., Bliss, T.*, et al.* (2007). Glycogen synthase kinase-3 inhibition is integral to long-term potentiation. Eur J Neurosci *25*, 81-86.

Hoover, B.R., Reed, M.N., Su, J., Penrod, R.D., Kotilinek, L.A., Grant, M.K., Pitstick, R., Carlson, G.A., Lanier, L.M., Yuan, L.L.*, et al.* (2010). Tau mislocalization to dendritic spines mediates synaptic dysfunction independently of neurodegeneration. Neuron *68*, 1067-1081.

Hu, Y., Chen, W., Wu, L., Jiang, L., Liang, N., Tan, L., Liang, M., and Tang, N. (2019). TGF-beta1 Restores Hippocampal Synaptic Plasticity and Memory in Alzheimer Model via the PI3K/Akt/Wnt/beta-Catenin Signaling Pathway. J Mol Neurosci *67*, 142-149.

Hughes, P.M., Botham, M.S., Frentzel, S., Mir, A., and Perry, V.H. (2002). Expression of fractalkine (CX3CL1) and its receptor, CX3CR1, during acute and chronic inflammation in the rodent CNS. Glia *37*, 314-327.

Inspector, M., Aharon-Perez, J., Glass-Marmor, L., and Miller, A. (2005). Matrix metalloproteinase-9, its tissue inhibitor(TIMP)-1 and CRP in Alzheimer's disease. Eur Neurol *53*, 155-157.

Izzo, N.J., Xu, J., Zeng, C., Kirk, M.J., Mozzoni, K., Silky, C., Rehak, C., Yurko, R., Look, G., Rishton, G.*, et al.* (2014). Alzheimer's therapeutics targeting amyloid beta 1-42 oligomers II: Sigma-2/PGRMC1 receptors mediate Abeta 42 oligomer binding and synaptotoxicity. PLoS One *9*, e111899.

Jack, C.R., Jr., Bennett, D.A., Blennow, K., Carrillo, M.C., Dunn, B., Haeberlein, S.B., Holtzman, D.M., Jagust, W., Jessen, F., Karlawish, J.*, et al.* (2018). NIA-AA Research Framework: Toward a biological definition of Alzheimer's disease. Alzheimers Dement *14*, 535-562.

Jack, C.R., Jr., Wiste, H.J., Vemuri, P., Weigand, S.D., Senjem, M.L., Zeng, G., Bernstein, M.A., Gunter, J.L., Pankratz, V.S., Aisen, P.S.*, et al.* (2010). Brain beta-amyloid measures and magnetic resonance imaging atrophy both predict time-to-progression from mild cognitive impairment to Alzheimer's disease. Brain *133*, 3336-3348.

Jackson, H.W., Defamie, V., Waterhouse, P., and Khokha, R. (2017). TIMPs: versatile extracellular regulators in cancer. Nat Rev Cancer *17*, 38-53.

Jacobsen, J.S., Wu, C.C., Redwine, J.M., Comery, T.A., Arias, R., Bowlby, M., Martone, R., Morrison, J.H., Pangalos, M.N., Reinhart, P.H.*, et al.* (2006). Early-onset behavioral and synaptic deficits in a mouse model of Alzheimer's disease. Proc Natl Acad Sci U S A *103*, 5161-5166.

Jadhav, S., Katina, S., Kovac, A., Kazmerova, Z., Novak, M., and Zilka, N. (2015). Truncated tau deregulates synaptic markers in rat model for human tauopathy. Front Cell Neurosci *9*, 24.

Jahn, H. (2013). Memory loss in Alzheimer's disease. Dialogues Clin Neurosci *15*, 445-454.

Jain, V., Baitharu, I., Prasad, D., and Ilavazhagan, G. (2013). Enriched environment prevents hypobaric hypoxia induced memory impairment and neurodegeneration: role of BDNF/PI3K/GSK3beta pathway coupled with CREB activation. PLoS One *8*, e62235.

Jansen, I.E., Savage, J.E., Watanabe, K., Bryois, J., Williams, D.M., Steinberg, S., Sealock, J., Karlsson, I.K., Hagg, S., Athanasiu, L.*, et al.* (2019). Genome-wide meta-analysis identifies new loci and functional pathways influencing Alzheimer's disease risk. Nat Genet *51*, 404-413.

Jansen, W.J., Ossenkoppele, R., Knol, D.L., Tijms, B.M., Scheltens, P., Verhey, F.R., Visser, P.J., Aalten, P., Aarsland, D., Alcolea, D.*, et al.* (2015). Prevalence of cerebral amyloid pathology in persons without dementia: a meta-analysis. JAMA *313*, 1924-1938.

Jarosz-Griffiths, H.H., Noble, E., Rushworth, J.V., and Hooper, N.M. (2016). Amyloid-beta Receptors: The Good, the Bad, and the Prion Protein. J Biol Chem *291*, 3174-3183.

Jaworski, D.M. (2000). Differential regulation of tissue inhibitor of metalloproteinase mRNA expression in response to intracranial injury. Glia *30*, 199-208.

John, G.R., Lee, S.C., Song, X., Rivieccio, M., and Brosnan, C.F. (2005). IL-1-regulated responses in astrocytes: relevance to injury and recovery. Glia *49*, 161-176.

Johnsen, B., Strand, B.H., Martinaityte, I., Lorem, G.F., and Schirmer, H. (2022). Leisure Time Physical Activities' Association With Cognition and Dementia: A 19 Years' Life Course Study. Front Aging Neurosci *14*, 906678.

Johnstone, M., Gearing, A.J., and Miller, K.M. (1999). A central role for astrocytes in the inflammatory response to beta-amyloid; chemokines, cytokines and reactive oxygen species are produced. J Neuroimmunol *93*, 182-193.

Joshi, C.R., Stacy, S., Sumien, N., Ghorpade, A., and Borgmann, K. (2020). Astrocyte HIV-1 Tat Differentially Modulates Behavior and Brain MMP/TIMP Balance During Short and Prolonged Induction in Transgenic Mice. Front Neurol *11*, 593188.

Jourquin, J., Tremblay, E., Bernard, A., Charton, G., Chaillan, F.A., Marchetti, E., Roman, F.S., Soloway, P.D., Dive, V., Yiotakis, A.*, et al.* (2005). Tissue inhibitor of metalloproteinases-1 (TIMP-1) modulates neuronal death, axonal plasticity, and learning and memory. Eur J Neurosci *22*, 2569-2578.

Jung, E.S., An, K., Hong, H.S., Kim, J.H., and Mook-Jung, I. (2012). Astrocyte-originated ATP protects Abeta(1-42)-induced impairment of synaptic plasticity. J Neurosci *32*, 3081-3087.

Jung, K.K., Liu, X.W., Chirco, R., Fridman, R., and Kim, H.R. (2006). Identification of CD63 as a tissue inhibitor of metalloproteinase-1 interacting cell surface protein. EMBO J *25*, 3934-3942.

Kaczmarek, L., Lapinska-Dzwonek, J., and Szymczak, S. (2002). Matrix metalloproteinases in the adult brain physiology: a link between c-Fos, AP-1 and remodeling of neuronal connections? EMBO J *21*, 6643-6648.

Kahlson, M.A., and Colodner, K.J. (2015). Glial Tau Pathology in Tauopathies: Functional Consequences. J Exp Neurosci *9*, 43-50.

Kang, J., Lemaire, H.G., Unterbeck, A., Salbaum, J.M., Masters, C.L., Grzeschik, K.H., Multhaup, G., Beyreuther, K., and Muller-Hill, B. (1987). The precursor of Alzheimer's disease amyloid A4 protein resembles a cell-surface receptor. Nature *325*, 733-736.

Karch, C.M., and Goate, A.M. (2015). Alzheimer's disease risk genes and mechanisms of disease pathogenesis. Biol Psychiatry *77*, 43-51.

Katzmarski, N., Ziegler-Waldkirch, S., Scheffler, N., Witt, C., Abou-Ajram, C., Nuscher, B., Prinz, M., Haass, C., and Meyer-Luehmann, M. (2020). Abeta oligomers trigger and accelerate Abeta seeding. Brain Pathol *30*, 36-45.

Keren-Shaul, H., Spinrad, A., Weiner, A., Matcovitch-Natan, O., Dvir-Szternfeld, R., Ulland, T.K., David, E., Baruch, K., Lara-Astaiso, D., Toth, B.*, et al.* (2017). A Unique Microglia Type Associated with Restricting Development of Alzheimer's Disease. Cell *169*, 1276-1290 e1217.

Khokha, R. (1994). Suppression of the tumorigenic and metastatic abilities of murine B16-F10 melanoma cells in vivo by the overexpression of the tissue inhibitor of the metalloproteinases-1. J Natl Cancer Inst *86*, 299-304.

Khuth, S.T., Akaoka, H., Pagenstecher, A., Verlaeten, O., Belin, M.F., Giraudon, P., and Bernard, A. (2001). Morbillivirus infection of the mouse central nervous system induces region-specific upregulation of MMPs and TIMPs correlated to inflammatory cytokine expression. J Virol *75*, 8268-8282.

Kim, D., and Tsai, L.H. (2009). Bridging physiology and pathology in AD. Cell *137*, 997-1000.

Kim, D.H., Choi, S.M., Jho, J., Park, M.S., Kang, J., Park, S.J., Ryu, J.H., Jo, J., Kim, H.H., and Kim, B.C. (2016). Infliximab ameliorates AD-associated object recognition memory impairment. Behav Brain Res *311*, 384-391.

Kimelberg, H.K. (2010). Functions of mature mammalian astrocytes: a current view. Neuroscientist *16*, 79-106.

Kimura, R., and Ohno, M. (2009). Impairments in remote memory stabilization precede hippocampal synaptic and cognitive failures in 5XFAD Alzheimer mouse model. Neurobiol Dis *33*, 229-235.

Kimura, T., Whitcomb, D.J., Jo, J., Regan, P., Piers, T., Heo, S., Brown, C., Hashikawa, T., Murayama, M., Seok, H.*, et al.* (2014). Microtubule-associated protein tau is essential for long-term depression in the hippocampus. Philos Trans R Soc Lond B Biol Sci *369*, 20130144.

Kishi, T., Matsunaga, S., Oya, K., Nomura, I., Ikuta, T., and Iwata, N. (2017). Memantine for Alzheimer's Disease: An Updated Systematic Review and Meta-analysis. J Alzheimers Dis *60*, 401-425.

Kitazawa, M., Medeiros, R., and Laferla, F.M. (2012). Transgenic mouse models of Alzheimer disease: developing a better model as a tool for therapeutic interventions. Curr Pharm Des *18*, 1131-1147.

Kivisakk, P., Carlyle, B.C., Sweeney, T., Quinn, J.P., Ramirez, C.E., Trombetta, B.A., Mendes, M., Brock, M., Rubel, C., Czerkowicz, J.*, et al.* (2022). Increased levels of the synaptic proteins PSD-95, SNAP-25, and neurogranin in the cerebrospinal fluid of patients with Alzheimer's disease. Alzheimers Res Ther *14*, 58.

Kjonigsen, L.J., Leergaard, T.B., Witter, M.P., and Bjaalie, J.G. (2011). Digital atlas of anatomical subdivisions and boundaries of the rat hippocampal region. Front Neuroinform *5*, 2.

Klaver, D.W., Wilce, M.C., Cui, H., Hung, A.C., Gasperini, R., Foa, L., and Small, D.H. (2010). Is BACE1 a suitable therapeutic target for the treatment of Alzheimer's disease? Current strategies and future directions. Biol Chem *391*, 849-859.

Koenigsknecht-Talboo, J., and Landreth, G.E. (2005). Microglial phagocytosis induced by fibrillar beta-amyloid and IgGs are differentially regulated by proinflammatory cytokines. J Neurosci *25*, 8240-8249.

Koffie, R.M., Hashimoto, T., Tai, H.C., Kay, K.R., Serrano-Pozo, A., Joyner, D., Hou, S., Kopeikina, K.J., Frosch, M.P., Lee, V.M.*, et al.* (2012). Apolipoprotein E4 effects in Alzheimer's disease are mediated by synaptotoxic oligomeric amyloid-beta. Brain *135*, 2155-2168.

Kraft, A.W., Hu, X., Yoon, H., Yan, P., Xiao, Q., Wang, Y., Gil, S.C., Brown, J., Wilhelmsson, U., Restivo, J.L., *et al.* (2013). Attenuating astrocyte activation accelerates plaque pathogenesis in APP/PS1 mice. FASEB J *27*, 187-198.

Krasemann, S., Madore, C., Cialic, R., Baufeld, C., Calcagno, N., El Fatimy, R., Beckers, L., O'Loughlin, E., Xu, Y., Fanek, Z., *et al.* (2017). The TREM2-APOE Pathway Drives the Transcriptional Phenotype of Dysfunctional Microglia in Neurodegenerative Diseases. Immunity *47*, 566-581 e569.

Kurt, M.A., Davies, D.C., and Kidd, M. (1999). beta-Amyloid immunoreactivity in astrocytes in Alzheimer's disease brain biopsies: an electron microscope study. Exp Neurol *158*, 221-228.

Lambert, E., Boudot, C., Kadri, Z., Soula-Rothhut, M., Sowa, M.L., Mayeux, P., Hornebeck, W., Haye, B., and Petitfrere, E. (2003). Tissue inhibitor of metalloproteinases-1 signalling pathway leading to erythroid cell survival. Biochem J *372*, 767-774.

Lambert, E., Bridoux, L., Devy, J., Dasse, E., Sowa, M.L., Duca, L., Hornebeck, W., Martiny, L., and Petitfrere-Charpentier, E. (2009). TIMP-1 binding to proMMP-9/CD44 complex localized at the cell surface promotes erythroid cell survival. Int J Biochem Cell Biol *41*, 1102-1115.

Landen, J.W., Zhao, Q., Cohen, S., Borrie, M., Woodward, M., Billing, C.B., Jr., Bales, K., Alvey, C., McCush, F., Yang, J., *et al.* (2013). Safety and pharmacology of a single intravenous dose of ponezumab in subjects with mild-to-moderate Alzheimer disease: a phase I, randomized, placebo-controlled, double-blind, dose-escalation study. Clin Neuropharmacol *36*, 14-23.

Lane, C.A., Hardy, J., and Schott, J.M. (2018). Alzheimer's disease. Eur J Neurol *25*, 59-70.

Lansita, J.A., Mease, K.M., Qiu, H., Yednock, T., Sankaranarayanan, S., and Kramer, S. (2017). Nonclinical Development of ANX005: A Humanized Anti-C1q Antibody for Treatment of Autoimmune and Neurodegenerative Diseases. Int J Toxicol *36*, 449-462.

Laskowitz, D.T., and Kolls, B.J. (2010). A phase 2 multiple ascending dose trial of bapineuzumab in mild to moderate Alzheimer disease. Neurology *74*, 2026; author reply 2026-2027.

Lautenschlager, N.T., Cupples, L.A., Rao, V.S., Auerbach, S.A., Becker, R., Burke, J., Chui, H., Duara, R., Foley, E.J., Glatt, S.L., *et al.* (1996). Risk of dementia among relatives of Alzheimer's disease patients in the MIRAGE study: What is in store for the oldest old? Neurology *46*, 641-650.

Lauterborn, J.C., Scaduto, P., Cox, C.D., Schulmann, A., Lynch, G., Gall, C.M., Keene, C.D., and Limon, A. (2021). Increased excitatory to inhibitory synaptic ratio in parietal cortex samples from individuals with Alzheimer's disease. Nat Commun *12*, 2603.

Lawson, L.J., Perry, V.H., and Gordon, S. (1992). Turnover of resident microglia in the normal adult mouse brain. Neuroscience *48*, 405-415.

Lee, C.H., Jeon, S.J., Cho, K.S., Moon, E., Sapkota, A., Jun, H.S., Ryu, J.H., and Choi, J.W. (2018). Activation of Glucagon-Like Peptide-1 Receptor Promotes Neuroprotection in Experimental Autoimmune Encephalomyelitis by Reducing Neuroinflammatory Responses. Mol Neurobiol *55*, 3007-3020.

Lee, D.C., Sunnarborg, S.W., Hinkle, C.L., Myers, T.J., Stevenson, M.Y., Russell, W.E., Castner, B.J., Gerhart, M.J., Paxton, R.J., Black, R.A., *et al.* (2003). TACE/ADAM17 processing of EGFR ligands indicates a role as a physiological convertase. Ann N Y Acad Sci *995*, 22-38.

Li, C., and Gotz, J. (2017). Tau-based therapies in neurodegeneration: opportunities and challenges. Nat Rev Drug Discov *16*, 863-883.

Li, C., Zhao, R., Gao, K., Wei, Z., Yin, M.Y., Lau, L.T., Chui, D., and Yu, A.C. (2011). Astrocytes: implications for neuroinflammatory pathogenesis of Alzheimer's disease. Curr Alzheimer Res *8*, 67-80.

Li, G., Fridman, R., and Kim, H.R. (1999). Tissue inhibitor of metalloproteinase-1 inhibits apoptosis of human breast epithelial cells. Cancer Res *59*, 6267-6275.

Lian, H., Litvinchuk, A., Chiang, A.C., Aithmitti, N., Jankowsky, J.L., and Zheng, H. (2016). Astrocyte-Microglia Cross Talk through Complement Activation Modulates Amyloid Pathology in Mouse Models of Alzheimer's Disease. J Neurosci *36*, 577-589.

Lian, H., Yang, L., Cole, A., Sun, L., Chiang, A.C., Fowler, S.W., Shim, D.J., Rodriguez-Rivera, J., Taglialatela, G., Jankowsky, J.L*., et al.* (2015). NFkappaB-activated astroglial release of complement C3 compromises neuronal morphology and function associated with Alzheimer's disease. Neuron *85*, 101-115.

Lian, H., and Zheng, H. (2016). Signaling pathways regulating neuron-glia interaction and their implications in Alzheimer's disease. J Neurochem *136*, 475-491.

Liddelow, S.A., and Barres, B.A. (2017). Reactive Astrocytes: Production, Function, and Therapeutic Potential. Immunity *46*, 957-967.

Liu, X., Yan, J., Liu, F., Zhou, P., Lv, X., Cheng, N., and Liu, L. (2022). Overexpression of REST Causes Neuronal Injury and Decreases Cofilin Phosphorylation in Mice. J Alzheimers Dis *87*, 873-886.

Liu, X.W., Bernardo, M.M., Fridman, R., and Kim, H.R. (2003). Tissue inhibitor of metalloproteinase-1 protects human breast epithelial cells against intrinsic apoptotic cell death via the focal adhesion kinase/phosphatidylinositol 3-kinase and MAPK signaling pathway. J Biol Chem *278*, 40364-40372.

Liu, X.W., Taube, M.E., Jung, K.K., Dong, Z., Lee, Y.J., Roshy, S., Sloane, B.F., Fridman, R., and Kim, H.R. (2005). Tissue inhibitor of metalloproteinase-1 protects human breast epithelial cells from extrinsic cell death: a potential oncogenic activity of tissue inhibitor of metalloproteinase-1. Cancer Res *65*, 898-906.

LoBue, C., Wadsworth, H., Wilmoth, K., Clem, M., Hart, J., Jr., Womack, K.B., Didehbani, N., Lacritz, L.H., Rossetti, H.C., and Cullum, C.M. (2017). Traumatic brain injury history is associated with earlier age of onset of Alzheimer disease. Clin Neuropsychol *31*, 85-98.

Long, J.M., and Holtzman, D.M. (2019). Alzheimer Disease: An Update on Pathobiology and Treatment Strategies. Cell *179*, 312-339.

Lorenzl, S., Albers, D.S., LeWitt, P.A., Chirichigno, J.W., Hilgenberg, S.L., Cudkowicz, M.E., and Beal, M.F. (2003). Tissue inhibitors of matrix metalloproteinases are elevated in cerebrospinal fluid of neurodegenerative diseases. J Neurol Sci *207*, 71-76.

Loy, C.T., Schofield, P.R., Turner, A.M., and Kwok, J.B. (2014). Genetics of dementia. Lancet *383*, 828-840.

McAlpine, F.E., Lee, J.K., Harms, A.S., Ruhn, K.A., Blurton-Jones, M., Hong, J., Das, P., Golde, T.E., LaFerla, F.M., Oddo, S*., et al.* (2009). Inhibition of soluble TNF signaling in a mouse model of Alzheimer's disease prevents pre-plaque amyloid-associated neuropathology. Neurobiol Dis *34*, 163-177.

McConlogue, L., Buttini, M., Anderson, J.P., Brigham, E.F., Chen, K.S., Freedman, S.B., Games, D., Johnson-Wood, K., Lee, M., Zeller, M*., et al.* (2007). Partial reduction of BACE1 has dramatic effects on Alzheimer plaque and synaptic pathology in APP Transgenic Mice. J Biol Chem *282*, 26326-26334.

McGeer, E.G., and McGeer, P.L. (2010). Neuroinflammation in Alzheimer's disease and mild cognitive impairment: a field in its infancy. J Alzheimers Dis *19*, 355-361.

McLarnon, J.G., and Ryu, J.K. (2008). Relevance of abeta1-42 intrahippocampal injection as an animal model of inflamed Alzheimer's disease brain. Curr Alzheimer Res *5*, 475-480.

Medeiros, R., Kitazawa, M., Passos, G.F., Baglietto-Vargas, D., Cheng, D., Cribbs, D.H., and LaFerla, F.M. (2013). Aspirin-triggered lipoxin A4 stimulates alternative activation of microglia and reduces Alzheimer disease-like pathology in mice. Am J Pathol *182*, 1780-1789.

Meeks, T.W., Ropacki, S.A., and Jeste, D.V. (2006). The neurobiology of neuropsychiatric syndromes in dementia. Curr Opin Psychiatry *19*, 581-586.

Mendoza-Naranjo, A., Contreras-Vallejos, E., Henriquez, D.R., Otth, C., Bamburg, J.R., Maccioni, R.B., and Gonzalez-Billault, C. (2012). Fibrillar amyloid-beta1-42 modifies actin organization affecting the cofilin phosphorylation state: a role for Rac1/cdc42 effector proteins and the slingshot phosphatase. J Alzheimers Dis *29*, 63-77.

Meng, X.F., Yu, J.T., Wang, H.F., Tan, M.S., Wang, C., Tan, C.C., and Tan, L. (2014). Midlife vascular risk factors and the risk of Alzheimer's disease: a systematic review and meta-analysis. J Alzheimers Dis *42*, 1295-1310.

Meucci, O., Fatatis, A., Simen, A.A., and Miller, R.J. (2000). Expression of CX3CR1 chemokine receptors on neurons and their role in neuronal survival. Proc Natl Acad Sci U S A *97*, 8075-8080.

Miller, G.A. (1956). The magical number seven plus or minus two: some limits on our capacity for processing information. Psychol Rev *63*, 81-97.

Mondragon-Rodriguez, S., Trillaud-Doppia, E., Dudilot, A., Bourgeois, C., Lauzon, M., Leclerc, N., and Boehm, J. (2012). Interaction of endogenous tau protein with synaptic proteins is regulated by N-methyl-D-aspartate receptor-dependent tau phosphorylation. J Biol Chem *287*, 32040-32053.

Morizawa, Y.M., Hirayama, Y., Ohno, N., Shibata, S., Shigetomi, E., Sui, Y., Nabekura, J., Sato, K., Okajima, F., Takebayashi, H*., et al.* (2017). Reactive astrocytes function as phagocytes after brain ischemia via ABCA1-mediated pathway. Nat Commun *8*, 28.

Morris, J.C. (1997). Clinical dementia rating: a reliable and valid diagnostic and staging measure for dementia of the Alzheimer type. Int Psychogeriatr *9 Suppl 1*, 173-176; discussion 177-178.

Morris, J.C. (2006). Mild cognitive impairment is early-stage Alzheimer disease: time to revise diagnostic criteria. Arch Neurol *63*, 15-16.

Morris, J.C., Heyman, A., Mohs, R.C., Hughes, J.P., van Belle, G., Fillenbaum, G., Mellits, E.D., and Clark, C. (1989). The Consortium to Establish a Registry for Alzheimer's Disease (CERAD). Part I. Clinical and neuropsychological assessment of Alzheimer's disease. Neurology *39*, 1159-1165.

Morris, J.C., Mohs, R.C., Rogers, H., Fillenbaum, G., and Heyman, A. (1988). Consortium to establish a registry for Alzheimer's disease (CERAD) clinical and neuropsychological assessment of Alzheimer's disease. Psychopharmacol Bull *24*, 641-652.

Morris, M., Knudsen, G.M., Maeda, S., Trinidad, J.C., Ioanoviciu, A., Burlingame, A.L., and Mucke, L. (2015). Tau post-translational modifications in wild-type and human amyloid precursor protein transgenic mice. Nat Neurosci *18*, 1183-1189.

Morris, R.G., Garrud, P., Rawlins, J.N., and O'Keefe, J. (1982). Place navigation impaired in rats with hippocampal lesions. Nature *297*, 681-683.

Mrak, R.E., and Griffin, W.S. (2001). Interleukin-1, neuroinflammation, and Alzheimer's disease. Neurobiol Aging *22*, 903-908.

Murphy, G. (2011). Tissue inhibitors of metalloproteinases. Genome Biol *12*, 233.

Murray, M.E., Graff-Radford, N.R., Ross, O.A., Petersen, R.C., Duara, R., and Dickson, D.W. (2011). Neuropathologically defined subtypes of Alzheimer's disease with distinct clinical characteristics: a retrospective study. Lancet Neurol *10*, 785-796.

Nagai, M., Re, D.B., Nagata, T., Chalazonitis, A., Jessell, T.M., Wichterle, H., and Przedborski, S. (2007). Astrocytes expressing ALS-linked mutated SOD1 release factors selectively toxic to motor neurons. Nat Neurosci *10*, 615-622.

Nalluri, S., Ghoshal-Gupta, S., Kutiyanawalla, A., Gayatri, S., Lee, B.R., Jiwani, S., Rojiani, A.M., and Rojiani, M.V. (2015). TIMP-1 Inhibits Apoptosis in Lung Adenocarcinoma Cells via Interaction with Bcl-2. PLoS One *10*, e0137673.

Nasrallah, I., and Dubroff, J. (2013). An overview of PET neuroimaging. Semin Nucl Med *43*, 449-461.

Nelson, P.T., Alafuzoff, I., Bigio, E.H., Bouras, C., Braak, H., Cairns, N.J., Castellani, R.J., Crain, B.J., Davies, P., Del Tredici, K.*, et al.* (2012a). Correlation of Alzheimer disease neuropathologic changes with cognitive status: a review of the literature. J Neuropathol Exp Neurol *71*, 362-381.

Nelson, T.E., Olde Engberink, A., Hernandez, R., Puro, A., Huitron-Resendiz, S., Hao, C., De Graan, P.N., and Gruol, D.L. (2012b). Altered synaptic transmission in the hippocampus of transgenic mice with enhanced central nervous systems expression of interleukin-6. Brain Behav Immun *26*, 959-971.

Norden, D.M., Fenn, A.M., Dugan, A., and Godbout, J.P. (2014). TGFbeta produced by IL-10 redirected astrocytes attenuates microglial activation. Glia *62*, 881-895.

Novak, P., Schmidt, R., Kontsekova, E., Zilka, N., Kovacech, B., Skrabana, R., Vince-Kazmerova, Z., Katina, S., Fialova, L., Prcina, M.*, et al.* (2017). Safety and immunogenicity of the tau vaccine AADvac1 in patients with Alzheimer's disease: a randomised, double-blind, placebo-controlled, phase 1 trial. Lancet Neurol *16*, 123-134.

O'Keefe, J., and Dostrovsky, J. (1971). The hippocampus as a spatial map. Preliminary evidence from unit activity in the freely-moving rat. Brain Res *34*, 171-175.

Oberheim, N.A., Goldman, S.A., and Nedergaard, M. (2012). Heterogeneity of astrocytic form and function. Methods Mol Biol *814*, 23-45.

Oberheim, N.A., Takano, T., Han, X., He, W., Lin, J.H., Wang, F., Xu, Q., Wyatt, J.D., Pilcher, W., Ojemann, J.G.*, et al.* (2009). Uniquely hominid features of adult human astrocytes. J Neurosci *29*, 3276-3287.

Oberheim, N.A., Tian, G.F., Han, X., Peng, W., Takano, T., Ransom, B., and Nedergaard, M. (2008). Loss of astrocytic domain organization in the epileptic brain. J Neurosci *28*, 3264-3276.

Oberheim, N.A., Wang, X., Goldman, S., and Nedergaard, M. (2006). Astrocytic complexity distinguishes the human brain. Trends Neurosci *29*, 547-553.

Oddo, S., Caccamo, A., Shepherd, J.D., Murphy, M.P., Golde, T.E., Kayed, R., Metherate, R., Mattson, M.P., Akbari, Y., and LaFerla, F.M. (2003). Triple-transgenic model of Alzheimer's disease with plaques and tangles: intracellular Abeta and synaptic dysfunction. Neuron *39*, 409-421.

Olabarria, M., Noristani, H.N., Verkhratsky, A., and Rodriguez, J.J. (2010). Concomitant astroglial atrophy and astrogliosis in a triple transgenic animal model of Alzheimer's disease. Glia *58*, 831-838.

Olry, A., Chastagner, P., Israel, A., and Brou, C. (2005). Generation and characterization of mutant cell lines defective in gamma-secretase processing of Notch and amyloid precursor protein. J Biol Chem *280*, 28564-28571.

Ozben, T., and Ozben, S. (2019). Neuro-inflammation and anti-inflammatory treatment options for Alzheimer's disease. Clin Biochem *72*, 87-89.

Paidi, R.K., Nthenge-Ngumbau, D.N., Singh, R., Kankanala, T., Mehta, H., and Mohanakumar, K.P. (2015). Mitochondrial Deficits Accompany Cognitive Decline Following Single Bilateral Intracerebroventricular Streptozotocin. Curr Alzheimer Res *12*, 785-795.

Paidi, R.K., Sarkar, S., Ambareen, N., and Biswas, S.C. (2022). Medha Plus - A novel polyherbal formulation ameliorates cognitive behaviors and disease pathology in models of Alzheimer's disease. Biomed Pharmacother *151*, 113086.

Panza, F., Lozupone, M., Logroscino, G., and Imbimbo, B.P. (2019). A critical appraisal of amyloid-beta-targeting therapies for Alzheimer disease. Nat Rev Neurol *15*, 73-88.

Park, D.S., Morris, E.J., Padmanabhan, J., Shelanski, M.L., Geller, H.M., and Greene, L.A. (1998). Cyclin-dependent kinases participate in death of neurons evoked by DNA-damaging agents. J Cell Biol *143*, 457-467.

Park, J.H., and Lee, S.A. (2021). The Fragility of Temporal Memory in Alzheimer's Disease. J Alzheimers Dis *79*, 1631-1646.

Pasqualetti, P., Bonomini, C., Dal Forno, G., Paulon, L., Sinforiani, E., Marra, C., Zanetti, O., and Rossini, P.M. (2009). A randomized controlled study on effects of ibuprofen on cognitive progression of Alzheimer's disease. Aging Clin Exp Res *21*, 102-110.

Patterson, S.L., Grover, L.M., Schwartzkroin, P.A., and Bothwell, M. (1992). Neurotrophin expression in rat hippocampal slices: a stimulus paradigm inducing LTP in CA1 evokes increases in BDNF and NT-3 mRNAs. Neuron *9*, 1081-1088.

Peineau, S., Nicolas, C.S., Bortolotto, Z.A., Bhat, R.V., Ryves, W.J., Harwood, A.J., Dournaud, P., Fitzjohn, S.M., and Collingridge, G.L. (2009). A systematic investigation of the protein kinases involved in NMDA receptor-dependent LTD: evidence for a role of GSK-3 but not other serine/threonine kinases. Mol Brain *2*, 22.

Pekny, M., Pekna, M., Messing, A., Steinhauser, C., Lee, J.M., Parpura, V., Hol, E.M., Sofroniew, M.V., and Verkhratsky, A. (2016). Astrocytes: a central element in neurological diseases. Acta Neuropathol *131*, 323-345.

Pekny, M., Wilhelmsson, U., and Pekna, M. (2014). The dual role of astrocyte activation and reactive gliosis. Neurosci Lett *565*, 30-38.

Pepeu, G., and Giovannini, M.G. (2010). Cholinesterase inhibitors and memory. Chem Biol Interact *187*, 403-408.

Pepeu, G., Giovannini, M.G., and Bracco, L. (2013). Effect of cholinesterase inhibitors on attention. Chem Biol Interact *203*, 361-364.

Pereira, C.F., Middel, J., Jansen, G., Verhoef, J., and Nottet, H.S. (2001). Enhanced expression of fractalkine in HIV-1 associated dementia. J Neuroimmunol *115*, 168-175.

Pickett, E.K., Koffie, R.M., Wegmann, S., Henstridge, C.M., Herrmann, A.G., Colom-Cadena, M., Lleo, A., Kay, K.R., Vaught, M., Soberman, R.*, et al.* (2016). Non-Fibrillar Oligomeric Amyloid-beta within Synapses. J Alzheimers Dis *53*, 787-800.

Pike, C.J., Cummings, B.J., and Cotman, C.W. (1995). Early association of reactive astrocytes with senile plaques in Alzheimer's disease. Exp Neurol *132*, 172-179.

Plassman, B.L., Langa, K.M., Fisher, G.G., Heeringa, S.G., Weir, D.R., Ofstedal, M.B., Burke, J.R., Hurd, M.D., Potter, G.G., Rodgers, W.L.*, et al.* (2007). Prevalence of dementia in the United States: the aging, demographics, and memory study. Neuroepidemiology *29*, 125-132.

Pooler, A.M., Noble, W., and Hanger, D.P. (2014). A role for tau at the synapse in Alzheimer's disease pathogenesis. Neuropharmacology *76 Pt A*, 1-8.

Porter, J.T., and McCarthy, K.D. (1996). Hippocampal astrocytes in situ respond to glutamate released from synaptic terminals. J Neurosci *16*, 5073-5081.

Prange, O., Wong, T.P., Gerrow, K., Wang, Y.T., and El-Husseini, A. (2004). A balance between excitatory and inhibitory synapses is controlled by PSD-95 and neuroligin. Proc Natl Acad Sci U S A *101*, 13915-13920.

Puzzo, D., Lee, L., Palmeri, A., Calabrese, G., and Arancio, O. (2014). Behavioral assays with mouse models of Alzheimer's disease: practical considerations and guidelines. Biochem Pharmacol *88*, 450-467.

Py, N.A., Bonnet, A.E., Bernard, A., Marchalant, Y., Charrat, E., Checler, F., Khrestchatisky, M., Baranger, K., and Rivera, S. (2014). Differential spatio-temporal regulation of MMPs in the 5xFAD mouse model of Alzheimer's disease: evidence for a pro-amyloidogenic role of MT1-MMP. Front Aging Neurosci *6*, 247.

Qi, Y., Klyubin, I., Cuello, A.C., and Rowan, M.J. (2018). NLRP3-dependent synaptic plasticity deficit in an Alzheimer's disease amyloidosis model in vivo. Neurobiol Dis *114*, 24-30.

Qiu, C., Kivipelto, M., and von Strauss, E. (2009). Epidemiology of Alzheimer's disease: occurrence, determinants, and strategies toward intervention. Dialogues Clin Neurosci *11*, 111-128.

Rajan, K.B., Barnes, L.L., Wilson, R.S., McAninch, E.A., Weuve, J., Sighoko, D., and Evans, D.A. (2017). Racial Differences in the Association Between Apolipoprotein E Risk Alleles and Overall and Total Cardiovascular Mortality Over 18 Years. J Am Geriatr Soc *65*, 2425-2430.

Regan, P., Piers, T., Yi, J.H., Kim, D.H., Huh, S., Park, S.J., Ryu, J.H., Whitcomb, D.J., and Cho, K. (2015). Tau phosphorylation at serine 396 residue is required for hippocampal LTD. J Neurosci *35*, 4804-4812.

Ries, M., and Sastre, M. (2016). Mechanisms of Abeta Clearance and Degradation by Glial Cells. Front Aging Neurosci *8*, 160.

Rodrigues, E.M., Scudder, S.L., Goo, M.S., and Patrick, G.N. (2016). Abeta-Induced Synaptic Alterations Require the E3 Ubiquitin Ligase Nedd4-1. J Neurosci *36*, 1590-1595.

Rogers, J., Kirby, L.C., Hempelman, S.R., Berry, D.L., McGeer, P.L., Kaszniak, A.W., Zalinski, J., Cofield, M., Mansukhani, L., Willson, P.*, et al.* (1993). Clinical trial of indomethacin in Alzheimer's disease. Neurology *43*, 1609-1611.

Ronnemaa, E., Zethelius, B., Lannfelt, L., and Kilander, L. (2011). Vascular risk factors and dementia: 40-year follow-up of a population-based cohort. Dement Geriatr Cogn Disord *31*, 460-466.

Rossi, F., and Bianchini, E. (1996). Synergistic induction of nitric oxide by beta-amyloid and cytokines in astrocytes. Biochem Biophys Res Commun *225*, 474-478.

Rowan, M.S., Neymotin, S.A., and Lytton, W.W. (2014). Electrostimulation to reduce synaptic scaling driven progression of Alzheimer's disease. Front Comput Neurosci *8*, 39.

Rubio-Perez, J.M., and Morillas-Ruiz, J.M. (2012). A review: inflammatory process in Alzheimer's disease, role of cytokines. ScientificWorldJournal *2012*, 756357.

Rukenstein, A., Rydel, R.E., and Greene, L.A. (1991). Multiple agents rescue PC12 cells from serum-free cell death by translation- and transcription-independent mechanisms. The Journal of neuroscience : the official journal of the Society for Neuroscience *11*, 2552-2563.

Rush, T., Martinez-Hernandez, J., Dollmeyer, M., Frandemiche, M.L., Borel, E., Boisseau, S., Jacquier-Sarlin, M., and Buisson, A. (2018). Synaptotoxicity in Alzheimer's Disease Involved a Dysregulation of Actin Cytoskeleton Dynamics through Cofilin 1 Phosphorylation. J Neurosci *38*, 10349-10361.

Russo, I., Caracciolo, L., Tweedie, D., Choi, S.H., Greig, N.H., Barlati, S., and Bosetti, F. (2012). 3,6'-Dithiothalidomide, a new TNF-alpha synthesis inhibitor, attenuates the effect of Abeta1-42 intracerebroventricular injection on hippocampal neurogenesis and memory deficit. J Neurochem *122*, 1181-1192.

Ryman, D.C., Acosta-Baena, N., Aisen, P.S., Bird, T., Danek, A., Fox, N.C., Goate, A., Frommelt, P., Ghetti, B., Langbaum, J.B.*, et al.* (2014). Symptom onset in autosomal dominant Alzheimer disease: a systematic review and meta-analysis. Neurology *83*, 253-260.

Saha, A., Saleem, S., Paidi, R.K., and Biswas, S.C. (2021). BH3-only proteins Puma and Beclin1 regulate autophagic death in neurons in response to Amyloid-beta. Cell Death Discov *7*, 356.

Saha, P., Sarkar, S., Paidi, R.K., and Biswas, S.C. (2020). TIMP-1: A key cytokine released from activated astrocytes protects neurons and ameliorates cognitive behaviours in a rodent model of Alzheimer's disease. Brain Behav Immun *87*, 804-819.

Saleem, S., and Biswas, S.C. (2017). Tribbles Pseudokinase 3 Induces Both Apoptosis and Autophagy in Amyloid-beta-induced Neuronal Death. J Biol Chem *292*, 2571-2585.

Samaey, C., Schreurs, A., Stroobants, S., and Balschun, D. (2019). Early Cognitive and Behavioral Deficits in Mouse Models for Tauopathy and Alzheimer's Disease. Front Aging Neurosci *11*, 335.

Sando, S.B., Melquist, S., Cannon, A., Hutton, M., Sletvold, O., Saltvedt, I., White, L.R., Lydersen, S., and Aasly, J. (2008). Risk-reducing effect of education in Alzheimer's disease. Int J Geriatr Psychiatry *23*, 1156-1162.

Sanphui, P., and Biswas, S.C. (2013). FoxO3a is activated and executes neuron death via Bim in response to beta-amyloid. Cell Death Dis *4*, e625.

Sanphui, P., Pramanik, S.K., Chatterjee, N., Moorthi, P., Banerji, B., and Biswas, S.C. (2013). Efficacy of Cyclin Dependent Kinase 4 Inhibitors as Potent Neuroprotective Agents against Insults Relevant to Alzheimer's Disease. PloS one *8*, e78842.

Sarkar, S., and Biswas, S.C. (2021). Astrocyte subtype-specific approach to Alzheimer's disease treatment. Neurochem Int *145*, 104956.

Sarter, M., and Bruno, J.P. (1997). Cognitive functions of cortical acetylcholine: toward a unifying hypothesis. Brain Res Brain Res Rev *23*, 28-46.

Sastre, M., and Gentleman, S.M. (2010). NSAIDs: How they Work and their Prospects as Therapeutics in Alzheimer's Disease. Front Aging Neurosci *2*, 20.

Schroeder, A., Fahrenholz, F., and Schmitt, U. (2009). Effect of a dominant-negative form of ADAM10 in a mouse model of Alzheimer's disease. J Alzheimers Dis *16*, 309-314.

Schumann, G., Huell, M., Machein, U., Hocke, G., and Fiebich, B.L. (1999). Interleukin-6 activates signal transducer and activator of transcription and mitogen-activated protein kinase signal transduction pathways and induces de novo protein synthesis in human neuronal cells. J Neurochem *73*, 2009-2017.

Scoville, W.B., and Milner, B. (1957). Loss of recent memory after bilateral hippocampal lesions. J Neurol Neurosurg Psychiatry *20*, 11-21.

Selkoe, D.J. (2002). Alzheimer's disease is a synaptic failure. Science *298*, 789-791.

Selkoe, D.J. (2008). Soluble oligomers of the amyloid beta-protein impair synaptic plasticity and behavior. Behav Brain Res *192*, 106-113.

Senechal, Y., Kelly, P.H., and Dev, K.K. (2008). Amyloid precursor protein knockout mice show age-dependent deficits in passive avoidance learning. Behav Brain Res *186*, 126-132.

Serrano-Pozo, A., Mielke, M.L., Gomez-Isla, T., Betensky, R.A., Growdon, J.H., Frosch, M.P., and Hyman, B.T. (2011). Reactive glia not only associates with plaques but also parallels tangles in Alzheimer's disease. Am J Pathol *179*, 1373-1384.

Shi, J.Q., Shen, W., Chen, J., Wang, B.R., Zhong, L.L., Zhu, Y.W., Zhu, H.Q., Zhang, Q.Q., Zhang, Y.D., and Xu, J. (2011). Anti-TNF-alpha reduces amyloid plaques and tau phosphorylation and induces CD11c-positive dendritic-like cell in the APP/PS1 transgenic mouse brains. Brain Res *1368*, 239-247.

Shimohama, S., Kamiya, S., Taniguchi, T., Akagawa, K., and Kimura, J. (1997). Differential involvement of synaptic vesicle and presynaptic plasma membrane proteins in Alzheimer's disease. Biochem Biophys Res Commun *236*, 239-242.

Singh, A., and Abraham, W.C. (2017). Astrocytes and synaptic plasticity in health and disease. Exp Brain Res *235*, 1645-1655.

Sipos, E., Kurunczi, A., Kasza, A., Horvath, J., Felszeghy, K., Laroche, S., Toldi, J., Parducz, A., Penke, B., and Penke, Z. (2007). Beta-amyloid pathology in the entorhinal cortex of rats induces memory deficits: implications for Alzheimer's disease. Neuroscience *147*, 28-36.

Sirko, S., Behrendt, G., Johansson, P.A., Tripathi, P., Costa, M., Bek, S., Heinrich, C., Tiedt, S., Colak, D., Dichgans, M.*, et al.* (2013). Reactive glia in the injured brain acquire stem cell properties in response to sonic hedgehog. [corrected]. Cell Stem Cell *12*, 426-439.

Small, D.H., Mok, S.S., and Bornstein, J.C. (2001). Alzheimer's disease and Abeta toxicity: from top to bottom. Nat Rev Neurosci *2*, 595-598.

Smith, L.A., and McMahon, L.L. (2018). Deficits in synaptic function occur at medial perforant path-dentate granule cell synapses prior to Schaffer collateral-CA1 pyramidal cell synapses in the novel TgF344-Alzheimer's Disease Rat Model. Neurobiol Dis *110*, 166-179.

Soeda, Y., and Takashima, A. (2020). New Insights Into Drug Discovery Targeting Tau Protein. Front Mol Neurosci *13*, 590896.

Sofroniew, M.V. (2009). Molecular dissection of reactive astrogliosis and glial scar formation. Trends Neurosci *32*, 638-647.

Sofroniew, M.V. (2015). Astrocyte barriers to neurotoxic inflammation. Nat Rev Neurosci *16*, 249-263.

Solmaz, V., Cinar, B.P., Yigitturk, G., Cavusoglu, T., Taskiran, D., and Erbas, O. (2015). Exenatide reduces TNF-alpha expression and improves hippocampal neuron numbers and memory in streptozotocin treated rats. Eur J Pharmacol *765*, 482-487.

Solomon, A., Kivipelto, M., Wolozin, B., Zhou, J., and Whitmer, R.A. (2009). Midlife serum cholesterol and increased risk of Alzheimer's and vascular dementia three decades later. Dement Geriatr Cogn Disord *28*, 75-80.

Song, G., Xu, S., Zhang, H., Wang, Y., Xiao, C., Jiang, T., Wu, L., Zhang, T., Sun, X., Zhong, L.*, et al.* (2016). TIMP1 is a prognostic marker for the progression and metastasis of colon cancer through FAK-PI3K/AKT and MAPK pathway. J Exp Clin Cancer Res *35*, 148.

Sperling, R.A., Aisen, P.S., Beckett, L.A., Bennett, D.A., Craft, S., Fagan, A.M., Iwatsubo, T., Jack, C.R., Jr., Kaye, J., Montine, T.J.*, et al.* (2011). Toward defining the preclinical stages of Alzheimer's disease:

recommendations from the National Institute on Aging-Alzheimer's Association workgroups on diagnostic guidelines for Alzheimer's disease. Alzheimers Dement *7*, 280-292.

Spinney, L. (2014). Alzheimer's disease: The forgetting gene. Nature *510*, 26-28.

Squire, L.R., Knowlton, B., and Musen, G. (1993). The structure and organization of memory. Annu Rev Psychol *44*, 453-495.

Squire, L.R., and Zola-Morgan, S. (1991). The medial temporal lobe memory system. Science *253*, 1380-1386.

Staff, R.T., Hogan, M.J., Williams, D.S., and Whalley, L.J. (2018). Intellectual engagement and cognitive ability in later life (the "use it or lose it" conjecture): longitudinal, prospective study. BMJ *363*, k4925.

Stephen, R., Barbera, M., Peters, R., Ee, N., Zheng, L., Lehtisalo, J., Kulmala, J., Hakansson, K., Chowdhary, N., Dua, T.*, et al.* (2021). Development of the First WHO Guidelines for Risk Reduction of Cognitive Decline and Dementia: Lessons Learned and Future Directions. Front Neurol *12*, 763573.

Stern, Y. (2002). What is cognitive reserve? Theory and research application of the reserve concept. J Int Neuropsychol Soc *8*, 448-460.

Stern, Y. (2012). Cognitive reserve in ageing and Alzheimer's disease. Lancet Neurol *11*, 1006-1012.

Subhadeep, D., Srikumar, B.N., Shankaranarayana Rao, B.S., and Kutty, B.M. (2021). Exposure to Short Photoperiod Regime Restores Spatial Cognition in Ventral Subicular Lesioned Rats: Potential Role of Hippocampal Plasticity, Glucocorticoid Receptors, and Neurogenesis. Mol Neurobiol *58*, 4437-4459.

Summers, W.K., Majovski, L.V., Marsh, G.M., Tachiki, K., and Kling, A. (1986). Oral tetrahydroaminoacridine in long-term treatment of senile dementia, Alzheimer type. N Engl J Med *315*, 1241-1245.

Sung, S., Yang, H., Uryu, K., Lee, E.B., Zhao, L., Shineman, D., Trojanowski, J.Q., Lee, V.M., and Pratico, D. (2004). Modulation of nuclear factor-kappa B activity by indomethacin influences A beta levels but not A beta precursor protein metabolism in a model of Alzheimer's disease. Am J Pathol *165*, 2197-2206.

Suryadevara, R., Holter, S., Borgmann, K., Persidsky, R., Labenz-Zink, C., Persidsky, Y., Gendelman, H.E., Wu, L., and Ghorpade, A. (2003). Regulation of tissue inhibitor of metalloproteinase-1 by astrocytes: links to HIV-1 dementia. Glia *44*, 47-56.

Swerdlow, R.H. (2007). Is aging part of Alzheimer's disease, or is Alzheimer's disease part of aging? Neurobiol Aging *28*, 1465-1480.

Szczepanik, A.M., and Ringheim, G.E. (2003). IL-10 and glucocorticoids inhibit Abeta(1-42)- and lipopolysaccharide-induced pro-inflammatory cytokine and chemokine induction in the central nervous system. J Alzheimers Dis *5*, 105-117.

Takeda, S., Hashimoto, T., Roe, A.D., Hori, Y., Spires-Jones, T.L., and Hyman, B.T. (2013). Brain interstitial oligomeric amyloid beta increases with age and is resistant to clearance from brain in a mouse model of Alzheimer's disease. FASEB J *27*, 3239-3248.

Tang, Y., and Le, W. (2016). Differential Roles of M1 and M2 Microglia in Neurodegenerative Diseases. Mol Neurobiol *53*, 1181-1194.

Tejima, E., Guo, S., Murata, Y., Arai, K., Lok, J., van Leyen, K., Rosell, A., Wang, X., and Lo, E.H. (2009). Neuroprotective effects of overexpressing tissue inhibitor of metalloproteinase TIMP-1. J Neurotrauma *26*, 1935-1941.

Termini, C.M., and Gillette, J.M. (2017). Tetraspanins Function as Regulators of Cellular Signaling. Front Cell Dev Biol *5*, 34.

Terry, R.D., Masliah, E., Salmon, D.P., Butters, N., DeTeresa, R., Hill, R., Hansen, L.A., and Katzman, R. (1991). Physical basis of cognitive alterations in Alzheimer's disease: synapse loss is the major correlate of cognitive impairment. Ann Neurol *30*, 572-580.

Thal, D.R., Schultz, C., Dehghani, F., Yamaguchi, H., Braak, H., and Braak, E. (2000). Amyloid beta-protein (Abeta)-containing astrocytes are located preferentially near N-terminal-truncated Abeta deposits in the human entorhinal cortex. Acta Neuropathol *100*, 608-617.

Then, F.S., Luck, T., Luppa, M., Arelin, K., Schroeter, M.L., Engel, C., Loffler, M., Thiery, J., Villringer, A., and Riedel-Heller, S.G. (2014). Association between mental demands at work and cognitive functioning in the general population - results of the health study of the Leipzig research center for civilization diseases (LIFE). J Occup Med Toxicol *9*, 23.

Tobinick, E., Gross, H., Weinberger, A., and Cohen, H. (2006). TNF-alpha modulation for treatment of Alzheimer's disease: a 6-month pilot study. MedGenMed *8*, 25.

Troy, C.M., Friedman, J.E., and Friedman, W.J. (2002). Mechanisms of p75-mediated death of hippocampal neurons. Role of caspases. The Journal of biological chemistry *277*, 34295-34302.

Troy, C.M., Rabacchi, S.A., Friedman, W.J., Frappier, T.F., Brown, K., and Shelanski, M.L. (2000). Caspase-2 mediates neuronal cell death induced by beta-amyloid. J Neurosci *20*, 1386-1392.

Tsai, K.J., Tsai, Y.C., and Shen, C.K. (2007). G-CSF rescues the memory impairment of animal models of Alzheimer's disease. J Exp Med *204*, 1273-1280.

Tuna, G., Yener, G.G., Oktay, G., Islekel, G.H., and FG, K.I. (2018). Evaluation of Matrix Metalloproteinase-2 (MMP-2) and -9 (MMP-9) and Their Tissue Inhibitors (TIMP-1 and TIMP-2) in Plasma from Patients with Neurodegenerative Dementia. J Alzheimers Dis *66*, 1265-1273.

Ultsch, M., Li, B., Maurer, T., Mathieu, M., Adolfsson, O., Muhs, A., Pfeifer, A., Pihlgren, M., Bainbridge, T.W., Reichelt, M.*, et al.* (2016). Structure of Crenezumab Complex with Abeta Shows Loss of beta-Hairpin. Sci Rep *6*, 39374.

Um, J.W., Kaufman, A.C., Kostylev, M., Heiss, J.K., Stagi, M., Takahashi, H., Kerrisk, M.E., Vortmeyer, A., Wisniewski, T., Koleske, A.J.*, et al.* (2013). Metabotropic glutamate receptor 5 is a coreceptor for Alzheimer abeta oligomer bound to cellular prion protein. Neuron *79*, 887-902.

Usardi, A., Pooler, A.M., Seereeram, A., Reynolds, C.H., Derkinderen, P., Anderton, B., Hanger, D.P., Noble, W., and Williamson, R. (2011). Tyrosine phosphorylation of tau regulates its interactions with Fyn SH2 domains, but not SH3 domains, altering the cellular localization of tau. FEBS J *278*, 2927-2937.

Vagelatos, N.T., and Eslick, G.D. (2013). Type 2 diabetes as a risk factor for Alzheimer's disease: the confounders, interactions, and neuropathology associated with this relationship. Epidemiol Rev *35*, 152-160.

Valori, C.F., Guidotti, G., Brambilla, L., and Rossi, D. (2019). Astrocytes: Emerging Therapeutic Targets in Neurological Disorders. Trends Mol Med *25*, 750-759.

van der Poel, A.M. (1967). Ethological study of the behaviour of the albino rat in a passive-avoidance test. Acta Physiol Pharmacol Neerl *14*, 503-505.

Van Eldik, L.J., and Wainwright, M.S. (2003). The Janus face of glial-derived S100B: beneficial and detrimental functions in the brain. Restor Neurol Neurosci *21*, 97-108.

van Es, J.H., van Gijn, M.E., Riccio, O., van den Born, M., Vooijs, M., Begthel, H., Cozijnsen, M., Robine, S., Winton, D.J., Radtke, F.*, et al.* (2005). Notch/gamma-secretase inhibition turns proliferative cells in intestinal crypts and adenomas into goblet cells. Nature *435*, 959-963.

Vandenabeele, P., and Fiers, W. (1991). Is amyloidogenesis during Alzheimer's disease due to an IL-1-/IL-6-mediated 'acute phase response' in the brain? Immunol Today *12*, 217-219.

Vanderwolf, C.H. (1964). Effect of Combined Medial Thalamic and Septal Lesions on Active-Avoidance Behavior. J Comp Physiol Psychol *58*, 31-37.

Verkhratsky, A., Parpura, V., Rodriguez-Arellano, J.J., and Zorec, R. (2019). Astroglia in Alzheimer's Disease. In:Verkhratsky, A, Ho, M, Zorec, R, Parpura, V (Eds) editors Neuroglia in Neurodegenerative Diseases Springer Singapore.

Verkhratsky, A., Zorec, R., and Parpura, V. (2017). Stratification of astrocytes in healthy and diseased brain. Brain Pathol *27*, 629-644.

Verkhratsky, A., Zorec, R., Rodriguez, J.J., and Parpura, V. (2016). Astroglia dynamics in ageing and Alzheimer's disease. Curr Opin Pharmacol *26*, 74-79.

Verma, M., and Howard, R.J. (2012). Semantic memory and language dysfunction in early Alzheimer's disease: a review. Int J Geriatr Psychiatry *27*, 1209-1217.

Wakida, N.M., Cruz, G.M.S., Ro, C.C., Moncada, E.G., Khatibzadeh, N., Flanagan, L.A., and Berns, M.W. (2018). Phagocytic response of astrocytes to damaged neighboring cells. PLoS One *13*, e0196153.

Walsh, D.M., Klyubin, I., Fadeeva, J.V., Cullen, W.K., Anwyl, R., Wolfe, M.S., Rowan, M.J., and Selkoe, D.J. (2002). Naturally secreted oligomers of amyloid beta protein potently inhibit hippocampal long-term potentiation in vivo. Nature *416*, 535-539.

Walsh, D.M., and Selkoe, D.J. (2004). Deciphering the molecular basis of memory failure in Alzheimer's disease. Neuron *44*, 181-193.

Wang, D., Zhang, X., Wang, M., Zhou, D., Pan, H., Shu, Q., and Sun, B. (2018). Early Activation of Astrocytes does not Affect Amyloid Plaque Load in an Animal Model of Alzheimer's Disease. Neurosci Bull *34*, 912-920.

Wang, H.W., Pasternak, J.F., Kuo, H., Ristic, H., Lambert, M.P., Chromy, B., Viola, K.L., Klein, W.L., Stine, W.B., Krafft, G.A.*, et al.* (2002). Soluble oligomers of beta amyloid (1-42) inhibit long-term potentiation but not long-term depression in rat dentate gyrus. Brain Res *924*, 133-140.

Wang, L., Benzinger, T.L., Su, Y., Christensen, J., Friedrichsen, K., Aldea, P., McConathy, J., Cairns, N.J., Fagan, A.M., Morris, J.C.*, et al.* (2016a). Evaluation of Tau Imaging in Staging Alzheimer Disease and Revealing Interactions Between beta-Amyloid and Tauopathy. JAMA Neurol *73*, 1070-1077.

Wang, Q., Wu, J., Rowan, M.J., and Anwyl, R. (2005). Beta-amyloid inhibition of long-term potentiation is mediated via tumor necrosis factor. Eur J Neurosci *22*, 2827-2832.

Wang, X.X., Tan, M.S., Yu, J.T., and Tan, L. (2014). Matrix metalloproteinases and their multiple roles in Alzheimer's disease. Biomed Res Int *2014*, 908636.

Wang, Z.X., Tan, L., Liu, J., and Yu, J.T. (2016b). The Essential Role of Soluble Abeta Oligomers in Alzheimer's Disease. Mol Neurobiol *53*, 1905-1924.

Wilcox, K.C., Lacor, P.N., Pitt, J., and Klein, W.L. (2011). Abeta oligomer-induced synapse degeneration in Alzheimer's disease. Cell Mol Neurobiol *31*, 939-948.

Wirths, O., Dins, A., and Bayer, T.A. (2012). AbetaPP accumulation and/or intraneuronal amyloid-beta accumulation? The 3xTg-AD mouse model revisited. J Alzheimers Dis *28*, 897-904.

Wischik, C.M., Novak, M., Edwards, P.C., Klug, A., Tichelaar, W., and Crowther, R.A. (1988). Structural characterization of the core of the paired helical filament of Alzheimer disease. Proc Natl Acad Sci U S A *85*, 4884-4888.

Wong, G.T., Manfra, D., Poulet, F.M., Zhang, Q., Josien, H., Bara, T., Engstrom, L., Pinzon-Ortiz, M., Fine, J.S., Lee, H.J.*, et al.* (2004). Chronic treatment with the gamma-secretase inhibitor LY-411,575 inhibits beta-amyloid peptide production and alters lymphopoiesis and intestinal cell differentiation. J Biol Chem *279*, 12876-12882.

Woo, J.A., Zhao, X., Khan, H., Penn, C., Wang, X., Joly-Amado, A., Weeber, E., Morgan, D., and Kang, D.E. (2015). Slingshot-Cofilin activation mediates mitochondrial and synaptic dysfunction via Abeta ligation to beta1-integrin conformers. Cell Death Differ *22*, 921-934.

Wyss-Coray, T., Loike, J.D., Brionne, T.C., Lu, E., Anankov, R., Yan, F., Silverstein, S.C., and Husemann, J. (2003). Adult mouse astrocytes degrade amyloid-beta in vitro and in situ. Nat Med *9*, 453-457.

Xiao, Q., Yan, P., Ma, X., Liu, H., Perez, R., Zhu, A., Gonzales, E., Burchett, J.M., Schuler, D.R., Cirrito, J.R.*, et al.* (2014). Enhancing astrocytic lysosome biogenesis facilitates Abeta clearance and attenuates amyloid plaque pathogenesis. J Neurosci *34*, 9607-9620.

Yamaguchi, H., Sugihara, S., Ogawa, A., Saido, T.C., and Ihara, Y. (1998). Diffuse plaques associated with astroglial amyloid beta protein, possibly showing a disappearing stage of senile plaques. Acta Neuropathol *95*, 217-222.

Yamamoto, M., Kiyota, T., Horiba, M., Buescher, J.L., Walsh, S.M., Gendelman, H.E., and Ikezu, T. (2007). Interferon-gamma and tumor necrosis factor-alpha regulate amyloid-beta plaque deposition and beta-secretase expression in Swedish mutant APP transgenic mice. Am J Pathol *170*, 680-692.

Yang, F., Ueda, K., Chen, P., Ashe, K.H., and Cole, G.M. (2000). Plaque-associated alpha-synuclein (NACP) pathology in aged transgenic mice expressing amyloid precursor protein. Brain Res *853*, 381-383.

Yin, K.J., Cirrito, J.R., Yan, P., Hu, X., Xiao, Q., Pan, X., Bateman, R., Song, H., Hsu, F.F., Turk, J.*, et al.* (2006). Matrix metalloproteinases expressed by astrocytes mediate extracellular amyloid-beta peptide catabolism. J Neurosci *26*, 10939-10948.

Yun, S.P., Kam, T.I., Panicker, N., Kim, S., Oh, Y., Park, J.S., Kwon, S.H., Park, Y.J., Karuppagounder, S.S., Park, H.*, et al.* (2018). Block of A1 astrocyte conversion by microglia is neuroprotective in models of Parkinson's disease. Nat Med *24*, 931-938.

Zamanian, J.L., Xu, L., Foo, L.C., Nouri, N., Zhou, L., Giffard, R.G., and Barres, B.A. (2012). Genomic analysis of reactive astrogliosis. J Neurosci *32*, 6391-6410.

Zhang, H., Ben Zablah, Y., Liu, A., Lee, D., Meng, Y., Zhou, C., Liu, X., Wang, Y., and Jia, Z. (2021). Overexpression of LIMK1 in hippocampal excitatory neurons improves synaptic plasticity and social recognition memory in APP/PS1 mice. Mol Brain *14*, 121.

Zhang, J., Wu, T., Zhan, S., Qiao, N., Zhang, X., Zhu, Y., Yang, N., Sun, Y., Zhang, X.A., Bleich, D.*, et al.* (2017). TIMP-1 and CD82, a promising combined evaluation marker for PDAC. Oncotarget *8*, 6496-6512.

Zhang, L., Shu, R., Wang, C., Wang, H., Li, N., and Wang, G. (2014). Hydrogen-rich saline controls remifentanil-induced hypernociception and NMDA receptor NR1 subunit membrane trafficking through GSK-3beta in the DRG in rats. Brain Res Bull *106*, 47-55.

Zhong, F., Liu, L., Wei, J.L., and Dai, R.P. (2019). Step by Step Golgi-Cox Staining for Cryosection. Front Neuroanat *13*, 62.

Zhou, Y., Song, W.M., Andhey, P.S., Swain, A., Levy, T., Miller, K.R., Poliani, P.L., Cominelli, M., Grover, S., Gilfillan, S*., et al.* (2020). Human and mouse single-nucleus transcriptomics reveal TREM2-dependent and TREM2-independent cellular responses in Alzheimer's disease. Nat Med *26*, 131-142.

Zhou, Z., Meng, Y., Asrar, S., Todorovski, Z., and Jia, Z. (2009). A critical role of Rho-kinase ROCK2 in the regulation of spine and synaptic function. Neuropharmacology *56*, 81-89.

Zhu, L.Q., Liu, D., Hu, J., Cheng, J., Wang, S.H., Wang, Q., Wang, F., Chen, J.G., and Wang, J.Z. (2010). GSK-3 beta inhibits presynaptic vesicle exocytosis by phosphorylating P/Q-type calcium channel and interrupting SNARE complex formation. J Neurosci *30*, 3624-3633.

Zhu, L.Q., Wang, S.H., Liu, D., Yin, Y.Y., Tian, Q., Wang, X.C., Wang, Q., Chen, J.G., and Wang, J.Z. (2007). Activation of glycogen synthase kinase-3 inhibits long-term potentiation with synapse-associated impairments. J Neurosci *27*, 12211-12220.

Zorec, R., Horvat, A., Vardjan, N., and Verkhratsky, A. (2015). Memory Formation Shaped by Astroglia. Front Integr Neurosci *9*, 56.

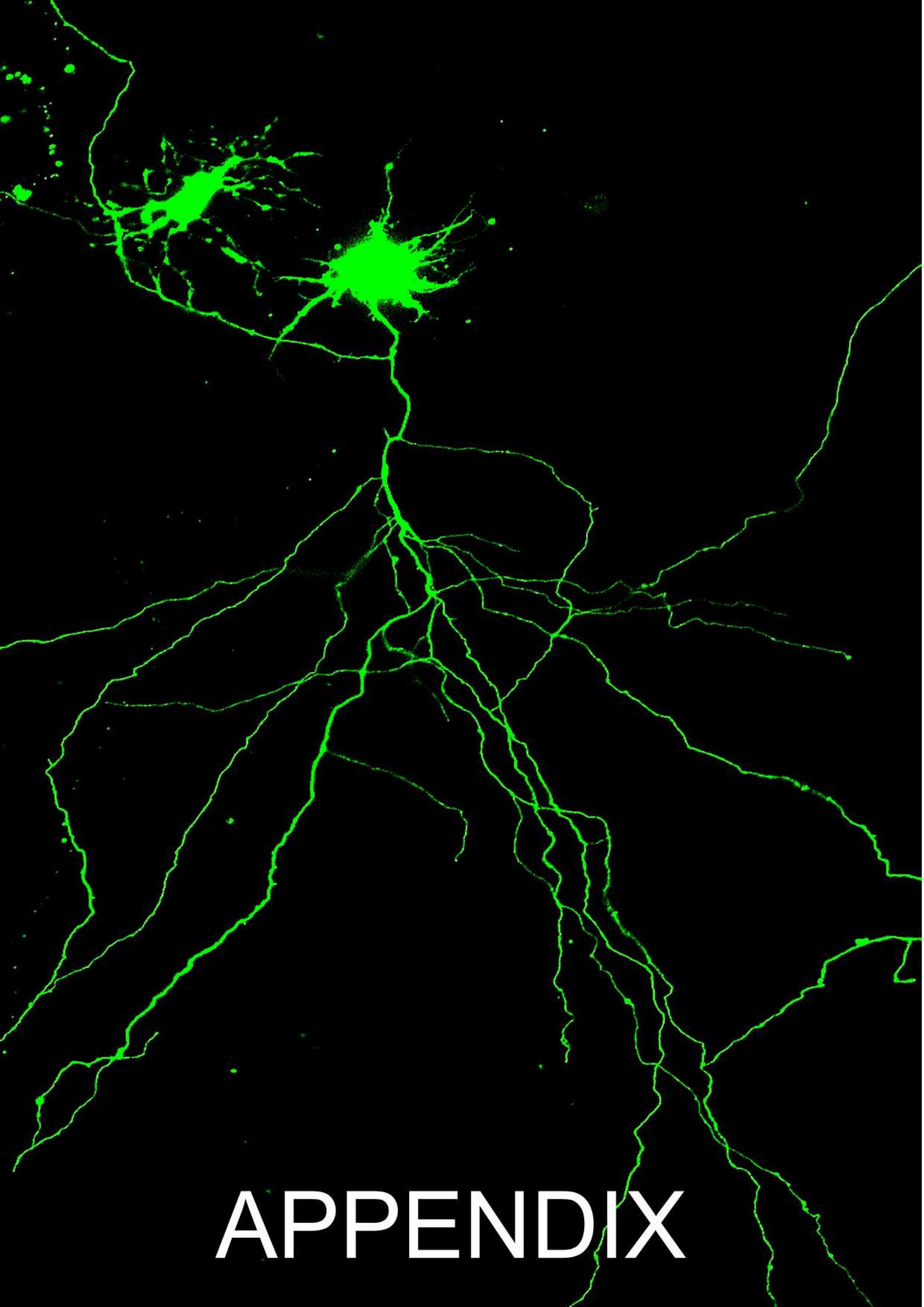

APPENDIX

APPENDIX

Scientific Publications:

Articles

1. Saha P*, **Sarkar S***, Paidi RK, Biswas SC. TIMP-1: A key cytokine released from activated astrocytes protects neurons and ameliorates cognitive behaviours in a rodent model of Alzheimer's disease. **Brain Behav Immun. 2020** Jul;87:804-819. doi: 10.1016/j.bbi.2020.03.014. Epub 2020 Mar 16. PMID: 32194232.

   **Co-first author*

2. Paidi RK, **Sarkar S,** Ambareen N, Biswas SC. Medha Plus - A novel polyherbal formulation ameliorates cognitive behaviors and disease pathology in models of Alzheimer's disease. Biomed Pharmacother. 2022 Jul;151:113086. doi: 10.1016/j.biopha.2022.113086. Epub 2022 May 24. PMID: 35617801.

3. Das H, **Sarkar S,** Paidi RK, Biswas SC. Subtle genomic DNA damage induces intraneuronal production of Amyloid-β (1-42) by increasing β-secretase activity. **FASEB J., 2021**, May;35(5):e21569. doi: 10.1096/fj.202001676RR. PMID: 33864420.

4. Mahapatra A, **Sarkar S**, Biswas SC, Chattopadhyay K. An aminoglycoside antibiotic inhibits both lipid-induced and solution-phase fibrillation of α-synuclein in vitro. **Chem Commun (Camb). 2019** Sep 21;55(74):11052-11055. doi: 10.1039/c9cc04251b. Epub 2019 Aug 27. PMID: 31453599.

5. Mahapatra A, **Sarkar S**, Biswas SC, Chattopadhyay K. Modulation of α-Synuclein Fibrillation by Ultrasmall and Biocompatible Gold Nanoclusters. **ACS Chem Neurosci. 2020** Oct 21;11(20):3442-3454. doi: 10.1021/acschemneuro.0c00550. Epub 2020 Oct 12. PMID: 33044818.

Reviews

1. **Sarkar S** and Biswas SC. Astrocyte subtype-specific approach to Alzheimer's disease treatment. **Neurochem Int. 2021** Epub 2021 Jan 24. https://doi.org/10.1016/j.neuint.2021.104956.

2. Mondal R, Lahiri D, Deb S, Bandyopadhyay D, Shome G, **Sarkar S**, Paria SR, Thakurta TG, Singla P, Biswas SC. COVID-19: Are we dealing with a multisystem vasculopathy in disguise of a viral infection? **J Thromb Thrombolysis. 2020** Oct;50(3):567-579. doi: 10.1007/s11239-020-02210-8. PMID: 32627126; PMCID: PMC7335630.

3. Lahiri D, Mondal R, Deb S, Bandyopadhyay D, Shome G, **Sarkar S**, Biswas SC. Neuroinvasive potential of a primary respiratory pathogen SARS- CoV2: Summarizing the evidences. **Diabetes Metab Syndr. 2020** Sep-Oct;14(5):1053-1060. doi: 10.1016/j.dsx.2020.06.062. Epub 2020 Jul 2. PMID: 32640417; PMCID: PMC7331527.

Book Chapters

1. **Sarkar S**, Guha S and Biswas SC. Role of reactive astrocytes in Alzheimer's Disease. The Biology of Glial Cells: Recent Advances by Springer 2022, pg 199-242.

2. Ambareen N, **Sarkar S**, Saha A, Biswas SC. Autophagy: Role in Alzheimer's disease pathophysiology and therapeutic avenues. Alzheimer's disease by the Royal Society of Chemistry 2022 Ch-10, pg 287-328, http://pubs.rsc.org/en/content/ebook/978-1-83916-230-5.

Conference abstract

1. **Sarkar S**, Paidi RK, Biswas SC. Astrocyte-secreted TIMP-1 binds to CD63 and differentially phosphorylates Akt in protecting neurons and promoting cognitive recovery in 5xFAD mice, Alzheimer's & dementia: the journal of the Alzheimer's Association 17, Suppl 3. DOI: 10.1002/alz.052606, Conference - Alzheimer's Association International Conference, 2021.

2. **Sarkar S**, Gharami K., Paidi RK, Biswas SC. Reactive astrocyte-secreted TIMP-1 rescues memory deficits and synaptic health in 5xFAD mouse model of Alzheimer's disease. Indian Academy of Neurosciences (IAN) meeting, 2021 Abstract book. Theme: Neuroglia in Health and disease, pg-140.

International and National Conferences attended

2022	Oral & Poster	BAW 2022, Outreach Activities: Advances in Biology Research, Education, and Teaching, organized by IISER Kolkata, June 14th-June 20th, 2022 at Ooty, India
2021	Oral	XXXIX Annual Meeting of Indian Academy of Neurosciences (IAN), Kolkata, India
2021	Oral	3rd Satellite Symposium for Indian Academy of Neurosciences (IAN)
2021	Participation	NeuroUpdate, IICB, Kolkata, India
2021	Poster	Alzheimer's Association International Conference (AAIC), 26th-30th July 2021, Denver, USA and online.
2021	Participation	23rd Biennial Meeting of the International Society for Developmental Neuroscience (ISDN 2021), Online
2020	Participation	XXXVIII Annual meeting of Indian Academy of Neurosciences International E-conference, Hyderabad, India
2020	Participation	NeuroEunoia 2020: A Neuroscience Affair, International E-conference, India
2020	Participation	NeuroUpdate, Kolkata, India
2020	Participation	3rd Symposium on Physiology and Pathology of Neuroglia, International E-conference
2019	Oral	Neurocon-2019; Disorders of Brain: Molecules, Models and Clinical Practice, Haryana, India
2019	Oral	Annual Conference on Frontiers in Biological Chemistry, Society of Biological Chemists (I) of Kolkata, Puri, India
2019	Poster	Symposium of Bridging Chemistry and Biology for Human Health and Disease, Society of Biological Chemists (I) of Kolkata and CSIR-IICB Kolkata, India
2019	Participation	NeuroUpdate, Kolkata, India
2018	Poster	International Congress of Cell Biology, a joint meeting of ISCB, APOCB and IFCB, Hyderabad, India
2017	Participation	NeuroUpdate, IICB, Kolkata, India

Awards and Honors:

1. **Travel award** for 4th ISN-JNC Flagship School "Brain Metabolism in Health and Disease" Sept 25th – Oct 2nd, 2022 in Schmerlenbach, Germany.
2. **Travel award** and **Young Members' Symposia selection** for ISN-APSN 2022 meeting, Aug 28th – Sep 1st, Honolulu, USA.
3. **Best Oral presentation award** at BAW 2022, Outreach Activities: Advances in Biology Research, Education, and Teaching, organized by IISER Kolkata, June 14th-June 20th, 2022 at Ooty, India
4. **Selected for Oral presentation** in D.M. Kar award category in Indian Academy of Neurosciences Annual Conference, 2021.
5. **First prize in Oral Presentation** in IBRO-APRC Associate School of Neuroscience "Biophysical to Molecular Techniques: An interface in Neurobiology Research" (August 23-27, 2021) by Indira Gandhi National Tribal University Amarkantak (MP), India.
6. **Best Poster Presentation** at the IBRO-APRC Georgian Associate School of Neuroscience held virtually, 21-25 August in Tbilisi, Georgia, 2021.
7. **Travel fellowship** by International Brain Research Organization and partial travel fellowship from Alzheimer's association for attending Alzheimer's Association International Conference (AAIC), 26th-30th July 2021, Denver, USA and online.
8. **Innovation in Science Pursuit for Inspired Research (INSPIRE) Fellowship** (IF160470) by Department of Science and Technology (DST), Government of India, in 2017 for pursuing doctoral (PhD) program in science.

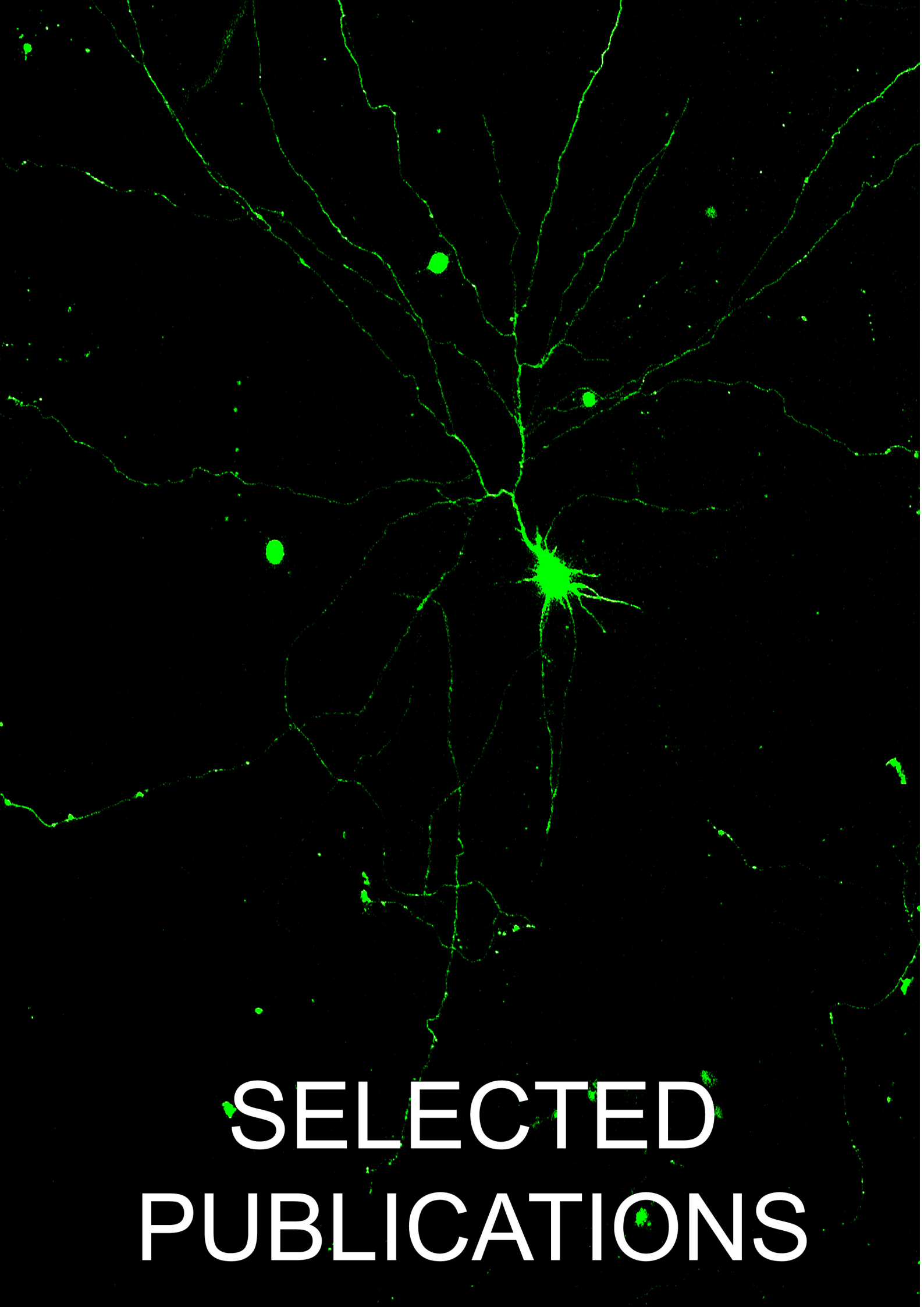

SELECTED PUBLICATIONS

Brain, Behavior, and Immunity 87 (2020) 804–819

Contents lists available at ScienceDirect

Brain, Behavior, and Immunity

journal homepage: www.elsevier.com/locate/ybrbi

Full-length Article

TIMP-1: A key cytokine released from activated astrocytes protects neurons and ameliorates cognitive behaviours in a rodent model of Alzheimer's disease

Pampa Saha[1,2], Sukanya Sarkar[1], Ramesh Kumar Paidi, Subhas C. Biswas*

Cell Biology and Physiology Division, CSIR-Indian Institute of Chemical Biology, 4 Raja S. C. Mullick Road, Kolkata 700 032, India

ARTICLE INFO

Keywords:
TIMP-1
Reactive astrogliosis
Amyloid-β
Rodent model
Neuroprotection
Cognitive dysfunctions
Akt
Alzheimer's disease
Cytokines

ABSTRACT

Alzheimer's disease (AD) is characterized by two pathologic species, extracellular amyloid-β (Aβ) plaques and intracellular neurofibrillary tangles. Astrocytes that maintain normal homeostasis in the brain undergo a set of molecular, cellular and functional changes called reactive astrogliosis in various neurological diseases including AD. It is hypothesized that reactive astrocytes initially tend to protect neurons by reducing Aβ load and by secreting a plethora of cytokines, however, their functions have only been poorly investigated. Our studies on the kinetics of activation of cortical astrocytes following Aβ-exposure revealed significant level of activation as early as in 6 h. The astrocyte conditioned medium (ACM) from 6 h Aβ-treated astrocytes (Aβ-ACM) provided significant neuroprotection of cultured cortical neurons against Aβ insults. Analysis of the secreted proteins in Aβ-ACM revealed a marked increase of Tissue inhibitor of Metalloproteinase-1 (TIMP-1) within 6 h. Interestingly, we found that neutralization of TIMP-1 with antibody or knockdown with siRNA in astrocytes abolished most of the neuroprotective ability of the 6 h Aβ-ACM on Aβ-treated cultured neurons. Furthermore addition of exogenous rat recombinant TIMP-1 protein protects primary neurons from Aβ mediated toxicity. In a well characterized Aβ-infused rodent model of AD, intra-cerebroventricular administration of TIMP-1 revealed a reduction in Aβ load and apoptosis in hippocampal and cortical regions. Finally, we found that TIMP-1 can ameliorate Aβ-induced cognitive dysfunctions through restoration of Akt and its downstream pathway and maintenance of synaptic integrity. Thus, our results not only provide a functional clarity for TIMP-1, secreted by activated astrocytes, but also support it as a major candidate in cytokine-mediated therapy of AD especially at the early phase of disease progression.

1. Introduction

Alzheimer's disease (AD) is an age-related neurodegenerative disorder associated with impairment of synaptic plasticity, neuronal apoptosis and severe loss of cognition and memory. Extracellular deposition of amyloid β (Aβ) as senile plaques and intracellular tangle formation are the two central events that trigger the pathogenesis (De Strooper and Karran, 2016).

In normal healthy brain, astrocytes play a major role in maintaining homeostasis by supplying energy to neurons, maintaining ionic balance and synaptic functions, removing excess glutamate to avoid glutamate excitotoxicity and supplying antioxidants like glutathione and ascorbic acid (Belanger and Magistretti, 2009). However, in most CNS injury or disease, astrocytes undergo a set of biochemical, morphological and genetic changes called reactive astrogliosis – a phenomenon characterized by hypertrophy, proliferation and altered gene expression leading to release of a myriad of anti- and pro-inflammatory cytokines (Olabarria et al., 2010; Sofroniew, 2014). While it is well known that continuous CNS insult leads to secretion of pro-inflammatory agents resulting in degeneration and death of neurons, much recent evidence indicates that during the early phase of disease, astrocytes play a critical neuroprotective role limiting apoptosis and providing trophic support to neurons (Anderson et al., 2014; Cregg et al., 2014; Teo and Bourne, 2018).

Two distinct reactive astrocyte populations were identified recently by the Ben Barres group using gene expression analysis (Zamanian et al., 2012; Liddelow et al., 2017). The neurotoxic A1 astrocytes are induced by microglia following neuroinflammation, and the

* Corresponding author.
E-mail address: subhasbiswas@iicb.res.in (S.C. Biswas).
[1] Contributed equally to this work.
[2] Current address: Department of Neurological Surgery, University of Pittsburgh, 200 Lothrop Street, Scaife Hall, Pittsburgh 15213, USA.

https://doi.org/10.1016/j.bbi.2020.03.014
Received 18 September 2019; Received in revised form 29 February 2020; Accepted 15 March 2020
Available online 16 March 2020
0889-1591/

neurotrophic A2 astrocytes are induced by ischemic injury. While both shared some common genes, A1 lacked the phagocytic activity and actively induced apoptosis by secreting toxic proteins and A2 possessed the neuroprotective property. A large proportion of astrocytes in the prefrontal cortex of AD post mortem brain are A1 (Liddelow et al., 2017). Since aging or disease increases A1 astrocytes, there might be more A2 in the prodromal stage of the disease which are converted to A1 with the progress of the disease or with age (Clarke et al., 2018).

Reactive astrocytes play a vital role in neuronal survival in AD through secretion of cytokines, chemokines and growth factors (Gadea et al., 2008; Belanger and Magistretti, 2009; Garwood et al., 2011). Tissue inhibitor of Metalloproteinase-1 (TIMP-1) is one such cytokine secreted from astrocytes in the early phase of inflammation and found to be increased in CSF of AD patient (Inspector et al., 2005; Wang et al., 2014). It is upregulated at protein level in many neuroinflammatory diseases (Rivera et al., 1997; Pagenstecher et al., 1998; Bugno et al., 1999; Jaworski, 2000; Szymocha et al., 2000; Khuth et al., 2001; Gardner and Ghorpade, 2003; Suryadevara et al., 2003) and at mRNA level in both the subtypes of reactive astrocytes (later named as A1 and A2) within 24 h of inflammatory as well as ischemic insult (Zamanian et al., 2012). In acute and chronic inflammatory conditions, the respective rise and fall of TIMP-1/MMP-9 ratio is a strong indication of neuroprotective attempt by TIMP-1 in the early phase of the disease (Gardner and Ghorpade, 2003). Nevertheless, none of the above studies reported the kinetics of astrocyte activation along with TIMP-1 expression or secretion which is essential to evaluate the temporal changes in TIMP-1 activity.

In the present study, we have investigated the kinetics of activation of astrocytes along with release of cytokines. We found that TIMP-1 is a major cytokine in astrocyte conditioned medium (ACM) from early Aβ-treated astrocytes which not only protects neurons from Aβ-induced toxicity but also improves cognitive behaviours including learning and memory in Aβ-induced rat model of AD.

2. Materials and methods

2.1. Materials

Cell culture media Dulbecco's modified Eagle's medium (DMEM), DMEM-F12, Neurobasal medium, B27 supplement, Fetal Bovine Serum (FBS), Horse Serum (HS), Penstrep antibiotic, Lipofectamine 2000, AlexaFluor, Sypro Ruby were purchased from Thermo Fisher Scientific (Waltham, MA, USA). Insulin, progesterone, putrescine, selenium, apotransferrin, nerve growth factor (NGF), poly-D-lysine (PDL), di-methyl sulfoxide (DMSO), paraformaldehyde (PFA) and 1,1,1,3,3,3 hexafluoro-2-propanol (HFIP) were purchased from Sigma-Aldrich (St.Louis, MO, USA). Primary culture instruments were from Roboz Surgical Instrument Co. (Gaithersburg, MD, USA). $A\beta_{1-42}$ was purchased from American Peptide (Sunnyvale, CA, USA) and Alexotech (Umea, Vasterbotten County, Sweden). Horseradish peroxidase conjugated secondary antibodies, normal IgG, TIMP-1, β3 tubulin, MAP2, IL-1β, SNAP25 and Actin antibodies were from SantaCruz Biotechnology (Santa Cruz, CA, USA). Vimentin, pAkt, tAkt, NF-kB, and PARP antibodies were purchased from Cell Signaling Technology (Danvers, MA, USA). Ki67, S100B, Bim, $A\beta_{1-42}$ and COX-2 antibodies were purchased from Abcam (Cambridge, UK). ECL reagent and polyvinylidenedifluoride (PVDF) membrane were purchased from GE Healthcare (Buckinghamshire, UK). Sodium dodecyl sulphate (SDS), Akt inhibitor II, Nestin and PSD95 antibodies were purchased from Merck (Darmstadt, Germany). Trypsin and Bovine Serum Albumin (BSA) were purchased from Sisco Research Laboratories Pvt. Ltd (Mumbai, India). All other fine chemicals were procured from standard local suppliers.

2.2. Cell cultures

2.2.1. Primary astrocyte culture

Primary astrocytes were cultured following the protocol that has been described earlier (Garwood et al., 2011; Saha and Biswas, 2015). In short, newborn Sprague Dawley rat pups were taken and the whole brain was dissected out and meninges were removed carefully. Neocortex parts were isolated and cut into pieces. The small cortical tissue pieces were minced and subjected to trypsinization for 30 min at 37 °C. Trypsinized brain tissue was triturated in DMEM medium supplemented with 10% FBS and passed through nylon mesh to avoid clumps. This single cell suspension was then added onto PDL (working concentration 0.1 mg/ml) coated plate and incubated for 2–3 min for preferential sticking of neurons. Next, the unattached cells were collected and harvested by centrifugation. Cells were resuspended in fresh medium and seeded at a density of 1.2 million/35 mm plate or 0.4 million/well of a 24-well plate. Cells were maintained for 13–14 days *in vitro* with medium change given every other day.

2.2.2. Primary cortical neuron culture

We performed the primary cortical neuron culture following the method which has been described earlier (Park et al., 1998; Troy et al., 2000). In brief, the neocortex part of E16-18 of rat were dissected out in serum free medium [DMEM/F12 (1:1)] supplemented with 6 mg/ml D-glucose, 100 μg/ml apo-transferrin, 25 μg/ml insulin, 20 nM progesterone, 60 μM putrescine, 30 nM selenium) and triturated into single cell suspension which was seeded at a density of 2.5 million/35 mm plate or 0.4 million/well of a 24-well PDL coated plate. The neurons were treated with oligomeric beta-amyloid ($A\beta_{1-42}$) after five days.

2.2.3. Astrocyte-neuron co-culture

To check the physical interaction between astrocytes and neurons, we adopted a co-culture system where primary cortical neurons were seeded onto mature astrocyte feeder layer (Haidet-Phillips et al., 2011). In short, cortical neurons were isolated from E16 rat embryos and seeded onto a feeder layer of primary astrocyte culture of 8DIV. After six days of seeding, the astrocyte-neuron co-culture was treated with Aβ with or without TIMP-1 neutralizing antibody.

2.2.4. Pheochromocytoma-12 (PC-12 cell) maintenance and differentiation

PC-12 cells were cultured as mentioned previously by Greene and Tischler (Greene and Tischler, 1976). They were maintained in DMEM supplemented with 10% HS and 5% FBS with passage at confluency. For differentiation, NGF at a concentration of 50 ng/ml and 1% HS were introduced to basic DMEM and added to cells. Cells were kept in this medium for five days. On the sixth day, all treatments were given.

2.3. Preparation of oligomeric Aβ

Lyophilized $A\beta_{1-42}$ peptide was resuspended in 100% HFIP to 1 mM concentration followed by vacuum centrifugation in a speed vac (Eppendorf, Hamburg, Germany). The peptide pellet was again suspended in DMSO at 5 mM concentration and subjected to sonication in 37 °C water bath for 10 min. Then it was diluted with phosphate-buffered saline (PBS: NaCl 137 mmole/L, KCL 2.7 mmole/L, Na_2HPO_4 10 mmole/L, KH_2PO_4 2 mmole/L, pH7.2) and SDS (0.2%) to a concentration of 400 μM and incubated for 6–18 h at 37 °C. Finally PBS was added to achieve a final concentration 100 μM and again incubated for 18–24 h at 37 °C. This preparation of Aβ was checked for oligomeric species by SDS–polyacrylamide gel electrophoresis (SDS-PAGE) followed by Sypro Ruby protein gel stain as described before (Saha and Biswas, 2015).

2.4. siTIMP-1 delivery to astrocytes

Primary astrocyte cultures were introduced to a smart pool of siTIMP-1 following the manufacturer's protocol (AccellsiRNA delivery, Dharmacon, Laffayette, CO, USA). According to this protocol, siTIMP-1 (1 μM) along with the positive control were dissolved in accellsiRNA delivery medium and directly added to cells. Successful knock down was verified after 72 h of incubation by western blot and immunocytochemistry with TIMP-1 antibody. The ACM from different experimental sets were then transferred to neuron after 72 h for further checking the effect of ACM deprived of TIMP-1 on neurons.

2.5. Treatments on cells

To minimize several growth factor and cytokine contaminations coming from FBS, we pretreated astrocyte cultures overnight with sera free medium (DMEM/F-12) and washed the cells twice with the same medium before giving any treatment. 14DIV astrocytes were treated with 1.5 μM of Aβ for different time points as indicated in the figures. For neutralization experiments, mature cultures were treated with TIMP-1 neutralizing antibody (AbDSerotec, Raleigh, UK) at 1 μg/ml concentration, or normal IgG at a concentration of 1 μg/ml, both in the presence and absence of Aβ.

Cortical neurons were treated with 1.5 μM Aβ for 24 h, or co-treated with rat recombinant TIMP-1 protein (R&D systems, Minneapolis, USA) at 25 ng/ml, 50 ng/ml and 100 ng/ml concentrations for 24 h and ACMs were taken from different experimental conditions as indicated in the figures.

PC-12 cells were treated with Aβ at 5 μM for 16 h, or co-treated with rat recombinant TIMP-1 protein at concentrations of 25 ng/ml, 50 ng/ml and 100 ng/ml for 16 h and with Akt inhibitor II at a concentration of 100 μM.

2.6. Survival assays

Plasmid DNA constructs were prepared with Plasmid Maxi kit (Qiagen, Germantown, MD, USA). For survival assay, primary cortical neuron culture was transfected with 0.5 μg of pSIREN-ZsGreen scrambled construct in complete cortical medium using lipofectamine 2000. After 6 h of incubation at 37 °C & 5% CO_2, lipofectamine containing medium was replaced by complete cortical medium. 48 h post transfection, cells were treated with Aβ and ACM from different experimental conditions. ZsGreen expressing viable cells were counted at 0 h, 24 h and 48 h under fluorescent microscope and represented.

Survival assay of cultured neurons was performed by a method that has been routinely used to assess viability of neuronal cells (Rukenstein et al., 1991; Troy et al., 2002; Sanphui et al., 2013). Cells were lysed in a detergent containing buffer that dissolves cell membrane but not nuclear membrane. The intact nuclei were then counted on a haemocytometer.

2.7. Immunocytochemistry

Immunocytochemistry was performed following the methods described previously (Biswas et al., 2005, 2007). Briefly, cells (either astrocytes or neurons as indicated in the figure) cultured on PDL-coated glass cover slips were fixed with 4% PFA in PBS for 10 min at room temperature followed by two washes with PBS. The fixed cells were permeabilized and blocked with 3% goat serum, 0.3% Triton X-100 in PBS for 1–2 h. Cells were then incubated with Ki67 (1:40), GFAP (1:50, Sigma-Aldrich, St. Louis, MO, USA), TIMP-1 (1:20), S100β (1:50), Vimentin (1:100), Nestin (1:100), p-Akt and t-Akt (1:50), β3 tubulin (1:50), or MAP2 (1:50) antibodies overnight at 4 °C. Following the primary antibody incubation, they were incubated with specific species matched secondary antibodies Alexafluor 546/488 for 1–2 h at room temperature. Nuclei were stained with Hoechst 33342 (Molecular Probes, Invitrogen, MA, USA) at a concentration of 2 μg/ml in PBS for 30 min at room temperature. Pictures were taken under LeicaCTR4000 Fluorescence Microscope or Leica TCS SP8 Confocal Microscope (Wetzlar, Germany) at 20× or higher magnifications as mentioned. The corrected total cell fluorescence (CTCF) was calculated by including integrated density of staining, area of the cell, and the background fluorescence of different experimental conditions. CTCF = Integrated density − (area of selected cell × mean fluorescence of background readings).

To evaluate neuronal arborization in different treatment conditions, we performed sholl analysis using NIH-ImageJ software which has widely been used elsewhere (Sholl, 1953; Cuesto et al., 2011; Sanphui and Biswas, 2013). Primary cultures of cortical neurons with different treatments along with control condition were immunostained with β3-tubulin and single neuron images were taken at low magnification. With the help of ImageJ, first the images were magnified and the processes were traced and a number of concentric circles were drawn from the neuron cell body with a 10 μm increasing radius. We performed a two-dimensional analysis where the number of intersecting points was calculated at each concentric circle. Data have been represented as the mean ± S.E.M. of five neurons from three independent experiments.

2.8. Preparation of cell or tissue lysate and western blotting

After the treatment, cells were washed with PBS and collected by means of scraping from wells in PBS and harvested by centrifugation at 1200 rpm at 4 °C for 5 min. Cells were lysed by lysis buffer (10 mM Tris (pH 7.4), 150 mM NaCl, 1% Triton X-100, 0.5% NP-40, 1 mM EDTA, 1 mM EGTA, 20mM NaF, 0.2mM Orthovanadate, Protease Inhibitors) and incubated for 10 min on ice. The lysed cells were centrifuged at 14,000 rpm at 4 °C for 15 min. For brain tissues, hippocampal samples were collected in radioimmunoprecipitation assay (RIPA – 50 mM Tris-HCl, 1 mM EDTA sodium salt, 150 mM NaCl, 1% Nonidet P-40, 0.25% soidium deoxycholate) buffer mixed with protease inhibitor cocktail followed by sonication, and same incubation and centrifugation steps as in case of cell samples. Supernatant in both cases were collected and proteins were estimated by Lowry method. Fifty μg of protein of each condition was resolved in SDS-PAGE. The proteins were transferred to PVDF membrane. After blocking with 5% BSA for 1 h at room temperature, the membranes were incubated with primary antibodies p-Akt (1:500), t-Akt (1:500), Actin (1:2000), IL-1β (1:1000), NF-kβ (1:1000), Bim (1:1000), PARP (1:1000), or TIMP-1 (1:500), for overnight at 4 °C. Membranes were washed three times with TBST [1.5 M NaCl, 1 M Tris (pH 7.5), 0.1% Tween20] followed by incubation with HRP tagged secondary antibody for 1–2 h at room temperature. Protein bands were detected on X-Ray film or UVP bioimager (anlytikjena, Upland, USA) by using ECL reagents after three times wash with TBST. Densitometric quantitation of each band was done by NIH-ImageJ software (NIH, Bethesda, MD, USA).

2.9. ELISA

For quantitative analysis of astrocyte secreted TIMP-1, we performed ELISA technique by using a kit (Rat TIMP-1 quantikine ELISA kit, R&D systems, Minneapolis, USA). According to the kit protocol, this assay employs the quantitative sandwich enzyme immunoassay technique. A monoclonal antibody specific for rat TIMP-1 was pre-coated onto a microplate. Standard, control and samples were added into the wells and any rat TIMP-1 present in these samples was trapped by the immobilized antibody. After washing away the unbound substances, an enzyme-linked polyclonal antibody specific for rat TIMP-1 was added to the wells. Following a wash to remove any unbound antibody-enzyme reagent, a substrate solution was added to the wells and protected from light. The enzyme-substrate reaction yielded a blue product that turned yellow when the stop solution was added. The intensity of the colour was measured spectrophotometrically at 450 nm and it was in

proportion to the amount of rat TIMP-1 bound in the initial step.

2.10. Cytokine array

The qualitative analysis of several cytokines along with TIMP-1 secreted from astrocytes, was performed by Proteome profiler rat cytokine array kit (R&D systems, Minneapolis, USA). 6 h, 16 h or 24 h ACM from control and Aβ treated astrocytes were subjected to conjugation with biotinylated antibodies. Then this cocktail was incubated with cytokine array membranes (embedded with 29 cytokines antibodies) overnight. On the next day, membranes were washed and streptavidin-HRP conjugates were added. Chemiluminescence was detected by UVP bioimager (anlytikjena, Upland, USA). Images were captured at different exposures to minutely detect the changes between the control and the treated dot blots for each of the cytokines. Dot intensities were analysed by the help of ImageJ software.

2.11. Animal housing and care

Adult male Sprague Dawley rats weighing between 280 and 320 g were housed maximum three per cage in a temperature-controlled room (24 ± 2 °C), with 12–12 h light-dark cycle, humidity (60 ± 5%) and access to food and water *ad libitum* in the animal house of CSIR-Indian Institute of Chemical Biology, Kolkata. All the studies were conducted in accordance with the guidelines formulated by the Committee for the Purpose of Control and Supervision of Experiments on Animals (Animal Welfare Divisions, Ministry of Environments and Forests, Govt. Of India), with approval from the Institutional Animal Ethics Committee (IAEC).

2.12. Stereotaxy

Rats were anesthetized with 50 mg/kg sodium thiopentone (Thiosol, Neon laboratories, Mumbai, India) intraperitoneally (i.p.) in 0.9% normal saline according to the protocol reported earlier (Paidi et al., 2015). The animals were positioned in a stereotactic frame (Stoelting, MO, USA) with the incision bar initially placed at the Bregma point. The body temperature of the animal was maintained at 37 °C using a homeothermic blanket (Harvard apparatus, U.K.). An oligomeric solution of Aβ, as mentioned in Section 2.3, was infused bilaterally at 2.25 μg in 5 μl per side of the brain into the hippocampus (lateral, 0.21 cm from the bregma; anteroposterior, 0.36 cm; dorsoventral, 0.28 cm, according to the atlas of Paxinos and Watson). The flow rate was kept at 0.5 μl/min utilizing a worker bee syringe pump (BAS, West Lafayette, USA). Aβ was allowed to diffuse for an extra 5 min after its delivery. Same volume of PBS was bilaterally injected in the control rats. rrTIMP-1 was stereotactically injected in the ventricle region of rat brain (lateral, 0 cm from the bregma; anteroposterior, 0.36 cm; dorsoventral, 0.38 cm) and the protein was allowed to diffuse for an additional 5 min after its injection.

2.13. Behavioural studies protocol

The experimental rats were randomly divided into five groups, namely, Control, only TIMP-1 (5 ng), only Aβ, Aβ + TIMP-1 (2.5 ng) and Aβ + TIMP-1 (5 ng). The control rats received PBS whereas the Aβ rats received freshly prepared oligomeric Aβ in each side of the brain. On the 7th day following Aβ or PBS infusion, some of the animals were injected with rat recombinant TIMP-1 (rrTIMP-1) at a dose of 2.5 ng or 5 ng per animal, dissolved in artificial cerebro spinal fluid, in a total volume of 5 μl into the ventricle region of the brain.

To evaluate Aβ induced memory deficits and their recovery with rrTIMP-1, rats from all the five groups were assessed sequentially by open-field or locomotion test, novel object recognition test, elevated plus maze test, passive avoidance test and fear conditioning tests starting on the 15th day onward following Aβ or PBS infusion, as per the schedule indicated below:

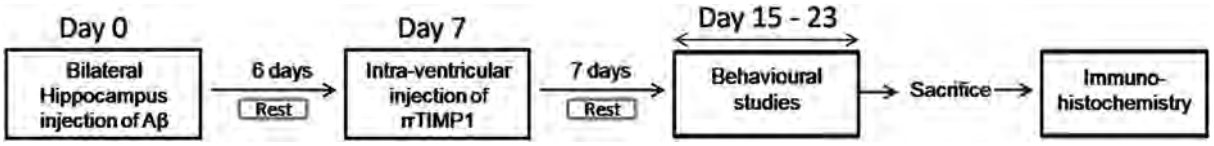

The behavioural tests were performed by an investigator completely blind to the treatment. Animal number in each group for each behavioural experiment has been given in Supplementary Table 1.

2.13.1. Locomotion test

It is broadly used to understand general activity and exploratory behaviour in rats and mice (Crusio, 2001). Locomotion apparatus (IR Actimeter, Panlab, Barcelona, Spain) consisted of an open field Plexiglas arena (278 × 236 × 300 mm) with the photocell emitters and receptors equally placed along the perimeter. These emitters and receptors build an x-y grid of invisible infrared rays. Animals placed in this chamber while moving caused beam breaks and subsequently data were recorded and analyzed by the analyzer. The rats were allowed to explore the arena for 10 min and the distances travelled by rats were determined.

2.13.2. Novel object recognition (NOR) test

This test is based on the innate tendency of rodents to explore a novel object instead of a familiar object, providing an index for recognition memory (Ennaceur, 2010). Each rat was placed in an open-field arena (50 cm × 30 cm × 40 cm) with two identical (same diameter, colour and length) cylindrical objects placed at parallel corners and was allowed to explore them for 5 min on the first day. On the second day, one of the cylindrical objects was swapped with a rectangular object of a different colour and each rat was again placed in the field for 5 min to explore the objects. The length of time spent in exploring each of the objects on day two was calculated and designated as time spent at novel object (TN) and time spent at familiar object (TF) values. Discrimination index (DI) and preference index (PI) were derived according to the formulas – DI = (TN − TF)/(TN + TF), PI = TN/(TN + TF) × 100 (Janus et al., 2000; Bryan et al., 2009; Antunes and Biala, 2012).

2.13.3. Elevated plus maze (EPM) test

The elevated plus maze (EPM) test is widely known for assessing anxiety and cognition in rodent models (Belzung and Griebel, 2001; Paidi et al., 2015). The test apparatus comprised of a plus-shaped wooden maze raised to a height of 60 cm from the floor with two open arms (50 cm × 10 cm, with a very small, 1 cm-wall) across from one another and at 90° to the two closed arms of same dimensions but with tall walls (50 cm).

On day one, the rat was placed at the edge of one of the open arms of plus maze with its face away from the centre and then allowed to explore the plus maze freely. The time taken by the animal to move from the open arm to the closed arm was termed as the transfer latency

and recorded as initial transfer latency (ITL) and the task was terminated once the animal moved into the closed arm. On day two, the same procedure was followed, and the transfer latency was recorded as retention transfer latency (RTL). The maximum time given per animal was 5 min.

2.13.4. Passive avoidance test

The instrument is comprised of two dimensionally identical chambers – a white (well-lit) chamber and a dark chamber partitioned with automated guillotine door for the rat to pass through (SHUTTLEBOX, Panlab, Barcelona, Spain). Initially, the animal was allowed to habituate for 5 min in the white compartment in door closed condition. This was followed by the acquisition stage or training stage where the animal was kept in the white chamber with door open condition for a maximum of 5 min. It is the innate tendency of rodents to gravitate towards darkness but once it reaches the dark chamber from the white chamber it received a mild aversive stimulus (foot-shock of 0.7 mA for 2 s). On the following day (Probe stage), each animal was similarly placed in the white chamber and the latency period to enter into the dark chamber was determined using SHUTAVOID software (Panlab, Barcelona, Spain) (McGaugh, 1966; Lawlor et al., 2007; Senechal et al., 2008; Bryan et al., 2009).

2.13.5. Fear conditioning tests

Fear conditioning tests are vastly used to evaluate hippocampal dependent associative learning and also useful to understand amygdala-hippocampal communication (Fanselow, 1980; Fanselow and Tighe, 1988; Hamann et al., 2002; Bryan et al., 2009). In this study, rats were individually placed in a sound-attenuating chamber with a stainless-steel grid floor that delivers shock and equipped with a recorder that records the freezing behaviour. Several studies have shown that rodents express their defensive behaviour related to fear in the form of freezing: total absence of motion excluding breathing movements. One ml of 10% vanilla extract was used in this conditioning chamber as the odour cue. The testing paradigm (Bubser et al., 2014) was appropriately followed as described below:

2.13.5.1. Contextual fear conditioning test. On the day of training, the rat was placed in the conditioning chamber and allowed to habituate for a 2 min period. After habituation, the animal was exposed to four sessions of an unconditioned stimulus (89 sec pre-shock interval; 0.7 mA 1-sec foot-shock), ending with a 2 min period without stimuli (10 min total). Approximately 24 h after the training (probe stage), the rat was returned to the chamber maintaining identical context and odour cue except shock stimuli. Freezing behaviour was assessed by PACKWIN 2.0 software (Panlab, Barcelona, Spain) during an 8 min period.

2.13.5.2. Cue dependent fear conditioning test. On the day of acquisition, each rat was placed in the conditioning chamber as previously mentioned and allowed to explore the chamber for an initial 2 min period. Following habituation, four 29 sec sessions of light and sound (90 dB, 4000 Hz) co-terminating with a foot-shock (0.6 mA, 1 sec) were delivered with an intersession interval of 1 min, after this a 2 min rest period was given to the animal before it was removed from the chamber (10 min in total). In the probe stage (24 h after training), the context of the box was tweaked by addition of white sheets to two walls and the floor, and a different odour cue (camphor) was used. Each rat was returned to this novel context and exposed to the same testing sessions as on day one but without unconditional stimuli. Freezing behaviour was assessed by PACKWIN 2.0 software (Panlab, Barcelona, Spain) without shock for 8 min.

2.14. Immunohistochemistry

Twenty three days following Aβ infusion, perfusion was performed transcardially under deep anaesthesia (1 g/kg of urethane, MP Biomedicals, lllkirch, France, in 0.9% NaCl solution, i.p.) with 50 ml of chilled 100 mM PBS (pH 7.4) followed by 50 ml of 4% (w/v) PFA and then the rat was decapitated and the brain was removed from the skull. The brain was submerged in 4% PFA overnight at 4 °C and then transferred in 30% (w/v) sucrose solution in PBS for cryopreservation at 4 °C. Coronal sections (20 μm thick) were taken through the hippocampus using a cryotome (Thermo Shandon, Pittsburg, PA, USA). The sections were carefully allowed to attach to gelatine-coated slides for histological staining. For immunofluorescence studies, the sections were rinsed with PBS thrice followed by permeabilization with PBS + 0.4% Triton-X for 40 min while for bright field imaging sections were incubated in 3% hydrogen peroxide/10% methanol solution for 10 min to quench endogenous peroxidase activity. Afterwards for both the studies, sections were washed with PBS + 0.1% Triton-X three times 5 min each. This was followed by blocking with 4% BSA in 0.1% PBST for 1 h. Primary antibodies used included $A\beta_{1-42}$ (1:100), TIMP-1 (1:100), GFAP (1:50), CD11b (1:500, Bio-Rad, USA), COX 2 (1:500), PSD95 (1:50) and SNAP25 (1:100). Primary antibody was diluted in the blocking solution and the sections were incubated with it for 48 h at 4 °C. This was followed by three washes with PBST (0.1%). For immunofluorescence, sections were incubated with appropriate Alexafluor-tagged secondary antibodies at RT for 2 h followed by staining in Hoechst solution for 30 min at 37 °C, rinsed thrice with PBS and then mounted with Prolong Gold Antifade with DAPI (Thermo Fisher Scientific, Waltham, MA, USA) for microscopic analysis. For bright field imaging, biotinylated secondary antibodies (Vector Laboratories USA) were used appropriately before incubation with streptavidin ABC solution (Vector Laboratories, Burlingame, CA, USA) and visualized by diaminobenzidine (Bio-Rad, USA) chromogen.

$A\beta_{1-42}$ labelled plaques were analysed quantitatively by calculating a percentage of plaque area or number of plaques and apoptotic cells were quantified by number of TUNEL positive cells by ImageJ software. Microglial counts were performed on images captured from 3 coronal sections/rat where cell counts were based on activated microglial morphology for CD11b positive cells and COX-2 positive microglia. Quantitative analysis (cells/mm2) was conducted using ImageJ software. CD11b and COX-2 positive cells were expressed as cell numbers per mm^2.

2.15. Terminal deoxynucleotidyl transferase dUTP nick end labeling (TUNEL) staining

The TUNEL staining was performed to assess apoptosis using Clonetech ApoAlert DNA Fragmentation kit (Takara, Kusatsu, Shiga, Japan) according to the manufacturer's protocol. Briefly, the tissue sections (as prepared earlier) were washed with PBS twice. The sections were then digested in Proteinase K solution (20μg/ml, diluted from concentration stock provided in the kit) for 20 min. The reaction was stopped by washing with PBS followed by addition of 4% PFA/PBS to the sections. The tissues were again washed in PBS. For tissue sections thus prepared, cells were equilibrated in Equilibriation buffer at RT for 10 min. The experimental samples were then incubated in a solution containing the nucleotide mix and Tdt enzyme in equilibriation buffer for 1 h at 37 °C in dark. The tailing reaction was terminated by 2XSSC buffer at RT for 15 min. Samples were washed twice with PBS. Following this, they were stained with Hoechst solution for 30 min at 37 °C and then washed with PBS two times before mounting with Prolong Gold Antifade with DAPI for microscopic analysis. The percentage of apoptotic cells were calculated by dividing the number of TUNEL-positive cells with the total number of cells (Hoechst stained nuclei) multiplied by 100.

2.16. Statistical analysis

All data were analyzed by one way ANOVA analysis followed by

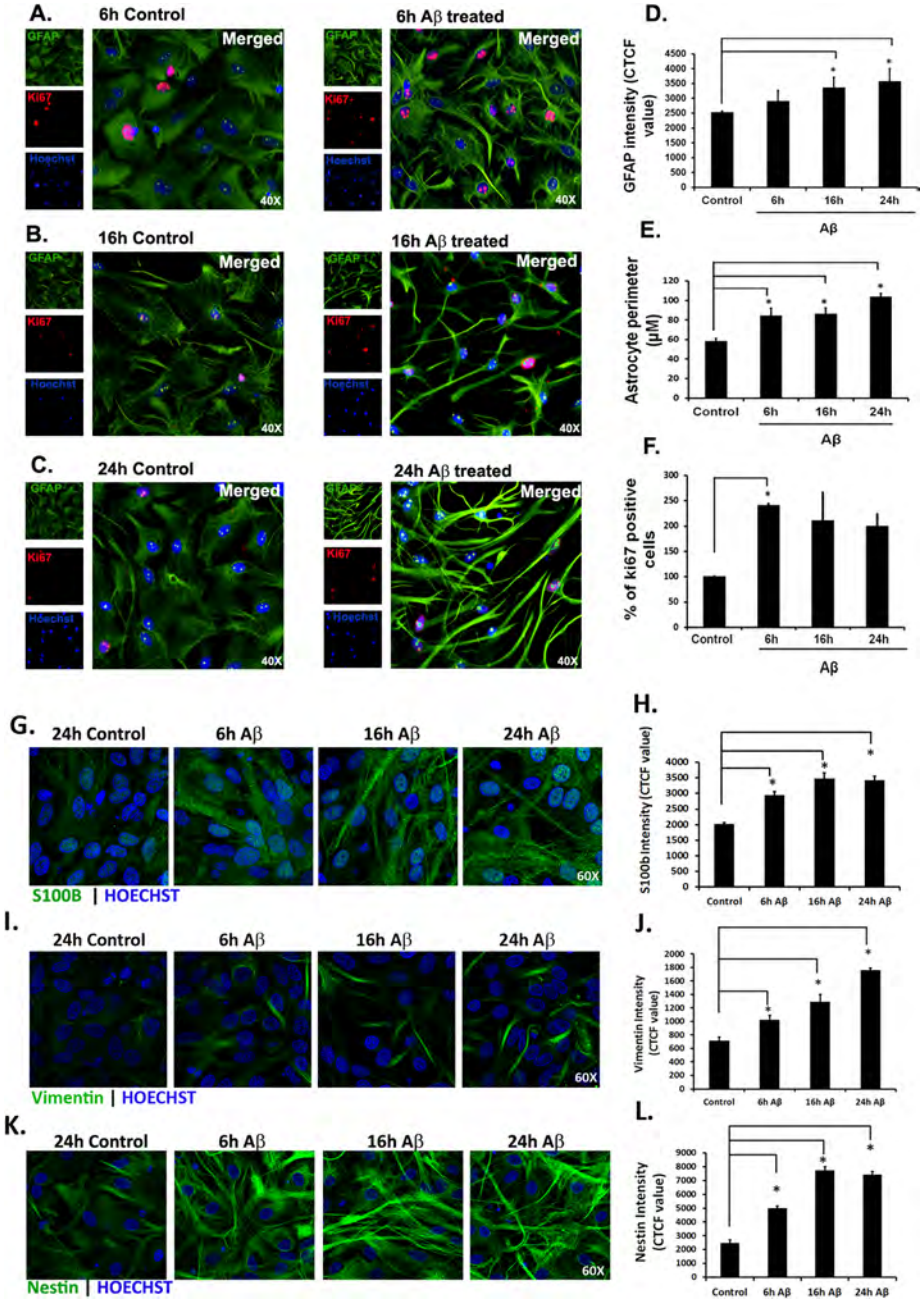

Fig. 1. Kinetics of morphological changes and cell proliferation upon Aβ treatment of cortical astrocytes. Astrocytes (14DIV), treated with 1.5 μM Aβ for 6 h (A), 16 h (B), and 24 h (C), were subjected to immunocytochemical staining with GFAP and Ki67 antibody followed by nuclear staining with Hoechst. Images were taken at a magnification of 40×. Both control and treated conditions in (A), (B), (C) figures represent a vertical panel of GFAP, Ki67 and Hoechst and the corresponding merged images (right of the vertical panel). (D), (E), (F) Bar diagrams represent quantitative analysis of GFAP intensity expressed as corrected total cell fluorescence (CTCF), astrocyte perimeter in μM and % of Ki67+ nuclei respectively at different time points of Aβ treatment. Values are expressed as Mean ± SEM of three independent experiments; *p ≤ 0.05. (G), (I), (K) panels represent 6 h, 16 h and 24 h Aβ treated astrocytes along with 24 h control samples, stained with S100B, vimentin and nestin respectively along with Hoechst stain. Images were taken at a magnification of 60x. (H), (J) and (L) bar diagrams are indicating the quantitative analysis of S100B, vimentin and nestin respectively which are expressed as CTCF values. Values are expressed as Mean ± SEM of three independent experiments; *p ≤ 0.05.

tukey's multiple comparison of means post hoc test by using graph pad software for comparing more than two experimental groups. For comparison of significant difference between two groups, student's *t*-test analysis was used. Data are presented as mean ± standard error of mean, and $p < 0.05$ was considered to be statistically significant.

3. Results

3.1. Kinetics of Aβ-induced activation of astrocytes in culture

We studied the activation of astrocytes upon Aβ exposure at different time points and subsequently checked the effect of activation on the health of neurons. Kinetics of activation was monitored following exposure of primary astrocyte cultures to Aβ for 6 h, 16 h and 24 h. GFAP expression, morphological changes and proliferation, three important hallmarks of astrocyte activation, were checked by immunocytochemical staining with GFAP and Ki67. Robust activation of astrocytes was evident within as early as 6 h of Aβ exposure, as characterized by a significant change in morphology from flat polygonal to long process bearing cells which has been expressed as astrocyte perimeter measurement (Fig. 1A, E, $p \leq 0.05$). This result can be corroborated to our previous report where the morphological changes of the Aβ-treated astrocytes were validated as characteristics of astrogliosis both *in vitro* and *in vivo* (Saha and Biswas, 2015). Along with that we found a marked increase in cell proliferation in terms of Ki67 positive cells (2.5 fold compared to control cells) upon 6 h of Aβ treatment (Fig. 1A, F, $p \leq 0.05$). But we did not find any significant change in GFAP expression at 6 h time point (Fig. 1A, D). At 16 h and 24 h, although the astrocyte perimeter showed a significant change (Fig. 1B–E) with appearance of longer process bearing cells and in GFAP intensity, but cell proliferation did not increase further (Fig. 1F). Hence to confirm astrogliosis in culture condition we further checked with other important activation markers such as S100B, vimentin and nestin. Each marker was found to be increased significantly within 6 h of Aβ

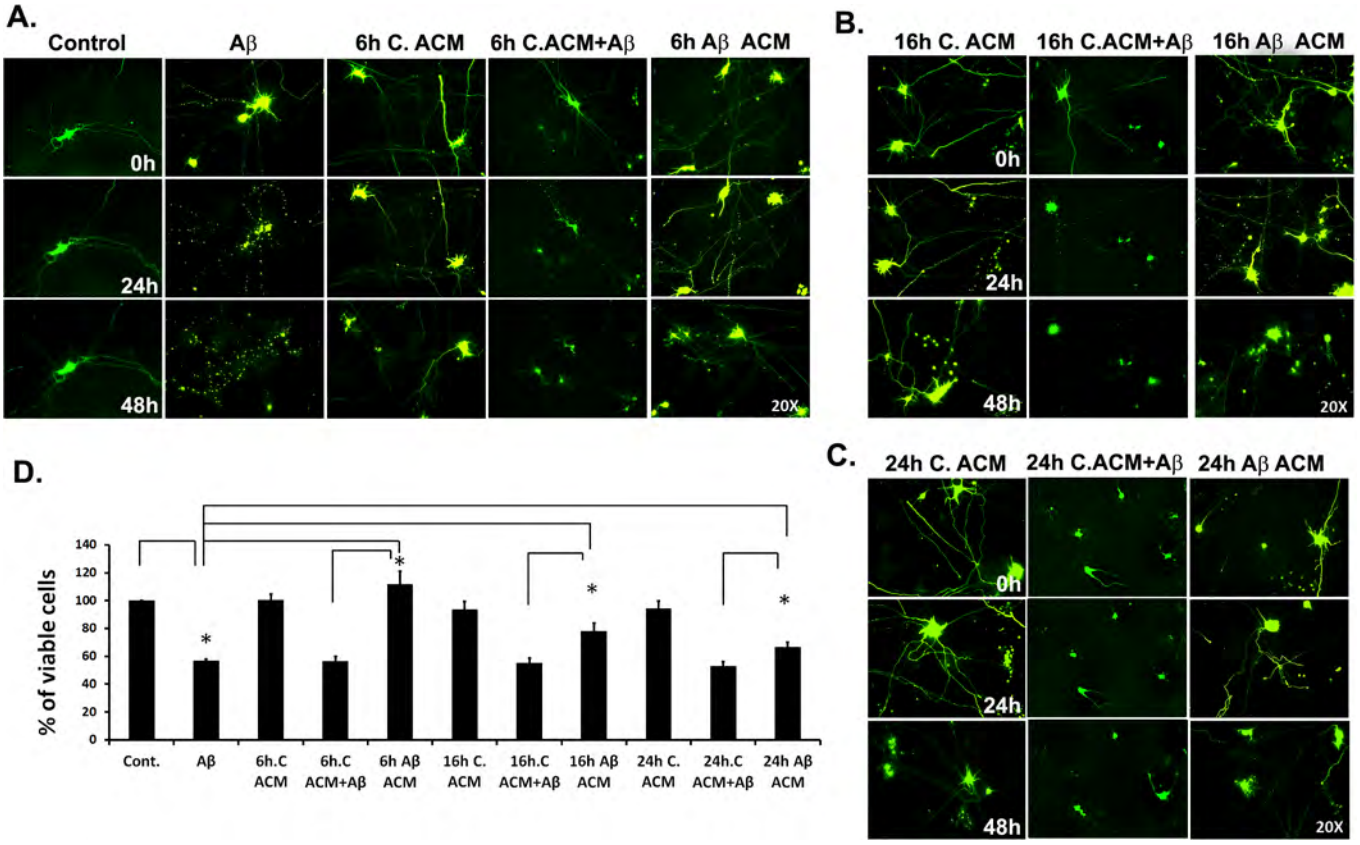

Fig. 2. Effect of conditioned medium from Aβ-exposed activated astrocytes on cultured cortical neurons. (A–C) ZsGreen transfected 6DIV cultures of cortical neurons were treated with 6 h, 16 h & 24 h control ACMs in presence or absence of Aβ or Aβ-treated ACM. Along with that only control neurons and direct Aβ treated neurons were taken. Pictures of viable green transfected cells were taken at 20× at 0 h, 24 h and 48 h of incubation. (D) Astrocytes were treated with Aβ for different time durations (6 h, 16 h or 24 h), then Aβ-treated or untreated ACMs were transferred to neurons in presence or absence of Aβ as indicated and after 24 h of incubation, the viable cells were counted by intact nuclei counting method. Data represents % of viable cells against different ACM treatment along with control neurons with or without Aβ. Values are expressed as Mean ± SEM of five independent experiments; *$p \leq 0.05$. (For interpretation of the references to colour in this figure legend, the reader is referred to the web version of this article.)

exposure to astrocytes compared to control and that continued at later time points as well (Fig. 1G–L, $p \leq 0.05$). Collectively, these results suggest that astrocytes in cultured condition are significantly activated within the first six hours following Aβ exposure.

3.2. Astrocyte conditioned medium (ACM) from Aβ-treated astrocyte cultures display neuroprotective properties

To investigate the effect of ACM which was collected at different time points following Aβ exposure to astrocytes, on the morphology and survival of Aβ-treated neurons (Nagai et al., 2007), ZsGreen-transfected cortical neurons were incubated with ACM collected at 6 h, 16 h and 24 h from control and Aβ-treated astrocytes in the presence or absence of Aβ as indicated in figure (Fig. 2). Images were taken at 0 h, 24 h and 48 h and total cell numbers were obtained by nuclei counting at 24 h of ACM treatment. Fig. 2A, B, C and D show that in the absence of ACM, Aβ-treatment on cultures of cortical neurons led to progressive degeneration of neuritis (Fig. 2A–C) and a significant death of neurons (≈40%) at 24 h (Fig. 2D, $p \leq 0.05$). In contrast, in the presence of control ACM or Aβ-treated ACM, the overall morphology in terms of dendrite retention and viability of neurons were protected significantly. However, control ACM did not provide any protection against Aβ-induced degeneration of neurites and death. In contrast, 6 h Aβ-treated ACM provided better protection to neurons in terms of retention of processes and number of viable cells compared to that from 16 h and 24 h Aβ-treated ACMs (Fig. 2A–D, $p \leq 0.05$).

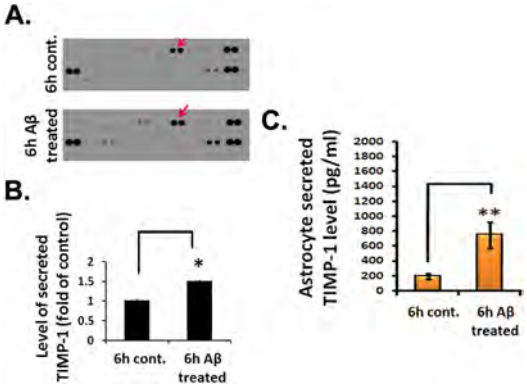

Fig. 3. Aβ significantly enhances secretion of TIMP-1 from astrocytes. Cultured astrocytes (14DIV), treated with 1.5 μM Aβ for 6 h, were used for all experiments along with untreated controls. (A) Cytokine array analysis of ACM from control and Aβ-treated astrocytes. Arrows indicate the dots which correspond to TIMP-1. (B) Densitometric analysis of the spots shown in (A) indicating the relative levels of secreted TIMP-1 in 6 h control and Aβ-treated ACMs; *$p < 0.05$. (C) Quantitation of TIMP-1 in the ACMs from control and Aβ-treated samples were performed by ELISA. Bar diagram represents TIMP-1 level in pg/ml in control and the Aβ-treated samples. Values are expressed as Mean ± SEM of three independent experiments;**$p < 0.05$.

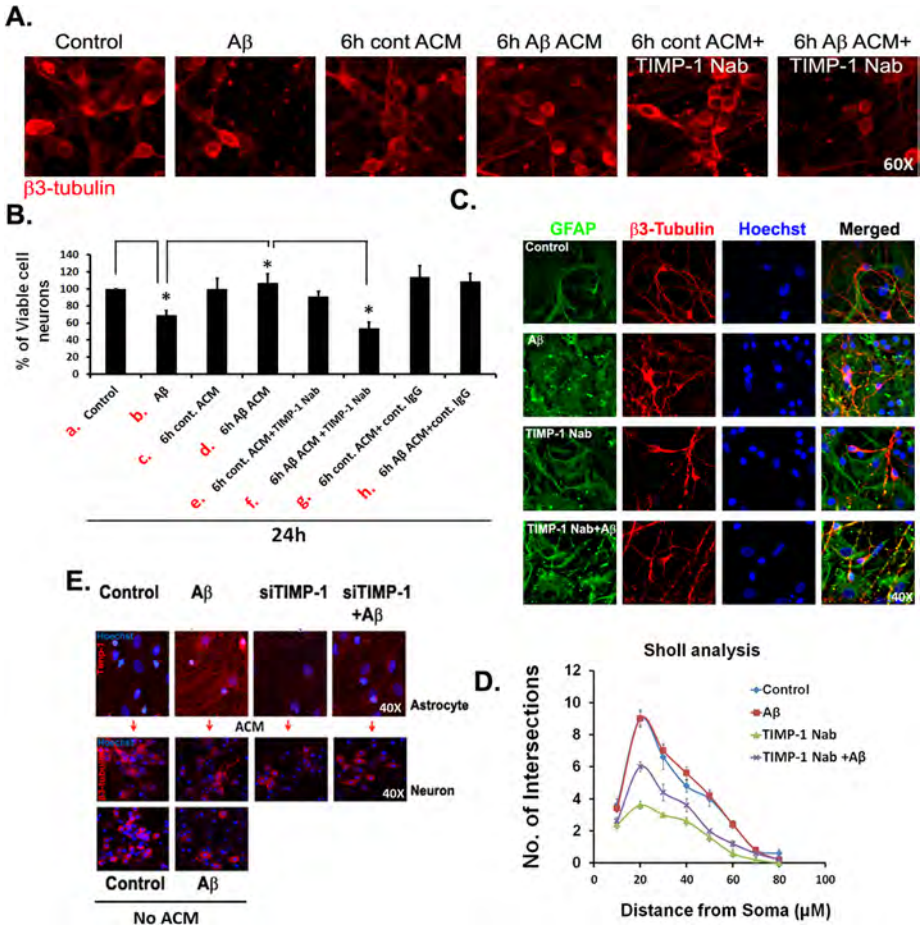

Fig. 4. Effect of TIMP-1 enriched and TIMP-1 neutralized ACM from 6 h control and 6 h Aβ-treated astrocytes on the viability and survival of neurons. (A) Cortical neuron cultures were treated with none (control), Aβ, 6 h control ACM, 6 h Aβ-treated ACM, 6 h control ACM + TIMP-1 Nab, 6 h Aβ-treated ACM + TIMP-1 Nab (as indicated in panels) for 24 h and subjected to immunocytochemistry with β3-tubulin antibody. Pictures were taken at 60×. (B) Primary cultures of cortical neurons (6DIV) were treated as indicated below the bars for 24 h and then the viable neurons were assayed by nuclei counting. a) Control neurons-no ACM; b) Aβ (1.5 μM) treated neurons-no ACM; c) 6 h control ACM (before TIMP-1 neutralization); d) 6 h Aβ treated ACM (before TIMP-1neutralization); e) 6 h control ACM after TIMP-1 neutralization with TIMP-1 NAb; f) 6 h Aβ treated ACM after TIMP-1 neutralization with TIMP-1 NAb; g) 6 h control ACM plus normal IgG; h) 6 h Aβ treated ACM plus normal IgG. Note the protection of neurons enabled by TIMP-1-containing ACM (d) and the loss of the protective effect following treatment of the ACM with TIMP-1 antibody (f) but not by treatment with control or normal IgG. Values are expressed as Mean ± SEM of four experiments; *$p < 0.05$. (C) Astrocyte-neuron co-cultures were treated with TIMP-1 Nab in presence or absence of Aβ for 6 h. Immunocytochemistry with GFAP and β3-tubulin antibody was performed. Pictures were taken at 40× under confocal microscope. Panels from left to right represent immunostaining with GFAP, β3-tubulin, Hoechst, and merged. Panels from top to bottom show control, Aβ-treated, TIMP-1 Nab and TIMP-1 Nab + Aβ treated cells. (D) Represents the corresponding sholl analysis for the arborisation of neurons present in co-cultured condition and under different treatment as in fig (C). (E) Astrocyte cultures (14 DIV) were transfected with siTIMP-1 and after 72 h, cells were treated with Aβ for 6 h. After the incubation period, 6 h ACMs were collected from control, Aβ-treated, siTIMP-1, and Aβ + siTIMP-1 treated astrocytes and transferred to 6DIV cultures of cortical neurons (middle panel). The remaining astrocytes were immunostained with TIMP-1 antibody along with nuclear staining with Hoechst to validate the knock down (Upper panel). After 24 h of 6 h Aβ-ACM treatment, neurons were immunostained with β3-tubulin antibody along with Hoechst to check their process integrity. In the lower panel, only control and Aβ-treated neurons (without ACM) are shown. Note the reduced expression of TIMP-1 in si-TIMP-1 treated astrocytes (upper panel) and the degeneration of the neurons in the presence of siTIMP-1 treated Aβ-ACM (middle panel). Pictures were taken at 40× magnification.

3.3. Aβ significantly induces secretion of TIMP-1 from astrocytes within 6 h of exposure

In view of the robust activation of astrocytes within 6 h of Aβ exposure and the maximum protection offered by the 6 h Aβ-treated ACM to cultures of Aβ-treated neurons, we analyzed the cytokine content of 6 h control and 6 h Aβ-treated ACM using a cytokine array kit (Proteome profiler Rat cytokine array kit, R&D). Comparison of the relative cytokine contents of ACMs from 6 h control and Aβ-treated samples showed that TIMP-1 is upregulated significantly in the Aβ-treated ACM (Fig. 3A and B, $p < 0.05$). The dot blots revealed changes in the expression of a number of other cytokines such as sICAM-1, CINC-1, MIP-1α, VEGF, IL-2 etc. (Supplementary Fig. 1 A and D). Consistent with this finding, ELISA assay also showed that at 6 h there was a three to four fold significant increase of TIMP-1 in ACM upon Aβ-exposure compared to control samples (Fig. 3C, $p < 0.05$). We also found that in cytokine arrays at later time points (16 h and 24 h), TIMP-1 level was reduced whereas cytokines like fractalkine, MIP 3α and CINC2 α/β were upregulated (Supplementary Fig. 1B–D). These findings justify why 6 h Aβ-treated ACM provided better neuroprotection compared to that of later time points.

3.4. ACM deprived of TIMP-1 loses neuroprotective activity

In order to assess the specific contribution of TIMP-1 present in ACM in neuroprotection of Aβ-treated neurons, we compared the relative neuroprotective activity of TIMP-1 enriched ACM with that of TIMP-I deprived ACM where TIMP-1 was inactivated by using a neutralizing antibody (TIMP-1 Nab). For this experiment, cultures of 6DIV cortical neurons (control and control + Aβ) were treated with 6 h control ACM, 6 h Aβ-treated ACM, 6 h control ACM + TIMP-1 Nab, 6 h Aβ-treated ACM + TIMP-1 Nab. After 24 h of incubation, the integrity of the neuronal processes was checked by immunochemical staining with β3-tubulin antibody.

The results revealed a significant loss of neurons and their processes when secreted TIMP-1 in ACM was neutralized by using a neutralizing antibody, compared to untreated ACM taken from either control or Aβ-treated astrocytes (Fig. 4A). To strengthen the data, we also treated astrocytes with 6 h control ACM + normal IgG, 6 h Aβ-treated ACM with normal IgG along with previous conditions and performed nuclei counting of viable neurons following 24 h of exposure (Fig. 4B). In the absence of ACM, Aβ-treatment led to a loss of 30% neurons (Fig. 4B, a and b, $p < 0.05$) and this was prevented by ACM from both 6 h control and 6 h Aβ-treated astrocytes (Fig. 4B, c and d, $p < 0.05$). Neutralization of TIMP-1 antibody in the 6 h control ACM partially loses the neuroprotective effect retaining 80–90% viability (Fig. 4B, e), which is presumably due to other neuroprotective factors present in the 6 h ACM. In contrast, neutralization of TIMP-1 in the 6 h Aβ-treated ACM (Fig. 4B, f) led to significant loss of neuroprotective effect (50% cell death at 24 h, $p < 0.05$). The specificity of TIMP-1 is evident from the

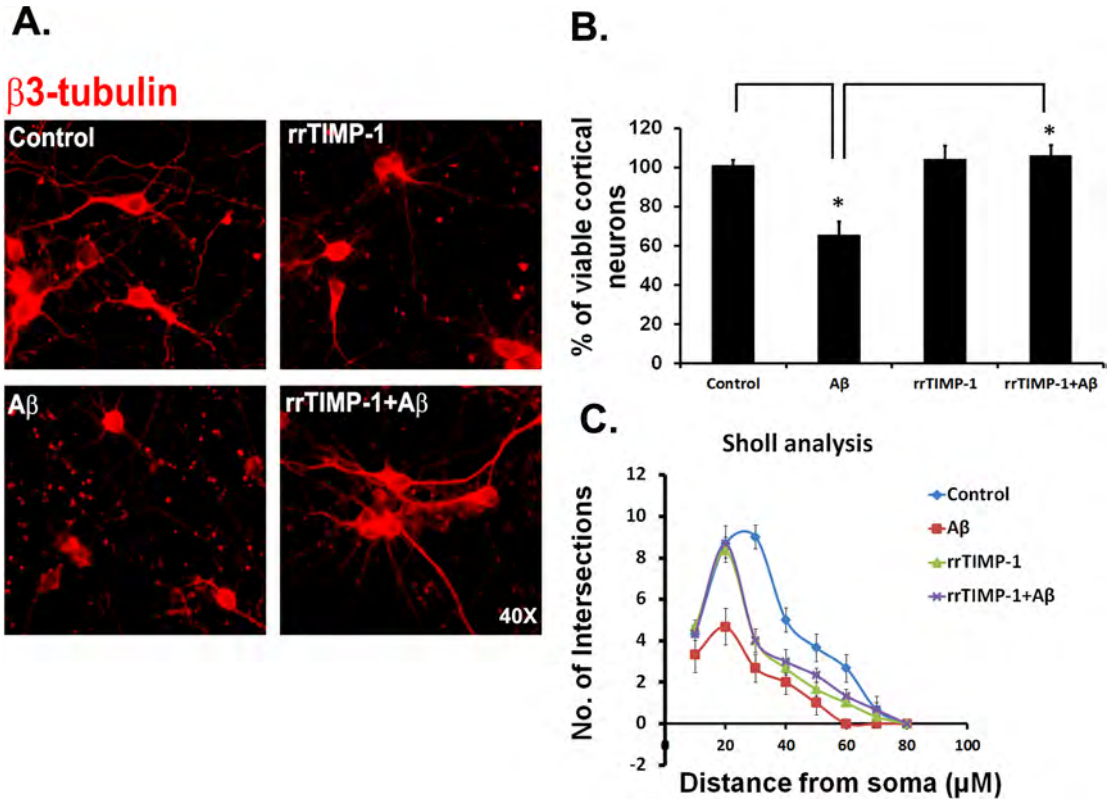

Fig. 5. Effect of rat recombinant TIMP-1 (rrTIMP-1) on the survival of primary cortical neurons in presence of Aβ: (A) Primary cortical neurons were treated with or without Aβ in the presence of rrTIMP-1 as indicated for 24 h. Cells were fixed and subjected to immunostaining with β3-tubulin antibody. Pictures were taken at 40× magnification. (B) Cell lysates from all samples were also collected and subjected to nuclei counting. Bar diagrams indicate the % of viable neurons at 24 h. Values are expressed as Mean ± SEM of three experiments; *p < 0.05. (C) Sholl analysis for the arborisation of neurons in fig (A) at different treatment conditions. Values are expressed as Mean ± SEM of three experiments; *p < 0.05.

fact that no such protection was observed when TIMP-1 antibody was replaced by normal IgG (Fig. 4B, g and h).

The neuroprotective effect of TIMP-1 was also evident in a co-culture model, where astrocyte-neuron co-cultures were treated with TIMP-1 Nab in the presence and absence of Aβ and after 6 h of incubation, cells were immunostained with GFAP and β3-tubulin to check the integrity of neuronal processes and astrocyte-neuron interactions. We performed sholl analysis and found a significant reduction in neurite retention and interaction with astrocytes in co-cultures treated with TIMP-1 Nab + Aβ compared to the control conditions where co-cultures were exposed to Aβ only (Fig. 4C, D).

Further evidence was obtained by knocking down TIMP-1 by introducing a smart pool of siTIMP-1 to primary mature astrocyte cultures both in control and Aβ-treated conditions for 72 h. Efficacy of the siTIMP-1 was checked by western blot and immunocytochemical analysis in PC12 cells (Supplementary Fig. 2A, B). Aβ-induced over-expression of TIMP-1 in primary astrocytes was prominently knocked down in the presence of siTIMP-1 (Fig. 4E). As described earlier, ACMs from control, Aβ, siTIMP-1 and Aβ + siTIMP-1 exposed astrocytes were taken and transferred to 6DIV cortical neuron cultures. After 24 h, the integrity of the neuronal processes was significantly lost where TIMP-1 was specifically downregulated (Fig. 4E). These observations led us to conclude that TIMP-1 secreted from Aβ-treated astrocytes has a beneficial role in maintaining neuronal health.

3.5. Rat recombinant TIMP-1 (rrTIMP-1) offers neuroprotection against Aβ-mediated neurotoxicity

Protection enabled by Aβ-induced TIMP-1 in ACM to cortical neurons led us to investigate the effect of rat recombinant TIMP-1 (rrTIMP-1) on the survival of Aβ-treated neurons. For these experiments, cultured cortical neurons or neuronally differentiated PC12 cells were treated with rrTIMP-1 (25 ng/ml, 50 ng/ml and 100 ng/ml) in the presence or absence of Aβ for 24 h. Cells were then fixed for immunocytochemical staining or subjected to survival assay by intact nuclei counting. Staining with β3-tubulin antibody for cortical neurons revealed that rrTIMP-1 at 100 ng/ml offered significant protection to cortical neurons against neuronal degeneration in terms of cell morphology (Fig. 5A). Our sholl analysis data is showing a quantitative restoration of neuronal process arborisation in Aβ treated neurons in presence of rrTIMP-1 protein (Fig. 5C). The results were consistent in differentiated PC12 cells (Supplementary Fig. 3A, B). Quantitative nuclei counting data showed that treatment with rrTIMP-1 at 100 ng/ml prevented the Aβ-induced death of the cortical neurons. No significant protection was observed at 25 ng/ml and 50 ng/ml doses of rrTIMP-1 (data not shown). Hence, all further experiments were conducted at 100 ng/ml dose of rrTIMP-1. Here, both control neurons and Aβ-treated neurons were treated with rrTIMP-1. Not only the control cells treated with rrTIMP-1 remained intact but also the rrTIMP-1 added Aβ-treated neurons were significantly protected against Aβ induced toxicity as observed at 24 h (Fig. 5B, $p < 0.05$). Similar significant protection from Aβ was found in PC-12 cells upon rrTIMP-1 treatment (Supplementary Fig. 3, $p < 0.05$).

3.6. TIMP-1 promotes survival of Aβ-treated neurons by activating the Akt signaling pathway

Next, we explored the possible mechanism and the signal transduction pathway involved in the protection of neurons by TIMP-1 from Aβ induced cytotixicity. In thyroid cancer, TIMP-1 is known to play an important role by binding to its receptor CD63 and activating the Akt signaling pathway which in turn is responsible for its anti-apoptotic

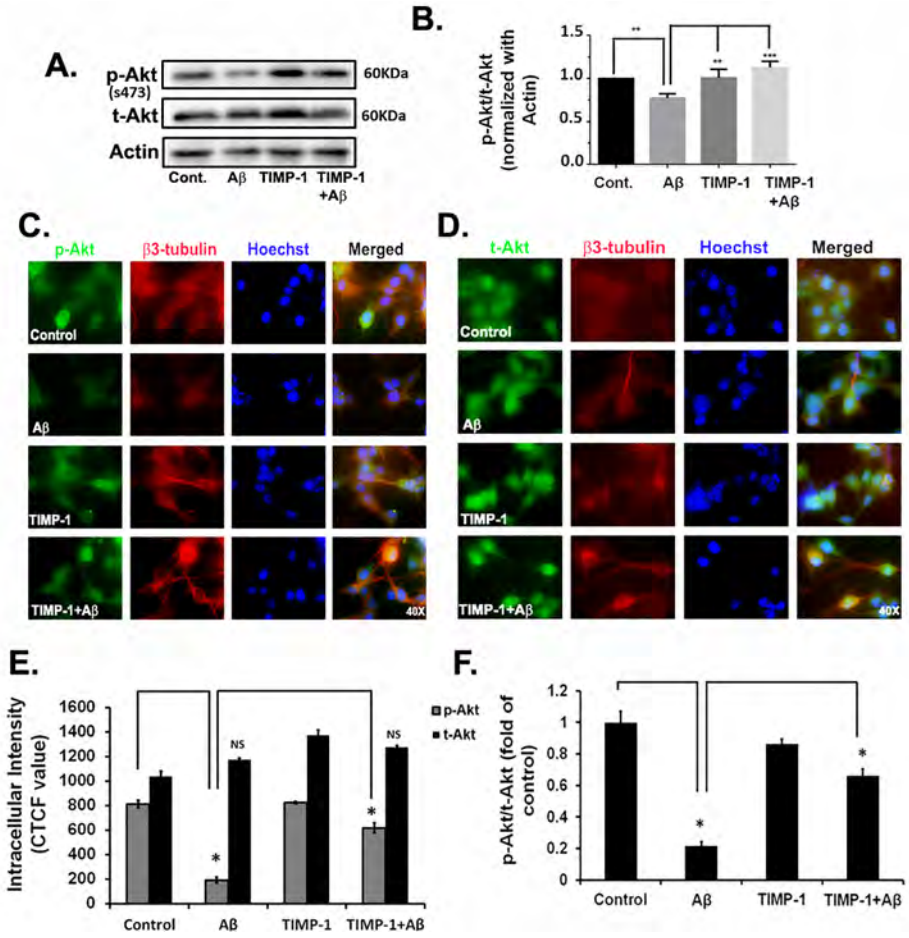

Fig. 6. TIMP-1 mediates neuroprotection by activating the Akt signalling pathway. In (A) and (B) primary cortical neurons were treated with Aβ, TIMP-1 and TIMP-1 + Aβ for 16 h. Control and the treated cells were harvested and the lysates were subjected to western blot analysis using p-Akt and t-Akt antibodies. Actin was used as a loading control (A). Bar diagram shows the ratio of p-Akt/t-Akt (normalized with Actin) derived from densitometric analysis of the blot using the Image J software. Values are expressed as Mean ± SEM from three independent experiments; **$p < 0.01$, ***$p < 0.001$ (B). (C) and (D) show immunostaining of PC-12 cells treated with Aβ, TIMP-1 and TIMP-1 + Aβ for 16 h with p-Akt and t-Akt antibodies respectively along with β3-tubulin antibody and nuclear staining with Hoechst reagent. Pictures were taken at 40× magnification. (E) and (F) represent the quantitative analysis of the intracellular intensities of p-Akt and t-Akt and their ratio respectively. Values are expressed as Mean ± SEM from three independent experiments.*$p < 0.05$.

activity (Bommarito et al., 2011). Other reports also indicate that Akt signalling pathway is affected in Aβ-mediated cellular toxicity in neuronal cells (Chen et al., 2009). In response to Aβ treatment Akt is inactivated due to dephosphorylation which in turn results in activation of Foxo3a due to its dephosphorylation at Akt sites and its translocation to nuclei to trigger the expression of apoptotic genes (Sanphui and Biswas, 2013; Saha and Biswas, 2015).

Consistent with the above reports, our western blot analysis indicated that Aβ-treatment of cortical neurons led to a significant reduction of phosphorylation of Akt (s473) compared to that of untreated controls (Fig. 6A, B $p < 0.01$). Interestingly, this reduced phosphorylation is markedly reversed by TIMP-1, as seen in the changes in normalized values of pAkt with tAkt from densitometric analysis of the blots (Fig. 6A and B, $p < 0.001$). Changes in the level of total Akt as well as Actin were insignificant across the treatment conditions. Similar results were obtained in western blot analysis in PC12 cells (Supplementary Fig. 4A). Consistent evidence was also obtained by simultaneous immunostaining of PC12 cells with pAkt, tAkt and β3-tubulin antibodies (Fig. 6C and D). We found that there is a significant decrease in p-Akt intensity which is expressed in CTCF value, in Aβ-treated PC-12 cells compared to control cells ($p < 0.05$). But upon introduction of rrTIMP-1 to Aβ-treated cells, we obtained a significant restoration of intracellular p-Akt intensity (Fig. 6E, $p < 0.05$). Furthermore, the ratio of intracellular intensity of p-Akt and t-Akt was found to be significantly restored by adding rrTIMP-1 to Aβ-treated cells (Fig. 6F, $p < 0.05$). The dependence of TIMP-1 mediated neuroprotection on the Akt signaling pathway was also observed by blocking Akt activation with Akt inhibitor II (Akt i), in the presence of which TIMP-1 was totally unable to protect neurons against Aβ-induced cell death (Supplementary Fig. 4B, $p < 0.05$).

3.7. TIMP-1 helps in Aβ clearance and blocks apoptosis through Akt/Bim/caspase axis in Aβ infused rat brain

To generate an *in vivo* model of AD, we infused Aβ stereotaxically in the rat brain as mentioned earlier and evaluated different inflammatory and gliosis markers (Supplementary Fig. 5A–I). The western blot data show that there is a significant increase in pro-IL-1β and NF-kβ, two potential inflammatory markers, in the Aβ infused hippocampal tissues (Supplementary Fig. 5A, B $p < 0.01$). Immunohistochemical studies also revealed that there is a significant increase in GFAP intensity and astrocyte perimeter in Aβ infused rat brain hippocampal and cortical regions near the site of infusion (HCSI) (Supplementary Fig. 5C–E). In addition, microglial activation was checked with CD11b and COX-2 staining which were found to be significantly upregulated in the HCSI of Aβ (Supplementary Fig. 5F–I).

Now, we were interested to check the underlying molecular mechanisms through which TIMP-1 renders neuroprotection *in vivo*. Twenty three days following Aβ infusion in rats, $Aβ_{1-42}$ plaques were abundantly detected by $Aβ_{1-42}$ antibody in the HCSI. In contrast, the vehicle controls presented no such labelling (Fig. 7Ai). HCSI of Aβ-infused rats injected with rrTIMP-1 showed marked reduction in plaque number ($p < 0.0001$) and plaque burden (%) ($p < 0.0001$) compared to Aβ rats (Fig. 7Ai, ii, iii). The diffusion of rrTIMP-1 was also confirmed by TIMP-1 antibody. rrTIMP-1 infused rats showed significant labelling for TIMP-1 protein throughout the brain whereas the control rats presented negligible TIMP-1 levels (Supplementary Fig. 6). This showed that intracerebroventricularly injected rrTIMP-1 got distributed in hippocampal and cortical regions under our experimental conditions. Thus, these results indicate that TIMP-1 might clear the $Aβ_{1-42}$ accumulation due to Aβ infusion in the HCSI of rat brains.

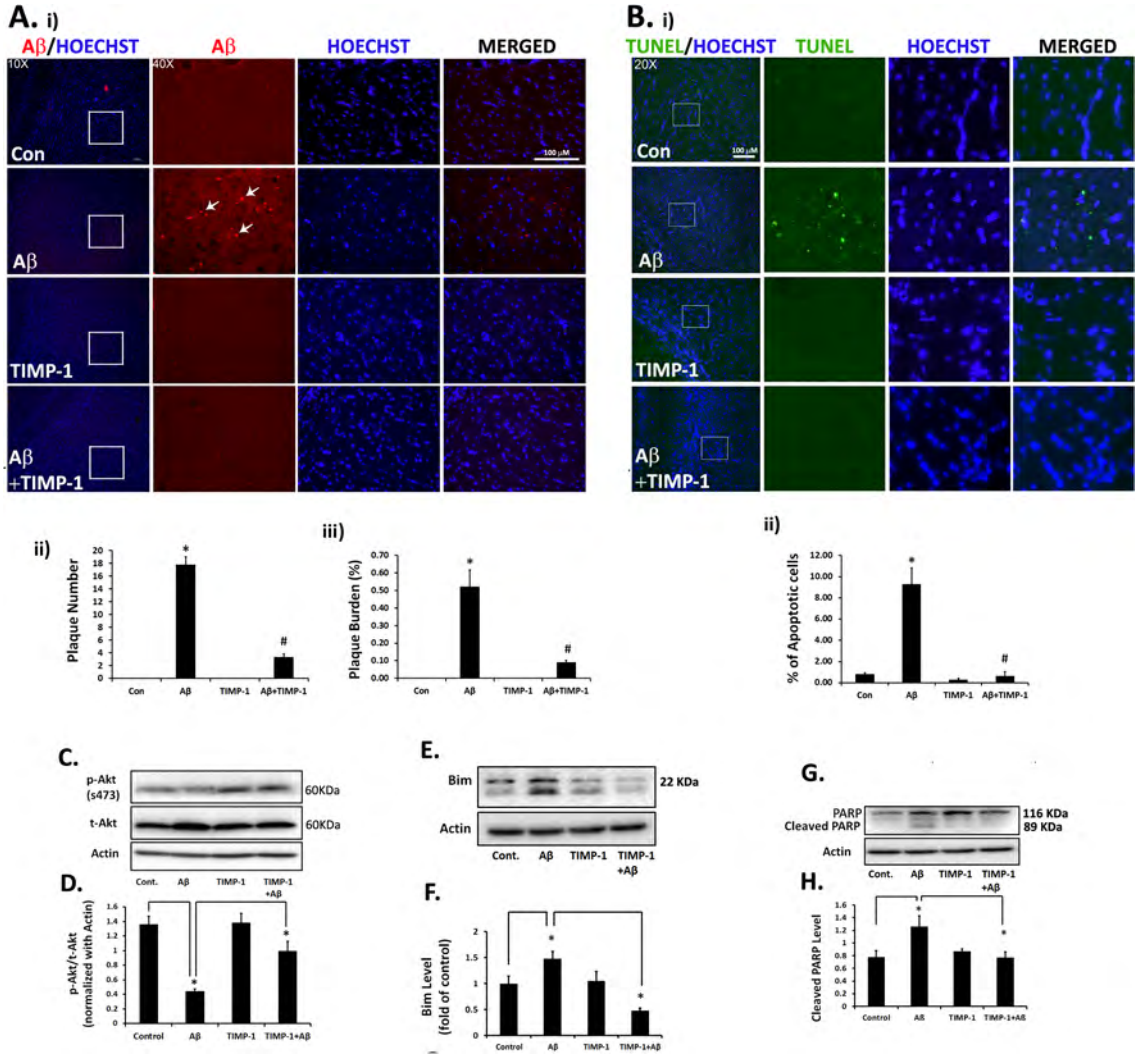

Fig. 7. TIMP-1 treatment induces Aβ clearance and protection against apoptosis in Aβ-infused rat brain. (A) Aβ plaques deposited extracellularly were detected by immunolabelling with $A\beta_{1-42}$ antibody in the hippocampal and cortical region near the site of infusion (HCSI) in brain of the different treatment groups, 23 days following Aβ infusion (i). The left vertical panel represents double-labelled images taken at 10× magnification for each experimental group (top to bottom) – Control, Aβ, TIMP-1 and Aβ + TIMP-1 (5 ng). Note the region marked for higher magnification view near the site of infusion (white boxes). The other 3 vertical panels (left to right) – $A\beta_{1-42}$ labelled (red), Hoechst stain (blue) and merged images were taken at 40× magnification (scale bar – 100 μm). Note the punctated $A\beta_{1-42}$ labelling in the HCSI of Aβ-infused brain (white arrows). Treatment with rrTIMP-1 significantly reduced the plaque number (ii) and plaque burden (%) (iii) compared to Aβ infusion alone (n = 3 for each group, 3 slices of each rat brain at 40×). *p < 0.0001, #p < 0.0001. (B) TUNEL assay stained the apoptotic cells green and were considered TUNEL positive while the total number of cells in the section was visualized by nuclear staining with Hoechst (blue). The left vertical panel represents 20× (scale bar – 100 μm) merged image from each group (top to bottom) – Control, Aβ, TIMP-1 and Aβ + TIMP-1 (5 ng). Note the region marked for zoomed viewing near the site of infusion (white boxes). The other 3 vertical panels show the enlarged images (left to right) – TUNEL staining, Hoechst staining and merged. Each row represents each experimental group. Aβ + TIMP-1 (5 ng) treated group showed a significant reduction in the % of apoptotic cells compared to Aβ alone group (n = 3 for each group, 3 slices of each rat brain, 500 cells/ slice at 20×); *p < 0.0001, #p < 0.0001. (*) indicates p-values in comparison to Control group and (#) indicates p-values in comparison to Aβ group. (C–H) Control, Aβ, TIMP-1 and TIMP-1 + Aβ brain tissues were subjected to western blot analysis with p-Akt, t-Akt, Bim and cleaved PARP antibodies. Actin was taken as loading control. Bar diagrams are representing corresponding densitometric analysis of the blots. Values are expressed as Mean ± SEM from three independent experiments; *p < 0.01. (For interpretation of the references to colour in this figure legend, the reader is referred to the web version of this article.)

Additionally, in tissue sections from Aβ-infused rats, the % of apoptotic or TUNEL–positive cells was significantly higher in the HCSI than the control sections. However, treatment with rrTIMP-1 markedly reduced the percentage of apoptotic cells (Fig. 7Bi, ii, p < 0.0001). Overall, the results indicate that Aβ induced an increase in apoptotic cells in the vicinity of infusion compared to control groups and TIMP-1 significantly prevented Aβ-induced apoptosis.

Our *in vitro* studies indicated that TIMP-1 could protect neurons through the Akt pathway upon Aβ exposure. This prompted us to check similar possibilities under *in vivo* conditions. For that, hippocampal tissues from control, Aβ, TIMP-1 and TIMP-1 + Aβ infused brains were subjected to western blot analysis with p-Akt (s473) and t-Akt. We found that TIMP-1 restored back the Akt activation state *in vivo* in Aβ-infused rats (Fig. 7C, D). Additionally, we also found that TIMP-1 injection significantly blocked the induction of Bim, a pro-apoptotic protein playing an essential role in neuronal death (Biswas et al., 2005),

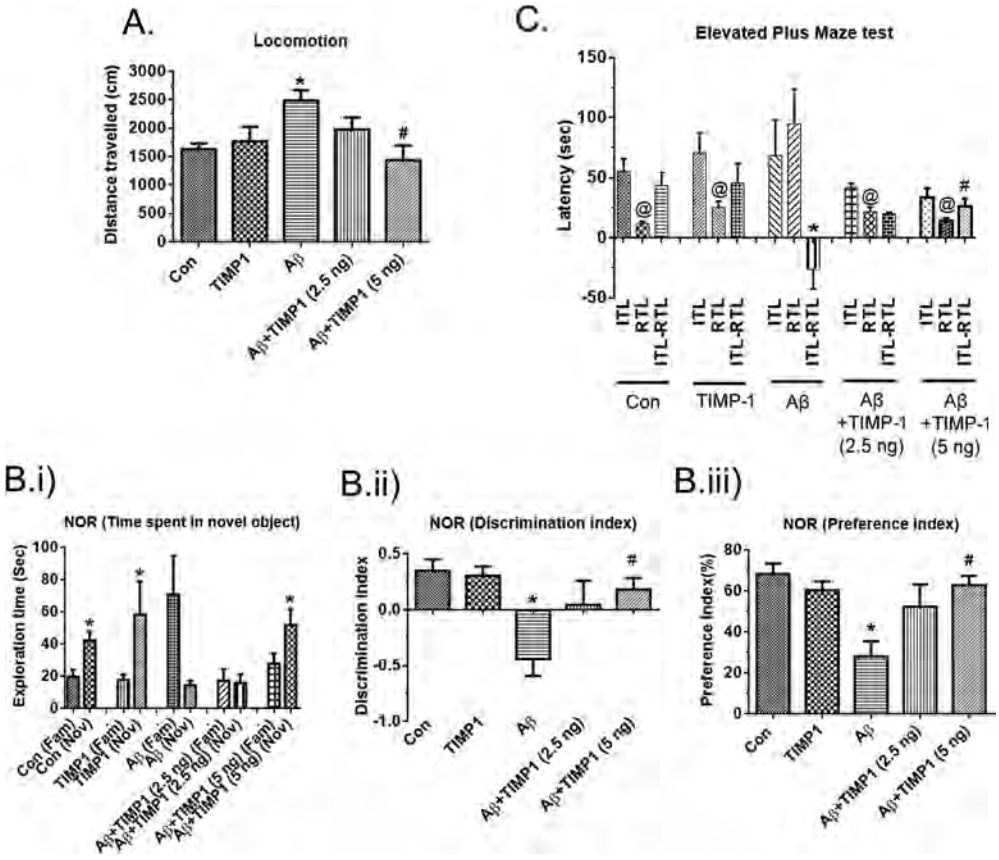

Fig. 8. Effect of TIMP-1 on cognitive abilities of Aβ-infused rats. (A) Locomotion test – Hyperlocomotion, measured as total distance travelled (cm), induced by Aβ (*$p < 0.01$) was significantly reduced by 5 ng of rrTIMP-1 (#$p < 0.01$). Control n = 9, TIMP-1 n = 4, Aβ n = 5, Aβ + TIMP-1 (2.5 ng) n = 3, Aβ + TIMP-1 (5 ng) n = 4. (B) Novel object recognition test - On day-2 (i) Compared to control and TIMP-1 only treated groups, exploration time of Aβ infused animals at the novel (Nov) object was reduced than the familiar (Fam) object while Aβ + TIMP-1 (5 ng) group spent significantly longer time with the novel object than familiar object (*$p < 0.05$). (ii) Aβ animals gave a negative discrimination index value (*$p < 0.05$) while for Aβ + TIMP-1 it was significantly positive (#$p < 0.05$) (iii) Preference index for the novel object was significantly lowered in the Aβ group (*$p < 0.05$) while it was significantly higher in the Aβ + TIMP-1 (5 ng) group than the Aβ group (#$p < 0.05$). Control n = 6, TIMP-1 n = 6, Aβ n = 8, Aβ + TIMP-1 (2.5 ng) n = 3, Aβ + TIMP-1 (5 ng) n = 6. (C) In Elevated plus maze test, retention transfer latency (RTL) on day-2 was significantly less than the initial transfer latency (ITL) on day-1 in all the experimental groups except Aβ animals (@ $p < 0.05$). The difference between ITL and RTL (ITL-RTL) was significantly negative for Aβ group (*$p < 0.05$) which was reversed to positive values by treatment with 5 ng TIMP-1 (#$p < 0.05$). Values are expressed as Mean ± SEM. (*) indicates p-values in comparison to Control group and (#) indicates p-values in comparison to Aβ group. Control n = 11, TIMP-1 n = 7, Aβ n = 9, Aβ + TIMP-1 (2.5 ng) n = 3, Aβ + TIMP-1 (5 ng) n = 7.

and PARP cleavage, a caspase 3 substrate, in Aβ infused rat hippocampal tissue (Fig. 7E-H).

3.8. TIMP-1 improves cognitive deficits in Aβ-infused rat by restoring synaptic integrity

Finally, we have examined several cognitive tasks performed by Aβ infused rats and effect of TIMP-1 thereon using a battery of behavioural experiments (see section 2 for details).

3.8.1. Locomotion test

Fig. 8A and supplementary Fig. 7 show that hyperlocomotion of Aβ infused rats was significantly reduced by treatment with 5 ng of rrTIMP-1 ($p < 0.01$) as evident from the distance travelled by the corresponding groups.

3.8.2. NOR test

Fig. 8Bi shows that Aβ infusion caused a significant reduction in novel object exploration time compared to familiar object with a negative DI (Fig. 8Bii, $p < 0.05$) and a reduced PI (Fig. 8Biii,$p < 0.05$) compared to the control group on the second day of test. Negative DI score for Aβ group indicated more time spent with the familiar object over the novel object, in contrast to the control group, while PI value below 50% indicated their preference towards familiar object as against the values in control (Antunes and Biala, 2012). rrTIMP-1 (5 ng) treated group showed a significant increase in exploration time (Fig. 8Bi, $p < 0.05$), positive DI score (Fig. 8Bii,$p < 0.05$) and above 50% PI value (Fig. 8Biii,$p < 0.05$), depicting that TIMP-1 improves recognition and learning memory.

3.8.3. EPM test

Fig. 8C shows that Aβ infusion in rats induced a significantly higher RTL (Day-2) than ITL (Day-1) which is in stark contrast to that seen in all other groups. The difference between ITL and RTL (ITL-RTL) was considered as the parameter to assess cognitive memory in EPM test. Notably, a negative difference was obtained in the Aβ infused animals indicating a loss of memory on day-two ($p < 0.05$). However, rrTIMP-1 (5 ng) treated Aβ rats gave positive ITL-RTL values significantly improving the score compared to Aβ group ($p < 0.05$) and thus overcoming the Aβ-induced cognitive loss.

3.8.4. Passive avoidance test

Fig. 9Ai shows no significant difference in performance between the treatment groups in the acquisition stage (Day-1). In the probe stage (Day-2), compared to the control group, Aβ-infused animals displayed a marked reduction the latency towards the dark chamber ($p < 0.0001$) (Fig. 9Aii). Both the rrTIMP-1-injected groups (2.5 ng and 5 ng), however, reversed the Aβ induced memory and learning impairments, evidenced by a significantly increased latency in the rrTIMP-1 (5 ng) group ($p < 0.001$).

3.8.5. Contextual and Cue-dependent fear conditioning tests

In contextual fear conditioning test, we measured the mean of the percent freezing in the four trials in the probe stage. Injection of Aβ hindered the acquisition of contextual fear conditioning estimated 24 h later in the probe stage as a significantly reduced percentage of freezing behaviour compared to control (Fig. 9Bi, $p < 0.005$). Upon rrTIMP-1 treatment, there was a dose-dependent reversal of the Aβ-induced reduction in percent freezing. rrTIMP-1 (5 ng) showed a significant increase in percent freezing compared to Aβ rats ($p < 0.005$).

In cue-dependent fear conditioning test, Aβ-infused animals showed

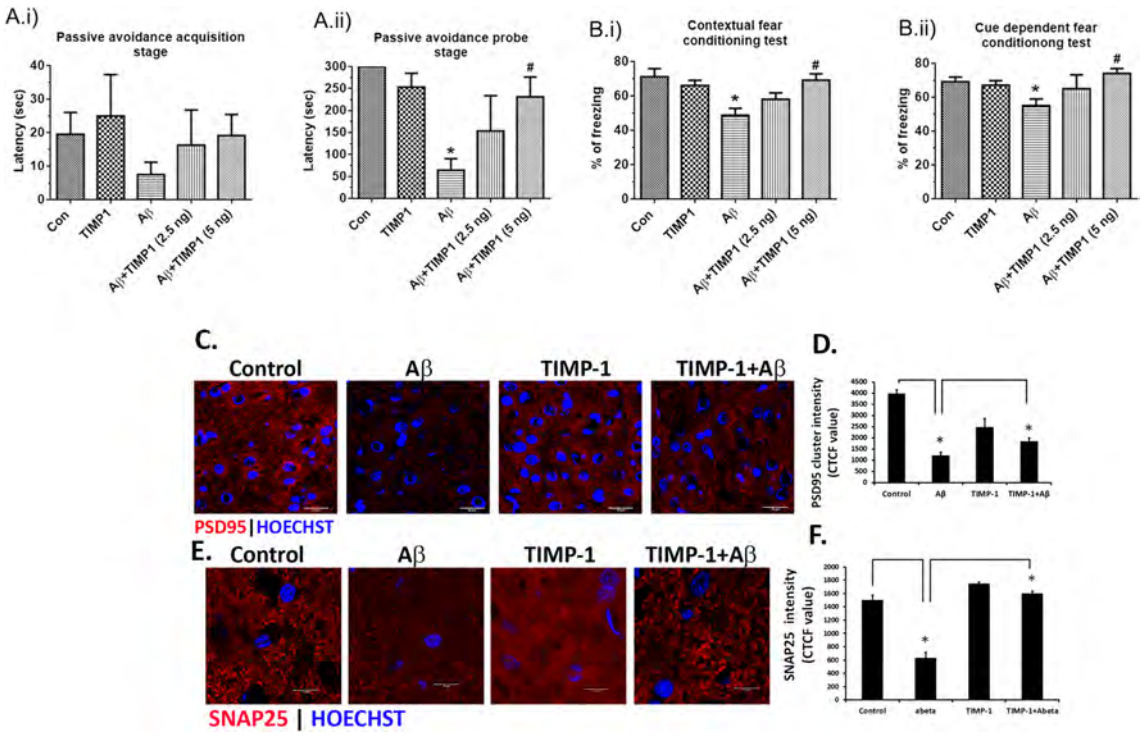

Fig. 9. TIMP-1 improves memory including associative learning in Aβ-infused rats by restoring synaptic integrity. (A) Passive avoidance test – (i) shows the latency of animals to the dark chamber on day-1 (acquisition stage) and (ii) shows that on day-2 probe stage, latency of animals to step into the dark chamber was markedly reduced in the Aβ group (*$p < 0.0001$) while it was significantly recovered in the Aβ + TIMP-1 (5 ng) group (#$p < 0.001$). Control n = 12, TIMP-1 n = 10, Aβ n = 6, Aβ + TIMP-1 (2.5 ng) n = 3, Aβ + TIMP-1 (5 ng) n = 7. Probe stages in B(i) Contextual fear conditioning test, the percent freezing was significantly attenuated in Aβ-infused rats (*$p < 0.005$) and this effect was reversed by TIMP-1 in a dose dependent manner that was statistically significant at 5 ng (#$p < 0.005$). Control n = 6, TIMP-1 n = 4, Aβ n = 7, Aβ + TIMP-1 (2.5 ng) n = 3, Aβ + TIMP-1 (5 ng) n = 6. B (ii) Cue-dependent fear conditioning test showed that TIMP-1 reversed the decreased percent freezing induced by Aβ in AD animals (*$p < 0.05$, #$p < 0.01$). Control n = 10, TIMP-1 n = 6, Aβ n = 7, Aβ + TIMP-1 (2.5 ng) n = 3, Aβ + TIMP-1 (5 ng) n = 7. Values are expressed as Mean ± SEM. (*) indicates p-values in comparison to Control group and (#) indicates p-values in comparison to Aβ group. (C-F) Immunohistochemical analysis was performed on control, Aβ, TIMP-1 and Aβ + TIMP-1 infused rat brain sections with PSD95 and SNAP25 antibodies. Images were taken at 40× magnification under confocal microscope (zoomed in images represented). Bar diagrams are representing the quantitative analysis of intensity of both the markers as CTCF values.

pronounced decrease in percent freezing in the probe stage ($p < 0.05$) (Fig. 9Bii). Administration of rrTIMP-1 alone did not have any significant effect on control rats; however, when injected in Aβ rats, the animals in probe stage exhibited a dose dependent improvement in percent freezing behaviours where the 5 ng dose was statistically significant ($p < 0.01$). Collectively, these results indicate that both context-dependent and cue-dependent hippocampal associated memory and learning were affected in Aβ-infused rat model and TIMP-1 helped in ameliorating these cognitive deficits.

Finally, we checked the levels of pre- and post-synaptic markers, SNAP25 and PSD95 respectively in control, Aβ, TIMP-1 and Aβ + TIMP-1 infused rat brain by immunohistochemistry (Fig. 9C-F). We found that, there was a significant decrease in both the synaptic markers in the HCSI of Aβ infused brain whereas infusion with TIMP-1 could significantly rescue the levels of both the synaptic markers implying that TIMP-1 could maintain the synaptic integrity in the Aβ-infused rat brains (Fig. 9D, F, $p < 0.01$).

4. Discussion

The different states of reactive astrocytes which determine their beneficial or detrimental roles in CNS are a major focus of research in neurodegenerative diseases. In this study, we investigated the beneficial roles of astrocyte-secreted protein, TIMP-1, in Aβ-treated primary cultures of neurons and Aβ-infused rats. A number of our experimental observations suggest that TIMP-1 is rapidly secreted from astrocytes in response to Aβ treatment and promotes neuronal survival by activation of Akt pathway, and improves cognitive functions such as learning and memory of Aβ-infused rats by reducing Aβ load and apoptosis, and maintaining synaptic integrity. First, we demonstrate that ACM from primary cultures of 6 h Aβ-treated astrocytes protected cortical neurons significantly from Aβ-induced death. Second, TIMP-1 secretion from astrocytes is greatly increased within 6 h of Aβ treatment. Third, TIMP-1 renders the neuroprotective efficacy of Aβ-treated ACM since neutralization of TIMP-1 with specific antibody diminishes the effect. Fourth, recombinant TIMP-1 protects neurons by blocking Aβ-induced inhibition of Akt and induction of Bim and caspases. Fifth, TIMP-1 injection in rat brain reduces Aβ-load and apoptosis in the vicinity of Aβ-infusion site. Finally a battery of behavioural studies indicates that TIMP-1 restores learning, memory and other cognitive deficits of rat those were impaired by Aβ-infusion. This observation was further supported by the fact that TIMP-1 restores the expression of pre- and post-synaptic proteins, markers of synaptic integrity, in Aβ-infused rat brain.

Although degeneration of Aβ-treated neurons is prompted by proinflammatory cytokines secreted by reactive astrocytes (Garwood et al., 2011; Li et al., 2011), several reports suggest a beneficial role of astrocyte activation in the early stage of the disease. WyssCorey et al. first showed that astrocytes were able to uptake and degrade Aβ in cultured mouse astrocytes (Wyss-Coray et al., 2003). Aβ containing astrocytes have been reported in human patient brain (Funato et al., 1998; Thal et al., 2000). Moreover, it has been shown that activated astrocytes are present even before the appearance of amyloid plaques (Wang et al., 2018) and that attenuating astrocyte activation accelerated amyloid pathology in AD mice (Kraft et al., 2013).These reports suggest that the activated astrocytes are protective by virtue of

their ability to facilitate Aβ-clearance and degradation but the molecular basis of this effect was unknown. One possibility is that TIMP-1 can promote Aβ clearance by astrocytes. There is a report that suggests TIMP-1 can induce astrocyte reactivity and that the reactivated astrocytes surrounding the Aβ deposition can increase the levels of astrocytic MMPs that degrade Aβ depositions and remove them from the brain (Hernandez-Guillamon et al., 2009). We report here that TIMP-1, secreted from astrocytes, plays an essential role in neuroprotection and in the clearance of Aβ-plaques from hippocampus and cortex of Aβ-infused rat brain.

TIMP-1 has been shown to have neuroprotective potential in several cases including HIV-1 infection (Ashutosh et al., 2012) and retinal neuron degeneration (Kim et al., 2018). Interestingly, in an AD model (5XFAD mice) TIMP-1 expression progressively increases between 4 and 6 months and then declines at 6 months when neurodegeneration starts, suggesting a neuroprotective role of TIMP-1 in the early phase of disease (Py et al., 2014). Our data corroborated with these findings, however, few other reports differ from the present findings. In another AD model (APP/PS1mice), MMP-2 and −9 has been reported to be involved in the digestion of Aβ-aggregates, these proteases are in turn inhibited by TIMP-1 (Yin et al., 2006). However, in our *in vitro* model we did not find any significant change in the secretion or at the intracellular level of MMP-2 among the four treatment groups (Control, Aβ, TIMP-1 and Aβ + TIMP-1) while MMP-9 was not detected at the secretion level and its intracellular level remained unchanged in all the four treatment conditions in neurons (data not shown). Moreover, it has been shown that TIMP-1 -/- condition can restore some of the seizure mediated neuron loss in hippocampus region, based on its MMP inhibitory roles. Paradoxically, these mice have also shown severe impairments in learning and memory functions (Jourquin et al., 2005) corroborating with our results.

Hence, the most important question is how TIMP-1 exerts its effect on neuroprotection. How does it interact with neurons? What signalling pathways are altered or modulated further in response to TIMP-1? How does it help in the recovery of memory and cognitive deficits? Most of these questions still remain unanswered. However, accumulating evidences imply TIMP-1 as a multifunctional protein which can act as a protease inhibitor and as a signaling molecule independently in several pathologic conditions (Stetler-Stevenson, 2008; Grunwald et al., 2019). In some instances, both of these functions of TIMP-1 are required such as in wound healing and fibrosis. However, in cancer the scenario is mostly inconclusive. Since TIMP-1 is a natural potent MMP inhibitor, a number of reports suggested its tumour suppressor activity, contrarily, through CD63/PI3K signalling it can also act as a cancer promoting agent (Stetler-Stevenson, 2008; Grunwald et al., 2019). Importantly, a number of recent clinical studies have associated it with an unfavourable prognosis in a series of cancers (Hawthorn et al., 2004; Wurtz et al., 2008; Wang et al., 2013; Song et al., 2016; Zurac et al., 2016). Intriguingly, these paradoxical reports can be traced from the fact that TIMP-1 has a large network of binding partners (Grunwald et al., 2019). During different biological contexts, these interaction partners compete for mutual interaction sites on TIMP-1 orchestrating its independent and opposing roles manifested through physiological or pathological effects. Hence, it is imperative to understand the fine tuning of its interactions with receptors. Besides CD63, one recent study has identified CD82 as another TIMP-1 receptor which helps its internalization in cancer cells (Zhang et al., 2017). It has also been shown that primary cortical neurons internalized TIMP-1 through a mechanism mediated by Low density receptor-related protein-1 (Thevenard et al., 2014). Overall, these intricate interactions of TIMP-1 with its different receptors affect its localization and mediate activation of several signalling pathways including MAPK, FAK and PI3K/Akt (Jung et al., 2006; Song et al., 2016). We and others have shown earlier that Akt pathway plays a central role in the survival of neurons in various AD models (Chen et al., 2009; Lee et al., 2009; Sanphui and Biswas, 2013). Collectively, these reports support our work where neuroprotection by TIMP-1 is mediated by upregulation of Akt phosphorylation, followed by inhibition of Bim and caspases in neurons. However, further investigations are required for the identification of specific TIMP-1 receptors and the signalling pathway that mediate its action on neurons.

TIMP-1 plays an important role in synaptic plasticity that underlies learning and memory (Kaczmarek, 2018). Magnowska et al., also reported that TIMP-1 critically regulates dendritic spine maturation and long term potentiation (Magnowska et al., 2016). These results are consistent with our present finding that intracerebroventricular infusion of TIMP-1 helps in recovery of a number of learning and memory related behaviours of Aβ-infused rats probably by maintaining active synapses as it restored pre- and post-synaptic proteins which were reduced in Aβ-infused brain. We further show that TIMP-1 has excellent potential in ameliorating AD pathology by reducing Aβ-depositions in Aβ-infused rat brain. Although further validation is required in other AD model, our study hugely contributes to the growing body of literature that focuses on the intriguing role of TIMP-1 in neurodegenerative diseases.

In conclusion, we identified TIMP-1 as a neuroprotective agent, secreted rapidly from astrocytes following Aβ-treatment. It confers neuroprotection by activating Akt signalling pathway and possibly clearing Aβ-plaques in Aβ-induced rat brain. Interestingly, recently two types of reactive astrocytes were identified in various neurological conditions namely the neurotoxic A1 astrocytes and the neurotrophic A2 astrocytes (Zamanian et al., 2012; Liddelow et al., 2017). It remains to be investigated whether it is an A2-specific phenomenon in AD or not. It is now well established that neuroinflammation in AD is associated with the release of a myriad of pro- and anti- inflammatory cytokines some of which are neuroprotective (Domingues et al., 2017) In this context, the present investigation revealing the neuroprotective properties of TIMP-1 suggest that it might be a potentially promising cytokine in treating AD and other neurodegenerative diseases.

Declaration of Competing Interest

The authors declare that they have no known competing financial interests or personal relationships that could have appeared to influence the work reported in this paper.

Acknowledgements

We, the authors, would like to thank Dr. P. K. Sarkar for critical reading of this manuscript and helpful discussions. We would also like to thank Dr. Rebecca Banerjee for her help in immunohistochemical studies and Mr. Diptesh Roy for his assistance during the revision work. We would also like to extend our gratitude towards Mr. Sounak Bhattacharya for his technical assistance in confocal microscopy.The work was supported in part by one of the 12th Five Year Plan Projects, miND (BSC0115) of CSIR, Govt. of India and by the Department of Biotechnology, Govt. of India, Project BT/PR14383/MED/12/475/2010.

Appendix A. Supplementary data

Supplementary data to this article can be found online at https://doi.org/10.1016/j.bbi.2020.03.014.

References

Anderson, M.A., Ao, Y., Sofroniew, M.V., 2014. Heterogeneity of reactive astrocytes. Neurosci. Lett. 565, 23–29.

Antunes, M., Biala, G., 2012. The novel object recognition memory: neurobiology, test procedure, and its modifications. Cogn. Process. 13, 93–110.

Ashutosh, Chao C, Borgmann, K., Brew, K., Ghorpade, A., 2012. Tissue inhibitor of metalloproteinases-1 protects human neurons from staurosporine and HIV-1-induced apoptosis: mechanisms and relevance to HIV-1-associated dementia. Cell Death Dis. 3, e332.

Belanger, M., Magistretti, P.J., 2009. The role of astroglia in neuroprotection. Dialogues Clin. Neurosci. 11, 281–295.
Belzung, C., Griebel, G., 2001. Measuring normal and pathological anxiety-like behaviour in mice: a review. Behav. Brain Res. 125, 141–149.
Biswas, S.C., Liu, D.X., Greene, L.A., 2005. Bim is a direct target of a neuronal E2F-dependent apoptotic pathway. J. Neurosci. 25, 8349–8358.
Biswas, S.C., Shi, Y., Sproul, A., Greene, L.A., 2007. Pro-apoptotic Bim induction in response to nerve growth factor deprivation requires simultaneous activation of three different death signaling pathways. J. Biol. Chem. 282, 29368–29374.
Bommarito, A., Richiusa, P., Carissimi, E., Pizzolanti, G., Rodolico, V., Zito, G., Criscimanna, A., Di Blasi, F., Pitrone, M., Zerilli, M., Amato, M.C., Spinelli, G., Carina, V., Modica, G., Latteri, M.A., Galluzzo, A., Giordano, C., 2011. BRAFV600E mutation, TIMP-1 upregulation, and NF-kappaB activation: closing the loop on the papillary thyroid cancer trilogy. Endocr. Relat. Cancer 18, 669–685.
Bryan, K.J., Lee, H., Perry, G., Smith, M.A., Casadesus, G., 2009. Transgenic mouse models of Alzheimer's disease. Behav. Test. Considerations.
Bubser, M., Bridges, T.M., Dencker, D., Gould, R.W., Grannan, M., Noetzel, M.J., Lamsal, A., Niswender, C.M., Daniels, J.S., Poslusney, M.S., Melancon, B.J., Tarr, J.C., Byers, F.W., Wess, J., Duggan, M.E., Dunlop, J., Wood, M.W., Brandon, N.J., Wood, M.R., Lindsley, C.W., Conn, P.J., Jones, C.K., 2014. Selective activation of M4 muscarinic acetylcholine receptors reverses MK-801-induced behavioral impairments and enhances associative learning in rodents. ACS Chem. Neurosci. 5, 920–942.
Bugno, M., Witek, B., Bereta, J., Bereta, M., Edwards, D.R., Kordula, T., 1999. Reprogramming of TIMP-1 and TIMP-3 expression profiles in brain microvascular endothelial cells and astrocytes in response to proinflammatory cytokines. FEBS Lett. 448, 9–14.
Chen, T.J., Wang, D.C., Chen, S.S., 2009. Amyloid-beta interrupts the PI3K-Akt-mTOR signaling pathway that could be involved in brain-derived neurotrophic factor-induced arc expression in rat cortical neurons. J. Neurosci. Res. 87, 2297–2307.
Clarke, L.E., Liddelow, S.A., Chakraborty, C., Munch, A.E., Heiman, M., Barres, B.A., 2018. Normal aging induces A1-like astrocyte reactivity. Proc. Natl. Acad. Sci. U.S.A. 115, E1896–E1905.
Cregg, J.M., DePaul, M.A., Filous, A.R., Lang, B.T., Tran, A., Silver, J., 2014. Functional regeneration beyond the glial scar. Exp. Neurol. 253, 197–207.
Crusio, W.E., 2001. Genetic dissection of mouse exploratory behaviour. Behav. Brain Res. 125, 127–132.
Cuesto, G., Enriquez-Barreto, L., Carames, C., Cantarero, M., Gasull, X., Sandi, C., Ferrus, A., Acebes, A., Morales, M., 2011. Phosphoinositide-3-kinase activation controls synaptogenesis and spinogenesis in hippocampal neurons. J. Neurosci. 31, 2721–2733.
De Strooper, B., Karran, E., 2016. The cellular phase of Alzheimer's disease. Cell 164, 603–615.
Domingues, C., da Cruz, E.S.O.A.B., Henriques, A.G., 2017. Impact of cytokines and chemokines on Alzheimer's disease neuropathological hallmarks. Curr. Alzheimer Res. 14, 870–882.
Ennaceur, A., 2010. One-trial object recognition in rats and mice: methodological and theoretical issues. Behav. Brain Res. 215, 244–254.
Fanselow, M.S., 1980. Conditioned and unconditional components of post-shock freezing. Pavlov. J. Biol. Sci. 15, 177–182.
Fanselow, M.S., Tighe, T.J., 1988. Contextual conditioning with massed versus distributed unconditional stimuli in the absence of explicit conditional stimuli. J. Exp. Psychol. Anim. Behav. Process. 14, 187–199.
Funato, H., Yoshimura, M., Yamazaki, T., Saido, T.C., Ito, Y., Yokofujita, J., Okeda, R., Ihara, Y., 1998. Astrocytes containing amyloid beta-protein (Abeta)-positive granules are associated with Abeta40-positive diffuse plaques in the aged human brain. Am. J. Pathol. 152, 983–992.
Gadea, A., Schinelli, S., Gallo, V., 2008. Endothelin-1 regulates astrocyte proliferation and reactive gliosis via a JNK/c-Jun signaling pathway. J. Neurosci. 28, 2394–2408.
Gardner, J., Ghorpade, A., 2003. Tissue inhibitor of metalloproteinase (TIMP)-1: the TIMPed balance of matrix metalloproteinases in the central nervous system. J. Neurosci. Res. 74, 801–806.
Garwood, C.J., Pooler, A.M., Atherton, J., Hanger, D.P., Noble, W., 2011. Astrocytes are important mediators of Abeta-induced neurotoxicity and tau phosphorylation in primary culture. Cell Death Dis. 2, e167.
Greene, L.A., Tischler, A.S., 1976. Establishment of a noradrenergic clonal line of rat adrenal pheochromocytoma cells which respond to nerve growth factor. Proc. Natl. Acad. Sci. U.S.A. 73, 2424–2428.
Grunwald, B., Schoeps, B., Kruger, A., 2019. Recognizing the molecular multifunctionality and interactome of TIMP-1. Trends Cell Biol. 29, 6–19.
Haidet-Phillips, A.M., Hester, M.E., Miranda, C.J., Meyer, K., Braun, L., Frakes, A., Song, S., Likhite, S., Murtha, M.J., Foust, K.D., Rao, M., Eagle, A., Kammesheidt, A., Christensen, A., Mendell, J.R., Burghes, A.H., Kaspar, B.K., 2011. Astrocytes from familial and sporadic ALS patients are toxic to motor neurons. Nat. Biotechnol. 29, 824–828.
Hamann, S., Monarch, E.S., Goldstein, F.C., 2002. Impaired fear conditioning in Alzheimer's disease. Neuropsychologia 40, 1187–1195.
Hawthorn, L., Stein, L., Varma, R., Wiseman, S., Loree, T., Tan, D., 2004. TIMP1 and SERPIN-A overexpression and TFF3 and CRABP1 underexpression as biomarkers for papillary thyroid carcinoma. Head Neck 26, 1069–1083.
Hernandez-Guillamon, M., Delgado, P., Ortega, L., Pares, M., Rosell, A., Garcia-Bonilla, L., Fernandez-Cadenas, I., Borrell-Pages, M., Boada, M., Montaner, J., 2009. Neuronal TIMP-1 release accompanies astrocytic MMP-9 secretion and enhances astrocyte proliferation induced by beta-amyloid 25–35 fragment. J. Neurosci. Res. 87, 2115–2125.
Inspector, M., Aharon-Perez, J., Glass-Marmor, L., Miller, A., 2005. Matrix metalloproteinase-9, its tissue inhibitor (TIMP)-1 and CRP in Alzheimer's disease. Eur. Neurol. 53, 155–157.
Janus, C., Pearson, J., McLaurin, J., Mathews, P.M., Jiang, Y., Schmidt, S.D., Chishti, M.A., Horne, P., Heslin, D., French, J., Mount, H.T., Nixon, R.A., Mercken, M., Bergeron, C., Fraser, P.E., St George-Hyslop, P., Westaway, D., 2000. A beta peptide immunization reduces behavioural impairment and plaques in a model of Alzheimer's disease. Nature 408, 979–982.
Jaworski, D.M., 2000. Differential regulation of tissue inhibitor of metalloproteinase mRNA expression in response to intracranial injury. Glia 30, 199–208.
Jourquin, J., Tremblay, E., Bernard, A., Charton, G., Chaillan, F.A., Marchetti, E., Roman, F.S., Soloway, P.D., Dive, V., Yiotakis, A., Khrestchatisky, M., Rivera, S., 2005. Tissue inhibitor of metalloproteinases-1 (TIMP-1) modulates neuronal death, axonal plasticity, and learning and memory. Eur. J. Neurosci. 22, 2569–2578.
Jung, K.K., Liu, X.W., Chirco, R., Fridman, R., Kim, H.R., 2006. Identification of CD63 as a tissue inhibitor of metalloproteinase-1 interacting cell surface protein. EMBO J. 25, 3934–3942.
Kaczmarek, L., 2018. From c-Fos to MMP-9: in control of synaptic plasticity to produce healthy and diseased mind, a personal view. Postepy Biochem. 64, 101–109.
Khuth, S.T., Akaoka, H., Pagenstecher, A., Verlaeten, O., Belin, M.F., Giraudon, P., Bernard, A., 2001. Morbillivirus infection of the mouse central nervous system induces region-specific upregulation of MMPs and TIMPs correlated to inflammatory cytokine expression. J. Virol. 75, 8268–8282.
Kim, H.S., Vargas, A., Eom, Y.S., Li, J., Yamamoto, K.L., Craft, C.M., Lee, E.J., 2018. Tissue inhibitor of metalloproteinases 1 enhances rod survival in the rd1 mouse retina. PLoS One 13, e0197322.
Kraft, A.W., Hu, X., Yoon, H., Yan, P., Xiao, Q., Wang, Y., Gil, S.C., Brown, J., Wilhelmsson, U., Restivo, J.L., Cirrito, J.R., Holtzman, D.M., Kim, J., Pekny, M., Lee, J.M., 2013. Attenuating astrocyte activation accelerates plaque pathogenesis in APP/PS1 mice. FASEB J. 27, 187–198.
Lawlor, P.A., Bland, R.J., Das, P., Price, R.W., Holloway, V., Smithson, L., Dicker, B.L., During, M.J., Young, D., Golde, T.E., 2007. Novel rat Alzheimer's disease models based on AAV-mediated gene transfer to selectively increase hippocampal Abeta levels. Mol. Neurodegener. 2, 11.
Lee, H.K., Kumar, P., Fu, Q., Rosen, K.M., Querfurth, H.W., 2009. The insulin/Akt signaling pathway is targeted by intracellular beta-amyloid. Mol. Biol. Cell 20, 1533–1544.
Li, C., Zhao, R., Gao, K., Wei, Z., Yin, M.Y., Lau, L.T., Chui, D., Yu, A.C., 2011. Astrocytes: implications for neuroinflammatory pathogenesis of Alzheimer's disease. Curr. Alzheimer Res. 8, 67–80.
Liddelow, S.A., Guttenplan, K.A., Clarke, L.E., Bennett, F.C., Bohlen, C.J., Schirmer, L., Bennett, M.L., Munch, A.E., Chung, W.S., Peterson, T.C., Wilton, D.K., Frouin, A., Napier, B.A., Panicker, N., Kumar, M., Buckwalter, M.S., Rowitch, D.H., Dawson, V.L., Dawson, T.M., Stevens, B., Barres, B.A., 2017. Neurotoxic reactive astrocytes are induced by activated microglia. Nature 541, 481–487.
Magnowska, M., Gorkiewicz, T., Suska, A., Wawrzyniak, M., Rutkowska-Wlodarczyk, I., Kaczmarek, L., Wlodarczyk, J., 2016. Transient ECM protease activity promotes synaptic plasticity. Sci. Rep. 6, 27757.
McGaugh, J.L., 1966. Time-dependent processes in memory storage. Science 153, 1351–1358.
Nagai, M., Re, D.B., Nagata, T., Chalazonitis, A., Jessell, T.M., Wichterle, H., Przedborski, S., 2007. Astrocytes expressing ALS-linked mutated SOD1 release factors selectively toxic to motor neurons. Nat. Neurosci. 10, 615–622.
Olabarria, M., Noristani, H.N., Verkhratsky, A., Rodriguez, J.J., 2010. Concomitant astroglial atrophy and astrogliosis in a triple transgenic animal model of Alzheimer's disease. Glia 58, 831–838.
Pagenstecher, A., Stalder, A.K., Kincaid, C.L., Shapiro, S.D., Campbell, I.L., 1998. Differential expression of matrix metalloproteinase and tissue inhibitor of matrix metalloproteinase genes in the mouse central nervous system in normal and inflammatory states. Am. J. Pathol. 152, 729–741.
Paidi, R.K., Nthenge-Ngumbau, D.N., Singh, R., Kankanala, T., Mehta, H., Mohanakumar, K.P., 2015. Mitochondrial deficits accompany cognitive decline following single bilateral intracerebroventricular streptozotocin. Curr. Alzheimer Res. 12, 785–795.
Park, D.S., Morris, E.J., Padmanabhan, J., Shelanski, M.L., Geller, H.M., Greene, L.A., 1998. Cyclin-dependent kinases participate in death of neurons evoked by DNA-damaging agents. J. Cell Biol. 143, 457–467.
Py, N.A., Bonnet, A.E., Bernard, A., Marchalant, Y., Charrat, E., Checler, F., Khrestchatisky, M., Baranger, K., Rivera, S., 2014. Differential spatio-temporal regulation of MMPs in the 5xFAD mouse model of Alzheimer's disease: evidence for a pro-amyloidogenic role of MT1-MMP. Front. Aging Neurosci. 6, 247.
Rivera, S., Tremblay, E., Timsit, S., Canals, O., Ben-Ari, Y., Khrestchatisky, M., 1997. Tissue inhibitor of metalloproteinases-1 (TIMP-1) is differentially induced in neurons and astrocytes after seizures: evidence for developmental, immediate early gene, and lesion response. J. Neurosci. 17, 4223–4235.
Rukenstein, A., Rydel, R.E., Greene, L.A., 1991. Multiple agents rescue PC12 cells from serum-free cell death by translation- and transcription-independent mechanisms. J. Neurosci. 11, 2552–2563.
Saha, P., Biswas, S.C., 2015. Amyloid-beta induced astrocytosis and astrocyte death: Implication of FoxO3a-Bim-caspase3 death signaling. Mol. Cell. Neurosci. 68, 203–211.
Sanphui, P., Biswas, S.C., 2013. FoxO3a is activated and executes neuron death via Bim in response to beta-amyloid. Cell Death Dis. 4, e625.
Sanphui, P., Pramanik, S.K., Chatterjee, N., Moorthi, P., Banerji, B., Biswas, S.C., 2013. Efficacy of cyclin dependent kinase 4 inhibitors as potent neuroprotective agents against insults relevant to Alzheimer's disease. PLoS One 8, e78842.
Senechal, Y., Kelly, P.H., Dev, K.K., 2008. Amyloid precursor protein knockout mice show age-dependent deficits in passive avoidance learning. Behav. Brain Res. 186, 126–132.
Sholl, D.A., 1953. Dendritic organization in the neurons of the visual and motor cortices

of the cat. J. Anat. 87, 387–406.
Sofroniew, M.V., 2014. Astrogliosis. Cold Spring Harb. Perspect. Biol. 7, a020420.
Song, G., Xu, S., Zhang, H., Wang, Y., Xiao, C., Jiang, T., Wu, L., Zhang, T., Sun, X., Zhong, L., Zhou, C., Wang, Z., Peng, Z., Chen, J., Wang, X., 2016. TIMP1 is a prognostic marker for the progression and metastasis of colon cancer through FAK-PI3K/AKT and MAPK pathway. J. Exp. Clin. Cancer Res. 35, 148.
Stetler-Stevenson, W.G., 2008. Tissue inhibitors of metalloproteinases in cell signaling: metalloproteinase-independent biological activities. Sci. Signal. 1, re6.
Suryadevara, R., Holter, S., Borgmann, K., Persidsky, R., Labenz-Zink, C., Persidsky, Y., Gendelman, H.E., Wu, L., Ghorpade, A., 2003. Regulation of tissue inhibitor of metalloproteinase-1 by astrocytes: links to HIV-1 dementia. Glia 44, 47–56.
Szymocha, R., Akaoka, H., Brisson, C., Beurton-Marduel, P., Chalon, A., Bernard, A., Didier-Bazes, M., Belin, M.F., Giraudon, P., 2000. Astrocytic alterations induced by HTLV type 1-infected T lymphocytes: a role for Tax-1 and tumor necrosis factor alpha. AIDS Res. Hum. Retroviruses 16, 1723–1729.
Teo, L., Bourne, J.A., 2018. Current opinion on a role of the astrocytes in neuroprotection. Neural Regen. Res. 13, 797–798.
Thal, D.R., Schultz, C., Dehghani, F., Yamaguchi, H., Braak, H., Braak, E., 2000. Amyloid beta-protein (Abeta)-containing astrocytes are located preferentially near N-terminal-truncated Abeta deposits in the human entorhinal cortex. Acta Neuropathol. 100, 608–617.
Thevenard, J., Verzeaux, L., Devy, J., Etique, N., Jeanne, A., Schneider, C., Hachet, C., Ferracci, G., David, M., Martiny, L., Charpentier, E., Khrestchatisky, M., Rivera, S., Dedieu, S., Emonard, H., 2014. Low-density lipoprotein receptor-related protein-1 mediates endocytic clearance of tissue inhibitor of metalloproteinases-1 and promotes its cytokine-like activities. PLoS One 9, e103839.
Troy, C.M., Friedman, J.E., Friedman, W.J., 2002. Mechanisms of p75-mediated death of hippocampal neurons. Role of caspases. J. Biol. Chem. 277, 34295–34302.
Troy, C.M., Rabacchi, S.A., Friedman, W.J., Frappier, T.F., Brown, K., Shelanski, M.L., 2000. Caspase-2 mediates neuronal cell death induced by beta-amyloid. J. Neurosci. 20, 1386–1392.
Wang, D., Zhang, X., Wang, M., Zhou, D., Pan, H., Shu, Q., Sun, B., 2018. Early activation of astrocytes does not affect amyloid plaque load in an animal model of Alzheimer's disease. Neurosci. Bull. 34, 912–920.
Wang, X.X., Tan, M.S., Yu, J.T., Tan, L., 2014. Matrix metalloproteinases and their multiple roles in Alzheimer's disease. Biomed Res. Int. 2014, 908636.
Wang, Y.Y., Li, L., Zhao, Z.S., Wang, H.J., 2013. Clinical utility of measuring expression levels of KAP1, TIMP1 and STC2 in peripheral blood of patients with gastric cancer. World J. Surg. Oncol. 11, 81.
Wurtz, S.O., Schrohl, A.S., Mouridsen, H., Brunner, N., 2008. TIMP-1 as a tumor marker in breast cancer–an update. Acta Oncol. 47, 580–590.
Wyss-Coray, T., Loike, J.D., Brionne, T.C., Lu, E., Anankov, R., Yan, F., Silverstein, S.C., Husemann, J., 2003. Adult mouse astrocytes degrade amyloid-beta in vitro and in situ. Nat. Med. 9, 453–457.
Yin, K.J., Cirrito, J.R., Yan, P., Hu, X., Xiao, Q., Pan, X., Bateman, R., Song, H., Hsu, F.F., Turk, J., Xu, J., Hsu, C.Y., Mills, J.C., Holtzman, D.M., Lee, J.M., 2006. Matrix metalloproteinases expressed by astrocytes mediate extracellular amyloid-beta peptide catabolism. J. Neurosci. 26, 10939–10948.
Zamanian, J.L., Xu, L., Foo, L.C., Nouri, N., Zhou, L., Giffard, R.G., Barres, B.A., 2012. Genomic analysis of reactive astrogliosis. J. Neurosci. 32, 6391–6410.
Zhang, J., Wu, T., Zhan, S., Qiao, N., Zhang, X., Zhu, Y., Yang, N., Sun, Y., Zhang, X.A., Bleich, D., Han, X., 2017. TIMP-1 and CD82, a promising combined evaluation marker for PDAC. Oncotarget 8, 6496–6512.
Zurac, S., Neagu, M., Constantin, C., Cioplea, M., Nedelcu, R., Bastian, A., Popp, C., Nichita, L., Andrei, R., Tebeica, T., Tanase, C., Chitu, V., Caruntu, C., Ghita, M., Popescu, C., Boda, D., Mastalier, B., Maru, N., Daha, C., Andreescu, B., Marinescu, I., Rebosapca, A., Staniceanu, F., Negroiu, G., Ion, D.A., Nikitovic, D., Tzanakakis, G.N., Spandidos, D.A., Tsatsakis, A.M., 2016. Variations in the expression of TIMP1, TIMP2 and TIMP3 in cutaneous melanoma with regression and their possible function as prognostic predictors. Oncol. Lett. 11, 3354–3360.

Neurochemistry International 145 (2021) 104956

Contents lists available at ScienceDirect

Neurochemistry International

journal homepage: www.elsevier.com/locate/neuint

Mini review

Astrocyte subtype-specific approach to Alzheimer's disease treatment

Sukanya Sarkar, Subhas C. Biswas *

Cell Biology and Physiology Division, CSIR-Indian Institute of Chemical Biology, 4 Raja S. C. Mullick Road, Kolkata, 700 032, India

ARTICLE INFO

Keywords:
Reactive astrocyte
Astrocyte reactivity
Cytokine
Alzheimer's disease
Central nervous system
Astrocyte subtype

ABSTRACT

Astrocytes respond to any pathological condition in the central nervous system (CNS) including Alzheimer's disease (AD), and this response is called astrocyte reactivity. Astrocyte reaction to a CNS insult is a highly heterogeneous phenomenon in which the astrocytes undergo a set of morphological, molecular and functional changes with a characteristic secretome profile. Such astrocytes are termed as 'reactive astrocytes'. Controversies regarding the reactive astrocytes abound. Recently, a continuum of reactive astrocyte profiles with distinct transcriptional states has been identified. Among them, disease-associated astrocytes (DAA) were uniquely present in AD mice and expressed a signature set of genes implicated in complement cascade, endocytosis and aging. Earlier, two stimulus-specific reactive astrocyte subtypes with their unique transcriptomic signatures were identified using mouse models of neuroinflammation and ischemia and termed as A1 astrocytes (detrimental) and A2 astrocytes (beneficial) respectively. Interestingly, although most of the A1 signature genes were also detected in DAA, as opposed to A2 astrocyte signatures, some of the A1 specific genes were expressed in other astrocyte subtypes, indicating that these nomenclature-based signatures are not very specific. In this review, we elaborate the disparate functions and cytokine profiles of reactive astrocyte subtypes in AD and tried to distinguish them by designating neurotoxic astrocytes as A1-like and neuroprotective ones as A2-like without directly referring to the A1/A2 original nomenclature. We have also focused on the dual nature from a functional perspective of some cytokines depending on AD-stage, highlighting a number of them as major candidates in AD therapy. Therefore, we suggest that promoting subtype-specific beneficial roles, inhibiting subtype-specific detrimental roles or targeting subtype-specific cytokines constitute a novel therapeutic approach to AD treatment.

Introduction

Alzheimer's disease (AD) is the most prevalent neurodegenerative disease with no cure to date. The major obstacle in therapy development is the incomplete understanding of disease evolution, especially in the context of cell-cell interactions. Existing literature mainly delves into neuronal damage downstream of toxic insults to understand AD pathogenesis. This neuron-centric view of AD pathogenesis has failed to translate into effective therapeutic strategies. This failure mirrors the lack of appreciation of pathological alterations in glial cells as an integral part of the central nervous system (CNS) and in intercellular interactions in disease pathogenesis. Astrocytes are the major players in maintaining brain homeostasis by supplying energy to neurons, maintaining ionic balance, recycling excess glutamate to avoid glutamate excitotoxicity and supplying antioxidants such as glutathione and ascorbic acid. In the last decade they have emerged as the primary cells playing a crucial role in regulating neuronal excitation-inhibition balance, in synaptic functioning, in learning and memory development and in maintaining blood brain barrier integrity in the CNS (Giaume et al., 2007; Burda and Sofroniew, 2014; Pekny et al., 2016; Verkhratsky et al., 2017; Arranz and De Strooper, 2019; Valori et al., 2019). In addition to these homeostatic functions in a healthy CNS, astrocytes undergo a process called astrocyte reaction in response to CNS insult (Escartin et al., 2019). The association of reactive astrocytes with pathological hallmarks and its functional consequences in AD are reported elsewhere (Gonzalez-Reyes et al., 2017; Perez-Nievas and Serrano-Pozo, 2018). Recently, distinct subtypes of reactive astrocytes with either defensive or detrimental properties with characteristic cytokine profiles have been identified. Cytokines, a heterogenous group of small proteins, are the major cellular mediators that are rapidly altered in response to any CNS insult and are attractive candidates for investigating different stages in AD with translational possibilities. Importantly, recent literatures suggest that astrocytes may be intentionally targeted for more effective therapeutic outcomes (Assefa et al., 2018; Sadick and Liddelow, 2019). Thus, this review attempts to unravel

* Corresponding author. ,
E-mail addresses: biswassc@gmail.com, subhasbiswas@iicb.res.in (S.C. Biswas).

https://doi.org/10.1016/j.neuint.2021.104956
Received 23 June 2020; Received in revised form 1 January 2021; Accepted 5 January 2021
Available online 24 January 2021

Abbreviations

TNFα	Tumor necrosis factor α
LRP1	lipoprotein receptor-related protein 1
DAA	disease-associated astrocytes
SRB1	scavenger receptor class B member 1
NEP	neprilysin
RAGE	Receptor for Advanced Glycation End Products
NF-κβ	nuclear factor κβ
IL	interleukin
IFNγ	interferon-γ
S100β	S100 calcium-binding protein β
TIMP-1	tissue inhibitor of matrix metalloproteinase 1
sICAM-1	soluble intercellular adhesion molecule 1
CXCL	C-X-C motif chemokine ligand
LPS	lipopolysaccharide
MCAO	Milddle Cerebral Artery Occlusion
H2-D1	histocompatibility 2, D region locus 1
SSP1	Sporulation-specific protein 1
s100a10	S100 calcium-binding protein a10
LIF	leukemia inhibitory factor
TGFβ	transforming growth factor β
CINC	cytokine-induced neutrophil chemoattractant
MIP-1α	Macrophage inflammatory protein-1 α
VEGF	Vascular endothelial growth factor
CJD	Creutzdfeldt-Jakob disease
NSAIDs	nonsteroidal anti-inflammatory drugs
MCP-1	monocyte chemoattractant protein-1
G-CSF	granulocyte colony stimulating factor

the different reactive states of astrocytes, especially focusing on their secreted cytokine composition and related functions with major implications in the development of novel reactive astrocyte subtype-specific therapeutic strategies for AD.

Pathophysiology of AD

AD is characterized by the presence of extracellular senile plaques consisting mainly of amyloid-β (Aβ) protein, intraneuronal neurofibrillary tangles (NFT) due to hyperphophorylation of tau, excessive neuroinflammation, and extensive synapse and neuronal loss in the brain (De Strooper and Karran, 2016). Normally, amyloid precursor protein (APP), a transmembrane protein highly expressed in the CNS, is cleaved sequentially either by α- and γ-secretases or by β- and γ-secretases, and produces different fragments of Aβ. However, in certain conditions, APP is cleaved mainly by β- and γ-secretases, and produces predominantly $Aβ_{1-42}$ (Kim and Tsai, 2009). Mutations in APP or in subunits of γ-secretase, presinilin 1/presinilin 2 result in more production of $Aβ_{1-42}$ and lead to early onset of the disease in cases of familial AD (FAD). However, most of the cases are sporadic AD (SAD) and etiologies remain elusive (Ribe et al., 2008).

Recent literatures suggest that NFT is directly linked to neurodegeneration and clinical symptoms of AD. Interestingly, it has been shown that Aβ deposition is required for the progression of tau pathology as well as neurodegeneration in AD (Wang et al., 2016). NFT is made up of paired helical filaments of aberrantly hyperphosphorylated forms of microtubule-associated protein tau. The primary function of tau protein, which is particularly abundant in neuronal axons, is to stabilize microtubules. However when it is aberrantly hyperphosphorylated, its binding affinity for microtubules is reduced, resulting in an abnormal increase in the levels of the unbound tau fractions that in turn lead to the aggregation of tau.

Pathophysiology of AD was first explained by Hardy and Higgins in 1992 in their "amyloid cascade hypothesis". They proposed that the faulty processing, accumulation and clearance of $Aβ_{1-42}$ is central to AD (Hardy and Higgins, 1992). However, this hypothesis is controversial as there is no direct link between amount of Aβ deposition and degree of cognitive decline in cases of SAD (Nelson et al., 2012). Thus, the "amyloid cascade hypothesis" has been revised over time and recently, Bart De Strooper and Eric Karran (De Strooper and Karran, 2016) proposed that AD pathogenesis involves a complex long cellular phase consisting of feedback and feedforward responses of astrocytes, microglia and vasculature. They considered Aβ and tau accumulations as risk factors in SAD and their accumulation as a sign of increased proteopathic stress. Defective clearance of Aβ and tau, the dysfunction of the neurovascular unit, aberrant neuronal network activity, impaired astrocyte and microglia homeostatic functions and possible gain-of toxic functions underlie the cellular phase. Astrocytes play a central role in the cellular phase to maintain homeostasis, and disease progresses inexorably when this homeostasis mechanism fails (De Strooper and Karran, 2016).

Although astrocyte reaction is not exclusive to AD pathology, it has been shown that reactive astrocytes (explained in detail later) occur both around dense-core Aβ plaques and in the proximity of NFTs and it increases linearly through the entire course of the disease (Serrano-Pozo et al., 2011). In fact, Aβ plaques are characterized by the presence of reactive astrocytes that penetrates the Aβ deposits with their processes and isolate the plaques from surrounding healthy neurons (Sofroniew, 2014). In addition, tau can even accumulate in astrocytes and thorn-shaped astrocytes featuring perinuclear tau deposits are relatively more common in AD. Furthermore, tau pathology influences astrocyte functions leading to an array of deleterious consequences both within the astrocytes themselves as well as on neuronal health (Kahlson and Colodner, 2015).

Stages in AD and astrocytic response

Recently National Institute on Aging and Alzheimer's association (NIA-AA) created a 'research framework" and defined AD as a biological construct in living people. It is based on biomarkers that detect specific pathological AD hallmarks: Aβ (A), phospho/pathologic tau (T) and neurodegeneration (N), regarded as the AT(N) classification (Jack et al., 2018) and is not focused on clinical outcomes. Biomarkers of neurodegeneration are labeled as "(N)" since they include atrophy on magnetic resonance imaging (MRI), 18-fluorodeoxyglucose positron emission tomography ([^{18}F]-FDG PET) hypometabolism and CSF total tau which are not specific for AD. Previously, NIA-AA created diagnostic guidelines for three stages of AD: pre-clinical, mild cognitive impairment (MCI) and dementia (Albert et al., 2011; Jack et al., 2011; McKhann et al., 2011; Sperling et al., 2011). However, since cognitive decline associated with AD occurs continuously over a long time (more than 20 years), the disease is more suitably regarded as a continuum than three distinct clinical entities (Dubois et al., 2016). Thus, recently NIA-AA took an initiative and updated the stages of AD based on biomarkers with the goal to create a common language for researchers to accurately understand the sequence of pathologic processes that leads to the cognitive symptoms associated with AD. However, this staging is for research purpose and its use is not recommended for clinical practice. Notably, although this AT(N) classification system focuses on neuron-centric aspects, for the first time it has been mentioned that astrocytes are emerging as potential biomarker targets (Jack et al., 2018).

The framework defined that a person diagnosed positive for a biomarker detecting Aβ deposition alone (low CSF $Aβ_{42}$ or $Aβ_{42}/Aβ_{40}$ ratio or abnormal Aβ by PET scan) and negative for a pathologic tau

biomarker (A + T-) among the three biomarker groups [AT(N)] would be categorized as "Alzheimer's pathologic change". An individual would only be assigned the label "Alzheimer's disease" if evidence for the biomarkers Aβ and pathologic tau, both, was present (A + T+). Alzheimer's pathologic change and AD are the initial and the later phases in the "Alzheimer's continuum" (see glossary) and is presented as a part of "Biomarker profiles and categories" by Jack et al., independent of the clinical symptoms (Jack et al., 2018). Aβ biomarker is the determining factor to include an individual in the Alzheimer's continuum while a biomarker for pathologic tau will dictate the labeling of an individual in the Alzheimer's continuum as having AD. Thus, it can be stated that presence of Aβ alone is essential but not sufficient for defining AD.

Stages in AD were also defined by NIA-AA based on disease severity guided by (1) biomarker profiles and (2) cognitive impairment independent of each other (Jack et al., 2018). Staging severity based on biomarkers can be accomplished by a combination of information from each member of the AT(N) biomarker system, more the number of abnormal biomarker groups among the three, more the advancement in severity/pathologic stage. Since cognitive performance is also present on a continuum, two cognitive schemes were outlined to define the stages in cognitive impairment independent of the biomarker profiles: syndromal categorical cognitive staging and numeric clinical staging. In the syndromal categorical cognitive staging, the cognitive continuum is divided into three traditional groups – cognitively unimpaired (CU), MCI and dementia sub-divided further into mild, moderate and severe dementia. A CU individual has a cognitive performance within the expected range calculated for that person, according to all the available details, based on cognitive test performance and/or clinical judgment. A person in the MCI stage shows a cognitive performance below his/her expected range. The person continues to perform day-to-day activities independently but cognitive deficits may result in mild yet detectable functional impact in performing more complex daily life activities. In the dementia stage, an individual displays significant cognitive impairment and/or neuro-behavioural symptoms having a consequential impact on daily life. The person is no longer completely independent and requires assistance in performing daily activities. This feature differentiates a person with dementia from MCI.

Numeric clinical staging scheme does not use the traditional categories and includes participants only from the Alzheimer's continuum. This staging scheme clearly defines the sequence of events that lead to the evolution of AD from an initial state marked by the appearance of pathologic biomarkers of AD in an asymptomatic individual. In this scheme, the cognitive continuum is divided into 6 stages - Stage-1 to 6 (Jack et al., 2018). Stage 1 includes cognitively unimpaired individuals with biomarker evidence as in the AD continuum. Stage 2 describes the earliest clinical outcomes of the Alzheimer's continuum, not necessarily presented as cognitive difficulties, and shares similarities with 'Preclinical AD' in the NIA-AA guideline, 2011 (Sperling et al., 2011). Preclinical AD has been earlier described by Dubious (2016) as a stage in AD marked by the complete absence of any clinical signs and/or symptoms but with the presence of both Aβ and tau biomarkers beyond their pathologic thresholds (Dubois et al., 2016). This stage has gained immense importance for studies targeted at the prevention of disease progression to its clinical state and also for investigations into novel biomarkers that will help verify therapies aimed at early disease intervention. Stage 3 describes cognitive decline short of dementia and is same as the MCI stage in syndromal categorical cognitive staging. Stages 4–6 define progressively worse functional impact on day-to-day life and are identical to the mild, moderate and severe dementia stages of the syndromal cognitive staging scheme. According to the 2018 research framework, a person can be completely staged based on severity by a combination of biomarker profile and cognitive/clinical stage described in either of the two schemes (Jack et al., 2018).

The last three numeric clinical stages may be collectively referred as 'advanced or late-AD stage'. Although Aβ deposition reaches a plateau at the onset of clinical dementia, cognitive impairments correlate with tau accumulation which starts spreading from the medial temporal lobe into the neocortex during the clinical phases [reviewed in (Long and Holtzman, 2019)].

As already mentioned, pre-clinical stages and MCI may extend up to two decades before the clinical symptoms and are largely considered as an 'early phase in AD'. Astrocytes are activated in this stage of AD (Schipper et al., 2006; Owen et al., 2009) and astrocyte reaction to AD may be considered as a prodromal AD phenomenon (Carter et al., 2012). Astrocytes may alter their phenotype through this early phase of AD depending upon disease progression which in turn can be related to aging since AD is generally considered as a disease of aging (Swerdlow, 2007a,b). There is probably an apparent overlapping and dynamic continuum between aging and AD. Hence, in order to present a clear view of astrocyte response through disease staging, we will try to explain astrocyte reactivity as a function of Aβ accumulation, the essential pathologic hallmark, which is easier to be detected, analysed and interpreted in AD patients. In SAD, it is often considered that an imbalance between Aβ production and removal due to impaired Aβ clearance with advent of aging may contribute to the high levels of extracellular Aβ deposition that trigger Aβ plaque pathogenesis (Lomakin et al., 1997; Xiao et al., 2014). Reactive astrocytes play a significant role in Aβ uptake and clearance in the early phase of AD (Basak et al., 2012). Astrocytes, at first, may attempt in this early phase to counteract the Aβ accumulation since ablation of glial fibrillary acidic protein (GFAP) and vimentin result in an enhanced plaque load (Kraft et al., 2013). However, the major concern is Aβ degradation following its uptake by astrocytes and that efficiency will ultimately determine whether Aβ will be cleared or astrocytes will themselves becomes a propagator of AD since death of these Aβ-loaded astrocytes creates secondary plaques (Garwood et al., 2017). Thus when and how the astrocyte efficiency change or their phenotype transitions from a friend to a foe is a major question that we attempt to answer.

Following Aβ phagocytosis various changes may occur within the astrocytes. Aβ may be trafficked for lysosomal degradation (Basak et al., 2012). However, with aging-associated AD progression through the early phase over years, lysosomal functioning may be impaired progressively resulting in increased accumulation of Aβ within astrocytes and further release extracellularly, contributing to plaque progression (Xiao et al., 2014). The initial Aβ accumulation can itself induce the expression of BACE-1, APP, γ-secretase and β-secretase processing within the astrocytes leading to an enhanced oligomeric Aβ production thus altering the astrocyte reaction or astrocytic phenotype itself (Grolla et al., 2013a, 2013b; Garwood et al., 2017). For example, BACE-1 which is primarily expressed within neurons is also found to show expression in activated astrocytes around Aβ plaques in advanced transgenic models of AD and in AD patients (Hartlage-Rubsamen et al., 2003; Rossner et al., 2005; Jin et al., 2012). This may occur over time through progression from early to late-stage of AD. Aβ can influence astrocyte signaling to secrete several cytokines that can trigger amyloidogenic processing of APP in astrocytes (Garwood et al., 2017). Tumor necrosis factor α (TNFα) is one such cytokine whose paracrine secretion is often linked with enhanced BACE-1 activity and further Aβ production. Additionally, the amyloidogenic as well as non-amyloidogenic processing of APP give rise to the APP intracellular domain (AICD) which is reportedly a negative regulator of low density lipoprotein receptor-related protein 1 (LRP1) expression. Since AICD shows an enhanced expression in reactive astrocytes near Aβ plaques, it can be involved in the prevention of astrocytic LRP1-directed Aβ uptake (Osborn et al., 2016).

Thus, the duration of presence and the amount of Aβ may themselves act as triggers and signal the astrocyte to modify themselves slowly from a phenotype that is capable of uptaking and degrading Aβ (protective) to a phenotype that may uptake Aβ but not degrade it effectively (detrimental). Obviously, 'age' has an important role to play here in correlation to AD stages (Garwood et al., 2017). Astrocytes from older AD mice phagocytosed 20% and 35% less amounts of Aβ in comparison to younger AD mice *in vitro* and *in vivo,* respectively (Iram et al., 2016).

This report strongly emphasizes that aging and AD progression go hand-in-hand through the early phase that alters the astrocyte phenotype as a function of Aβ accumulation which progressively causes synaptic dysfunction, neuron loss and clinically diagnosable cognitive symptoms. They further showed that astrocytes from older AD mice have a reduced scavenger receptor class B member 1 (SRB1) expression in comparison to younger ones, and thus may be the reason behind reduced Aβ uptake. In agreement, others also reported downregulations of astrocyte secreted Aβ-degrading enzymes. For example, neprilysin (NEP) expression was reduced in aged Tg2576 mice (Carter et al., 2019). There is also a notable metabolic alteration in astrocytes that can upregulate the expression of Receptor for Advanced Glycation End Products (RAGE) and downregulate LRP1 receptor increasing RAGE-mediated Aβ uptake, triggering the nuclear factor κβ (NF-κβ) pathway and the subsequent pro-inflammatory cytokine secretion and reduced Aβ phagocytosis. It is worth mentioning here that the relative expression levels of RAGE and LRP1 receptors play a critical role in AD progression (Zulfiqar et al., 2019).

REACTIVE ASTROCYTES – neurotoxic or neuroprotective?

In a fascinating review article by Escartin et al. (2019), the authors present an agglomeration of consensus and controversies across the world in the field of reactive astrocytes starting with the nomenclature itself. They summarize the disparate views to provide the readers with a broad definition of reactive astrocytes. They have defined 'reactive astrocytes' which we attempt to describe as follows – (i) Astrocytes can sense and in turn respond to an abnormal circumstance in the brain. (ii) They show changes at the transcriptional, morphological, biochemical and functional levels in response to such circumstances. (iii) The alterations persist while the pathological insult is present, but some of the changes may resolve. (iv) Reactive astrocytes are a heterogenous population and may have disparate effects on disease progression. In this review, we use the most consensual nomenclature of the astrocyte community that is 'reactive astrocytes' or 'astrocyte reaction' to discuss and explain our views (Escartin et al., 2019). Conventionally, astrocyte reaction is considered a commonality of neuroinflammatory processes involved in all kinds of neurological disorders including AD. Pro-inflammatory cytokines such as interleukin 1 (IL-1), IL-6, TNFα, interferon-γ (IFNγ) etc. are heavily secreted from reactive astrocytes surrounding Aβ plaques in rodent models and human patients of AD (Li et al., 2011). The majority of the reports depicting both transcriptomic (Orre et al., 2014; Garwood et al., 2017) and proteomic alterations in reactive astrocytes are evidently inclined towards neurotoxicity leading to neuronal death in AD (Garwood et al., 2011; Furman et al., 2012; Iram et al., 2016). Calcineurin/NFAT (Norris et al., 2005; Wu et al., 2010; Furman et al., 2012) and NF-κβ pathways are the major inflammatory pathways regulating the pro-inflammatory responses of reactive astrocytes accentuating their detrimental cytokine production (Bales et al., 1998). Interference with the Calcineurin/NFAT pathway in APP/PS1 mice (refer Supplementary Table 1) suppressed astrocyte reaction by reducing reactive astrocytes and Aβ deposition and improved cognitive functions (Furman et al., 2012). Strengthening this evidence, reports also suggest that the Calcineurin/NFAT pathway is involved in triggering dendritic spine loss thus propagating the pathophysiology in AD (Norris et al., 2005; Wu et al., 2010). The NF-κβ pathway, on the other hand, is instigated by Aβ in primary astrocyte cultures and can further enhance the expression of several pro-inflammatory cytokines such as IL-6, IL-1 etc (Bales et al., 1998). This pro-inflammatory signaling can remain activated for a prolonged period of time by reactive astrocyte-secreted S100 calcium-binding protein β (S100β) acting in an autocrine manner (Lam et al., 2001). Furthermore, complement protein C3 is also induced downstream of the NF-κβ pathway and has been highly implicated in the pro-inflammatory phenotype of reactive astrocytes (Liddelow et al., 2017; Perez-Nievas and Serrano-Pozo, 2018). Additionally, detrimental cytokine IL-1β also secreted downstream of this pathway acts on the reactive astrocytes themselves, triggering Aβ production and upregulating pro-inflammatory cytokine secretion (Gonzalez-Reyes et al., 2017). Pro-inflammatory cytokines thus secreted elevate astrocytic production and release of Aβ (Blasko et al., 2000), influence neighboring microglia to reduce phagocytosis (Koenigsknecht-Talboo and Landreth, 2005), dictate synapse loss (Norris et al., 2005; Wu et al., 2010) and eventual neurodegeneration. Contrary to popular belief, emerging evidence increasingly contradicts such a linear presentation of a rather complex multi-faceted phenomenon comprising both neuroprotective as well as neurotoxic aspects.

Findings that reactive astrocyte detection occurs even before the appearance of Aβ plaques (Wang et al., 2018) and that astrocyte reaction inhibition propagates plaque pathology in AD mice (Kraft et al., 2013) allude towards a neuroprotective role of astrocytes. Wyss-Coray (2003) first indicated that reactive astrocytes may trigger Aβ clearance through its degradation following uptake (Wyss-Coray et al., 2003), although evidence of Aβ-loaded astrocytes were already present in the literature (Funato et al., 1998; Thal et al., 2000) especially in those near Aβ plaques (Yamaguchi et al., 1998; Kurt et al., 1999). Phagocytosis and the secretion of Aβ-degrading enzymes may be regarded as the major mechanisms of astrocyte-mediated Aβ clearance (Perez-Nievas and Serrano-Pozo, 2018). Several receptors such as LRP-1 (Kim et al., 2009; Basak et al., 2012; Garwood et al., 2017), low density lipoprotein receptor (Katsouri and Georgopoulos, 2011; Basak et al., 2012) and SRB1 (Wyss-Coray et al., 2003; Mulder et al., 2012) show enhanced expression on reactive astrocytes and can mediate Aβ uptake. The phagocytosed Aβ is degraded within the astrocytes via lysosomal degradation especially at the early stages in AD (Xiao et al., 2014). Furthermore, Aβ-degrading enzymes such as insulin degrading enzyme, NEP, endothelin-converting enzyme-2 and matrix metalloproteinases are also highly expressed by reactive astrocytes as revealed from AD postmortem studies and in rodent models of AD (Carter et al., 2019). α1-21 antichymotrypsin, α2-macroglobulin and apolipoprotein J secreted from astrocytes also help in Aβ degradation (Ries and Sastre, 2016; Carter et al., 2019). Indeed, transplantation of astrocytes in plaque-bearing mouse models of AD fortified the role of astrocyte-mediated Aβ degradation (Koistinaho et al., 2004; Pihlaja et al., 2008; Nielsen et al., 2009, 2010). Additionally, reactive astrocyte-secreted anti-inflammatory cytokines such as tissue inhibitor of matrix metalloproteinase 1 (TIMP-1), soluble intercellular adhesion molecule 1 (sICAM-1) and transforming growth factor beta (TGFβ) also influence plaque clearance in a rat model of AD (Chen et al., 2015; Saha et al., 2020). The Sofroniew group emphasized the role of astrocytic scarring in separating Aβ plaques from the surrounding healthy neurons (Sofroniew, 2009) and also in preventing CNS-entry of inflammatory cells, further restricting cytotoxic brain inflammation in neurological diseases (Sofroniew, 2015). Studies in transgenic loss-of-function models revealed the ability of reactive astrocytes in blood brain barrier (BBB) repair following traumatic injury, especially depended on their ability to proliferate and form glial scars (Bush et al., 1999; Faulkner et al., 2004; Sofroniew, 2015). The JAK-STAT pathway may be the most prominent pathway regulating the anti-inflammatory functions of reactive astrocytes during CNS insults among others (Okada et al., 2006; Herrmann et al., 2008; Wanner et al., 2013). Astrocyte-secreted anti-inflammatory cytokines and growth factors including IL-6, IL-11, IL-19, IL-27 and sonic hedgehog induce several positive intracellular signaling pathways besides maintaining BBB integrity and/or leading to astrocytic-scar formation (Meeuwsen et al., 2003; John et al., 2005; Hamby et al., 2012; Zamanian et al., 2012; Jensen et al., 2013; Cooley et al., 2014; Pitter et al., 2014). C-X-C motif chemokine ligand 8 (CXCL8), one of the very first chemokines found in the brain, can exert both protective and detrimental effects in the CNS (Mamik and Ghorpade, 2016). Contrarily, substantial evidence also suggests that CXCL8 is elevated in the CSF of AD patients, detected at higher levels in serum associated with cognitive deficits and shows a positive association with Aβ levels (Correa et al., 2011; Mamik and Ghorpade, 2016). Similarly, some of the anti-inflammatory cytokines

namely IL-6 and IL-11 (Sofroniew, 2015) may also be involved in inducing pro-inflammatory responses depending on the intracellular pathway they activate. Coherently, pro-inflammatory cytokine TNF-α can induce pro-inflammatory regulator NF-κβ or can conversely upregulate astrocytic A20 production, an ubiquitin-modifying protein that inhibits NF-κβ signaling (Catrysse et al., 2014), eventually suppressing autoimmune inflammation and leukocyte-recruiting chemokine production from astrocytes (Wang et al., 2013). Pro-inflammatory cytokines TNF-α, IFNγ and IL-1β can also induce astrocytic galectin-9 expression that inhibits autoimmune inflammation (Steelman et al., 2013). Thus, these types of evidence raise a critical point for speculation about intracellular temporal regulation in production of astrocytic cytokines mediating disparate effects along the inflammatory scale in neurodegenerative diseases including AD. Furthermore, whether pro- and anti-inflammatory cytokines or pro- and anti-inflammatory behaviours of the same cytokine are dependent on the nature of the reactive state of astrocytes is a subject for vigorous investigation. The dichotomy of a particular cytokine may also depend on the neurodegenerative disease model and additionally on the nature of events that have induced the degenerative process. Recently, the Barres's group identified distinct reactive astrocyte subtypes with their unique transcriptomic signatures and cytokine profiles in two different injury models as described below, and thus can provide a major clue in identifying astrocyte-subtype-specific cytokine profiles (Liddelow and Barres, 2017; Liddelow et al., 2017).

ASTROCYTE SUBTYPES – heterogeneity in relation to function

Escartin et al. (2019) nicely illustrated the heterogeneity of astrocyte reaction in relation to different disease stages or age, species and gender, or on the basis of morphological, signaling, molecular, and functional changes (Escartin et al., 2019). Describing different subtypes in various diseases or on the basis of origin, lineage etc. is out of the scope of this review. Here, we describe AD related heterogeneity of reactive astrocytes and the major subtypes that are functionally different, in particular, either beneficial or detrimental.

The heterogeneity of reactive astrocytes in AD is mainly evident based on brain regions, site of Aβ plaques, signaling and functions. Hoke et al. (1994) have reported that astrocytes are regionally heterogeneous in their response to Aβ. They found marked astrocyte reaction in response to Aβ only in cortical and hippocampal astrocytes (Hoke et al., 1994). Accumulating evidence also suggests that reactive astrocytes are mainly observed in the micro-environment of Aβ plaques (Nagy et al., 1996; Burbach et al., 2004; Olabarria et al., 2010; Delekate et al., 2014). Interestingly, Olabarria et al. (2010) have observed astroglial hypertrophy surrounding plaques and astroglial atrophy away from plaques as a generalized process (Olabarria et al., 2010). Moreover, astroglial hyperactivity is mediated by purinergic signaling in reactive astrocytes surrounding plaques (Delekate et al., 2014).

With the advent of transcriptomic profiling tools, Zamanian et al. (2012) described two molecular classes of reactive astrocytes. Striking evidences showed that two injury models in mice – neuroinflammation (induced by lipopolysaccharide (LPS)) and ischemic stroke (induced by Milddle Cerebral Artery Occlusion (MCAO)) were associated with very distinct reactive astrocyte subtypes exhibiting disparate molecular phenotypes. While the ischemia-associated reactive astrocyte population essentially demonstrated a protective or beneficial phenotype, the LPS model showed a detrimental effect (Zamanian et al., 2012). The two subtypes were eventually termed as A1 (detrimental) and A2 (beneficial) in analogy with the two polarized phenotypes demonstrated by microglia – M1 and M2 (Martinez and Gordon, 2014; Heppner et al., 2015; Liddelow et al., 2017). A1s activated the pro-inflammatory NF-κβ pathway leading to the upregulated expression of complement proteins including C1r, C1s, C3 and C4 in which C3 is increasingly being recognized as a defining marker of the A1 phenotype. The other marker genes that can define the A1 subtype are histocompatibility 2, D region locus 1 (H2-D1) and Serping1. Genes such as CXCL1, CXCL2 and Sporulation-specific protein 1 (SSP1) encoding pro-inflammatory cytokines are induced in astrocytes following LPS treatment and are commonly involved in the recruitment of immune cells in the CNS (Zamanian et al., 2012; Liddelow et al., 2017). The A1 phenotype itself is triggered by three essential cytokines or complement proteins released by activated microglia – TNF-α, IL-1α and C1q (Liddelow et al., 2017). A1s showed diminished ability to phagocytose neuronal or synaptic debris and to promote neuronal growth and support. C3-expressing astrocytes were extensively identified in the pre-frontal cortex of human AD brains (Liddelow et al., 2017). Furthermore, C3 thus secreted can bind to C3aR receptors on neurons, disrupting their dendritic morphology and synaptic functions, or may bind to C3aR on microglia, inhibiting their ability to phagocytose toxic Aβ (Arranz and De Strooper, 2019). C3 and C1q showed enhanced expressions in exosomes derived from reactive astrocytes in AD patients compared to healthy individuals (Goetzl et al., 2018). Additionally, A1 supposedly secretes a yet-to-be identified neurotoxin that can induce neuronal and oligodendroglial apoptosis (Liddelow and Barres, 2017).

Transcriptomic profiling of A2 depicted upregulated expression of anti-inflammatory genes such as cardiotrophin-like cytokine factor 1, S100 calcium-binding protein a10 (s100a10), pentraxin 3, sphingosine kinase 1, IL-6, leukemia inhibitory factor (LIF) and transglutaminase 1 and other neurotrophic factors including Arginase-1 and nuclear factor erythroid 2-related factor 2 (Zamanian et al., 2012; Liddelow and Barres, 2017). Evidence suggests that LIF can protect against Aβ-induced neurotoxicity by activating Akt-mediated autophagy signaling especially in hippocampal cells (Lee et al., 2019). Barres's group however proposed that the STAT-3 pathway may be regulating the A2 phenotype in reference to Sofroniew's work which emphasized the major role of STAT-3 in inducing anti-inflammatory cytokine production (Sofroniew, 2015; Liddelow and Barres, 2017). A highly reported beneficial cytokine, IL-10, can induce astrocytic TGFβ secretion, improving microglial ability to phagocytose Aβ, thus protecting neurons from Aβ toxicity (Norden et al., 2014). Notably, the STAT3 pathway and TGFβ have often been positively correlated with the microglial M2 phenotype (Lee et al., 2020). Overall, it may thus be predicted that A2s are regulated by STAT3 signalling releasing a series of beneficial cytokines including TGFβ.

Recently, Habib et al. (2020) identified a unique reactive astrocyte subtype specific to AD and termed them as disease-associated astrocytes (DAA). DAA appear at an early stage (before cognitive decline) in the disease and increased manifold with disease progression. Furthermore, DAA-like populations emerge with aging in both wild type (WT) mice as well as in human brains and are mainly localized around Aβ plaques both in the hippocampus and subiculum, regions adversely affected in AD. The authors used single-nucleus RNA sequencing to create a cellular-molecular map of the hippocampal regions of 7-month old 5xFAD mice (refer to Supplementary Table 1 for details) alongside that of age-matched WT mice. They described a continuum of astrocyte profiles with distinct transcriptional states, reflecting a very dynamic astrocyte reaction process. Three distinct transcriptional states were identified – GFAP-low, GFAP-high and DAA and the cells were further grouped into transcriptional sub-clusters revealing transitional-like intermediate states that either reflected a transition between GFAP-low expressing astrocytes and GFAP-high ones or that reflected a transition from GFAP-low to DAA state. DAA were however uniquely present in AD mice and expressed a signature set of genes implicated in the complement cascade, endocytosis and aging. Interestingly, the authors showed that although most of the A1/inflammation signature genes were also detected in DAA, as opposed to A2 astrocyte signatures, some of the A1 specific genes were expressed in other astrocyte sub-clustures indicating that these nomenclature-based signatures are not very specific and rather identify a mixed astrocyte population (Habib et al., 2020).

Hence, the simple binarization may be quite restrictive to define other potential subtypes of reactive astrocytes, dependent on AD stage and brain topography. Barres's group also indicated that several more

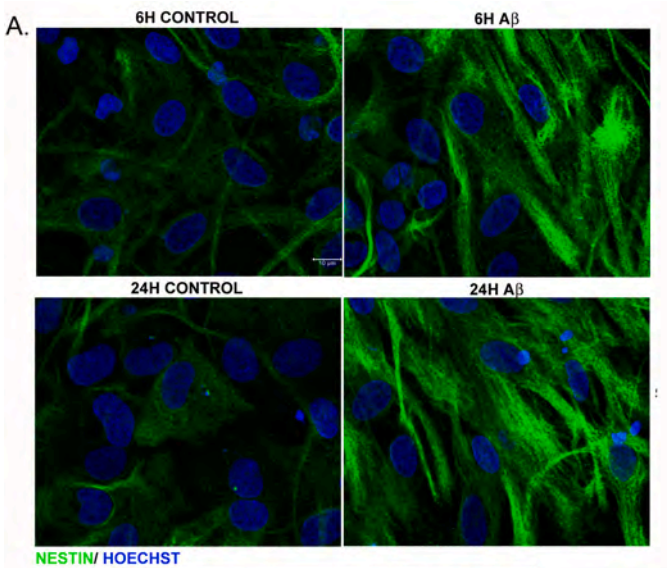

B.

	Cytokines	6h Aβ	24h Aβ
1	TIMP-1	↑	↓
2	sICAM-1	↑	↓
3	CINC-1	↑	—
4	MIP-1α	↑	—
5	VEGF	↑	↓
6	IL-2	↑	—
7	IP-10	—	↓
8	RANTES	—	↓
9	CINC-2α/β	—	↑
10	Fractalkine	—	↑
11	MIP-3α	—	↑

Fig. 1. Morphological changes of cortical astrocytes upon Aβ treatment and the associated cytokine secretion profile. A. Astrocytes (14DIV), treated with 1.5 μM Aβ for 6 h (upper panel) and 24 h (lower panel), were subjected to immunocytochemical staining with Nestin antibody followed by nuclear staining with Hoechst. Images were taken at a magnification of 60 × . Aβ treatment induced significant activation in astrocytes with morphological changes from flat polygonal to elongated shape with enhanced Nestin expression at both the time points. B. The associated cytokines secreted upon Aβ treatment at each time point are indicated in the table below the images. Green arrows indicate cytokines that were significantly upregulated in the Aβ-treated astrocyte secretome compared to control cells whereas red arrows indicate cytokines that were significantly downregulated in the same manner at each time point. It was observed that the cytokines upregulated at the 6 h time point were well-known anti-inflammatory cytokines whereas those upregulated at 24 h were generally pro-inflammatory in nature. Note that some of the anti-inflammatory cytokines (as indicated at 6 h) – TIMP-1, sICAM-1 and VEGF were downregulated at 24 h in the Aβ -treated astrocyte secretome.

reactive astrocyte subtypes may exist beyond the mentioned two, representing extreme ends of a rather complex continuum of reactive astrocyte states (Liddelow and Barres, 2017). However, in an attempt to present a comprehensive review of a highly complex subject – 'astrocyte subtypes in AD' to the readers, we have only discussed papers that give us an idea of the distinct functional profiles of reactive astrocytes in AD and have tried to draw a clearer picture by designating neurotoxic astrocytes as A1-like and neuroprotective ones as A2-like (a new nomenclature, with no relation to A1/A2 specific gene signatures unless stated otherwise).

Heneka et al. (2015) reported that microglial activation shifted from an initial M2 (beneficial) phenotype to a later M1 (detrimental) phenotype in response to CNS insults such as Aβ with their characteristic cytokine profiles (Heneka et al., 2015). Hence, a similar transition may be expected in activated astrocyte states and their related secretomes.

Our group has performed a kinetic study of astrocytic reaction upon Aβ-treatment in a primary culture model, revealing a plethora of upregulated beneficial cytokines such as TIMP-1, sICAM-1, cytokine-induced neutrophil chemoattractant-1 (CINC-1), Macrophage inflammatory protein-1 α (MIP-1α), Vascular endothelial growth factor (VEGF) and IL-2 at early hours of treatment, while cytokines such as Fractalkine, MIP-3α and CINC-2α/β were enriched at the later time points in the astrocyte conditioned medium that showed detrimental effects on neuronal health and survival (Fig. 1). We have also shown that rat recombinant TIMP-1 offered significant protection to primary cortical neurons against Aβ-induced neurodegeneration (Fig. 2) (Saha et al., 2020). Hence, we speculate that stage in AD progression can be a crucial factor in determining astrocyte fate – A1-like or A2-like reactive astrocytes.

Role of astrocyte-derived cytokines on neurons

Some astrocyte derived cytokine and chemokine molecules act directly on neurons and others act indirectly by activating non-neuronal cells in the brain. Nevertheless, the whole system of intercellular communication especially under pathological stress in brain is a highly complex and diverse phenomenon with most of the cytokines acting in an autocrine or paracrine manner.

IL-1β of the IL-1 family of cytokines is a major pro-inflammatory cytokine detected in the plasma and CSF of AD patients (Brosseron et al., 2014) and reportedly released by reactive astrocytes (Sofroniew, 2015). Besides being a well-recognized initiator of the immune response in AD, it triggers synthesis and amyloidogenic processing of APP in neurons (Griffin et al., 1998). It also acts in an autocrine manner inducing IL-6 production and s100β overexpression from the reactive astrocytes themselves, stimulates iNOS activity (Rossi and Bianchini, 1996) and further macrophage colony stimulating factor production leading to neuronal degeneration (Rubio-Perez and Morillas-Ruiz, 2012). Additonally, IL-1 upregulates neuronal acetylcholinesterase activity and further IL-1 production and astrocyte reaction, establishing a self-propagating continuous cycle (Griffin et al., 1998; Mrak and Griffin, 2001).

IL-6 thus induced in astrocytes can drive both pro-inflammatory and anti-inflammatory pathways in neurons (Sofroniew, 2015). In the CNS, IL-6 is implicated in neuronal health since it shares the receptor gp130 with growth factors like ciliary neurotrophic factor, oncostatin M, LIF and IL-11 that trigger JAK-STAT pathway promoting neuronal growth. Contrarily, IL-6 like cytokines may have detrimental effects on neurogenesis during development (John et al., 2005). While some data suggest that IL-6 inhibits the expression of proinflammatory cytokines like IL-1β and TNFα (John et al., 2005), others show that it may induce APP synthesis (Vandenabeele and Fiers, 1991). In AD, it may trigger ERK1/ERK2 and STAT3 (Schumann et al., 1999) as well as induce the expression of acute phase proteins including α2-macroglobulin and metallothionine in neurons (Ganter et al., 1991; Bauer et al., 1993; Akiyama et al., 2000).

TNFα, another important pro-inflammatory cytokine secreted by reactive astrocytes, renders its neurotoxic effect by promoting detrimental cell cycle events within these terminally differentiated cells during AD pathogenesis (Yamamoto et al., 2007). Moreover, soluble TNFα can activate TNFR1 with an intracellular 'death domain' which upon activation is involved in neuroinflammation and neuronal death not only in AD, but also in Parkinson's disease (PD), Amyotrophic lateral sclerosis and Multiple sclerosis (Antel et al., 1996; Akiyama et al., 2000).

Fractalkine or CX3CL1 constitutively expressed in the neurons in the resting CNS, under a pathological insult may be expressed and secreted by astrocytes (Pereira et al., 2001; Hughes et al., 2002). Emerging data suggest a role for fractalkine-CX3CR1 signaling in AD (Chen et al., 2016). Fractalkine can bind to its cognate receptor CX3CR1 on hippocampal neurons, activating the Akt pathway and rendering neuroprotection (Meucci et al., 2000). CXCL8 is expressed by astrocytes and

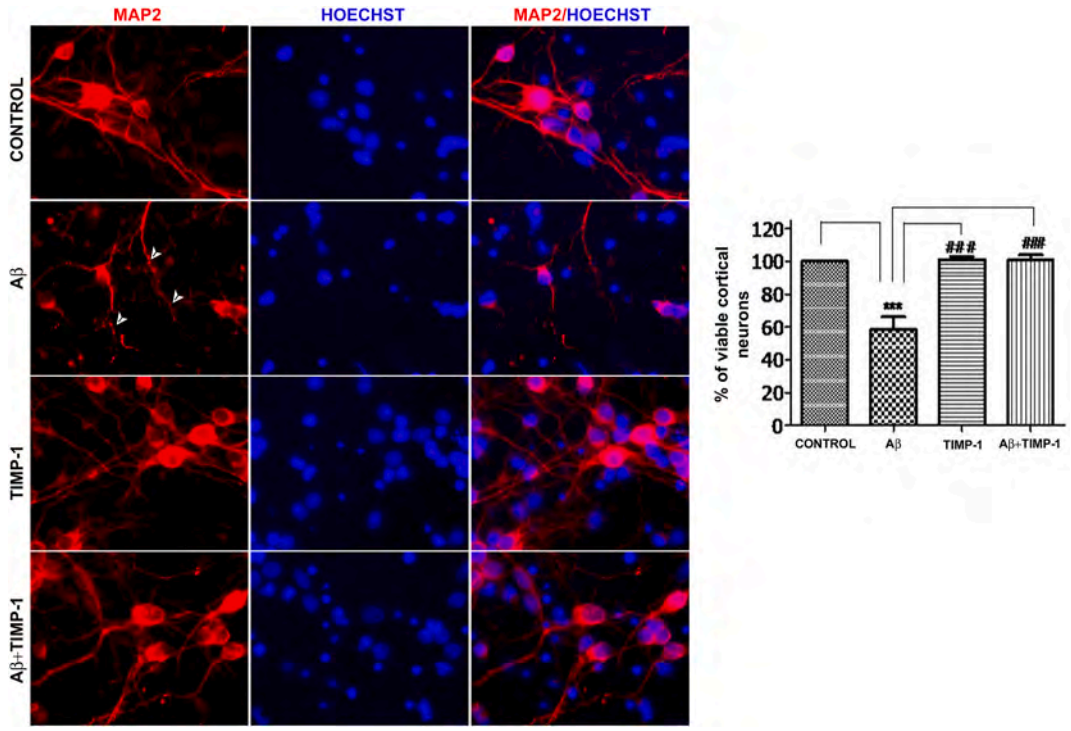

Fig. 2. Role of TIMP-1 on the viability of primary cortical neurons in presence of Aβ. Primary cortical neuron culture was given Aβ treatment alone or along with TIMP-1 for 24 h. Cells were subsequently fixed and immunostained with MAP2 antibody followed by Hoechst. Pictures were taken at 60 × magnification. Cells from all samples were also collected in nuclei counting buffer and counted for intact nuclei. Bar diagrams indicate the percentage of viable cortical neurons at 24 h following treatment. Values are expressed as Mean ± SEM of three experiments; ***$p < 0.05$, compared to control, ###$p < 0.05$, compared to Aβ. The figure has been adapted from an earlier publication of our group (Saha et al., 2020).

microglia as well as neurons upon Aβ treatment and can protect neurons by inducing brain derived neurotrophic factor production and by inhibiting Aβ-triggered neuronal apoptosis through autocrine or paracrine mechanisms (Ashutosh et al., 2011).

Astrocyte secreted cytokines can mediate their functions on neurons indirectly by activating microglial cells. TGF-β from activated astrocytes helps in inhibiting neuroinflammation by regulating microglial activation. Interestingly, IL-10 is the upstream regulator cytokine secreted from activated microglia that induces astrocytic TGF-β production. Thus, the presence of astrocytes is imperative to drive IL-10-mediated anti-inflammatory responses including attenuated expression of pro-inflammatory IL-1β and enhanced expression of anti-inflammatory fractalkine receptors (CX3CR1) and IL-4 receptors (IL-4Rα) in microglia (Cekanaviciute et al., 2014; Norden et al., 2014). In GFAP-IL-6 mice, IL-6 production from reactive astrocytes induces microgliosis and chronic neuroinflammation, and thus indirectly causes loss of synapses and calbindin-containing neurons leading to the cognitive impairment observed in these mice (Heyser et al., 1997). Several reports in PD models showed a protective phenotype mediated by Fractalkine, especially by virtue of its ability to transform the phenotype of microglia from the detrimental M1 to the protective M2 state (Morganti et al., 2012; Nash et al., 2013, 2015; Pabon et al., 2011; Wang et al., 2014). However, its nature of involvement in AD models remains controversial to date. There may be several other cytokine and chemokine molecules that may act directly or indirectly on neurons, but encompassing all of them is beyond the scope of this review.

Reactive astrocyte biomarkers

Cytokines and chemokines are the effector molecules that dictate the role of reactive astrocytes especially under a pathological condition and yet are not specifically released only by these cells. For identifying reactive astrocytes which are intimately related to different neurodegenerative diseases including AD, biomarkers of reactive astrocytes have emerged. Reactive astrocytes are slowly but surely getting integrated into the biomarker framework alongside already established neuronal biomarkers for real-time detection of human AD and its stages.

Biomarkers are molecules that are disease-specific and are present at detectable levels in body fluids such as saliva, urine, blood or CSF or that can be imaged using sophisticated analytical techniques including PET and MRI. For the CNS, fluid markers are typically quantified in the CSF or blood (serum/plasma). In AD, GFAP and S100β are reactive astrocyte biomarkers that are detected in both blood and CSF while D-serine, a gliotransmitter released by activated astrocytes, and YKL-40 are the other classical CSF biomarkers (Carter et al., 2019). However, GFAP levels are also found to be elevated in the CSF of frontotemporal lobar degeneration, dementia with Lewy bodies and Creutzdfeldt-Jakob disease (CJD) patients and some reports found that s100β is elevated in CJD but not in AD when compared to controls (Perez-Nievas and Serrano-Pozo, 2018).

PET is a non-invasive method for quantifying pharmacological and biological processes within the brain using special radioisotopes that emit positrons (for example, ^{18}F, ^{11}C, ^{15}O) commonly called radiotracers. It is a highly versatile and sensitive functional imaging technique that can help visualize different biochemical processes at the molecular level *in vivo*. Astrocyte reactivity can be quantified using two currently available radiotracers: [^{11}C]BU99008 and [^{11}C]deuterium-L-deprenyl ([^{11}C]DED) both of which uses the ^{11}C isotope (Carter et al., 2019). The molecular target of [^{11}C]BU99008 is imidazoline2-binding sites (I2BSs) present on mitochondrial membranes in astrocytes and are enhanced in AD post-mortem brains. The first human PET study with [^{11}C]BU99008 demonstrated that the brain delivery of the radiotracer was good and its binding was specific and consistent with the distribution of I2BS (Tyacke et al., 2018). [^{11}C]DED binds to an enzyme specifically expressed in astrocytes, monoamine oxidase B (MAO-B). This radiotracer has been used for imaging in different diseases including

ALS, focal epilepsy and CJD (Kumlien et al., 2001; Engler et al., 2003; Johansson et al., 2007). In transgenic models of AD, the initial phases of Aβ accumulation are linked to an upregulated expression of MAO-B whereas in the later stages of Aβ deposition the MAO-B level does not increase significantly but other astrocyte biomarkers namely GFAP are increased. Interestingly, GFAP and MAO-B do not colocalize in the mouse models indicating that they measure different populations of astrocytes (Olsen et al., 2018). A study in human demonstrates that [^{11}C]DED binding to MAO-B is significantly elevated by around 17% in early AD patients in comparison to cognitively normal candidates in the frontal and parietal cortices (Carter et al., 2012). Similarly, an increased binding was observed in carriers of autosomal dominant AD mutation around 30 years before the clinical onset of symptoms (Scholl et al., 2015).

[^{18}F]-FDG, a radiofluorinated analog of glucose, visualized by PET in the brain has been traditionally used as a biomarker measuring neuronal activity and for the diagnosis of AD stages (Chen et al., 2011). However, a recent report by Zimmer et al. has highlighted the contribution of astrocytes in the [^{18}F]-FDG PET signal (Zimmer et al., 2017). Interestingly, astrocyte glutamate transport specifically through glutamate transporter-1 (GLT-1) and glutamate/aspartate transporter (GLAST) acts as a trigger for uptake of glucose by astrocytes (Pellerin and Magistretti, 1994). Hence, it seems highly likely that the [^{18}F]-FDG signal probably reflects to a great extent the glucose consumption by astrocytes than that by neurons. Indeed, both human stem cell-derived astrocytes and neurons treated with Aβ oligomers display prominent glucose hypometabolism (Tarczyluk et al., 2015). Post mortem AD brains displayed reduced expression of the glucose transporters, glucose transporter 1 (GLUT1) (expressed predominantly on astrocytes and endothelial cells) and glucose transporter 3 (GLUT3) (expressed specifically on neurons) (Simpson et al., 1994; Liu et al., 2008) reinforcing that hypometabolism in AD estimated by [^{18}F]-FDG PET is not only a marker of neuronal dysfunction but also a non-specific indicator of astrocyte metabolic alterations in AD. Astrocyte reactivity especially in the early stages in AD has been estimated by multi-tracer PET where besides specific biomarker [^{11}C]DED, [^{18}F]-FDG PET was also used in human patients (Carter et al., 2012; Scholl et al., 2015). The major concern in these types of PET studies is that they can only be conducted in special facilities or research centers.

The most promising reactive astrocyte biomarker in CSF is YKL-40. It has been highly useful for predicting AD progression through its stages – pre-clinical to MCI to AD-related dementia. YKL-40, also known as Chitinase-3-like-1 (CHI3L1), is a 40 kDa human cartilage glycoprotein-39 (HC-gp39) and chondrex that is reportedly upregulated in AD brain and is involved in inflammation and tissue remodeling (Craig-Schapiro et al., 2010; Antonell et al., 2014; Alcolea et al., 2015a). A correlation was found between CSF YKL-40 levels and neurodegeneration biomarkers such as phospho-tau and total-tau levels in the CSF, and also with the cortical Aβ load especially at the early stage of AD (Antonell et al., 2014; Alcolea et al., 2015b). Immunoreactivity studies show that it was specifically observed in a subset of reactive astrocytes near AD-associated plaques and in some rare cases in microglia and neurons of white matter (Querol-Vilaseca et al., 2017). Interestingly, earlier studies indicated that transcription of YKL-40 is induced in astrocytes by pro-inflammatory factors such as TNFα and IL-1β released from activated macrophages. TNFα is one of the cytokines released from activated microglia (the resident macrophages of the brain) that is responsible for the conversion of astrocytes to the A1 phenotype (Liddelow et al., 2017). Furthermore, Zamanian et al. showed that YKL-40 (*chi3l1*) is one of the top 50 genes upregulated in detrimental astrocytes but does not appear in the top 50 upregulated genes in the protective subtype although it is expressed in both the reactive subtypes in mice (Zamanian et al., 2012). Thus, YKL-40 can be considered as a prominent reactive astrocyte biomarker that can differentiate A1-like and A2-like populations. Another known reactive astrocyte biomarker tenascin c, which is an extracellular matrix protein released by reactive astrocytes, was activated only in the A2 model (Laywell et al., 1992; Zamanian et al., 2012). Surprisingly, GFAP and vimentin were both highly upregulated in the A1-like and A2-like astrocyte populations. Hence, it may be suggested that although these biomarkers are well established reactive astrocyte biomarkers and help in the distinction between astrocytes' quiescent and reactive states, their level of expression changes may vary among different reactive astrocyte subpopulations.

Lipocalin-2 and Serpina3n have also been indicated as putative reactive astrocyte biomarkers because these two secretory protein genes were actively and significantly induced in both A1-like and A2-like astrocytes (Zamanian et al., 2012). The difference in each of their fold-changes between the LPS-induced and MCAO-induced models provides an insight in their ability to distinguish between the two subtypes, and may be able to do the same among many more subtypes in future. C3, complement factor B and Myxovirus resistance gene MX dynamin like GTPase 1 have recently emerged as specific markers for A1-like (Liddelow et al., 2017) while s100a10 has been utilized as a specific marker for A2-like astrocytes (Fujita et al., 2018). However, till now they have not evolved as reactive astrocyte subtype-specific biomarkers per se, but are potential candidates for further investigation.

ASTROCYTIC SUBTYPE-BASED THERAPIES – where do the cytokines stand?

In light of the aforementioned plausible transition in secretion profiles of reactive astrocyte subtypes during AD progression, subtype-targeting therapies may be a novel approach to AD treatment where cytokines pose as attractive targets. Additionally, cell-specific therapies accentuating the beneficial role of reactive astrocytes in AD and/or suppressing toxic gain-of-function in astrocytes may provide further opportunities in AD restriction, prevention or cure.

Blocking the activation of detrimental A1-like astrocytes is already being investigated through (a) inhibition of microglial activation (b) inhibition of microglia-secreted cytokines – IL-1α, TNFα and C1q that trigger the A1 phenotype. Microglial activation can be inhibited by using NLY01 (Yun et al., 2018) or exendin4 (Goncalves et al., 2016; Gullo et al., 2017; Lee et al., 2018; Garabadu and Verma, 2019), both agonists of the long-acting glucagon-like peptide-1 receptor, and are potential candidates in AD treatment. TNFα inhibition has been particularly relevant since the use of Etanercept (a TNFα inhibitor) in rheumatoid arthritis patients diminished their relative risk of developing AD compared to controls (Chou et al., 2016; Ekert et al., 2018), but the drug met with inconclusive outcomes in phase-2 clinical trials (Decourt et al., 2017). Similarly, anti-C1q antibody and a recombinant antagonist of IL-1α (Anakinra) are also being investigated at the pre-clinical and clinical levels (Lansita et al., 2017; Liddelow and Barres, 2017; Qi et al., 2018). A1-secreted IL-1α, IL-6 and IFNγ instigate neighboring neurons towards degeneration through induction of caspase-3 activity and hyperphosphorylated tau cleavage. Minocycline which reportedly targets these pro-inflammatory cytokine secretions was able to inhibit neuronal degeneration even in Aβ presence (Garwood et al., 2010). In addition, targeting C3 through inhibitors (Lian et al., 2015; Lian and Zheng, 2016) or blocking C3aR (Lian et al., 2016), its receptor, may inhibit A1-like astrocytes (Lian et al., 2015). Additionally, nonsteroidal anti-inflammatory drugs (NSAIDs) attenuate the release of pro-inflammatory cytokines, arresting neuronal death in AD (Gasparini et al., 2004; Sastre and Gentleman, 2010). However, to date NSAIDs have been mostly unsuccessful in clinical trials for AD (de Jong et al., 2008). Glucocortocoids also reduce IL-1α, IL-1β, IL-6 etc. secretions from A1-like astrocytes (Szczepanik and Ringheim, 2003; Fakhoury, 2018). Treatment with molecules/drugs targeting pro-inflammatory cytokine secretion has met limited success at the clinical level to date largely because they fail to take into account the AD stage-specific presence of target astrocyte subtypes. For example, anti-TNFα treatment may inhibit A1-like astrocyte activation in advanced AD-stage patients but may contrarily instigate a detrimental effect at the prodromal AD stage since

Table 1
Probable A1-like and A2-like astrocyte subtype-specific therapeutic targets in Alzheimer's disease (AD).

A1-like astrocyte targeted strategies in AD treatment					
Target	**Therapeutic molecule/ drug**	**Experimental model**	**Route of drug/ molecule administration**	**Age of administration**	**Reference**
		Cytokine-based inhibition			
TNFα	Etanercept (TNFα inhibitor, used in standard RA therapy)	Human AD patients[b]	s.c.	Average age, 76.5 years	Chou et al. (2016)
		Human AD patients[a]	s.c.	Average age, 72.4 ± 9.7 years	Butchart et al. (2015)
		Human AD patients[a,c]	Perispinal	Average age, 76.7 ± 10.9 years	Tobinick et al. (2006)
	Xpro1595 (TNFα inhibitor)	TgCRND8 mice	s.c.	1-month old (Pre-plaque stage)	Cavanagh et al. (2016)
	TNFR2:Fc (anti-TNFα biologics)	$A\beta_{25-35}$-injected mice	s.c.	6-week old (2nd, 4th and 6th day following Aβ administration)	Detrait et al. (2014)
	3,6′-dithiothalidomide (small molecule	3xTg-AD Mice	i.p.	4-month old (Pre-plaque stage with mild intraneuronal Aβ)	Gabbita et al. (2012)
	TNFα inhibitor)	$A\beta_{1-42}$-injected mice	i.p.	3-month old (Administered 7 days prior to Aβ injection)	Russo et al. (2012)
	Thalidomide (small molecule TNFα inhibitor)	APP23 mice	i.p.	Long term treatment- 9 to 12-month-old, Short term treatment – 12-month old	He et al. (2013)
	Infliximab (monoclonal anti-TNFα antibody)	$A\beta_{1-42}$-injected mice	i.c.v.	6-week old (co-administered with Aβ)	Kim et al. (2016)
		APP/PS1 mice	i.c.v.	12-month old	Shi et al. (2011)
	XENP345 (Dominant negative TNFα inhibitor selective for soluble TNF)	3xTg-AD mice	i.c.v.	4.5-month old	McAlpine et al. (2009)
C1q	ANX005 (anti-C1q antibody)	Sprague-Dawley (SD) rats	i.v.	8–9 weeks	Lansita et al. (2017)
		Cynomolgus monkeys	i.v.	2–4 years	
	ANX-M1 (anti-C1q antibody)	$A\beta_{1-40}$-oligomer injected mice	i.p. and i.c.v.	3-month old (co-administered with Aβ)	Hong et al. (2016)
IL1α	Anakinra (recombinant IL1α receptor antagonist)	McGill-Thy1-APP-TG rats	s.c.	6-month old (Pre-plaque stage)	Qi et al. (2018)
IL-6, MCP-1	Minocycline (an antibiotic)	Htau mice	i.p.	3–4 month old	Garwood et al. (2010)
IL1β, TNFα, IL-6	NSAIDs -Ibuprofen	Human AD patients[a]	oral	≥65 years	Pasqualetti et al. (2009)
		Tg2576 mice	oral	3-month old (Pre-plaque Stage with high levels of soluble Aβ)	Eriksen et al. (2003)
	Indomethacin	Human AD patients[a]	oral	Average age 78 ± 2 years	Rogers et al. (1993)
		Human AD patients[a]	oral	Average age 72.7 ± 6.9 years	de Jong et al. (2008)
	Naproxen	Human AD patients[a]	oral	Average age 74.1 ± 7.8 years	Aisen et al. (2003)
IL1α, IL1β, IL-6, MCP-1	Glucocorticoids (prednisolone and dexamethasone)	$A\beta_{1-42}$-injected mice	i.p.	50–60 days old (30 min prior to Aβ injection by i.c.v.)	Szczepanik and Ringheim (2003)
		Microglial activation inhibition			
Glucagon-like peptide-1 receptor agonists	Exendin-4[d]	Streptozotocin (STZ) injected rat AD model	i.p.	Male mature rats weighing between 200 and 220 g (Administered for 14 days following i.c.v. STZ)	Solmaz et al. (2015)
		$A\beta_{1-42}$-injected rat	i.p.	6–8 weeks (weighing 180 ± 20 g, administered from Day-1 to Day-14 following Aβ i.c.v. on Day-1)	Garabadu and Verma (2019)
NF-κβ	NSAIDs-Indomethacin	Tg2576 mice	oral	8-month old	Sung et al. (2004)
	Aspirin	Tg2576 mice	s.c.	12-month old	Medeiros et al. (2013)
C3	C3aR antagonist	APP/TTA double transgenic mice	i.p.	8-month old	Lian et al. (2015)
	C3aR antagonist or genetic deletion of C3aR	APP/TTA mice	i.p.	7.25-month old	Lian and Zheng (2016)

(*continued on next page*)

Table 1 (*continued*)

A2-like astrocyte targeted strategies in AD treatment

TIMP-1	-do-	$A\beta_{1-42}$-injected rat	i.c.v.	Adult male SD rats weighing 280–320 g (Administered on the 7th day following Aβ i.c.v.)	Saha et al. (2020)
ICAM-1	-do-	$A\beta_{1-42}$-injected rat 5xFAD mice	i.p. i.p.	Adult male SD rats weighing 280–320 g (Drug injection started on the 7th day following Aβ i.c.v.) 6-month old	S. Guha, R. K. Paidi, P. Saha, S.C. Biswas (Unpublished)
TGFβ	-do-	$A\beta_{1-42}$-injected rat	i.c.v. i.n.	4-month old (1 h before Aβ i.c.v.) (7th-day after Aβ i.c.v.)	Chen et al. (2015)
		3xTg mice	i.c.v.	2–3 month	Hu et al. (2019)
IL-10	-do-	$A\beta_{1-42}$-injected mice	i.v.	50–60 days old (Administered 10 min before the Aβ i.c.v. injection)	Szczepanik and Ringheim (2003)
IFNβ	-do-	Lentiviral (LV) mediated overexpression of mutant APP in hippocampus of adult rat	i.n.	12 week old male Wister rats (240–260g) (Administered on Day-23 following icv of LV-APP and continued on alternate days till day-48)	Chavoshinezhad et al. (2019)
IL33	-do-	APP/PS1 mice	i.p.	6–25 month old mice	Fu et al. (2016)
G-CSF	-do-	Tg2576 mice $A\beta_{1-42}$-injected mice	s.c. s.c.	10–12 month old 8-week old (Administration started on the 7th day following Aβ i.c.v.)	Tsai et al. (2007)

This table presents a collection of strategies by which the A1-like (detrimental) and A2-like (protective) astrocyte-subtypes can be targeted, especially by utilizing cytokines secreted by the reactive astrocytes. This table also provides a comprehensive view of the age of administration of the putative therapeutic molecule/drug in both human AD patients and animal models for targeting reactive astrocyte subtypes in disease prevention or treatment. Further information regarding experimental models has been provided in Supplementary Table 1.

Abbreviations: C3aR - C3 receptor, i.c.v. - intracerebroventricular, i.n. - intranasal, i.p. – intraperitoneal, i.v. – intravenous, NSAIDs - nonsteroidal anti-inflammatory drugs, RA – rheumatoid arthritis, s.c. – subcutaneous, TNFR2:Fc - TNF receptor 2 fused to a Fc domain, -do- - same as the previous cell.

[a] Probable AD according to National Institute of Neurological and Communicative Disorders and Stroke and the Alzheimer's Disease and Related Disorders Association (NINCDS-ADRDA) Criteria.

[b] As per International Classification of Diseases, Ninth Revision (ICD-9) code for rheumatoid arthritis (RA), along with a diagnosis of AD made at least 120 days after the diagnosis of RA.

[c] Diagnostic and Statistical Manual of Mental Disorders, Fourth Edition (DSM-IV) criteria for AD, mild-to-severe AD.

[d] A site-specific pegylated form of exendin-4, NLY01 produced by Neuraly company (http://www.ddpharmatech.com/) has been approved for Phase 2B trial in patients with MCI due to AD after it was well-tolerated in Phase-1 trial (NCT03672604) in healthy volunteers.

TNFα is also known to trigger the beneficial A20 (Sofroniew, 2015). Nevertheless, there are still ongoing clinical trials targeted at inflammatory cytokines (Long and Holtzman, 2019; Hampel et al., 2020).

Direct A2-like astrocyte specific cytokine application may be considered as a novel approach in AD treatment. Recently, we have elegantly demonstrated that intracerebroventricular introduction of the beneficial cytokine TIMP-1, released by the protective state of Aβ-activated astrocytes in an Aβ-infused rat model of AD, ameliorated cognitive deficits besides inducing Aβ clearance, inhibiting neuronal apoptosis and improving synaptic health through activation of the Akt pathway (Saha et al., 2020). Intranasal (IN) administration of TGFβ in an Aβ-injected rat AD model alleviated cognitive deficits and neuronal apoptosis (Chen et al., 2015), and direct hippocampal infusion of TGFβ in an AD mouse ameliorated AD-induced memory impairments and synaptic plasticity through activation of the PI3K/Akt/Wnt/β-catenin signaling pathway (Hu et al., 2019), exemplify promising cytokine-mediated strategies in AD treatment. In support of this, IN administration of IFNβ, expressed by both glia and neurons, can alleviate cognitive deficits in a rat model of AD by modulating apoptosis and hippocampal neurogenesis (Chavoshinezhad et al., 2019). Intravenous administration of the anti-inflammatory cytokine IL-10 in Aβ or LPS-injected mice inhibited the overwhelming production of pro-inflammatory cytokines such as IL-1β, IL-1α, IL-6 and monocyte chemoattractant protein-1 (MCP-1) in the hippocampal and cortical regions (Szczepanik and Ringheim, 2003). Intraperitoneal (i.p.) administration of IL-33 into APP/PS1 mice reduced Aβ plaques by inducing microglial phagocytosis of Aβ and by downregulating the expression of pro-inflammatory genes and improving cognitive functions (Fu et al., 2016). Recently, we have also found that i.p. administration of ICAM-1 ameliorates cognitive behavioral deficits in $A\beta_{1-42}$-infused rats and 5xFAD transgenic mice by reducing elevated levels of NF-κB (Guha et al. unpublished data). Subcutaneous administration of granulocyte colony stimulating factor (G-CSF) into Aβ-induced mouse models of AD and Tg2576 mice (refer to Supplementary Table 1 for details) presents yet another therapeutic strategy that significantly ameliorated their memory functions. Furthermore, the recovery was associated with G-CSF induced bone marrow-derived hematopoietic stem cell mobilization and local neurogenesis near the Aβ plaques. Since G-CSF is already being used as a drug for the treatment of chemotherapy-induced neutropenia, it would be an excellent candidate for cytokine-mediated non-invasive treatment in AD (Tsai et al., 2007). However, these strategies are still at their preliminary stages requiring further investigation. A list of probable A1-like and A2-like astrocyte specific targets is given in Table 1.

Conclusion

A linear understanding of astrocyte reaction as a function of age is becoming irrelevant with the emergence of complex concepts of 'reactive astrocyte subtypes'. Beyond the under-appreciated immense role played by astrocytes in a healthy CNS, a critical understanding of reactive astrocytes is pivotal for neurological disease diagnosis or treatment. Compelling evidence emphasizes the transition of protective astrocytes probably existing at the prodromal stage with their signatory beneficial cytokine profile towards a detrimental profile at the later stages in AD. Whether these profiles are directly linked to astrocyte

subtypes need to be further investigated, but they definitely validates the role of cytokines in mediating astrocyte-subtype-specific functions. However, the failures of cytokine-mediated therapy stems from the lack of complete knowledge of each cellular state of reactive astrocytes involving analysis of subtype-specific morphology, transcriptomics, proteomics and metabolomics. For example, STAT3 and NF-κβ-targeting may seem like tantalizing options in regulating subtype-specific cytokine production, but a hurried approach without appreciating their bigger role in the total physiology will only result in catastrophic outcomes, even astrocytomas. Single-cell transcriptomics provide an incredible opportunity to deeply analyze each astrocyte state and its transition. This, in future, may help correlate each subtype and its signatory cytokines with specific AD stages. Hence, better and comprehensive understanding of astrocyte-subtype specific profiles, broad yet nuanced study of the balance between the newly emerging astrocyte subtypes and the nature of the transition between the activated states with an eye for the inter- and intra-cellular changes/molecules leading towards altering cytokine production is prudent in the present scenario of astro-centric neurodegeneration research.

Declaration of competing interest

The authors have no conflict of interest.

Acknowledgements

We would like thank Prof. Lloyd A. Greene, Department of Pathology and Cell Biology, Columbia University, New York for reading this manuscript, correcting errors relating to grammar and improving the flow. We would like to thank CSIR, Govt. of India for funding (BSC0115) and DST, govt. of India for Inspire fellowship to Sukanya Sarkar.

Appendix A. Supplementary data

Supplementary data to this article can be found online at https://doi.org/10.1016/j.neuint.2021.104956.

References

Aisen, P.S., Schafer, K.A., Grundman, M., Pfeiffer, E., Sano, M., Davis, K.L., Farlow, M.R., Jin, S., Thomas, R.G., Thal, L.J., 2003. Effects of rofecoxib or naproxen vs placebo on Alzheimer disease progression: a randomized controlled trial. JAMA 289, 2819–2826.

Akiyama, H., Barger, S., Barnum, S., Bradt, B., Bauer, J., Cole, G.M., Cooper, N.R., Eikelenboom, P., Emmerling, M., Fiebich, B.L., Finch, C.E., Frautschy, S., Griffin, W. S., Hampel, H., Hull, M., Landreth, G., Lue, L., Mrak, R., Mackenzie, I.R., McGeer, P. L., O'Banion, M.K., Pachter, J., Pasinetti, G., Plata-Salaman, C., Rogers, J., Rydel, R., Shen, Y., Streit, W., Strohmeyer, R., Tooyoma, I., Van Muiswinkel, F.L., Veerhuis, R., Walker, D., Webster, S., Wegrzyniak, B., Wenk, G., Wyss-Coray, T., 2000. Inflammation and Alzheimer's disease. Neurobiol. Aging 21, 383–421.

Albert, M.S., DeKosky, S.T., Dickson, D., Dubois, B., Feldman, H.H., Fox, N.C., Gamst, A., Holtzman, D.M., Jagust, W.J., Petersen, R.C., Snyder, P.J., Carrillo, M.C., Thies, B., Phelps, C.H., 2011. The diagnosis of mild cognitive impairment due to Alzheimer's disease: recommendations from the National Institute on Aging-Alzheimer's Association workgroups on diagnostic guidelines for Alzheimer's disease. Alzheimers Dement 7, 270–279.

Alcolea, D., Martinez-Lage, P., Sanchez-Juan, P., Olazaran, J., Antunez, C., Izagirre, A., Ecay-Torres, M., Estanga, A., Clerigue, M., Guisasola, M.C., Sanchez Ruiz, D., Marin Munoz, J., Calero, M., Blesa, R., Clarimon, J., Carmona-Iragui, M., Morenas-Rodriguez, E., Rodriguez-Rodriguez, E., Vazquez Higuera, J.L., Fortea, J., Lleo, A., 2015a. Amyloid precursor protein metabolism and inflammation markers in preclinical Alzheimer disease. Neurology 85, 626–633.

Alcolea, D., Vilaplana, E., Pegueroles, J., Montal, V., Sanchez-Juan, P., Gonzalez-Suarez, A., Pozueta, A., Rodriguez-Rodriguez, E., Bartres-Faz, D., Vidal-Pineiro, D., Gonzalez-Ortiz, S., Medrano, S., Carmona-Iragui, M., Sanchez-Saudinos, M., Sala, I., Anton-Aguirre, S., Sampedro, F., Morenas-Rodriguez, E., Clarimon, J., Blesa, R., Lleo, A., Fortea, J., 2015b. Relationship between cortical thickness and cerebrospinal fluid YKL-40 in predementia stages of Alzheimer's disease. Neurobiol. Aging 36, 2018–2023.

Antel, J.P., Becher, B., Owens, T., 1996. Immunotherapy for multiple sclerosis: from theory to practice. Nat. Med. 2, 1074–1075.

Antonell, A., Mansilla, A., Rami, L., Llado, A., Iranzo, A., Olives, J., Balasa, M., Sanchez-Valle, R., Molinuevo, J.L., 2014. Cerebrospinal fluid level of YKL-40 protein in preclinical and prodromal Alzheimer's disease. J Alzheimers Dis 42, 901–908.

Arranz, A.M., De Strooper, B., 2019. The role of astroglia in Alzheimer's disease: pathophysiology and clinical implications. Lancet Neurol. 18, 406–414.

Ashutosh, Kou, W., Cotter, R., Borgmann, K., Wu, L., Persidsky, R., Sakhuja, N., Ghorpade, A., 2011. CXCL8 protects human neurons from amyloid-beta-induced neurotoxicity: relevance to Alzheimer's disease. Biochem. Biophys. Res. Commun. 412, 565–571.

Assefa, B.T., Gebre, A.K., Altaye, B.M., 2018. Reactive astrocytes as drug target in Alzheimer's disease. BioMed Res. Int. 2018, 4160247.

Bales, K.R., Du, Y., Dodel, R.C., Yan, G.M., Hamilton-Byrd, E., Paul, S.M., 1998. The NF-kappaB/Rel family of proteins mediates Abeta-induced neurotoxicity and glial activation. Brain Res Mol Brain Res 57, 63–72.

Basak, J.M., Verghese, P.B., Yoon, H., Kim, J., Holtzman, D.M., 2012. Low-density lipoprotein receptor represents an apolipoprotein E-independent pathway of Abeta uptake and degradation by astrocytes. J. Biol. Chem. 287, 13959–13971.

Bauer, J., Ganter, U., Abel, J., Strauss, S., Jonas, U., Weiss, R., Gebicke-Haerter, P., Volk, B., Berger, M., 1993. Effects of interleukin-1 and interleukin-6 on metallothionein and amyloid precursor protein expression in human neuroblastoma cells. Evidence that interleukin-6 possibly acts via a receptor different from the 80-kDa interleukin-6 receptor. J. Neuroimmunol. 45, 163–173.

Blasko, I., Veerhuis, R., Stampfer-Kountchev, M., Saurwein-Teissl, M., Eikelenboom, P., Grubeck-Loebenstein, B., 2000. Costimulatory effects of interferon-gamma and interleukin-1beta or tumor necrosis factor alpha on the synthesis of Abeta1-40 and Abeta1-42 by human astrocytes. Neurobiol. Dis. 7, 682–689.

Brosseron, F., Krauthausen, M., Kummer, M., Heneka, M.T., 2014. Body fluid cytokine levels in mild cognitive impairment and Alzheimer's disease: a comparative overview. Mol. Neurobiol. 50, 534–544.

Burbach, G.J., Dehn, D., Del Turco, D., Staufenbiel, M., Deller, T., 2004. Laser microdissection reveals regional and cellular differences in GFAP mRNA upregulation following brain injury, axonal denervation, and amyloid plaque deposition. Glia 48, 76–84.

Burda, J.E., Sofroniew, M.V., 2014. Reactive gliosis and the multicellular response to CNS damage and disease. Neuron 81, 229–248.

Bush, T.G., Puvanachandra, N., Horner, C.H., Polito, A., Ostenfeld, T., Svendsen, C.N., Mucke, L., Johnson, M.H., Sofroniew, M.V., 1999. Leukocyte infiltration, neuronal degeneration, and neurite outgrowth after ablation of scar-forming, reactive astrocytes in adult transgenic mice. Neuron 23, 297–308.

Butchart, J., Brook, L., Hopkins, V., Teeling, J., Puntener, U., Culliford, D., Sharples, R., Sharif, S., McFarlane, B., Raybould, R., Thomas, R., Passmore, P., Perry, V.H., Holmes, C., 2015. Etanercept in Alzheimer disease: A randomized, placebo-controlled, double-blind, phase 2 trial. Neurology 84, 2161–2168.

Carter, S.F., Herholz, K., Rosa-Neto, P., Pellerin, L., Nordberg, A., Zimmer, E.R., 2019. Astrocyte biomarkers in Alzheimer's disease. Trends Mol. Med. 25, 77–95.

Carter, S.F., Scholl, M., Almkvist, O., Wall, A., Engler, H., Langstrom, B., Nordberg, A., 2012. Evidence for astrocytosis in prodromal Alzheimer disease provided by 11C-deuterium-L-deprenyl: a multitracer PET paradigm combining 11C-Pittsburgh compound B and 18F-FDG. J. Nucl. Med. 53, 37–46.

Catrysse, L., Vereecke, L., Beyaert, R., van Loo, G., 2014. A20 in inflammation and autoimmunity. Trends Immunol. 35, 22–31.

Cavanagh, C., Tse, Y.C., Nguyen, H.B., Krantic, S., Breitner, J.C., Quirion, R., Wong, T.P., 2016. Inhibiting tumor necrosis factor-alpha before amyloidosis prevents synaptic deficits in an Alzheimer's disease model. Neurobiol. Aging 47, 41–49.

Cekanaviciute, E., Dietrich, H.K., Axtell, R.C., Williams, A.M., Egusquiza, R., Wai, K.M., Koshy, A.A., Buckwalter, M.S., 2014. Astrocytic TGF-beta signaling limits inflammation and reduces neuronal damage during central nervous system Toxoplasma infection. J. Immunol. 193, 139–149.

Chavoshinezhad, S., Mohseni Kouchesfahani, H., Ahmadiani, A., Dargahi, L., 2019. Interferon beta ameliorates cognitive dysfunction in a rat model of Alzheimer's disease: modulation of hippocampal neurogenesis and apoptosis as underlying mechanism. Prog. Neuro-Psychopharmacol. Biol. Psychiatry 94, 109661.

Chen, J.H., Ke, K.F., Lu, J.H., Qiu, Y.H., Peng, Y.P., 2015. Protection of TGF-beta1 against neuroinflammation and neurodegeneration in Abeta1-42-induced Alzheimer's disease model rats. PloS One 10, e0116549.

Chen, K., Ayutyanont, N., Langbaum, J.B., Fleisher, A.S., Reschke, C., Lee, W., Liu, X., Bandy, D., Alexander, G.E., Thompson, P.M., Shaw, L., Trojanowski, J.Q., Jack Jr., C. R., Landau, S.M., Foster, N.L., Harvey, D.J., Weiner, M.W., Koeppe, R.A., Jagust, W. J., Reiman, E.M., 2011. Characterizing Alzheimer's disease using a hypometabolic convergence index. Neuroimage 56, 52–60.

Chen, P., Zhao, W., Guo, Y., Xu, J., Yin, M., 2016. CX3CL1/CX3CR1 in Alzheimer's disease: a target for neuroprotection. BioMed Res. Int. 2016, 8090918.

Chou, R.C., Kane, M., Ghimire, S., Gautam, S., Gui, J., 2016. Treatment for rheumatoid arthritis and risk of Alzheimer's disease: a nested case-control analysis. CNS Drugs 30, 1111–1120.

Cooley, I.D., Chauhan, V.S., Donneyz, M.A., Marriott, I., 2014. Astrocytes produce IL-19 in response to bacterial challenge and are sensitive to the immunosuppressive effects of this IL-10 family member. Glia 62, 818–828.

Correa, J.D., Starling, D., Teixeira, A.L., Caramelli, P., Silva, T.A., 2011. Chemokines in CSF of Alzheimer's disease patients. Arq Neuropsiquiatr 69, 455–459.

Craig-Schapiro, R., Perrin, R.J., Roe, C.M., Xiong, C., Carter, D., Cairns, N.J., Mintun, M. A., Peskind, E.R., Li, G., Galasko, D.R., Clark, C.M., Quinn, J.F., D'Angelo, G., Malone, J.P., Townsend, R.R., Morris, J.C., Fagan, A.M., Holtzman, D.M., 2010. YKL-40: a novel prognostic fluid biomarker for preclinical Alzheimer's disease. Biol. Psychiatr. 68, 903–912.

de Jong, D., Jansen, R., Hoefnagels, W., Jellesma-Eggenkamp, M., Verbeek, M., Borm, G., Kremer, B., 2008. No effect of one-year treatment with indomethacin on Alzheimer's disease progression: a randomized controlled trial. PloS One 3, e1475.

De Strooper, B., Karran, E., 2016. The cellular phase of Alzheimer's disease. Cell 164, 603–615.
Decourt, B., Lahiri, D.K., Sabbagh, M.N., 2017. Targeting tumor necrosis factor Alpha for Alzheimer's disease. Curr. Alzheimer Res. 14, 412–425.
Delekate, A., Fuchtemeier, M., Schumacher, T., Ulbrich, C., Foddis, M., Petzold, G.C., 2014. Metabotropic P2Y1 receptor signalling mediates astrocytic hyperactivity in vivo in an Alzheimer's disease mouse model. Nat. Commun. 5, 5422.
Detrait, E.R., Danis, B., Lamberty, Y., Foerch, P., 2014. Peripheral administration of an anti-TNF-alpha receptor fusion protein counteracts the amyloid induced elevation of hippocampal TNF-alpha levels and memory deficits in mice. Neurochem. Int. 72, 10–13.
Dubois, B., Hampel, H., Feldman, H.H., Scheltens, P., Aisen, P., Andrieu, S., Bakardjian, H., Benali, H., Bertram, L., Blennow, K., Broich, K., Cavedo, E., Crutch, S., Dartigues, J.F., Duyckaerts, C., Epelbaum, S., Frisoni, G.B., Gauthier, S., Genthon, R., Gouw, A.A., Habert, M.O., Holtzman, D.M., Kivipelto, M., Lista, S., Molinuevo, J.L., O'Bryant, S.E., Rabinovici, G.D., Rowe, C., Salloway, S., Schneider, L.S., Sperling, R., Teichmann, M., Carrillo, M.C., Cummings, J., Jack Jr., C.R., 2016. Preclinical Alzheimer's disease: definition, natural history, and diagnostic criteria. Alzheimers Dement 12, 292–323.
Ekert, J.O., Gould, R.L., Reynolds, G., Howard, R.J., 2018. TNF alpha inhibitors in Alzheimer's disease: a systematic review. Int. J. Geriatr. Psychiatr. 33, 688–694.
Engler, H., Lundberg, P.O., Ekbom, K., Nennesmo, I., Nilsson, A., Bergstrom, M., Tsukada, H., Hartvig, P., Langstrom, B., 2003. Multitracer study with positron emission tomography in Creutzfeldt-Jakob disease. Eur. J. Nucl. Med. Mol. Imag. 30, 85–95.
Eriksen, J.L., Sagi, S.A., Smith, T.E., Weggen, S., Das, P., McLendon, D.C., Ozols, V.V., Jessing, K.W., Zavitz, K.H., Koo, E.H., Golde, T.E., 2003. NSAIDs and enantiomers of flurbiprofen target gamma-secretase and lower Abeta 42 in vivo. J. Clin. Invest. 112, 440–449.
Escartin, C., Guillemaud, O., Carrillo-de Sauvage, M.A., 2019. Questions and (some) answers on reactive astrocytes. Glia 67, 2221–2247.
Fakhoury, M., 2018. Microglia and astrocytes in Alzheimer's disease: implications for therapy. Curr. Neuropharmacol. 16, 508–518.
Faulkner, J.R., Herrmann, J.E., Woo, M.J., Tansey, K.E., Doan, N.B., Sofroniew, M.V., 2004. Reactive astrocytes protect tissue and preserve function after spinal cord injury. J. Neurosci. 24, 2143–2155.
Fu, A.K., Hung, K.W., Yuen, M.Y., Zhou, X., Mak, D.S., Chan, I.C., Cheung, T.H., Zhang, B., Fu, W.Y., Liew, F.Y., Ip, N.Y., 2016. IL-33 ameliorates Alzheimer's disease-like pathology and cognitive decline. Proc. Natl. Acad. Sci. U. S. A. 113, E2705–E2713.
Fujita, A., Yamaguchi, H., Yamasaki, R., Cui, Y., Matsuoka, Y., Yamada, K.I., Kira, J.I., 2018. Connexin 30 deficiency attenuates A2 astrocyte responses and induces severe neurodegeneration in a 1-methyl-4-phenyl-1,2,3,6-tetrahydropyridine hydrochloride Parkinson's disease animal model. J. Neuroinflammation 15, 227.
Funato, H., Yoshimura, M., Yamazaki, T., Saido, T.C., Ito, Y., Yokofujita, J., Okeda, R., Ihara, Y., 1998. Astrocytes containing amyloid beta-protein (Abeta)-positive granules are associated with Abeta40-positive diffuse plaques in the aged human brain. Am. J. Pathol. 152, 983–992.
Furman, J.L., Sama, D.M., Gant, J.C., Beckett, T.L., Murphy, M.P., Bachstetter, A.D., Van Eldik, L.J., Norris, C.M., 2012. Targeting astrocytes ameliorates neurologic changes in a mouse model of Alzheimer's disease. J. Neurosci. 32, 16129–16140.
Gabbita, S.P., Srivastava, M.K., Eslami, P., Johnson, M.F., Kobritz, N.K., Tweedie, D., Greig, N.H., Zemlan, F.P., Sharma, S.P., Harris-White, M.E., 2012. Early intervention with a small molecule inhibitor for tumor necrosis factor-alpha prevents cognitive deficits in a triple transgenic mouse model of Alzheimer's disease. J. Neuroinflammation 9, 99.
Ganter, U., Strauss, S., Jonas, U., Weidemann, A., Beyreuther, K., Volk, B., Berger, M., Bauer, J., 1991. Alpha 2-macroglobulin synthesis in interleukin-6-stimulated human neuronal (SH-SY5Y neuroblastoma) cells. Potential significance for the processing of Alzheimer beta-amyloid precursor protein. FEBS Lett. 282, 127–131.
Garabadu, D., Verma, J., 2019. Exendin-4 attenuates brain mitochondrial toxicity through PI3K/Akt-dependent pathway in amyloid beta (1-42)-induced cognitive deficit rats. Neurochem. Int. 128, 39–49.
Garwood, C.J., Cooper, J.D., Hanger, D.P., Noble, W., 2010. Anti-inflammatory impact of minocycline in a mouse model of tauopathy. Front. Psychiatr. 1, 136.
Garwood, C.J., Pooler, A.M., Atherton, J., Hanger, D.P., Noble, W., 2011. Astrocytes are important mediators of Abeta-induced neurotoxicity and tau phosphorylation in primary culture. Cell Death Dis. 2, e167.
Garwood, C.J., Ratcliffe, L.E., Simpson, J.E., Heath, P.R., Ince, P.G., Wharton, S.B., 2017. Review: astrocytes in Alzheimer's disease and other age-associated dementias: a supporting player with a central role. Neuropathol. Appl. Neurobiol. 43, 281–298.
Gasparini, L., Ongini, E., Wenk, G., 2004. Non-steroidal anti-inflammatory drugs (NSAIDs) in Alzheimer's disease: old and new mechanisms of action. J. Neurochem. 91, 521–536.
Giaume, C., Kirchhoff, F., Matute, C., Reichenbach, A., Verkhratsky, A., 2007. Glia: the fulcrum of brain diseases. Cell Death Differ. 14, 1324–1335.
Goetzl, E.J., Schwartz, J.B., Abner, E.L., Jicha, G.A., Kapogiannis, D., 2018. High complement levels in astrocyte-derived exosomes of Alzheimer disease. Ann. Neurol. 83, 544–552.
Goncalves, A., Lin, C.M., Muthusamy, A., Fontes-Ribeiro, C., Ambrosio, A.F., Abcouwer, S.F., Fernandes, R., Antonetti, D.A., 2016. Protective effect of a GLP-1 analog on ischemia-reperfusion induced blood-retinal barrier breakdown and inflammation. Invest. Ophthalmol. Vis. Sci. 57, 2584–2592.
Gonzalez-Reyes, R.E., Nava-Mesa, M.O., Vargas-Sanchez, K., Ariza-Salamanca, D., Mora-Munoz, L., 2017. Involvement of astrocytes in Alzheimer's disease from a neuroinflammatory and oxidative stress perspective. Front. Mol. Neurosci. 10, 427.
Griffin, W.S., Sheng, J.G., Royston, M.C., Gentleman, S.M., McKenzie, J.E., Graham, D.I., Roberts, G.W., Mrak, R.E., 1998. Glial-neuronal interactions in Alzheimer's disease: the potential role of a 'cytokine cycle' in disease progression. Brain Pathol. 8, 65–72.
Grolla, A.A., Fakhfouri, G., Balzaretti, G., Marcello, E., Gardoni, F., Canonico, P.L., DiLuca, M., Genazzani, A.A., Lim, D., 2013a. Abeta leads to Ca(2)(+) signaling alterations and transcriptional changes in glial cells. Neurobiol. Aging 34, 511–522.
Grolla, A.A., Sim, J.A., Lim, D., Rodriguez, J.J., Genazzani, A.A., Verkhratsky, A., 2013b. Amyloid-beta and Alzheimer's disease type pathology differentially affects the calcium signalling toolkit in astrocytes from different brain regions. Cell Death Dis. 4, e623.
Gullo, F., Ceriani, M., D'Aloia, A., Wanke, E., Constanti, A., Costa, B., Lecchi, M., 2017. Plant polyphenols and exendin-4 prevent hyperactivity and TNF-alpha release in LPS-treated in vitro neuron/astrocyte/microglial networks. Front. Neurosci. 11, 500.
Habib, N., McCabe, C., Medina, S., Varshavsky, M., Kitsberg, D., Dvir-Szternfeld, R., Green, G., Dionne, D., Nguyen, L., Marshall, J.L., Chen, F., Zhang, F., Kaplan, T., Regev, A., Schwartz, M., 2020. Disease-associated astrocytes in Alzheimer's disease and aging. Nat. Neurosci. 23, 701–706.
Hamby, M.E., Coppola, G., Ao, Y., Geschwind, D.H., Khakh, B.S., Sofroniew, M.V., 2012. Inflammatory mediators alter the astrocyte transcriptome and calcium signaling elicited by multiple G-protein-coupled receptors. J. Neurosci. 32, 14489–14510.
Hampel, H., Caraci, F., Cuello, A.C., Caruso, G., Nistico, R., Corbo, M., Baldacci, F., Toschi, N., Garaci, F., Chiesa, P.A., Verdooner, S.R., Akman-Anderson, L., Hernandez, F., Avila, J., Emanuele, E., Valenzuela, P.L., Lucia, A., Watling, M., Imbimbo, B.P., Vergallo, A., Lista, S., 2020. A path toward precision medicine for neuroinflammatory mechanisms in Alzheimer's disease. Front. Immunol. 11, 456.
Hardy, J.A., Higgins, G.A., 1992. Alzheimer's disease: the amyloid cascade hypothesis. Science 256, 184–185.
Hartlage-Rubsamen, M., Zeitschel, U., Apelt, J., Gartner, U., Franke, H., Stahl, T., Gunther, A., Schliebs, R., Penkowa, M., Bigl, V., Rossner, S., 2003. Astrocytic expression of the Alzheimer's disease beta-secretase (BACE1) is stimulus-dependent. Glia 41, 169–179.
He, P., Cheng, X., Staufenbiel, M., Li, R., Shen, Y., 2013. Long-term treatment of thalidomide ameliorates amyloid-like pathology through inhibition of beta-secretase in a mouse model of Alzheimer's disease. PLoS One 8, e55091.
Heneka, M.T., Carson, M.J., El Khoury, J., Landreth, G.E., Brosseron, F., Feinstein, D.L., Jacobs, A.H., Wyss-Coray, T., Vitorica, J., Ransohoff, R.M., Herrup, K., Frautschy, S. A., Finsen, B., Brown, G.C., Verkhratsky, A., Yamanaka, K., Koistinaho, J., Latz, E., Halle, A., Petzold, G.C., Town, T., Morgan, D., Shinohara, M.L., Perry, V.H., Holmes, C., Bazan, N.G., Brooks, D.J., Hunot, S., Joseph, B., Deigendesch, N., Garaschuk, O., Boddeke, E., Dinarello, C.A., Breitner, J.C., Cole, G.M., Golenbock, D. T., Kummer, M.P., 2015. Neuroinflammation in Alzheimer's disease. Lancet Neurol. 14, 388–405.
Heppner, F.L., Ransohoff, R.M., Becher, B., 2015. Immune attack: the role of inflammation in Alzheimer disease. Nat. Rev. Neurosci. 16, 358–372.
Herrmann, J.E., Imura, T., Song, B., Qi, J., Ao, Y., Nguyen, T.K., Korsak, R.A., Takeda, K., Akira, S., Sofroniew, M.V., 2008. STAT3 is a critical regulator of astrogliosis and scar formation after spinal cord injury. J. Neurosci. 28, 7231–7243.
Heyser, C.J., Masliah, E., Samimi, A., Campbell, I.L., Gold, L.H., 1997. Progressive decline in avoidance learning paralleled by inflammatory neurodegeneration in transgenic mice expressing interleukin 6 in the brain. Proc. Natl. Acad. Sci. U. S. A. 94, 1500–1505.
Hoke, A., Canning, D.R., Malemud, C.J., Silver, J., 1994. Regional differences in reactive gliosis induced by substrate-bound beta-amyloid. Exp. Neurol. 130, 56–66.
Hong, S., Beja-Glasser, V.F., Nfonoyim, B.M., Frouin, A., Li, S., Ramakrishnan, S., Merry, K.M., Shi, Q., Rosenthal, A., Barres, B.A., Lemere, C.A., Selkoe, D.J., Stevens, B., 2016. Complement and microglia mediate early synapse loss in Alzheimer mouse models. Science 352, 712–716.
Hu, Y., Chen, W., Wu, L., Jiang, L., Liang, N., Tan, L., Liang, M., Tang, N., 2019. TGF-beta1 restores hippocampal synaptic plasticity and memory in alzheimer model via the PI3K/Akt/Wnt/beta-Catenin signaling pathway. J. Mol. Neurosci. 67, 142–149.
Hughes, P.M., Botham, M.S., Frentzel, S., Mir, A., Perry, V.H., 2002. Expression of fractalkine (CX3CL1) and its receptor, CX3CR1, during acute and chronic inflammation in the rodent CNS. Glia 37, 314–327.
Iram, T., Trudler, D., Kain, D., Kanner, S., Galron, R., Vassar, R., Barzilai, A., Blinder, P., Fishelson, Z., Frenkel, D., 2016. Astrocytes from old Alzheimer's disease mice are impaired in Abeta uptake and in neuroprotection. Neurobiol. Dis. 96, 84–94.
Jack Jr., C.R., Albert, M.S., Knopman, D.S., McKhann, G.M., Sperling, R.A., Carrillo, M. C., Thies, B., Phelps, C.H., 2011. Introduction to the recommendations from the National Institute on Aging-Alzheimer's Association workgroups on diagnostic guidelines for Alzheimer's disease. Alzheimers Dement 7, 257–262.
Jack Jr., C.R., Bennett, D.A., Blennow, K., Carrillo, M.C., Dunn, B., Haeberlein, S.B., Holtzman, D.M., Jagust, W., Jessen, F., Karlawish, J., Liu, E., Molinuevo, J.L., Montine, T., Phelps, C., Rankin, K.P., Rowe, C.C., Scheltens, P., Siemers, E., Snyder, H.M., Sperling, R., 2018. NIA-AA Research Framework: toward a biological definition of Alzheimer's disease. Alzheimers Dement 14, 535–562.
Jensen, C.J., Massie, A., De Keyser, J., 2013. Immune players in the CNS: the astrocyte. J. Neuroimmune Pharmacol. 8, 824–839.
Jin, S.M., Cho, H.J., Kim, Y.W., Hwang, J.Y., Mook-Jung, I., 2012. Abeta-induced Ca(2+) influx regulates astrocytic BACE1 expression via calcineurin/NFAT4 signals. Biochem. Biophys. Res. Commun. 425, 649–655.
Johansson, A., Engler, H., Blomquist, G., Scott, B., Wall, A., Aquilonius, S.M., Langstrom, B., Askmark, H., 2007. Evidence for astrocytosis in ALS demonstrated by [11C](L)-deprenyl-D2 PET. J. Neurol. Sci. 255, 17–22.
John, G.R., Lee, S.C., Song, X., Rivieccio, M., Brosnan, C.F., 2005. IL-1-regulated responses in astrocytes: relevance to injury and recovery. Glia 49, 161–176.

Kahlson, M.A., Colodner, K.J., 2015. Glial tau pathology in tauopathies: functional consequences. J. Exp. Neurosci. 9, 43–50.
Katsouri, L., Georgopoulos, S., 2011. Lack of LDL receptor enhances amyloid deposition and decreases glial response in an Alzheimer's disease mouse model. PloS One 6, e21880.
Kim, D.H., Choi, S.M., Jho, J., Park, M.S., Kang, J., Park, S.J., Ryu, J.H., Jo, J., Kim, H.H., Kim, B.C., 2016. Infliximab ameliorates AD-associated object recognition memory impairment. Behav. Brain Res. 311, 384–391.
Kim, D., Tsai, L.H., 2009. Bridging physiology and pathology in AD. Cell 137, 997–1000.
Kim, J., Castellano, J.M., Jiang, H., Basak, J.M., Parsadanian, M., Pham, V., Mason, S.M., Paul, S.M., Holtzman, D.M., 2009. Overexpression of low-density lipoprotein receptor in the brain markedly inhibits amyloid deposition and increases extracellular A beta clearance. Neuron 64, 632–644.
Koenigsknecht-Talboo, J., Landreth, G.E., 2005. Microglial phagocytosis induced by fibrillar beta-amyloid and IgGs are differentially regulated by proinflammatory cytokines. J. Neurosci. 25, 8240–8249.
Koistinaho, M., Lin, S., Wu, X., Esterman, M., Koger, D., Hanson, J., Higgs, R., Liu, F., Malkani, S., Bales, K.R., Paul, S.M., 2004. Apolipoprotein E promotes astrocyte colocalization and degradation of deposited amyloid-beta peptides. Nat. Med. 10, 719–726.
Kraft, A.W., Hu, X., Yoon, H., Yan, P., Xiao, Q., Wang, Y., Gil, S.C., Brown, J., Wilhelmsson, U., Restivo, J.L., Cirrito, J.R., Holtzman, D.M., Kim, J., Pekny, M., Lee, J.M., 2013. Attenuating astrocyte activation accelerates plaque pathogenesis in APP/PS1 mice. Faseb. J. 27, 187–198.
Kumlien, E., Nilsson, A., Hagberg, G., Langstrom, B., Bergstrom, M., 2001. PET with 11C-deuterium-deprenyl and 18F-FDG in focal epilepsy. Acta Neurol. Scand. 103, 360–366.
Kurt, M.A., Davies, D.C., Kidd, M., 1999. beta-Amyloid immunoreactivity in astrocytes in Alzheimer's disease brain biopsies: an electron microscope study. Exp. Neurol. 158, 221–228.
Lam, A.G., Koppal, T., Akama, K.T., Guo, L., Craft, J.M., Samy, B., Schavocky, J.P., Watterson, D.M., Van Eldik, L.J., 2001. Mechanism of glial activation by S100B: involvement of the transcription factor NFkappaB. Neurobiol. Aging 22, 765–772.
Lansita, J.A., Mease, K.M., Qiu, H., Yednock, T., Sankaranarayanan, S., Kramer, S., 2017. Nonclinical development of ANX005: a humanized anti-C1q antibody for treatment of autoimmune and neurodegenerative diseases. Int. J. Toxicol. 36, 449–462.
Laywell, E.D., Dorries, U., Bartsch, U., Faissner, A., Schachner, M., Steindler, D.A., 1992. Enhanced expression of the developmentally regulated extracellular matrix molecule tenascin following adult brain injury. Proc. Natl. Acad. Sci. U. S. A. 89, 2634–2638.
Lee, C.H., Jeon, S.J., Cho, K.S., Moon, E., Sapkota, A., Jun, H.S., Ryu, J.H., Choi, J.W., 2018. Activation of glucagon-like peptide-1 receptor promotes neuroprotection in experimental autoimmune encephalomyelitis by reducing neuroinflammatory responses. Mol. Neurobiol. 55, 3007–3020.
Lee, H.J., Lee, J.O., Lee, Y.W., Kim, S.A., Seo, I.H., Han, J.A., Kang, M.J., Kim, S.J., Cho, Y.H., Park, J.J., Choi, J.I., Park, S.H., Kim, H.S., 2019. LIF, a novel myokine, protects against amyloid-beta-induced neurotoxicity via akt-mediated autophagy signaling in hippocampal cells. Int. J. Neuropsychopharmacol. 22, 402–414.
Lee, N.Y., Kim, Y., Kim, Y.S., Shin, J.H., Rubin, L.P., 2020. beta-Carotene exerts anti-colon cancer effects by regulating M2 macrophages and activated fibroblasts. J. Nutr. Biochem. 82, 108402.
Li, C., Zhao, R., Gao, K., Wei, Z., Yin, M.Y., Lau, L.T., Chui, D., Yu, A.C., 2011. Astrocytes: implications for neuroinflammatory pathogenesis of Alzheimer's disease. Curr. Alzheimer Res. 8, 67–80.
Lian, H., Litvinchuk, A., Chiang, A.C., Aithmitti, N., Jankowsky, J.L., Zheng, H., 2016. Astrocyte-microglia cross talk through complement activation modulates amyloid pathology in mouse models of Alzheimer's disease. J. Neurosci. 36, 577–589.
Lian, H., Yang, L., Cole, A., Sun, L., Chiang, A.C., Fowler, S.W., Shim, D.J., Rodriguez-Rivera, J., Taglialatela, G., Jankowsky, J.L., Lu, H.C., Zheng, H., 2015. NFkappaB-activated astroglial release of complement C3 compromises neuronal morphology and function associated with Alzheimer's disease. Neuron 85, 101–115.
Lian, H., Zheng, H., 2016. Signaling pathways regulating neuron-glia interaction and their implications in Alzheimer's disease. J. Neurochem. 136, 475–491.
Liddelow, S.A., Barres, B.A., 2017. Reactive astrocytes: production, function, and therapeutic potential. Immunity 46, 957–967.
Liddelow, S.A., Guttenplan, K.A., Clarke, L.E., Bennett, F.C., Bohlen, C.J., Schirmer, L., Bennett, M.L., Munch, A.E., Chung, W.S., Peterson, T.C., Wilton, D.K., Frouin, A., Napier, B.A., Panicker, N., Kumar, M., Buckwalter, M.S., Rowitch, D.H., Dawson, V. L., Dawson, T.M., Stevens, B., Barres, B.A., 2017. Neurotoxic reactive astrocytes are induced by activated microglia. Nature 541, 481–487.
Liu, Y., Liu, F., Iqbal, K., Grundke-Iqbal, I., Gong, C.X., 2008. Decreased glucose transporters correlate to abnormal hyperphosphorylation of tau in Alzheimer disease. FEBS Lett. 582, 359–364.
Lomakin, A., Teplow, D.B., Kirschner, D.A., Benedek, G.B., 1997. Kinetic theory of fibrillogenesis of amyloid beta-protein. Proc. Natl. Acad. Sci. U. S. A. 94, 7942–7947.
Long, J.M., Holtzman, D.M., 2019. Alzheimer disease: an update on pathobiology and treatment strategies. Cell 179, 312–339.
Mamik, M.K., Ghorpade, A., 2016. CXCL8 as a potential therapeutic target for HIV-associated neurocognitive disorders. Curr. Drug Targets 17, 111–121.
Martinez, F.O., Gordon, S., 2014. The M1 and M2 paradigm of macrophage activation: time for reassessment. F1000Prime Rep 6, 13.
McAlpine, F.E., Lee, J.K., Harms, A.S., Ruhn, K.A., Blurton-Jones, M., Hong, J., Das, P., Golde, T.E., LaFerla, F.M., Oddo, S., Blesch, A., Tansey, M.G., 2009. Inhibition of soluble TNF signaling in a mouse model of Alzheimer's disease prevents pre-plaque amyloid-associated neuropathology. Neurobiol. Dis. 34, 163–177.
McKhann, G.M., Knopman, D.S., Chertkow, H., Hyman, B.T., Jack Jr., C.R., Kawas, C.H., Klunk, W.E., Koroshetz, W.J., Manly, J.J., Mayeux, R., Mohs, R.C., Morris, J.C., Rossor, M.N., Scheltens, P., Carrillo, M.C., Thies, B., Weintraub, S., Phelps, C.H., 2011. The diagnosis of dementia due to Alzheimer's disease: recommendations from the National Institute on Aging-Alzheimer's Association workgroups on diagnostic guidelines for Alzheimer's disease. Alzheimers Dement 7, 263–269.
Medeiros, R., Kitazawa, M., Passos, G.F., Baglietto-Vargas, D., Cheng, D., Cribbs, D.H., LaFerla, F.M., 2013. Aspirin-triggered lipoxin A4 stimulates alternative activation of microglia and reduces Alzheimer disease-like pathology in mice. Am. J. Pathol. 182, 1780–1789.
Meeuwsen, S., Persoon-Deen, C., Bsibsi, M., Ravid, R., van Noort, J.M., 2003. Cytokine, chemokine and growth factor gene profiling of cultured human astrocytes after exposure to proinflammatory stimuli. Glia 43, 243–253.
Meucci, O., Fatatis, A., Simen, A.A., Miller, R.J., 2000. Expression of CX3CR1 chemokine receptors on neurons and their role in neuronal survival. Proc. Natl. Acad. Sci. U. S. A. 97, 8075–8080.
Morganti, J.M., Nash, K.R., Grimmig, B.A., Ranjit, S., Small, B., Bickford, P.C., Gemma, C., 2012. The soluble isoform of CX3CL1 is necessary for neuroprotection in a mouse model of Parkinson's disease. J Neurosci 32, 14592–14601.
Mrak, R.E., Griffin, W.S., 2001. Interleukin-1, neuroinflammation, and Alzheimer's disease. Neurobiol. Aging 22, 903–908.
Mulder, S.D., Veerhuis, R., Blankenstein, M.A., Nielsen, H.M., 2012. The effect of amyloid associated proteins on the expression of genes involved in amyloid-beta clearance by adult human astrocytes. Exp. Neurol. 233, 373–379.
Nagy, J.I., Li, W., Hertzberg, E.L., Marotta, C.A., 1996. Elevated connexin43 immunoreactivity at sites of amyloid plaques in Alzheimer's disease. Brain Res. 717, 173–178.
Nash, K.R., Lee, D.C., Hunt Jr., J.B., Morganti, J.M., Selenica, M.L., Moran, P., Reid, P., Brownlow, M., Guang-Yu Yang, C., Savalia, M., Gemma, C., Bickford, P.C., Gordon, M.N., Morgan, D., 2013. Fractalkine overexpression suppresses tau pathology in a mouse model of tauopathy. Neurobiol. Aging 34, 1540–1548.
Nash, K.R., Moran, P., Finneran, D.J., Hudson, C., Robinson, J., Morgan, D., Bickford, P. C., 2015. Fractalkine over expression suppresses alpha-synuclein-mediated neurodegeneration. Mol. Ther. 23, 17–23.
Nelson, P.T., Alafuzoff, I., Bigio, E.H., Bouras, C., Braak, H., Cairns, N.J., Castellani, R.J., Crain, B.J., Davies, P., Del Tredici, K., Duyckaerts, C., Frosch, M.P., Haroutunian, V., Hof, P.R., Hulette, C.M., Hyman, B.T., Iwatsubo, T., Jellinger, K.A., Jicha, G.A., Kovari, E., Kukull, W.A., Leverenz, J.B., Love, S., Mackenzie, I.R., Mann, D.M., Masliah, E., McKee, A.C., Montine, T.J., Morris, J.C., Schneider, J.A., Sonnen, J.A., Thal, D.R., Trojanowski, J.Q., Troncoso, J.C., Wisniewski, T., Woltjer, R.L., Beach, T. G., 2012. Correlation of Alzheimer disease neuropathologic changes with cognitive status: a review of the literature. J. Neuropathol. Exp. Neurol. 71, 362–381.
Nielsen, H.M., Mulder, S.D., Belien, J.A., Musters, R.J., Eikelenboom, P., Veerhuis, R., 2010. Astrocytic A beta 1-42 uptake is determined by A beta-aggregation state and the presence of amyloid-associated proteins. Glia 58, 1235–1246.
Nielsen, H.M., Veerhuis, R., Holmqvist, B., Janciauskiene, S., 2009. Binding and uptake of A beta1-42 by primary human astrocytes in vitro. Glia 57, 978–988.
Norden, D.M., Fenn, A.M., Dugan, A., Godbout, J.P., 2014. TGFbeta produced by IL-10 redirected astrocytes attenuates microglial activation. Glia 62, 881–895.
Norris, C.M., Kadish, I., Blalock, E.M., Chen, K.C., Thibault, V., Porter, N.M., Landfield, P. W., Kraner, S.D., 2005. Calcineurin triggers reactive/inflammatory processes in astrocytes and is upregulated in aging and Alzheimer's models. J. Neurosci. 25, 4649–4658.
Okada, S., Nakamura, M., Katoh, H., Miyao, T., Shimazaki, T., Ishii, K., Yamane, J., Yoshimura, A., Iwamoto, Y., Toyama, Y., Okano, H., 2006. Conditional ablation of Stat3 or Socs3 discloses a dual role for reactive astrocytes after spinal cord injury. Nat. Med. 12, 829–834.
Olabarria, M., Noristani, H.N., Verkhratsky, A., Rodriguez, J.J., 2010. Concomitant astroglial atrophy and astrogliosis in a triple transgenic animal model of Alzheimer's disease. Glia 58, 831–838.
Olsen, M., Aguilar, X., Sehlin, D., Fang, X.T., Antoni, G., Erlandsson, A., Syvanen, S., 2018. Astroglial responses to amyloid-beta progression in a mouse model of Alzheimer's disease. Mol. Imag. Biol. 20, 605–614.
Orre, M., Kamphuis, W., Osborn, L.M., Jansen, A.H.P., Kooijman, L., Bossers, K., Hol, E. M., 2014. Isolation of glia from Alzheimer's mice reveals inflammation and dysfunction. Neurobiol. Aging 35, 2746–2760.
Osborn, L.M., Kamphuis, W., Wadman, W.J., Hol, E.M., 2016. Astrogliosis: an integral player in the pathogenesis of Alzheimer's disease. Prog. Neurobiol. 144, 121–141.
Owen, J.B., Di Domenico, F., Sultana, R., Perluigi, M., Cini, C., Pierce, W.M., Butterfield, D.A., 2009. Proteomics-determined differences in the concanavalin-A-fractionated proteome of hippocampus and inferior parietal lobule in subjects with Alzheimer's disease and mild cognitive impairment: implications for progression of AD. J. Proteome Res. 8, 471–482.
Pabon, M.M., Bachstetter, A.D., Hudson, C.E., Gemma, C., Bickford, P.C., 2011. CX3CL1 reduces neurotoxicity and microglial activation in a rat model of Parkinson's disease. J. Neuroinflammation 8, 9.
Pasqualetti, P., Bonomini, C., Dal Forno, G., Paulon, L., Sinforiani, E., Marra, C., Zanetti, O., Rossini, P.M., 2009. A randomized controlled study on effects of ibuprofen on cognitive progression of Alzheimer's disease. Aging Clin. Exp. Res. 21, 102–110.
Pekny, M., Pekna, M., Messing, A., Steinhauser, C., Lee, J.M., Parpura, V., Hol, E.M., Sofroniew, M.V., Verkhratsky, A., 2016. Astrocytes: a central element in neurological diseases. Acta Neuropathol. 131, 323–345.
Pellerin, L., Magistretti, P.J., 1994. Glutamate uptake into astrocytes stimulates aerobic glycolysis: a mechanism coupling neuronal activity to glucose utilization. Proc. Natl. Acad. Sci. U. S. A. 91, 10625–10629.
Pereira, C.F., Middel, J., Jansen, G., Verhoef, J., Nottet, H.S., 2001. Enhanced expression of fractalkine in HIV-1 associated dementia. J. Neuroimmunol. 115, 168–175.

Perez-Nievas, B.G., Serrano-Pozo, A., 2018. Deciphering the astrocyte reaction in Alzheimer's disease. Front. Aging Neurosci. 10, 114.
Pihlaja, R., Koistinaho, J., Malm, T., Sikkila, H., Vainio, S., Koistinaho, M., 2008. Transplanted astrocytes internalize deposited beta-amyloid peptides in a transgenic mouse model of Alzheimer's disease. Glia 56, 154–163.
Pitter, K.L., Tamagno, I., Feng, X., Ghosal, K., Amankulor, N., Holland, E.C., Hambardzumyan, D., 2014. The SHH/Gli pathway is reactivated in reactive glia and drives proliferation in response to neurodegeneration-induced lesions. Glia 62, 1595–1607.
Qi, Y., Klyubin, I., Cuello, A.C., Rowan, M.J., 2018. NLRP3-dependent synaptic plasticity deficit in an Alzheimer's disease amyloidosis model in vivo. Neurobiol. Dis. 114, 24–30.
Querol-Vilaseca, M., Colom-Cadena, M., Pegueroles, J., San Martin-Paniello, C., Clarimon, J., Belbin, O., Fortea, J., Lleo, A., 2017. YKL-40 (Chitinase 3-like I) is expressed in a subset of astrocytes in Alzheimer's disease and other tauopathies. J. Neuroinflammation 14, 118.
Ribe, E.M., Serrano-Saiz, E., Akpan, N., Troy, C.M., 2008. Mechanisms of neuronal death in disease: defining the models and the players. Biochem. J. 415, 165–182.
Ries, M., Sastre, M., 2016. Mechanisms of abeta clearance and degradation by glial cells. Front. Aging Neurosci. 8, 160.
Rogers, J., Kirby, L.C., Hempelman, S.R., Berry, D.L., McGeer, P.L., Kaszniak, A.W., Zalinski, J., Cofield, M., Mansukhani, L., Willson, P., Kogan, F., 1993. Clinical trial of indomethacin in Alzheimer's disease. Neurology 43, 1609–1611.
Rossi, F., Bianchini, E., 1996. Synergistic induction of nitric oxide by beta-amyloid and cytokines in astrocytes. Biochem. Biophys. Res. Commun. 225, 474–478.
Rossner, S., Lange-Dohna, C., Zeitschel, U., Perez-Polo, J.R., 2005. Alzheimer's disease beta-secretase BACE1 is not a neuron-specific enzyme. J. Neurochem. 92, 226–234.
Rubio-Perez, J.M., Morillas-Ruiz, J.M., 2012. A review: inflammatory process in Alzheimer's disease, role of cytokines. Sci. World J. 756357, 2012.
Russo, I., Caracciolo, L., Tweedie, D., Choi, S.H., Greig, N.H., Barlati, S., Bosetti, F., 2012. 3,6'-Dithiothalidomide, a new TNF-alpha synthesis inhibitor, attenuates the effect of Abeta1-42 intracerebroventricular injection on hippocampal neurogenesis and memory deficit. J. Neurochem. 122, 1181–1192.
Sadick, J.S., Liddelow, S.A., 2019. Don't forget astrocytes when targeting Alzheimer's disease. Br. J. Pharmacol. 176, 3585–3598.
Saha, P., Sarkar, S., Paidi, R.K., Biswas, S.C., 2020. TIMP-1: a key cytokine released from activated astrocytes protects neurons and ameliorates cognitive behaviours in a rodent model of Alzheimer's disease. Brain Behav. Immun. 87, 804–819.
Sastre, M., Gentleman, S.M., 2010. NSAIDs: how they work and their prospects as therapeutics in Alzheimer's disease. Front. Aging Neurosci. 2, 20.
Schipper, H.M., Bennett, D.A., Liberman, A., Bienias, J.L., Schneider, J.A., Kelly, J., Arvanitakis, Z., 2006. Glial heme oxygenase-1 expression in Alzheimer disease and mild cognitive impairment. Neurobiol. Aging 27, 252–261.
Scholl, M., Carter, S.F., Westman, E., Rodriguez-Vieitez, E., Almkvist, O., Thordardottir, S., Wall, A., Graff, C., Langstrom, B., Nordberg, A., 2015. Early astrocytosis in autosomal dominant Alzheimer's disease measured in vivo by multi-tracer positron emission tomography. Sci. Rep. 5, 16404.
Schumann, G., Huell, M., Machein, U., Hocke, G., Fiebich, B.L., 1999. Interleukin-6 activates signal transducer and activator of transcription and mitogen-activated protein kinase signal transduction pathways and induces de novo protein synthesis in human neuronal cells. J. Neurochem. 73, 2009–2017.
Serrano-Pozo, A., Mielke, M.L., Gomez-Isla, T., Betensky, R.A., Growdon, J.H., Frosch, M. P., Hyman, B.T., 2011. Reactive glia not only associates with plaques but also parallels tangles in Alzheimer's disease. Am. J. Pathol. 179, 1373–1384.
Shi, J.Q., Shen, W., Chen, J., Wang, B.R., Zhong, L.L., Zhu, Y.W., Zhu, H.Q., Zhang, Q.Q., Zhang, Y.D., Xu, J., 2011. Anti-TNF-alpha reduces amyloid plaques and tau phosphorylation and induces CD11c-positive dendritic-like cell in the APP/PS1 transgenic mouse brains. Brain Res. 1368, 239–247.
Simpson, I.A., Chundu, K.R., Davies-Hill, T., Honer, W.G., Davies, P., 1994. Decreased concentrations of GLUT1 and GLUT3 glucose transporters in the brains of patients with Alzheimer's disease. Ann. Neurol. 35, 546–551.
Sofroniew, M.V., 2009. Molecular dissection of reactive astrogliosis and glial scar formation. Trends Neurosci. 32, 638–647.
Sofroniew, M.V., 2014. Astrogliosis. Cold Spring Harb Perspect Biol 7, a020420.
Sofroniew, M.V., 2015. Astrocyte barriers to neurotoxic inflammation. Nat. Rev. Neurosci. 16, 249–263.
Solmaz, V., Cinar, B.P., Yigitturk, G., Cavusoglu, T., Taskiran, D., Erbas, O., 2015. Exenatide reduces TNF-alpha expression and improves hippocampal neuron numbers and memory in streptozotocin treated rats. Eur. J. Pharmacol. 765, 482–487.
Sperling, R.A., Aisen, P.S., Beckett, L.A., Bennett, D.A., Craft, S., Fagan, A.M., Iwatsubo, T., Jack Jr., C.R., Kaye, J., Montine, T.J., Park, D.C., Reiman, E.M., Rowe, C.C., Siemers, E., Stern, Y., Yaffe, K., Carrillo, M.C., Thies, B., Morrison-Bogorad, M., Wagster, M.V., Phelps, C.H., 2011. Toward defining the preclinical stages of Alzheimer's disease: recommendations from the National Institute on Aging-Alzheimer's Association workgroups on diagnostic guidelines for Alzheimer's disease. Alzheimers Dement 7, 280–292.
Steelman, A.J., Smith 3rd, R., Welsh, C.J., Li, J., 2013. Galectin-9 protein is up-regulated in astrocytes by tumor necrosis factor and promotes encephalitogenic T-cell apoptosis. J. Biol. Chem. 288, 23776–23787.
Sung, S., Yang, H., Uryu, K., Lee, E.B., Zhao, L., Shineman, D., Trojanowski, J.Q., Lee, V. M., Pratico, D., 2004. Modulation of nuclear factor-kappa B activity by indomethacin influences A beta levels but not A beta precursor protein metabolism in a model of Alzheimer's disease. Am. J. Pathol. 165, 2197–2206.
Swerdlow, R.H., 2007a. Is aging part of Alzheimer's disease, or is Alzheimer's disease part of aging? Neurobiol. Aging 28, 1465–1480.
Swerdlow, R.H., 2007b. Pathogenesis of Alzheimer's disease. Clin. Interv. Aging 2, 347–359.
Szczepanik, A.M., Ringheim, G.E., 2003. IL-10 and glucocorticoids inhibit Abeta(1-42)- and lipopolysaccharide-induced pro-inflammatory cytokine and chemokine induction in the central nervous system. J Alzheimers Dis 5, 105–117.
Tarczyluk, M.A., Nagel, D.A., Rhein Parri, H., Tse, E.H., Brown, J.E., Coleman, M.D., Hill, E.J., 2015. Amyloid beta 1-42 induces hypometabolism in human stem cell-derived neuron and astrocyte networks. J. Cerebr. Blood Flow Metabol. 35, 1348–1357.
Thal, D.R., Schultz, C., Dehghani, F., Yamaguchi, H., Braak, H., Braak, E., 2000. Amyloid beta-protein (Abeta)-containing astrocytes are located preferentially near N-terminal-truncated Abeta deposits in the human entorhinal cortex. Acta Neuropathol. 100, 608–617.
Tobinick, E., Gross, H., Weinberger, A., Cohen, H., 2006. TNF-alpha modulation for treatment of Alzheimer's disease: a 6-month pilot study. MedGenMed 8, 25.
Tsai, K.J., Tsai, Y.C., Shen, C.K., 2007. G-CSF rescues the memory impairment of animal models of Alzheimer's disease. J. Exp. Med. 204, 1273–1280.
Tyacke, R.J., Myers, J.F.M., Venkataraman, A., Mick, I., Turton, S., Passchier, J., Husbands, S.M., Rabiner, E.A., Gunn, R.N., Murphy, P.S., Parker, C.A., Nutt, D.J., 2018. Evaluation of (11)C-BU99008, a PET ligand for the Imidazoline2 binding site in human brain. J. Nucl. Med. 59, 1597–1602.
Valori, C.F., Guidotti, G., Brambilla, L., Rossi, D., 2019. Astrocytes: emerging therapeutic targets in neurological disorders. Trends Mol. Med. 25, 750–759.
Vandenabeele, P., Fiers, W., 1991. Is amyloidogenesis during Alzheimer's disease due to an IL-1-/IL-6-mediated 'acute phase response' in the brain? Immunol. Today 12, 217–219.
Verkhratsky, A., Zorec, R., Parpura, V., 2017. Stratification of astrocytes in healthy and diseased brain. Brain Pathol. 27, 629–644.
Wang, Y., Fu, Y., Xue, S., Ai, A., Chen, H., Lyu, Q., Kuang, Y., 2014. The M2 polarization of macrophage induced by fractalkine in the endometriotic milieu enhances invasiveness of endometrial stromal cells. Int. J. Clin. Exp. Pathol. 7, 194–203.
Wang, D., Zhang, X., Wang, M., Zhou, D., Pan, H., Shu, Q., Sun, B., 2018. Early activation of astrocytes does not affect amyloid plaque load in an animal model of Alzheimer's disease. Neurosci Bull 34, 912–920.
Wang, L., Benzinger, T.L., Su, Y., Christensen, J., Friedrichsen, K., Aldea, P., McConathy, J., Cairns, N.J., Fagan, A.M., Morris, J.C., Ances, B.M., 2016. Evaluation of tau imaging in staging alzheimer disease and revealing interactions between beta-amyloid and tauopathy. JAMA Neurol 73, 1070–1077.
Wang, X., Deckert, M., Xuan, N.T., Nishanth, G., Just, S., Waisman, A., Naumann, M., Schluter, D., 2013. Astrocytic A20 ameliorates experimental autoimmune encephalomyelitis by inhibiting NF-kappaB- and STAT1-dependent chemokine production in astrocytes. Acta Neuropathol. 126, 711–724.
Wanner, I.B., Anderson, M.A., Song, B., Levine, J., Fernandez, A., Gray-Thompson, Z., Ao, Y., Sofroniew, M.V., 2013. Glial scar borders are formed by newly proliferated, elongated astrocytes that interact to corral inflammatory and fibrotic cells via STAT3-dependent mechanisms after spinal cord injury. J. Neurosci. 33, 12870–12886.
Wu, H.Y., Hudry, E., Hashimoto, T., Kuchibhotla, K., Rozkalne, A., Fan, Z., Spires-Jones, T., Xie, H., Arbel-Ornath, M., Grosskreutz, C.L., Bacskai, B.J., Hyman, B.T., 2010. Amyloid beta induces the morphological neurodegenerative triad of spine loss, dendritic simplification, and neuritic dystrophies through calcineurin activation. J. Neurosci. 30, 2636–2649.
Wyss-Coray, T., Loike, J.D., Brionne, T.C., Lu, E., Anankov, R., Yan, F., Silverstein, S.C., Husemann, J., 2003. Adult mouse astrocytes degrade amyloid-beta in vitro and in situ. Nat. Med. 9, 453–457.
Xiao, Q., Yan, P., Ma, X., Liu, H., Perez, R., Zhu, A., Gonzales, E., Burchett, J.M., Schuler, D.R., Cirrito, J.R., Diwan, A., Lee, J.M., 2014. Enhancing astrocytic lysosome biogenesis facilitates Abeta clearance and attenuates amyloid plaque pathogenesis. J. Neurosci. 34, 9607–9620.
Yamaguchi, H., Sugihara, S., Ogawa, A., Saido, T.C., Ihara, Y., 1998. Diffuse plaques associated with astroglial amyloid beta protein, possibly showing a disappearing stage of senile plaques. Acta Neuropathol. 95, 217–222.
Yamamoto, M., Kiyota, T., Horiba, M., Buescher, J.L., Walsh, S.M., Gendelman, H.E., Ikezu, T., 2007. Interferon-gamma and tumor necrosis factor-alpha regulate amyloid-beta plaque deposition and beta-secretase expression in Swedish mutant APP transgenic mice. Am. J. Pathol. 170, 680–692.
Yun, S.P., Kam, T.I., Panicker, N., Kim, S., Oh, Y., Park, J.S., Kwon, S.H., Park, Y.J., Karuppagounder, S.S., Park, H., Oh, N., Kim, N.A., Lee, S., Brahmachari, S., Mao, X., Lee, J.H., Kumar, M., An, D., Kang, S.U., Lee, Y., Lee, K.C., Na, D.H., Kim, D., Lee, S. H., Roschke, V.V., Liddelow, S.A., Mari, Z., Barres, B.A., Dawson, V.L., Dawson, T.M., Ko, H.S., 2018. Block of A1 astrocyte conversion by microglia is neuroprotective in models of Parkinson's disease. Nat. Med. 24, 931–938.
Zamanian, J.L., Xu, L., Foo, L.C., Nouri, N., Zhou, L., Giffard, R.G., Barres, B.A., 2012. Genomic analysis of reactive astrogliosis. J. Neurosci. 32, 6391–6410.
Zimmer, E.R., Parent, M.J., Souza, D.G., Leuzy, A., Lecrux, C., Kim, H.I., Gauthier, S., Pellerin, L., Hamel, E., Rosa-Neto, P., 2017. [(18)F]FDG PET signal is driven by astroglial glutamate transport. Nat. Neurosci. 20, 393–395.
Zulfiqar, S., Garg, P., Nieweg, K., 2019. Contribution of astrocytes to metabolic dysfunction in the Alzheimer's disease brain. Biol. Chem. 400, 1113–1127.

Glossary

Alzheimer's disease (AD): According to NIA-AA 2018 guidelines, AD refers to the mandatory presence of both abnormal levels of Aβ and pathologic tau biomarkers *in vivo*

Alzheimer's pathologic change: It is an early stage in the Alzheimer's continuum defined by the presence of an abnormal Aβ biomarker along with normal level of pathologic tau biomarker *in vivo*

Alzheimer's continuum: It is an umbrella term that includes individuals with biomarker profiles of either Alzheimer's pathologic change or AD

Amyloid β (Aβ) plaque: One of the histopathological features of Alzheimer's disease consisting of insoluble amyloid β of β-sheet conformation

Astrocytoma: a form of cancer that originate in the astrocytes in the brain

Astroglial atrophy: Decrease or shrinkage in the size of astrocytes in response to various stimuli, often associated with loss of functions

Astroglial hypertrophy: Increase in the size of astrocytes in response to various stimuli, often associated with gain of new functions

Astrocyte reaction/reactivity: is a highly heterogeneous phenomenon where the astrocytes undergo a set of morphological, molecular and functional changes with a characteristic secretome profile in response to a CNS insult

Astrocytic scar: primarily comprises of rapidly proliferated reactive astrocytes forming a compact structural barrier that isolates a region of tissue damage such as damaged neurons from the surrounding healthy cells in the CNS. It is also conventionally referred as **glial scars**

Blood brain barrier (BBB): A highly selective and protective physiological sieve that creates a separating memebrane between the circulating blood and the brain regulating the exchange of various molecules and ions between the two segments

Chemokines: They are considered as a small family of chemoattractant cytokines that are highly implicated in directing astrocytes towards areas of neuroinflammation and in regulating microglial migration in the CNS, especially during a pathological insult

Complement proteins: are the main players of the complement system that are involved in attacking intruding subjects and support phagocytosis of waste products contributing towards protection and cure of the host

Cytokines: a heterogeneous group of small proteins (molecular weights range from 8 kDa to 40 kDa) that are the major cellular mediators synthesized and secreted by almost all nucleated cells and are rapidly altered in response to any CNS insult

Glial fibrillary acidic protein (GFAP): an intermediate filament protein that is expressed mainly within astrocytes and its expression is increased in reactive astrocytes. It is often used as an astrocyte marker.

Gliotransmitters: Chemical transmitters secreted by astrocytes that include D-serine, glutamate and ATP

Microgliosis: It is a complex reaction of microglia to CNS insults marked by changes in morphology, gene expression and surface phenotype along with an increase in their number near the site of the insult. It is alternatively referred as **microglial activation**

Neurofibrillary tangles: One of the histopathological features of Alzheimer's disease, made up of insoluble aggregates of hyperphophorylated tau proteins

Neutropenia: It is a medical condition in a person with low levels of neutrophils

Reactive astrocyte: is a heterogeneous population of astrocytes that appear in response to an abnormal situation in the brain and may have disparate effects on disease progression

Tau protein: It is a microtubule-associated protein found extensively in the neurons and is highly involved in the maintenance of microtubule stability and functions

Vimentin: Another commonly used marker of astrocytes whose expression increases in reactive astrocytes

Biomedicine & Pharmacotherapy 151 (2022) 113086

Contents lists available at ScienceDirect

Biomedicine & Pharmacotherapy

journal homepage: www.elsevier.com/locate/biopha

Medha Plus – A novel polyherbal formulation ameliorates cognitive behaviors and disease pathology in models of Alzheimer's disease

Ramesh Kumar Paidi [a,1], Sukanya Sarkar [a], Naqiya Ambareen [a,b], Subhas Chandra Biswas [a,b,*]

[a] Cell Biology and Physiology Division, CSIR-Indian Institute of Chemical Biology, 4 Raja S. C. Mullick Road, Kolkata 700032, India
[b] Academy of Scientific and Innovative Research (AcSIR), Headquarters, CSIR-HRDC Campus, Sector 19, Kamla Nehru Nagar, Ghaziabad 201002, India

ARTICLE INFO

Keywords:
Aβ
5XFAD
Cognitive behaviors
Polyherbal formulation
Apoptosis
Alzheimer's disease

ABSTRACT

Alzheimer's disease (AD) is a multi-faceted neurodegenerative disorder that leads to drastic cognitive impairments culminating in death. Pathologically, it is characterized by amyloid-β (Aβ) plaques, neurofibrillary tangles and neurodegeneration in brain. Complete cure of AD remains elusive to date. Available synthetic drugs only provide symptomatic reliefs targeting single molecule, hence, are unable to address the multi-factorial aspects in AD pathogenesis. It is imperative to develop combinatorial drugs that address the multiple molecular targets in AD. We show a unique polyherbal formulation of Brahmi, Mandukaparni, Shankhpushpi, Yastimadhu, Kokilaksha and Shunthi called 'Medha Plus' (MP), conventionally used for improving memory and reducing anxiety, was able to ameliorate cognitive deficits and associated pathological hallmarks of AD. Viability assays revealed that MP prevented Aβ-induced loss of neurites as well as neuronal apoptosis in cellular models. An array of behavioral studies showed that MP was able to recover AD-associated memory deficits in both Aβ-injected rats and 5XFAD mice. Immunohistochemical studies further revealed that MP treatment reduced Aβ depositshpi and decreased apoptotic cell death in the hippocampus. Enzymatic assays demonstrated anti-oxidative and anti-acetyl cholinesterase properties of MP especially in hippocampus of Aβ-injected rats. An underlying improvement in synaptic plasticity was observed with MP treatment in 5XFAD mice along with an increased expression of phospho-Akt at serine 473 indicating a role of PI3K/Akt signaling in correcting these synaptic deficits. Thus, our strong experiment-driven approach shows that MP is an incredible combinatorial drug that targets multiple molecular targets with exemplary neuroprotective properties and is proposed for clinical trial.

1. Introduction

Alzheimer's disease (AD) is a chronic and progressive neurodegenerative disorder leading to cognitive and memory disabilities [1]. Accumulation of amyloid-β (Aβ) plaques and formation of neurofibrillary tangles (NFT) in the brain tissues are considered as the main pathological features of AD [2]. One of the major underlying causes is considered to be excessive ROS production due to oxidative stress, often correlated to aging [3]. The present treatments mainly comprise of palliative therapy which only partially lowers the rate of memory and learning dysfunctions in AD. Inhibition of acetylcholine esterase (AChE) activity is the most common therapeutic strategy with limited disease-modifying effect [4]. Several AChE inhibitors namely Donepezil [5], Rivastigmine [6] and Galantamine [7] are currently being used against AD. An NMDA receptor antagonist, Memantine [8] is often used as an alternative or in combination. However, these drugs are not bereft of side-effects and are only nominally helpful. There has been high rate of failures of several candidate drugs in clinical trials. Recently, FDA approved a drug Aducanumab (Aβ antibody) using the accelerated approval pathway which is showing some promise yet it is only effective in the early stages of the disease [9]. Attacking the disease from all possible avenues is the need of the hour. Lifestyle changes form an important aspect of present-day AD prevention strategies. This may include taking food-supplements or organic medicines on a daily basis

Abbreviations: AD, Alzheimer's disease; Aβ, amyloid-β; NFT, neurofibrillary tangle; BBB, blood-brain barrier; GABA, gamma-Aminobutyric acid; LTP, long-term potentiation; LTD, long-term depression; LPS, lipopolysaccharides; BDNF, brain-derived neurotrophic factor; PD, Parkinson's disease; NMDA, N-methyl-D-aspartate; ROS, reactive oxygen species; AChE, acetylcholinesterase.

* Corresponding author at: Cell Biology and Physiology Division, CSIR-Indian Institute of Chemical Biology, 4 Raja S. C. Mullick Road, Kolkata 700032, India.
E-mail address: subhasbiswas@iicb.res.in (S.C. Biswas).
[1] Current address: Department of Neurological Sciences, RUSH University Medical Center, Chicago, IL 60612, USA.

https://doi.org/10.1016/j.biopha.2022.113086
Received 15 February 2022; Received in revised form 29 April 2022; Accepted 4 May 2022

[10–14]. Herbal medicines are free from side effects, completely natural, affordable, can be taken early-on in life and in the long run may inhibit the occurrence of several age-related neurodegenerative disorders including AD or even complement the regular process of therapy.

Numerous reports suggest that medicinal plants have possible neuroprotective properties and some have been tested at preclinical levels and few have even advanced to clinical trials [15]. From ancient times 'Ayurvedic' or medicinal herbs have traditionally been applied for the treatment and management of neurodegenerative diseases in several countries including India. They are encouraging candidates in the advancement of safe, effective and multi-targeted therapies for the treatment of multifaceted neurological disorders such as AD. Phytochemical constituents including sterols, tannins, lignans, flavonoids, polyphenols, triterpenes and alkaloids in medicinal plants demonstrate several beneficial properties such as anti-inflammatory, anti--amyloidogenic, antioxidant, anti-cholinesterase, and hypolipidemic roles.

Bacopa monnieri, commonly known as Brahmi, belongs to the family Scrophulariaceae and has been widely implicated in the improvement of brain function and to treat epilepsy [16]. Earlier *in vitro* and *in vivo* studies showed that it has an antioxidant property as well [17]. *B. monnieri* extracts enhance memory and learning functions in various transgenic animal AD models by lowering the Aβ levels in the cortex and the hippocampus [18,19]. Reportedly, it lowers the whole brain AChE activity in aged mice and in cultured neurons [20,21]. Bacoside A is a saponin that is the major bioactive component of *B. monnieri* extract among others. Interestingly, it also inhibits ageing-associated etiologies in rodents, including reductions in brain acetyl choline, serotonin, and dopamine levels, elevation in neuroinflammatory cytokines, oxidative stress and lipofuscin levels, and abnormalities in hippocampal neuron morphology [18,22,23].

Centella asiatica (Mandukaparni) is enriched in saponin, belonging to Umbelliferae family. Accumulating evidence indicates that it possesses numerous health benefits including nerve stimulation, as a sedative tranquilizer, but particularly valued as a revitalizing herb in rejuvenation and enhancement of memory abilities. *C. asiatica* induces significant improvement in cognitive functions across different behavioral parameters in rodent models [24,25]. Moreover, asiatic acid, pentacyclic triterpene in *C. asiatica*, can cross the blood brain barrier (BBB) and inhibit mitochondrial impairment in a focal cerebral ischemia mouse model [26]. It improves hippocampal-dependent spatial memory by inducing hippocampal neurogenesis in adult rats [19]. *C. asiatica* enhances the dendritic arborization in CA3 region of the hippocampus [20]. Further, it acts as a free radical scavenger and is valued for its remarkable antioxidant properties [27].

Shankhpushpi or *Convolvulus pluricaulis* Choisy belonging to the family Convolvulaceae has been traditionally used in the management of disorders of the nervous system. It is used as a nervine tonic to boost memory and learning functions [28]. It especially demonstrates anti-depressant-like effects due to its ability to reduce pro-inflammatory cytokines namely IL-1β, IL-6 and TNF-α levels in a chronic depression model in rat [29]. It displays anti-oxidant properties, improves BBB integrity and neuronal morphology in a rat model of cerebral ischemia reperfusion injury [30]. Notably, *Convolvulus pluricaulis* extract improves synaptic plasticity by enhancing LTP/LTD ratio in healthy rat brain hippocampus. Electrophysiology experiments *ex vivo* also revealed that an active chemical component of *C. pluricaulis* called scopoletin is the major mediator in synaptic improvement observed in the rats [31]. Recently, all the above three herbs have been reviewed for their implications in AD [32].

The aqueous extract from the root of *Glycerrhiza glabra* or Yastimadhu of the family Papilionaceae shows improvement in learning and memory functions in diazepam and scopolamine induced amnestic rat models [33–35] and displays anti-inflammatory properties in LPS-induced mice [36]. Glycyrrhizin is one of the active components of *Glycerrhiza glabra* that attributes for its sweet taste. It reduces GABA and histamine levels in fusidic acid treated rats [37]. These effects were associated with an enhanced bioenergetics status of neurons and improvement in BDNF levels in the brain. Higher dose of the glycyrrhizin showed correction in FA induced behavioral alterations and oxidative damage via restoration of caspase-3 activity [38]. It also alleviated vascular dementia related cognitive deficits in rats resulting from oxidative damage and inhibition of voltage-gated ion channels in hippocampal CA1 neurons of a rat model [39].

Zingiber officinale is the scientific name for ginger or Sunthi and belongs to the Zingiberaceae family. It has been reported that an aqueous extract from the rhizomes of ginger has potent anti-cholinesterase activity, anti-inflammatory, antioxidant and neuroprotective capabilities [40]. Due to these excellent features, it corrects natural ageing induced amnesia [41]. Moreover, a unique mixture of extracts from *Cyperusrotundus* and *Zingiber officinale* can reverse the AF64A-mediated age-related dementia in male Wistar rats by improving cholinergic function and decreasing oxidative stress [42]. Extract of *Zingiber officinale* exhibits neuroprotective effect on dopaminergic neurons (DA) in a PD rodent model [43]. 6-shogaol, the major bioactive constituent of *Zingiber officinale*, exerts prominent neuroprotective effects in LPS treated astrocytes and rodent models of PD, in transient global ischemia and in LPS-mediated neuroinflammation. It could attenuate inflammatory glial cell reactivation in intrahippocampal Aβ-injected mice as well as alleviated Aβ or scopolamine induced memory deficits [44]. Its anti-inflammatory roles are further supported by its inhibitory effects on the production of prostaglandin E (2) [PGE(2)] and pro-inflammatory cytokines, such as interleukin 1β (IL-1β) and tumor necrosis factor–α (TNF-α). Additionally, it can downregulate cyclo-oxygenase-2 (COX-2), P-38 mitogen activated protein kinase (MAPK), and nuclear factor kappa B (NF–κB) expressions [37,42]. 6-shogaol reportedly acts as a CysLT1R/cathepsin B inhibitor and diminishes Aβ plaque deposition in APPSw/PS1-dE9 transgenic model of AD [45].

Roots, leaves and seeds of Kokilaksha or *Hygrophila schulli* belonging to Acanthaceae family have traditionally been used as diuretic agents. Extracts of *H. schulli* show antioxidative properties by enhancing superoxide dismutase and catalase activities [46]. Recently, an ethanolic extract of the herb demonstrated anti-inflammatory and anti-nociceptive activities in a paw edema mice model [47]. Although there is no direct evidence of any neuroprotective role of *H. schulli* in models of neurodegenerative diseases, its extracts are enriched in fixed oil containing linoleic and oleic acid [48] which have implications in neuroprotection. Linoleic acid protects against Aβ-induced neuroinflammation, detrimental glial reactivation, oxidative stress and cognitive impairments in rats [49] and mice [50].

The above-mentioned herbs display several neuroprotective properties including anti-inflammatory, anti-oxidative properties, promote synaptic plasticity, improve learning and memory, act as AChE inhibitors, lower Aβ levels in brain, improve mitochondrial bioenergetics, dendritic arborization, BBB integrity, neuronal morphology and in reduction of GABA levels. However, the extent to which each herb offers these benefits at an individual level is limited. We believe it would be extremely interesting to study their effects in combination to address multiple ailments associated with AD and to optimize all the neuroprotective benefits the herbs can offer. No study to date has extensively investigated the neuroprotective effects of a combinatorial formulation of all the above-mentioned herbs from a neurodegenerative disease aspect. Parker Robinson Pvt. Ltd. (India) has prepared a unique combination of aqueous extracts of six therapeutic plants indigenous to South-East Asia and hugely propagated across India - Brahmi, Mandukaparni, Shankhpushpi, Yastimadhu, Kokilaksha and Shunthi formulated as a sirup called 'Medha Plus' (MP). This novel polyherbal formulation, already marketed for general memory improvement in human, poses as an exciting candidate for investigating a combinatorial effect of the six herbal plants in AD prevention or therapy. In this work, we extensively study the different effects of MP in both *in vitro* and *in vivo* models of AD especially focusing on its role in alleviating AD-related

cognitive deficits.

2. Materials and methods

2.1. Materials

Neurobasal medium, Dulbecco's modified Eagle's medium (DMEM), DMEM-F12, B27 supplement, Fetal Bovine Serum (FBS), Horse Serum, Penstrep antibiotic, Lipofectamine 2000 and, AlexaFluor were procured from Thermo Fisher Scientific (Waltham, MA, USA). Poly-D-lysine (PDL), insulin, progesterone, putrescine, selenium, apo-transferrin, nerve growth factor (NGF), Di-methyl sulfoxide (DMSO), para-formaldehyde (PFA), acetylthiocholine iodide, actin antibody and, 1,1,1,3,3,3 hexafluoro-2-propanol (HFIP) were bought from Sigma-Aldrich (St.Louis, MO, USA). $A\beta_{1-42}$ was procured from Alexotech (Umea, Vasterbotten County, Sweden). Horseradish peroxidase conjugated secondary antibodies were obtained from Cell Signaling Technology (MA, USA). MAP2 antibody was purchased from SantaCruz Biotechnology (Santa Cruz, CA, USA). Polyvinylidene difluoride membrane (PVDF) membrane was bought from GE Healthcare (Buckinghamshire, UK). ECL reagent was obtained from Takara Bio Inc. (Japan). Sodium dodecyl sulfate (SDS) was procured from Merck (Darmstadt, Germany). Trypsin and Bovine Serum Albumin (BSA) were brought from Sisco Research Laboratories Pvt. Ltd (Mumbai, India). 'Medha Plus' Syrup' consisting of Brahmi, Mandukaparni, Shankhpushpi, Yastimadhu, Kokilaksha and Shunthi (the composition and major active components of each plant are given in Table 1) and its raw ingredients were from Parker Robinson Pvt Ltd. (India). The research and development work were undertaken for value addition of the product "Medha Plus". All other fine chemicals and primary culture instruments used in the present study were bought from standard local suppliers.

2.2. Cell culture

2.2.1. Pheochromocytoma-12 (PC-12) cell culture

PC-12 cells were initially isolated from rat adrenal medulla and can be differentiated into neuron-like cells. The cell line was obtained from ATCC and was maintained in DMEM supplemented with 10% HS and 5% FBS and passaged at confluency. For their differentiation, a differentiating media composed of basic DMEM supplemented with NGF (50 ng/ml) and 1% HS was added to cells and changed every alternative day for five days. On day 6, the differentiated cells were treated.

2.2.2. SHSY5Y cell culture

SHSY5Y is a cell line initially derived as a sub-clone of the original cell line named SK-N-SH isolated from the bone marrow of a four-year old female with neuroblastoma and upon differentiation can be used as a human neuronal cell line. The cell line was maintained in DMEM supplemented with 10% FBS and passaged at confluency. For differentiation, the medium was changed with the basic DMEM media supplemented with 10 μM of all-trans retinoic acid and 1% FBS every alternate day for 7–8 days until the cell is fully differentiated. All experiments were performed on the 9th day following differentiation.

2.2.3. Primary cortical neuron culture

Rat primary cortical neurons were cultured as per the method published previously [51,52]. Briefly, the neocortex region was isolated from E16–18 rat and meninges was removed. Following proper trituration to obtain a suspension of single cells, cell number was quantified and plated in DMEM/F12 [1:1] media supplemented with 100 μg/ml transferrin, 25 μg/ml insulin, 6 mg/ml D-glucose, 20 nM progesterone, 30 nM selenium and 60 μM putrescine onto PDL-coated tissue culture plates. The cells were maintained in same media with1:1 media change every 48 h for six days. All treatments were given on the 7th day.

Table 1
The composition and major active components of each plant present in Medha Plus.

S. no.	Name of the plant	Common name and family	Major active components	Refs.
1	*Bacopa monnieri*	Brahmi, Scrophulariaceae family	Bacoside A, bacoside B, bacogenin A1–A4, bacopasaponin C and bacopasides I and II, monnieraside I, monnieraside III, Monnierin, plantioside B, pseudojujubogenin. Other components are 3-O- [β-D-glucopyranosyl (1–3)-β-D-glucopyranosyl] Pseudojujubogenin, Wogonin, oroxindin luteolin, luteolin-7-glucoside, luteolin-7-glucuronide,apigenin-7-gluconide, nicotine, 3-formy1-4-hydroxy-2H-pyran. Bacosine, bacosterol, bacosterol 3-O-β-D-glucopyranoside, stigmasterol, stigmastanol. β-sitosterol, D-mannitol and other glycosides. The other chemicals are betulin and betulinic acids. Brahmine and herpestine, saponins, hersaponin and monnierin.	[16–23]
2	*Centella asiatica*	Mandukaparni, Umbelliferae family	Thankuniside and isothankuniside, asiaticoside A and B, Madecassoside, asiatic, madecassic, ascorbic, thankunic, pectic and brahmic acids. Other components are isobrahamic acid, brahmoside, isothankunic acid, glucosyl quercetin, 3-glucosyl kaempferol, 7-glucosylkaempferol and polyacetylenes.	[19,20, 24, 25–27]
3	*Convolvulus pluricaulis*	Shankhpushpi, Convolvulaceae family	Scopoletin, kaempferol-3-glucoside, kaempferol, 3,4-dihydroxycinnamic acids are the principal chemical components of the plant. Plant yields an alkaloid known as shankhpuspine. The other chemical components are β-sitosterol-β-D-glucoside, n-hexacosanol, n-triacontanol, n-dotriacontanol, n-octacosanol, n-triacotane,	[28–32]

(*continued on next page*)

Table 1 (*continued*)

S. no.	Name of the plant	Common name and family	Major active components	Refs.
			β-setosterol and microphyllic acid.	
4	*Glycerrhiza glabra*	Yastimadhu, Papilionacea Family	Glycyrrhizin, liquiritin, glycyrrhetinic acid. rhamnoglucoside. A Triterpenoid- liquoric acid from roots. Root extract estrogenic contains β- sitosterol and stigmasterol. It also contains herniarin and umbelliferone and flavones-liquiritin, liquiritigenin, isoliquiritin and isoliquiritigenin. The characteristic aroma of the volatile oil of liquorice is due to presence of a mixture of estragole, anethole, eugenol, indole, y-nonalactone and cumic alcohol	[33–38]
5	*Zingiber officinale*	Sunthi, Zingiberaceae family	Rhizomes of the plant contain acid oleoresin. Resin contains pungent principle gingerol, shogaols, gingeodiols, and gingediacetates. 6-Shogaol, 6- gingerol, zingiberol, β-phellandrene α-zingiberone, ar-curcumene, β-bisabolene. The other chemical components are also known from the rhizomes of ginger such as gingerenones A, B and C, isogingerenone B, hexahydrocurcumin, diarylheptanoids, gingerdiols, 6-ginge-sulfonic acid, ginger glycolipids A, B and C, gingerenones, (+)-angelicoidenol-2-O-β-D-glucopyranoside, geranial glycosides, α-santalol. β-endesmol, Nerolidol, farnesal, elemol, neral, geranial, α- and β-pinene, camphene, sabinene, myrcene, limonene,1,8-cineole, and aliphatic alkanes etc.	[39–45]
6	*Hygrophilaschulli*	Kokilaksha, Acanthaceae family	Linoleic and oleic acid. The other components are palmitic acid, stearic acids, myristic acids, polysaccharides, xylose, uronic acid, histidine, lysine, phenyl alanine and β-sitosterol. The aerial parts of the plant contain alkaloids, phytosterol, essential oil, mucilage, triterpene, lupeol, stigmasterol etc.	[46–50]

Table 1 (*continued*)

S. no.	Name of the plant	Common name and family	Major active components	Refs.

2.3. Dose calculation

MP composition in 10 ml syrup includes water extracts of Brahmi: 400 mg, Mandukaparni: 400 mg, Shankhpushpi: 200 mg, Kokilaksha: 200 mg, Yastimadhu: 200 mg, Shunthi: 50 mg. MP is prescribed at 400 mg, which is present in 10 ml tonic, per day for an adult person (60 kg body weight). From here, we calculated the rat equivalent dose (RED) considering the body weight of an adult rat to be 300 g and multiplying the scaled-down human dose by a factor of 6.2 [53]. It stands at 12.4 mg present in 310 μl of MP; correspondingly, the cellular dose was calculated by dividing the animal dose by a factor 5 for animal to cellular dose conversion. Hence the calculated dose of 2.4 mg present in 60 μl of the syrup was selected for viability assays. Effect of MP was also checked at 30 μl and 90 μl to study dose dependency in cellular models.

Dried form of three of MP's major constituent herbs that are Brahmi (*Bacopa monnieri*, BM), Mandukaparni (*Centella asiatica*, CA) and Shankhpushpi (*Convolvulus pluricaulis*, CP) were procured from Parker Robinson Pvt. Ltd. (India). Extracts were prepared according to the protocol described earlier for BM [54], CA [55] and CP [56]. Each of these extracts were checked for toxicity towards SHSY5Y cells and dose for checking neuroprotection in each case was deduced following the above mentioned references (data not shown). SHSY5Y cells were pre-treated for 2 h with BM, CA and CP extracts at 100 μg/ml, 100 μg/ml and 100 μg/ml respectively followed by Aβ treatment and viability was assessed at 24 h using MTT assay.

2.4. Cell Viability assays

2.4.1. Trypan blue exclusion assay

This is a standard assay for cell viability assessment. It is based on the principle that live cells based on the virtue of their intact cell membranes exclude certain dyes such as trypan blue, eosin and propidium while dead cells do not. Upon staining viable cells have a clear cytoplasm while non-viable cells have a blue cytoplasm. Trypan blue solution was prepared as a 0.4% solution in PBS as a stock and for counting mixed with diluted cell suspension as 1:1 mixture. The live (unstained) cells were then counted in a haemocytometer and number of live cells per ml was calculated. Primed PC12 cells were treated with 4 μM Aβ alone as well as Aβ along with 3 different doses of MP – 30 μl/ml, 60 μl/ml and 90 μl/ml and corresponding doses of vehicle for 24 h before staining with Trypan blue and counting the viable cells.

2.4.2. MTT assay

MTT is a sensitive and reliable indicator of the cellular metabolic activity and correspondingly the cell viability. NAD(P)H-dependent cellular oxido-reductase enzymes are present primarily in the mitochondria of live cells and can reduce the tetrazolium dye i.e.MTT into insoluble formazan crystals deposited within cells seen as purple color and can be quantified colorimetrically. Differentiated PC12 cells were treated with 4 μM Aβ and Aβ along with 3 doses of MP – 30 μl/ml, 60 μl/ml and 90 μl/ml and corresponding doses of vehicle for 24 h. Differentiated SH-SY5Y cells were treated with 3 μM Aβ and Aβ along with 60 μl/ml MP and corresponding dose of vehicle for 24 h. MTT solution was freshly prepared in PBS and added to cells at 0.5 mg/ml, incubated in dark for 4 h to allow formazan crystal formations. The resultant

formazan crystals were then dissolved in DMSO and quantified at 570 nm.

2.4.3. Intact nuclei counting method

Viability of primary cortical neurons was estimated by intact nuclei counting that is routinely used for neuronal cells as described earlier [57–59]. Trypsinized cells were firstly lysed in a buffer (with detergent) that dissolves cellular membrane but keeps the nuclear membrane intact. The number of intact nuclei was counted in a haemocytometer. The treatment conditions were similar as in SHSY5Y, only the Aβ dose was kept at 1.5 μM. The selection of Aβ dose in various cell types was based on previous reports [57].

2.5. Immunocytochemistry in primary neurons

To understand the morphological changes of primary neurons under different conditions – Control, Vehicle Control (VC), Aβ (1.5 μM) and Aβ + MP60, we performed immunocytochemistry 24 h following treatment as described previously [60,61]. Neurons cultured on PDL-coated glass cover slips were fixed in freshly prepared 4% PFA in PBS for 10–15 min at room temperature and then washed with PBS. The fixed cells were then blocked with 3% goat serum in 0.3% Triton X-100 solution in PBS for 1 h at RT. Cells were incubated overnight with MAP-2 (1:50) in blocking solution at 4℃. Following proper washing, the cells were incubated in secondary antibody Alexafluor 488 for 1–2 h at room temperature in dark. Nuclei were stained with Hoechst 33342 solution in PBS for 30 min, washed carefully and mounted in Prolong Gold Anti-fade reagent (Invitrogen) for long-term storage. Images were taken in Leica CTR4000 fluorescence microscope at 63X objective.

2.6. Terminal deoxynucleotidyl transferase dUTP nick end labeling (TUNEL) staining

The TUNEL assay was performed according to the manufacturer's protocol (Clontech, ApoAlert DNA Fragmentation kit, Takara). Briefly, adherent cells grown on glass coverslips were fixed with freshly prepared 4% PFA for 15 min following which they were washed with PBS twice. Cells were then permeabilized with pre-chilled 0.1% Triton-X in 0.1% Sodium Citrate solution for 5 min on ice. For tissues, coronal sections of rodent brain were used for this study. Initially sections were washed with PBS three times (5 min each). The tissue was then digested in Proteinase K solution (20 μg/ml, diluted from concentrated stock provided in the kit) for 20 min. The reaction was terminated by rinsing with excess PBS and this was followed by addition of 4% PFA to the sections. Next, for tissue sections or cells, both were washed twice with PBS. The specimens were then equilibrated in equilibration buffer at RT for 10 min. The samples were incubated in a solution containing the nucleotide mix and Tdt enzyme for 1 h at 37 °C in dark. The reaction was stopped by 2X SSC buffer provided in the kit at RT for 15 min. Samples were rinsed with PBS. Following this, they were stained with Hoechst solution for 30 min at 37 °C and then washed with PBS before mounting with Prolong Gold Antifade with DAPI for microscopic analysis. For quantitative analysis in cells, 4–5 equal window images were taken from different regions of the coverslip at 63 × magnification, following which total number of cells in each field (Hoechst stained) and total number of TUNEL positive cells in each field (fluorescein+Hoechst+) were counted and percentage of TUNEL positive cell was calculated by dividing the TUNEL positive cell count with the total number of cells multiplied by 100. To study apoptosis of primary neurons under different conditions – Control, VC, Aβ (1.5 μM) and Aβ + MP60, we performed TUNEL assay 24 h following treatment.

2.7. Sholl analysis

Sholl analysis was performed to assess neuronal arborization under different treatment conditions by NIH-ImageJ software, widely reported earlier [62–64]. Primary cortical neurons were transfected with 0.5 μg of pSIREN-ZsGreen empty scrambled construct in neurobasal medium with lipofectamine 2000. Following 6 h incubation at 37 °C & 5% CO_2, fresh media was replaced. After 48 h, cells were treated with Vehicle, Aβ and Aβ + MP60 for 24 h. GFP expressing viable cells were imaged under fluorescence microscope at 10 × magnification. The processes of individual neurons were traced and a number of concentric circles were drawn from the neuron cell body with an increasing radius of 25 μm. Two-dimensional analysis was performed where the number of intersecting points of the neuronal processes at each concentric circle was calculated. Data have been represented as the mean ± S.E.M. of five to six neurons from three independent experiments.

2.8. Preparation of oligomeric Aβ

Oligomeric preparation of $A\beta_{1–42}$ was performed following the steps reported earlier [60]. Briefly, lyophilized form of $A\beta_{1–42}$ peptide was reconstituted in 100% HFIP followed by evaporation of HFIP in a speed vac (Eppendorf, Hamburg, Germany). The resulting pellet was carefully re-suspended in DMSO to 5 mM and stored in aliquots at − 80 °C for long term use. The stock was diluted in PBS with SDS (SDS final concentration - 0.2%) to 400 μM and incubated in a dry bath for 18–24 h at 37 °C. It was further diluted to 100 μM in PBS and re-incubated for 18–24 h at 37 °C before use.

2.9. Animal housing and care

Adult Sprague Dawley rats (weighing between 280 and 320 g) or 5-month-old male 5XFAD mice were housed in three per cage, which contained sterile paddy husk as bedding with free access to water and food under a 12–12 h light -dark cycle. Constant temperature (24 ± 2 °C), and humidity (60 ± 5%), were maintained in the animal house of CSIR-Indian Institute of Chemical Biology (IICB), Kolkata. All the experiments were performed in accordance with the Institutional Animal Ethics Committee (IAEC) and as per the National Guidelines (CPCSEA) on the required care and use of animals in laboratory research (Indian National Science academy, INSA, New Delhi, 2000). The animals were habituated in laboratory conditions before the experiments.

2.10. Stereotaxy

Rats were anesthetized with 50 mg/kg Sodium thiopentone (Thiosol, Neon laboratories, Mumbai, India) in 0.9% normal saline according to the procedure reported by Paidi et al., 2015 [65]. The animal was placed in a stereotactic frame (Stoelting, MO, USA) with the incision bar initially placed at the Bregma point. Oligomeric solution of 4.5 μg Aβ peptide (prepared as per the protocol mentioned by Saha et al [60,66]) was injected bilaterally, 5μl per side, in the CA1 region of the hippocampus in adult male Sprague-Dawley rats. The co-ordinates are, lateral, ± 0.21 cm from the bregma; anteroposterior, 0.36 cm; dorsoventral, 0.28 cm, according to the atlas of Paxinos and Watson. The flow rate was kept at0.5 μl/min by using a worker bee syringe pump (BAS, West Lafayette, USA). Aβ was allowed to diffuse for an extra 5 min after its delivery. Same volume of PBS was bilaterally injected in the control rats. Homeothermic blanket (Harvard apparatus, U.K.) was used to maintain the body temperature of the animals (37 °C).

2.11. Behavioral analysis protocol

The animals were randomly divided into 5 groups: Control (PBS infused), MP (only MP infused), Aβ ($A\beta_{1–42}$), Aβ plus human equivalent dose (HED) of MP and Aβ plus rat equivalent dose (RED) [17] of MP. The animals were administered with MP orally daily till their sacrifice. After six days of $A\beta_{1–42}$ infusion, MP treatment was started. After ten days of MP treatment, behavioral tests were performed. Similar groups were maintained in 5XFAD mice as in rats; except we included mice

equivalent dose (MED) [27] instead of RED. Both MED and RED doses were calculated from the HED dose prescribed earlier where dose calculation in different animal models is based on body metabolic rate and body weight [53]. An additional group of Donepezil (10 mg/kg, an acetyl cholinesterase inhibitor) treated 5XFAD mice was used as a standard drug control for behavioral experiments performed in the transgenic mice. The number of animals used in each of the behavioral experiments are given in Tables 2A (rats) and 2B (mice).

According to USFDA (2005) guidelines, we calculated RED from the recommended human dose as mentioned earlier; there 310 μl of MP was given per rat per day. For mouse, considering average body weight as 30 g and by multiplying the human dose by a factor 12.3, 61.5 μl of MP was given per mouse per day and the dose was termed as MED [67]. HED in rat or MED in mouse was calculated from the human dose (average human body weight 60 kg) with respect to individual animal's average body weight. Open-field test, novel object recognition test, passive avoidance test, contextual and cue-dependent fear conditioning test, and elevated plus maze test were used to evaluate the cognitive changes in both the AD models - Aβ-infused rats and 5XFAD transgenic mice and the effect of MP on them.

2.11.1. Open-field test

Locomotor activity levels in rats or mice can be comprehensively assessed by the open field activity monitoring system as described earlier [68–71]. An open-field arena with a x-y grid of invisible infrared rays is used to record the distance and regions traveled by the rodent in the arena in 10 min.

2.11.2. Novel object recognition

This behavioral test is dependent on the innate tendency of rodents to explore a novel object more than a familiar object as described earlier [60,72,73]. Briefly, the animal was placed in a rectangular box with two identical objects on Day-1. On Day-2, one of the objects was replaced by differently shaped object and the animal was tested for its ability to distinguish the novel object from the familiar for 5 min. The length of time spent in inspecting each of the objects on both the days was noted and discrimination index (DI) and preference index (PI) calculated according to the formulas $DI = (TN - TF)/(TN + TF)$, $PI = TN/(TN + TF) * 100$. (TN = Time spent exploring the novel object and TF = Time Spent exploring the familiar object).

2.11.3. Passive avoidance test

The instrument used in this test contains two chambers that are dimensionally identical, but one is white (well-lit) chamber and another is a dark chamber separated by an automated guillotine door. The test was performed over two days as previously reported [60,68,72]. In short, on day-1 acquisition stage, the animals were placed in the white chamber and the time taken by the animal to move to the dark chamber where it instantly received a mild foot-shock (0.7 mA for 2 s) was recorded. On the next day (Probe stage), the latency to the dark chamber was recorded by SHUTAVOID software (Panlab, Barcelona, Spain).

Table 2A
Total number of rats involved in behavioral experiments.

Cognitive tests	Experimental animal groups (rats)				
	Vehicle treated (Con)	MP (RED)	Aβ	Aβ + MP (HED)	Aβ + MP (RED)
Open Field Test	8	5	5	7	8
Elevated plus maze (Cognition)	9	8	8	9	8
Novel object recognition	5	8	6	6	5
Passive Avoidance	9	8	6	9	9
Contextual Fear conditioning	6	5	8	6	5
Cue Dependent Fear conditioning	8	6	8	7	6

2.11.4. Fear conditioning test

It is employed to assess hippocampal dependent associative learning and is helpful to understand amygdala-hippocampal communication.

2.11.4.1. Contextual fear-conditioning test. On the day of training, the rat was positioned in a sound-proof chamber and following a 2-min habituation, the animal was subjected to four sessions of an unconditioned stimulus (each session - 89 s pre-shock interval; 0.7 mA 1-s foot-shock) terminating in a 2 min relaxation period without stimuli (10 min total). 24 h later, the animals were placed in the same context but this time the shock was absent. Freezing behavior defined as complete absence of motion excluding breathing movements was recorded by PACKWIN 2.0 software (Panlab) during an 8 min testing period [68].

2.11.4.2. Cue dependent fear conditioning test. Cue dependent test was performed as described previously [60,72]. Briefly after an initial habituation, four 29 s sessions of light and sound (90 dB, 4000 Hz for rats; 80 dB, 2500 Hz for mice) co-terminating in a foot-shock (0.6 mA, 1 s for rats; 0.4 mA, 1 s for mice) were delivered to the animal placed in the sound-proof Panlab chamber with an inter trial interval of 1 min. The animal was allowed to relax for an additional 2-min period before it was removed from the chamber (10 min in total). 24 h later, the context of the box was modified. Rodents were exposed to the same cues as on day-1 but without shock. Freezing behavior was recorded during an 8 min test period by using PACKWIN automated software.

2.11.5. Elevated plus maze (EPM) test

The elevated plus maze (EPM) test is employed to assess anxiety and cognitive ability in rodent models and has been described previously [65]. Briefly, on the first day, the animal was allowed to explore the arms of the plus maze and the time taken for it to move from the open arm to the closed arm was recorded as initial transfer latency (ITL) [74]. On day 2, the same protocol was followed and the transfer latency to the closed arm was recorded as retention transfer latency (RTL). The maximum duration of exploration for each animal each day was 300 s.

2.12. Immunohistochemistry

Transcardial perfusion of animals were performed under deep anesthesia 60 mg/kg Sodium thiopentone (Thiosol, Neon laboratories, Mumbai, India) with 50 ml of chilled 100 mM PBS (pH 7.4) followed by 4% PFA and then the animal was decapitated and the brain was separated from the skull. Following additional fixation in 4% PFA overnight at 4 °C, the brain was transferred in 30% (w/v) sucrose solution in PBS at 4 °C. With a cryotome (thermo Shandon, Pittsburg, PA, USA), coronal sections (20 μm thick) were taken on gelatin-coated slides for histological staining. Immunohistochemistry was performed as described earlier [14,69,75]. The sections were washed in PBS three times and then permeabilized with PBS + 0.4% Triton-X for 40 min. Later, sections were rinsed with PBS + 0.1% Triton-X and then blocked with 4% BSA in 0.1% PBST for 1 h. Primary antibodies including polyclonal rabbit anti-rat $A\beta_{1-42}$ antibody (1:100, Abcam), polyclonal rabbit anti-mouse SNAP25 (1:100, Santacruz Biotechnology) and PSD95 (1: 50, Merck Millipore) antibodies were diluted in the blocking solution (4% BSA in 0.1% PBST) and added to the sections for a 48 h incubation at 4 °C. Following washing with PBST (0.1%) to remove unbound primary antibodies, specific Alexa fluor-tagged secondary antibodies were added to sections at room temperature in dark for 2 h. Hoechst solution was used to stain the nucleus for 30 min at 37 °C. Finally, the sections were washed few times more in PBS and then mounted with Prolong Gold Antifade (Invitrogen) for confocal microscopic imaging. Quantification

Table 2B
Total number of mice involved in behavioral experiments.

Cognitive tests	Experimental animal groups (mice)					
	Vehicle treated (WT)	MP (MED)	5XFAD	5XFAD + MP (HED)	5XFAD + MP (MED)	5XFAD + Donepezil
Open Field Test	8	5	5	7	6	5
Elevated plus maze (Cognition)	9	8	8	8	8	7
Novel object recognition	9	8	6	5	8	6
Contextual Fear conditioning	6	7	8	7	6	7
Cue dependent fear conditioning	7	5	6	7	6	5

Con, control; WT, wild type; MP, Medha Plus; RED, Rat equivalent dose; MED, mouse equivalent dose; HED, human equivalent dose.

of fluorescence intensity was done by quantifying corrected total cell fluorescence (CTCF). It is calculated from integrated density of staining, area of the cell, and the background fluorescence of different experimental conditions using the formulae CTCF = Integrated density − (area of selected cell × mean fluorescence of background readings).

2.13. Western Blotting

The animals were decapitated, and the hippocampus tissue was collected and kept in − 80 °C for long term storage. 60 μg of protein was run in SDS-PAGE and transferred to PVDF membrane. Blocking was done in 5% BSA solution in TBST [1.5 M NaCl, 1 M Tris (pH7.5), 0.1% Tween20] for 1 h at room temperature and then the membranes were incubated with primary antibodies for phosphorylated-Akt at serine 473 (1:500, Cell Signaling Technology, MA, USA), Akt (1:500, Cell Signaling Technology, MA, USA), polyclonal rabbit anti-mouse SNAP 25 (1:1000, Santacruz Biotechnology) and PSD 95 (1: 1000, Merck Millipore) antibodies or Actin (1:10,000) overnight at 4°C. Membranes were washed with TBST followed by HRP-tagged secondary antibody incubation for 1–2 h at room temperature. Following further washing in TBST to remove unbound antibodies, the blots were imaged using western blot ECL substrate in ChemiDoc MP imaging system (BIO-RAD). Densitometric quantitation of each band was done by NIH-ImageJ software (NIH, Bethesda, MD, USA).

2.14. Acetyl cholinesterase (AChE) assay

AChE activity was measured by Ellman et al. method [76]. This assay is based on the formation of a yellow reaction product when thiocholine is released from acetylthiocholine and combine with the test reagent, 5, 5′-dithio-bis-(2-nitrobenzoic acid) (DTNB). For the in vitro experiment, a 2% homogenate of rat brain cortex prepared in 100 mM phosphate buffer (pH 8.0) was centrifuged very briefly at 1000 *g* at 4 °C and the supernatants were used for the estimation of AChE activity. The reaction mixture contained 0.1 M sodium phosphate buffer (pH 8.0), DTNB (10 mM), acetylthiocholine iodide (75 mM) and 80 μl of tissue homogenate. Different doses of aqueous drug (individually) and donepezil (1 μM) were incubated with rat brain cortical tissue homogenate and DTNB for 15 min at 37 °C, and the reaction was initiated by addition of acetylthiocholine iodide. The kinetic profile of enzymatic activity was measured at 412 nm for 2 min at 15 s intervals by spectrophotometer. The specific activity of AChE was calculated in μmoles/min/mg of protein. For in vivo estimation of acetylcholine esterase activity, rats (treated or untreated) were sacrificed by decapitation and immediately hippocampal and cortical tissue were collected in 100 mM phosphate buffer (pH 8.0). Afterwards, the same protocol was employed as mentioned above. Following calculation for specific activity of AChE, results were presented as percent of control group.

2.15. ROS generation assay

Following treatment, animals were sacrificed by decapitation. Mitochondrial P_2 fractions were prepared from the hippocampus and cerebral cortex of control, Aβ and Aβ+MP treated rats as elucidated previously by Thomas and Mohanakumar [77]. Briefly, animals were sacrificed by decapitation, the hippocampus and cortex immediately dissected out and homogenized individually in 10-times volumes of ice-cold mitochondrial isolation buffer comprising 225 mM mannitol, 75 mM sucrose, 5 mM MOPS, 1 mM EGTA and 1 mg/ml BSA, pH 7.4. Centrifugation of the homogenate was done at 1000 *g* for 10 min at 4 °C. The pellet was thrown away and the supernatant centrifuged at 9500 *g* for 30 min at 4 °C. The pellet hereby obtained was rinsed in cold 50 mM Tris-HCl, pH 7.2 (centrifuged at 9500 *g* for 30 min at 4°C). Cold 10 mM potassium phosphate buffer at pH 7.2 was then used to re-suspend this resulting mitochondrial pellet. Rat brain hippocampal and cortical ROS generation was evaluated by H2DCF-DA method [78]. Mitochondrial P_2 fraction was collected from the hippocampal and cortical regions of the control and treated rat brains [79]. Following normalization, the mitochondrial P_2 fraction was allowed to incubate with H_2DCF-DA for 30 min and a spectrofluorimetric (Perkin Elmer, USA) determination of fluorescence intensity was performed setting the excitation and emission at 495 nm and 529 nm respectively.

2.16. Statistical analysis

All data for comparing more than two experimental groups were analyzed by one-way ANOVA analysis followed by tukey's multiple comparison post hoc test using graph pad software. For comparison of significant difference between two groups, unpaired two-tailed student's 't' test analysis was used. Data are presented as mean ± standard error of mean (SEM), and $p < 0.05$ was considered to be statistically significant.

3. Results

3.1. Medha Plus (MP) shows neuroprotective activity against Aβ-mediated neurotoxicity in vitro

MP is a novel polyherbal formulation of six herbs those are individually beneficial for the improvement of brain functions including memory. We studied the combinatorial effect of these six herbs present in MP in both *in vitro* and *in vivo* models of AD to check its neuroprotective ability and its role in alleviating AD-related cognitive deficits.

As discussed in the materials and methods section, three different doses of MP – 30 μl/ml, 60 μl/ml and 90 μl/ml were initially selected to check for neuroprotective ability in Aβ-treated neuronally differentiated PC12 cells alongside concomitant vehicle controls (VC, at the select doses). We found that MP at 60 μl/ml dose recovered cell viability by 30% in Aβ-treated PC12 cells as opposed to those treated with Aβ alone in both trypan blue exclusion (Fig. 1a) and MTT assays (Fig. 1b). The recovery in viability was not significant at 30 μl/ml dose while recovery at 90 μl/ml was same as 60 μl/ml suggesting it as an optimal dose of MP. We then checked its efficacy in a human derived cell line and proceeded with the 60 μl/ml dose for further viability study with MTT in SHSY5Y cells treated with Aβ. We observed more than 40% recovery in cell viability against those treated with Aβ alone (Fig. 1c). Next, we checked for the neuroprotective efficacy of MP in more relevant primary rat cortical neurons and found that MP at 60 μl/ml significantly recovered

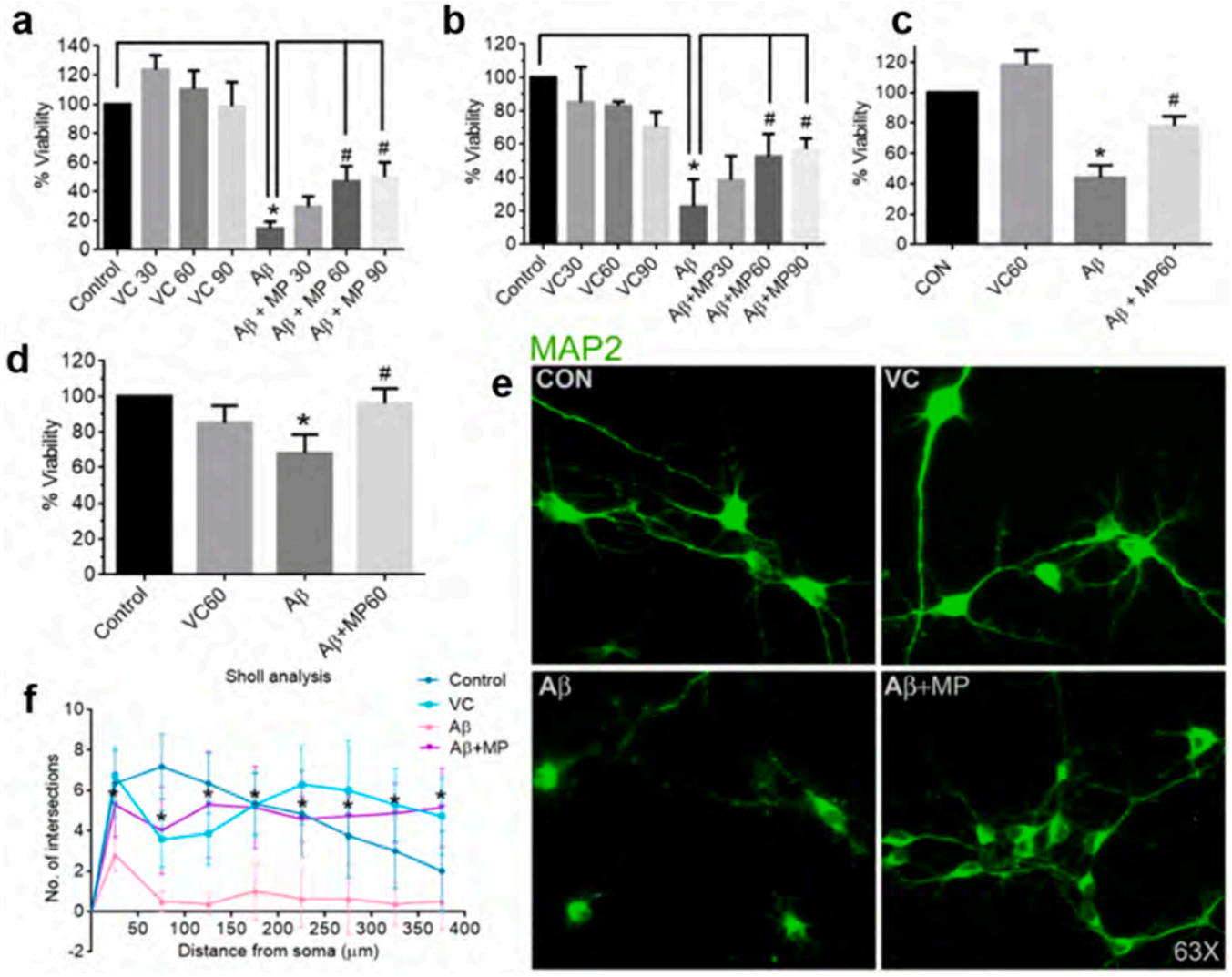

Fig. 1. Medha Plus (MP) protects neurons against Aβ toxicity *in vitro*. (a) Viability assay of PC12 by Trypan Blue exclusion method: Primed PC12 cells were treated with Aβ and Aβ along with different doses of MP – 30 μl/ml (MP30), 60 μl/ml (MP60), and 90 μl/ml (MP90) in addition to vehicle controls (VC) at each dose. Data from 3 independent experiments were analyzed by One-way ANOVA, Tukey's post hoc test. (*) denotes p-value < 0.0001 compared to control group, (#) denotes p-value < 0.05 compared to Aβ group. (b) Viability assay of PC12 by MTT: Primed PC12 cells were similarly treated as above. Data from 4 independent experiments were analyzed by One-way ANOVA, Tukey's post hoc test. (*) denotes p-value < 0.0001, compared to control group (#) denotes p-value < 0.05 and (##) denotes p-value < 0.005 compared to Aβ group. (c) Viability assay in SHSY5Y by MTT: Differentiated SHSY5Y cells were treated with Aβ and with Aβ+MP60. Data from 4 independent experiments were analyzed by One-way ANOVA, Tukey's post hoc test. (*) denotes p-value < 0.0001 compared to control group, (#) denotes p-value < 0.0001 compared to Aβ group. (d) Viability assay by intact nuclei counting method: Primary cortical neurons were treated with Aβ and Aβ+MP60. Data from 3 independent experiments were analyzed by One-way ANOVA, Tukey's post hoc test. (*) denotes p-value < 0.05 compared to control group, (#) denotes p-value < 0.05 compared to Aβ group. (e) Primary cortical neurons were stained with MAP2 antibody following treatment with Aβ and Aβ+MP60 besides appropriate controls. All images were taken at 63× magnification. (f) Sholl analysis was performed to quantify neuronal arborizations in figure (e) under the above-mentioned treatment conditions. Values are expressed as Mean±SEM from three independent experiments. (*) denotes p-value < 0.05 compared to Aβ.

cell viability of Aβ treated primary neurons, that is, comparable to control (Fig. 1d). We further checked for recovery in neuronal morphology by ICC with MAP2, 24 h following Aβ, with or without MP treatment and observed visible improvement in neurite morphology and neuronal arborizations quantified by Sholl analysis as against the loss of neurites observed under Aβ treated condition (Fig. 1e–f). In all the cases there was no significant effect on cells treated with VC. Since we found optimal beneficial effect with 60 μl/ml dose of MP, we used this dose in all the following cellular experiments. We further compared the effect of MP at 60 μl/ml dose on Aβ-treated SHSY5Y cells with that of extracts of CA (at 100 μg/ml), CP (at 100 μg/ml) and BM (at 100 μg/ml) for 24 h. Each of these herbal extracts rendered significant protection against Aβ toxicity. We further found that MP induced higher protection against Aβ compared to each of the above-mentioned extracts which were statistically significant (Supplementary Fig. 1).

3.2. *MP protects primary cortical neurons against Aβ-induced apoptosis*

TUNEL assay is routinely performed to assess apoptosis in cells as described earlier. In all the four treatment groups – Control, Aβ, VC and Aβ + MP, the percent of TUNEL + cells among all the randomly counted cells were calculated. We found that Aβ treatment induced a significant level of apoptosis as about 60% TUNEL + cells counted in primary neurons in 24 h while upon Aβ and MP co-treatment there was significant reduction (< 20%) in apoptotic cells which is comparable to control and VC (Fig. 2a–b). Taken together, our *in vitro* data suggest that MP protects neuronal cells significantly from Aβ induced toxicity.

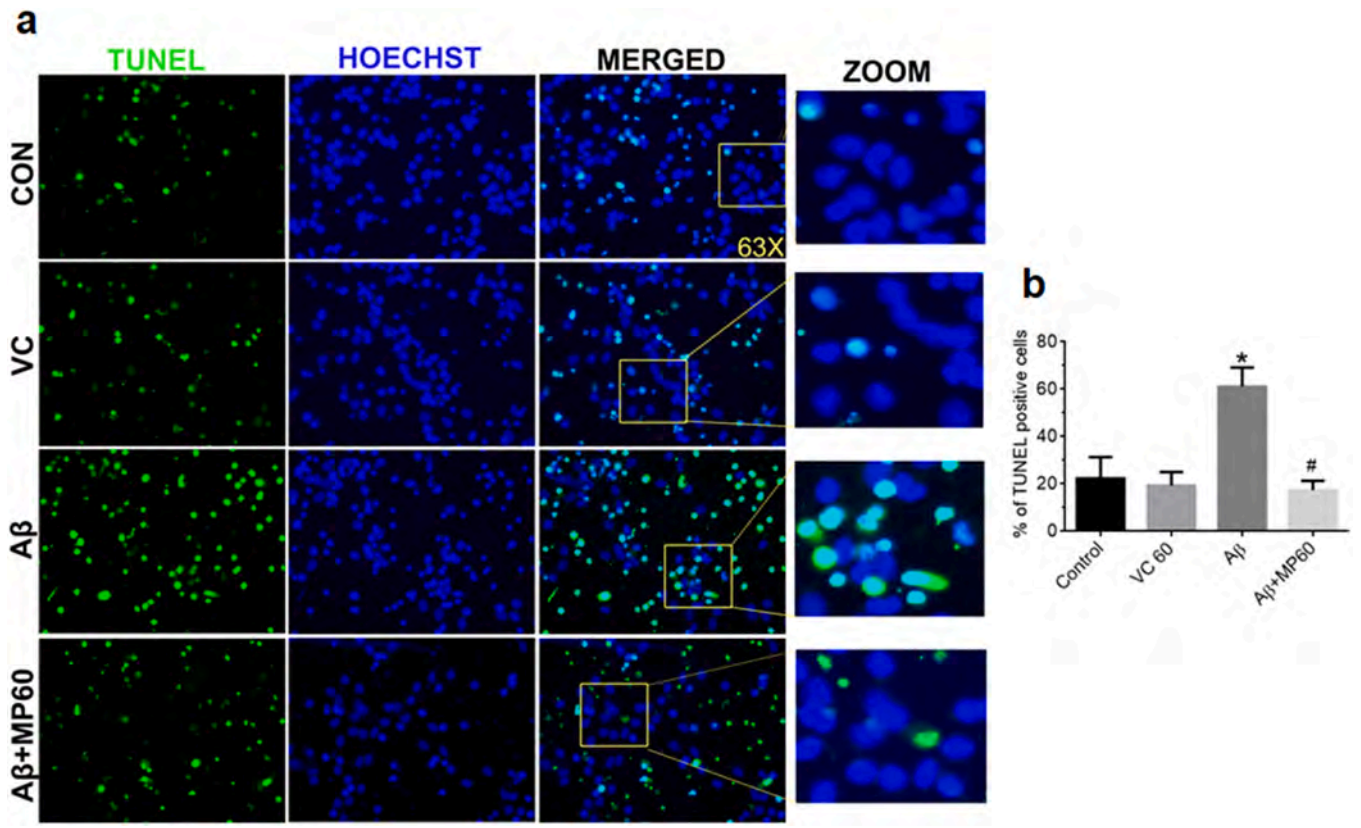

Fig. 2. Medha Plus (MP) prevents Aβ-induced apoptosis in primary cortical neurons quantified by TUNEL assay: (a) Left to right – First panel shows TUNEL positive cells (green), second panel shows nuclei of primary cortical neurons stained by Hoechst (blue), third panel shows the merged images and the fourth panel shows the magnified versions of the area marked by the box (yellow) in the third panel. Each row denotes the treatment conditions as mentioned. All images in first to third panel were taken at 63X magnification. (b) Quantification of TUNEL positive cells compared to total number of cells in each field in terms of percentage. (*) denotes p-value < 0.001 compared to control group, (#) denotes p-value < 0.001 compared to Aβ group.

3.3. MP administration attenuates learning and memory deficits in Aβ-infused rat

Stereotactic infusion of toxic oligomeric Aβ near the CA1 region of hippocampus in adult rat (described in materials and methods) represents a sporadic AD model and has been reported by us earlier [72]. The timeline of Aβ infusion, MP treatment and subsequent behavioral tests in rats is outlined in Fig. 3a. Initially, we performed open-field test which helps to determine the locomotor activity and anxiety-like behavior in rodents. In the duration of 10 min of the test, the Aβ-infused rats traveled significantly longer distance (in cm) compared to control animals. RED significantly reduced the hyperlocomotor activity of Aβ animals while HED did not have any significant effect (Fig. 3b, Supplementary Fig. 2).

Novel object Recognition (NOR) was used to test the effect of MP on working memory in Aβ-infused rats. On the first day rats in all the groups spent equal time with the identical objects placed in the NOR box (Fig. 3c). On the second day, Aβ-infused rats spent significantly less time with the novel object compared to familiar object resulting in a negative DI and 40% PI indicating an inability to distinguish the novel object from the familiar one and reduced preference for the novel object respectively, contrary to the score of control animals [81]. Both doses of MP (HED and RED) improved the DI and PI scores of Aβ rats to a positive and $> 50\%$ values respectively (Fig. 3d–f). Fig. 3g, EPM test shows Aβ-infused rats exhibited increased RTL (retention transfer latency) (Day-2) compared to ITL (initial transfer latency) (Day-1), contrary to the other groups which displayed reduced RTL values compared to corresponding ITL. The difference between ITL and RTL values (ITL-RTL) is used as an attribute to depict memory retention. Aβ-infused animals displayed a negative value signifying cognitive loss, however, both the HED and RED treated Aβ animals scored positive ITL-RTL values denoting cognitive recovery.

The passive avoidance works on the principle based on the animal's ability to learn to withdraw from a specific behavior to evade an aversive stimulus. The acquisition or training day results do not show any significant difference among the four groups (Fig. 3h). In the probe stage that is on the next day, Aβ-infused rats displayed diminished latency to the dark chamber while MP administered Aβ-infused animals (both HED and RED groups) retained the memory from day-1 and showed a higher transfer latency to the dark chamber (Fig. 3i).

Fig. 3j shows the mean of %freezing of animals in all the four trials in Probe stage (day-2) of the contextual fear conditioning test. Aβ-infused rats displayed significantly reduced %freezing (40%) compared to control groups. However, the freezing behavior recovered in the Aβ-infused rats treated with either HED or RED of MP signifying retention of context dependent associative memory. In the probe stage (day-2) of cue-dependent fear conditioning test, the Aβ-infused animals showed significantly reduced freezing (around 45%) in response to the cues while MP administered Aβ-infused rats (both HED and RED groups) displayed improved freezing behavior that is comparable to the control groups (Fig. 3k). This result indicates that MP treatment improves cue-dependent associative learning and memory in a sporadic model of AD.

3.4. MP treatment induces Aβ clearance and inhibits apoptosis in Aβ-infused rats

Bilateral injection of Aβ near the CA1 region of hippocampus leads to deposition of Aβ aggregates near the site of infusion in rats. We tested the effect of MP in reducing the toxic Aβ accumulation in the Aβ-infused rats near the site of infusion (See Fig. 4a). We found prominent $A\beta_{1-42}$

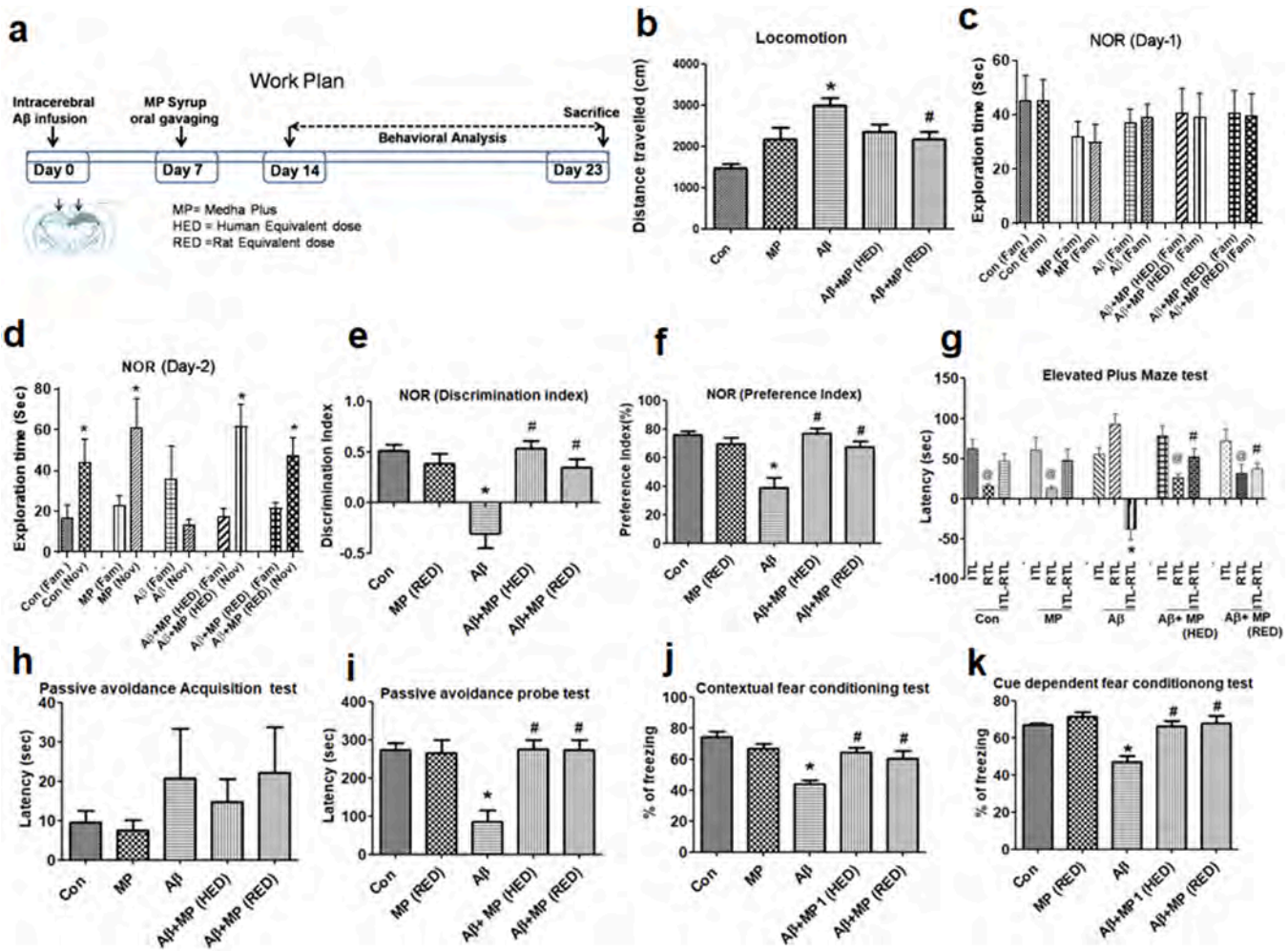

Fig. 3. Medha Plus (MP) ameliorates learning and memory deficits in Aβ-infused rat: Aβ-infused rats were treated with MP at two doses - human equivalent dose (HED) and rat equivalent dose (RED) and used for all the behavioral studies along with Aβ-infused rats and PBS infused controls as per the schematic diagram shown in (a). Data are represented as Mean ± S.E.M and for comparisons between more than two groups one-way ANOVA analysis followed by Tukey's post hoc comparison test was used for all the experiments except mentioned otherwise. (**b) Open field test-** graph shows the average distance traveled by the rats in each treatment group in cm *$p < 0.05$, #$p < 0.05$. **Novel object recognition (NOR) test -(c)** The bar graph depicts the average time spent by the animals with two similar objects (familiar - fam) on day-1 of NOR test. (d) Depicts the average time spent by the animals with the novel object [2] and familiar object (Fam) on day-2 of the test in each group and analyzed by student's t-test between the two durations in each group of animals. (*) denotes p-value < 0.05. **(e)** Shows the discrimination index calculated for each group on day-2. *$p < 0.05$, #$p < 0.05$. (**f)** Preference index for novel object is shown,*$p < 0.05$, #$p < 0.05$. (**g) Elevated plus maze test** - retention transfer latency (RTL) of day-2 was markedly reduced compared to initial transfer latency (ITL) [74] of day-1 within each group in all the experimental groups except Aβ treated animals (@$p < 0.05$, unpaired two-tailed t-test). ITL-RTL values were compared between groups (*$p < 0.05$, #$p < 0.05$). (**h**) **Passive avoidance test -** shows the acquisition stage in which the step through latency (sec) of animals to t**h**e dark chamber on day-1 is presented and (**i)** on day-2 probe stage, latency of animals to step into the dark chamber was again recorded and analyzed (*$p < 0.0001$, #$p < 0.001$) [80]. **(j)** Results of Contextual fear conditioning test day-2 results are shown and analyzed (*$p < 0.005$, #$p < 0.005$). (**k)** Represents the results of Cue-dependent fear conditioning tests that were conducted on the 2nd day following day-1 of acquisition (training). The results show that MP reversed the reduction in %freezing that was induced by Aβ in the rats (*$p < 0.05$, #$p < 0.005$) (*) indicates p-values in comparison to control group and (#) indicates p-values in comparison to Aβ group. The number of animals used in each of the rat behavioral experiments are given in Table 2A.

plaque formation near the infusion site twenty-three days post Aβ infusion in rats detected by anti-$A\beta_{1-42}$ antibody (Fig. 4b–d). On the other hand, bilateral intracerebral vehicle administered rats did not show any Aβ plaque formation near the infusion site. On the 7th day following Aβ infusion, we started the administration of HED and RED of MP. Both the doses of MP diminished $A\beta_{1-42}$ accumulation near the infusion site in Aβ-infused rat brains. Fig. 4e–f show the increased TUNEL + cells (green puncta) in the Aβ-infused rat brains in the hippocampus and cortical regions near the site of infusion compared to control groups. However, the number was significantly reduced in both the HED and RED treatment groups denoting that apoptosis was inhibited by MP administration in Aβ-infused rats.

3.5. Administration of MP lowers ROS production and inhibits acetyl choline esterase (AChE) activity in Aβ-infused rat brain

To study the effect of MP formulation on ROS generation, we used H2-DCFDA assay as mentioned in the materials and methods. Two-fold increase in ROS production was observed in the hippocampus of the Aβ-infused rats compared to vehicle treated rats. Both the doses of MP treatment in Aβ-infused rats significantly lowered ROS generation in the hippocampus compared to the Aβ-infused group (Fig. 5a). However, in cortex the upregulation in ROS generation in Aβ rats was not statistically significant in comparison to vehicle treated rats and hence the effect of MP treatment could not be estimated (Fig. 5b).

To check the AChE inhibitory activity of MP, we initially checked it

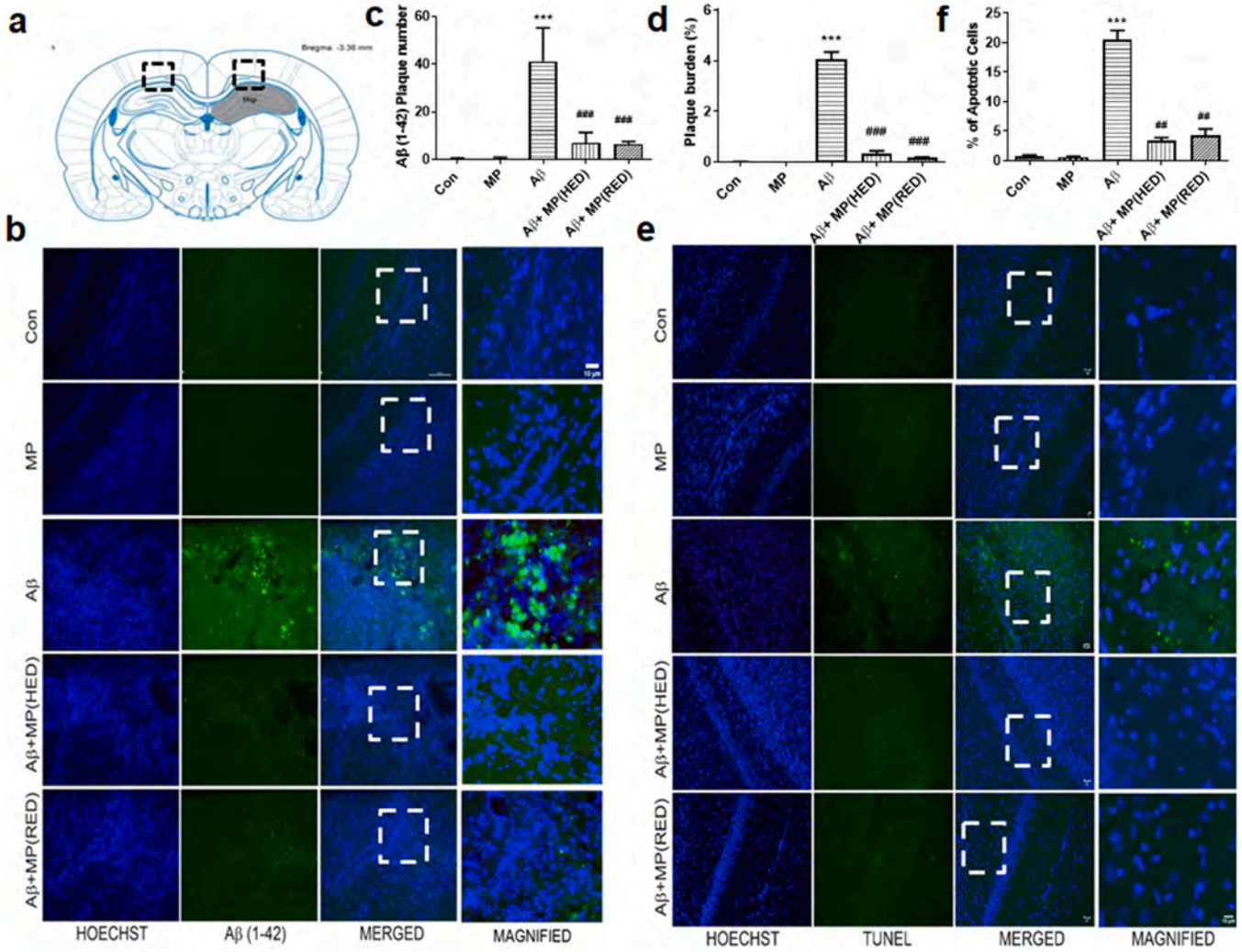

Fig. 4. Medha Plus (MP) administration induces Aβ clearance and protects against Aβ induced apoptosis in Aβ-infused rat brain. (a) Schematic diagram shows the infusion sites of Aβ oligomers in rat brain **(B)** Accumulation of Aβ plaques were observed by immunolabelling with $A\beta_{1-42}$ antibody in 20 μm coronal sections from the hippocampal region near the site of infusion in Aβ injected rat brain 23 days following infusion and visualized with fluorescent tagged secondary antibodies. The horizontal panels show double-labeled images taken for each experimental group (top to bottom) – Control, only MP (RED), Aβ, Aβ + MP (HED) and Aβ + MP (RED). The 4 vertical panels (left to right) – Hoechst stain (blue), $A\beta_{1-42}$ labeled (green) and, merged images were taken at 20X magnification (scale bar 100 μm). Magnified merged images (scale bar - 10 μm) are also shown. Note the region marked for higher magnification near the site of infusion (white boxes). Note the punctated $A\beta_{1-42}$ labeling in the Aβ rat brain in the hippocampal region near the site of infusion. Oral administration of MP significantly reduced the plaque number **(c)** and plaque burden (%) **(d)** compared to Aβ infusion alone (n = 3 for each group, 3 slices of each rat brain at 20X). *p < 0.0001, #p < 0.0001. (e) TUNEL assay was performed through hippocampal region to identify the apoptotic cells. TUNEL positive cells appeared as green puncta in the Aβ-infused rat hippocampus near CA1 region, while the total number of cells in the section was visualized with Hoechst (blue). The horizontal panels represent 20x (scale bar – 10 μm) images of sections from each group (top to bottom) – Control, only MP (RED), Aβ, Aβ+MP (HED), Aβ + MP (RED). The regions of interest are marked in white boxes in 20x images. Left to right TUNEL staining, Hoechst staining, merged and magnified merged image of region of interest. Note the increased number of TUNEL positive cells in the Aβ-infused brain sections while very few TUNEL positive cells were present in the MP administered Aβ group. (f) Depicts the percent of apoptotic cells. Aβ infused animals treated with MP group showed a significant reduction in the % of apoptotic cells compared to Aβ alone group (n = 3 for each group, 3 slices of each rat brain, 500 cells/slice at 20x); *p < 0.0001, #p < 0.0001. One way ANOVA was used to compare among groups (*) indicates p-values in comparison to control group and (#) indicates p-values in comparison to Aβ group.

in naive rat brain cortical tissue by employing the Ellman method [76]. MP at 30 μl and 60 μl doses (equal to RED and HED doses) in the *in vitro* study showed significant inhibition of AChE activity compared to control tissue (Supplementary Fig. 4). Moreover, MP showed similar activity like donepezil at 1 μM dose (used as a standard AChE inhibitor). Next, we validated the effect of MP on AChE activity in vivo. We show that Aβ infusion in rats induced a significant increase in the AChE activity in both the hippocampus and cortical regions compared to vehicle treated rats (Fig. 5c–d). MP treatment to Aβ-infused rats (RED groups) significantly inhibited the AChE activity in the hippocampus and cortical regions of the brain.

3.6. MP treatment ameliorates cognitive deficits in a familial AD model

5XFAD is the most advanced familial model of AD carrying five genetic mutations. To study the effect of MP in familial model of AD, the polyherbal formulation was fed to 5-month-old 5XFAD mice for a specific duration as demonstrated in a schematic in Fig. 6a. The animals were randomly divided into six treatment groups as indicated and their cognitive performances were studied through a battery of behavioral tests similar to those in rats. As expected, MP at both HED and MED attenuated the hyperlocomotory behavior (Fig. 6b, Supplementary Fig. 3), improved exploration time with the novel object in day-2 of NOR, generated positive DI scores and > 50% PI values in 5XFAD mice

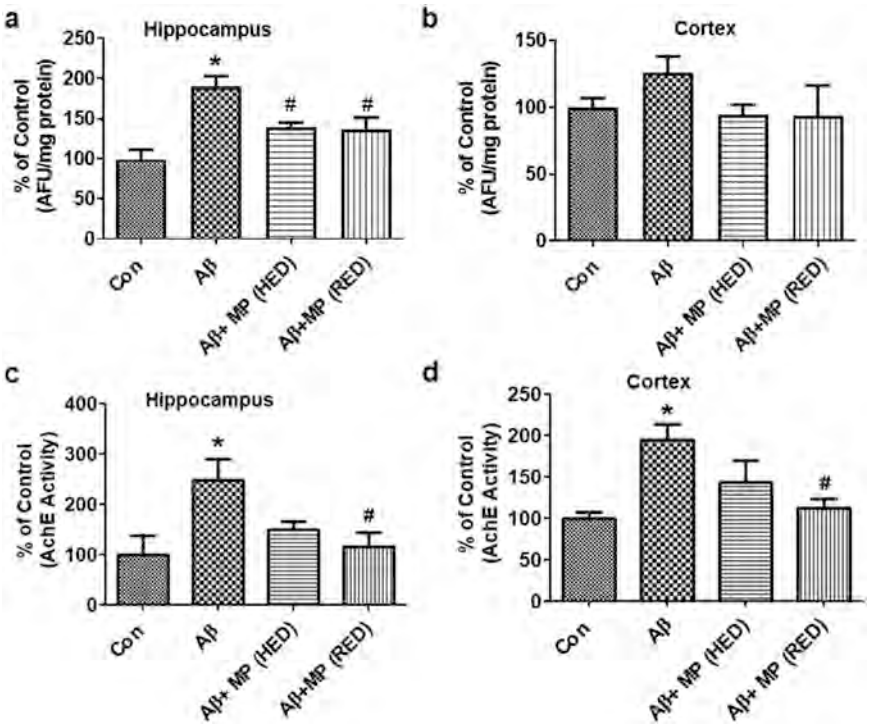

Fig. 5. Medha Plus (MP) attenuates Aβ-induced ROS production and acetyl choline esterase activity in rats. Graph represents the arbitrary fluorescence unit (AFU) for ROS production per milligram (mg) of protein as a percentage of control in hippocampus (a) and cortical region (b) of the rat brain. Different doses of MP (HED and RED) lower the $A\beta_{1-42}$ induced AChE activity in rat brain hippocampus (c) and cortex (d) as micromoles per minute per milligram protein. ($*p < 0.05$ and $\#p < 0.05$, Control $n = 3$, $A\beta$ $n = 4$, $A\beta$ + MP (HED)= 3, $A\beta$ + MP (RED) = 3). Values are expressed as AChE activity as a percentage of control. One-way ANOVA analysis, tukey's post hoc test, was used. (*) indicates p-values in comparison to control group and (#) indicates p-values in comparison to Aβ group.

(Fig. 6c–f). Notably in NOR, there was indication of better memory retention with MED compared to HED in MP treated 5XFAD mice and the MED group's results were comparable to the WT and 5XFAD + Donepezil groups. Further, MP treated 5XFAD mice (MED group) showed significantly improved ITL-RTL values in EPM test compared to 5XFAD mice (Fig. 6g). Finally, in both context-dependent and cue-dependent fear conditioning tests, both HED and MED treatments equivalently improved the %freezing of 5XFAD mice (around 70%) denoting the retention of associative fear memory in the MP treated groups (Fig. 6h–i).

3.7. MP treatment improves synaptic protein expressions in 5XFAD mice

We checked for the expression levels of SNAP 25 (pre-synaptic) and PSD 95 (post-synaptic) in the treatment groups through immunohistochemistry (IHC) and western blotting (WB) to understand the effect of MP on pre- and post-synaptic protein levels. 5XFAD mice brain exhibited significantly lower expressions of SNAP 25 and PSD 95 compared to respective age-matched wild type controls in the hippocampal and cortical regions near the site of infusion (Fig. 7a–b, e). Quantitative analysis of IHC data reveal that both HED and MED of MP treatment to 5XFAD alleviated the low-level expressions of both the synaptic proteins. However, we observed the recovery in synaptic protein expressions were better in MED treated 5XFAD compared to the HED treated group of MP. Similar results were observed in WB analysis for SNAP 25 and PSD 95 following MP treatment to 5XFAD mice (Fig. 7c–d, f). We next predicted that AKT (protein kinase B) signaling pathway may play a role in this improvement of synaptic functions [82]. We observed that MED of MP in 5XFAD mice significantly enhanced the phosphorylation levels of Akt at serine 473 compared to untreated 5XFAD mice. However, the HED of MP did not show any significant changes compared to 5XFAD group. Immunoblotting results with phospho-Akt (s473) from primary cortical neurons co-treated with Aβ and MP showed a similar effect of MP (Supplementary Fig. 5). Taken together, these results indicate an improvement in pre- and post-synaptic structures that may be correlated to behavioral improvements with an underlying activation of Akt pathway.

4. Discussion

In this study, we evaluated the neuroprotective effect of a unique polyherbal formulation derived from six herbs (Brahmi, Mandukaparni, Shankhpushpi, Yastimadhu, Kokilaksha and Shunthi) marketed as Parker's Medha Plus (MP) in both cellular and animal models of AD. We initially found that MP protected neuronally differentiated PC12 and SHSY5Y cells, and primary rat cortical neurons against Aβ oligomer induced toxicity and offered an improvement in neuroprotection to SHSY5Y cells compared to atleast three of its major constituent herbs – Mandukaparni, Shankhpushpi and Brahmi. MP protected Aβ-treated neurons by blocking apoptosis. We further detected significant recovery in neuronal morphology in MP treated primary neurons from Aβ-induced degeneration of neuronal processes. In order to assess the effect of MP on AD-related cognitive behavioral parameters, we employed an array of behavioral tests in two different rodent models. MP attenuated hyperlocomotor activity, improved short-term and spatial memory, reduced anxiety-related cognitive deficits and ameliorated hippocampal dependent fear memory in Aβ-injected adult rats. Similar results were observed with MP treatment in an advanced familial model of AD, 5XFAD mouse. Further we observed that oral treatment of MP reduced Aβ plaque burden as well as number of apoptotic cells in the hippocampal regions of Aβ-injected rats. Moreover, H2-DCFDA assay showed that MP was able to significantly decrease Aβ induced ROS generation in the hippocampi in Aβ-infused rats. Additionally, MP reduced AChE activity in both hippocampus and cortex in Aβ-infused rat. Finally, we found that MP treatment improved pre- and post-synaptic protein expressions in the hippocampi of 5XFAD mice which may be regulated by an increased phosphorylation of Akt at serine 473.

No stone should remain unturned in the fight against AD especially when some therapeutic recipes may be hidden in the most commonly found herbs. However, herbal products are often not regarded as highly as conventional medicine due to lack of strong evidence-based science. Traditional Chinese medicine has been more scientifically propagated into modern therapies than traditional Indian medicine (Ayurveda) which still requires an extensive scientific approach. Polyherbal formulations are more widely used than single herb extracts since they are

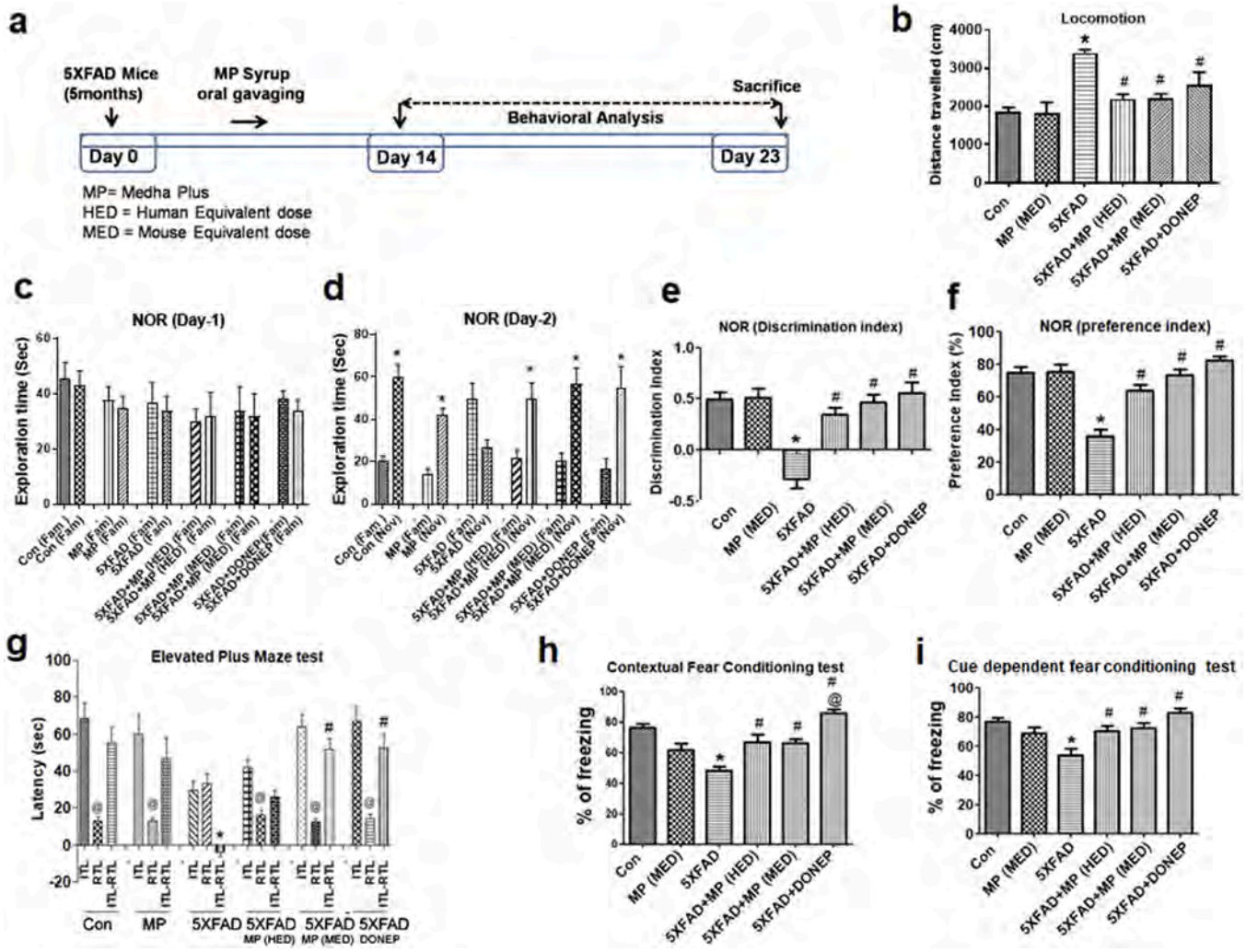

Fig. 6. Medha Plus (MP) rescues learning and memory deficits in 5XFAD mice (a) Experimental protocol for MP treatment in 5 month old 5XFAD transgenic mouse **(b) Open field test -** graph depicts the average distance covered in cm in all the six groups – Control (Vehicle treated wild type), mouse equivalent dose (MED) of MP treated control mice, 5XFAD, human equivalent dose (HED) of MP treated 5XFAD, MED of MP treated 5XFAD and Donepezil (Donep) treated 5XFAD mice. The same groups are shown in all the other behavioral tests in mice and data presented as Mean ± S.E.M. ANOVA followed by Tukey's post hoc comparison test was used for comparisons among more than two groups and student's t-test between two groups. In **novel object recognition (NOR)** test **(c)** there is no statistical difference in time spent with two familiar (fam) objects on day-1 among the mice groups. (d) 5XFAD animals spent significantly less time with the novel (nov) object than the familiar (Fam) object on day-2 as shown by the exploration time while 5XFAD + HED and 5XFAD + MED groups spent significantly longer time with the novel object than familiar object similar to the control (*$p < 0.05$, two-tailed t-test within each group) **(e)** Discrimination index calculated from NOR test and compared among groups (*$p < 0.05$, #$p < 0.05$) **(f)** Preference index for the novel object calculated from NOR test is also shown and analyzed (*$p < 0.05$, #$p < 0.05$). **(g)** In **Elevated plus maze test**, retention transfer latency (RTL) of day-2 is compared to day-1 initial transfer latency in each of the experimental groups and analyzed (@$p < 0.05$, unpaired two-tailed t-test). ITL-RTL values are presented to compare among six groups (*$p < 0.05$, #$p < 0.05$). **(h)** Percent freezing of animals in each experimental group in the probe day of contextual fear conditioning testis shown (*$p < 0.005$, #$p < 0.05$). **(i)** Depicts the percent freezing of mice in Cue-dependent fear conditioning probe tests that were conducted on the 2nd day following day-1 of acquisition. (*$p < 0.05$, #$p < 0.05$) (*) indicates p-values in comparison to Control group and (#) indicates p-values in comparison to 5XFAD group. The number of animals used in each of the mouse behavioral experiments are given in Table 2B.

thought to provide a synergistic effect that would surpass the benefits of individual herbs [42]. Moreover, they would be more effective in treating multi-faceted diseases like AD with a wide range of pathological pathways and multiple targets involved. Few polyherbal formulations from China have progressed to clinical trial level in AD namely Ba Wei Di Huang Wan (a mixture of Rehmannia along with seven plants) [83] and Yi-Gan San formula (a mixture of seven different branches and root stocks) [84]. Ayurveda has shown the use of medicinal plants in treating or managing several neurological disorders either individually or as polyherbal formulations collectively termed as *Medhya Rasayana*. Several of the compound *Rasayana* drugs include the herbal components present in MP and each single herb has been reported to be effective in regulating one or multiple targets in AD [85]. Clinical trials with traditional herbs have been limited to small studies. There is a lack of well-controlled large-scale trials in patients with dementia or AD. In healthy humans, treatment with Brahmi for three months enhanced spatial working memory [86,87]. In another study, 12-week treatment with standardized dose of Brahmi extract improved the response of participating volunteers without dementia (≥ 65 years) in a delayed recall and Stroop test (it tests the ability to decipher relevant and irrelevant information) [88]. Mandukaparni treatment also showed cognitive improvement with respect to working memory and self-rated mood in elderly participants without dementia [89]. However, most of these studies focused on healthy individuals without dementia, were performed with small groups over a short duration of trial and were poorly designed making them less reliable [85].

Recently, Brahmi Nei (BN), traditionally used for its immunomodulatory effects and in treating anxiolytic disorders, was tested for its

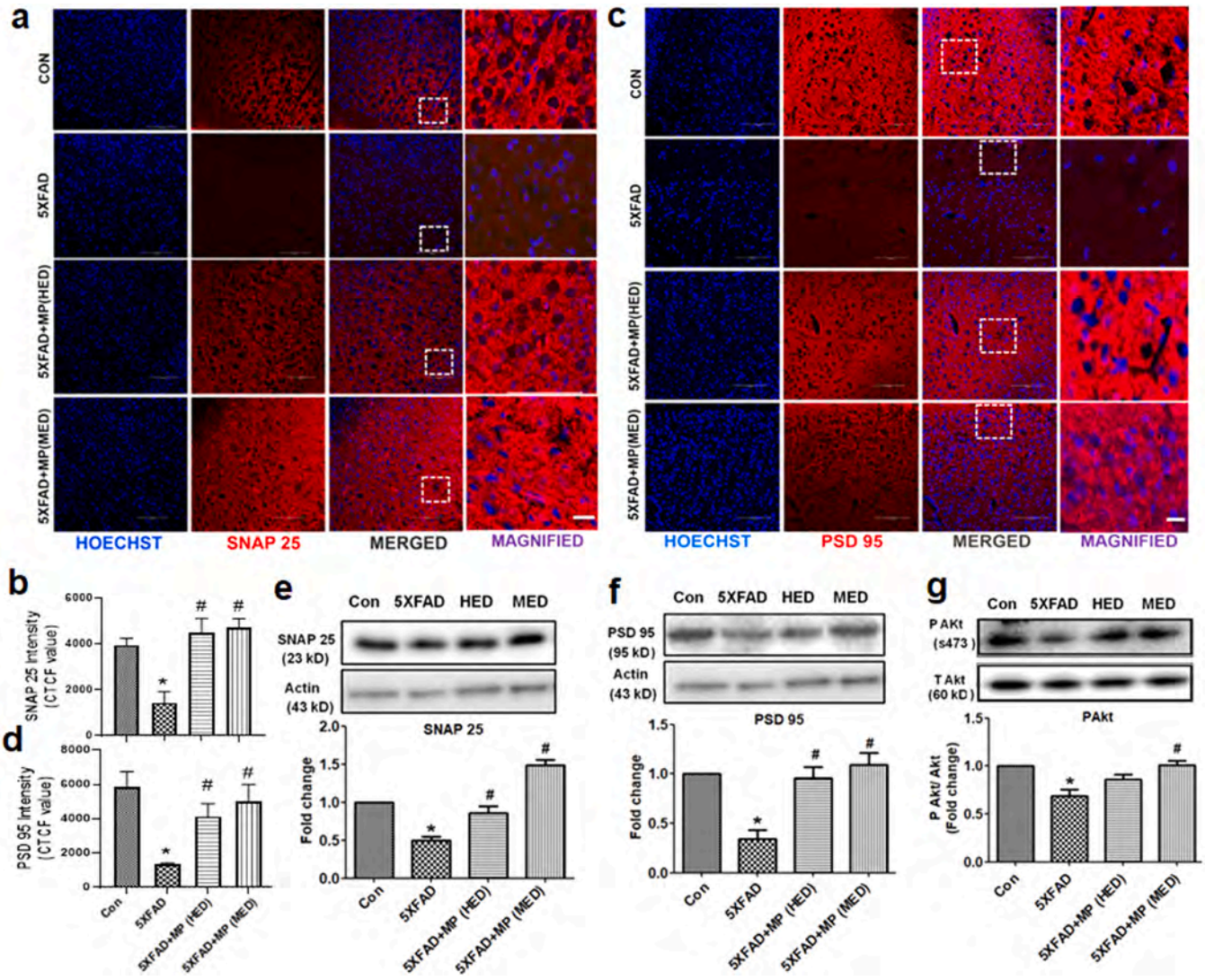

Fig. 7. Medha Plus (MP) rescues neurons from synaptoxicity in 5XFAD mice. Immunohistochemical staining shows SNAP 25 and PSD 95 expressions in mice 20 μm brain coronal sections in all the four groups. The horizontal panels in (a) and (b) represent images taken at 20X magnification in confocal microscope for each experimental group (top to bottom) – Control, 5XFAD, 5XFAD+MP (HED), 5XFAD+MP (MED). The 4 vertical panels (left to right) – Hoechst stain (blue), SNAP 25 or PSD 95 (red), merged images (scale bar - 100 μm) and magnified merged images (10 μm). SNAP 25 (b) and PSD 95 (c) fluorescence intensities were measured in the respective groups by using ImageJ software. Bar diagrams represent corresponding Mean ± S.E.M CTCF values of the respective groups, *$p < 0.05$, #$p < 0.05$ (three images per animal and $n = 3$ per group). Hippocampal tissue lysates from the above-mentioned four groups were subjected to immunoblot analysis and SNAP 25 (e) and PSD 95 (f) expressions are shown and quantified. Actin was taken as the loading control. Densitometric analysis of the blots was performed by ImageJ software. Values are expressed as Mean ± SEM *$p < 0.05$, #$p < 0.05$ ($n = 3$ per group). (**g**) Phosphorylation of AKT at ser473 was checked as an upstream regulator of the synaptic signaling pathway through immunoblotting and the total AKT level was checked as the loading control. Bar diagram shows the ratio of pAkt/tAkt derived from densitometric analysis of the blot using the ImageJ software. Values are expressed as Mean ± SEM. *$p < 0.05$,#$p < 0.05$)($n = 3$ per group). (*) indicates p-values in comparison to Control group and (#) indicates p-values in comparison to Aβ group.

ability to ameliorate cognitive deficits in a model of AD. BN is composed of eleven plant-derived components and it significantly prevented neurodegeneration, improved neuritic spine morphology, diminished amyloid plaque deposits, attenuated inflammatory damage, and enhanced working memory in scopolamine-administered rat model showing pathological features of AD. Indeed, it also upregulated pro-survival protein expressions and genes responsible for memory consolidation and growth of axons [90]. However, scopolamine-administered rat model does not manifest all features of AD and the study requires validation in a proper AD model.

We show that MP which combines six extremely common herbs, native to South-East Asia, already marketed as a novel polyherbal formulation for memory boosting, improving concentration and relieving anxiety and stress, display remarkable neuroprotective properties in models of AD. We performed extensive behavioral, histological and enzymatic studies in both sporadic model of AD (Aβ-injected rats) [60] as well as in an advanced familial AD model (5XFAD mice)[91] to strongly confirm the neuroprotective results we initially observed in neuronal cells *in vitro*. Aβ-injected rats display hyperexploratory behavior, increased anxiety level, attenuated short-term memory and impaired fear memory. Additionally, immunohistochemistry revealed strong amyloid plaque depositions and increased number of apoptotic cells in the hippocampal region near the site of injection of Aβ. Aβ-infused rats also displayed increased ROS production in the hippocampus but not in cortex. The reason for this discrepancy may be the site of infusion of Aβ (in the hippocampus) and hence, the ROS generation may not have reached the detectable level for our assay in the cortex at the time of experiment. AChE activity was also significantly upregulated in both hippocampus and cortex. All these features are coherent with that of a sporadic AD model, displaying a direct effect of oligomeric Aβ

accumulation.Thus, Aβ injection majorly dictates the development of all pathological features of AD including disrupted cholinergic system [92], ROS production [93] and neuronal apoptosis [60,66,74,75,94]. MP was able to ameliorate all these abnormalities to a significant level. Notably, the ability of MP to reduce Aβ plaques makes it a very good natural anti-amyloid agent. Further, its ability to target all these pathological aspects of AD with no side effects provides a holistic treatment strategy. 5XFAD is the most advanced familial AD model with five AD-related genetic mutations which show additional pathological features that go beyond the sporadicAβ-injected model (https://www.alzforum.org/research-models/5xfad-b6sjl). Hence, in order to reaffirm our results as well as to observe whether MP was effective for individuals with a family history of AD, this model was the most suitable since it displayed diminished level of synaptic protein expressions in the hippocampus along with a robust level of cognitive decline [95]. Reduced synaptic proteins - pre-synaptic SNAP 25 and post-synaptic PSD 95 expressions are sufficient markers to predict decreased synaptic plasticity [96]. Alteration of synaptic plasticity is implicated in learning and memory impairments correlated with numerous neurological disorders and psychiatric diseases including AD [96]. MP was able to recover 5-month old 5XFAD from the cognitive decline and improved synaptic integrity. An upregulated expression of phospho-Akt in MP treated 5XFAD mice further supported our results since PI3k/Akt signaling is shown to underlie GSK 3β regulation implicated in synaptic plasticity [97,98]. The present work investigated two different doses of MP in Aβ-injected rat model and 5XFAD mouse model individually. The higher dose applied in each model correlates with the metabolic rate in each type of rodent and was calculated according to a previous report [53] while the HED was calculated from the daily traditionally recommended dose taken by an individual. MP at its higher dose (RED in rat and MED in mouse) in each study was able to significantly recover the different types of cognitive abilities (spatial, associated, short term memories) and the underlying pathological changes in both the rodent models of AD. However, HED in each case induced a change that was either equivalent to the effect seen with the higher dose or at least indicated a similar trend (in a few studies the recovery was not statistically significant). This may be attributed to the superior performance of the animal with the more metabolically suitable dose in coherence to the fact that MP was given orally and hence this aspect should be considered in calculating dosing for future clinical trials with the drug. Moreover, the active components of these herbs that render the cognitive benefits and ameliorate pathological lesions in AD animal models are not determined in this study. Further studies are required to analyze the components of MP and identify its active ingredients.

Nonetheless, these results showcase the ability of multi-constituent MP in reversing cognitive deficits and underlying synaptic health in two different rodent models relevant to both sporadic and familial forms of AD. Its traditional use by people of India without any report of toxicity to date in addition to our study adding a scientific anti-AD aspect to its existing benefits, promote it as a frontline candidate drug for clinical trials in AD.

CRediT authorship contribution statement

Ramesh Kumar Paidi: Conceptualization, Methodology, Investigation, Data curation, Writing – original draft. **Sukanya Sarkar**: Conceptualization, Methodology, Investigation, Data curation, Writing – review & editing. **Naqiya Ambareen**: Methodology, Investigation. **Subhas C Biswas**: Conceptualization, Supervision, Funding acquisition, Writing – review & editing.

Data availability

Data will be made available on request.

Acknowledgement

The work has been supported by M/S Parker Robinson Pvt. Ltd. (http://www.parkerrobinson.org/Medha_Plus) who developed and supplied the “Medha Plus” formulation. We sincerely thank Mr. B. K. Sarkar, MD, Parker’s Robinson Pvt. Ltd, 1, Nimak Mahal Road, Kolkata 700043 for providing financial and logistic support. We acknowledge Mr. Ashish Kumar and Ms. Amrutha K. for their assistance in the preparation of CA, CP and BM extracts. We would like to thank DST, Govt. of India for Inspire fellowship to Sukanya Sarkar, CSIR, Govt. of India for Junior Research Fellowship to Naqiya Ambareen and CSIR-IICB for infrastructural facilities.

Appendix A. Supporting information

Supplementary data associated with this article can be found in the online version at doi:10.1016/j.biopha.2022.113086.

References

[1] S. Davinelli, N. Sapere, D. Zella, R. Bracale, M. Intrieri, G. Scapagnini, Pleiotropic protective effects of phytochemicals in Alzheimer’s disease, Oxid. Med. Cell. Longev. 2012 (2012), 386527.
[2] V.J. De-Paula, M. Radanovic, B.S. Diniz, O.V. Forlenza, Alzheimer’s disease, Subcell. Biochem 65 (2012) 329–352.
[3] C. Behl, B. Moosmann, Antioxidant neuroprotection in Alzheimer’s disease as preventive and therapeutic approach, Free Radic. Biol. Med. 33 (2) (2002) 182–191.
[4] E. Giacobini, The cholinergic system in Alzheimer disease, Prog. Brain Res. 84 (1990) 321–332.
[5] A. Venneri, R. Lane, Effects of cholinesterase inhibition on brain white matter volume in Alzheimer’s disease, Neuroreport 20 (3) (2009) 285–288.
[6] S. Muthuraju, P. Maiti, P. Solanki, A.K. Sharma, S.B. Amitabh, D. Singh, G. Prasad, Ilavazhagan, Acetylcholinesterase inhibitors enhance cognitive functions in rats following hypobaric hypoxia, Behav. Brain Res. 203 (1) (2009) 1–14.
[7] E. Giacobini, Cholinesterase inhibitors: new roles and therapeutic alternatives, Pharm. Res. 50 (4) (2004) 433–440.
[8] W. Danysz, C.G. Parsons, The NMDA receptor antagonist memantine as a symptomatological and neuroprotective treatment for Alzheimer’s disease: preclinical evidence, Int. J. Geriatr. Psychiatry 18 (Suppl. 1) (2003) S23–S32.
[9] L. Schneider, A resurrection of aducanumab for Alzheimer’s disease, Lancet Neurol. 19 (2) (2020) 111–112.
[10] B. Miziak, B. Blaszczyk, S.J. Czuczwar, Some candidate drugs for pharmacotherapy of Alzheimer’s disease, Pharmaceuticals 14 (5) (2021).
[11] R.J. Williams, K.P. Mohanakumar, P.M. Beart, Neuro-nutraceuticals: natural products nourish the brain but be aware of contrary effects, Neurochem. Int. 150 (2021), 105159.
[12] M. Govindarajulu, S. Ramesh, L. Neel, M. Fabbrini, M. Buabeid, A. Fujihashi, D. Dwyer, T. Lynd, K. Shah, K.P. Mohanakumar, F. Smith, T. Moore, M. Dhanasekaran, Nutraceutical based SIRT3 activators as therapeutic targets in Alzheimer’s disease, Neurochem. Int. 144 (2021), 104958.
[13] R.K. Paidi, Tetra hydro isoquinoline (TIQ), an ayurvedic herbal molecule ameliorates STZ-induced Alzheimer’s like phenotypes and neuropathology in rats, Alzheimer’s Dement. (2019) 274.
[14] D. Dutta, M. Majumder, R.K. Paidi, K. Pahan, Alleviation of Huntington pathology in mice by oral administration of food additive glyceryl tribenzoate, Neurobiol. Dis. 153 (2021), 105318.
[15] P. Upadhyay, A. Sadhu, P.K. Singh, A. Agrawal, K. Ilango, S. Purohit, G.P. Dubey, Revalidation of the neuroprotective effects of a United States patented polyherbal formulation on scopolamine induced learning and memory impairment in rats, Biomed. Pharmacother. = Biomed. Pharmacother. 97 (2018) 1046–1052.
[16] A. Mishra, A.K. Mishra, S. Jha, Effect of traditional medicine brahmi vati and bacoside A-rich fraction of Bacopa monnieri on acute pentylenetetrzole-induced seizures, amphetamine-induced model of schizophrenia, and scopolamine-induced memory loss in laboratory animals, Epilepsy Behav.: EB 80 (2018) 144–151.
[17] R.V. Rao, O. Descamps, V. John, D.E. Bredesen, Ayurvedic medicinal plants for Alzheimer’s disease: a review, Alzheimers Res. Ther. 4 (3) (2012) 22.
[18] R. Kapoor, S. Srivastava, P. Kakkar, Bacopa monnieri modulates antioxidant responses in brain and kidney of diabetic rats, Environ. Toxicol. Pharm. 27 (1) (2009) 62–69.
[19] T. Dubey, S. Chinnathambi, Brahmi (Bacopa monnieri): an ayurvedic herb against the Alzheimer’s disease, Arch. Biochem. Biophys. 676 (2019), 108153.
[20] T. Peth-Nui, J. Wattanathorn, S. Muchimapura, T. Tong-Un, N. Piyavhatkul, P. Rangseekajee, K. Ingkaninan, S. Vittaya-Areekul, Effects of 12-week Bacopa monnieri consumption on attention, cognitive processing, working memory, and functions of both cholinergic and monoaminergic systems in healthy elderly volunteers, Evid. Based Complement. Altern. Med. 2012 (2012), 606424.
[21] N. Limpeanchob, S. Jaipan, S. Rattanakaruna, W. Phrompittayarat, K. Ingkaninan, Neuroprotective effect of Bacopa monnieri on beta-amyloid-induced cell death in primary cortical culture, J. Ethnopharmacol. 120 (1) (2008) 112–117.

[22] S.K. Bhattacharya, A. Bhattacharya, A. Kumar, S. Ghosal, Antioxidant activity of Bacopa monniera in rat frontal cortex, striatum and hippocampus, Phytother. Res. 14 (3) (2000) 174–179.
[23] K. Anbarasi, G. Vani, K. Balakrishna, C.S. Devi, Effect of bacoside A on brain antioxidant status in cigarette smoke exposed rats, Life Sci. 78 (12) (2006) 1378–1384.
[24] N.E. Gray, A. Alcazar Magana, P. Lak, K.M. Wright, J. Quinn, J.F. Stevens, C. S. Maier, A. Soumyanath, Centella asiatica – phytochemistry and mechanisms of neuroprotection and cognitive enhancement, Phytochem. Rev. 17 (1) (2018) 161–194.
[25] J.U. Welbat, P. Chaisawang, W. Pannangrong, P. Wigmore, Neuroprotective properties of asiatic acid against 5-fluorouracil chemotherapy in the hippocampus in an adult rat model, Nutrients 10 (8) (2018).
[26] R.G. Krishnamurthy, M.C. Senut, D. Zemke, J. Min, M.B. Frenkel, E.J. Greenberg, S. W. Yu, N. Ahn, J. Goudreau, M. Kassab, K.S. Panickar, A. Majid, Asiatic acid, a pentacyclic triterpene from Centella asiatica, is neuroprotective in a mouse model of focal cerebral ischemia, J. Neurosci. Res. 87 (11) (2009) 2541–2550.
[27] R. Tabassum, K. Vaibhav, P. Shrivastava, A. Khan, M. Ejaz Ahmed, H. Javed, F. Islam, S. Ahmad, M. Saeed Siddiqui, M.M. Safhi, Centella asiatica attenuates the neurobehavioral, neurochemical and histological changes in transient focal middle cerebral artery occlusion rats, Neurol. Sci. 34 (6) (2013) 925–933.
[28] N.K. Sethiya, A. Nahata, P.K. Singh, S.H. Mishra, Neuropharmacological evaluation on four traditional herbs used as nervine tonic and commonly available as Shankhpushpi in India, J. Ayurv. Integr. Med. 10 (1) (2019) 25–31.
[29] G.L. Gupta, J. Fernandes, Protective effect of Convolvulus pluricaulis against neuroinflammation associated depressive behavior induced by chronic unpredictable mild stress in rat, Biomed. Pharmacother. = Biomed. Pharmacother. 109 (2019) 1698–1708.
[30] M.H. Shalavadi, V.M. Chandrashekhar, I.S. Muchchandi, Neuroprotective effect of Convolvulus pluricaulis choisy in oxidative stress model of cerebral ischemia reperfusion injury and assessment of MAP2 in rats, J. Ethnopharmacol. 249 (2020), 112393.
[31] R. Das, T. Sengupta, S. Roy, S. Chattarji, J. Ray, Convolvulus pluricaulis extract can modulate synaptic plasticity in rat brain hippocampus, Neuroreport 31 (8) (2020) 597–604.
[32] J. Mehla, P. Gupta, M. Pahuja, D. Diwan, D. Diksha, Indian medicinal herbs and formulations for Alzheimer's disease, from traditional knowledge to scientific assessment, Brain Sci. 10 (12) (2020).
[33] K.K. Chakravarthi, R. Avadhani, Beneficial effect of aqueous root extract of Glycyrrhiza glabra on learning and memory using different behavioral models: an experimental study, J. Nat. Sci. Biol. Med. 4 (2) (2013) 420–425.
[34] Y.M. Cui, M.Z. Ao, W. Li, L.J. Yu, Effect of glabridin from Glycyrrhiza glabra on learning and memory in mice, Planta Med. 74 (4) (2008) 377–380.
[35] D. Dhingra, M. Parle, S.K. Kulkarni, Memory enhancing activity of Glycyrrhiza glabra in mice, J. Ethnopharmacol. 91 (2–3) (2004) 361–365.
[36] M.J. Cho, J.H. Kim, C.H. Park, A.Y. Lee, Y.S. Shin, J.H. Lee, C.G. Park, E.J. Cho, Comparison of the effect of three licorice varieties on cognitive improvement via an amelioration of neuroinflammation in lipopolysaccharide-induced mice, Nutr. Res. Pract. 12 (3) (2018) 191–198.
[37] E.O. Farombi, A.O. Abolaji, B.O. Adetuyi, O. Awosanya, M. Fabusoro, Neuroprotective role of 6-Gingerol-rich fraction of Zingiber officinale (Ginger) against acrylonitrile-induced neurotoxicity in male Wistar rats, J. Basic Clin. Physiol. Pharm. 30 (3) (2018).
[38] O.A. Ahmed-Farid, S.A. Haredy, R.M. Niazy, R.J. Linhardt, M. Warda, Dose-dependent neuroprotective effect of oriental phyto-derived glycyrrhizin on experimental neuroterminal norepinephrine depletion in a rat brain model, Chem.-Biol. Interact. 308 (2019) 279–287.
[39] J. Guo, C.X. Yang, J.J. Yang, Y. Yao, Glycyrrhizic acid ameliorates cognitive impairment in a rat model of vascular dementia associated with oxidative damage and inhibition of voltage-gated sodium channels, CNS Neurol. Disord. - Drug Targets 15 (8) (2016) 1001–1008.
[40] N. Palachai, J. Wattanathorn, S. Muchimapura, W. Thukham-Mee, Phytosome loading the combined extract of mulberry fruit and ginger protects against cerebral ischemia in metabolic syndrome rats, Oxid. Med. Cell. Longev. 2020 (2020) 5305437.
[41] B. Topic, E. Tani, K. Tsiakitzis, P.N. Kourounakis, E. Dere, R.U. Hasenohrl, R. Hacker, C.M. Mattern, J.P. Huston, Enhanced maze performance and reduced oxidative stress by combined extracts of Zingiber officinale and Ginkgo biloba in the aged rat, Neurobiol. Aging 23 (1) (2002) 135–143.
[42] C. Sutalangka, J. Wattanathorn, Neuroprotective and cognitive-enhancing effects of the combined extract of Cyperus rotundus and Zingiber officinale, BMC Complement. Alter. Med. 17 (1) (2017) 135.
[43] D.K. Khatri, A.R. Juvekar, Neuroprotective effect of curcumin as evinced by abrogation of rotenone-induced motor deficits, oxidative and mitochondrial dysfunctions in mouse model of Parkinson's disease, Pharm. Biochem. Behav. 150–151 (2016) 39–47.
[44] M. Moon, H.G. Kim, J.G. Choi, H. Oh, P.K. Lee, S.K. Ha, S.Y. Kim, Y. Park, Y. Huh, M.S. Oh, 6-Shogaol, an active constituent of ginger, attenuates neuroinflammation and cognitive deficits in animal models of dementia, Biochem. Biophys. Res. Commun. 449 (1) (2014) 8–13.
[45] J.Y. Na, K. Song, J.W. Lee, S. Kim, J. Kwon, 6-Shogaol has anti-amyloidogenic activity and ameliorates Alzheimer's disease via CysLT1R-mediated inhibition of cathepsin B, Biochem. Biophys. Res. Commun. 477 (1) (2016) 96–102.
[46] A. Mahima, R. Rahal, S.K. Deb, H. Latheef, R. Abdul Samad, A.K. Tiwari, A. Verma, K. Kumar, Dhama, Immunomodulatory and therapeutic potentials of herbal, traditional/indigenous and ethnoveterinary medicines, Pak. J. Biol. Sci.: PJBS 15 (16) (2012) 754–774.
[47] G.H. Tekulu, A. Desta, M.G. Hiben, E.M. Araya, Anti-nociceptive and anti-inflammatory activity of Hygrophila schulli leaves, J. Inflamm. Res. 13 (2020) 497–505.
[48] M.G. Akimov, P.V. Dudina, E.V. Fomina-Ageeva, N.M. Gretskaya, A.A. Bosaya, E. V. Rudakova, G.F. Makhaeva, G.O. Kagarlitsky, S.A. Eremin, V.I. Tsetlin, V. V. Bezuglov, Neuroprotective and antioxidant activity of arachidonoyl choline, its bis-quaternized analogues and other acylcholines, Dokl. Biochem. Biophys. 491 (1) (2020) 93–97.
[49] N. Tofighi, M. Asle-Rousta, M. Rahnema, R. Amini, Protective effect of alpha-linoleic acid on Abeta-induced oxidative stress, neuroinflammation, and memory impairment by alteration of alpha7 nAChR and NMDAR gene expression in the hippocampus of rats, Neurotoxicology 85 (2021) 245–253.
[50] W. Ali, M. Ikram, H.Y. Park, M.G. Jo, R. Ullah, S. Ahmad, N.B. Abid, M.O. Kim, Oral administration of alpha linoleic acid rescues abeta-induced glia-mediated neuroinflammation and cognitive dysfunction in C57BL/6N mice, Cells 9 (3) (2020).
[51] D.S. Park, E.J. Morris, J. Padmanabhan, M.L. Shelanski, H.M. Geller, L.A. Greene, Cyclin-dependent kinases participate in death of neurons evoked by DNA-damaging agents, J. Cell Biol. 143 (2) (1998) 457–467.
[52] C.M. Troy, S.A. Rabacchi, W.J. Friedman, T.F. Frappier, K. Brown, M.L. Shelanski, Caspase-2 mediates neuronal cell death induced by beta-amyloid, J. Neurosci. 20 (4) (2000) 1386–1392.
[53] A.B. Nair, S. Jacob, A simple practice guide for dose conversion between animals and human, J. Basic Clin. Pharm. 7 (2) (2016) 27–31.
[54] M. Rastogi, R.P. Ojha, B.P. Devi, A. Aggarwal, A. Agrawal, G.P. Dubey, Amelioration of age associated neuroinflammation on long term bacosides treatment, Neurochem. Res. 37 (4) (2012) 869–874.
[55] Y.K. Gupta, M.H. Veerendra Kumar, A.K. Srivastava, Effect of Centella asiatica on pentylenetetrazole-induced kindling, cognition and oxidative stress in rats, Pharm. Biochem. Behav. 74 (3) (2003) 579–585.
[56] J. Malik, S. Choudhary, P. Kumar, Protective effect of Convolvulus pluricaulis standardized extract and its fractions against 3-nitropropionic acid-induced neurotoxicity in rats, Pharm. Biol. 53 (10) (2015) 1448–1457.
[57] A. Rukenstein, R.E. Rydel, L.A. Greene, Multiple agents rescue PC12 cells from serum-free cell death by translation- and transcription-independent mechanisms, J. Neurosci.: Off. J. Soc. Neurosci. 11 (8) (1991) 2552–2563.
[58] P. Sanphui, S.K. Pramanik, N. Chatterjee, P. Moorthi, B. Banerji, S.C. Biswas, Efficacy of cyclin dependent kinase 4 inhibitors as potent neuroprotective agents against insults relevant to Alzheimer's disease, PLoS One 8 (11) (2013), e78842.
[59] C.M. Troy, J.E. Friedman, W.J. Friedman, Mechanisms of p75-mediated death of hippocampal neurons. Role of caspases, J. Biol. Chem. 277 (37) (2002) 34295–34302.
[60] P. Saha, S. Sarkar, R.K. Paidi, S.C. Biswas, TIMP-1: a key cytokine released from activated astrocytes protects neurons and ameliorates cognitive behaviours in a rodent model of Alzheimer's disease, Brain Behav. Immun. 87 (2020) 804–819.
[61] H. Das, S. Sarkar, R.K. Paidi, S.C. Biswas, Subtle genomic DNA damage induces intraneuronal production of amyloid-beta (1–42) by increasing beta-secretase activity, FASEB J.: Off. Publ. Fed. Am. Soc. Exp. Biol. 35 (5) (2021), e21569.
[62] D.A. Sholl, Dendritic organization in the neurons of the visual and motor cortices of the cat, J. Anat. 87 (4) (1953) 387–406.
[63] G. Cuesto, L. Enriquez-Barreto, C. Carames, M. Cantarero, X. Gasull, C. Sandi, A. Ferrus, A. Acebes, M. Morales, Phosphoinositide-3-kinase activation controls synaptogenesis and spinogenesis in hippocampal neurons, J. Neurosci. 31 (8) (2011) 2721–2733.
[64] P. Sanphui, S.C. Biswas, FoxO3a is activated and executes neuron death via Bim in response to beta-amyloid, Cell Death Dis. 4 (2013), e625.
[65] R.K. Paidi, D.N. Nthenge-Ngumbau, R. Singh, T. Kankanala, H. Mehta, K. P. Mohanakumar, Mitochondrial deficits accompany cognitive decline following single bilateral intracerebroventricular streptozotocin, Curr. Alzheimer Res. 12 (8) (2015) 785–795.
[66] A. Saha, S. Saleem, R.K. Paidi, S.C. Biswas, BH3-only proteins Puma and Beclin1 regulate autophagic death in neurons in response to Amyloid-beta, Cell Death Discov. 7 (1) (2021) 356.
[67] V. Sharma, J.H. McNeill, To scale or not to scale: the principles of dose extrapolation, Br. J. Pharm. 157 (6) (2009) 907–921.
[68] S. Guha, R.K. Paidi, S. Goswami, P. Saha, S.C. Biswas, ICAM-1 protects neurons against Amyloid-beta and improves cognitive behaviors in 5xFAD mice by inhibiting NF-kappaB, Brain Behav. Immun. 100 (2021) 194–210.
[69] R.K. Paidi, M. Jana, R.K. Mishra, D. Dutta, K. Pahan, Selective inhibition of the interaction between SARS-CoV-2 spike S1 and ACE2 by SPIDAR peptide induces anti-inflammatory therapeutic responses, J. Immunol. 207 (10) (2021) 2521–2533.
[70] R.K. Paidi, M. Jana, S. Raha, M. McKay, M. Sheinin, R.K. Mishra, K. Pahan, Eugenol, a component of Holy Basil (Tulsi) and common spice clove, inhibits the interaction between SARS-CoV-2 spike S1 and ACE2 to induce therapeutic responses, J. NeuroImmune Pharm.: Off. J. Soc. NeuroImmune Pharm. (2021).
[71] R.K. Paidi, M. Jana, R.K. Mishra, D. Dutta, S. Raha, K. Pahan, ACE-2-interacting domain of SARS-CoV-2 (AIDS) peptide suppresses inflammation to reduce fever and protect lungs and heart in mice: implications for COVID-19 therapy, J. NeuroImmune Pharm.: Off. J. Soc. NeuroImmune Pharm. 16 (1) (2021) 59–70.
[72] D. De, I. Mukherjee, S. Guha, R.K. Paidi, S. Chakrabarti, S.C. Biswas, S. N. Bhattacharyya, Rheb-mTOR activation rescues Abeta-induced cognitive impairment and memory function by restoring miR-146 activity in glial cells, Molecular therapy, Nucleic Acids 24 (2021) 868–887.

[73] S. Sarkar, R.K. Paidi, S.C. Biswas, Astrocyte-secreted TIMP-1 binds to CD63 and differentially phosphorylates Akt in protecting neurons and promoting cognitive recovery in 5xFAD mice, Alzheimer's Dement. 17 (2021).
[74] M.P. Bordone, M.M. Salman, H.E. Titus, E. Amini, J.V. Andersen, B. Chakraborti, A. V. Diuba, T.G. Dubouskaya, E. Ehrke, A. Espindola de Freitas, G. Braga de Freitas, R.A. Goncalves, D. Gupta, R. Gupta, S.R. Ha, I.A. Hemming, M. Jaggar, E. Jakobsen, P. Kumari, N. Lakkappa, A.P.L. Marsh, J. Mitlohner, Y. Ogawa, R. K. Paidi, F.C. Ribeiro, A. Salamian, S. Saleem, S. Sharma, J.M. Silva, S. Singh, K. Sulakhiya, T.W. Tefera, B. Vafadari, A. Yadav, R. Yamazaki, C.I. Seidenbecher, The energetic brain – a review from students to students, J. Neurochem. 151 (2) (2019) 139–165.
[75] P. Saha, S. Guha, S.C. Biswas, P38K and JNK pathways are induced by amyloid-beta in astrocyte: implication of MAPK pathways in astrogliosis in Alzheimer's disease, Mol. Cell. Neurosci. 108 (2020), 103551.
[76] G.L. Ellman, K.D. Courtney, V. Andres Jr., R.M. Feather-Stone, A new and rapid colorimetric determination of acetylcholinesterase activity, Biochem. Pharm. 7 (1961) 88–95.
[77] B. Thomas, K.P. Mohanakumar, Melatonin protects against oxidative stress caused by 1-methyl-4-phenyl-1,2,3,6-tetrahydropyridine in the mouse nigrostriatum, J. Pineal Res. 36 (1) (2004) 25–32.
[78] J. Luo, R. Shi, Acrolein induces oxidative stress in brain mitochondria, Neurochem. Int. 46 (3) (2005) 243–252.
[79] M. Pandey, M. Varghese, K.M. Sindhu, S. Sreetama, A.K. Navneet, K. P. Mohanakumar, R. Usha, Mitochondrial NAD^+-linked state 3 respiration and complex-I activity are compromised in the cerebral cortex of 3-nitropropionic acid-induced rat model of Huntington's disease, J. Neurochem. 104 (2) (2008) 420–434.
[80] A. Sirichoat, W. Chaijaroonkhanarak, P. Prachaney, W. Pannangrong, R. Leksomboon, A. Chaichun, P. Wigmore, J.U. Welbat, Effects of asiatic acid on spatial working memory and cell proliferation in the adult rat hippocampus, Nutrients 7 (10) (2015) 8413–8423.
[81] M. Antunes, G. Biala, The novel object recognition memory: neurobiology, test procedure, and its modifications, Cogn. Process. 13 (2) (2012) 93–110.
[82] F. Ahmad, K. Singh, D. Das, R. Gowaikar, E. Shaw, A. Ramachandran, K. V. Rupanagudi, R.P. Kommaddi, D.A. Bennett, V. Ravindranath, Reactive oxygen species-mediated loss of synaptic Akt1 SIgnaling Leads to Deficient Activity-dependent Protein Translation Early in Alzheimer's disease, Antioxid. Redox Signal. 27 (16) (2017) 1269–1280.
[83] K. Iwasaki, S. Kobayashi, Y. Chimura, M. Taguchi, K. Inoue, S. Cho, T. Akiba, H. Arai, J.C. Cyong, H. Sasaki, A randomized, double-blind, placebo-controlled clinical trial of the Chinese herbal medicine "ba wei di huang wan" in the treatment of dementia, J. Am. Geriatr. Soc. 52 (9) (2004) 1518–1521.
[84] K. Iwasaki, T. Satoh-Nakagawa, M. Maruyama, Y. Monma, M. Nemoto, N. Tomita, H. Tanji, H. Fujiwara, T. Seki, M. Fujii, H. Arai, H. Sasaki, A randomized, observer-blind, controlled trial of the traditional Chinese medicine Yi-Gan San for improvement of behavioral and psychological symptoms and activities of daily living in dementia patients, J. Clin. Psychiatry 66 (2) (2005) 248–252.
[85] R. Sharma, K. Kuca, E. Nepovimova, A. Kabra, M.M. Rao, P.K. Prajapati, Traditional Ayurvedic and herbal remedies for Alzheimer's disease: from bench to bedside, Expert Rev. Neurother. 19 (5) (2019) 359–374.
[86] C. Stough, J. Lloyd, J. Clarke, L.A. Downey, C.W. Hutchison, T. Rodgers, P. J. Nathan, The chronic effects of an extract of Bacopa monniera (Brahmi) on cognitive function in healthy human subjects, Psychopharmacology 156 (4) (2001) 481–484.
[87] C. Stough, L.A. Downey, J. Lloyd, B. Silber, S. Redman, C. Hutchison, K. Wesnes, P. J. Nathan, Examining the nootropic effects of a special extract of Bacopa monniera on human cognitive functioning: 90 day double-blind placebo-controlled randomized trial, Phytother. Res. 22 (12) (2008) 1629–1634.
[88] C. Calabrese, W.L. Gregory, M. Leo, D. Kraemer, K. Bone, B. Oken, Effects of a standardized Bacopa monnieri extract on cognitive performance, anxiety, and depression in the elderly: a randomized, double-blind, placebo-controlled trial, J. Altern. Complement. Med. 14 (6) (2008) 707–713.
[89] J. Wattanathorn, L. Mator, S. Muchimapura, T. Tongun, O. Pasuriwong, N. Piyawatkul, K. Yimtae, B. Sripanidkulchai, J. Singkhoraard, Positive modulation of cognition and mood in the healthy elderly volunteer following the administration of Centella asiatica, J. Ethnopharmacol. 116 (2) (2008) 325–332.
[90] K. Rajendran, D.R. Chellappan, S. Sankaranarayanan, V. Ramakrishnan, U. M. Krishnan, Investigations on a polyherbal formulation for treatment of cognitive impairment in a cholinergic dysfunctional rodent model, Neurochem. Int. 141 (2020), 104890.
[91] A.L. Oblak, P.B. Lin, K.P. Kotredes, R.S. Pandey, D. Garceau, H.M. Williams, A. Uyar, R. O'Rourke, S. O'Rourke, C. Ingraham, D. Bednarczyk, M. Belanger, Z. A. Cope, G.J. Little, S.G. Williams, C. Ash, A. Bleckert, T. Ragan, B.A. Logsdon, L. M. Mangravite, S.J. Sukoff Rizzo, P.R. Territo, G.W. Carter, G.R. Howell, M. Sasner, B.T. Lamb, Comprehensive evaluation of the 5XFAD mouse model for preclinical testing applications: a MODEL-AD study, Front. Aging Neurosci. 13 (2021), 713726.
[92] M. Telles-Longui, D. Mourelle, N.M. Schowe, G.C. Cipolli, H.N. Malerba, H.S. Buck, T.A. Viel, alpha7 nicotinic ACh receptors are necessary for memory recovery and neuroprotection promoted by attention training in amyloid-beta-infused mice, Br. J. Pharm. 176 (17) (2019) 3193–3205.
[93] T. Schilling, C. Eder, Amyloid-beta-induced reactive oxygen species production and priming are differentially regulated by ion channels in microglia, J. Cell. Physiol. 226 (12) (2011) 3295–3302.
[94] A. Saha, S. Saleem, P.R. Kumar, S.C. Biswas, BH3-only proteins Puma and Beclin1 regulate autophagic death in neurons in response to Amyloid-beta, Cell Death Discov. 7 (1) (2021) 356.
[95] S. Kang, S. Ha, H. Park, E. Nam, W.H. Suh, Y.H. Suh, K.A. Chang, Effects of a dehydroevodiamine-derivative on synaptic destabilization and memory impairment in the 5xFAD, Alzheimer's disease mouse model, Front. Behav. Neurosci. 12 (2018) 273.
[96] N. Schaefer, C. Rotermund, E.M. Blumrich, M.V. Lourenco, P. Joshi, R. U. Hegemann, S. Jamwal, N. Ali, E.M. Garcia Romero, S. Sharma, S. Ghosh, J. K. Sinha, H. Loke, V. Jain, K. Lepeta, A. Salamian, M. Sharma, M. Golpich, K. Nawrotek, R.K. Paidi, S.M. Shahidzadeh, T. Piermartiri, E. Amini, V. Pastor, Y. Wilson, P.A. Adeniyi, A.K. Datusalia, B. Vafadari, V. Saini, E. Suarez-Pozos, N. Kushwah, P. Fontanet, A.J. Turner, The malleable brain: plasticity of neural circuits and behavior – a review from students to students, J. Neurochem. 142 (6) (2017) 790–811.
[97] A. Naskar, T. Manivasagam, J. Chakraborty, R. Singh, B. Thomas, M. Dhanasekaran, K.P. Mohanakumar, Melatonin synergizes with low doses of L-DOPA to improve dendritic spine density in the mouse striatum in experimental Parkinsonism, J. Pineal Res. 55 (3) (2013) 304–312.
[98] B. Shal, W. Ding, H. Ali, Y.S. Kim, S. Khan, Anti-neuroinflammatory potential of natural products in attenuation of Alzheimer's disease, Front. Pharm. 9 (2018) 548.

Received: 9 July 2020 | Revised: 12 March 2021 | Accepted: 17 March 2021

DOI: 10.1096/fj.202001676RR

RESEARCH ARTICLE

THE FASEB JOURNAL

Subtle genomic DNA damage induces intraneuronal production of amyloid-β (1-42) by increasing β-secretase activity

Hrishita Das | **Sukanya Sarkar** | **Ramesh K. Paidi** | **Subhas C. Biswas**

Cell Biology and Physiology Division, CSIR-Indian Institute of Chemical Biology, Kolkata, India

Correspondence
Subhas C. Biswas, Cell biology and Physiology Division, CSIR-Indian Institute of Chemical Biology, 4 Raja S. C. Mullick Road, Kolkata 700 032, India.
Email: biswassc@gmail.com; subhasbiswas@iicb.res.in

Funding information
SERB Projects, Grant/Award Number: EEQ/2018/000997

Abstract

Aberrant accumulation of amyloid-β (Aβ) in brain is the major trigger for pathogenesis in Alzheimer's disease (AD). It is imperative to understand how Aβ attains such toxic levels in the brain parenchyma. We detected that a subtle and tolerable amount of DNA damage, related to aging, increased intraneuronal $A\beta_{1\text{-}42}$ production both in cultured neuron and in cortex of rodent brain. Strikingly, we also observed elevated levels of mitochondrial fusion and of its major driver protein, MFN2. Hyperfusion of mitochondria may be seen as an adaptive stress response resulting from the induction of ER stress since we detected the activation of both PERK and IRE1α arms of unfolded protein response of ER stress. We found increased phosphorylation of PERK substrate eukaryotic initiation factor 2 α (eIF2α), and upregulation of the downstream effector proteins, ATF4 and CHOP. Concomitantly, increased XBP1 level, the direct effecter protein of IRE-1α, was observed. Reports suggest that eIF2α phosphorylation can increase BACE1 activity, the rate limiting enzyme in Aβ production. Here, we show that inhibiting PERK, decreased $A\beta_{1\text{-}42}$ level while direct BACE1 inhibition, reduced the mitochondrial fusion. We found increased MFN2 expression in young 5xFAD mice when Aβ plaques and neurodegeneration were absent. Thus, our study indicates that mild DNA damage leads to increased $A\beta_{1\text{-}42}$ production almost as a consequence of an initial ER stress-directed protective mitochondrial fusion in brain. We propose that an age-related subtle genomic DNA damage may trigger enhanced intraneuronal $A\beta_{1\text{-}42}$ production in an apparently healthy neuron way before the appearance of clinical symptoms in AD.

KEYWORDS

amyloid-β, DNA damage, BACE1, PERK, eIF2α, 5xFAD, MFN2

Abbreviations: Aβ, amyloid-β; AD, Alzheimer's disease; APP, amyloid precursor protein; MFN2, Mitofusin-2; BACE1, beta-site APP cleaving enzyme 1; CHL1, close homolog of L1; ATF4, activating transcription factor 4; CHOP, C/EBP homologous protein; XBP1, X-box-binding protein 1; PERK, protein kinase R-like endoplasmic reticulum kinase; DAPT, *N*-[*N*-(3,5-difluorophenacetyl)-l-alanyl]-*S*-phenylglycine *t*-butyl ester; SIME, stress-induced mitochondrial elongation; PTPRF, the protein tyrosine phosphatase receptor type f; MAM, mitochondria-associated membrane; eIF2α, eukaryotic initiation factor 2 α.

1 | INTRODUCTION

Alzheimer's disease (AD) is a progressive neurodegenerative disease with complex pathobiology. AD is recognized clinically by progressive cognitive decline and pathologically by the presence of extracellular senile plaques composed primarily of amyloid-$\beta_{1\text{-}42}$ ($A\beta_{1\text{-}42}$) peptide and by intracellular neurofibrillary tangles comprising hyperphosphorylated tau.[1] The majority of the AD cases is sporadic in nature and occurs after the age of 65 while few cases occur at an early age and are inherited in an autosomal fashion. The cause of sporadic AD is still a mystery. Age is the most consistent and a major risk factor for sporadic AD.[2]

Besides extracellular amyloid deposition in the brain parenchyma, emerging evidence indicates that Aβ peptides can accumulate intraneuronally. A large number of careful immunohistochemical studies using $A\beta_{1\text{-}42}$-specific antibodies, have shown an increase of intracellular Aβ in postmortem AD brains, especially in AD-susceptible brain regions, and in young transgenic mice way before the eventual extracellular plaque depositions, NFT formation, and cognitive impairments (reviewed in[1,3]). Interestingly, it has been shown that human neurons in AD-vulnerable regions specifically accumulate $A\beta_{1\text{-}42}$[3] and this intraneuronal accumulation precedes both Aβ plaque and neurofibrillary tangle formation.[4] It has also been shown that intraneuronal Aβ accumulation may contribute to hyperphosphorylation of tau[5] and cause synaptic dysfunction without the involvement of plasma membrane receptors.[6,7] This initial $A\beta_{1\text{-}42}$ accumulation is one of the earliest pathological events, thereby triggering the cascade leading to neurodegeneration.[1] However, how $A\beta_{1\text{-}42}$ is produced during aging and how it attains the eventual toxic level in the brain remains elusive.

Amyloid precursor protein (APP) is present in plasma membrane and it has a role in cell adhesion and cell movement.[3] APP is also present in the trans-Golgi network, endoplasmic reticulum (ER), endosomal, lysosomal, and mitochondrial membranes. The synthesis of Aβ could potentially occur wherever APP and the APP processing enzyme, β- and γ-secretases are localized, and it is likely that this occurs in several cellular compartments.[3] It has also been shown that presenilin-1 and presenilin-2 of γ-secretase complex are located at the interface between mitochondria and the ER.[8] The ER-mitochondria interface, commonly known as mitochondria-associated membrane (MAM) plays an essential role in Ca^{2+} signaling, lipid metabolism, mitochondrial morphology, apoptosis, etc. The communication between these two organelles has been shown to be dysregulated in AD.[9] Mitochondrial dysfunction has already been implicated in AD. Aβ has been shown to bind with alcohol dehydrogenase and directly leads to mitochondrial toxicity in AD patient and transgenic mice.[10] It has also been shown that Aβ progressively accumulate in mitochondria and lead to reduced oxygen consumption and decreased enzymatic activity of respiratory chain complexes (III and IV) and cytochrome c oxidase activity.[11,12] Impaired balance of mitochondrial fusion and fission plays an important role in synaptic dysfunction and its loss in AD.[13] Mitochondrial fusion boosts mitochondrial bioenergetics, increases ATP production, help in the exchange of mitochondrial DNA (mtDNA), and inhibit autophagy of mitochondria during stress conditions.[14] Increased fusion of mitochondria could be a result of early ER stress response that actually precedes mitochondrial fission.[15] Stress-induced mitochondrial hyperfusion (SIMH) is a dynamic remodeling of mitochondrial morphology that suppresses the pathologic mitochondrial fragmentation and promotes mitochondrial function. UV irradiation, thapsigargin, actinomycin D, and cycloheximide treatment can induce SIMH. It is considered as an adaptive stress response of a cell before succumbing to the stress.[16] In response to ER stress, cells induce a highly conserved stress response to maintain cellular homeostasis, termed as unfolded protein response (UPR).[17] It has been shown that UPR arm of ER stress is activated in early stages of AD in apparently healthy looking neurons which might be a part of protective mechanism.[18] In response to the misfolding of newly synthesized proteins inside ER, interplay between active ATF6, IRE-1α, and PERK initiate parallel signaling cascades that selectively promote the expression of UPR-target genes important for mitigating damage. IRE-1α as well as PERK indirectly helps in reducing the amount of unfolded polypeptide present inside the ER for more effective chaperone-mediated folding of proteins in a well saturated ER lumen. The dimerization of PERK leads to the activation of its cytosolic kinases, which subsequently phosphorylate serine 51 on the α-subunit of eukaryotic initiation factor 2α (eIF2α). Phosphorylation of eIF2α prevents conventional global translation. This halt of translation in this manner increases the probability that ribosomes will scan past inhibitory upstream open reading frames, resulting in increased translation of a specific subset of mRNAs, UPR responsive genes, antioxidants, molecular chaperons, most notably an mRNA that encodes ATF4. In addition to promoting an adaptive response, ATF4 regulates the transcription of the gene encoding pro-apoptotic factor CCAAT-enhancer-binding protein homologous protein (CHOP). Sustained UPR will thus lead to the expression of pro-apoptotic genes leading to activation of cell death in a later period.[17] During this time, strong association of ER-mitochondria contact sites is also observed, reasonably in order to support the high energy demand of ER stress-induced transcriptional machinery.[19]

Mitofusin 1 (MFN1) and mitofusin 2 (MFN2), integral proteins of the mitochondrial outer membrane, are required for fusion of adjacent mitochondria.[19,20] Although both MFN1 and MFN2 are required for mitochondrial fusion, MFN2 is predominantly expressed in the brain and they have a certain degree of redundancy.[21] MFN2 is a important player in maintenance of mitochondrial dynamics. Moreover, it is also

involved in MAM formation. Accumulating evidences also suggest a role of MFN2 in AD. Its level is decreased in frontal cortex and hippocampus in postmortem AD patients.[13,22] MFN2 level also decreases with age in AD mice. However, in different AD models, an increased ER-mitochondria coupling has been observed at early stages of the disease.[19] In particular, it has been shown that Presinilin-2 mutations, as in familial AD, directly increased ER-mitochondria coupling by binding or sequestering to MFN-2.[8,19]

DNA damage is a stress that individuals experience throughout their life span but increases exponentially with aging. It has been reported that DNA double-strand breaks and DNA damage response activation occurs in primary neurons treated with camptothecin (CPT).[23] CPT is a topoisomerase-I (TOP1) inhibitor which binds with TOP1/DNA complex resulting in DNA strand breaks.[24] TOP1 is necessary to remove DNA supercoiling during transcription. It relaxes supercoiling by forming transient TOP1 cleavage complexes (TOP1cc), which are TOP1-linked DNA single-strand breaks. CPT traps the transient TOP1cc and forms DNA double-strand breaks.[25] Doxorubicin (Dox) is another widely used DNA damaging agent. It is reported that there is decline in cognitive function in patients in the later period of treatment with Dox mainly for breast cancer.[26] Dox can intercalate DNA in the nucleus and inhibits the enzyme topoisomerase II. In cultured neurons, it can cause neurotoxicity and subsequent cell death.[26]

DNA damage is implicated in many diseases and presents an important aspect in AD as the affected part of CNS also shows an increased sign of DNA damage.[27] It was hypothesized around 30 years ago that increased DNA damage may be associated with AD due to the observation of specific chromatin structure alteration in AD patients.[28] Subsequently there is at least twofold increase in DNA breaks in cortices of AD patients, underscoring the contribution of accumulated genomic damage.[29] Hippocampal DNA from late stage AD brain was shown to have a twofold acrolein/guanosine DNA adducts as compared to that of an unaffected brain.[28,30] Here, in this study we have investigated whether a subtle DNA damage leads to an increased Aβ synthesis in neurons or not. Interestingly, we found signs of ER stress and elongated mitochondrial morphology as a consequence of adaptive stress response induced by mild DNA damage. ER stress further triggered enhanced activity of β-secretase and subsequent Aβ production.

2 | MATERIALS AND METHODS

2.1 | Materials

Camptothecin (CPT), Doxorubicin (Dox) Methylthiazolyldiphenyl-tetrazolium bromide (MTT), Insulin, progesterone, putrescine, selenium, transferrin, poly-D-lysine, Tetramethylrhodamine methyl ester perchlorate (TMRM), and DCFDA probe were purchased from Sigma (St. Louis, MO, USA). (3,5-Difluorophenylacetyl)-L-alanyl-L-2-phenylglycine tert-butyl ester (DAPT) was purchased from TCI chemicals (Portland). Fetal bovine serum, Horse serum, Goat serum, Dulbecco's modified Eagle's Medium, penicillin-streptomycin solution were purchased from Gibco (Thermo Fisher Scientific). Anti-pH2AX, Anti-PERK, Anti-phospho-PERK, anti-eIF2α, anti-phospho-eIF2α, XBP1, IRE1α, ATF4, and CHOP antibodies were purchased from Cell Signaling Technology. Anti-$A\beta_{1\text{-}42}$, Anti-MFN2 antibody were purchased from Abcam. CHL-1 antibody was purchased from R&D systems. N-Cadherin, PTPRF, APP, BACE1 antibodies were purchased from ABclonal. Phospho-IRE1α antibody, Alexa Fluor 488, Alexa Fluor 568, and all the culture media were purchased from Invitrogen (Life Technologies). HRP-conjugated secondary mouse and rabbit antibodies were purchased from Santa Cruz Biotechnology. Fluorophore-conjugated pH2AX antibody suitable for flow cytometry was purchased from BD Biosciences. MitoTracker Red CMXRos, MitoSOX Red were purchased from molecular probes (Thermo Fisher Scientific). β-Secretase inhibitor IV and PERK inhibitor (GSK2656157) were purchased from Cayman chemical. siAPP and siBACE1 were purchased from ambion (Life Technologies). SH-SY5Y cell line was purchased from ATCC, MFN2 Knock out mouse embryonic fibroblast cell line and normal Mouse embryonic fibroblast (MEF) cell line were a kind gift from Dr Suvendra Nath Bhattacharya, IICB, Kolkata, India. PC12 cell were obtained from Dr Lloyd A. Greene, Columbia University, New York, USA. 5xFAD AD transgenic mice were purchased from the Jackson laboratory, USA. Male Sprague Dawley rats were purchased from IICB animal house.

2.2 | Cell culture and treatment

Rat pheochromocytoma cells (PC12) cells were cultured as described previously.[31] Cells were maintained in DMEM medium supplemented with 10% heat-inactivated horse serum (HS) and 5% heat-inactivated fetal bovine serum (FBS), and neuronally differentiated by NGF (50 ng/mL) in DMEM supplemented with 1% HS for 5-7 days. Experiments were performed after 5 days. SH-SY5Y cells were cultured in DMEM medium supplemented with 10% heat-inactivated FBS and differentiated in presence of Retinoic acid (10 μmol/L) for 7 days before the treatment. Primary cortical neurons were cultured from the neocortex of E-18 rat embryo in serum-free medium (DMEM/F12 [1:1]) supplemented with 6 mg/mL of D-glucose, 100 μg/mL of transferrin, 25 μg/mL of insulin, 20 nmol/L of progesterone, 60 μmol/L of putrescine, and 30 nmol/L of selenium) on poly-D-lysine coated plates as described previously.[32] After 5 days, the neurons were treated with CPT.

2.3 | Immunoblotting

Cortical neurons, neuronally differentiated PC12 and SH-SY5Y cells were lysed and proteins were analyzed by western blotting as described previously.[33,34] For quantification of secreted proteins, conditioned medium from treated SH-SY5Y cells was concentrated using Amicon Ultra Centrifugal Filter Devices 50K (Millipore) before western blot analysis. For each condition 50 μg of protein (cell lysate) or 100 μg protein (conditioned medium) were resolved in SDS-PAGE and then, transferred to PVDF membrane. HRP-conjugated secondary antibodies against the primary antibodies were used. Detection was carried out by Clarity Max western ECL substrate (BIO-RAD) detection reagent, according to the manufacturer's protocol. Imaging of all Western blots was performed using a ChemiDoc MP imaging system (BIO-RAD).

2.4 | CPT infusion in animals

Male Sprague Dawley rats were anesthetized by injecting sodium pentobarbital and placed on a stereotaxic frame, and then a volume of 5 μL of desired dose of CPT in DMSO was infused in the right cerebral cortex at stereotaxic coordinates from bregma (AP, −4.1 mm; L, 2.5 mm; DV, 1.3 mm) according to the rat brain atlas. The opposite side was considered as vehicle control infusion site which was infused with DMSO. After 2 days of injection, animals were sacrificed.

2.5 | Preparation of cells from rat brain cortex for FACS analysis

The protocol was used as described by Brewer et al[35] with few modifications. Neocortex region was taken from rat brain after sacrifice. The cortex was minced with razor blades on ice-cold glass plate and placed in a 1.5 mL eppendorf tube and weighed on a fine balance. Neurobasal medium (10 times of volume of the weight of the sample) was added and the tube was kept on ice. The minced tissue was incubated with 0.05% collagenase-containing fresh neurobasal medium for 30 minutes at 4°C. Cell pellet was collected by centrifuging at 425 × g for 2 minutes at 4ºC and the pellet was resuspended in ice-cold neurobasal medium replacing the previous collagenase-containing medium. To dissociate tissue, samples were triturated 10 times with fire-polished Pasteur pipette. To remove large debris and cell clusters from the cell suspension, the supernatant were filtered through pre-wetted 70 μm cell strainers on ice. Small cellular debris was removed by density centrifugation through a three density step gradient of percoll, 1ml of each solution (high density solution: 3.426 mL neurobasal medium +824.5 μL percoll +97.8 μL of 1 mol/L NaCl), (medium density solution: 3.600 mL neurobasal medium +650.5 μL percoll +76.5 μL of 1 mol/L NaCl), and (low density solution: 3.770 mL neurobasal medium +480.3 μL percoll +59.5 μL of 1 mol/L NaCl), was carefully layered in a 15 mL falcon tube with the highest density solution on the bottom. The filtered cell suspension was applied to the top of this gradient and centrifuged at 430 *g* for 3 minutes. The cloudy top layer (~2 mL) containing debris was discarded. Cells in the remaining layers were pelleted by centrifugation at 550 *g* for 5 minutes. The upper layer was removed and again centrifuged to see visible pellet. To fix the cell ice-cold 100% ethanol was added to each tube, gently vortexed, kept on ice for 15 minutes with occasional inversion. To remove the ethanol, cells were pelleted by centrifugation at 425 *g* for 2 minutes and then, processed for FACS. Cells were incubated with primary antibody conjugated with secondary fluorophore and incubated in room temperature for 30 minutes. After washing in wash buffer (PBST) the cells were suspended in staining buffer. Staining buffer was prepared from 0.05% FBS and 0.09% sodium azide. Samples were then placed in FACS tube and analyzed in Flow cytometry.[35]

2.6 | Transfection

SH-SY5Y cells were plated in 24-well plate on coverslips and primed for 2 days in the presence of RA. Transfection was done on second day of priming in sera and antibiotic-free growth medium using lipofectamine 2000. Annealed validated siRNA against APP, BACE1, and MFN2 purchased from ambion were used for the downregulation. Six-hours post-transfection the sera-free medium was replaced with priming medium. Cells were maintained for 48 hours before treatment. On the fifth day, treatment was done in sera free medium and cells or conditioned media were harvested for further experiments.

2.7 | Immunochemistry

Cortical neurons and neuronally differentiated SH-SY5Y cells plated on Poly-D-lysine coated cover slips were fixed with 4% paraformaldehyde for 10 minutes. Cells were then washed thrice with PBS for 5 minutes each, then blocked in 3% goat serum in PBS containing 0.3% Triton-X 100 (PBST) for 2 hours at room temperature. The cells were immunolabeled with primary antibody in a blocking solution overnight at 4°C. The next day cells were washed thrice for 10 minutes each in PBST, followed by incubation with the appropriate secondary antibody for 2 hours at room temperature in blocking solution. Again cells were washed thrice each for 10 minutes in PBST. Nuclei were stained with Hoechst 33342 (Molecular Probes, Invitrogen) at a concentration of 2 μg/mL in PBS for 30 minutes at room temperature. The pictures were taken under a confocal microscope (Leica). The corrected total cell fluorescence (CTCF) was

determined by considering the integrated density of staining, area of the cell, and the background fluorescence of different experimental conditions. CTCF = Integrated density – (area of selected cell × mean fluorescence of background readings).[33]

Twenty micrometers of cryosections of the brain from CPT-infused or PBS-infused rats and wild-type or transgenic mice were immunostained as described previously.[34] In brief, the sections were blocked with 5% goat serum in PBS containing 0.3% Triton-X 100 for 1 hour at room temperature. Brain slices were incubated in primary antibody in a blocking solution overnight at 4°C. Sections were washed thrice with PBST and incubated with a fluorescence-tagged secondary antibody for 2 hours at room temperature. Following three washes with PBST and Hoechst staining, the sections were mounted and observed under fluorescence or confocal microscopes.

2.8 | Extracellular flux (XF) analysis

Oxygen consumption rate (OCR) was measured as described previously (Qian and Van Houten, 2010). Cells were seeded in XFe24 cell culture plates at 1×10^4 cells/well and incubated in 5% CO_2 at 37°C. Prior to the analysis, cells were washed and growth medium was replaced with bicarbonate-free modified RPMI 1640 medium, the "assay medium" (Molecular Devices, Sunnyvale, CA). Cells were then incubated for another 60 minutes in a 37°C incubator without CO_2. Oxygen consumption rate were then performed simultaneously using a Seahorse XFe24 Extracellular Flux Analyzer (Seahorse Bioscience, North Billerica, MA).

2.9 | Mitochondrial membrane potential, superoxide generation, and morphology

To measure mitochondrial membrane potential and superoxide generation, cells were incubated in either 25 nmol/L of TMRM (to measure mitochondrial membrane potential) or 3 μmol/L of MitoSox (to measure mitochondrial ROS) or 1 μmol/L of DCFDA (to measure total cellular ROS) for 20 minutes at 37°C, respectively, in dark. At first cells were trypsinized and suspended in HBSS containing 1% BSA or DPBS. Then, the appropriate dye was added in the same solvent and incubated. After the incubation, cells were pelleted down in 600 *g* for 5 minutes and washed thrice in the same solvent. DCF, TMRM, and MitoSox fluorescence intensity were analyzed using flow cytometer.

To study mitochondrial morphology, cells were incubated with 20 nmol/L MitoTracker red dissolved in growth medium for 20 minutes at 37°C and washed in PBS/media thrice for 5 minutes each to remove the excess dye. Then the cells were fixed in ice-cold methanol for 15 minutes at −20°C, washed thrice with PBS for 5 minutes each and then, nuclei were stained with Hoechst. After mounting the cells were visualized under a confocal microscope.

2.10 | ELISA of $A\beta_{1\text{-}42}$

Secretary level of $A\beta_{1\text{-}42}$ was measured from the spent medium of cultured SH-SY5Y cells and primary cortical neurons using Human/Rat β-amyloid $_{1\text{-}42}$ ELISA kit from Wako, USA (cat no. 290-62601) and R&D systems (Cat no. DAB142) following the manufacturer's protocol.

2.11 | MTT assay

Cells were incubated with 0.5 mg/mL MTT dissolved in the growth media. Cells were kept in 37°C for 4-6 hours until the purple formazan complex is formed. The media is then discarded slowly without disturbing the formazan complex. DMSO is added to dissolve the complex and OD was measured at 550 nm.

2.12 | BACE1 activity

The activity of the enzyme was measured using the β-secretase activity assay kit from Calbiochem (cat no. 565785) following the manufacturer's protocol.

2.13 | sAPPβ ELISA

sAPPβ was quantified using ELISA kit from mybiosource, San Diego, USA (cat no. MBS018909) following the manufacturer's protocol.

2.14 | Imaging and analysis of mitochondrial size

Cells were seeded on cover slips for immunofluorescence and stained as described earlier. Fixed cells were imaged under confocal microscope (Leica TCS SP8) using a 63X oil objective. LAS X software is used for exporting the images. The size of mitochondria was measured using Image J software.

2.15 | Statistics

All experimental results are reported as mean ± SEM. Student's *t*-test was performed as unpaired, two-tailed sets

of arrays to evaluate the significance of difference between the means and are presented as *P* values. One-way ANOVA was performed for experiments containing more than two groups.

3 | RESULTS

3.1 | Camptothecin induces DNA damage but not death in neurons at low doses

It has been reported that CPT induces DNA double-strand breaks and DNA damage response (DDR) activation with the formation of nuclear DDR foci-containing pH2AX (phosphorylated form of H2AX) in primary neurons.[23] It has also been shown that 10 μmol/L CPT induces massive cell death in primary neurons after 24 hours.[36] First, we performed a dose-response study to find a window of doses of CPT that do not induce death after 24 hours in neuronally differentiated SH-SY5Y cells (Figure 1A). We found that induction of death occurred starting from the dose of 500 nmol/L in SH-SY5Y cells following 24 hours of CPT treatment. Next, we checked the effect of the non-lethal doses of CPT in primary cortical neurons (Figure 1B) and we observed no induction of significant death up to 50 nmol/L CPT after 24 hours. Interestingly, though there was no induction of neuron death following 24 hours of incubation with CPT in the selected range of doses, accumulation of pH2AX (a marker for DNA damage)[37] took place starting from the dose of 5 nmol/L. Immunocytochemical analysis showed increased number of pH2AX foci in the nucleus compared to control when SH-SY5Y cells were treated with 5, 10, or 25 nmol/L CPT (Figure 1C,D). Hence, the 10 nmol/L dose was mostly chosen for further studies. For the in vivo study, 100 nmol/L CPT was infused stereotaxically (about 10-fold of the in vitro dose) in rat brain, single cell suspension was prepared from the infused area of the cortex, fixed, stained with antibodies against pH2AX and cleaved caspase-3, and flow cytometry analysis was done (see methods for details). Results revealed an increased number of the pH2AX-positive cells after 48 hours of 100 nmol/L CPT treatment which are represented by the Q4 quadrant (Figure 1E,F). In contrast, there was no significant increase in the cleaved caspase-3-positive cells which are represented by the Q1 quadrant (Figure 1E).

3.2 | Level of $A\beta_{1\text{-}42}$ is increased in response to mild DNA damage in neuron

Since aging is considered as one of the major risk factors for AD, we were curious to find out whether a mild DNA damage induces Aβ production in neurons as a stress response or not. Using transgenic AD mice and human AD patients' vulnerable brain regions, several studies have shown that early accumulation of Aβ peptides inside neurons is one of the earliest pathological events leading to synaptic dysfunction and neurodegeneration.[1,4] We checked the level of intracellular Aβ in differentiated SH-SY5Y cells treated with 10 nmol/L concentration of CPT for 24 hours by $A\beta_{1\text{-}42}$ immunostaining using confocal microscope. It was observed that there was increased $A\beta_{1\text{-}42}$ immunoreactivity in differentiated SH-SY5Y cells as compared to untreated control cells (Figure 2A,B). The level of $A\beta_{1\text{-}42}$ was also checked in the spent media of SH-SY5Y cells by sandwich ELISA against $A\beta_{1\text{-}42}$. The secretory level of $A\beta_{1\text{-}42}$ was also increased significantly in CPT-treated cells as compared to control cells (Figure 2C). Increased levels of $A\beta_{1\text{-}42}$ were also found in primary cortical neurons when treated with 10 nmol/L dose of CPT (Figure 2D-F). Moreover, immunohistochemistry of rat brains infused with CPT using an anti-$A\beta_{1\text{-}42}$ antibody showed that there was accumulation of $A\beta_{1\text{-}42}$ in the cortex (Figure 2G,H). To check the specificity of staining for $A\beta_{1\text{-}42}$, we performed siRNA-mediated downregulation of APP and BACE1 in differentiated SH-SY5Y cells. We detected that transfection of siAPP and siBACE1 caused 60% and 70% knockdown of APP and BACE1, respectively, (Figure S1A-D) which proves the efficacy of the siRNAs. Downregulation with each of the siRNAs reduced the intensity of Aβ staining even in the presence of CPT in differentiated SH-SY5Y cells (Figure S1E,F). Similar finding was observed with DAPT, a γ-secretase inhibitor,[38] treatment in differentiated SH-SY5Y cells. Pre-treatment with DAPT (250 nmol/L) for 2 hours diminished the increment of Aβ observed after CPT treatment (Figure S1E,F). The secretory level of Aβ was also reduced significantly after downregulation of APP, BACE1 and treatment with DAPT (Figure S1G). Taken together, these results validate the specificity of the $A\beta_{1\text{-}42}$ antibody and suggest that production of $A\beta_{1\text{-}42}$ was increased in neuronal cells and brain cortex in response to mild DNA damage.

There are plenty of evidences that support the fact that Aβ and oxidative stress are linked together.[39,40] We were interested to see whether the mild DNA damage-induced $A\beta_{1\text{-}42}$ production is mediated by oxidative stress in our model system. Interestingly, we found that increased $A\beta_{1\text{-}42}$ levels in neurons were not dependent on generation of hydroxyl and superoxide radicals. When differentiated SH-SY5Y cells were treated with 5 nmol/L to 50 nmol/L CPT for 24 hours, increase in total cellular ROS was not observed (Figure 2I). Moreover, another neuronal cell line, differentiated PC12 cells when treated with 10 nmol/L CPT, neither death nor increase in total cellular ROS or mitochondrial ROS were observed (Figure S1H-J). These results indicate that $A\beta_{1\text{-}42}$ could be generated in neurons independent of oxidative stress.

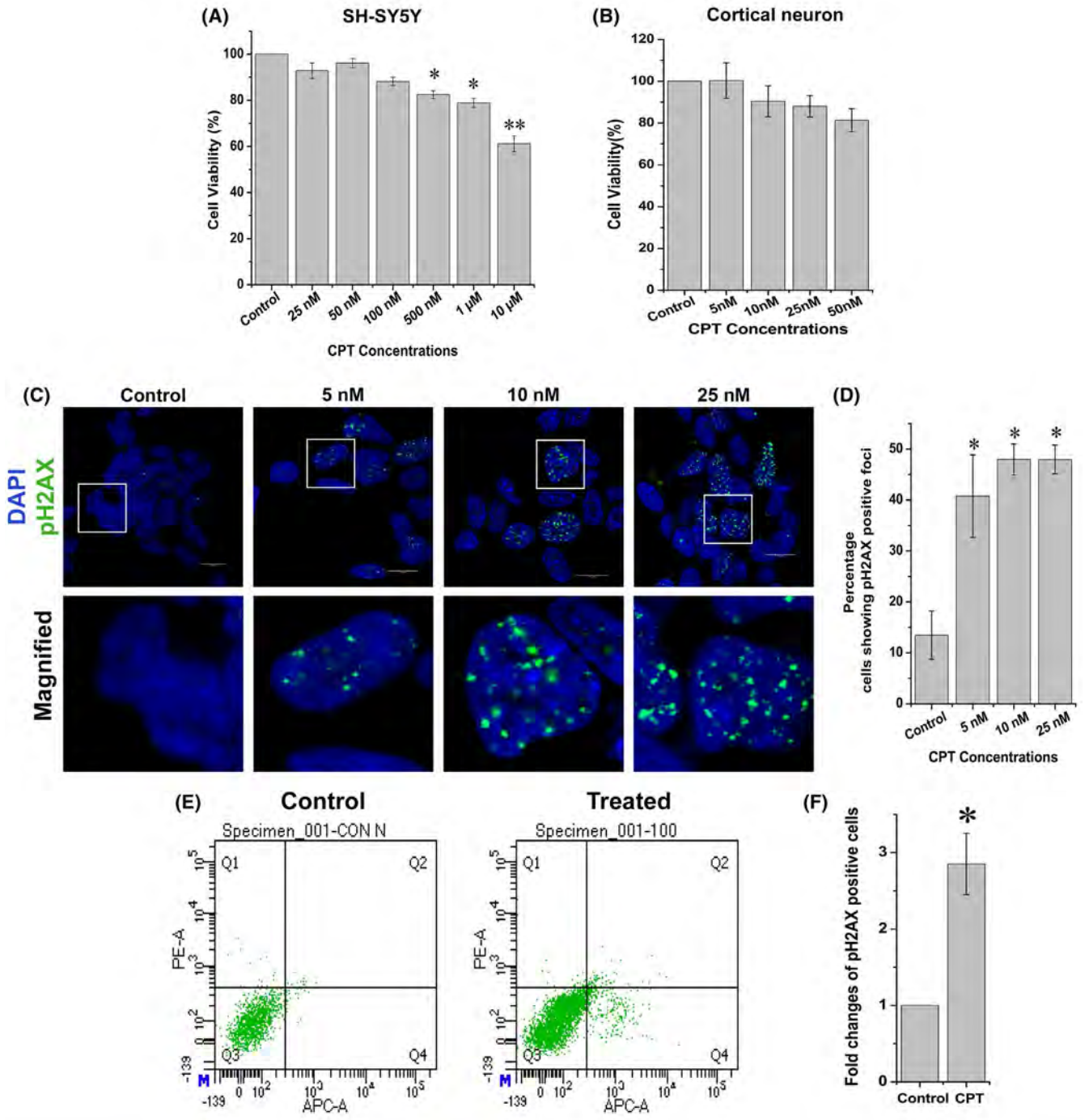

FIGURE 1 Camptothecin (CPT) induces genomic DNA damage but not neuron death at low doses. A and B, Neuronally differentiated, SH-SY5Y cells (A) and primary cortical neurons (B) were treated with CPT (5 nmol/L-10 μmol/L) for 24 h. Cell viability was checked by MTT assay. Data are represented as mean ± SEM (*$P < .05$; **$P < .01$; n = 3). C, Differentiated SH-SY5Y cells were treated with CPT for 24 h, and then subjected to immunocytochemical staining with DNA damage marker pH2AX antibody followed by nuclear staining with Hoechst. Note the pH2AX-positive foci (green dots) in nuclei having DNA double-strand breaks. D, Number of cells positive for pH2AX foci were counted from random fields of three independent experiments and represented as percentage of cells showing pH2AX-positive foci. Data are represented as mean ± SEM (*$P < .05$). E, Induction of DNA damage in rat brain cortex after infusion with 100 nmol/L CPT for 48 h. The Q4 quadrant is presenting cells which are positive for pH2AX and Q1 showing cells positive for cleaved caspase-3. F, Quantitative representation of the flow cytometric analysis of cells showing pH2AX-positive foci. Data are represented as mean ± SEM (*$P < .05$, n = 3)

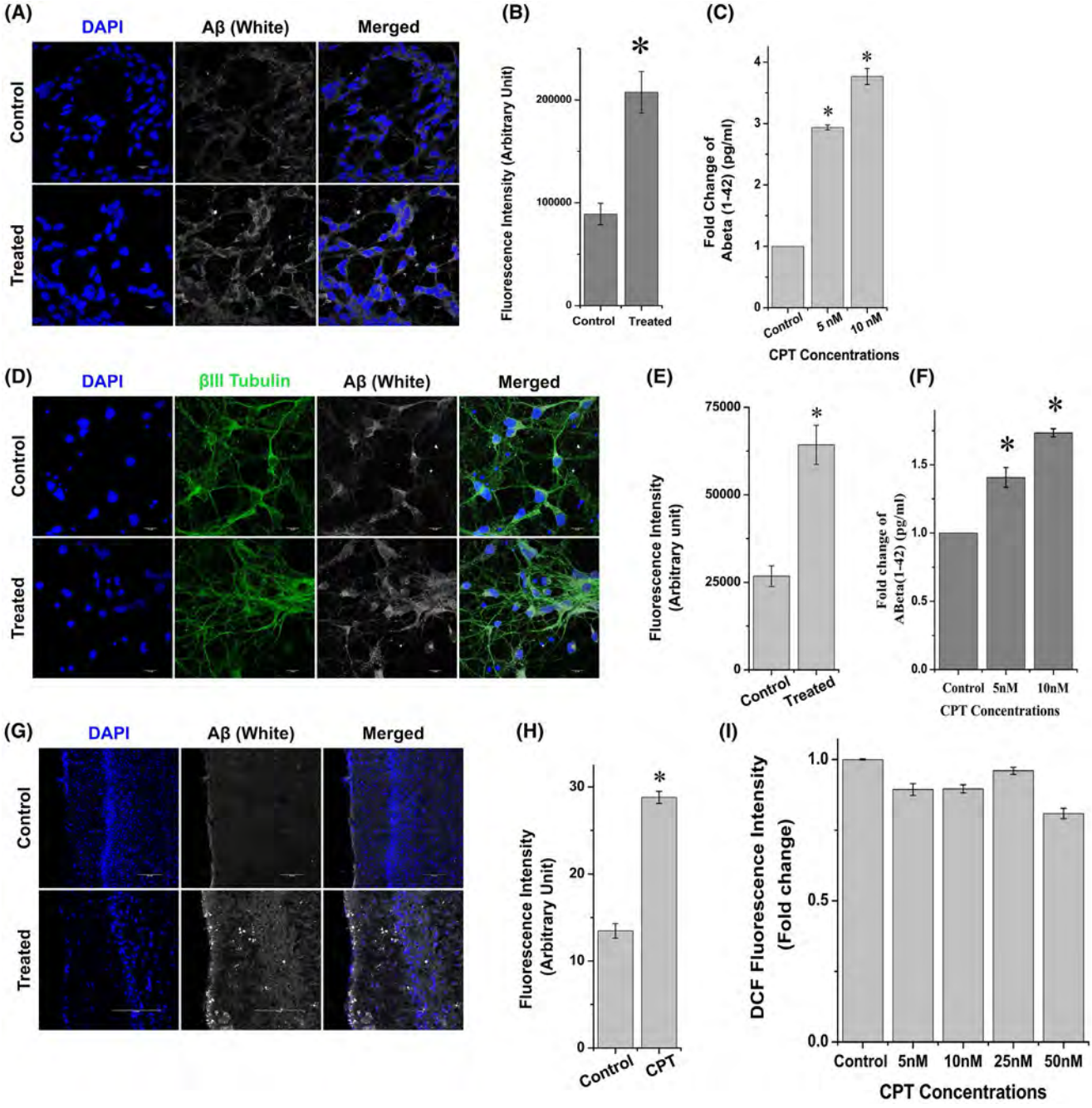

FIGURE 2 **Levels of $A\beta_{1\text{-}42}$ are increased under subtle induction of DNA damage in neurons**. A, Immunocytochemical staining with $A\beta_{1\text{-}42}$ antibody (white), followed by nuclei staining with DAPI (blue) in differentiated SH-SY5Y cells after 24 h of 10 nmol/L CPT treatment. B, The CTCF (calculated total cell fluorescence) values of 25 cells from random fields were calculated using ImageJ software and data are represented as mean ± SEM (*$P < .05$). Anti-$A\beta_{1\text{-}42}$ antibody which is reactive with $A\beta_{1\text{-}42}$ and does not cross-react with $A\beta_{1\text{-}40}$, full-length APP, sAPP-beta or sAPP-alpha is used for the staining. C, Sandwich ELISA of $A\beta_{1\text{-}42}$ in the spent media of differentiated SH-SY5Y cells after 5 nmol/L and 10 nmol/L CPT treatment for 24 h. D, Immunocytochemical staining with $A\beta_{1\text{-}42}$ antibody (white), β3-Tubulin antibody (green), followed by nuclei staining with DAPI (blue) in primary cortical neurons after 24 h of 10 nmol/L CPT treatment. E, Quantification of fluorescence intensity of (D). The CTCF values of 25 cells from random fields were calculated using ImageJ software and data are represented as mean ± SEM (*$P < .05$). F, Sandwich ELISA of $A\beta_{1\text{-}42}$ in the spent media of cultured primary cortical neurons after 5 nmol/L and 10 nmol/L CPT treatment for 24 h. Data are represented as mean ± SEM (*$P < .05$; n = 3). G, Immunohistochemical staining with $A\beta_{1\text{-}42}$ antibody (white) followed by nuclei staining with DAPI (blue) of sections obtained from rat brain cortex infused with 100 nmol/L CPT for 48 h. H, Quantification of fluorescence intensity of $A\beta_{1\text{-}42}$ using ImageJ software. Each group contained three numbers of animals. Intensity of 25 images from each group were calculated and data are represented as mean ± SEM (*$P < .05$) n = 25. (I) Quantification of DCF fluorescence obtained from flow cytometry for the measurement of total cellular ROS in differentiated SH-SY5Y cells under different concentrations of CPT treatment for 24 h

3.3 | Subtle DNA damage induces ER stress that leads to Aβ production by increasing BACE1 activity

Next, we addressed how $A\beta_{1\text{-}42}$ is generated in response to subtle DNA damage. Besides plasma membrane, APP has also been reported to be present in intracellular organelles including ER and accumulating evidences from transgenic mice and human patients suggest that $A\beta_{1\text{-}42}$ can also be generated and accumulated intraneuronally.[3] It is also known that γ-secretase complex along with APP is enriched at the interface between mitochondria and the ER.[9] To check whether subtle doses of CPT can induce ER stress in neurons, a prominent marker of ER stress—PERK, which is an important factor of the UPR, was investigated. ER stress activates PERK which subsequently phosphorylates eIF2α resulting in global transient suppression of translation and transcription of cytoprotective factors.[41] Interestingly, we found increased phosphorylation of PERK at a early time point (2 hours) in response to 10 nmol/L CPT treatment (Figure 3A,B; Figure S2A).

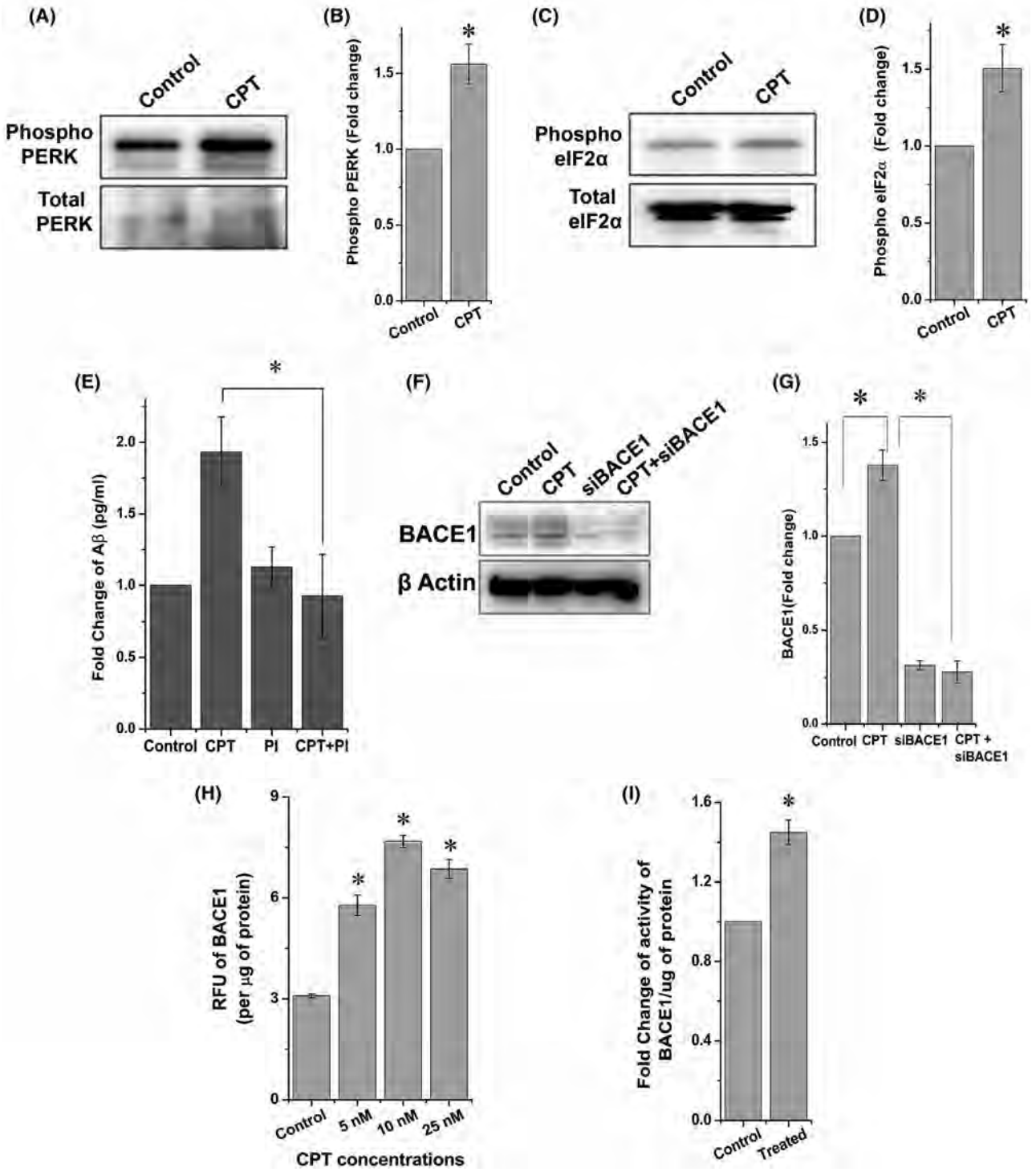

FIGURE 3 ER stress is induced and BACE activity is increased due to subtle DNA damage. A, Differentiated SH-SY5Y cells were treated with CPT for 2 h. Control and the treated cells were harvested and the lysates were subjected to western blot analysis using phospho-PERK and PERK antibodies. B, Bar diagram shows the levels of phospho-PERK normalized with total-PERK derived from densitometric analysis of the blot using the ImageJ software. Values are expressed as mean ± SEM from three independent experiments;*$P < .05$. C, Differentiated SH-SY5Y cells were treated with CPT for 2 h. Control and the treated cells were harvested and the lysates were subjected to western blot analysis using phospho-eIF2α and eIF2α antibodies. D, Bar diagram shows the levels of phospho-eIF2α normalized with total-eIF2α derived from densitometric analysis of the blot using the ImageJ software. Data are represented as mean ± SEM (*$P < .05$; n = 3). E, Quantitation of $A\beta_{1\text{-}42}$ in the spent media from differentiated SH-SY5Y cells after 24 h of treatment with 10 nmol/L CPT in presence or absence of 10 μmol/L PERK inhibitor (PI) were performed by ELISA. Bar diagram represents $A\beta_{1\text{-}42}$ level in pg/mL in control and the CPT-treated samples. Data are represented as mean ± SEM (*$P < .05$; n = 3). F, Differentiated SH-SY5Y cells were transfected with siBACE1, 48 h post-transfection treated with or without 10 nmol/L CPT for 24h and western blot analysis of cell lysates was performed using BACE1 antibody. G, Bar diagram shows the levels of BACE1 normalized with β-Actin derived from densitometric analysis of the blot using the ImageJ software. Data are represented as mean ± SEM (*$P < .05$; n = 3). H, Differentiated SH-SY5Y cells were treated with different doses of CPT as indicated for 24 h. BACE1 activity was measured from whole-cell lysate using the manufacturer's protocol of BACE1 activity measurement kit. I, Rat brain cortex was infused with 100 nmol/L CPT. After 48 h, animal was sacrificed and the activity of BACE1 was measured in the infused brain tissue lysate using the above mentioned kit. Data are represented as mean ± SEM (*$P < .05$; n = 3)

The phosphorylation levels of eIF2α were also increased under similar conditions (Figure 3C,D; Figure S2B). This finding indicates that mild DNA damage induces UPR-mediated ER stress in differentiated SH-SY5Y cells within 2 hours. To strengthen our finding of UPR-mediated ER stress, we checked downstream effector proteins of PERK arm of UPR and activation of IRE1α. We found marked increase of the effector proteins namely ATF4 and CHOP and increased phosphorylation of eIF2α after 2 hours of CPT treatment and a sharp decrease at 24 hours (Figure S1C-F). Interestingly we also found increased level of phospho-IRE-1α, and its direct effector XBP1, a parallel arm of UPR response, under similar time points which further strengthen the evidence of UPR in our model (Figure S1C,G,H).

To further confirm the contribution of PERK in increased Aβ load, GSK2656157 (PI), an established inhibitor of PERK at a concentration of 10 μmol/L was used for co-treatment with 10 nmol/L CPT for 24 hours and the level of extracellular $A\beta_{1\text{-}42}$ was measured in the spent media of neurons (Figure 3E). It was observed that PI reduced the level of $A\beta_{1\text{-}42}$ which was otherwise raised by 10 nmol/L CPT after 24 hours. These results suggest that the PERK arm of UPR contributes toward the increased $A\beta_{1\text{-}42}$ production in response to mild DNA damage.

It has been reported that energy deprivation leads to phosphorylation of eIF2α, which increases the translation of BACE1 and elevates Aβ production in neurons.[42] BACE1 is the rate limiting enzyme for $A\beta_{1\text{-}42}$ production. It gives an indication that under stress conditions, BACE1 could be a target of eIF2α. Hence, we checked the protein level of BACE1 and its activity in response to CPT treatments. We found that there was significant increase in protein level at 10 nmol/L CPT which was diminished in presence of si-BACE1 (3F-G). We also observed increased activity of BACE1 at 5, 10, and 25 nmol/L of CPT in differentiated SH-SY5Y cells (Figure 3H). Moreover, there was a significant increase in BACE1 activity in the tissue lysate of 100 nmol/L CPT infused rat brain cortex (Figure 3I). To further validate BACE1 activity in our model, we checked for other substrates of BACE1. Besides APP, BACE1 also cleaves seizureprotein 6, L1, CHL1 and contactin-2 etc in neuron.[43] We checked the levels of CHL1 and sAPPβ after 10 nmol/L CPT treatment in differentiated SH-SY5Y cells. Increased level of secretory sAPPβ was observed after 24 hours CPT treatment in differentiated SH-SY5Y cells (Figure S2I). Increased level of soluble CHL1 in conditioned medium was detected after 24h CPT treatment and that level was decreased following knockdown of BACE1 (Figure S2J,K). N-Cadherin and PTPRF were taken as negative controls which are not substrates of/dependent on BACE1 but are readily released in conditioned medium.[43] Hence, knocking down BACE1 did not change their levels in the conditioned medium. These results suggest that mild DNA damage induced an ER stress leading to an increase in $A\beta_{1\text{-}42}$ production by enhancing BACE1 activity via the PERK arm of UPR.

3.4 | Mitochondrial elongation occurs as an adaptive stress response due to subtle DNA damage

It has been reported that early ER stress leads to mitochondrial fusion which increases metabolic performance to cope with the stress.[41] This adaptive stress response also protects mitochondria from fission and autophagosomal degradation.[14,41] Since mild DNA damage led to ER stress in our model, we checked whether it causes mitochondrial fusion as well. We found elongated mitochondrial morphology under subtle induction of DNA damage which we describe as stress-induced mitochondrial elongation (SIME) (Figure 4A). Mitochondrial membrane potential was also increased as reflected by increased TMRM intensity under similar conditions (Figure 4B). Next we focused on the respiration of mitochondria by measuring the basal respiration and total ATP production in

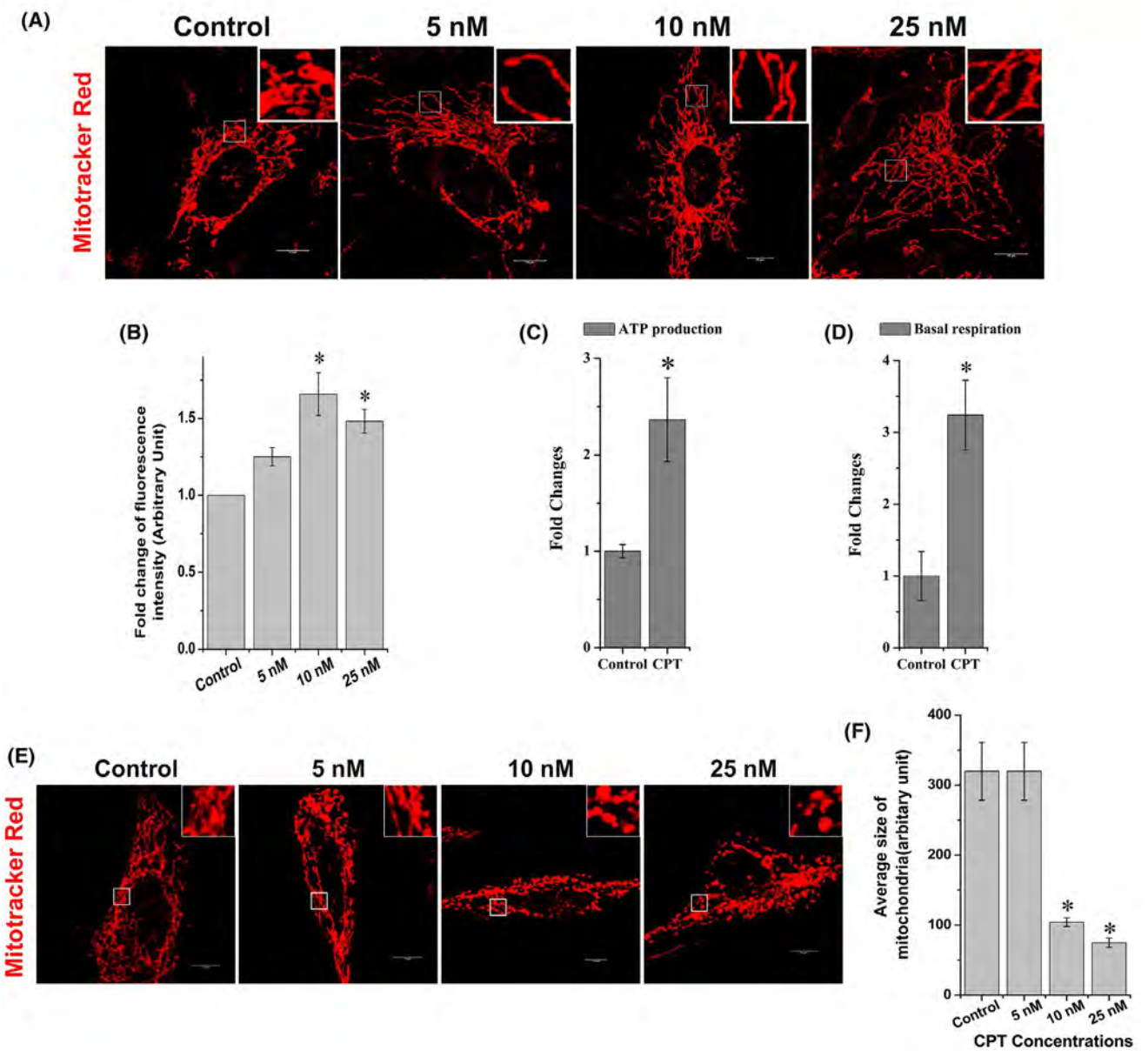

FIGURE 4 Subtle DNA damage causes stress-induced mitochondrial elongation (SIME) and boosts mitochondrial respiration in neurons. A, Differentiated SH-SY5Y cells were treated with different doses of CPT as indicated for 24 h. Mitochondria were stained with MitoTracker red and imaged under a confocal microscope. Note the elongated mitochondrial structures in zoomed insets. B, Differentiated SH-SY5Y cells were treated with different doses of CPT as indicated for 24 h. Quantitative analysis of mitochondrial membrane potential was performed after staining with TMRM followed by flow cytometry. Data are represented as mean ± SEM (*$P < .05$; n = 3). C and D, Differentiated SH-SY5Y cells were treated with different doses of CPT for 24 h. Bioenergetic flux was assessed using the Seahorse XFe24 analyzer and OCR was measured. Bar diagram represents changes in basal respiration and ATP production. Data are represented as mean ± SEM (*$P < .05$; n = 3). E, Differentiated SH-SY5Y cells were treated with indicated doses (5-25nM) of CPT for 48 h. MitoTracker red staining of mitochondria was done and pictures were taken under a confocal microscope. F, Sizes of mitochondria were determined using ImageJ software. Data are represented as mean ± SEM (*$P < .05$; n = 20 cells from three independent experiments)

differentiated SH-SY5Y cells treated with 10 nmol/L CPT for 24 hours. Using Seahorse XFe24 analyzer we found an increase in the basal respiration and ATP production in response to mild DNA damage (Figure 4C,D). These results suggest that mitochondrial fusion could be an adaptive stress response of a cell to promote mitochondrial metabolism as reflected by increased respiration and ATP production.[15,16,44]

We also assessed the fate of mitochondria when neuronal cells were exposed to mild DNA damage for a prolonged period. We observed mitochondrial fragmentation when neurons were treated with 10 nmol/L and 25 nmol/L CPT for 48 hours (Figure 4E,F). It is well known that mitochondrial fragmentation can lead to apoptosis.[45] Since AD is a progressive disease, it may be correlated with the scenario observed

in the disease condition, that mitochondrial elongation occurs at the early stages of the disease as an adaptive stress response to mild DNA damage, later followed by mitochondrial fragmentation resulting in neurodegeneration.

3.5 | Doxorubicin acts similar to CPT in differentiated SH-SY5Y cells and can induce increased Aβ production at low doses

After studying the effect of the mild doses of CPT on Aβ production, we extended our study to another commonly used DNA damaging agent Dox. Dox inhibits topoisomerase II which relaxes supercoils in DNA for transcription. This drug induces DNA double-strand breaks in cultured neuron as it accumulates in the nucleus and causes synaptic damage and compromised neuronal survival. At first we performed a cell viability assay to find out a range of doses of Dox that will not kill neuron. The result of cell viability assay with Dox in differentiated SH-SY5Y cells revealed that there was no significant cell death up to 1 μmol/L for 24 hours (Figure 5A). Next, we treated cells with very lose doses of Dox (10 and 100 nmol/L) for 24 hours and checked the level of pH2AX (Figure 5B-E). We observed increased pH2AX-positive foci in nucleus and increased level of pH2AX in cell lysate of both 10 and 100 nmol/L Dox-treated differentiated SH-SY5Y cells. There was induction of DNA damage but that was devoid of any simultaneous increment of apoptosis as there was no change in PARP1 cleavage (Figure 5F). Next we checked intra-neuronal Aβ level by immunocytochemistry with antibody against $Aβ_{1-42}$. Interestingly we found that there was increased Aβ staining in 10 and 100 nmol/L Dox-treated samples of 24 hours compared to untreated control (Figure 5G-H). There was also a significant increase in secretory level of $Aβ_{1-42}$ after treatment with 100 nmol/L Dox for 48 hours (Figure 5I). These results corroborated our finding with CPT and strengthen our point that mild DNA damage can induce increased level of Aβ. Hyperfusion of mitochondria (Figure 5J-K) was also observed as a part of adaptive stress response after Dox treatment along with increased pPERK and peIF2α (Figure 5L-N). These findings altogether suggest that increased intra-neuronal Aβ is a by-product of a cell which is under mild DNA damage and associated early ER stress.

3.6 | MFN2 plays an essential role for mitochondrial fusion in response to mild DNA damage

MFN2 seems to have a critical role in mitochondrial fusion and dynamics in the brain. Moreover, its downregulation has been reported in AD postmortem brains which might affect the Aβ production.[19] Since we found an increased mitochondrial fusion in response to mild DNA damage, we determined the level of MFN2 in neurons. The dose of CPT that elevates $Aβ_{1-42}$ level, also increased the expression of MFN2 in neurons. Immunocytochemical study revealed that there was an increased expression of MFN2 in differentiated SH-SY5Y cells when treated with 10 nmol/L CPT for 24 hours (Figure 6A,B). There was also a dose-dependent increase in MFN2 levels in response to the sub-lethal doses of CPT as observed by western blot analysis (Figure 6C,D). To further validate the essential role of MFN2 in Aβ production, we downregulated MFN2 in differentiated SH-SY5Y cells and treated them with 10 nmol/L CPT. Immunocytochemistry and ELISA results revealed that knockdown of MFN2 reduced the level of Aβ which was upregulated due to CPT treatment (Figure 6E-G). Interestingly, no mitochondrial elongation was observed in MFN2 knock-out MEF cells in response to CPT treatment which indicates the essential role of MFN2 in SIME (Figure S3A). We then compared the levels of MFN2 at different ages in 5xFAD transgenic mice (2, 4, and 7 months) with age-matched wild-type controls and observed that prior to the development of AD pathology, that is, in the early age groups (2 and 4 months), MFN2 levels were significantly increased as compared to age-matched controls (Figure 6H-I, Figure S3B). This finding probably suggests that MFN2 is increased as an adaptive stress response leading to hyperfusion of mitochondria and Aβ production at the early stages of AD and later it decreases as fragmentation of mitochondria increases.

3.7 | ER stress-induced PERK and BACE1 are required for mitochondrial elongation

Finally, we addressed one interesting aspect that is whether ER stress-induced PERK and subsequent BACE1 activation have any contribution to the increased elongation of mitochondria. To clear that doubt we inhibited PERK and BACE1 by treating differentiated SH-SY5Y cells with PERK and BACE1 inhibitors, respectively, in presence of 10 nmol/L CPT and checked the effect on mitochondrial elongation. The result showed that there was significant reduction of mitochondrial fusion with inhibition of PERK as well as of BACE1 (Figure 7A,B). siRNA-mediated downregulation of BACE1 also showed similar effect on mitochondrial ultrastructure (Figure 7C,D) as observed by treatment with commercially available BACE1 inhibitor. This finding emphasizes the contribution of Aβ toward increased mitochondrial fusion under subtle DNA damage. Moreover, inhibition of PERK and BACE1 also blocked the increase in MFN2 levels in response to 10 nmol/L CPT

treatment (Figure 7E,F). Collectively, these results suggest that mild DNA damage-induced ER stress triggers an early protective stress response such as increased mitochondrial fusion by activating PERK and BACE1. However, $A\beta_{1-42}$ is also produced as a by-product following BACE1 activation and may eventually accumulate and lead to

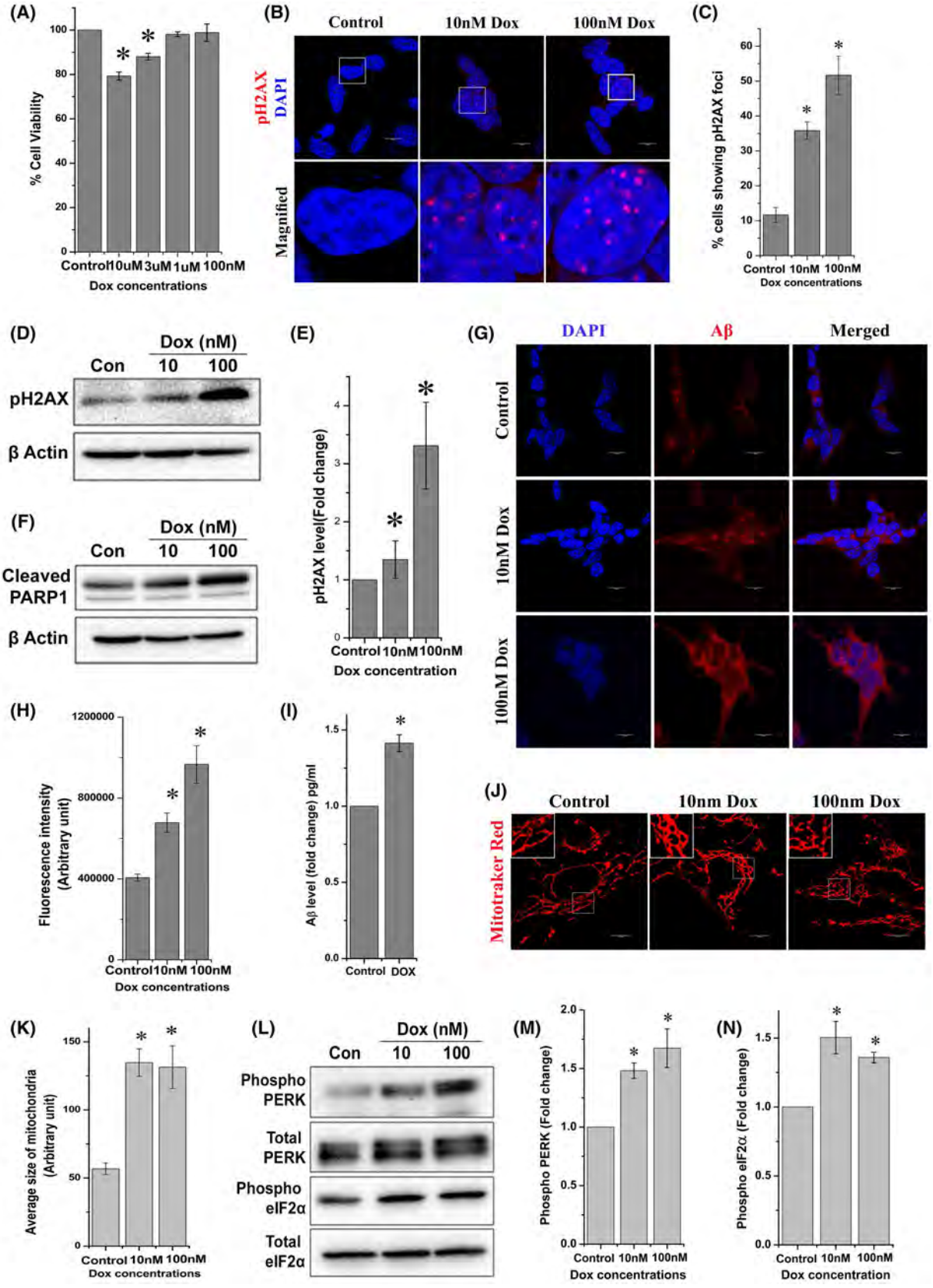

FIGURE 5 Doxorubicin (Dox) induces increased level of Aβ at low doses without inducing cell death. A, Differentiated SH-SY5Y cells were treated with Dox (100 nmol/L-10 μmol/L) for 24 h. Cell viability was checked by MTT assay. Data are represented as mean ± SEM (*$P < .05$; n = 3). B, C, Differentiated SH-SY5Y cells were treated with Dox for 24 h, and then subjected to immunocytochemical staining with DNA damage marker pH2AX antibody followed by nuclear staining with DAPI. Number of cells positive for pH2AX foci were counted from random fields of three independent experiments and represented as percentage of cells showing pH2AX-positive foci. Data are represented as mean ± SEM (*$P < .05$). D, E, Expression of pH2AX protein level was studied by western blot analysis. Bar diagram shows the levels of pH2AX normalized with β-Actin derived from densitometric analysis of the blot using the ImageJ software. Values are expressed as mean ± SEM from three independent experiments;*$P < .05$. F, Expression of cleaved PARP-1 protein level was studied by western blot. G, Immunocytochemical staining with $Aβ_{1-42}$ antibody (red), followed by nuclei staining with DAPI (blue) in differentiated SH-SY5Y cells after 24 h of 10 nmol/L and 100 nmol/L Dox treatment. H, The CTCF (calculated total cell fluorescence) values of 25 cells from random fields were calculated using ImageJ software and data are represented as mean ± SEM (*$P < .05$). I, Sandwich ELISA of $Aβ_{1-42}$ in the spent media of differentiated SH-SY5Y cells after 100 nmol/L Dox treatment for 48 h. J, Differentiated SH-SY5Y cells were treated with indicated doses of Dox for 24 h. MitoTracker red staining of mitochondria was done and pictures were taken under a confocal microscope. K, Sizes of mitochondria were determined using ImageJ software. Data are represented as mean ± SEM (*$P < .05$; n = 15 cells from three independent experiments). L, Markers of ER stress phospho-PERK normalized with total-PERK and phospho-eIF2α normalized with total-eIF2α were analyzed by western blot. M, N, Densitometry of the same is presented. Data are represented as mean ± SEM (*$P < .05$; n = 3)

neurodegeneration. The overall findings are summarized schematically in Figure 7G.

4 | DISCUSSION

A major concern in case of sporadic AD is how Aβ reaches at the toxic levels in the brain parenchyma. We report here that mild DNA damage leads to ER stress which activates BACE1 and thereby Aβ production. We hypothesized that age-related DNA damage that cannot be repaired efficiently with aging, might lead to an elevated production of Aβ. We introduced mild DNA damage using sub-lethal doses of CPT and Dox in cultured neurons and also in vivo by injecting CPT in the cortex. The doses we used induced DNA damage without any induction of oxidative stress or death in neurons. However, the mild DNA damage led to an increase in $Aβ_{1-42}$ levels in neurons in vitro and in vivo. Next we investigated the mechanism behind DNA damage-induced enhanced Aβ synthesis. We observed activation of PERK, its substrate eIF2α, and their downstream effector molecules ATF4 and CHOP as well as activation of IRE-1α and the associated effector protein XBP1. Both of these signaling pathways are recognized as parallel arms of UPR that may be induced by ER stress in response to the mild DNA damage. We also found increased BACE1 activity in response to the mild DNA damage since BACE1 is already recognized as the downstream target of eIF2α. Recently, Lebeau et al have reported that PERK arm of UPR protects mitochondria by dynamic remodeling of mitochondrial morphology and promoting stress-induced mitochondrial hyperfusion.[15] We observed that the subtle DNA damage led to mitochondrial elongation and boosted basal respiration and ATP production. However, prolonged application of the mild DNA damage led to mitochondrial fragmentation. Importantly, we found MFN2, an outer mitochondrial GTPase protein, plays an essential role in Aβ production and displayed increased levels in 5xFAD mice at early stages. Moreover, we found that both PERK activity and BACE1 activity are required for mild DNA damage-induced mitochondrial elongation.

Altogether, it apparently seems that the increased Aβ synthesis comes as a by-product of this adaptive stress response, seen as mitochondrial elongation, triggered by mild DNA damage. Subtle DNA damage is a prominent feature of an aging cell. Brain cells are much more susceptible to oxidative damage to their DNA, proteins, and lipids as brain consumes higher oxygen than any other organ.[46] Aging and AD both share many common features including DNA damage.[27] Accumulating evidence convincingly indicates to an intraneuronal accumulation of Aβ in AD brains at early stages.[46] It is an established fact that Aβ is mainly synthesized intracellularly [47] and its release is regulated by synaptic activity.[2] Since APP and its processing enzymes such as γ-secretase, are also present in many intracellular organelles namely endosomes, ER and mitochondria, Aβ can be synthesized at the organelle level.[3] UPR arm of ER stress is reportedly activated in response to mild stress such as energy deprivation which in turn can activate BACE1 and the following Aβ production.[42] Consistently, our work demonstrate that a mild DNA damage trigger ER stress, thereby BACE1 activation and Aβ production. CPT treatment of differentiated SH-SY5Y cells with very low doses led to the activation of PERK-eIF2α-ATF4 pathway as a part of UPR at a early time point. IRE-1α was also activated after CPT treatment within a short period of time. Both PERK and IRE-1α respond to ER stress in a similar manner. Along with IRE-1α, PERK indirectly reduces the quantity of unfolded polypeptide within the ER to allow for more efficient chaperone-mediated protein folding. Interestingly, the UPR response was induced at early time points and diminished after 24 hours while the BACE1 activity persisted and so did the Aβ level. Furthermore, although subtle DNA damage led to mitochondrial fusion at early time points, mitochondrial fission took place at 48 hours. Thus, sustained ER stress leads to cell death at later time points.

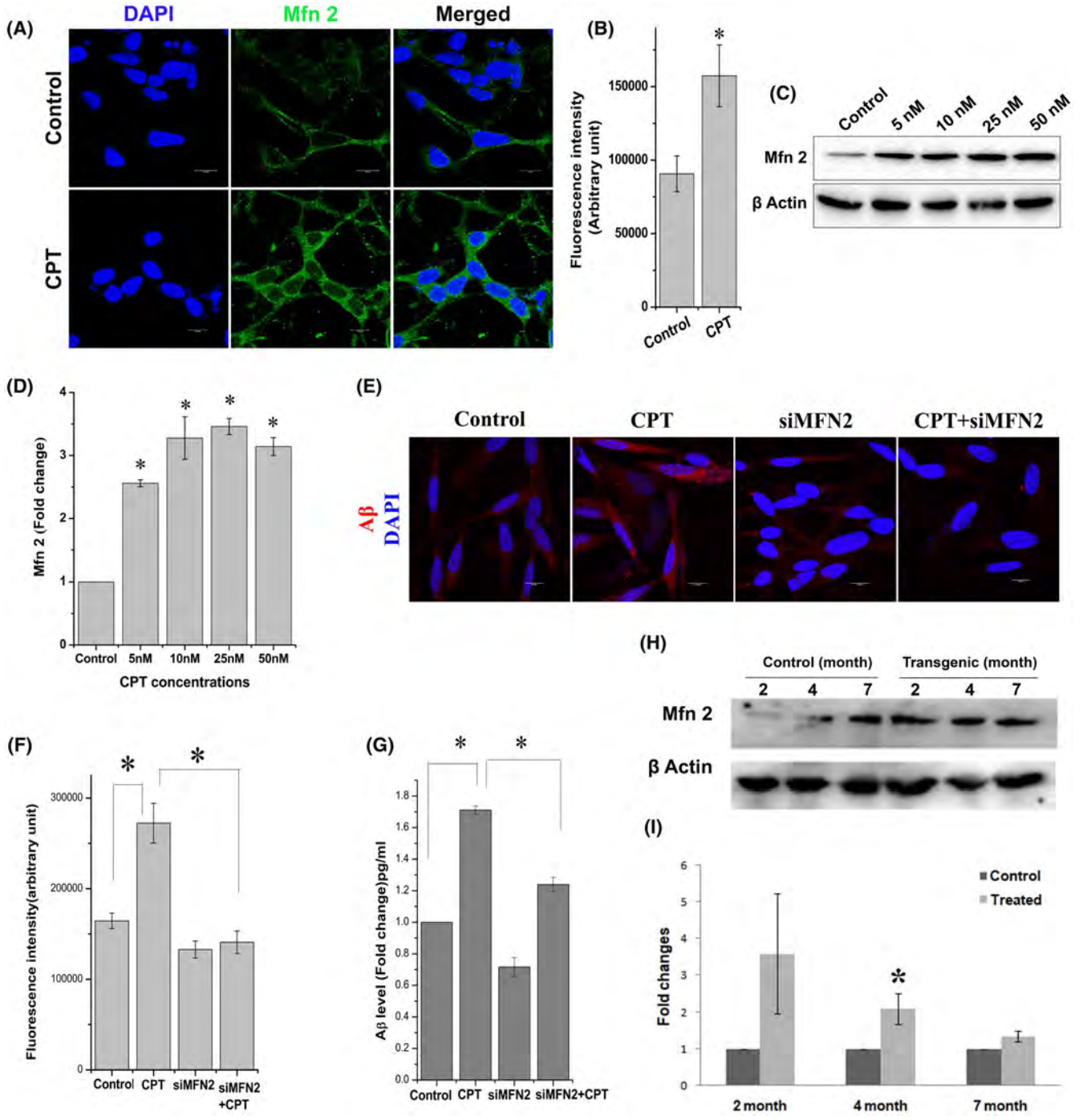

FIGURE 6 MFN2 plays a role in DNA damage-induced mitochondrial fusion. A, Immunocytochemistry of MFN2 in differentiated SH-SY5Y cells after treatment with 10 nmol/L CPT for 24 h. Blue represents DAPI and green represents MFN2. B, CTCF values were calculated and data are represented as mean ± SEM (*$P < .05$; n = 25 cells from random fields of three independent experiments). C, Differentiated SH-SY5Y cells were treated with different doses of CPT for 24 h. Control and the treated cells were harvested and the lysates were subjected to western blot analysis using MFN2 and β-actin antibodies. D, Bar diagram shows the levels of MFN2 normalized with β-actin derived from densitometric analysis of the blot using the ImageJ software. Data are represented as mean ± SD (*$P < .05$; n = 2). E, Differentiated SH-SY5Y cells were transfected with siMFN2, 48 h post-transfection treated with or without 10 nmol/L CPT for 24h and cells were immunostained with antibody against $A\beta_{1\text{-}42}$ (red). Nucleus was stained with DAPI. F, The CTCF values of 25 cells from random fields were calculated using ImageJ software and data are represented as mean ± SEM (*$P < .05$). G, Sandwich ELISA of $A\beta_{1\text{-}42}$ in the spent media of differentiated SHSY5Y cells transfected with siMFN2 for 48 h and treated with or without 10 nmol/L CPT post-transfection for 24 h was performed. Data are represented as mean ± SEM (*$P < .05$; n = 3). H, Western blot analysis of MFN2 using tissue lysates from different ages of wild-type and 5xFAD transgenic mice. Note the increased expression of MFN2 is observed in early months of transgenic AD mice compared to age-matched control. I, Bar diagram shows the levels of MFN2 normalized with β-actin derived from densitometric analysis of the blots using the ImageJ software. Data are represented as mean ± SEM (*$P < .05$; n = 3)

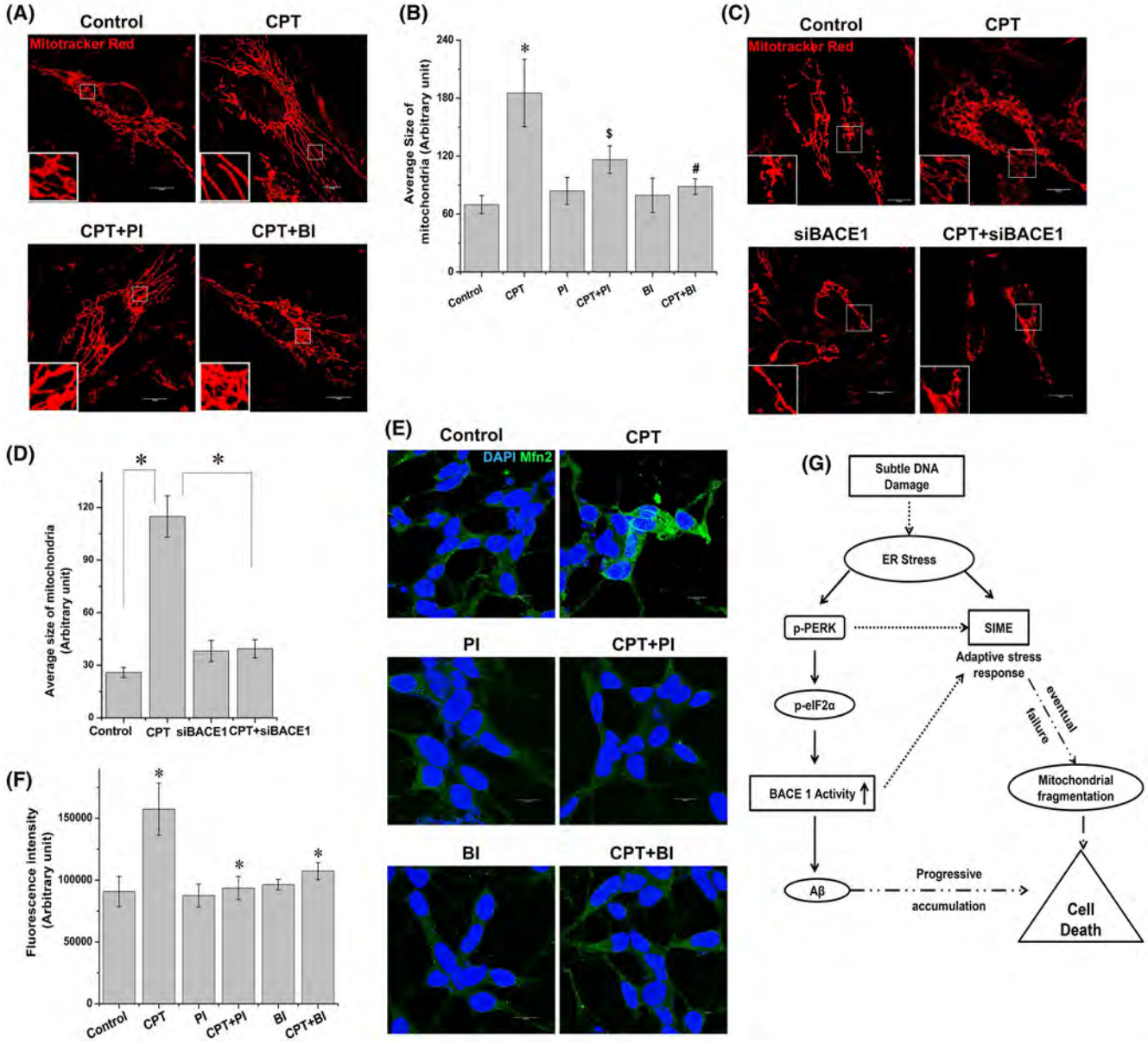

FIGURE 7 ER stress-induced PERK and BACE1 contributes to SIME caused by DNA damage. A, Shows the effect of PERK inhibitor (PI) and BACE1 inhibitor (BI) on mitochondrial dynamics. Differentiated SH-SY5Y cells were treated with 10 nmol/L CPT in presence or absence of 10 μmol/L PI and 5 μmol/L BI for 24 h. Mitochondria were stained with MitoTracker red and imaged under a confocal microscope. B, Quantification of mitochondrial size using ImageJ software. Data are represented as mean ± SEM; *: control vs CPT; $: CPT vs CPT+PI; #: CPT vs CPT+BI ($P < .05$ was considered as significant, n = 25 cells from three independent experiments). C, Differentiated SH-SY5Y cells were transfected with siBACE1, 48 h post-transfection, treated with or without 10 nmol/L CPT for 8 h and staining with MitoTracker red was done to see mitochondrial ultra-structure. D, Sizes of mitochondria were determined using ImageJ software. Data are represented as mean ± SEM (*$P < .05$; n = 15 cells from three independent experiments). E, Immunocytochemical staining with MFN2 antibody (green), followed by nuclei staining with DAPI (blue) in differentiated SH-SY5Y cells after 24 hours of 10 nmol/L CPT treatment in presence or absence of 10 μmol/L PI and 5 μmol/L BI. F, Quantification of fluorescence intensity of MFN2 using ImageJ software. CTCF values were calculated and data are represented as mean ± SEM (*$P < .05$; n = 25 cells from random fields of three independent experiments). G, Graphical representation of the proposed pathway leading to an increase in Aβ production and stress-induced mitochondrial changes in response to a mild DNA damage

Mitochondrial dysfunction is an integral part of AD. It has been extensively reported in models of AD and AD patients' brain cells. However, it has been suggested that mitochondrial dysfunction is an epiphenomenon of a dysfunctional neuron, and it occurs at a later stage in the disease.[48] Mitochondria do not work in isolation, but associate with other subcellular organelles including ER via mitochondria-associated ER membranes (MAM). Interestingly, it has been shown that components of γ-secretase, presenilin-1, presenilin-2, and γ-secretase activity itself are highly enriched

in MAM.[49] Therefore, changes in the function of MAM could have a role behind the production of Aβ. MFN2 is also enriched in MAM which is required for mitochondrial fusion.[29] Importantly, we found that mitochondrial elongation takes place due to ER stress in response to mild DNA damage and Aβ is apparently produced as a consequence. Inhibition or downregulation of BACE1 in presence of CPT treatment reduced elongation/fusion of mitochondria suggesting a possible role of Aβ in mitochondrial elongation which is an adaptive morphology of mitochondria coping with stress. The fusion of mitochondrial network promotes a resistance of mitochondria toward autophagosomal degradation.[44] It helps in buffering the damage caused to mitochondria by exchanging mtDNA and also helps to meet the energy demand of a cell by promoting ATP production.[50,51] DNA double-strand break activates DNA repair pathway in neurons which is very much energy demanding.[46] So, to meet the energy demand of DNA double-strand break, elongation of mitochondria could be one of the consequences as it boosts oxidative phosphorylation resulting in enhanced ATP production. Increase of intracellular Aβ may be seen as a consequence of adaptive stress response as it can bind and scavenge intracellular ROS via binding to heavy metals.[46] In this study, we observed that increase of intracellular Aβ occurred initially without any increase in ROS. We also observed fusion of mitochondria at the early time periods following the stress that may help to delay the process/progress of death. But after a certain point, this fusion shifts toward mitochondrial fragmentation which may accompany an increased ROS production.[52] Fragmented mitochondrial morphology is prominent in the affected regions of brain which is an important feature of a dying neuron.[13] AD is associated with mitochondrial fragmentation that is observed in the late stages of the disease but what precedes this detrimental mitochondrial morphology is not clearly known. To understand the correlation of this transition of mitochondrial morphology in the disease progression, we checked MFN2 levels in 5xFAD mice and notably, we found increased levels of MFN2 in the early months of transgenic AD mice brains prior to the appearance of plaques as compared to the wild-type mice.[53] It suggests that before the appearance of Aβ plaques, there could be an adaptive stress response manifested by elongation of mitochondria at the early stages of the disease. The switch from fusion to fission and its exact mechanism is not clear and demands further research. Altogether this study draws attention to a comparatively novel mitochondrial phenomenon that is stress-induced mitochondrial elongation in the scenario of AD. Unveiling this remodeling event could be beneficial to revisit the disease from a mitochondrial-ER perspective presenting new molecular players appearing early in AD progression.

Plenty of literature has already depicted the association of Aβ production and oxidative stress.[54] Jin et al[55] reported that oxidative stress induced by DNA damaging agents, Etoposide, and Camptothecin increased the γ secretase activity in CHO-C99 cell line. But the selected doses were 100 μmol/L for Etoposide and 25 μmol/L for CPT much higher than the dose range 5-25 nmol/L we used to induce the mild DNA damage. DNA damaging agents at higher doses induce oxidative stress and apoptosis. In that study, increment of ROS or RNS coincided with the increase of γ-secretase activity. Other studies have also shown an association of oxidative stress and BACE1 activity.[56] Oxidative stress may also be the cause of increased Aβ production. Oxidative stress inducing agent may increase APP expression and, therefore, enhance intracellular and secreted Aβ levels in neuronal and non-neuronal cells.[57-61] However, oxidative stress and associated apoptosis are a chronic condition that occurs at the late stages in a progressive disease like AD. In contrast to these reports, Wang et al[62] have shown that CPT and its analogs reduced Aβ levels in HEK and SH-SY5Y cell lines stably expressing AβPP with the Swedish mutation. However, unlike neuronal cells, these cancerous cell lines were resistant to CPT-induced death even at 1 μmol/L concentration. Primary neurons and differentiated SH-SY5Y cells are more prone to CPT-induced toxicity and 1 μmol/L CPT induces cell death in these cells.[36] Moreover, SH-SY5Y cell lines stably expressing AβPP with the Swedish mutation produced exogenous Aβ which was probably reduced by CPT. Whereas, in our study we only induced mild DNA damage using very low concentration of CPT in differentiated SH-SY5Y cells, primary neurons (10 nmol/L) or even in animals (100 nmol/L) to recapitulate an early phenomenon of AD which induced Aβ production without causing oxidative stress or apoptosis.

AD is a progressive neurodegenerative disease which extends through an asymptomatic stage called preclinical AD over few decades before the patient develops detectable amyloid pathology and other clinical manifestations. Despite significant advances in understanding the disease pathology, disease modifying drugs are yet to be achieved. Drugs targeting the amyloid pathology mainly targeted APP processing enzymes to block its synthesis or amyloid clearance by immunization[2] and have failed in clinical trials to date. We have investigated how $A\beta_{1\text{-}42}$ level increases in response to a subtle DNA damage in relation to aging. We demonstrated that mild DNA damage leads to ER stress and an adaptive mitochondrial response where an enhanced $A\beta_{1\text{-}42}$ production almost projects as a consequence. However, subsequent failure of this adaptive response alongside progressive $A\beta_{1\text{-}42}$ accumulation probably contributes toward the detrimental pathological signatures in the later stages of AD. Thus, this work may pave the way for many more investigations in understanding age-related sporadic AD where ER-mitochondrial interplay holds an unparalleled significance especially at the early disease stages.

ACKNOWLEDGMENTS

The authors thank Akash Saha for proof reading of this manuscript. The authors also thank Mr Sounak Bhattacharya for his technical assistance in confocal microscopy. The work was supported by SERB Projects (EEQ/2018/000997) of DST, Govt. of India and Counsil of Scientific and Industrial Research (CSIR), Govt.of India.

CONFLICT OF INTEREST

The authors have no conflict of interest.

AUTHOR CONTRIBUTIONS

HD and SCB conceived the problem and designed all experiments; HD performed all experiments. RKP helped in performing animal experiments; HD and SCB analyzed the data and wrote the paper. SS helped in performing experiments, analyzing the data and writing the paper during revision of the manuscript, and critical reading of this manuscript.

ORCID

Subhas C. Biswas https://orcid.org/0000-0002-1746-101X

REFERENCES

1. Bayer TA, Wirths O. Intracellular accumulation of amyloid-Beta - a predictor for synaptic dysfunction and neuron loss in Alzheimer's disease. *Front Aging Neurosci*. 2010;2:8.
2. Long JM, Holtzman DM. Alzheimer disease: an update on pathobiology and treatment strategies. *Cell*. 2019;179:312-339.
3. LaFerla FM, Green KN, Oddo S. Intracellular amyloid-beta in Alzheimer's disease. *Nat Rev Neurosci*. 2007;8:499-509.
4. Gouras GK, Tsai J, Naslund J, et al. Intraneuronal Abeta42 accumulation in human brain. *Am J Pathol*. 2000;156:15-20.
5. Takahashi RH, Almeida CG, Kearney PF, et al. Oligomerization of Alzheimer's beta-amyloid within processes and synapses of cultured neurons and brain. *J Neurosci*. 2004;24:3592-3599.
6. Ripoli C, Cocco S, Li Puma DD, et al. Intracellular accumulation of amyloid-beta (Abeta) protein plays a major role in Abeta-induced alterations of glutamatergic synaptic transmission and plasticity. *J Neurosci*. 2014;34:12893-12903.
7. Almeida CG, Tampellini D, Takahashi RH, et al. Beta-amyloid accumulation in APP mutant neurons reduces PSD-95 and GluR1 in synapses. *Neurobiol Dis*. 2005;20:187-198.
8. Area-Gomez E, del Carmen Lara Castillo M, Tambini MD, Guardia-Laguarta C, de Groof AJC, Madra M, Ikenouchi J, Umeda M, Bird TD, Sturley SL, Schon EA. Upregulated function of mitochondria-associated ER membranes in Alzheimer disease. *EMBO J*. 2012;31:4106-4123.
9. De Strooper B, Scorrano L. Close encounter: mitochondria, endoplasmic reticulum and Alzheimer's disease. *EMBO J*. 2012;31:4095-4097.
10. Lustbader JW, Cirilli M, Lin C, et al. ABAD directly links Abeta to mitochondrial toxicity in Alzheimer's disease. *Science*. 2004;304:448-452.
11. Caspersen C, Wang N, Yao J, et al. Mitochondrial Abeta: a potential focal point for neuronal metabolic dysfunction in Alzheimer's disease. *FASEB J*. 2005;19:2040-2041.
12. Manczak M, Anekonda TS, Henson E, Park BS, Quinn J, Reddy PH. Mitochondria are a direct site of A beta accumulation in Alzheimer's disease neurons: implications for free radical generation and oxidative damage in disease progression. *Hum Mol Genet*. 2006;15:1437-1449.
13. Wang X, Su B, Lee HG, et al. Impaired balance of mitochondrial fission and fusion in Alzheimer's disease. *J Neurosci*. 2009;29:9090-9103.
14. Rambold AS, Kostelecky B, Elia N, Lippincott-Schwartz J. Tubular network formation protects mitochondria from autophagosomal degradation during nutrient starvation. *Proc Natl Acad Sci USA*. 2011;108:10190-10195.
15. Lebeau J, Saunders JM, Moraes VWR, et al. The PERK arm of the unfolded protein response regulates mitochondrial morphology during acute endoplasmic reticulum stress. *Cell Rep*. 2018;22:2827-2836.
16. Tondera D, Grandemange S, Jourdain A, et al. SLP-2 is required for stress-induced mitochondrial hyperfusion. *EMBO J*. 2009;28:1589-1600.
17. Sprenkle NT, Sims SG, Sanchez CL, Meares GP. Endoplasmic reticulum stress and inflammation in the central nervous system. *Mol Neurodegener*. 2017;12:42.
18. Hoozemans JJ, Veerhuis R, Van Haastert ES, et al. The unfolded protein response is activated in Alzheimer's disease. *Acta Neuropathol*. 2005;110:165-172.
19. Filadi R, Pendin D, Pizzo P. Mitofusin 2: from functions to disease. *Cell Death Dis*. 2018;9:330.
20. Koshiba T, Detmer SA, Kaiser JT, Chen H, McCaffery JM, Chan DC. Structural basis of mitochondrial tethering by mitofusin complexes. *Science*. 2004;305:858-862.
21. Eura Y, Ishihara N, Yokota S, Mihara K. Two mitofusin proteins, mammalian homologues of FZO, with distinct functions are both required for mitochondrial fusion. *J Biochem*. 2003;134:333-344.
22. Manczak M, Calkins MJ, Reddy PH. Impaired mitochondrial dynamics and abnormal interaction of amyloid beta with mitochondrial protein Drp1 in neurons from patients with Alzheimer's disease: implications for neuronal damage. *Hum Mol Genet*. 2011;20:2495-2509.
23. Sordet O, Redon CE, Guirouilh-Barbat J, et al. Ataxia telangiectasia mutated activation by transcription- and topoisomerase I-induced DNA double-strand breaks. *EMBO Rep*. 2009;10:887-893.
24. Hsiang YH, Hertzberg R, Hecht S, Liu LF. Camptothecin induces protein-linked DNA breaks via mammalian DNA topoisomerase I. *J Biol Chem*. 1985;260:14873-14878.
25. Pommier Y. Topoisomerase I inhibitors: camptothecins and beyond. *Nat Rev Cancer*. 2006;6:789-802.
26. Manchon JF, Dabaghian Y, Uzor NE, Kesler SR, Wefel JS, Tsvetkov AS. Levetiracetam mitigates doxorubicin-induced DNA and synaptic damage in neurons. *Sci Rep*. 2016;6:25705.
27. Hegde ML, Hegde PM, Rao KS, Mitra S. Oxidative genome damage and its repair in neurodegenerative diseases: function of transition metals as a double-edged sword. *J Alzheimer's Dis*. 2011;24(Suppl 2):183-198.
28. Bradley-Whitman MA, Timmons MD, Beckett TL, Murphy MP, Lynn BC, Lovell MA. Nucleic acid oxidation: an early feature of Alzheimer's disease. *J Neurochem*. 2014;128:294-304.
29. de Brito OM, Scorrano L. Mitofusin 2 tethers endoplasmic reticulum to mitochondria. *Nature*. 2008;456:605-610.
30. Cotman CW, Su JH. Mechanisms of neuronal death in Alzheimer's disease. *Brain Pathol*. 1996;6:493-506.

31. Greene LA, Tischler AS. Establishment of a noradrenergic clonal line of rat adrenal pheochromocytoma cells which respond to nerve growth factor. *Proc Natl Acad Sci USA*. 1976;73:2424-2428.
32. Park DS, Morris EJ, Padmanabhan J, Shelanski ML, Geller HM, Greene LA. Cyclin-dependent kinases participate in death of neurons evoked by DNA-damaging agents. *J Cell Biol*. 1998;143:457-467.
33. Akhter R, Sanphui P, Biswas SC. The essential role of p53-up-regulated modulator of apoptosis (Puma) and its regulation by FoxO3a transcription factor in beta-amyloid-induced neuron death. *J Biol Chem*. 2014;289:10812-10822.
34. Biswas SC, Shi Y, Sproul A, Greene LA. Pro-apoptotic Bim induction in response to nerve growth factor deprivation requires simultaneous activation of three different death signaling pathways. *J Biol Chem*. 2007;282:29368-29374.
35. Brewer GJ. Isolation and culture of adult rat hippocampal neurons. *J Neurosci Methods*. 1997;71:143-155.
36. Morris EJ, Geller HM. Induction of neuronal apoptosis by camptothecin, an inhibitor of DNA topoisomerase-I: evidence for cell cycle-independent toxicity. *J Cell Biol*. 1996;134:757-770.
37. Kuo LJ, Yang LX. Gamma-H2AX - a novel biomarker for DNA double-strand breaks. *Vivo*. 2008;22:305-309.
38. Dovey HF, John V, Anderson JP, et al. Functional gamma-secretase inhibitors reduce beta-amyloid peptide levels in brain. *J Neurochem*. 2001;76:173-181.
39. Cheignon C, Tomas M, Bonnefont-Rousselot D, Faller P, Hureau C, Collin F. Oxidative stress and the amyloid beta peptide in Alzheimer's disease. *Redox Biol*. 2018;14:450-464.
40. Butterfield DA, Lauderback CM. Lipid peroxidation and protein oxidation in Alzheimer's disease brain: potential causes and consequences involving amyloid beta-peptide-associated free radical oxidative stress. *Free Radic Biol Med*. 2002;32:1050-1060.
41. Bravo R, Vicencio JM, Parra V, et al. Increased ER-mitochondrial coupling promotes mitochondrial respiration and bioenergetics during early phases of ER stress. *J Cell Sci*. 2011;124:2143-2152.
42. O'Connor T, Sadleir KR, Maus E, et al. Phosphorylation of the translation initiation factor eIF2alpha increases BACE1 levels and promotes amyloidogenesis. *Neuron*. 2008;60:988-1009.
43. Kuhn PH, Koroniak K, Hogl S, et al. Secretome protein enrichment identifies physiological BACE1 protease substrates in neurons. *EMBO J*. 2012;31:3157-3168.
44. Eisner V, Picard M, Hajnoczky G. Mitochondrial dynamics in adaptive and maladaptive cellular stress responses. *Nat Cell Biol*. 2018;20:755-765.
45. Young KW, Pinon LG, Bampton ET, Nicotera P. Different pathways lead to mitochondrial fragmentation during apoptotic and excitotoxic cell death in primary neurons. *J Biochem Mol Toxicol*. 2010;24:335-341.
46. Pan L, Penney J, Tsai LH. Chromatin regulation of DNA damage repair and genome integrity in the central nervous system. *J Mol Biol*. 2014;426:3376-3388.
47. Rajendran L, Annaert W. Membrane trafficking pathways in Alzheimer's disease. *Traffic*. 2012;13:759-770.
48. Morais VA, De Strooper B. Mitochondria dysfunction and neurodegenerative disorders: cause or consequence. *J Alzheimer's Dis*. 2010;20(Suppl 2):S255-S263.
49. Area-Gomez E, de Groof AJ, Boldogh I, et al. Presenilins are enriched in endoplasmic reticulum membranes associated with mitochondria. *Am J Pathol*. 2009;175:1810-1816.
50. Wang DB, Garden GA, Kinoshita C, et al. Declines in Drp1 and parkin expression underlie DNA damage-induced changes in mitochondrial length and neuronal death. *J Neurosci*. 2013;33:1357-1365.
51. Gomes LC, Di Benedetto G, Scorrano L. During autophagy mitochondria elongate, are spared from degradation and sustain cell viability. *Nat Cell Biol*. 2011;13:589-598.
52. Wang X, Wang W, Li L, Perry G, Lee HG, Zhu X. Oxidative stress and mitochondrial dysfunction in Alzheimer's disease. *Biochem Biophys Acta*. 2014;1842:1240-1247.
53. Oakley H, Cole SL, Logan S, et al. Intraneuronal beta-amyloid aggregates, neurodegeneration, and neuron loss in transgenic mice with five familial Alzheimer's disease mutations: potential factors in amyloid plaque formation. *J Neurosci*. 2006;26:10129-10140.
54. Tamagno E, Guglielmotto M, Aragno M, et al. Oxidative stress activates a positive feedback between the gamma- and beta-secretase cleavages of the beta-amyloid precursor protein. *J Neurochem*. 2008;104:683-695.
55. Jin SM, Cho HJ, Jung ES, Shim MY, Mook-Jung I. DNA damage-inducing agents elicit gamma-secretase activation mediated by oxidative stress. *Cell Death Differ*. 2008;15:1375-1384.
56. Tamagno E, Bardini P, Obbili A, et al. Oxidative stress increases expression and activity of BACE in NT2 neurons. *Neurobiol Dis*. 2002;10:279-288.
57. Frederikse PH, Garland D, Zigler JS Jr, Piatigorsky J. Oxidative stress increases production of beta-amyloid precursor protein and beta-amyloid (Abeta) in mammalian lenses, and Abeta has toxic effects on lens epithelial cells. *J Biol Chem*. 1996;271:10169-10174.
58. Misonou H, Morishima-Kawashima M, Ihara Y. Oxidative stress induces intracellular accumulation of amyloid beta-protein (Abeta) in human neuroblastoma cells. *Biochemistry*. 2000;39:6951-6959.
59. Murray IV, Liu L, Komatsu H, et al. Membrane-mediated amyloidogenesis and the promotion of oxidative lipid damage by amyloid beta proteins. *J Biol Chem*. 2007;282:9335-9345.
60. Patil S, Sheng L, Masserang A, Chan C. Palmitic acid-treated astrocytes induce BACE1 upregulation and accumulation of C-terminal fragment of APP in primary cortical neurons. *Neurosci Lett*. 2006;406:55-59.
61. Cheng SY, Trombetta LD. The induction of amyloid precursor protein and alpha-synuclein in rat hippocampal astrocytes by diethyldithiocarbamate and copper with or without glutathione. *Toxicol Lett*. 2004;146:139-149.
62. Wang J, Shi ZQ, Zhang M, et al. Camptothecin and its analogs reduce amyloid-beta production and amyloid-beta42-induced IL-1beta production. *J Alzheimer's Dis*. 2015;43:465-477.

SUPPORTING INFORMATION

Additional Supporting Information may be found online in the Supporting Information section.

How to cite this article: Das H, Sarkar S, Paidi RK, Biswas SC. Subtle genomic DNA damage induces intraneuronal production of amyloid-β (1-42) by increasing β-secretase activity. *The FASEB Journal*. 2021;35:e21569. https://doi.org/10.1096/fj.202001676RR

alzheimer's association

AAIC 21

ALZHEIMER'S ASSOCIATION INTERNATIONAL CONFERENCE®

JULY 26-30 > ONLINE AND IN PERSON

POSTER PRESENTER

SUKANYA SARKAR

presented "**Astrocyte-secreted TIMP-1 binds to CD63 and differentially phosphorylates Akt in protecting neurons and promoting cognitive recovery in 5xFAD mice** "

at the Alzheimer's Association International Conference® (AAIC®).

Delphine Boche, Ph.D.
Chair, Scientific Program Committee

Philip Scheltens, M.D., Ph.D., FAAN
Chair, Scientific Program Committee

Colorado Convention Center
Denver, Colorado, USA